The Pennsylvania State University

The Graduate School

DESTRUCTION AND REFORMATION OF AN IRON-SULFUR CLUSTER DURING CATALYSIS BY LIPOYL SYNTHASE

A Dissertation in

Biochemistry, Microbiology, and Molecular Biology

by

Erin L. McCarthy

© 2020 Erin McCarthy

Submitted in Partial Fulfillment
of the Requirements
for the Degree of

Doctor of Philosophy

May 2020

The dissertation of Erin L. McCarthy was reviewed and approved by the following:

Squire J. Booker
Evan Pugh University Professor of Chemistry
Professor of Biochemistry and Molecular Biology
Eberly Family Distinguished Chair in Chemistry
Howard Hughes Medical Investigator
Dissertation Advisor
Chair of Committee

Carsten Krebs
Professor of Chemistry
Professor of Biochemistry and Molecular Biology

Amie K. Boal
Associate Professor of Chemistry
Associate Professor of Biochemistry and Molecular Biology

Xin Zhang
Assistant Professor of Chemistry
Assistant Professor of Biochemistry and Molecular Biology
Paul Berg Early Career Professorship in the Eberly College of Science

Howard M. Salis
Associate Professor of Chemical Engineering
Associate Professor of Agricultural and Biological Engineering

Wendy Hanna-Rose
Head of the Department or Chair of the Graduate Program
Professor of Biochemistry and Molecular Biology

ABSTRACT

Lipoyl synthase (LipA in bacteria, LIAS in humans, Lip5 in yeast) is a radical SAM (RS) enzyme that catalyzes the second step of the *de novo* biosynthesis of lipoic acid, an essential cofactor known for its prominent roles in energy metabolism and the degradation of certain amino acids, among others. All RS enzymes contain one [4Fe–4S] cluster typically coordinated by cysteine residues lying in a highly conserved Cx_3Cx_2C motif. This iron-sulfur (Fe–S) cluster supplies the electron during the reductive cleavage of SAM to generate a 5′-deoxyadenosyl 5′-radical (5′-dA•) capable of hydrogen abstraction from an unactivated carbon center. Lipoyl synthase coordinates a second 'auxiliary' cluster that has been shown to be sacrificed as a sulfur source during catalysis, leaving LipA in an inactive state in the absence of a system to regenerate it. As such, LipA typically catalyzes no more than one turnover *in vitro.* This sacrificial role for an Fe–S cluster has been controversial because, in the proposed mechanism, LipA is a substrate consumed within the reaction, rather than an enzyme capable of catalysis.

In Chapter 2, the discovery of a novel protein factor, NfuA, is described. *E. coli* NfuA, an Fe–S cluster-containing protein suggested to serve as an intermediate in Fe–S cluster delivery, was found to restore *E. coli* LipA for subsequent turnover in a non-rate limiting step. This work explains why clinical patients with mutations in the gene encoding the human homolog NFU1 have fatal conditions associated with lipoic acid deficiency. Chapter 3 of this work describes studies to understand the mechanism by which *E. coli* NfuA targets and recognizes *E. coli* LipA. Importantly, we have discovered that *E. coli* NfuA is composed of two primary domains, and the N-terminal "A-type" domain is essential for tight complex formation with *E. coli* LipA both *in vitro* and *in vivo.* While the *E. coli* NfuA C-terminal domain can coordinate a [4Fe–4S] cluster, this truncated version is significantly impaired in its ability to activate *E. coli* LipA. Moreover, this study suggests that the architecture of *E. coli* NfuA is composed of two distinct components that have separate,

but essential, functions in the regeneration mechanism of *E. coli* LipA. Chapter 4 of this work describes strategies to understand the mechanism of cluster restoration in *E. coli* LipA.. Using a selenium labeled *E. coli* NfuA protein, we have discovered that *E. coli* LipA can utilize a [4Fe–4Se] cluster to produce selenolipoic acid; however, only exactly one equivalent of selenolipoic acid can be generated. These results have exciting potential applications for trapping an intermediate state in the NfuA-mediated cluster insertion mechanism. In Chapter 5, we have probed the specificity of NfuA for LipA by performing co-immunoprecipitation studies with NfuA that has an encoded FLAG epitope tag, we have pulled down endogenous proteins that interact with NfuA and identified them using mass spectrometry. Intriguingly, these proteins included LipA, as well as lipoylated proteins in the cell such as the pyruvate dehydrogenase complex and proteins involved in lipoic acid regulation such as ClpX. Other proteins involved in iron-sulfur cluster biogenesis and trafficking were also identified, including IscS and Mrp/AbpC. Lastly, other Fe–S cluster containing proteins, including RimO, MiaB, and RlmN, were also pulled down with NfuA. Additionally, through library construction and screening using a bacterial two hybrid approach, we have identified a single amino acid residue on NfuA, isoleucine at position 4, and a three amino acid motif isoleucine, proline, valine on LipA, at positions 22-24 that are involved in the protein-protein interaction. In Chapter 6, we have explored a conflicting hypothesis proposed in the literature that a different protein, ErpA, is the sole protein in the cell responsible for delivering Fe–S clusters in the cell. Rather, it was proposed that NfuA functions to stabilize the cofactor on ErpA rather than participate in the maturation of metalloproteins. Through a combination of *in vitro* and *in vivo* binding assays, as well as activity assays, we have shown that this hypothesis is unlikely, due to the lack of interaction between ErpA and LipA as well as limited effect on LipA activity. In addition, we characterized LipA from *S. aureus,* a pathogenic organism that has profound implications in human health and disease. The pathway of auxiliary cluster regeneration in this

organism was explored with subsequent characterizations of potentially involved proteins, including *S. aureus* SufT, *S. aureus* Nfu, and *S. aureus* SufA.

Collectively, this work addressed an outstanding fundamental question in the field of enzymology: what is the mechanism by which proteins that destroy their metallocofactors during their reaction mechanism get regenerated to support catalysis? While significant progress was made towards identifying and understanding the process by which the auxiliary cluster of *E. coli* LipA is regenerated during catalysis, many gaps still remain in our understanding. Indeed, future work will need to address many remaining questions which are discussed in the concluding future directions.

TABLE OF CONTENTS

LIST OF FIGURES

LIST OF TABLES

ACKNOWLEDGEMENTS

As I reflect upon the years spent towards earning my doctorate, it is difficult to put into words how grateful I am for all of the support I received along the way. It is truly incredible how many people contributed to my success. Being a part of the third floor is a unique experience and provides an unparalleled training environment.

First and foremost, I'd like to dedicate this thesis to my dad, Mike McCarthy. He was, and always will be, my biggest supporter. He was the funniest, smartest, and most generous person I have ever met. I miss you every day.

I am incredibly grateful to my thesis advisor, Squire Booker, for his endless support. I am constantly amazed by the depth of his knowledge spanning all areas of science. He has encouraged me to be fearless and to pursue difficult biological questions. Through his rigorous training, I have learned to be meticulous in both my research and scientific writing. Above all, his sheer enthusiasm and passion for science is infectious.

My committee provided a great deal of support to me over the years. Thank you to Howard Salis, Amie Boal, Xin Zhang, and Carsten Krebs. While not officially committee members, I am also grateful to Marty Bollinger and Alexey Silakov.

Carsten Krebs was an integral part of this chapter of my life and deserves special recognition. I think that all would agree that Carsten is truly the spirit of the third floor. He is the unifying force that lightens the many trials and tribulations that entail during a PhD program. It is true that a hoppy hour or a chocolate truffle can make even the worst research days a little brighter.

I am overwhelmed thinking of all the postdocs and graduate students who have helped me over the years. I am truly thankful to all current and previous members of the Silakov, Boal, Booker, and Bollinger/Krebs groups. Most importantly, Nick Lanz shaped me into the scientist I am today. His rigorous training at the beginning of my PhD was critical to my success. I am also thankful to Brad Landgraf, who helped me significantly during the early stages of my PhD. I am lucky to call Maria Pandelia a friend. Bo Zhang, thank you for your friendship and also for your tireless analyses of my complicated Mössbauer spectra. Debangsu Sil, more thanks for your patience and help deconvulating complicated Mössbauer spectra. As Maria would say, Mössbauer is unforgiving. I now fully understand that statement, as I am sure you do

also. To my friends Edward Badding, Liz Onderko, and Joey LaMattina, I had the most fun years of my PhD with you. Thanks for all the good times. Matt Bauerle and Erica Schwalm, thank you both for your light-heartedness at all stages during your time in the Booker lab. I will always appreciate your patience and willingness to help me. Bo Wang, thank you for all of your synthetic expertise. Thank you to undergraduate students Zerick Dill and Ananda Rankin who contributed to various aspects of my graduate work who I have had the privilege of mentoring. I can't wait to see what you accomplish in your future careers. Lastly, thanks to Patrick Corrigan, Hannah Rose, and Juan Pan for their friendship.

To my sister Shannon, thank you for everything you've done for me throughout my life. You are one of the most caring and dependable people I know, and I am thankful I have you. Aubrey and Chase are the light of my life. Aubrey, I am thankful for your past and future talented singing and acting performances, as well as your scholastic achievements. Chase, I am thankful for your quirky personality, your endless squishy hugs, and your genuine love and concern for the entire world. I look forward to seeing what the future holds for you both.

Mike Simon and Jack Cunningham, I am lucky to call you friends. Your support and heroic efforts during one of the most difficult times of my life will always be appreciated.

To the WABS: Kaylin, Ashley, JC, Lindsey, Christiana, Mike, and Abby, thank you for being the very best of friends over the past >15 years! It is rare to have such an unwavering friendship spanning so many stages of our lives.

Lastly, thank you to Chris Gray who has been supportive throughout the course of my graduate studies. His patience and calm demeanor has provided much needed balance to my life. I am so excited for our future together.

The authors acknowledge the following funding sources that supported the work in this document: NIH (GM-122595), National Science Foundation (MCB-1716686), and the Eberly Family Distinguished Chair in Science to SJB. SJB is an investigator of the Howard Hughes Medical Institute. The findings and conclusions presented within do not reflect the view of the above funding agencies.

Chapter 1

The Chemistry of Lipoic Acid Biosynthesis

This chapter was reproduced in part from "McCarthy, E.L., and Booker, S.J. The Chemistry of Lipoic Acid Biosynthesis. Comprehensive Natural Products III, *Submitted.*"

Historical Overview of Lipoic Acid

α-Lipoic acid (6,8-thioctic acid, (R)-5-(1,2-dithiolane-3-yl)pentanoic acid, or 6,8-dithiooctanoic acid) is a sulfur-containing molecule used as an essential cofactor by enzymes that catalyze the oxidative decarboxylation of various α-keto acids and glycine, as well as the breakdown of acetoin to acetaldehyde and acetyl-coA. In its functional form, it is covalently attached through an amide linkage to a specific lysyl residue on a lipoyl carrier protein (LCP), producing a 14 Å appendage. This so-called "swinging arm" allows the cofactor to transport reaction intermediates between successive active sites in the multienzyme complexes that require it. Its thiol groups at C6 and C8 allow for reversible disulfide bond formation—a two-electron oxidation—interchanging between free thiols and a 5-membered dithiolane ring. This dithiolane ring is a key property of this cofactor, which allows it to act both as an electron acceptor as well as a carrier of intermediates via a thioester linkage as detailed below **(Figure 1-1).**

Lipoic acid was originally discovered in the 1940s when it was identified as a factor that could support the growth of certain lactic acid bacteria (1,2). The growth of these particular bacteria relied heavily on the presence of acetate, a volatile compound that was largely lost from the media during the autoclave process, requiring supplementation of the cultures with acetate. Alternately, it was realized that an "acetate replacement factor" prepared by acid hydrolysis of liver could support growth (2-4). Research from another laboratory discovered that a different lactic acid bacteria grew on pyruvate only when supplied with a similarly prepared acetate-free acetate replacement factor, leading to the hypothesis that acetate was being synthesized by this compound through the decarboxylation of pyruvate (5-7). Together, these two groups solicited an industrial partnership with Eli Lilly, and, through a heroic effort, isolated 30 mgs of the acetate replacement/pyruvate oxidation factor from 10 tons of liver. This collaboration produced the first characterization of this compound, which was subsequently named lipoic acid, due to its physical properties such as its poor water solubility (8). Lipoic acid was found to be a sulfur-containing compound, though a nitroprusside assay to test for free thiols was negative. Treatment of the compound with sodium cyanide, an agent that can reduce dithiol bonds, resulted in a positive nitroprusside assay, which lead to the assignment of a dithiolane ring (9). A combination of elemental analysis, titration experiments, x-ray data, infrared spectroscopy, and polarographic studies revealed its molecular formula as $C_8H_{14}O_2S_2$. Taken together, these analyses led to the successful determination of the structure of lipoic acid by comparing the experimentally determined properties to those of chemically synthesized racemic thioctic acid (9,10). Lipoic acid was later found to have one chiral center at C6, an assignment that was made possible by the chemical synthesis of the two isomers by Merck (11,12). A number of experiments revealed that lipoic acid was enzyme-bound in the cell. The first indication of a covalent attachment was the observation that hydrolysis was required to isolate lipoic acid. This finding was further tested by isolating the pyruvate and α-ketoglutarate dehydrogenase complexes from bacterial cultures supplemented with ^{35}S-labeled lipoic acid (13).

The as-isolated enzymes contained ^{35}S-labeled lipoic acid which could be only be removed by hydrolysis, resulting in inactive enzymes and radioactive N^6-(6,8-disulfooctanoyl)-L-lysine.

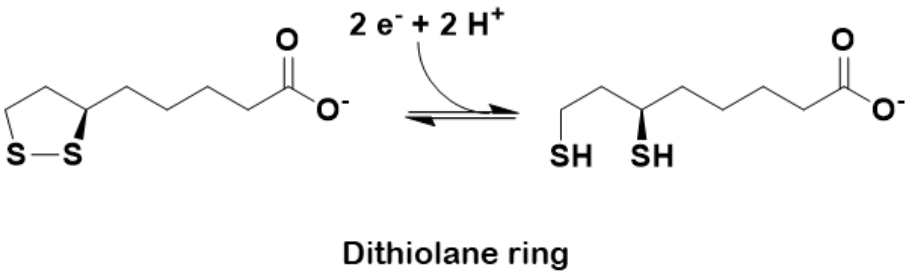

Figure 1-1: **Structure of lipoic acid.** Lipoic acid is an eight-carbon straight-chain fatty acid with thiol groups at C6 and C8, allowing reversible disulfide bond formation, interchanging between free thiols and a dithiolane ring.

Pathways for Biosynthesis of the Lipoyl Cofactor

Very little free lipoic acid exists in the cell. In its more biologically relevant form, lipoic acid is covalently attached via an amide linkage to a specific lysyl residue on a lipoyl carrier protein (LCP). The biosynthesis of the lipoyl cofactor has been best studied in *E. coli*. In this organism, two pathways exist for the production of the lipoyl cofactor. In the exogenous pathway, free lipoic acid is scavenged and ATP-activated to form a lipoyl-AMP intermediate. Subsequently, it is transferred to the lipoyl carrier protein to yield the lipoyl cofactor. In *E. coli*, both reactions are catalyzed by lipoate-protein ligase A. In humans and some other organisms, this reaction is catalyzed by two distinct proteins. Lipoate-activating enzyme (LAE) catalyzes the formation of the activated lipoyl-AMP, whereas lipoyltransferase (LT) catalyzes the subsequent transfer of the lipoyl group to the LCP. In the endogenous or *de novo* pathway, octanoyl-ACP is derived from the

type II fatty acid biosynthetic pathway. The octanoyltransferase LipB subsequently transfers the octanoyl group from the ACP to the LCP to generate octanoyl-LCP. LipA then catalyzes sulfur insertion at C6 and C8 of the octanoyl appendage to generate the lipoyl cofactor.

Lipoic Acid in Human Health

Lipoic acid is used therapeutically for a wide assortment of clinical conditions. In particular, its ability to readily cross the brain-blood barrier makes it an attractive clinical compound (14). Dihydrolipoic acid, the reduced form of lipoic acid, reacts with damaging oxidants such as superoxide radicals. It also participates in the recycling of other known antioxidants, including vitamin C, thioredoxin, and glutathione, which can then regenerate vitamin E (15,16). As a result of its antioxidant properties, lipoic acid has been shown to alleviate symptoms associated with oxidative stress, most notably in diabetes, a disease that afflicts more than 400 million people worldwide (17).

Lipoic acid has also been shown to modulate various signaling pathways, including insulin and NF-κB. In healthy individuals, insulin regulates glucose uptake in cells by directing the GLUT-4 glucose receptor to the plasma membrane, allowing it to facilitate glucose transport into the cells where it is phosphorylated and sequestered. Individuals suffering from type II diabetes develop insulin resistance, which is accompanied by a diminished ability to traffic GLUT-4 to the membrane surface. Lipoic acid has been shown to enhance GLUT-4 transport for more efficient glucose uptake, counteracting the negative effects arising from insulin resistance (18).

Defects in lipoic acid biosynthesis or in any of the enzymes that require it have resulted in clinical conditions that have been fatal in most cases (19). Mutations in the gene encoding lipoyl synthase (LIAS), which catalyzes the last step in the biosynthesis of the lipoyl cofactor, is a known cause of a condition known as glycine encephalopathy (also known as nonketoic hyperglycemia),

an autosomal recessive disorder affecting the glycine cleavage system (GCS), resulting in toxic accumulation of glycine in the body. Several cases describing extreme biochemical consequences as a result have been reported. Baker, *et al.*, described two patients with mutations in *LIAS* who suffered from variant non-ketotic hyperglycemia (20). The first patient had a mutation in *LIAS* that resulted in a glutamate 159 to lysine amino substitution. The patient presented systems neonatally of hypotonia, a state of low muscle tone. The patient later developed severe symptoms, including seizures, failure to thrive, severe psychomotor retardation, and acquired hearing lost, among other symptoms, which ultimately resulted in death before the age of 3. The second patient also had a mutation in *LIAS* which resulted in an aspartate 215 to glutamate amino acid substitution. Symptoms were observed two days after birth, which included hypotonia, seizures and severe developmental delays. At the age of 14, he functioned as if at the age of 7 and had immature physical functions. Western blot analysis of this patient's fibroblasts revealed significantly reduced levels of lipoylated proteins.

Tsurusaki *et al.* reported a patient with a novel mutation in *LIAS* resulting in a methionine 310 to threonine amino acid substitution and leading to glycine encephalopathy (21). In this case, the patient was normal until the age of 18 months when she suffered from an upper respiratory infection and subsequently developed severe symptoms including involuntary movements and seizures. This patient required tube feeding from the age of 19 months, and at 21 years, was bedridden and unable to form meaningful words. Mayr *et al.* described a patient with an arginine 294 to histidine amino substitution in *LIAS* resulting in pyruvate dehydrogenase deficiency (22). The patient presented with neonatal epilepsy and defective mitochondrial energy metabolism resulting in lactic acidosis. Western blot analysis confirmed depleted lipoic acid levels in the patient.

Mutations in genes outside of *LIAS* have also resulted in defects associated with insufficient lipoic acid production. Recently, mutations in the gene encoding the lipoyltransferase LIPT1 has been reported, resulting in pyruvate dehydrogenase and α-ketoglutarate dehydrogenase (KDH)

activities as well as Leigh disease, a neurometabolic disorder affecting the central nervous system (23). When this clinical case was documented, the role of ligase LIPT1 in human lipoic acid metabolism was unclear. However, the Cronan laboratory recently clarified the physiological role of LIPT1; it transfers the lipoyl group from the H protein, upon which it is synthesized, to the other LCPs that require it, explaining the observed clinical phenotypes (24).

Mutations in the genes encoding human NFU1 and BOLA3 have also been reported, which cause disastrous biochemical disorders that have been linked to lipoic acid deficiency (19,25,26). The underlying cause of the lipoic acid deficiency in humans with NFU1 mutations was recently uncovered when it was discovered that it is essential for restoring an essential cofactor of *E. coli* lipoyl synthase (LipA) during the biosynthesis of lipoic acid. However, the role of human BOLA3 and its possible role in lipoic acid biosynthesis is currently unknown. Indeed, these examples serve only to highlight some notable roles of lipoic acid, but are far from a comprehensive list of the extensive involvement of this essential molecule in human health and disease.

Biological Roles of the Lipoyl Cofactor

α-Keto-Acid Dehydrogenase Complexes. The role of lipoic acid in the α-ketoacid dehydrogenase complexes is well-established (27). The pyruvate dehydrogenase complex (PDC) and the α-ketoglutarate dehydrogenase complex (KDC) are required for carbon entry into the citric acid cycle as well as a key step in the citric acid cycle, whereas the branched-chain 2-oxoacid dehydrogenase complex (BCKDC) is responsible for the degradation of branched-chain amino acids (mammals), the synthesis of branched-chain fatty acids (bacteria), and the synthesis of branched-chain hydrocarbons (plants). In certain Gram-negative bacteria that undergo anaerobic respiration, the acetoin dehydrogenase complex (ADC) catalyzes the degradation of acetoin to acetaldehyde and acetyl-coenzyme A (CoA). These large multienzyme complexes contain a

dehydrogenase (E1), a dihydrolipoyl transacetylase (E2), and an FAD-dependent lipoamide dehydrogenase (E3) **(Figure 1-2).** E2 serves as the core of the complex and houses the lipoyl cofactor, which contains the 14 Å swinging arm that facilitates the translocation of intermediates between successive active sites of these elaborate protein complexes. The PDC mechanism is composed of five steps **(Figure 1-2).** The thiamine diphosphate (TDP)-dependent pyruvate dehydrogenase (E1) catalyzes the decarboxylation of pyruvate, generating CO_2. The resulting hydroxyethyl group is transferred from E1 to the lipoyl group on E2 with concomitant reduction of the disulfide bond. The thioester is cleaved by CoA to form acetyl-CoA. The dihydrolipoamide group is reoxidized by the FAD-dependent lipoamide dehydrogenase in the E3 subunit, regenerating the cofactor for subsequent turnovers. The reduced E3 subunit is in turn reoxidized at the expense of NAD^+, yielding NADH. The oxidative decarboxylation of α-ketoglutarate to succinyl-CoA, CO_2, and NADH in the KDC of the citric acid cycle, as well as the oxidative decarboxylation of the α-ketoacids generated from branched-chain amino acids in the BCKDC into acyl-CoA derivatives, occur through a mechanism that is similar to that described for the PDC. In contrast to the mechanism described for the PDC, the E1 complex of the ADC catalyzes the fragmentation of the α-hydroxyketone with formation of acetyl-TDP (acetoin is not a 2-oxoacid, so it cannot be decarboxylated). The same mechanism described for the PDC occurs in E2 and E3.

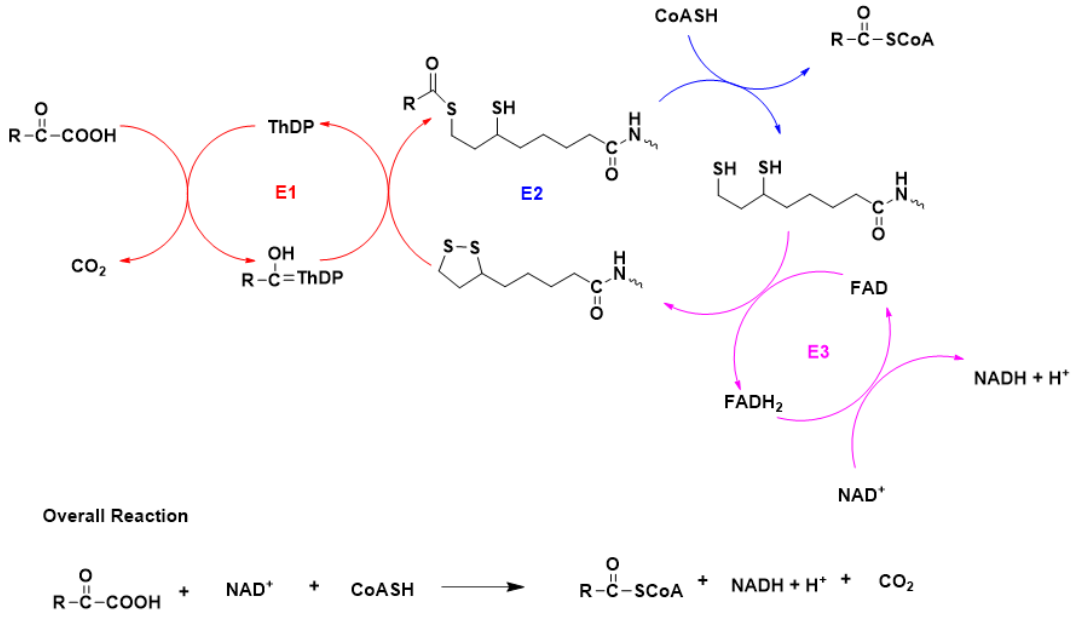

Figure 1-2: **Mechanism of α-Keto-Acid Dehydrogenase Complexes.** The E1 subunit binds thiamine diphosphate (ThDP); the E2 subunit contains lipoamide; the E3 subunit binds flavin adenine dinucleotide (FAD).

The Glycine Cleavage System. The glycine cleavage system (GCS, known as glycine decarboxylase in plants) catalyzes the reversible oxidative decarboxylation of glycine to CO_2, ammonia, and N^5,N^{10}-methylene-tetrahydrofolate (THF) **(Figure 1-3).** The GCS is composed of four loosely associated proteins (P, H, T, and L), unlike the PDC and KDC, which form multienzyme complexes containing tightly associated subunits. The P protein exists as a homodimer and catalyzes the PLP-dependent decarboxylation of glycine to yield CO_2. The resulting aminomethyl group is then transferred to the lipoylated aminomethyltransferase (H protein) with reduction of the lipoyl group to form an aminomethyl H protein intermediate. The T protein then catalyzes the formation of ammonia with the transfer of the methylene group from the lipoyl appendage on the H protein to THF, generating N^5,N^{10}-methylene-THF. The dihydrolipoyl

group is then reoxidized by the L protein. The GCS has been extensively studied and is the subject of many reviews (28). It is a also a vital component in the photorespiratory cycle in plants, where N^5,N^{10}-methylene-THF is used to form serine from glycine. The importance of the GCS is also highlighted above, where dysfunction of this system results in toxic accumulation of glycine in body tissues resulting in human disease.

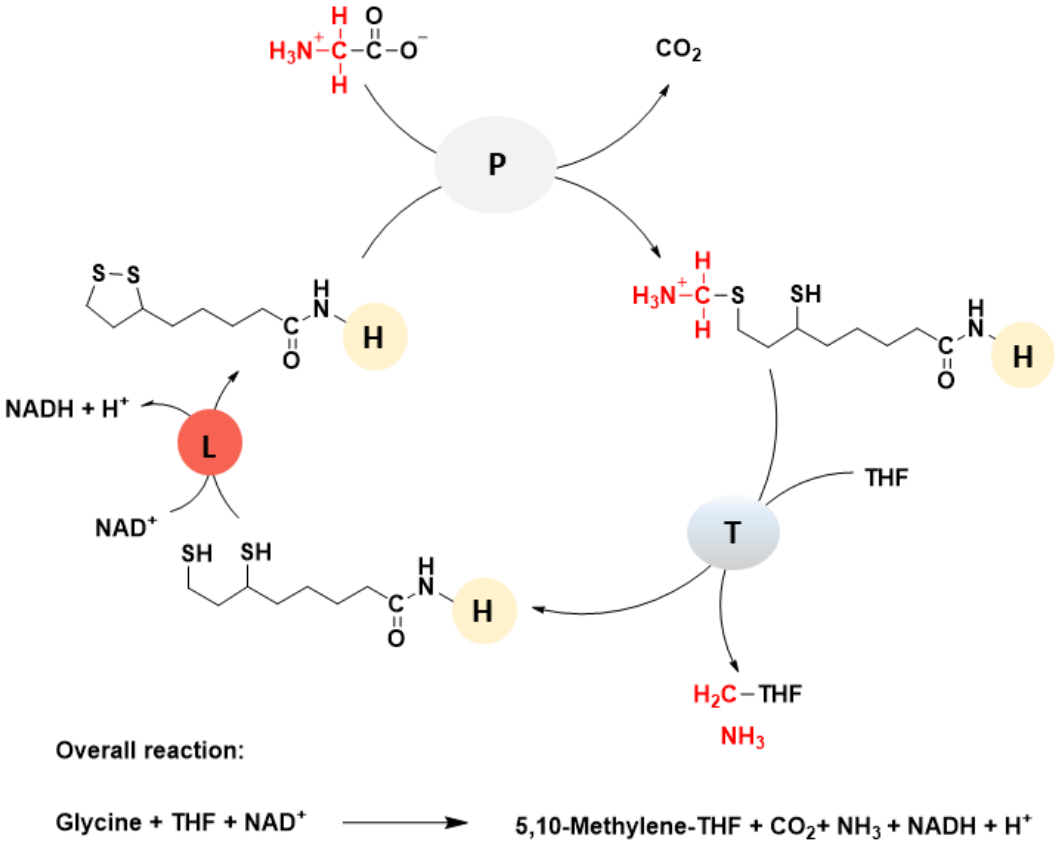

Figure 1-3: **Mechanism of Glycine Cleavage System**. The The P-protein binds pyridoxal 5′-phosphate (PLP); the T-protein contains lipoamide; the L-protein binds flavin adenine dinucleotide (FAD).

LipB and LipM: Characterization of Octanoyl-[Acyl Carrier Protein]-Protein Transferases

In vivo feeding studies using [^{35}S] lipoic acid or [^{14}C] octanoic acid demonstrated lipoylation or octanoylation in an *lplA* null *E. coli* strain, suggesting an alternative pathway for lipoylation which was later designated LipB (29-31). LipB is an octanoyltransferase that transfers an octanoyl group from octanoyl-ACP to an LCP, which is an off-shoot of the fatty acid biosynthetic pathway. The octanoyl-LCP then serves as the substrate for LipA, which subsequently inserts sulfur atoms at C6 and C8 to generate the final lipoyl product. The production of large quantities of LipB has been proposed to be toxic to *E. coli* cells, based on the observation that overexpression of the *lipB* gene impairs bacterial growth (32). Nevertheless, isolation of LipB has been successful both by immobilized metal-affinity chromatography using a hexahistidine tag and by conventional methods (33,34). The enzyme's turnover number, monitoring the transfer of a [1-^{14}C]-octanoyl group from [1-^{14}C]-octanoyl-ACP to the apo H protein, was determined to be 0.2 s^{-1}. *E. coli* LipB contains three cysteinyl residues, one of which reacts with 5,5′-dithiobis-2-nitrobenzoic acid at a rate that is 50-fold greater than that of the others, suggesting a possible role in covalent catalysis. Studies both by the Booker and by the Cronan laboratories, showed that the reaction proceeds via a ping-pong intermediate, involving a covalent octanoyl acyl-enzyme intermediate on cysteine 169 of *E. coli* LipB. A subsequent X-ray crystal structure of LipB from *Mycobacterium tuberculosis* suggested a role for a highly conserved lysine residue, leading to the assignment of LipB as a cysteine/lysine dyad acyltransferase (35). A proposed mechanism for LipB that is consistent with all experimental observations is shown in **Figure 1-4.** The octanoyl chain is transferred from octanoyl-ACP to the conserved LipB cysteine thiol. After release of the ACP, the LCP binds and the target lysine residue then attacks the thioester of the octanoyl-LipB intermediate, forming an amide linkage and releasing the regenerated LipB cysteine thiolate.

It was initially unclear why the genome of *Bacillus subtilis* encoded no LipB homologue, given that it contained a gene encoding LipA. To identify a possible protein with similar octanoyltransferase activity, a *B. subtilis* genomic DNA library was screened for the ability to rescue the growth of an *E. coli* LipB knockout strain (36). This study led to the identification of LipM, a protein that exhibits an activity that is identical to that of LipB, and that also catalyzes its reaction through a covalent acyl-enzyme intermediate involving a cystine thioester linkage. Though LipM was initially incorrectly annotated as a ligase, it is now realized that LipB and LipM belong to the same family and most likely have similar overall structures. However, their amino acid sequences are remarkably different, sharing only 20% identity despite using identical reaction mechanisms.

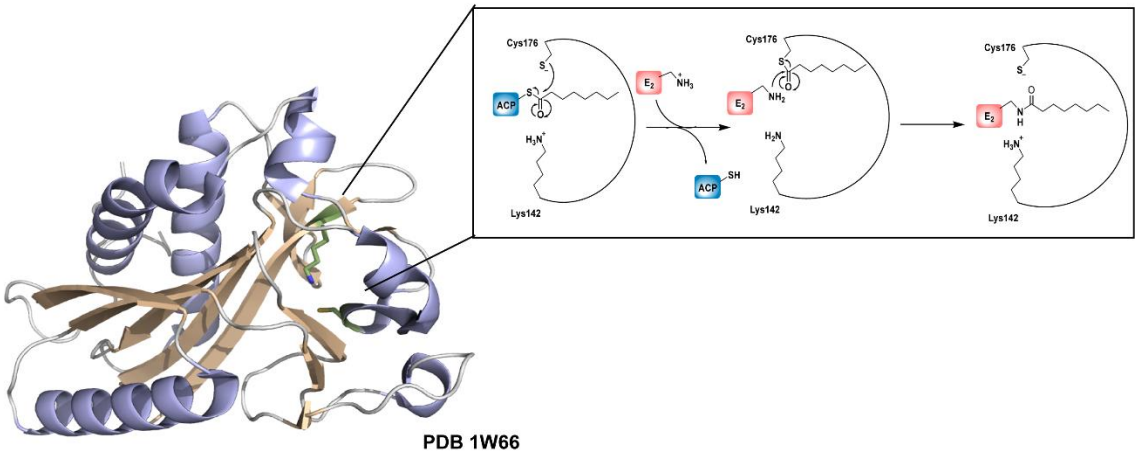

Figure 1-4: Octanoyltransferase LipB mechanism. Cys176 and Lys142 are proposed to act as an ion pair in a cysteine/lysine dyad. Briefly, an octanoyl group is transferred from an acyl-carrier protein in an off-shoot from fatty acid biosynthesis to a highly conserved cysteinyl residue (Cys176). The octanoyl chain is then transferred to a specific lysyl residue on the lipoyl carrier protein (E_2 in this case). Following release of the now octanoylated E_2, LipB is returned to its resting state.

An Introduction to Radical SAM Enzymes.

Although initially identified by Sofia *et. al* in 2001, the Radical *S*-adenosyl-L-methionine (SAM) superfamily is comprised of more than 115,000 distinct proteins, catalyzing an astonishing breadth of chemical transformations with new chemistry being uncovered every year (37,38). Indeed, RS enzymes catalyze methylation and methylthiolation of unactivated carbon or phosphinate phosphorus centers, oxidation of hydroxyl or thiol functional groups, 1,2-cross-migrations of functional groups, epimerizations, sulfur insertion, carbon-carbon bond formation, key steps in the biosynthesis of metallocofactors, and a variety of complex rearrangements, amongst others (39). All RS enzymes studied to date contain at least one [4Fe–4S] cluster typically coordinated by cysteinyl residues lying in a highly conserved Cx_3Cx_2C motif. One iron ion of the cluster, often referred to as the "unique" iron, is capable of ligating a molecule of *S*-adenosyl-L-methionine (SAM) in a bidentate fashion via its α-carboxylate and α-amino groups **(Figure 1-5).** *In vitro* reductants, such as dithionite, or an *in vivo* reducing system, such as flavodoxin/flavodoxin reductase/NADPH, reduce the [4Fe–4S] cluster to the +1 oxidation state, which then facilitates a reductive cleavage of SAM, affording L-methionine and a 5′-deoxyadenosyl 5′-radical (5′-dA•) **(Figure 1-6).** The 5'-dA•, a potent oxidant, initiates catalysis by abstracting a target hydrogen atom from the substrate, facilitating reactions with high energy barriers that cannot typically take place via polar mechanisms. The highly reactive 5′-dA• has never been directly observed; however, the use of a SAM analog 3′,4′-anhydro-*S*-adenosylmethionine in lysine 2,3-aminomutase has provided insight (40-42). In recent studies from the Broderick and Hoffman labs, rapid-mix freeze-quench technology with detection by electron paramagnetic resonance (EPR) spectroscopy was used to trap a catalytically competent intermediate in the reaction of pyruvate formate-lyase activating enzyme (PFL-AE), which was termed Ω (40). A detailed spectroscopic characterization of this intermediate led to its designation as an organometallic species in which the 5′-carbon of 5'-

deoxyadenosine is bound to the unique iron of the [4Fe–4S] **(Figure 1-7).** Although it was not initially clear whether Ω was specific to PFL-AE or a unifying feature of all RS enzymes, a subsequent study indicated its presence in several other RS enzymes that catalyze very different types of chemistry and implied that Ω is a characteristic feature of this superfamily (43).

RS enzymes often use SAM for multiple chemical roles, serving not only to initiate chemistry via the 5′-dA•, but also to use as an agent to methylate unactivated carbon centers, yielding *S*-adenosylhomocysteine (SAH) as another SAM-derived byproduct. Additionally, a subset of RS enzymes contains one or more additional Fe–S clusters, known as auxiliary clusters, or an additional cobalamin or PLP cofactor, which expand the diversity of reactions within the superfamily (44). One particular role for auxiliary clusters that has been described is as a sulfur source in which the metallocofactor is cannibalized during turnover to insert sulfur atom(s) into an organic substrate. To date, two RS enzymes have been characterized in detail to confirm this sacrificial mechanism, while others have been proposed but still lack experimental evidence **(Figure 1-8).** In addition to the canonical RS [4Fe–4S] cluster, biotin synthase, or BioB, contains a [2Fe–2S] auxiliary cluster. Using a sulfur atom derived from the auxiliary cluster, BioB generates a thioether bond between carbons 6 and 9 of dethiobiotin in the biosynthesis of the biotin cofactor (45-50) Lipoyl synthase, or LipA, coordinates a [4Fe–4S] auxiliary cluster, which it uses to insert two sulfur atoms at C6 and C8 of a protein-bound *n*-octanoyl chain (51-57). Recent evidence suggests that LipA may consume its entire cluster to produce two equivalents of lipoic acid per protein (58). Other RS enzymes involved in sulfur attachment include RimO, which catalyzes the methylthiolation of the β-carbon of an aspartyl residue within the S12 subunit of the ribosome, and MiaB which catalyzes the methylthiolation of an adenosine nucleotide at position 37 (A37) on several tRNAs (59-65). However, in these systems, the immediate source of the attached sulfur atoms is not as well-understood.

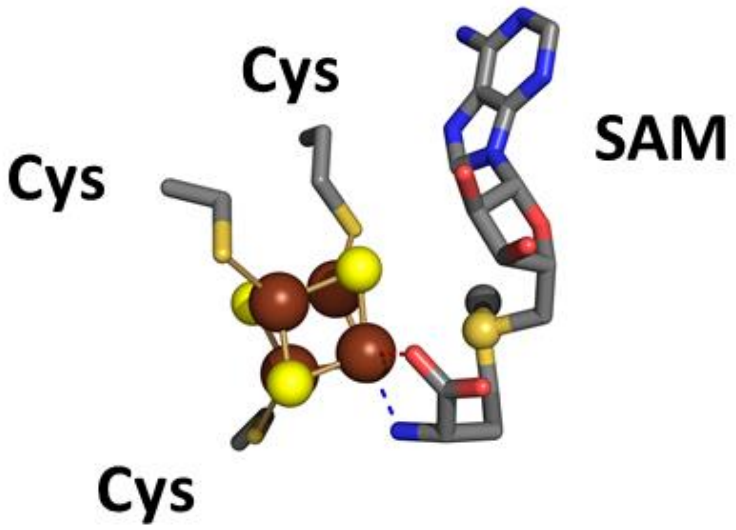

Figure 1-5: **Coordination of characteristic [4Fe–4S] cluster in RS enzymes.** RS enzymes coordinate a [4Fe–4S] cluster that is used to reductively cleave SAM. It is ligated by three highly conserved cysteinyl residues lying in a CX3CX2C motif, whereas the unique iron is coordinated by a molecule of *S*-adenosyl-L-methionine in a bidentate fashion.

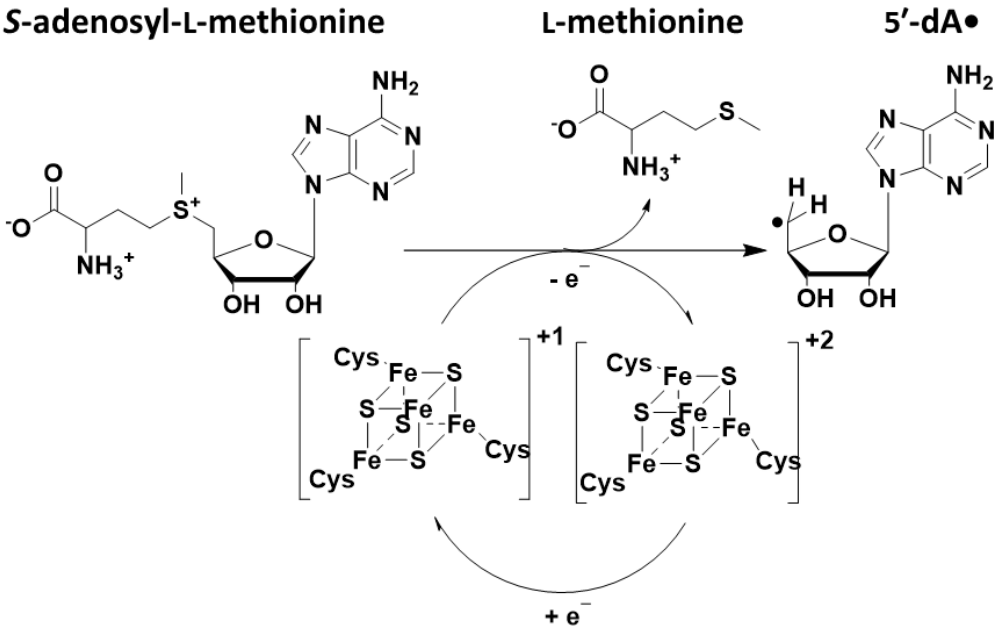

Figure 1-6: **Cleavage of *S*-adenosyl-L-methionine.** RS enzymes coordinate a [4Fe–4S] cluster, which, in its one electron reduced state, can reductively cleave *S*-adenosyl-L-methionine to L-methionine and 5′-deoxyadenosyl 5′-radical (5′-dA•) to initiate catalysis.

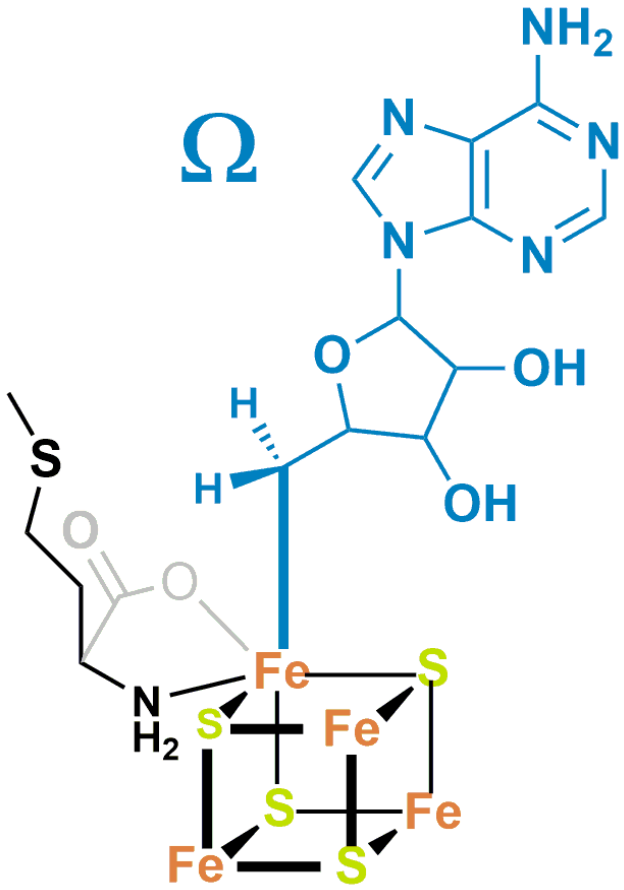

Figure 1-7: **Recently proposed organometallic intermediate Ω.** Newly proposed intermediate in RS enzymes termed "Ω." This species is defined as an organometallic intermediate in which the 5′-carbon of the deoxyadenosyl SAM-derived structure is bound to the unique iron of the [4Fe–4S].

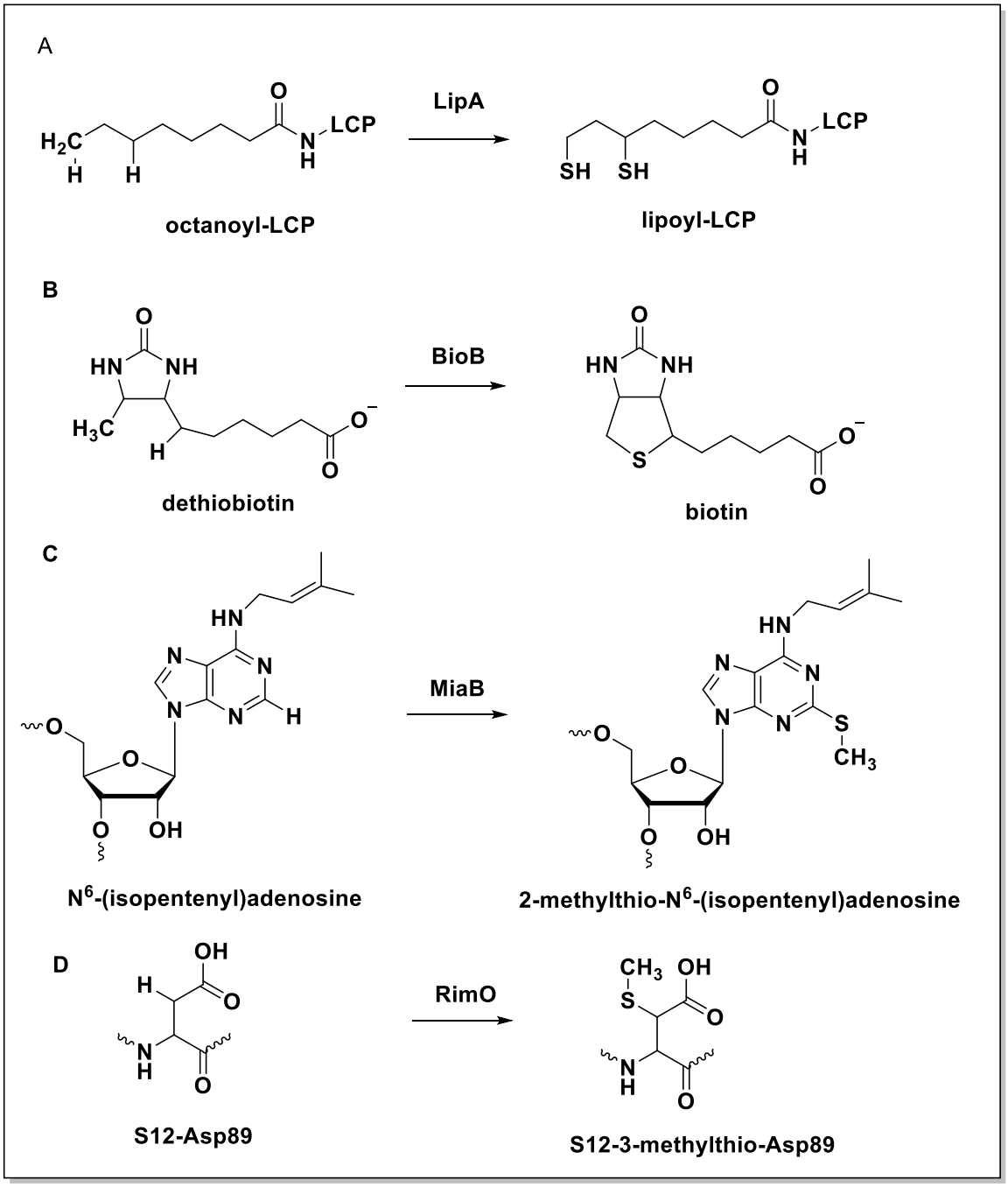

Figure 1-8: **RS enzymes that catalyze sulfur insertion reactions.** (A) LipA catalyzes the formation of lipoyl-LCP. (B) BioB catalyzes the conversion of dethiobiotin to biotin. (C) MiaB catalyzes the methylthiolation of an adenosine nucleotide at position 37 (A37) on tRNAs. (D) RimO catalyzes the methylthiolation of the β-carbon of an aspartyl residue within the S12 subunit of the ribosome.

Isolation and Characterization of LipA.

E. coli genetic studies and metabolic feeding experiments played a key role in the identification of the pathways for the biosynthesis of the lipoyl cofactor, the biologically relevant form of lipoic acid in which a molecule of lipoic acid is covalently attached to a lipoyl carrier protein (66). Early mutagenesis studies generated two mutant *E. coli* strains that were lipoic acid auxotrophs (67). Both lipoic acid auxotrophic strains were found to have mutations in the gene encoding *lipA.* The auxotrophs could be rescued if the cultures were supplied with acetate or succinate which bypass the need for lipoic acid in the citric acid cycle, or with lipoic acid indicating that the *lipA* gene product was involved in the *de novo* biosynthesis of the lipoyl cofactor, rather than its attachment to the enzymes that require it. Metabolic feeding of two *E. coli* lipoic acid auxotrophic strains designated W1485-*lip2* and JRG33-*lip9* containing point mutations in the *lipA* gene showed that supplying the cultures with 8-mercaptooctanoic acid could support growth, while 6-mercaptooctanoic acid could not (68). However, a second independent study that instead used strains that had transposon insertions in the *lipA* gene confirmed that 8-mercaptooctanoic acid could support growth but that 6-mercaptooctanoic acid also could support growth if supplied in great excess (69). These studies suggest that another enzyme *in vivo* could perform a moonlighting function and insert sulfur into these substrates in the absence of LipA.

The sequence of the *lipA* gene from *Escherichia coli* was first reported in the early 1990's in two independent studies by the Cronan and Ashley laboratories (70,71). The characterization of the LipA protein was of great interest, because at the time, very little was known about the chemistry of how sulfur was attached to unactivated carbon centers. However, isolation of the LipA protein proved to be exceptionally difficult, which hindered the characterization of the enzyme activity.

The isolation of *E. coli* LipA was first reported by the laboratory of Michael Marletta and also independently by the laboratory of Marc Fontecave (72,73). In the first isolation, the protein had a brown color, and the UV-visible spectrum as well as Raman spectra were consistent with the presence of [4Fe–4S] clusters. However, iron and sulfide analyses revealed the protein only contained approximately 1.8 mol iron and 2.2 mol sulfide per mol of protein, indicating very poor cofactor incorporation, and no activity was reported (72). From the study conducted by the Fontecave laboratory, overexpression of the *lipA* gene recombinantly in *E. coli* resulted in insoluble aggregates. To overcome this, the inclusion bodies found in the protein pellet were resolubilized and refolded and subsequently chemically reconstituted to re-introduce the [4Fe–4S] cofactor. Similarly, their preparation resulted in a LipA protein that contained only 1.8-2.3 mol of iron and sulfide per mol of protein, though they were able to obtain an EPR spectrum indicative of a $[4Fe–4S]^{+}$ cluster following reduction with 5-deazaflavin and light (73).

The difficulty in obtaining robust protein inhibited detailed mechanistic characterization of LipA for many years. In an attempt to increase the amount of soluble LipA protein for biochemical characterization, the Peter Roach laboratory performed various co-expression studies with factors that were hypothesized to assist with protein folding. These factors included thioredoxin, which is suggested to increase solubility of proteins by changing the redox potential of the cytosol and GroESL, a chaperone that assists with *in vivo* protein folding (74,75). However, these factors were shown to have no significant effect on LipA solubility. A third attempt, which proved to be a hugely significant observation, showed that LipA solubility was enhanced three-fold when co-expressed with the gene cluster encoding for iron-sulfur machinery proteins, the iron sulfur cluster (*isc*) pathway (76).

Despite the progress made towards isolating LipA protein for analysis, no activity had been demonstrated in any of the described studies. The Cronan laboratory developed the first method to demonstrate LipA activity *in vitro* using an indirect spectrophotometric assay to analyze the LipA-

dependent formation of lipoyl-PDC. Using this strategy, reactions were conducted with what was thought to be the necessary components: LipA protein, SAM, octanoyl-ACP substrate, and sodium dithionite as a chemical reductant. At designated times, the octanoyltransferase LipB and apo E2 of the PDC were added in order to catalyze transfer of the lipoyl group from lipoyl-ACP to the target lysyl residue of the LCP for analysis of product formation. However, the resulting activity of LipA was reported to be only 0.032 mol product per mol LipA (77). As it was later discovered, this lackluster activity was attributed to the fact that octanoyl-ACP was not the true substrate for LipA, but rather octanoyl-PDC, which was discovered through several lines of evidence. First, it was observed that *E. coli* strains lacking the *lipB* gene could still grow on octanoic acid in the absence of lipoic acid if both LplA and LipA were present. This observation led to a new hypothesis, in which LplA was proposed to transfer octanoic acid to an LCP to subsequently serve as the substrate for LipA. To test this hypothesis, an *E. coli lipA lipB fadE* null (λ) mutant was created, which resulted in the accumulation of d_{15}-labeled octanoyl-E2 domain when cultured in the presence of d_{15}-octanoic acid (78). The null mutation in the *lipB* gene in the strain used prevented the accumulation of unlabeled octanoyl-E2 domains, whereas the *fadE* null mutation prevented the degradation of d_{15} -octanoic acid by β-oxidation. Once the labeled E2 domains were generated *in vivo,* LipA activity was introduced by transduction of the cells with phage particles containing a *lipA* cosmid. Upon isolation of the E2 domains and analysis by ES-MS, it was observed that the d_{15}-labeled octanoyl-E2 domains had been converted to d_{13}-labeled E2 domains, confirming the hypothesis that LipA acts on octanoyl-LCPs in the cell. *In vitro* reactions validated this model, demonstrating the LipA-dependent cleavage of SAM by monitoring the formation of 5′-deoxyadenosine. Significant accumulation of 5′-deoxyadenosine was observed in the presence of octanoyl-E2 but not in the presence of octanoyl-ACP (78). Additional evidence was provided by the Booker laboratory, in which the octanoyl-H protein was shown to be a substrate for LipA *in vitro* (52).

A detailed spectroscopic characterization was carried out in a collaboration between the Booker and Krebs laboratories (53). The *E. coli lipA* gene was inserted into a pET28a expression plasmid under the control of an isopropyl-β-$_D$-thiogalactopyranoside (IPTG) inducible promoter. The *lipA* gene was co-expressed with genes encoding proteins involved in iron-sulfur (FeS) cluster biosynthesis and trafficking from *Azotobacter vindelandii*, which were under the control of an arabinose-inducible promoter. As described previously, this co-expression strategy significantly enhanced the amount of soluble protein obtained when isolating LipA. Similarly, LipA could be overproduced in minimal media in the presence of ^{57}Fe, with limiting contamination from natural abundance ^{56}Fe. This ^{57}Fe enriched protein was analyzed by Mössbauer spectroscopy, a spectroscopic technique that is described in detail elsewhere (79), but which provides information about the configuration and oxidation state of iron. This technique, often applied in combination with EPR spectroscopy, is invaluable for identifying the nature of iron-containing cofactors, especially FeS clusters. When overproduced and isolated via immobilized metal affinity chromatography, LipA was found to contain 6.9 mol iron and 6.4 mol sulfur per LipA polypeptide, considerably higher than all other reported preparations (80). The UV-visible spectrum, as well as Mössbauer and EPR spectra all indicated the presence of [4Fe–4S] clusters. Following chemical reconstitution, the protein was found to contain13.8 mol iron and 13.1 mol sulfur per polypeptide, although 33% of the total iron was determined by Mössbauer spectroscopy to be non-specifically bound iron species, resulting in a normalized stoichiometry of 9.2 mol iron and 8.8 mol sulfur per polypeptide, suggestive of the presence of two [4Fe–4S] clusters. LipA contains eight total cysteine residues, of which six are absolutely conserved. Three lie in the Cx_3Cx_2C motif that is characteristic of RS enzymes, while three that in a Cx_4Cx_5C motif, which is found in all lipoyl synthases. Two triple variants were constructed, in which all of the conserved cysteines within either motif were replaced with alanines. Both triple variants contained close to one [4Fe–4S] per polypeptide, which is 50% of that observed for the WT protein, confirming the presence of two [4Fe–4S] clusters. In

addition, neither triple variant could catalyze formation of the lipoyl cofactor, suggesting that the cysteines lying within these two motifs are critical to the reaction.

The current working model for the LipA reaction mechanism is shown in **Figure 1-9.** Fully reconstituted LipA contains two [4Fe–4S] clusters. One cluster interacts with SAM to generate the 5'-dA•, while the second cluster (the auxiliary cluster) is degraded during turnover to provide the attached sulfur atoms. Catalysis is initiated by the reductive cleavage of SAM to afford a 5'-dA•, which abstracts the C6 *pro-R* hydrogen atom of a pendant *n*-octanoamide chain residing on an LCP. The resulting C6 substrate radical attacks one of the bridging μ-sulfido ions of the auxiliary cluster, which is accompanied by a reduction of one of the Fe^{3+} ions of the cluster to Fe^{2+}, as well as the loss of an Fe^{2+} ion and an electron to afford a [3Fe–3S–1(6*S*)-thio-octanoamide]LCP intermediate. This intermediate exhibits a core charge of $[3Fe–4S]^0$, containing one Fe^{3+} ion and a valence-delocalized Fe^{3+}-Fe^{2+} (i.e. 2 $Fe^{2.5+}$ ions) pair of ions. A second reductive cleavage of SAM generates a second 5′-dA•, which abstracts a hydrogen atom from C8 of the [3Fe–3S–1(6*S*)-thio-octanoamide]LCP intermediate. The resulting C8 substrate radical attacks a second bridging μ-sulfido ion of the auxiliary cluster with concomitant reduction of an Fe^{3+} ion to Fe^{2+}. The resulting cluster species is believed to be unstable, and falls apart to ferrous and sulfide ions, eliminating lipoic acid upon protonation of the sulfur atoms. The Mössbauer spectrum of the [3Fe–3S–1(6*S*)-thio-octanoamide]LCP intermediate clearly shows it to contain two Fe^{3+} ions and one Fe^{2+} ion rather than the expected one Fe^{3+} ion and two Fe^{2+} ions. It is not clear where the additional electron goes or how it is lost.

The proposed working hypothesis is consistent with all experimental evidence that has been accumulated to date. Firstly, it was determined that two equivalents of SAM are required to produce one equivalent of lipoic acid. In reactions that included 50 μM *E. coli* LipA, excess octanoyl-H protein substrate and the flavodoxin/flavodoxin reductase reducing system, 18 μM lipoyl-H protein and 50 μM 5′-deoxyadenosine was produced, indicating the cleavage of two

equivalents of SAM during the reaction (52). To probe the mechanism further, H protein containing a perdeuterated (i.e. d_{15}) octanoyl group was used as a substrate in the reaction. Analysis by GC-MS revealed the incorporation of deuterium into 5′-deoxyadenosine, as expected. Unexpectedly, only ~50% of the 5′-deoxyadenosine was formed when using the [d_{15}]-octanoyl-H protein as compared to the H protein containing an octanoyl chain at natural abundance. Moreover, the lipoyl product was not detected, suggesting a large kinetic isotope effect arising from abstraction of one of the deuterium atoms from the [d_{15}]-octanoyl-H protein substrate. Expanding on this work, the Roach laboratory used short octanoyl-lysine-containing peptide substrates to address the sequence of hydrogen-atom abstractions from the octanoyl-H protein substrate. The advantage of the short peptide substrates was that they could be separated from the lipoyl product by high-performance liquid chromatography (HPLC). When LipA from *Sulfolobus solfataricus* was incubated with a peptide substrate containing a [6,6-d_2]-octanoyl-lysine appendage, the corresponding lipoyl product was observed. By contrast, when the enzyme was incubated with a peptide substrate containing an [8,8,8-d_3]-octanoyl-lysine appendage, only minute quantities of the lipoyl product were observed, leading to the assignment of the large kinetic isotope effect to abstraction of a deuterium from C8 of the substrate **(Figure 1-10)** (54,81). To address the sequence of sulfur attachment in a manner unbiased by the isotope effect, reactions were conducted with substrate at natural abundance and then analyzed by nuclear magnetic resonance (NMR) and HPLC coupled with mass spectrometry (LC-MS). Three products were observed: one was a species containing one sulfur atom, while the remaining two were the lipoyl and dihydrolipoyl products. Interestingly, when the reaction was filtered through a membrane having a 5 kDa molecular weight cut-off to separate LipA from the small molecules, the monothiolated species in the filtrate was greatly reduced, suggesting that it remained tightly associated with LipA under nondenaturing conditions. The monothiolated species was alkylated with iodoacetamide under reducing conditions and then purified by HPLC before analyzing it by COSY (1H-1H **CO**rrelation **S**pectroscop**Y**) NMR, which revealed the exclusive

formation of the 6-thio-octanoyl-lysine intermediate. No 8-thio-octanoyl-lysine species was observed, leading to the conclusion that hydrogen atom abstraction and sulfur attachment occurs sequentially: first from C6 and then from C8 from the octanoyl-lysine peptide substrate.

The identity of the immediate source of the sulfur atom to be attached to the octaonyl group during the biosynthesis of lipoic acid was an outstanding key question. It was proposed by the Booker laboratory that LipA cannibalized its auxiliary iron-sulfur cluster to supply the sulfur atom; however, this proposal initially faced heavy criticism from the scientific community, given that cannibalization would result in an inactivated enzyme after the first turnover. Nevertheless, an abundance of experimental evidence was consistent with this unorthodox role for an FeS cluster. First, lipoylated product could be observed in the absence of an exogenously supplied sulfur source, hinting that the origin of the sulfur was the LipA protein itself. Isotopic labeling studies by Cicchillo and Booker sought to provide direct evidence for this proposal (51). LipA, containing ^{34}S at all sulfurs in the protein, including the [4Fe–4S] clusters, was generated by overproducing the protein in *E. coli* cultured in minimal medium in which the only sulfur source is exogenously added $Na_2{}^{34}S$. When the ^{34}S-labeled LipA was used in a typical reaction in the absence of any other sulfur source, only ^{34}S-labeled lipoyl product was formed, indicating that the added sulfurs are derived from LipA itself. To address whether both sulfurs come from the same polypeptide or cluster, a 1:1 mixture of ^{32}S-labeled (i.e. at natural abundance) LipA and ^{34}S-labeled LipA was used in the reaction, with the expectation of products containing solely ^{32}S-labeled sulfur and ^{34}S-labeled sulfur if both sulfurs in lipoic acid derive from the same polypeptide. By contrast, a 1:2:1 ratio of only ^{32}S-labeled, $^{32}S/^{34}S$-labeled, and only ^{34}S-labeled would be expected if each polypeptide contributes only one sulfur atom to the final product. When the products were isolated from this reaction, the overwhelming majority was ^{32}S-labeled only and ^{34}S-labeled only, with a minor fraction containing the mixed $^{32}S/^{34}S$-labeled species. This result confirmed that the sulfurs originate from the LipA protein itself, and that both sulfur atoms derive from the same LipA polypeptide. The final interpretation was that

both sulfurs derive from one [4Fe–4S] cluster, and that the mixed $^{32}S/^{34}S$-labeled species is a result of sulfide being released into solution during cluster degradation and then being used to reconstitute another cluster during the reaction.

Further evidence for the sacrificial role of the auxiliary cluster was provided by X-ray crystallographic and spectroscopic studies. The Roach group published the first X-ray crystal structures of LipA, which were of the protein from *Thermosynechococcus elongatus* (55). The structures revealed the presence of two [4Fe-4S] clusters, confirming what had been determined earlier by Mössbauer spectroscopy (56). One structure contained a bound molecule of SAH; however, only electron density corresponding to the homocysteine portion of the molecule and the 5'-carbon of the adenosyl group was observed. A second structure was obtained of a protein that was co-crystallized with SAM; however, only methylthioadenosine was observed in the structure, as was a molecule of dithiothreitol, which was bonded to the unique iron ion of the RS cluster where the methionine portion of SAM would normally coordinate. No structures with octanoyllysine-containing or related substrates were reported, although the authors modeled in N-octanoyllysine methylamide as a substrate surrogate. In this model, the distance between C5′ of SAM and C6 of the substrate was 4.4 Å, while the distance between C6 of the substrate and the nearest μ_3-sulfido ion of the auxiliary cluster was 6.4 Å. The most striking feature of the structures was the finding that the auxiliary cluster contained three cysteine ligands, as expected, but also a serine ligand. This serine ligand is found at the extreme C-terminus of the protein in a highly conserved RSSY motif, wherein the arginine (R) and second serine (S) are absolutely conserved. It was proposed that this unique serine ligand would enable dissociation to allow the loss of the iron ion so that the second sulfur atom could be accessible during the second half-reaction. A similar structure of LipA from *M. tuberculosis* was subsequently reported by the Drennan and laboratories.

The Booker laboratory used electron paramagnetic resonance (EPR) spectroscopy in concert with a 2,4-hexadienoyl-containing substrate analogue attached to the H protein to demonstrate that LipA's auxiliary cluster and its substrate are within bonding distance (82). Upon abstraction of the C6 hydrogen atom of this substrate analogue, a highly stabilized substrate radical was detected by EPR, and the multiline pattern of the spectrum indicated an unpaired electron with strong ^{1}H hyperfine interactions with multiple ^{1}H nuclei. When this experiment was repeated with a [6,6,6,-d_3]-2,4-hexadienoyl-containing H protein, a substantially simplified EPR spectrum was obtained, indicating that two of the hyperfine interactions observed with the substrate at natural abundance are from protons at C6. Additional labeling of the C5 position using a [5,6,6,6,-d_3]-2,4-hexadienoyl-containing H protein resulted in further simplification of the EPR spectrum, and an anisotropic ^{2}H signal was observed in the ^{2}H HYSCORE (hyperfine sublevel correlation) spectrum. Simulation of the EPR spectra suggested that the unpaired electron was predominantly at C5 (~65% total spin); however, the hyperfine coupling constants suggested that the electronic structure of the species was significantly perturbed from the expected planar arrangement with a conjugated radical. Interestingly, the optimum temperature for observing the radical signal was 25 to 35 K, which is considerably lower than for typical organic radicals, suggesting that it could be perturbed by electron spin–spin interactions with a nearby [4Fe–4S] cluster.

The dramatic isotope effect observed when using the [8,8,8,-d_3]-octanoyl-lysine peptide was exploited to generate the monothiolated intermediate in sufficient yields to perform a detailed Mössbauer spectroscopic analysis (56). In this analysis, unreacted ^{57}Fe labelled LipA contained two intact [4Fe–4S] clusters, its radical SAM cluster used to reductively cleave SAM to initiate radical chemistry and its auxiliary cluster which was the hypothesized sulfur source. Upon reaction of the LipA with either the [8,8,8,-*d3*]-octanoyl-lysine peptide or 1 eq SAM, a species was observed that was consistent with a a [3Fe–3S–1(6-thiooctanoyl)LCP] cluster, corresponding to an intermediate in which an iron atom has been lost and the first sulfur has been inserted at C6. This

intermediate was shown to be both catalytically and kinetically competent through biochemical assays. This work ultimately trapped the LipA protein in the act of destroying its auxiliary cluster and provided the first direct evidence for the sacrificial role of its iron sulfur cluster. The first crystal structure of LipA from *Thermosynechococcus elongatus* containing both intact iron-sulfur clusters **(Figure 1-11)** was solved by the laboratory of Peter Roach. The structure revealed a highly unusual serine residue coordinating the unique iron of the auxiliary cluster. It was proposed that this unique serine ligand enabled dissociation to allow the loss of the iron atom so that the second sulfur atom could be accessible. Crystallographic snapshots of the LipA reaction were provided in a collaborative effort between the Booker and Drennan laboratories (83). By reacting LipA from *Mycobacterium tuberculosis* using the octanoyl-lysine peptide mimic and 1 equivalent of SAM, the authors were able to arrest the reaction at the monothiolated intermediate state and crystallize the resulting protein, providing a clear image of the [3Fe–3S–1(6-thiooctanoyl)LCP] cluster **(Figure 1-12).** The structural, biochemical, and spectroscopic characterization of this species provided robust evidence for the destruction of the auxiliary cluster during LipA's reaction mechanism.

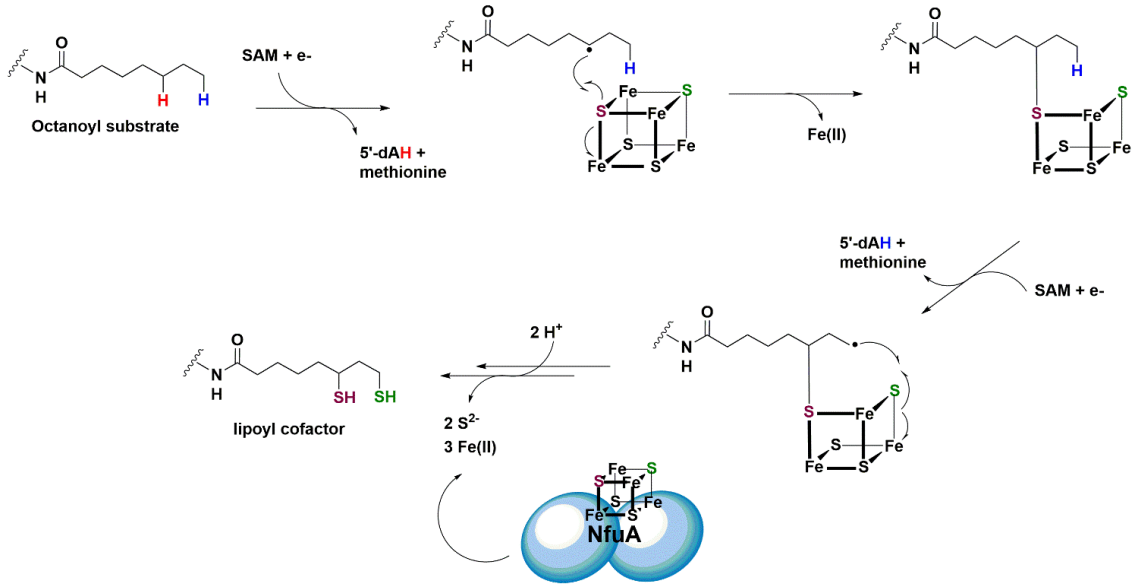

Figure 1-9: **Current proposed mechanism for LipA.** , LipA contains two [4Fe–4S] clusters, one of which (the auxiliary cluster) is sacrificed during turnover. Catalysis proceeds by reductive cleavage of SAM to render a 5′-deoxyadenosyl 5′-radical (5′-dA•), which abstracts the C6 hydrogen atom of a pendant *n*-octanoamide chain residing on a lipoyl carrier protein. The resulting C6 substrate radical attacks one of the sulfide ions of the auxiliary cluster, which is followed by loss of an Fe^{2+} ion to afford a [3Fe–3S–1(6S)-thio-octanoamide]H protein intermediate. A second reductive cleavage of SAM generates a second 5′-dA•, which abstracts an H• from C8 of the thio-octanoamide intermediate. The resulting C8 substrate radical attacks a second sulfide ion of the auxiliary cluster, which is followed by the addition of two protons and the loss of three Fe^{2+} ions and two S^{2-} ions to generate the lipoyl group in its reduced form. Following its destruction, iron-sulfur cluster carrier protein NfuA regenerates the auxiliary cluster for subsequent turnover.

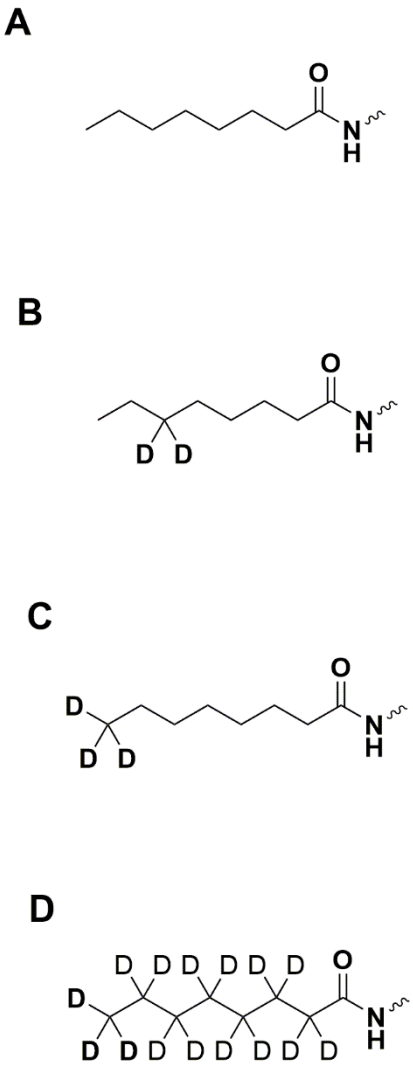

Figure 1-10: **Deuterated peptide substrates used for kinetic isotope effect.** Structures of peptide substrates used to determine kinetic isotope effect are as follows: **(A)** octanoyl-lysyl peptide **(B)** [6,6-d_2]-octanoyl-lysine peptide substrate **(C)** [8,8,8-d_3]-octanoyl-lysine peptide substrate **(D)** [d_{15}]-octanoyl-lysine peptide substrate

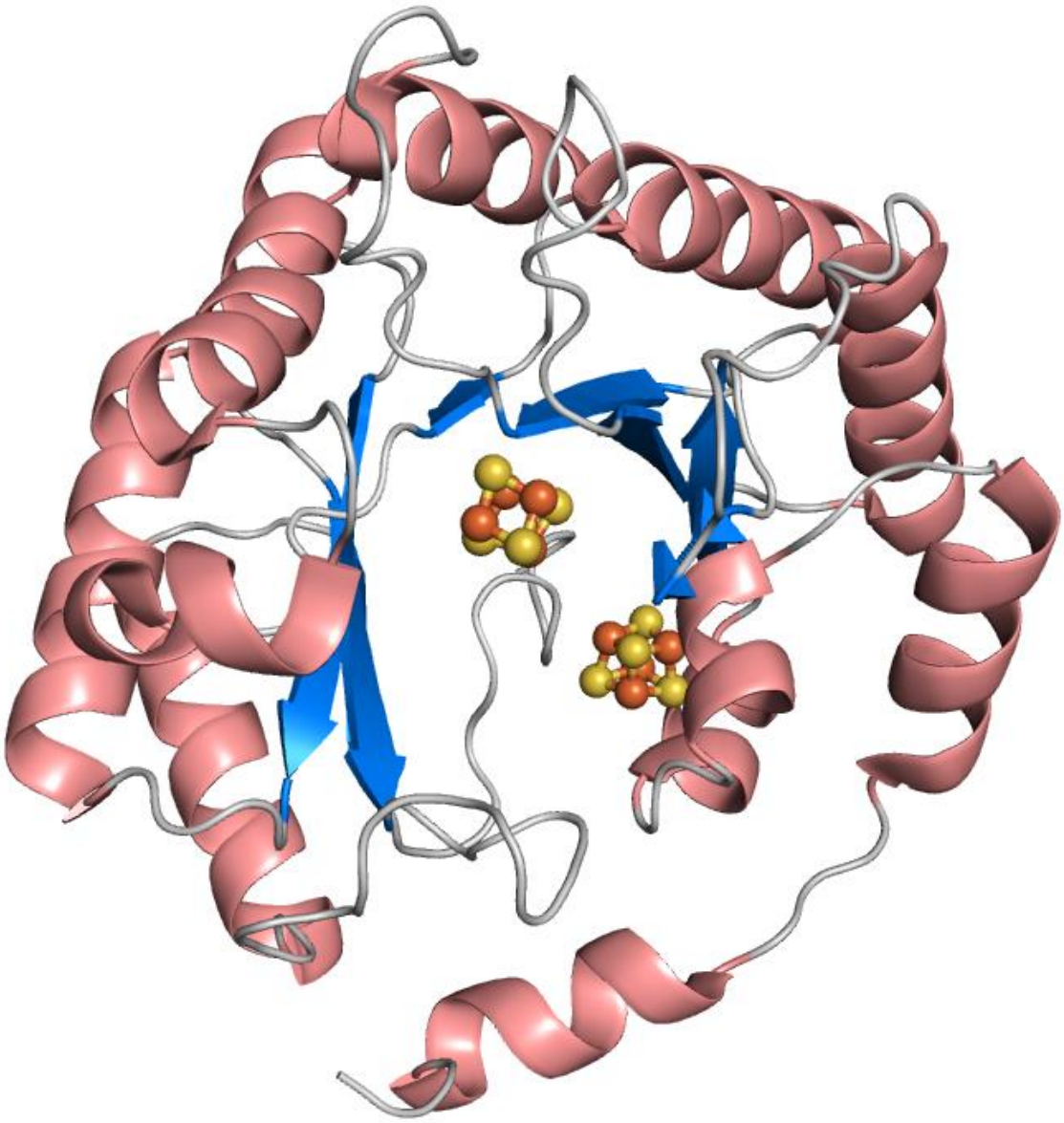

Figure 1-11: **Crystal structure of LipA from *Thermosynechococcus elongatus.*** The first crystal structure of *T. elongatus* LipA (PDB 4U0P) was solved to 1.6 Å by the Peter Roach laboratory. The characteristic TIM barrel (shown in blue) houses two [4Fe–4S] clusters.

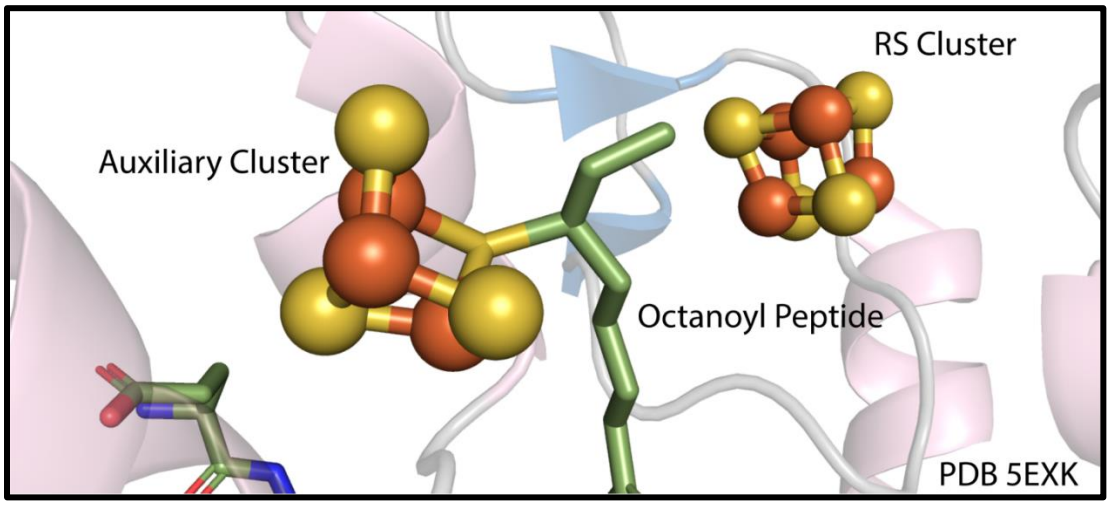

Figure 1-12: **Crystal structure of monothiolated intermediate in LipA from *Mycobacterium tuberculosis.*** The structure of LipA from *M. tuberculosis* was solved to 1.8 Å in a collaboration between the Drennan and Booker laboratories. By first reacting the protein with 1 eq. of SAM and an octanoyl peptide substrate, the authors were able to trap the protein in the act of consuming its cluster, arresting the reaction at the monothiolated intermediate state shown above.

Reactivation of LipA by NfuA

Until recently, the fate of the auxiliary cluster at the end of the reaction mechanism has been entirely unknown. The obligate destruction of the auxiliary cluster rendered LipA in an inactive state, incapable of catalysis in the absence of a system to regenerate it. An insightful paper published by the Weissman laboratory used ribosomal profiling techniques to provide the first quantitative analysis of translation rates *in vivo* (84). The resulting data indicated that 1,100 LipA molecules must modify 25,000 2-oxoacid dehydrogenase molecules plus 4,000 molecules of GcvH in cells grown during log phase in minimal media. The exceptionally slow rate of LipA synthesis almost certainly eliminates the possibility of LipA catalyzing only a single turnover in the cell. Indeed, it is likely that a mechanism exists that either repairs or replaces the auxiliary cluster to support catalysis *in vivo,* given that established pathways for FeS cluster biosynthesis and

trafficking exist and are highly regulated to avoid the toxic accumulation of metals in the cell. Though there are distinct differences between organisms, a similar basic framework exists for the biosynthesis of FeS clusters. In *E. coli*, the protein IscU serves as a central scaffold upon which FeS clusters are assembled **(Figure 1-13).** Sulfur is provided through a cysteine desulfurase in a PLP-dependent mechanism, and electrons are inputted through a ferredoxin/ferredoxin reductase, while the source of iron is still debated. The newly assembled iron-sulfur cluster is then transferred with the help of co-chaperones to an intermediate carrier protein, which subsequently targets and re-inserts the clusters into the metalloprotein that requires it in a process that is still very poorly understood (85-88). While several intermediate carrier proteins have been identified, their targets as well as the mechanistic details of recognition and maturation have not been fully characterized.

One initial hypothesis was that the cysteine desulfurase (IscS in *E. coli*) could simply repair the LipA auxiliary cluster by reinserting the sulfur atoms that were lost during the reaction; however, *in vitro* experiments with IscS showed that it had a minimal effect on LipA activity (58). Initial efforts to identify the missing factor were largely unsuccessful. However, several reports in the literature described clinical cases in which patients had an ultimately fatal condition that was linked to mutations in the gene encoding *NFU1 (22,89-91).* Interestingly, western blots using anti-lipoic acid antibodies revealed significantly decreased lipoic acid levels in clinical samples, leading to a new hypothesis that the protein encoding by that particular gene was involved in lipoic acid biosynthesis. The *E. coli* homolog of NFU1, NfuA, had previously been characterized, as well as the NfuAs from other organisms, though its potential role in lipoic acid biosynthesis had never been explored (92-95).

Previous studies demonstrated that *E. coli* NfuA could be isolated in an apo form, and then could incorporate a [4Fe–4S] cofactor upon chemical reconstitution (94,95). *E. coli* NfuA was later isolated with the [4Fe–4S] cofactor intact by co-expressing the gene encoding *nfuA* with genes involved in FeS cluster biosynthesis using methods previously described for LipA (58,96).

Formation of a tight complex between *E. coli* LipA and *E. coli* NfuA was observed using analytical size exclusion chromatography. The most exciting results came from LipA activity assays in which the monothiolated intermediate and the lipoyl product formation could be monitored by liquid chromatography-mass spectrometry (LC-MS) when using an octanoyl-lysine-containing peptide substrate. Consistent with its mechanistic proposal, LipA can only catalyze one turnover due to the destruction of its auxiliary cluster. In one experiment, LipA was reacted to completion, wherein it catalyzed its usual one turnover. Surprisingly, when [4Fe–4S]-loaded NfuA was then added to the assay mixture, LipA immediately began reforming additional monothiolated intermediate and lipoyl product. When the reaction conditions were altered such that NfuA was added at the beginning of the assay in excess of LipA, LipA was able to catalyze more than 10 turnovers exhibiting catalytic behavior for the first time *in vitro,* and the extent of turnover was related to the concentration of added NfuA. It is known that non-physiological cluster transfer can occur through chemical reconstitution of Fe-S cluster containing proteins in the presence of iron, sulfide, and reductant. As a result, several control experiments were performed in order to ensure that the enhanced activity was a direct result of a protein-catalyzed cluster insertion mechanism. LipA was reacted under normal assay conditions, but in the presence of free iron, sulfide, and reductant. While some activity enhancement was observed, the enhanced activity was relatively low compared to the robust catalysis observed in the presence of NfuA. The non-physiological mechanism was also rejected by a control experiment containing LipA and NfuA in buffer containing excess ^{34}sulfide. If LipA was scavenging metals from solution, it would be expected that the final lipoyl product would have ^{34}S incorporation. However, no labelled product was observed which is consistent with a role for NfuA in direct cluster insertion. The possibility of LipA scavenging metal from solution was also rejected using a second method in which the chelating agent citrate was included in the assay. In this case, if LipA was scavenging metals from solution, product inhibition would be observed in the presence of a chelating agent that removes the free metals from solution. When

reactions were performed with LipA and NfuA in the presence and absence of citrate, no product inhibition was observed. Cumulatively, these control experiments allowed the confident assignment of a role for NfuA in the regeneration of LipA's auxiliary cluster.

An isotopic labelling strategy was employed to probe the reaction in further detail. NfuA was isolated in its apo form, and then chemically resconstituted to contain an Fe–^{34}S cluster. When using LipA protein that was isolated using sulfur at natural abundance (i.e. ^{32}S) in an assay with [4Fe–4^{34}S]-loaded NfuA, the source of the sulfur incorporated in the final lipoyl cofactor could be tracked **(Figure 1-14).** It was expected that one equivalent of unlabeled lipoyl product would be formed from LipA's unlabeled cluster followed by ^{34}S-labeled lipoyl product from NfuA's labeled cluster. However, surprisingly two equivalents of unlabeled lipoyl product were observed, which was followed by the ^{34}S-labeled product, suggesting that LipA could mobilize all four of its sulfur atoms in the presence of NfuA.

Significant gaps in our understanding of the regeneration mechanism for the auxiliary cluster of LipA. The mechanism by which NfuA recognizes and interacts with LipA is a largely unanswered question. Building upon previously published data that suggested a role for the N-terminal domain of NfuA in protein-protein interactions, it was shown that the N-terminal domain was essential for binding LipA and for efficiently restoring its catalytic activity (95,97). Nfu-like proteins lacking the N-terminal domain, such as from *Staphylococcus aureus*, were significantly diminished in their ability to activate LipA, though a genetic fusion of the N-terminal domain to the Nfu-like protein fully restored its activity. Additionally, though the isotopic ^{34}S labelling studies demonstrated that LipA uses the sulfur from NfuA's cluster, the state of the iron-sulfur cluster and the details of the maturation mechanism are unknown. The fate of the iron atoms liberated when the sulfur atoms are consumed is also not known. Indeed, much work remains to be done to fully understand the process.

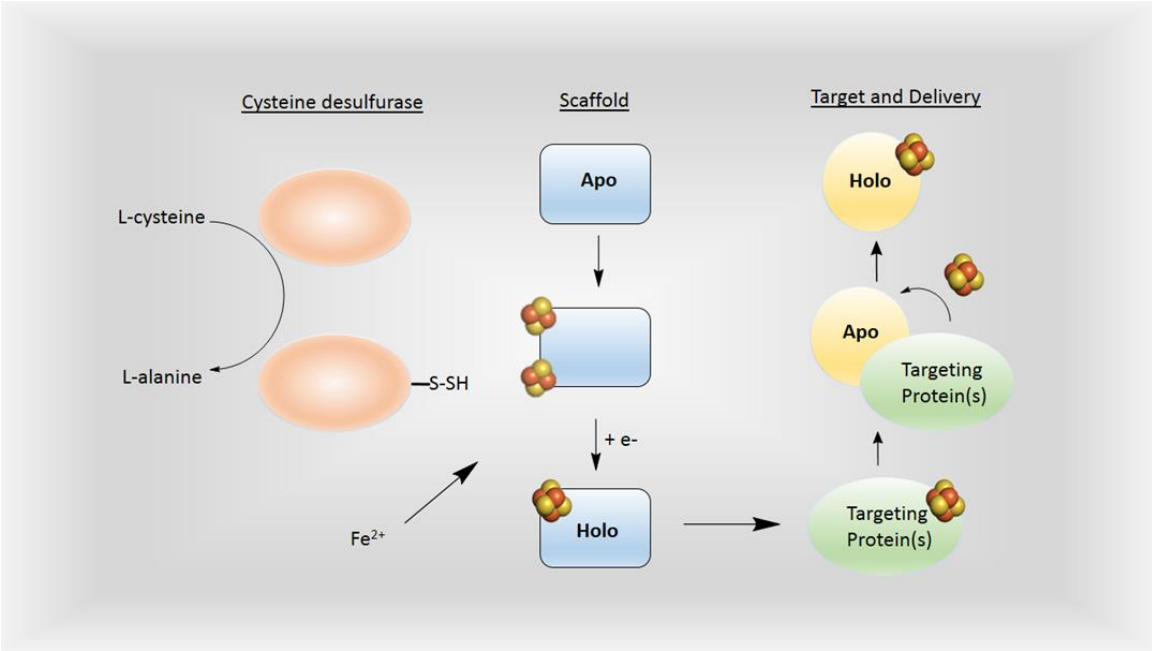

Figure 1-13: **General overview of iron-sulfur cluster assembly in *E. coli.*** A cysteine desulfurase converts cysteine to alanine using a PLP-dependent mechanism to supply sulfur, whereas the iron source is still debated. The iron-sulfur cluster is first assembled on a general scaffold protein. In a poorly understood mechanism, the newly assembled cluster is then transferred to a targeting protein with the help of chaperones, which then delivers and the cluster to the apo-proteins that require it.

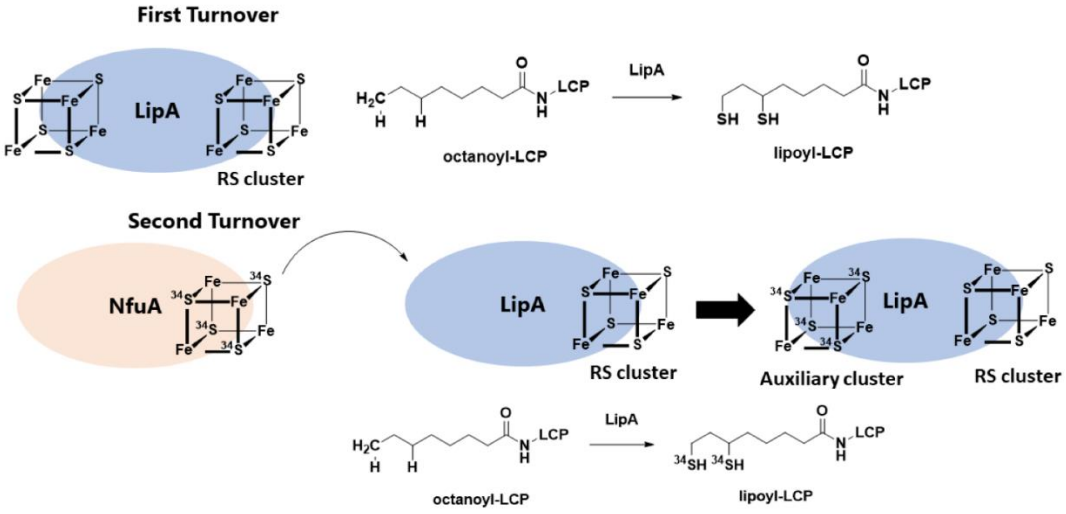

Figure 1-14: **Probing cluster regeneration using 34-S labeled NfuA.** LipA that was isolated with natural abundance was reacted in the presence of NfuA that was loaded with [4Fe–4^{34}S] cluster. The expectation was that one equivalent of unlabeled lipoyl product would be observed while subsequent turnover would generate ^{34}S incorporated lipoyl product that was a result of LipA being regenerated and subsequently using its new cluster for catalysis. However, surprisingly, two equivalents of unlabeled lipoyl product were observed in the presence of NfuA, suggesting that LipA can mobilize all four of its sulfur atoms.

Lipoate Protein Ligase A and Lipoate Activating Enzyme

The second avenue for the biosynthesis of the lipoyl cofactor is known as the endogenous pathway in which free lipoic acid is scavenged from the environment **(Figure 1-15).** In *E. coli*, the enzyme responsible for this activity is known as lipoate protein ligase A (LplA). *E. coli* LplA has been extensively studied and catalyzes the ATP-dependent activation and subsequent attachment of free lipoic acid to LCPs that require it. Early studies were conducted in the lipoic acid deficient *Streptococcus faecalis*,(also known as also known as *Enterococcus faecalis*), strain 10C1. Using this organism, Reed *et al.* first demonstrated that the lipoate activating system required ATP, lipoic

acid, Mg^{2+}, and two unidentified components that were separable, one of which was heat stable and one of which was heat labile (98). In the *E. coli* system, individual components were unable to be isolated, suggesting either a tightly bound complex, or, alternatively, that the same enzyme was responsible for both activation and transfer of the lipoic acid to LCPs.

The gene encoding LplA was discovered in the 1990s. *E. coli* strains with a null mutation in the *lplA* gene were able to successfully transport lipoic acid in the cell, but were unable to attach it to LCPs (99). Interestingly, this null strain was shown to grow normally in the presence of selenolipoate, a compound that was previously shown to inhibit *E. coli* growth, presumably due to its inability to be reductively acylated, its essential role in the pyruvate dehydrogenase complex (100). Enzyme assays using [^{35}S]labeled lipoic acid confirmed that this gene encoded a lipoate protein ligase that catalyzes the ATP-dependent attachment of lipoic acid to apo LCPs.

Since its identification, LplA has been routinely used to understand lipoic acid biosynthesis, but also as a novel protein labelling reagent by substituting other residues for the tryptophan-37, an amino acid at the end of the lipoic acid binding site. By substituting this residue, the active site is enlarged, allowing alternate substrates other than its natural substrate lipoic acid are able to bind (101). Similar to the observations in *S. faecalis,* lipoate protein ligase activity was determined to be catalyzed by two distinct enzymes in mammals. Contrary to *E. coli,* the ATP activation of lipoic acid to lipoyl-AMP is catalyzed by lipoate activating enzyme, whereas a second enzyme lipoyltransferase is then responsible for transferring the lipoyl group to the LCP.

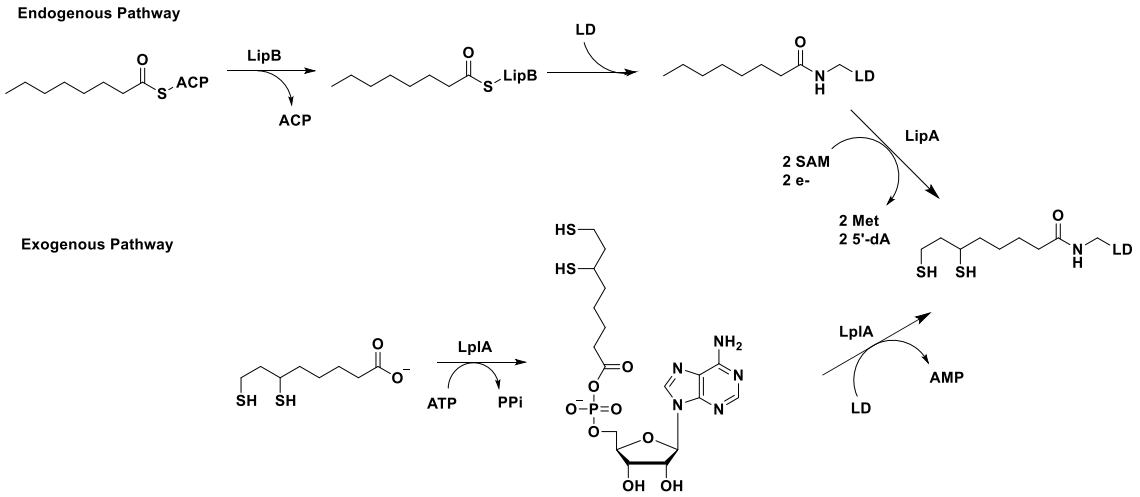

Figure 1-15: **Pathways for the biosynthesis of the lipoyl cofactor in *E. coli.*** Two pathways exist for the biosynthesis of the lipoyl cofactor in *E. coli*. In the endogenous pathway (top), octanoyl-transferase LipB transfers the octanoyl group from an acyl-carrier protein (ACP) to the lipoyl domain (LD). The RS enzyme LipA then inserts the sulfur atoms to generate the cofactor. In the exogenous pathway (bottom), lipoic acid is scavenged and ATP-activated by LplA and then subsequently transferred to the lipoyl domain.

Lipoamidase

Lipoamidase (Lpa) catalyzes the cleavage of the amide bond that covalently links lipoic acid to the lysyl residue of the LCP. Because lipoic acid is assembled on a cognate protein, lipoamidase (or an enzyme that catalyzes a similar reaction) is thought to be responsible for the free lipoate found in Nature. The activity of this enzyme was first reported in 1958 and given the name “lipoyl-X hydrolase” (98). Early experiments designed to test the reactions involved in generating protein-bound lipoate in cell-free extracts of *S. faecalis* (also known as *E. faecalis)* found that amide-containing lipoic acid compounds lacking a free carboxylate group did not inhibit pyruvate dehydrogenase complex as would be expected. Surprisingly, these amide-containing compounds were found to activate the activity of the pyruvate dehydrogenase complex, but only in

the presence of ATP. This unexpected result was hypothesized to be a result of the amide bonds being cleaved during incubation, whereas a second report of an enzyme from yeast was described with similar properties (102). The enzyme was later renamed lipoamidase after it was found to act on a variety of substrates, proving it to be more diverse than initially thought (103). *E. coli*, the organism in which lipoic acid biosynthesis is best understood, lacks Lpa activity, whereas lipoic acid biosynthesis in *S. faecalis* is distinct, with its genome lacking genes encoding LipA and LipB making it a lipoic acid auxotroph. Cloning and characterization of Lpa from *S. faecalis* proved difficult because Lpa heterologously expressed in *E. coli* proved to be highly toxic to the cells. In fact, *lpa* gene expression was only achieved when T7 RNA polymerase was introduced through λCE6 phage. Once successfully isolated, Lpa was found to be an 80 kDa protein containing an amidase domain with a classic Ser-Ser-Lys catalytic triad that was essential for activity (104). Lpa activity has also been characterized in the pathogenic bacteria *Listeria monocytogenes* (105). Recently, Lpa has been used as a probe to gain new insight in lipoate metabolism in *Plasmodium falciparum* (106).

Lipoic Acid Biosynthesis in Pathogenic Bacteria and Protozoa

While the *de novo* biosynthesis of the lipoyl cofactor in *E. coli* only requires two dedicated enzymes (LipB and LipA), a much more elaborate pathway exists in some other organisms, such as *B. subtilis*. *B. subtilis* encodes a ligase, LplJ, which has a similar scavenging activity as *E. coli* LplA **(Figure 1-16).** In the *de novo* endogeneous pathway in *B. subtilis*, the H protein, GcvH, from the glycine cleavage system is the sole substrate for lipoic acid assembly, such that all enzymes requiring a lipoyl domain require lipoyl transfer from lipoylated GcvH. The study of endogenous lipoic acid biosynthesis in this system was initially puzzling, due to the lack of a gene encoding LipB, although a gene for LipA was present. A protein with an identical function, LipM, was later discovered, which helped to solve this mystery (36). LipM catalyzes the transfer of an octanoyl

group from octanoyl-ACP to octanoyl-GcvH. Once the GcvH has been lipoylated, an amidotransferase, LipL, transfers the group from the GcvH to all other LCPs that require lipoate **(Figure 1-16)** (107).

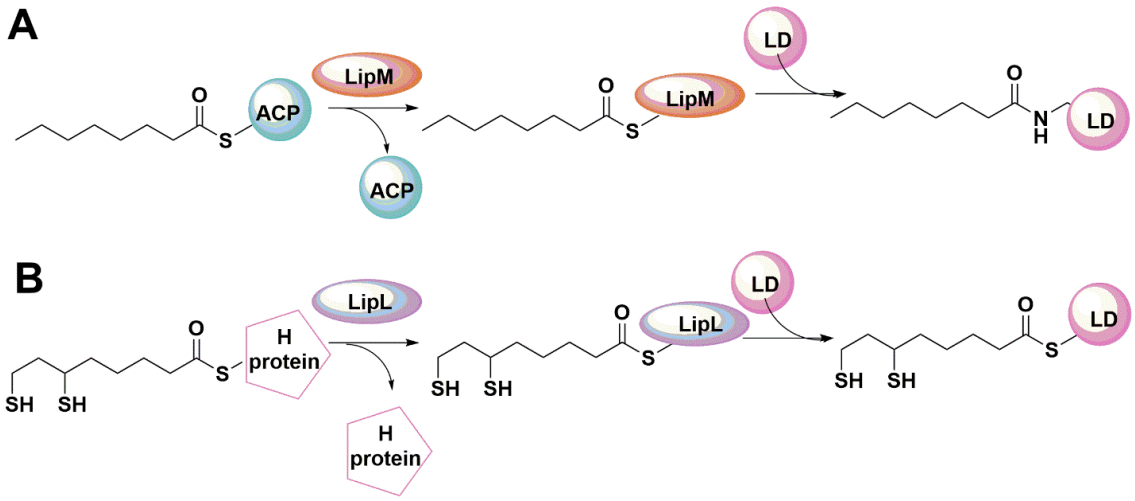

Figure 1-16: **Lipoic acid biosynthesis in *B. subtilis* and *L. monocytogenes.*** (A) Mechanism of LipM which performs the same mechanism as LipB in *B. subtilis*. (B) Lipoic acid attachment to lipoyl carrier proteins in some organisms require that it first be attached to the H protein in the GCS and then transferred to the other enzymes that require lipoate. In *B. subtilis* and *L. monocytogenes*, it is catalyzed by the protein LipL.

The pathogenic organism *L. monocytogenes* lacks genes encoding for LipA or LipM and scavenges its lipoic acid from its mammalian host via a lipoamidase. Similar to *B. subtilis*, the lipoic acid is first required to be attached to GcvH using the ligase LplA1, and then is subsequently transferred to its target LCP by the amidotransferase LipL to generate the lipoylated proteins required for its survival **(Figure 1-16)** (105,108). The essential role of lipoic acid makes the cofactor an intriguing target for new antibiotic and anti-parasitic pharmaceuticals. Contrary to *L. monocyotogenes*, which relies on a scavenging mechanism, notably, many pathogenic bacteria lack

the salvage pathway and instead rely completely on the *de novo* biosynthesis pathway, including *Mycobacterium tuberculosis* (tuberculosis), *Rickettsia prowazekii* (epidemic typhus), *Rickettsia rickettsia* (Rocky mountain spotted fever), *Neisseria gonorrheae* (gonorrhea), *Corynebacterium diphtheriae* (diphtheria), *Neisseria meningitides* (bacterial meningitis), *Burkholderia pseudomallei* (melioidosis), *Legionella pneumophila* (Legionnaire's disease), and *Heliobacter pyloria* (stomach disorders) (109,110). Interestingly, in *Helicobacter pylori*, no proteins associated with lipoic acid metabolism have been identified to date (111,112).

Lipoic acid biosynthesis in the apicoplexan parasite *Plasmodium*, the cause of malaria, has been intensely studied. In this organism, lipoic acid biosynthesis occurs in the apicoplast, a degenerate nonphotosynthetic plastid organelle that is thought to have resulted from endosymbiosis by a red algal cell (113). The apicoplast contains many proteins that are synthesized in the nucleus of the cell and directed to the apioplast through a localization signal. In *Plasmodium,* the LipA homologue is found only in the apicoplast along with LipB, the same enzymes required for the *de novo* biosynthesis of lipoic acid in *E. coli*. The fatty acid biosynthetic pathway along with pyruvate dehydrogenase are also found in the apicoplast, while the other lipoylated complexes (glycine cleavage system, branched-chain dehydrogenase, 2-oxoglutarate dehydrogenase) reside in the mitochondria. A scavenging pathway also exists in the mitochondria of *Plasmodium* through the use of two ligases LplA1 and LplA2. Because *de novo* biosynthesis of lipoic acid occurs in the apicoplast, the scavenging pathway is the source of lipoic acid for the lipoylated protein complexes in the mitochondrion. LplA2 can also be targeted to the apicoplast and provide a scavenging pathway (108,111).

Lipoic Acid Biosynthesis in Plants

Lipoic acid biosynthesis is pivotal for plant survival. Leaf mitochondria require robust amounts of lipoylated H protein to maintain the photorespiratory cycle, in which two molecules of glycine are converted to serine. During photosynthesis, nearly half of the protein content in the mitochondria are composed of proteins involved in the glycine cleavage pathway to support this process. Plants also have their lipoylated protein complexes divided in two distinct organelles, similar to what was described for the apicoplexan parasites. The plant mitochondrion contains the pyruvate dehydrogenase complex, the 2-oxoketoglutarate dehydrogenase complex, the branched chain-dehydrogenase complex, and the glycine cleavage system. The pyruvate dehydrogenase complex is also redundantly found in the plastid. Contrary to the apicoplexan parasites, fatty acid biosynthesis occurs both in the mitochondrion and in the plastid, and each has a *de novo* pathway for the biosynthesis of the lipoyl cofactor from octanoyl-ACP (114). LipB activity has been observed in plant mitochondrial lysate, and three genes have been identified that encode an octanoyltransferase with a LipB-like function. Lip2 has been shown to functionally replace LipB in *E. coli* (115), whereas Lip2p is a second non-essential protein with LipB-activity that is specifically targeted to the plastid (116). A second LipB-like protein that is targeted to the plant plastid, Lip2p2, is non-essential, though a double mutant of Lip2p and Lip2p2 cannot survive (117). Similar to the LipB homologues, two LipA-like proteins have been identified, each with a specific organelle localization (118,119). Lip1 is targeted to the mitochondrion and was shown to functionally replace *E. coli* LipA, whereas Lip1p is targeted to the plastids. Plant mitochondria also contain a ligase that can functionally replace *E. coli* LplA, which is essential for the plant leaves and roots.

Future Outlook and Conclusions

Understanding the biosynthesis of lipoic acid has been a journey spanning many decades. The progress made thus far is truly remarkable considering the technical challenges that have been encountered over the years. From the very beginning, it required an astounding 10 tons of liver to isolate 30 mg of lipoic acid for its initial characterization (2,8). An extreme hurdle that cannot be understated is the amount of dedicated effort by many laboratories spent isolating LipA for biochemical analysis, as well as identifying the correct substrate. An immense effort was put forth to exhaustively demonstrate that LipA destroys its auxiliary cluster to use as a sulfur source—an unconventional mechanism that was not universally accepted by the scientific community initially. Even many years later, an outstanding question still remained: what is the fate of the auxiliary cluster of LipA following its destruction during the biosynthesis of lipoic acid? Only recently has this question been resolved, when *E. coli* LipA catalysis was demonstrated for the first time *in vitro* in the presence of the intermediate iron-sulfur cluster carrier *E. coli* NfuA (58). Several clinical reports identifying lipoic acid deficiencies in patients with mutations in the gene encoding the human homolog, NFU1, were key for defining NfuA's role in *E. coli* lipoic acid biosynthesis (22,89,90,120).

Despite the measurable progress, many questions still remain. The detailed mechanism by which *E. coli* NfuA recognizes *E. coli* LipA and subsequently regenerates its auxiliary cluster is largely unknown. Similarly, the fate of the residual iron following the consumption of the sulfur atoms of the auxiliary cluster isn't clear. It seems unlikely that the iron would be released into the environment given that iron is tightly regulated within the cell due to its toxicity at high concentrations. Additionally, several other factors have had dramatic effects on lipoic acid biosynthesis when mutations arise, or when knocked out in genetic experiments. For example, mutations within the human gene BOLA3 have lead to lipoic acid deficiency in clinical patients similarly to NFU1, though the role of this gene is unknown (89,90). Similarly, a protein in the

pathogenic bacterium *S. aureus*, SufT, has been reported to have drastic effects on lipoic acid requiring enzymes, although its biological role is not yet known (121,122). Indeed, it is clear that many interesting discoveries will be made in the future!

References

1. Snell, E. E. (1992) Microorganisms in vitamin and biofactor research. *Journal of nutritional science and vitaminology* **Spec No**, 34-39
2. Reed, L. J., De, B. B., Johnston, P. M., and Getzendaner, M. E. (1951) Acetate-replacing factors for lactic acid bacteria. I. Nature, extraction, and distribution. *The Journal of biological chemistry* **192**, 851-858
3. Reed, L. J. (1998) From lipoic acid to multi-enzyme complexes. *Protein science : a publication of the Protein Society* **7**, 220-224
4. Reed, L. J. (2001) A trail of research from lipoic acid to alpha-keto acid dehydrogenase complexes. *The Journal of biological chemistry* **276**, 38329-38336
5. O'Kane D, J., and Gunsalus, I. C. (1948) Pyruvic Acid Metabolism: A Factor Required for Oxidation by Streptococcus faecalis. *J Bacteriol* **56**, 499-506
6. Gunsalus, I. C. (1953) The chemistry and function of the pyruvate oxidation factor (lipoic acid). *Journal of cellular physiology. Supplement* **41**, 113-136
7. Gunsalus, I. C., Struglia, L., and O'Kane, D. J. (1952) Pyruvic acid metabolism. IV. Occurrence, properties, and partial purification of pyruvate oxidation factor. *The Journal of biological chemistry* **194**, 859-869
8. Reed, L. J., De, B. B., Gunsalus, I. C., and Hornberger, C. S., Jr. (1951) Crystalline alpha-lipoic acid; a catalytic agent associated with pyruvate dehydrogenase. *Science (New York, N.Y.)* **114**, 93-94
9. Reed, L. J., Gunsalus, I. C., Schnakenberg, G. H. F., Soper, Q. F., Boaz, H. E., Kern, S. F., and Parke, T. V. (1953) Isolation, Characterization and Structure of α-Lipoic Acid1. *Journal of the American Chemical Society* **75**, 1267-1270
10. Bullock, M. W., Brockman, J. A., Patterson, E. L., Pierce, J. V., and Stokstad, E. L. R. (1952) SYNTHESIS OF COMPOUNDS IN THE THIOCTIC ACID SERIES. *Journal of the American Chemical Society* **74**, 3455-3455
11. Walton, E., Wagner, A. F., Peterson, L. H., Holly, F. W., and Folkers, K. (1954) THE SYNTHESIS OF (+)-α-LIPOIC ACID AND ITS OPTICAL ANTIPODE. *Journal of the American Chemical Society* **76**, 4748-4748
12. Mislow, K., and Meluch, W. C. (1956) The Stereochemistry of α-Lipoic Acid1. *Journal of the American Chemical Society* **78**, 5920-5923
13. Koike, M., and Reed, L. J. (1960) alpha-Keto acid dehydrogenation complexes. II. The role of protein-bound lipoic acid and flavin adenine dinucleotide. *The Journal of biological chemistry* **235**, 1931-1938
14. Schreibelt, G., Musters, R. J., Reijerkerk, A., de Groot, L. R., van der Pol, S. M., Hendrikx, E. M., Dopp, E. D., Dijkstra, C. D., Drukarch, B., and de Vries, H. E. (2006) Lipoic acid affects cellular migration into the central nervous system and stabilizes

blood-brain barrier integrity. *Journal of immunology (Baltimore, Md. : 1950)* **177**, 2630-2637

15. Zhang, J., Zhou, X., Wu, W., Wang, J., Xie, H., and Wu, Z. (2017) Regeneration of glutathione by alpha-lipoic acid via Nrf2/ARE signaling pathway alleviates cadmium-induced HepG2 cell toxicity. *Environmental toxicology and pharmacology* **51**, 30-37
16. Kagan, V. E., Shvedova, A., Serbinova, E., Khan, S., Swanson, C., Powell, R., and Packer, L. (1992) Dihydrolipoic acid--a universal antioxidant both in the membrane and in the aqueous phase. Reduction of peroxyl, ascorbyl and chromanoxyl radicals. *Biochemical pharmacology* **44**, 1637-1649
17. Golbidi, S., Badran, M., and Laher, I. (2011) Diabetes and alpha lipoic Acid. *Frontiers in pharmacology* **2**, 69-69
18. Estrada, D. E., Ewart, H. S., Tsakiridis, T., Volchuk, A., Ramlal, T., Tritschler, H., and Klip, A. (1996) Stimulation of glucose uptake by the natural coenzyme alpha-lipoic acid/thioctic acid: participation of elements of the insulin signaling pathway. *Diabetes* **45**, 1798-1804
19. Landgraf, B. J., McCarthy, E. L., and Booker, S. J. (2016) Radical S-Adenosylmethionine Enzymes in Human Health and Disease. *Annual review of biochemistry* **85**, 485-514
20. Baker, P. R., II, Friederich, M. W., Swanson, M. A., Shaikh, T., Bhattacharya, K., Scharer, G. H., Aicher, J., Creadon-Swindell, G., Geiger, E., MacLean, K. N., Lee, W.-T., Deshpande, C., Freckmann, M.-L., Shih, L.-Y., Wasserstein, M., Rasmussen, M. B., Lund, A. M., Procopis, P., Cameron, J. M., Robinson, B. H., Brown, G. K., Brown, R. M., Compton, A. G., Dieckmann, C. L., Collard, R., Coughlin, C. R., II, Spector, E., Wempe, M. F., and Van Hove, J. L. K. (2013) Variant non ketotic hyperglycinemia is caused by mutations in LIAS, BOLA3 and the novel gene GLRX5. *Brain : a journal of neurology* **137**, 366-379
21. Tsurusaki, Y., Tanaka, R., Shimada, S., Shimojima, K., Shiina, M., Nakashima, M., Saitsu, H., Miyake, N., Ogata, K., Yamamoto, T., and Matsumoto, N. (2015) Novel compound heterozygous LIAS mutations cause glycine encephalopathy. *Journal Of Human Genetics* **60**, 631
22. Mayr, Johannes A., Zimmermann, Franz A., Fauth, C., Bergheim, C., Meierhofer, D., Radmayr, D., Zschocke, J., Koch, J., and Sperl, W. (2011) Lipoic Acid Synthetase Deficiency Causes Neonatal-Onset Epilepsy, Defective Mitochondrial Energy Metabolism, and Glycine Elevation. *The American Journal of Human Genetics* **89**, 792-797
23. Soreze, Y., Boutron, A., Habarou, F., Barnerias, C., Nonnenmacher, L., Delpech, H., Mamoune, A., Chrétien, D., Hubert, L., Bole-Feysot, C., Nitschke, P., Correia, I., Sardet, C., Boddaert, N., Hamel, Y., Delahodde, A., Ottolenghi, C., and de Lonlay, P. (2013) Mutations in human lipoyltransferase gene LIPT1cause a Leigh disease with secondary deficiency for pyruvate and alpha-ketoglutarate dehydrogenase. *Orphanet Journal of Rare Diseases* **8**, 192
24. Cao, X., Zhu, L., Song, X., Hu, Z., and Cronan, J. E. (2018) Protein moonlighting elucidates the essential human pathway catalyzing lipoic acid assembly on its cognate enzymes. *Proceedings of the National Academy of Sciences* **115**, E7063-E7072
25. Navarro-Sastre, A., Tort, F., Stehling, O., Uzarska, Marta A., Arranz, José A., del Toro, M., Labayru, M. T., Landa, J., Font, A., Garcia-Villoria, J., Merinero, B., Ugarte, M., Gutierrez-Solana, Luis G., Campistol, J., Garcia-Cazorla, A., Vaquerizo, J., Riudor, E., Briones, P., Elpeleg, O., Ribes, A., and Lill, R. (2011) A Fatal Mitochondrial Disease Is

Associated with Defective NFU1 Function in the Maturation of a Subset of Mitochondrial Fe-S Proteins. *The American Journal of Human Genetics* **89**, 656-667
26. Cameron, Jessie M., Janer, A., Levandovskiy, V., MacKay, N., Rouault, Tracey A., Tong, W.-H., Ogilvie, I., Shoubridge, Eric A., and Robinson, Brian H. (2011) Mutations in Iron-Sulfur Cluster Scaffold Genes NFU1 and BOLA3 Cause a Fatal Deficiency of Multiple Respiratory Chain and 2-Oxoacid Dehydrogenase Enzymes. *The American Journal of Human Genetics* **89**, 486-495
27. Reed, L. J. (1998) From lipoic acid to multi-enzyme complexes. *Protein Science* **7**, 220-224
28. Douce, R., Bourguignon, J., Neuburger, M., and Rébeillé, F. (2001) The glycine decarboxylase system: a fascinating complex. *Trends in Plant Science* **6**, 167-176
29. Reed, K. E., and Cronan, J. E., Jr. (1993) Lipoic acid metabolism in Escherichia coli: sequencing and functional characterization of the lipA and lipB genes. *Journal of bacteriology* **175**, 1325-1336
30. Green, D. E., Morris, T. W., Green, J., Cronan, J. E., Jr., and Guest, J. R. (1995) Purification and properties of the lipoate protein ligase of Escherichia coli. *The Biochemical journal* **309 (Pt 3)**, 853-862
31. Morris, T. W., Reed, K. E., and Cronan, J. E., Jr. (1995) Lipoic acid metabolism in Escherichia coli: the lplA and lipB genes define redundant pathways for ligation of lipoyl groups to apoprotein. *J Bacteriol* **177**, 1-10
32. Vaisvila, R., Rasmussen, L. J., Lobner-Olesen, A., von Freiesleben, U., and Marinus, M. G. (2000) The LipB protein is a negative regulator of dam gene expression in Escherichia coli. *Biochimica et biophysica acta* **1494**, 43-53
33. Jordan, S. W., and Cronan, J. E., Jr. (2003) The Escherichia coli lipB gene encodes lipoyl (octanoyl)-acyl carrier protein:protein transferase. *Journal of bacteriology* **185**, 1582-1589
34. Nesbitt, N. M., Baleanu-Gogonea, C., Cicchillo, R. M., Goodson, K., Iwig, D. F., Broadwater, J. A., Haas, J. A., Fox, B. G., and Booker, S. J. (2005) Expression, purification, and physical characterization of Escherichia coli lipoyl(octanoyl)transferase. *Protein expression and purification* **39**, 269-282
35. Ma, Q., Zhao, X., Nasser Eddine, A., Geerlof, A., Li, X., Cronan, J. E., Kaufmann, S. H., and Wilmanns, M. (2006) The Mycobacterium tuberculosis LipB enzyme functions as a cysteine/lysine dyad acyltransferase. *Proceedings of the National Academy of Sciences of the United States of America* **103**, 8662-8667
36. Christensen, Q. H., and Cronan, J. E. (2010) Lipoic Acid Synthesis: A New Family of Octanoyltransferases Generally Annotated as Lipoate Protein Ligases. *Biochemistry* **49**, 10024-10036
37. Sofia, H. J., Chen, G., Hetzler, B. G., Reyes-Spindola, J. F., and Miller, N. E. (2001) Radical SAM, a novel protein superfamily linking unresolved steps in familiar biosynthetic pathways with radical mechanisms: functional characterization using new analysis and information visualization methods. *Nucleic acids research* **29**, 1097-1106
38. Holliday, G. L., Akiva, E., Meng, E. C., Brown, S. D., Calhoun, S., Pieper, U., Sali, A., Booker, S. J., and Babbitt, P. C. (2018) Chapter One - Atlas of the Radical SAM Superfamily: Divergent Evolution of Function Using a “Plug and Play” Domain. in *Methods in enzymology* (Bandarian, V. ed.), Academic Press. pp 1-71
39. Broderick, J. B., Duffus, B. R., Duschene, K. S., and Shepard, E. M. (2014) Radical S-Adenosylmethionine Enzymes. *Chemical Reviews* **114**, 4229-4317
40. Horitani, M., Shisler, K., Broderick, W. E., Hutcheson, R. U., Duschene, K. S., Marts, A. R., Hoffman, B. M., and Broderick, J. B. (2016) Radical SAM catalysis via an

organometallic intermediate with an Fe–[5′-C]-deoxyadenosyl bond. *Science (New York, N.Y.)* **352**, 822-825

41. Magnusson, O. T., Reed, G. H., and Frey, P. A. (2001) Characterization of an allylic analogue of the 5'-deoxyadenosyl radical: an intermediate in the reaction of lysine 2,3-aminomutase. *Biochemistry* **40**, 7773-7782
42. Magnusson, O. T., Reed, G. H., and Frey, P. A. (1999) Spectroscopic Evidence for the Participation of an Allylic Analogue of the 5‘-Deoxyadenosyl Radical in the Reaction of Lysine 2,3-Aminomutase. *Journal of the American Chemical Society* **121**, 9764-9765
43. Byer, A. S., Yang, H., McDaniel, E. C., Kathiresan, V., Impano, S., Pagnier, A., Watts, H., Denler, C., Vagstad, A. L., Piel, J., Duschene, K. S., Shepard, E. M., Shields, T. P., Scott, L. G., Lilla, E. A., Yokoyama, K., Broderick, W. E., Hoffman, B. M., and Broderick, J. B. (2018) Paradigm Shift for Radical S-Adenosyl-l-methionine Reactions: The Organometallic Intermediate Omega Is Central to Catalysis. *Journal of the American Chemical Society* **140**, 8634-8638
44. Lanz, N. D., and Booker, S. J. (2015) Auxiliary iron-sulfur cofactors in radical SAM enzymes. *Biochimica et biophysica acta* **1853**, 1316-1334
45. Fugate, C. J., and Jarrett, J. T. (2012) Biotin synthase: Insights into radical-mediated carbon–sulfur bond formation. *Biochimica et Biophysica Acta (BBA) - Proteins and Proteomics* **1824**, 1213-1222
46. Guianvarc'h, D., Florentin, D., Bui, B. T. S., Nunzi, F., and Marquet, A. (1997) Biotin Synthase, a New Member of the Family of Enzymes Which Uses S-Adenosylmethionine as a Source of Deoxyadenosyl Radical. *Biochemical and biophysical research communications* **236**, 402-406
47. Shaw, N. M., Birch, O. M., Tinschert, A., Venetz, V., Dietrich, R., and Savoy, L. A. (1998) Biotin synthase from Escherichia coli: isolation of an enzyme-generated intermediate and stoichiometry of S-adenosylmethionine use. *The Biochemical journal* **330 (Pt 3)**, 1079-1085
48. Escalettes, F., Florentin, D., Tse Sum Bui, B., Lesage, D., and Marquet, A. (1999) Biotin Synthase Mechanism: Evidence for Hydrogen Transfer from the Substrate into Deoxyadenosine. *Journal of the American Chemical Society* **121**, 3571-3578
49. Hewitson, K. S., Baldwin, J. E., Shaw, N. M., and Roach, P. L. (2000) Mutagenesis of the proposed iron-sulfur cluster binding ligands in Escherichia coli biotin synthase. *FEBS Letters* **466**, 372-376
50. Hewitson, K. S., Ollagnier-de Choudens, S., Sanakis, Y., Shaw, N. M., Baldwin, J. E., Munck, E., Roach, P. L., and Fontecave, M. (2002) The iron-sulfur center of biotin synthase: site-directed mutants. *Journal of biological inorganic chemistry : JBIC : a publication of the Society of Biological Inorganic Chemistry* **7**, 83-93
51. Cicchillo, R. M., and Booker, S. J. (2005) Mechanistic Investigations of Lipoic Acid Biosynthesis in Escherichia coli: Both Sulfur Atoms in Lipoic Acid are Contributed by the Same Lipoyl Synthase Polypeptide. *Journal of the American Chemical Society* **127**, 2860-2861
52. Cicchillo, R. M., Iwig, D. F., Jones, A. D., Nesbitt, N. M., Baleanu-Gogonea, C., Souder, M. G., Tu, L., and Booker, S. J. (2004) Lipoyl synthase requires two equivalents of S-adenosyl-L-methionine to synthesize one equivalent of lipoic acid. *Biochemistry* **43**, 6378-6386
53. Cicchillo, R. M., Lee, K. H., Baleanu-Gogonea, C., Nesbitt, N. M., Krebs, C., and Booker, S. J. (2004) Escherichia coli lipoyl synthase binds two distinct [4Fe-4S] clusters per polypeptide. *Biochemistry* **43**, 11770-11781

54. Douglas, P., Kriek, M., Bryant, P., and Roach, P. L. (2006) Lipoyl synthase inserts sulfur atoms into an octanoyl substrate in a stepwise manner. *Angewandte Chemie (International ed. in English)* **45**, 5197-5199
55. Harmer, J. E., Hiscox, M. J., Dinis, P. C., Fox, S. J., Iliopoulos, A., Hussey, J. E., Sandy, J., Van Beek, F. T., Essex, J. W., and Roach, P. L. (2014) Structures of lipoyl synthase reveal a compact active site for controlling sequential sulfur insertion reactions. *The Biochemical journal* **464**, 123-133
56. Lanz, N. D., Pandelia, M. E., Kakar, E. S., Lee, K. H., Krebs, C., and Booker, S. J. (2014) Evidence for a catalytically and kinetically competent enzyme-substrate cross-linked intermediate in catalysis by lipoyl synthase. *Biochemistry* **53**, 4557-4572
57. Lanz, N. D., Rectenwald, J. M., Wang, B., Kakar, E. S., Laremore, T. N., Booker, S. J., and Silakov, A. (2015) Characterization of a Radical Intermediate in Lipoyl Cofactor Biosynthesis. *Journal of the American Chemical Society* **137**, 13216-13219
58. McCarthy, E. L., and Booker, S. J. (2017) Destruction and reformation of an iron-sulfur cluster during catalysis by lipoyl synthase. *Science (New York, N.Y.)* **358**, 373-377
59. Landgraf, B. J., Arcinas, A. J., Lee, K. H., and Booker, S. J. (2013) Identification of an intermediate methyl carrier in the radical S-adenosylmethionine methylthiotransferases RimO and MiaB. *Journal of the American Chemical Society* **135**, 15404-15416
60. Landgraf, B. J., and Booker, S. J. (2016) Stereochemical Course of the Reaction Catalyzed by RimO, a Radical SAM Methylthiotransferase. *Journal of the American Chemical Society* **138**, 2889-2892
61. Forouhar, F., Arragain, S., Atta, M., Gambarelli, S., Mouesca, J. M., Hussain, M., Xiao, R., Kieffer-Jaquinod, S., Seetharaman, J., Acton, T. B., Montelione, G. T., Mulliez, E., Hunt, J. F., and Fontecave, M. (2013) Two Fe-S clusters catalyze sulfur insertion by radical-SAM methylthiotransferases. *Nature chemical biology* **9**, 333-338
62. Lee, K. H., Saleh, L., Anton, B. P., Madinger, C. L., Benner, J. S., Iwig, D. F., Roberts, R. J., Krebs, C., and Booker, S. J. (2009) Characterization of RimO, a new member of the methylthiotransferase subclass of the radical SAM superfamily. *Biochemistry* **48**, 10162-10174
63. Anton, B. P., Saleh, L., Benner, J. S., Raleigh, E. A., Kasif, S., and Roberts, R. J. (2008) RimO, a MiaB-like enzyme, methylthiolates the universally conserved Asp88 residue of ribosomal protein S12 in Escherichia coli. *Proceedings of the National Academy of Sciences of the United States of America* **105**, 1826-1831
64. Pierrel, F., Douki, T., Fontecave, M., and Atta, M. (2004) MiaB protein is a bifunctional radical-S-adenosylmethionine enzyme involved in thiolation and methylation of tRNA. *The Journal of biological chemistry* **279**, 47555-47563
65. Pierrel, F., Bjork, G. R., Fontecave, M., and Atta, M. (2002) Enzymatic modification of tRNAs: MiaB is an iron-sulfur protein. *The Journal of biological chemistry* **277**, 13367-13370
66. Parry, R. J. (1983) Biosynthesis of some sulfur-containing natural products investigations of the mechanism of carbon-sulfur bond formation. *Tetrahedron* **39**, 1215-1238
67. Herbert, A. A., and Guest, J. R. (1968) Biochemical and genetic studies with lysine+methionine mutants of Escherichia coli: lipoic acid and alpha-ketoglutarate dehydrogenase-less mutants. *Journal of general microbiology* **53**, 363-381
68. Hayden, M. A., Huang, I. Y., Iliopoulos, G., Orozco, M., and Ashley, G. W. (1993) Biosynthesis of lipoic acid: characterization of the lipoic acid auxotrophs Escherichia coli W1485-lip2 and JRG33-lip9. *Biochemistry* **32**, 3778-3782

69. Reed, K. E., and Cronan, J. E., Jr. (1993) Lipoic acid metabolism in Escherichia coli: sequencing and functional characterization of the lipA and lipB genes. *J Bacteriol* **175**, 1325-1336
70. Hayden, M. A., Huang, I., Bussiere, D. E., and Ashley, G. W. (1992) The biosynthesis of lipoic acid. Cloning of lip, a lipoate biosynthetic locus of Escherichia coli. *The Journal of biological chemistry* **267**, 9512-9515
71. Vanden Boom, T. J., Reed, K. E., and Cronan, J. E. (1991) Lipoic acid metabolism in Escherichia coli: isolation of null mutants defective in lipoic acid biosynthesis, molecular cloning and characterization of the E. coli lip locus, and identification of the lipoylated protein of the glycine cleavage system. *Journal of Bacteriology* **173**, 6411-6420
72. Busby, R. W., Schelvis, J. P. M., Yu, D. S., Babcock, G. T., and Marletta, M. A. (1999) Lipoic Acid Biosynthesis: LipA Is an Iron−Sulfur Protein. *Journal of the American Chemical Society* **121**, 4706-4707
73. Ollagnier-de Choudens, S., and Fontecave, M. (1999) The lipoate synthase from Escherichia coli is an iron-sulfur protein. *FEBS Letters* **453**, 25-28
74. Yasukawa, T., Kanei-Ishii, C., Maekawa, T., Fujimoto, J., Yamamoto, T., and Ishii, S. (1995) Increase of solubility of foreign proteins in Escherichia coli by coproduction of the bacterial thioredoxin. *The Journal of biological chemistry* **270**, 25328-25331
75. Iametti, S., Bera, A. K., Vecchio, G., Grinberg, A., Bernhardt, R., and Bonomi, F. (2001) GroEL-assisted refolding of adrenodoxin during chemical cluster insertion. *European journal of biochemistry* **268**, 2421-2429
76. Kriek, M., Peters, L., Takahashi, Y., and Roach, P. L. (2003) Effect of iron-sulfur cluster assembly proteins on the expression of Escherichia coli lipoic acid synthase. *Protein expression and purification* **28**, 241-245
77. Miller, J. R., Busby, R. W., Jordan, S. W., Cheek, J., Henshaw, T. F., Ashley, G. W., Broderick, J. B., Cronan, J. E., Jr., and Marletta, M. A. (2000) Escherichia coli LipA is a lipoyl synthase: in vitro biosynthesis of lipoylated pyruvate dehydrogenase complex from octanoyl-acyl carrier protein. *Biochemistry* **39**, 15166-15178
78. Zhao, X., Miller, J. R., Jiang, Y., Marletta, M. A., and Cronan, J. E. (2003) Assembly of the covalent linkage between lipoic acid and its cognate enzymes. *Chem Biol* **10**, 1293-1302
79. Pandelia, M. E., Lanz, N. D., Booker, S. J., and Krebs, C. (2015) Mossbauer spectroscopy of Fe/S proteins. *Biochimica et biophysica acta* **1853**, 1395-1405
80. Cicchillo, R. M., Lee, K.-H., Baleanu-Gogonea, C., Nesbitt, N. M., Krebs, C., and Booker, S. J. (2004) Escherichia coli Lipoyl Synthase Binds Two Distinct [4Fe−4S] Clusters per Polypeptide. *Biochemistry* **43**, 11770-11781
81. Bryant, P., Kriek, M., Wood, R. J., and Roach, P. L. (2006) The activity of a thermostable lipoyl synthase from Sulfolobus solfataricus with a synthetic octanoyl substrate. *Analytical Biochemistry* **351**, 44-49
82. Lanz, N. D., Rectenwald, J. M., Wang, B., Kakar, E. S., Laremore, T. N., Booker, S. J., and Silakov, A. (2015) Characterization of a Radical Intermediate in Lipoyl Cofactor Biosynthesis. *Journal of the American Chemical Society* **137**, 13216-13219
83. McLaughlin, M. I., Lanz, N. D., Goldman, P. J., Lee, K. H., Booker, S. J., and Drennan, C. L. (2016) Crystallographic snapshots of sulfur insertion by lipoyl synthase. *Proceedings of the National Academy of Sciences of the United States of America* **113**, 9446-9450
84. Li, G.-W., Burkhardt, D., Gross, C., and Weissman, Jonathan S. (2014) Quantifying Absolute Protein Synthesis Rates Reveals Principles Underlying Allocation of Cellular Resources. *Cell* **157**, 624-635

85. Ayala-Castro, C., Saini, A., and Outten, F. W. (2008) Fe-S cluster assembly pathways in bacteria. *Microbiology and molecular biology reviews : MMBR* **72**, 110-125, table of contents
86. Bai, Y., Chen, T., Happe, T., Lu, Y., and Sawyer, A. (2018) Iron–sulphur cluster biogenesis via the SUF pathway. *Metallomics* **10**, 1038-1052
87. Blanc, B., Gerez, C., and Ollagnier de Choudens, S. (2015) Assembly of Fe/S proteins in bacterial systems: Biochemistry of the bacterial ISC system. *Biochimica et biophysica acta* **1853**, 1436-1447
88. Fontecave, M., and Ollagnier-de-Choudens, S. (2008) Iron-sulfur cluster biosynthesis in bacteria: Mechanisms of cluster assembly and transfer. *Archives of biochemistry and biophysics* **474**, 226-237
89. Baker, P. R., 2nd, Friederich, M. W., Swanson, M. A., Shaikh, T., Bhattacharya, K., Scharer, G. H., Aicher, J., Creadon-Swindell, G., Geiger, E., MacLean, K. N., Lee, W. T., Deshpande, C., Freckmann, M. L., Shih, L. Y., Wasserstein, M., Rasmussen, M. B., Lund, A. M., Procopis, P., Cameron, J. M., Robinson, B. H., Brown, G. K., Brown, R. M., Compton, A. G., Dieckmann, C. L., Collard, R., Coughlin, C. R., 2nd, Spector, E., Wempe, M. F., and Van Hove, J. L. (2014) Variant non ketotic hyperglycinemia is caused by mutations in LIAS, BOLA3 and the novel gene GLRX5. *Brain : a journal of neurology* **137**, 366-379
90. Cameron, Jessie M., Janer, A., Levandovskiy, V., MacKay, N., Rouault, Tracey A., Tong, W.-H., Ogilvie, I., Shoubridge, Eric A., and Robinson, Brian H. (2011) Mutations in Iron-Sulfur Cluster Scaffold Genes NFU1 and BOLA3 Cause a Fatal Deficiency of Multiple Respiratory Chain and 2-Oxoacid Dehydrogenase Enzymes. *American Journal of Human Genetics* **89**, 486-495
91. Navarro-Sastre, A., Tort, F., Stehling, O., Uzarska, Marta A., Arranz, José A., del Toro, M., Labayru, M T., Landa, J., Font, A., Garcia-Villoria, J., Merinero, B., Ugarte, M., Gutierrez-Solana, Luis G., Campistol, J., Garcia-Cazorla, A., Vaquerizo, J., Riudor, E., Briones, P., Elpeleg, O., Ribes, A., and Lill, R. (2011) A Fatal Mitochondrial Disease Is Associated with Defective NFU1 Function in the Maturation of a Subset of Mitochondrial Fe-S Proteins. *American Journal of Human Genetics* **89**, 656-667
92. Bandyopadhyay, S., Naik, S. G., O'Carroll, I. P., Huynh, B. H., Dean, D. R., Johnson, M. K., and Dos Santos, P. C. (2008) A proposed role for the Azotobacter vinelandii NfuA protein as an intermediate iron-sulfur cluster carrier. *The Journal of biological chemistry* **283**, 14092-14099
93. Jin, Z., Heinnickel, M., Krebs, C., Shen, G., Golbeck, J. H., and Bryant, D. A. (2008) Biogenesis of iron-sulfur clusters in photosystem I: holo-NfuA from the cyanobacterium Synechococcus sp. PCC 7002 rapidly and efficiently transfers [4Fe-4S] clusters to apo-PsaC in vitro. *The Journal of biological chemistry* **283**, 28426-28435
94. Angelini, S., Gerez, C., Ollagnier-de Choudens, S., Sanakis, Y., Fontecave, M., Barras, F., and Py, B. (2008) NfuA, a new factor required for maturing Fe/S proteins in Escherichia coli under oxidative stress and iron starvation conditions. *The Journal of biological chemistry* **283**, 14084-14091
95. Py, B., Gerez, C., Angelini, S., Planel, R., Vinella, D., Loiseau, L., Talla, E., Brochier-Armanet, C., Garcia Serres, R., Latour, J. M., Ollagnier-de Choudens, S., Fontecave, M., and Barras, F. (2012) Molecular organization, biochemical function, cellular role and evolution of NfuA, an atypical Fe-S carrier. *Molecular microbiology* **86**, 155-171
96. McCarthy, E. L., and Booker, S. J. (2018) Biochemical Approaches for Understanding Iron-Sulfur Cluster Regeneration in Escherichia coli Lipoyl Synthase During Catalysis. *Methods in enzymology* **606**, 217-239

97. McCarthy, E. L., Rankin, A. N., Dill, Z. R., and Booker, S. J. (2019) The A-type domain in Escherichia coli NfuA is required for regenerating the auxiliary [4Fe-4S] cluster in Escherichia coli lipoyl synthase. *The Journal of biological chemistry* **294**, 1609-1617
98. Reed, L. J., Koike, M., Levitch, M. E., and Leach, F. R. (1958) Studies on the nature and reactions of protein-bound lipoic acid. *The Journal of biological chemistry* **232**, 143-158
99. Morris, T. W., Reed, K. E., and Cronan, J. E., Jr. (1994) Identification of the gene encoding lipoate-protein ligase A of Escherichia coli. Molecular cloning and characterization of the lplA gene and gene product. *The Journal of biological chemistry* **269**, 16091-16100
100. Reed, K. E., Morris, T. W., and Cronan, J. E., Jr. (1994) Mutants of Escherichia coli K-12 that are resistant to a selenium analog of lipoic acid identify unknown genes in lipoate metabolism. *Proceedings of the National Academy of Sciences of the United States of America* **91**, 3720-3724
101. Cohen, J. D., Zou, P., and Ting, A. Y. (2012) Site-specific protein modification using lipoic acid ligase and bis-aryl hydrazone formation. *Chembiochem : a European journal of chemical biology* **13**, 888-894
102. Seaman, G. R. (1959) Purification of an enzyme from yeast which liberates protein-bound thioctic acid. *The Journal of biological chemistry* **234**, 161-164
103. Suzuki, K., and Reed, L. J. (1963) LIPOAMIDASE. *The Journal of biological chemistry* **238**, 4021-4025
104. Jiang, Y., and Cronan, J. E. (2005) Expression Cloning and Demonstration of Enterococcus faecalis Lipoamidase (Pyruvate Dehydrogenase Inactivase) as a Ser-Ser-Lys Triad Amidohydrolase. *Journal of Biological Chemistry* **280**, 2244-2256
105. Christensen, Q. H., Hagar, J. A., O'Riordan, M. X. D., and Cronan, J. E. (2011) A Complex Lipoate Utilization Pathway in Listeria monocytogenes. *Journal of Biological Chemistry* **286**, 31447-31456
106. Jhun, H., Walters, M. S., and Prigge, S. T. (2018) Using Lipoamidase as a Novel Probe To Interrogate the Importance of Lipoylation in Plasmodium falciparum. *mBio* **9**, e01872-01818
107. Cao, X., Hong, Y., Zhu, L., Hu, Y., and Cronan, J. E. (2018) Development and retention of a primordial moonlighting pathway of protein modification in the absence of selection presents a puzzle. *Proceedings of the National Academy of Sciences* **115**, 647-655
108. Cronan, J. E. (2016) Assembly of Lipoic Acid on Its Cognate Enzymes: an Extraordinary and Essential Biosynthetic Pathway. *Microbiology and Molecular Biology Reviews* **80**, 429-450
109. Lanz, N. D., Lee, K. H., Horstmann, A. K., Pandelia, M. E., Cicchillo, R. M., Krebs, C., and Booker, S. J. (2016) Characterization of Lipoyl Synthase from Mycobacterium tuberculosis. *Biochemistry* **55**, 1372-1383
110. Spalding, M. D., and Prigge, S. T. (2010) Lipoic acid metabolism in microbial pathogens. *Microbiology and molecular biology reviews : MMBR* **74**, 200-228
111. Spalding, M. D., and Prigge, S. T. (2010) Lipoic acid metabolism in microbial pathogens. *Microbiology and molecular biology reviews : MMBR* **74**, 200-228
112. Kather, B., Stingl, K., van der Rest, M. E., Altendorf, K., and Molenaar, D. (2000) Another Unusual Type of Citric Acid Cycle Enzyme inHelicobacter pylori: the Malate:Quinone Oxidoreductase. *Journal of Bacteriology* **182**, 3204-3209
113. Gould, S. B., Waller, R. F., and McFadden, G. I. (2008) Plastid Evolution. *Annual Review of Plant Biology* **59**, 491-517

114. Wada, H., Shintani, D., and Ohlrogge, J. (1997) Why do mitochondria synthesize fatty acids? Evidence for involvement in lipoic acid production. *Proceedings of the National Academy of Sciences* **94**, 1591-1596
115. Wada, M., Yasuno, R., Jordan, S. W., Cronan Jr., J. E., and Wada, H. (2001) Lipoic Acid Metabolism in Arabidopsis thaliana: Cloning and Characterization of a cDNA Encoding Lipoyltransferase. *Plant and Cell Physiology* **42**, 650-656
116. Wada, M., Yasuno, R., and Wada, H. (2001) Identification of an Arabidopsis cDNA encoding a lipoyltransferase located in plastids11The nucleotide sequence data of the Arabidopsis thaliana LIP2p cDNA for a lipoyltransferase located in plastids were deposited in the DDBJ, EMBL, and GenBank nucleotide sequence databases with the accession number AB048535. *FEBS Letters* **506**, 286-290
117. Ewald, R., Hoffmann, C., Neuhaus, E., and Bauwe, H. (2014) Two redundant octanoyltransferases and one obligatory lipoyl synthase provide protein-lipoylation autonomy to plastids of Arabidopsis. *Plant Biology* **16**, 35-42
118. Yasuno, R., and Wada, H. (1998) Biosynthesis of Lipoic Acid in Arabidopsis: Cloning and Characterization of the cDNA for Lipoic Acid Synthase. *Plant Physiology* **118**, 935-943
119. Yasuno, R., and Wada, H. (2002) The biosynthetic pathway for lipoic acid is present in plastids and mitochondria in Arabidopsis thaliana 1. *FEBS Letters* **517**, 110-114
120. Navarro-Sastre, A., Tort, F., Stehling, O., Uzarska, M. A., Arranz, J. A., Del Toro, M., Labayru, M. T., Landa, J., Font, A., Garcia-Villoria, J., Merinero, B., Ugarte, M., Gutierrez-Solana, L. G., Campistol, J., Garcia-Cazorla, A., Vaquerizo, J., Riudor, E., Briones, P., Elpeleg, O., Ribes, A., and Lill, R. (2011) A fatal mitochondrial disease is associated with defective NFU1 function in the maturation of a subset of mitochondrial Fe-S proteins. *Am J Hum Genet* **89**, 656-667
121. Mashruwala, A. A., Bhatt, S., Poudel, S., Boyd, E. S., and Boyd, J. M. (2016) The DUF59 Containing Protein SufT Is Involved in the Maturation of Iron-Sulfur (FeS) Proteins during Conditions of High FeS Cofactor Demand in Staphylococcus aureus. *PLoS genetics* **12**, e1006233
122. Mashruwala, A. A., Pang, Y. Y., Rosario-Cruz, Z., Chahal, H. K., Benson, M. A., Mike, L. A., Skaar, E. P., Torres, V. J., Nauseef, W. M., and Boyd, J. M. (2015) Nfu facilitates the maturation of iron-sulfur proteins and participates in virulence in Staphylococcus aureus. *Molecular microbiology* **95**, 383-409

Chapter 2

Destruction and reformation of an iron-sulfur cluster during catalysis by lipoyl synthase

This chapter was reproduced from "McCarthy, E.L., and Booker, S.J. Destruction and reformation of an iron-sulfur cluster during catalysis by lipoyl synthase. Science. 2017; 358(6361): 373-377."

Abstract

Lipoyl synthase (LipA) catalyzes the last step in the biosynthesis of the lipoyl cofactor, which is the attachment of two sulfhydryl groups to C6 and C8 of a pendant octanoyl chain. The appended sulfur atoms derive from an auxiliary [4Fe-4S] cluster on the protein that is degraded during turnover, limiting LipA to one turnover in vitro. We found that the *Escherichia coli* iron-sulfur (Fe-S) cluster carrier protein NfuA efficiently reconstitutes the auxiliary cluster during LipA catalysis in a step that is not rate-limiting. We also found evidence for a second pathway for cluster regeneration involving the *E. coli* protein IscU. These results show that enzymes that degrade their Fe-S clusters as a sulfur source can nonetheless act catalytically. Our results also explain why patients with *NFU1* gene deletions exhibit phenotypes that are indicative of lipoyl cofactor deficiencies.

Introduction

Lipoic acid is an eight-carbon, straight-chain fatty acid containing sulfhydryl groups at C6 and C8, which undergo reversible disulfide-bond formation to generate a dithiolane ring (1,2). It is used as a redox-active cofactor in several multienzyme complexes that are involved in the oxidative decarboxylation of various α-keto acids and glycine, as well as in the oxidative degradation of acetoin (3-5). In these complexes, lipoic acid is attached through an amide linkage to a conserved lysyl residue of a lipoyl carrier protein (LCP), producing a 14 Å "swinging arm" that allows its dithiolane ring to access multiple active sites. A well-known role is in the pyruvate dehydrogenase complex (PDC), where it plays a central function in the conversion of pyruvate to acetyl–coenzyme A (3,4). Other complexes in which it functions in a similar capacity are the α-ketoglutarate dehydrogenase complex (KDC), the branched-chain α-ketoacid dehydrogenase complex, the acetoin dehydrogenase complex, and the glycine cleavage system (3-6). Deficiencies in the biosynthesis of the lipoyl cofactor or in any of the multienzyme complexes that require it result in a number of diseases, one of which is multiple mitochondrial dysfunctions syndrome, which leads to severe developmental delays, seizures, and death (7). In mammals, the complete inability to synthesize lipoic acid is embryonic lethal (8).

Although the lipoyl cofactor is structurally simple, its biosynthesis has been enigmatic. Seminal studies from the Cronan laboratory identified the pathway by which the lipoyl cofactor is biosynthesized de novo in *E. coli* and highlighted the roles of two dedicated proteins: octanoyltransferase (LipB), which catalyzes the transfer of an *n*-octanoyl moiety from octanoyl–acyl carrier protein to a conserved lysyl residue on an LCP; and lipoyl synthase (LipA; LIAS in humans and Lip5 in yeast), which catalyzes the subsequent attachment of two sulfur atoms at C6 and C8 of the aliphatic chain (9-12). This pathway is conserved in all organisms that synthesize the lipoyl cofactor de novo, although slight variations have been noted (9,13,14).

LipA is a member of the radical *S*-adenosylmethionine (SAM) superfamily of enzymes; as such, it uses a 5′-deoxyadenosyl 5′-radical (5′-dA•) that results from the reductive cleavage of SAM to abstract hydrogen atoms (H•)—first from C6 and then from C8—to activate the aliphatic chain for sulfur attachment (15-18). All radical SAM (RS) proteins contain one [4Fe-4S] cluster that supplies the electron during the reductive cleavage of SAM (19,20). However, lipoyl synthases contain a second [4Fe-4S] cluster that has been hypothesized to be the source of the attached sulfur atoms (17,21,22). Consistent with this hypothesis, LipA typically catalyzes no more than one turnover during in vitro reactions because of the obligate destruction of the iron-sulfur (Fe-S) cluster (16,18,23). The current working hypothesis for turnover by LipA is shown in **Figure 2-1** (16,17,24). SAM binds in contact with the RS [4Fe-4S] cluster—termed $[4Fe\text{-}4S]_{RS}$—and undergoes reductive cleavage to generate a 5′-dA•, which abstracts an H• from C6 of the octanoyllysyl group of an LCP. The resulting C6 radical attacks a bridging μ-sulfido ion of the auxiliary cluster, with concomitant reduction of one of the Fe^{3+} ions of the cluster to Fe^{2+} and loss of an Fe^{2+} ion, to afford a [3Fe-3S-1(6*S*)-thio-octanoyl-LCP] cluster (16,17). A second 5′-dA•, generated from the reductive cleavage of a second SAM molecule, abstracts a C8 H•, with subsequent attack of the resulting C8 radical onto a second bridging μ-sulfido ion of the auxiliary cluster. This step results in attachment of the second sulfur atom and concomitant full or partial destruction of the cluster upon protonation of the two sulfur atoms in the nascent lipoyl group.

If the current proposed mechanism for LipA catalysis reflects the in vivo mechanism, LipA would be a substrate rather than an enzyme, given that it is irreversibly consumed in the reaction. Hence, it is likely that there is a system responsible for either the repair of a partially degraded cluster or the insertion of a newly assembled [4Fe-4S] cluster into the LipA active site. Although Fe-S cluster assembly can occur spontaneously in vitro, it has been established that the in vivo process involves a complex network of proteins that is highly regulated (25-30). Herein, we provide

evidence that *E. coli* NfuA, an Fe-S cluster–containing protein that has been suggested to serve as an intermediate in Fe-S cluster delivery, confers catalytic properties on *E. coli* LipA.

A number of studies have provided strong evidence that NFU1 and BOLA3 are involved in lipoic acid production in mammalian and yeast cells. For example, mutations in either *NFU1* or *BOLA3*, previously considered to encode alternative scaffold proteins in Fe-S cluster biosynthesis, were found to cause a fatal deficiency of multiple respiratory chain and 2-oxoacid dehydrogenase enzymes. These deficiencies were thought to be due to a lack of the lipoyl group on the LCPs of the PDC and KDC, as well as defects in complexes I and II of the mitochondrial respiratory chain (31,32). More recent studies directly linked NFU1 and BOLA3 to lipoic acid biosynthesis in mammalian cells and yeast, and it was determined that the proteins participated at some late stage in the process (33).

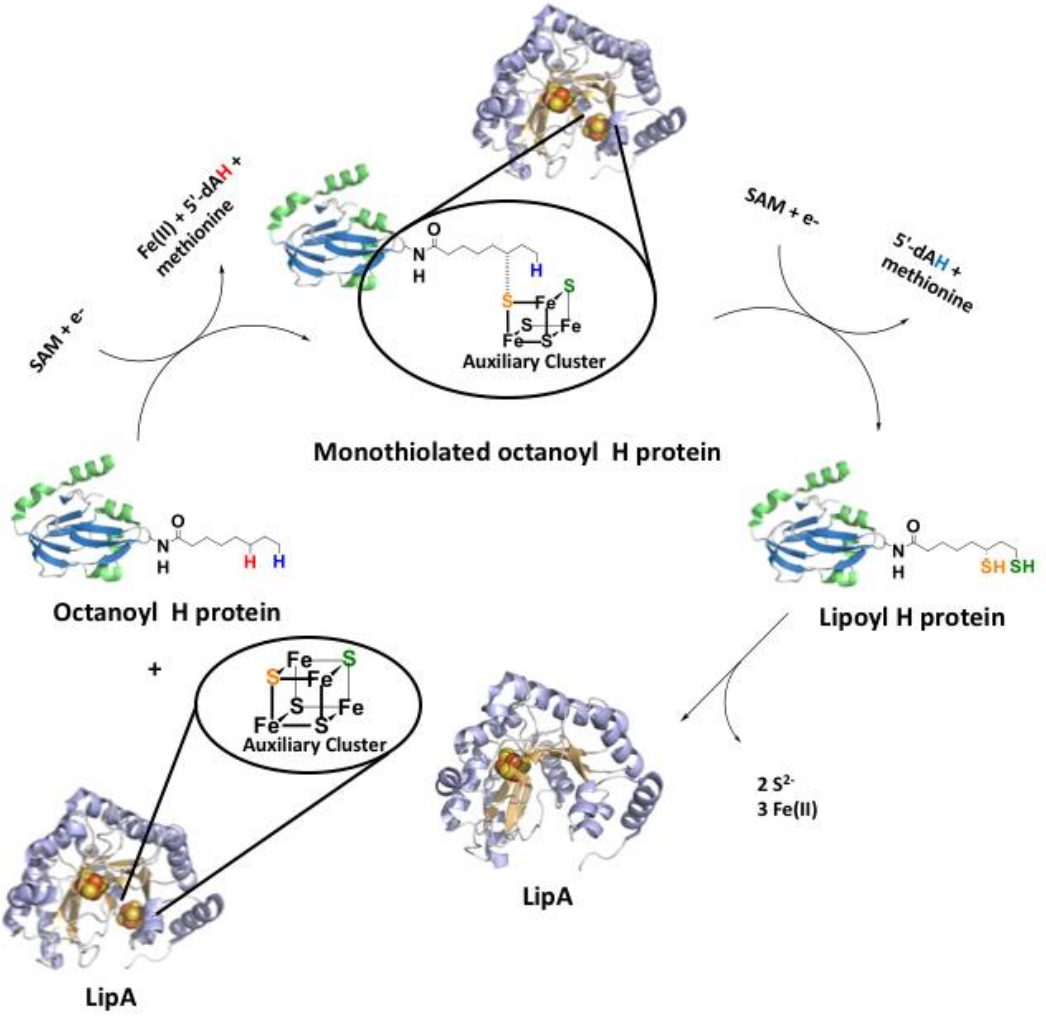

Figure 2-1: Catalysis by LipA. LipA contains two [4Fe-4S] clusters, one of which (the auxiliary cluster shown) is sacrificed during turnover. Catalysis proceeds by reductive cleavage of SAM to render a 5′-deoxyadenosyl 5′-radical (5′-dA•), which abstracts the C6 *pro-R* hydrogen atom of a pendant *n*-octanoamide chain residing on a lipoyl carrier protein (H protein of the glycine cleavage system shown). The resulting C6 substrate radical attacks one of the sulfide ions of the auxiliary cluster, which is followed by loss of an Fe^{2+} ion to afford a [3Fe-3S-1(6*S*)-thio-octanoamide]H protein intermediate (labeled as monothiolated octanoyl H protein). A second reductive cleavage of SAM generates a second 5′-dA•, which abstracts an H• from C8 of the thio-octanoamide H protein intermediate. The resulting C8 substrate radical attacks a second sulfide ion of the auxiliary cluster, which is followed by the addition of two protons and the loss of three Fe^{2+} ions and two S^{2-} ions to generate the lipoyl group in its reduced form.

Materials and Methods

Materials— Restriction enzymes and materials for cloning were obtained from New England Biolabs (Ipswich, MA). DNA isolation kits were purchased from Machery-Nagel (Dueren, Germany). Deoxynucleotides for PCR amplification were from Denville Scientific Corporation (South Plainfield, New Jersey). Kanamycin, arabinose, isopropyl β-D-thiogalactopyranoside (IPTG), tris (2-carboxyethyl) phosphine (TCEP), dithiothreitol, and ampicillin were from Gold Biotechnology (St. Louis, MO). Protein calibration standards, elemental ^{34}S, $FeCl_3$, L-cysteine, DNase I, β-mercaptoethanol (BME), pyridoxal 5′-phosphate (PLP), sodium dithionite, and (1,10)-phenanthroline were purchased from Sigma Co. (St. Louis, MO). Ni-NTA resin for protein isolation was obtained from Qiagen. HEPES (sodium salt) and potassium chloride were from Dot Scientific (Burton, MI). Imidazole and lysozyme were from Alfa Aesar (Haverhill, MA). Coomassie brilliant blue dye and Bradford reagent were from Amresco (Fountain Parkway Solon, OH). Unlabeled Na_2S and Bovine serum albumin (BSA) used for the Bradford standard were from Thermo Fisher Scientific (Waltham, MA). Materials used in LC-MS assays, including the lipoyl, octanoyl, and 6-thiooctanoyl peptides, SAH nucleosidase, external standard peptide, and SAM have been previously described (16). All chemicals and reagents were of the highest grade available.

General procedures— UV-visible spectra were recorded on a Varian Cary 50 spectrometer (Walnut Creek, CA) using the WinUV software package. Polymerase Chain Reaction (PCR) was performed using a Bio-Rad S1000 Thermal Cycler. High-performance liquid chromatography (HPLC) with detection by mass spectrometry (LC−MS) was conducted on an Agilent Technologies (Santa Clara, CA) 1200 system coupled to an Agilent Technologies 6410 QQQ mass spectrometer. The system was operated with the associated MassHunter software package, which was also used for data collection and analysis.

Plasmid Construction—The construction of the *E. coli lipA* expression vector has been previously described (21). *E. coli nfuA*, *hscA*, and *hscB* genes were PCR amplified from genomic DNA (W3110) and ligated into the expression plasmid pET28a using its *Hin*dIII/*Xho*I, and *Nde*I/*Xho*I restriction sites, respectively. *E. coli iscU* and *iscS* genes were PCR amplified from genomic DNA (W3110) and ligated into the expression plasmid pSUMO using the *Bsa*I/*Xho*I restriction sites. The resulting constructs were verified by DNA sequencing at the Genomics Core Facility (University Park, PA). Primers used for PCR amplification were purchased from Integrated DNA Technologies (Coralville, IA) and are listed in **Table 2-1**.

Table **2-1**: Oligonucleotides used for plasmid construction.

Gene	Vector		Oligonucleotide
nfuA	pET28a	forward	5' CGC GGC GTC AAG CTT ATG ATC CGT ATT TCC GAT GCT GC 3'
		reverse	5' CGC GGC GTC CTC GAG TTA GTA GTA GGA GTG TTC GCC GC 3'
lipA	pET28a	forward	5' GCG GCG TCC ATA TGA GTA AAC CCA TTG TGA TGG AAC GC 3'
		reverse	5′ GCC GGA ATT CTT ACT TAA CTT CCA TCC CTT TCG 3′
hscA	pET28a	forward	5' CGC GGC GTC CAT ATG GCC TTA TTA CAA ATT AGT GAA CCT GG 3'
		reverse	5' CGC GGC GTC CTC GAG TTA AAC CTC GTC CAC GGA ATG GC 3'
hscB	pET28a	forward	5' CGC GGC GTC CAT ATG GAT TAC TTC ACC CTC TTT GGC TTG C 3'
		reverse	5' CGC GGC GTC CTC GAG TTA AAA ATC GAG CAG TTT TTC TTC G 3'
iscU	pSUMO	forward	5' CGC GGC GTC GGTCTC G AGGT ATG GCT TAC AGC GAA AAA GTT ATC GAC CAT TAC G 3'
		reverse	5' CGC GGC GTC GGTCTC CTCGAG TTA TTT TGC TTC ACG TTT GCT TTT ATA GTC CGC 3'
iscS	pSUMO	forward	5' CGC GGC GTC GGTCTC G AGGT ATG AAA TTA CCG ATT TAT CTC G 3'
		reverse	5' CGC GGC GTC GGTCTC CTCGAG TTA ATG ATG AGC CCA TTC G 3'
Δ*nfuA*	N/A	forward	5' CGC GGC GTC G GTC TGG TGC CTT TGT CGA ACC TTG TAG 3'
		reverse	5' CGC GGC GTC TAC ACC GAT AGC AAC AAT GAC TAA TGG 3'

\

Strains and Growth Conditions—Overproduction of *E. coli* LipA has been previously described (21). For overproduction of NfuA, *E. coli* BL21(DE3) cells were transformed with the *pET28a-nfuA* construct along with plasmid pDB1282, which contains genes of the *isc* operon from

Azotobacter vinelandii (21). *E. coli* strains were grown at 37 °C and 180 rpm in M9 minimal media supplemented with 50 μM $FeCl_3$, ampicillin (100 μg/mL), and kanamycin (50 μg/mL). At an OD_{600}=0.3, 0.2% arabinose was added to induce expression of the *isc* genes contained on the pDB1282 plasmid. At an OD_{600}=0.6, *nfuA* gene expression was induced by addition of 200 μM IPTG (final concentration) at 18 °C, and expression was allowed to take place for 18 h. IscU and apo-NfuA were prepared using a similar procedure with some modifications. *E. coli* BL21(DE3) cells were transformed with the *iscU*-pSUMO plasmid in the absence of pDB1282 and was cultured in M9 minimal media. Gene expression was induced with 200 μM IPTG. For overproduction of apo-NfuA, the M9 minimal media was supplemented with the following metal mix (final concentrations): 3 nM $(NH_4)_2Mo_7O_{24}$, 30 nM $CoCl_2$•$6H_20$, 400 nM H_3BO_3, 10 nM $CuSO_4$•5H2O, 80 nM $MnCl_2$•$4H_20$, and 10 nM $ZnSO_4$•$7H_20$. At an OD_{600}=0.3, the cultures were supplemented with a mixture of essential amino acids, including alanine (800 μM), arginine (400 μM), asparagine (400 μM), aspartic acid (400 μM), cysteine (100 μM), glutamic acid (600 μM), glutamine (600 μM), glycine (800 μM), histidine (200 μM), isoleucine (400 μM), leucine (800 μM), lysine (400 μM), methionine (200 μM), phenylalanine (400 μM), proline (400 μM), serine (10 mM), threonine (400 μM), tryptophan (100 μM), tyrosine (200 μM), and valine (600 μM). At an OD_{600}=0.6, 75 μM 1,10-phenanthroline was added to the flasks, which were subsequently chilled on ice for 2 h. Gene expression was then induced with 200 μM IPTG for ~18 h at 18 °C. For *hscA*, *hscB*, and *iscS*, *E. coli* BL21(DE3) cells were transformed with the target plasmid, and was cultured at 37 °C in LB media supplemented with kanamycin (50 μg/mL). At an OD_{600}=0.6, gene expression was induced with 200 μM IPTG for ~7 h. In all instances, bacterial cells were harvested by centrifugation at 7,000 × g for 15 min at 4 °C. The resulting pellets were flash-frozen in liquid N_2 and stored in liquid N_2 until further use.

Purification of E. coli LipA, NfuA, HscA, and HscB— The purification of *E. coli* LipA has been previously described (21). Holo-NfuA, Apo-NfuA, HscA, and HscB were purified by immobilized metal affinity chromatography (IMAC) using the following procedure. All purification steps were carried out in an anaerobic chamber containing <1 ppm O_2 (Coy Laboratory Products, Grass Lake, Michigan), with the exception of the centrifugation steps in which centrifuge tubes were tightly sealed in the chamber before removing. The cellular pellet containing overproduced protein was re-suspended in Buffer A (50 mM HEPES, pH 7.5, 300 mM KCl, 20 mM imidazole, 10 mM BME). Lysozyme (1 mg/mL) and Dnase I (0.1 mg/mL) were added, and the solution was stirred for 30 min at room temperature. The cells were lysed by sonic disruption, and the resulting lysate was centrifuged at 45,000 x g for 1 h at 4 °C. The supernatant was applied to a column of Ni-NTA resin pre-equilibrated in Buffer A, and the column was washed with Buffer B (50 mM HEPES, pH 7.5, 300 mM KCl, 45 mM imidazole, 10 mM BME, and 10% glycerol). The protein was eluted with Buffer C (50 mM HEPES, pH 7.5, 300 mM KCl, 500 mM imidazole, 10 mM BME, and 10% glycerol) and then concentrated to 2.5 mL and exchanged into storage buffer (50 mM HEPES, pH 7.5, 300 mM KCl, 5 mM DTT, 15% glycerol) using a PD-10 column (GE Healthcare Life Sciences). The protein was aliquoted, flash-frozen, and stored in liquid N_2 until use. SDS-PAGE analysis performed using a mini vertical electrophoresis unit from Hoefer (Holliston MA). A 12.5% polyacrylamide gel stained with Coomassie brilliant blue revealed that the final protein was >95% pure. The protein concentration was determined using the Bradford method (34). Amino acid analysis, performed by the UC Davis Proteomics Core, revealed that the Bradford method overestimates the protein concentration of *Ec* NfuA by a factor of 1.18. Colorimetric iron and sulfide analyses normalized to protein concentration were used to estimate the iron and sulfide content per polypeptide (35,36).

Purification of E. coli IscU and IscS— IscU and IscS were each overproduced as a cleavable fusion with the protein SUMO, which contained an N-terminal hexahistidine-tag. This construct permitted the isolation of each of the proteins in their native states. The first step of the purification procedure was identical to the purification procedures described above, with the exception that the fusion protein was exchanged into Cleavage Buffer (50 mM HEPES, pH 7.5, 300 mM KCl, 10% glycerol, and 10 mM BME) using a PD-10 column following the protein elution step. ULP1 protease (50 μg per mg of protein to be cleaved) was added to the fusion protein to excise the hexahistidine-tagged SUMO protein from IscU or IscS, and the reaction was incubated on ice overnight. The following day, the protein solution was re-applied to a nickel column equilibrated in Cleavage Buffer, and the native IscU or IscS protein was collected in the flow-through. The protein was exchanged into storage buffer, concentrated, aliquoted, and flash-frozen in liquid N2. IscS was reconstituted with 5 mM DTT and 5 mM pyridoxal 5′-phosphate (PLP) overnight on ice, and unbound PLP was removed by gel filtration chromatography.

Chemical Reconstitution of NfuA—Wild-type NfuA was chemically reconstituted under anaerobic conditions to ensure full [4Fe–4S] cluster incorporation. A reaction containing 100 μM NfuA was slowly stirred on ice. DTT (5 mM final) was added in three increments every 20 min, and the solution was incubated for 1 h. Next, 500 μM $FeCl_3$ was added in five increments every 5 min, and the solution was incubated for 30 min. Finally, 500 μM Na_2S was added in five increments every 30 min, and the reaction was incubated on ice overnight. The following day, aggregates were removed by centrifugation at 14,000 × g for 10 min, and the protein was concentrated to 2.5 mL. The protein was then further purified by size-exclusion chromatography on a HiPrep 16/60 Sephacryl HR S-200 column (GE Health Sciences) equilibrated in storage buffer (flow-rate of 0.5 mL/min) and connected to an ÅKTA protein liquid chromatography system (GE Health Sciences) housed in an anaerobic chamber. For reconstitution of apo-NfuA with $^{34}S^{2-}$, the same procedure

was used with the following modification: 1.6 mM $Na_2{}^{34}S$ and 1.6 mM $FeCl_3$were used in the reaction. $Na_2{}^{34}S$ was synthesized from elemental ^{34}S as described below.

Biological Reconstitution of IscU—IscU was isolated in its apo-form and its cluster was reconstituted as described previously with the following slight modifications (37). Briefly, 4 mM BME was added to a 15 mL reaction containing 200 μM native IscU in gel filtration buffer (50 mM HEPES, pH 7.5, 300 mM KCl, 15% glycerol, 5 mM DTT). 1.6 mM $FeCl_3$ was added incrementally over a 30 min interval and then the solution was incubated for 30 min on ice. IscS (20 μM) was added, and the reaction was initiated with 5 mM cysteine, pH 7.5. The following day, aggregates were removed as described above for the reconstitution of NfuA.

Interaction between LipA and NfuA—The ability of LipA and NfuA to associate was investigated using size-exclusion chromatography. A 500 μL mixture of standards composed of cytochrome c (12.4 kDa), carbonic anhydrase (29 kDa), bovine serum albumin (66 kDa), alcohol dehydrogenase (150 kDa), α-amylase (200 kDa), and blue dextran (2000 kDa) was applied to a HiPrep 16/60 Sephacryl HR S-200 column (GE Healthcare) housed in a Coy anaerobic glovebox under strictly anaerobic conditions (<1 ppm O2) equilibrated in freshly prepared buffer (50 mM HEPES, pH 7.5, 150 mM KCl, 15% glycerol, and 1 mM DTT). The log MW of each standard was plotted against their respective elution volumes, corrected for the void volume of the column **(Figure 2-2).** The linear equation was then used to estimate the molecular weight of each sample. The following samples were applied to the column in a 500 μL volume: 100 μM NfuA, 100 μM LipA, and a mixture of 100 μM LipA and 100 μM NfuA. The interaction was judged both by the calculated experimental size of each of the peaks as well as by a shift in the elution volume. The presence of both LipA and NfuA was confirmed by SDS-PAGE.

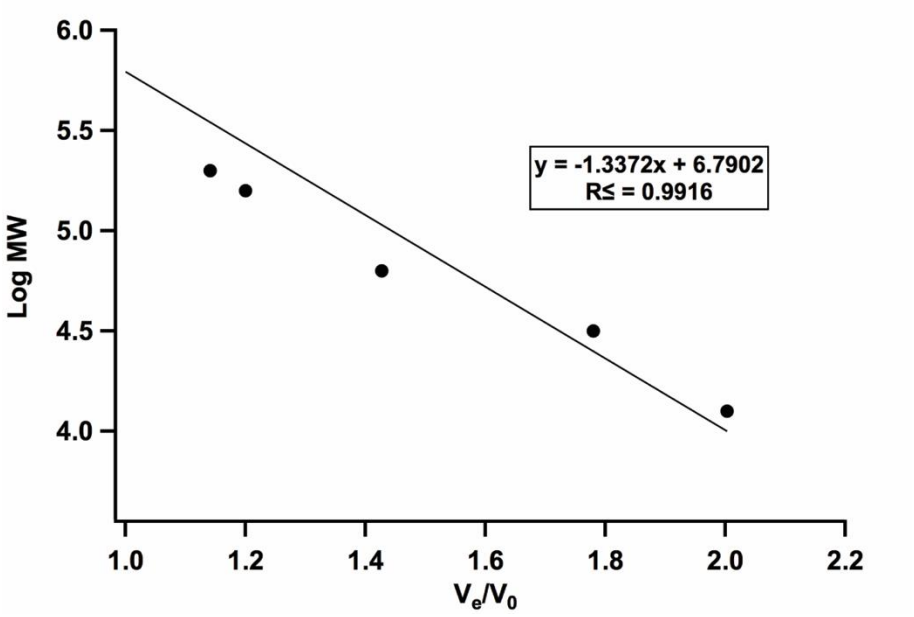

Figure **2-2**: Standard curve for size-exclusion chromatography included cytochrome c (12.4 kDa), carbonic anhydrase (29 kDa), bovine serum albumin (66 kDa), alcohol dehydrogenase (150 kDa), β-amylase (200 kDa), and blue dextran (2000 kDa).

Synthesis of $Na_2{}^{34}S$— Na234S was synthesized from ^{34}S using a previously published method with slight modifications (38). A two-neck 100 mL round bottom flask was cooled to -78 °C in a dry ice/acetone bath. Elemental ^{34}S (50 mg) was added to the cooled flask, and ammonia gas was passed through the attached Dewar condenser until 30 mL of liquid ammonia accumulated. A two-fold molar excess of sodium metal was added slowly and the reaction was stirred for 30 min. The solution was warmed to room temperature, and the ammonia was evaporated under a stream of nitrogen gas to yield a white precipitate. Isopropanol was used to quench the excess sodium metal, followed by the addition of 5 mL water. The solutions were removed *in vacuo* to yield a white precipitate. The concentration of sulfide was determined by the method of Beinert (36).

LC-MS Activity Assays— The experimental setup and assay conditions were described in detail elsewhere with a few notable exceptions (16). The multiple turnover assays using unlabeled NfuA

included either 50 μM LipA and 200 μM NfuA (**Figure 2-5, Panel E**), or 10 μM LipA and 400 μM NfuA (**Figure 2-5, Panel F**) in addition to 600 μM peptide substrate analog (Glu-Ser-Val-[*N*6-octanoyl]Lys-Ala-Ala-Ser-Asp), 0.5 μM S-adenosylhomocysteine (SAH) nucleosidase, 1 mM SAM, and buffer (100 mM HEPES, pH 7.5, 300 mM KCl, and 10% glycerol). When NfuA was added to a reaction that had already undergone turnover for 150 min in its absence (**Figure 2-5, Panel D**), its concentration was 200 μM, while that of LipA was 50 μM. All other reaction components were as listed above. Reactions were conducted at room temperature and were initiated by addition of sodium dithionite to a final concentration of 2 mM. The reactions were quenched at appropriate times with H_2SO_4 at a final concentration of 100 mM. The reaction testing the effect of IscU on LipA turnover contained 20 μM LipA, 400 μM IscU, 600 μM peptide substrate analog, 0.5 μM SAH nucleosidase, 2 mM ATP, 2 mM SAM, and 100 mM $MgCl_2$ **(Figure 2-7, Panel B).** When appropriate, 200 μM HscA and 200 μM HscB were included in reactions containing IscU or NfuA **(Figure 2-7, Panels C and D).** When ^{34}S-labeled NfuA was used, the reactions contained either 20 μM LipA and 100 μM ^{34}S-labeled NfuA (**Figure 2-6, Panels A**) or 10 μM LipA and 400 μM ^{34}S-labeled NfuA (**Figure 2-6, Panel B**), as well as 600 μM peptide substrate analog, 0.5 μM SAH nucleosidase, and 1 mM SAM. The ^{34}S-containing lipoyl peptide product was analyzed using the same conditions previously described. Detection of substrates and products was performed using electrospray ionization in positive mode (ESI+) with the following parameters: a nitrogen gas temperature of 340 °C and flow rate of 9.0 L/min, a nebulizer pressure of 40 PSI and a capillary voltage of 4000 V. Substrates and products were detected using multiple reaction monitoring **(Table 2-2).** The assay mixture was separated on an Agilent Technologies Zorbax Extend-C18 column Rapid Resolution HT (4.6 mm × 50 mm, 1.8 μm particle size) equilibrated in 98% Solvent A (0.1% formic acid, pH 2.6) and 2% Solvent B (100% acetonitrile). A gradient of 2-23% solvent B was applied from 0.8 min to 3.5 min and maintained at 23% solvent B until 8 min before returning to 2% solvent B from 8 min to 10 min. A flow-rate of 0.4 mL/min was maintained throughout the

method. The column was allowed to re-equilibrate for 2 min under the initial conditions between sample injections.

Table **2-2**: Fragmentation Products Monitored by LC-MS.

Compound	Parent Ion*	Product Ion 1$^{\Psi}$	Product Ion 2$^{\Psi}$
AtsA peptide	474.4 (135)	229.1 (12)	153.1 (26)
5'-dA	252.1 (90)	136 (13)	119 (50)
Trp	188 (130)	146.1 (10)	118 (21)
Octanoyl	932.5 (240)	552.3 (37)	210.1 (51)
Monothiolated ^{32}S	964.5 (240)	584.3 (37)	242.1 (51)
Lipoyl $^{32}S/^{32}S$	996.5 (240)	616.4 (37)	274.1 (51)
Monothiolated ^{34}S	966.5 (240)	586.3 (37)	244.1 (51)
Lipoyl $^{32}S/^{34}S$	998.5 (240)	618.4 (37)	276.1 (51)
Lipoyl $^{34}S/^{34}S$	1000.5 (240)	620.4 (37)	278.1 (51)

*Respective fragmentor voltages in parenthesis

$^{\Psi}$Respective collision energies in parenthesis

The effect of extraneous iron and sulfide on the activity of LipA was tested (**Figure 2-6, Panel C**) by including 0.8 mM $FeCl_3$ and 0.8 mM Na_2S in a reaction containing 50 μM LipA and no NfuA. The control reaction contained 200 μM NfuA in the absence of additional iron and sulfide. To assess whether IscS was capable of repairing the auxiliary cluster during turnover (**Figure 2-6, Panel D**), reactions contained 200 μM IscS, 5 mM cysteine, and 5 mM DTT.

In order to show that the cluster transfer from NfuA to LipA is direct rather than a passive diffusion mechanism, excess citrate was added to the buffer. Five-fold excess citrate (150 μM) was added to LipA or NfuA (30 μM) and incubated at room temperature for 2.5 hr. UV-visible spectra were obtained before and after citrate addition for each of the proteins to ensure citrate did not affect cluster incorporation on the respective proteins **(Figure 2-8).** Activity assays were then performed to test whether citrate inhibited the product formation catalyzed by LipA. The reaction

contained 100 μM LipA, 1 mM NfuA, 5 mM citrate, 700 μM octanoyllysyl peptide substrate, 0.5 μM SAH nucleosidase, and 2 mM SAM **(Figure 2-6, Panel E).**

A second method was used to confirm direct cluster transfer from NfuA and IscU to LipA in which excess ^{34}S was included in the buffer system, and assays were conducted using NfuA, IscU, and LipA with clusters containing natural abundance sulfur **(Figure 2-6, Panel F and 2-7, Panel E).** The reactions contained 25 μM LipA, 400 μM IscU or NfuA, 1 mM ^{34}S, 700 μM octanoyllsyl peptide substrate, 0.5 μM SAH nucleosidase, 2 mM SAM, and buffer (100 mM HEPES, pH 7.5, 300 mM KCl, 10% glycerol). Unlabeled product, mixed $^{32}S/^{34}S$ product, and $^{34}S/^{34}S$ labeled product formation was monitored via LC-MS as described above.

Growth study of Δnfu A strain—E. coli strain *BW25113* with a kanamycin cassette replacing the *nfuA* gene was obtained from the Keio collection (Yale Coli Genetic Stock Center). To confirm that the deletion was present, primers (**Table 2-1**) were used to amplify the region containing the kanamycin cassette using the PCR, and the resulting DNA fragment was sequenced. A single colony was used to inoculate 200 mL LB media supplemented with 25 μg/mL kanamycin. The culture was grown at 37 °C at 250 rpm overnight. The following day, 100 μL of the starter culture was centrifuged for 5 min at 14,000 × g, and the pellet was re-suspended in M9 media. The supernatant was removed, and the process was repeated three times. After the final wash, the re-suspended cells were used to inoculate 100 mL flasks containing M9 minimal media + 25 μg/mL kanamycin. The optical density at 600 nm was used to monitor cell growth over a period of 30 hr and compared to a BW25113 control strain, a *BW25113*: Δ*nfuA* + 25 μM lipoic acid, and *BW25113*: Δ*nfuA* + 5 mM succinate/5 mM acetate prepared under identical conditions **(Figure 2-7, Panel A).**

Results

To assess the effect of NfuA—a bacterial homolog of NFU1—on the LipA reaction, we carried out molecular sieve chromatography (MSC) to first establish whether NfuA associates with LipA. *E. coli* NfuA was overproduced with an N-terminal hexahistidine (His_6) tag to allow purification by immobilized metal affinity chromatography **(Figure 2-3).** The purified protein contained 1.8 ± 0.2 sulfide and 2.3 ± 0.2 iron ions per polypeptide; however, its ultraviolet-visible (UV-vis) spectrum suggested the presence of [4Fe-4S] clusters **(Figure 2-4, Panel A).** Moreover, reconstitution of as-isolated NfuA with additional iron and sulfide did not lead to more cluster incorporation. This stoichiometry is consistent with the presence of one [4Fe-4S] cluster per dimer of polypeptides. LipA alone **(Figure 2-5, dotted trace, Panel B)** eluted at 59.6 ml by MSC, exhibiting an experimentally calculated mass of 44.1 kDa (theoretical mass, 38.2 kDa) based on the elution profiles of a suite of standards **(Figure 2-2).** NfuA alone (dashed trace) eluted at 64.6 ml, exhibiting an experimentally calculated mass of 28.9 kDa (theoretical mass, 25.6 kDa). The sample containing both LipA and NfuA (solid trace) showed an elution at 54.6 ml, corresponding to an experimentally calculated mass of 67.2 kDa, which suggested a 1:1 heterodimer of LipA and NfuA (theoretical mass, 63.8 kDa). To confirm the results obtained by MSC, we subjected fractions from the two peaks observed in the LipA + NfuA trace to SDS–polyacrylamide gel electrophoresis (PAGE). As shown in **Figure 2-5, Panel C,** the major peak (lane 2) contained both NfuA and LipA. In these experiments, NfuA migrates as a monomer and can interact with LipA as a monomer. In previous similar characterizations of NfuA, it was stated to migrate as a homodimer by MSC; however, the experimental methods and data were not provided in detail (39,40). The UV-vis spectrum of NfuA alone upon elution from the column reveals that it had lost its cluster **(Figure 2-4, Panel B).** By contrast, LipA eluted from the column with both of its clusters intact. However, when NfuA was chromatographed at higher concentrations, as during its purification, it eluted with

its [4Fe-4S] cluster intact. These observations are consistent with a comparatively less stable cluster on NfuA that is required for dimerization, as has been suggested previously (39-41).

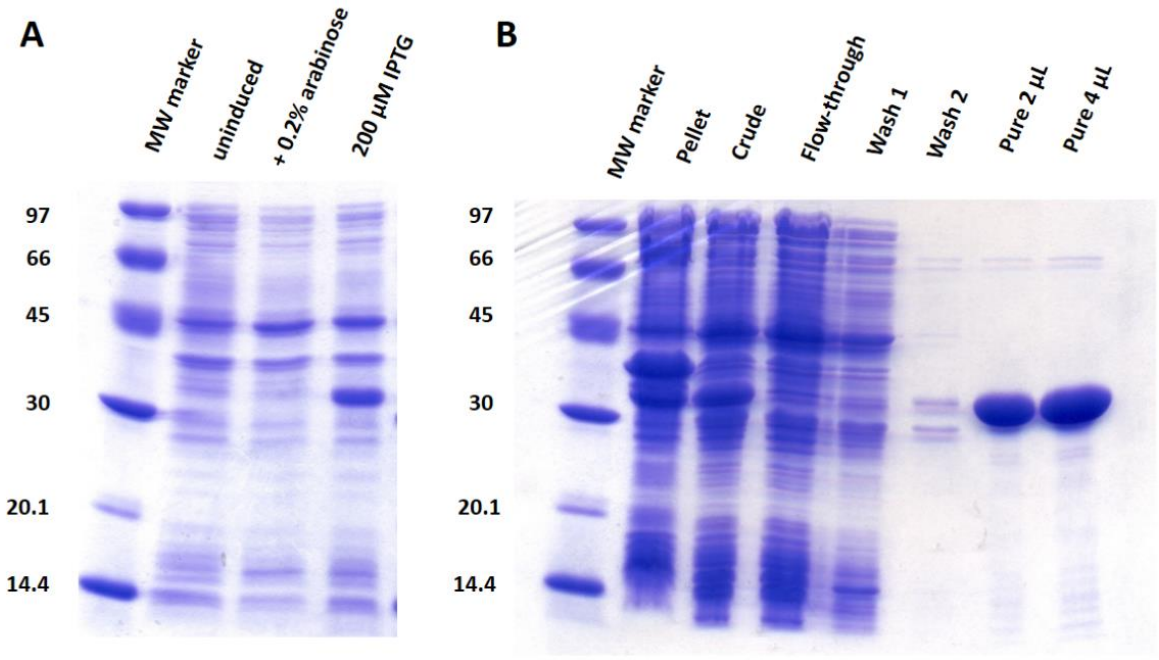

Figure **2-3**: SDS-PAGE of (A) Overproduction of *Ec* NfuA in M9 minimal media and (B) isolation of *Ec* NfuA via IMAC (Ni-NTA).

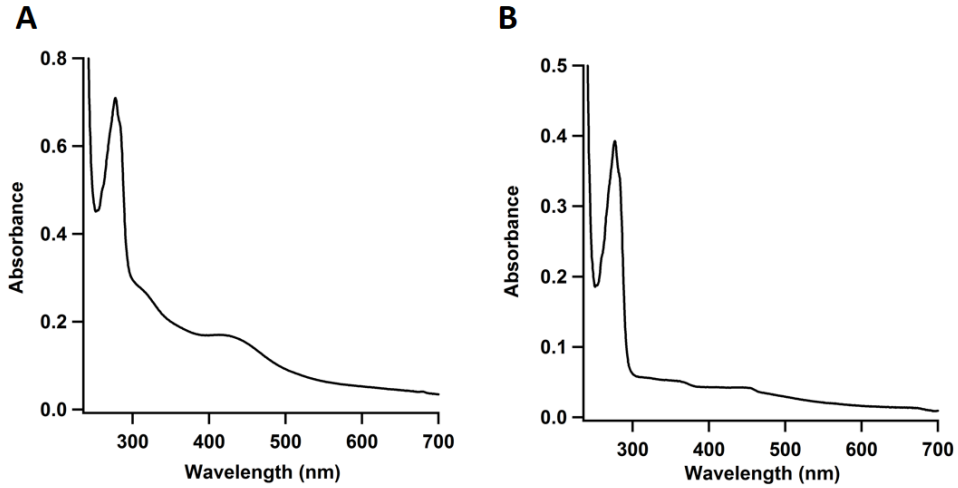

Figure **2-4**: UV-visible spectra of *Ec* NfuA (A) before analytical molecular-sieve chromatography (15 μM protein) and (B) after analytical molecular-sieve chromatography (8 μM protein).

Shown in **Figure 2-5, Panel D** is a reaction depicting LipA turnover using an 8–amino acid peptide substrate analog containing the octanoyllysyl residue [Glu-Ser-Val-(N^6-octanoyl)Lys-Ala-Ala-Ser-Asp] as it undergoes modification (16). The triangles show formation and decay of the monothiol-containing intermediate; the squares show formation of the lipoylated peptide product. As is typical, formation of the product leveled off around the concentration of the enzyme (50 μM). When NfuA (200 μM polypeptide; 100 μM [4Fe-4S] cluster) was injected into the reaction after a single turnover by LipA (150 min), rapid formation of additional lipoyl-containing product and monothiol-containing intermediate was observed. A similar result is shown in **Figure 2-5, Panel E**, wherein NfuA was added at the beginning of the reaction. In this instance, more than two additional turnovers (triangles) took place above that observed when NfuA was omitted (squares). Moreover, when the concentration of LipA in the reaction was lowered (7 μM) as the concentration of NfuA was raised (400 μM), the reaction became catalytic **(Figure 2-5, Panel F).**

The absence of an initial burst of 1 equivalent of product that is followed by a slow phase indicates that cluster transfer from NfuA to LipA is not rate-limiting during catalysis.

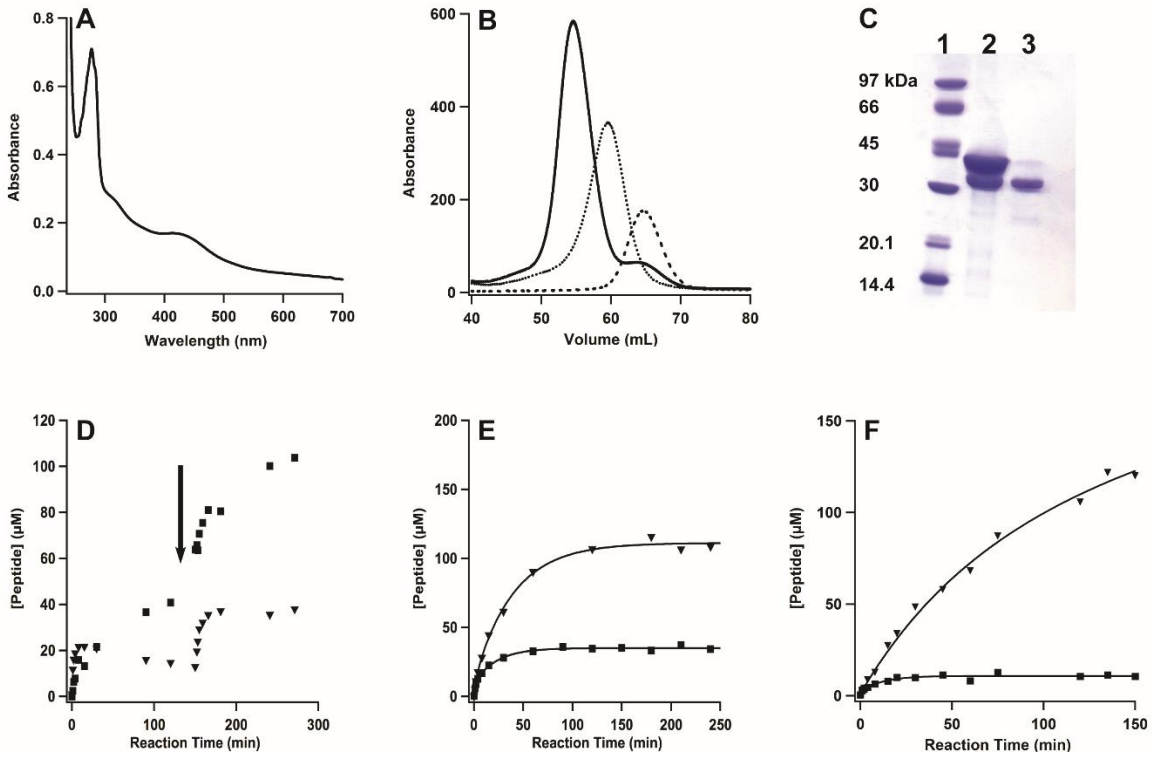

Figure 2-5: **(A)** UV-visible spectrum of 15 μM as-isolated *E. coli* NfuA**. (B)** Interaction between LipA and NfuA monitored by molecular sieve chromatography**.** Dashed line, 100 μM NfuA alone. NfuA elutes (64.6 mL) with an experimentally calculated molecular mass of 28.9 kDa (theoretical mass, 25.6 kDa). Dotted line, 100 μM LipA alone. LipA elutes (59.6 mL) with an experimentally calculated molecular mass of 44.1 kDa (theoretical mass, 38.2 kDa). Solid line, 100 μM LipA + 100 μM NfuA. A complex between LipA and NfuA elutes (54.6 mL) with an experimentally calculated molecular mass of 67.2 kDa (theoretical mass, 63.8 kDa). **(C)** SDS–PAGE gel of fraction represented by solid line in panel B (lane 2). NfuA standard (lane 3). Molecular mass markers (lane 1). (**D**) Addition of NfuA into a LipA reaction gives rise to additional turnovers. 6(*S*)-thio-octanoyllysyl intermediate (closed triangles). Lipoyllysyl product (closed squares). The reaction contained 50 μM LipA, 600 μM peptide substrate analog (Glu-Ser-Val-[N^6-octanoyl]Lys-Ala-Ala-Ser-Asp), 0.5 μM SAH nucleosidase, 2 mM dithionite and 1 mM SAM. Reactions were conducted at room temperature, and at the designated time indicated by the arrow, 200 μM NfuA was added to the reaction **(E)** Inclusion of NfuA (200 μM) in LipA reaction mixtures gives rise to multiple turnovers. Lipoyllysyl product in the absence of NfuA (closed squares). Lipoyllysyl product in the presence of NfuA (closed triangles). The reaction conditions were as described for panel **D**. **(F)** The LipA reaction under catalytic conditions. The reaction conditions were as described in panel A, except that the concentration of LipA was 10 μM (7 μM active) and the concentration of NfuA was 400 μM.

The model for LipA catalysis shown in **Figure 2-1** predicts that upon one full turnover, two sulfide ions from the auxiliary [4Fe-4S] cluster are incorporated into the lipoyl product, while the remaining two sulfide ions are released into solution along with four ferrous ions. To assess this stoichiometry more rigorously, we conducted reactions with NfuA that was overproduced in the absence of its Fe-S cluster and then reconstituted with iron and ^{34}S-labeled sulfide. Shown in **Figure 2-6, Panel A** is a reaction with 20 μM LipA containing Fe-S clusters composed of sulfide at natural abundance (~95% ^{32}S) and 100 μM NfuA containing Fe-S clusters composed of ^{34}S-labeled (~99%) sulfide. An initial burst of lipoyl product containing two ^{32}S sulfurs was observed (circles), which is consistent with previous results that indicate that the auxiliary cluster of LipA is used as the source of inserted sulfur atoms (16,17,38). Surprisingly, however, the amount of lipoyl product containing two ^{32}S atoms was more than 50% greater than that expected (33 μM versus 20 μM); this finding suggests that the enzyme can potentially direct all four sulfide ions from the cluster into the lipoyl product rather than release two of them into solution during each turnover. Lipoyl product containing two ^{34}S atoms was also observed (triangles), confirming that the [4Fe-4S] cluster on NfuA can be used to reconstitute the auxiliary cluster on LipA. Formation of the lipoyl product containing two ^{34}S atoms took place with a pronounced lag, as expected for a reaction in which the Fe-S cluster on LipA is consumed before NfuA transfers a labeled cluster to LipA. In this experiment, the amount of ^{34}S-labeled lipoyl product was limited by the concentration of holo NfuA in the reaction mixture. When the experiment was conducted with excess NfuA (400 μM NfuA and ~7 μM active LipA), production of ~1.5 equivalents of the ^{32}S-labeled lipoyl product was followed by production of multiple equivalents of the ^{34}4S-labeled lipoyl product **(Figure 2-6, Panel B).** We also observed the slow formation of a lipoyl group containing one ^{32}S atom and one ^{34}S atom **(Figure 2-6, Panel A),** which we believe derives from aberrantly released sulfide that is

subsequently used to reconstitute another auxiliary cluster during the reaction. Consistent with this explanation, when reactions were conducted in the presence of 0.8 mM sodium sulfide but in the absence of NfuA, additional product formation was observed; however, this additional formation of product was not as fast or as extensive as when NfuA was present **(Figure 2-6, Panel C).** Similarly, when IscS, cysteine, and dithiothreitol (DTT) were included in reaction mixtures, a slight increase in product was observed **(Figure 2-6, Panel D).**

To show that the effect of NfuA on the LipA reaction involves a direct transfer of the cluster from NfuA to LipA, rather than the release of iron and sulfide into solution followed by reconstitution of the auxiliary cluster, we conducted two additional experiments. In one experiment, the effect of NfuA (1 mM) on LipA (100 μM) catalysis was measured in the presence of 5 mM citrate, which can chelate released iron from NfuA and prevent it from being used in the reconstitution of LipA during turnover (42). The presence of citrate had no effect on NfuA's ability to enhance LipA turnover **(Figure 2-6, Panel E).** In a second experiment, the effect of NfuA (400 μM) on LipA (25 μM) catalysis was measured in the presence of 1 mM $Na_2{}^{34}S$. If the enhanced effect of NfuA were mediated through release of its iron and sulfide into solution, substantial incorporation of ^{34}S in the lipoyl product after the initial turnover would be expected (43). When the reaction was conducted in the presence of $Na_2{}^{34}S$, the formation of lipoyl product containing two ^{32}S atoms was similar to that when the reaction was conducted in the absence of $Na_2{}^{34}S$; a very small amount of lipoyl product containing one ^{34}S atom and one ^{32}S atom was observed, whereas virtually no product containing two ^{34}S atoms was observed **(Figure 2-6, Panel F).** These results indicate that release of iron and sulfide from NfuA into solution followed by its use in reconstituting the auxiliary cluster of LipA is unlikely.

The effect of NfuA on the growth and viability of *E. coli* was assessed in two previous studies (39,44). In one study, Δ*nfuA* strains grew as well as wild-type strains in enriched media, except under conditions of oxidative stress (paraquat administration) or iron starvation (2,2′-

dipyridyl administration) (39). In a second study, a Δ*nfuA* strain displayed a growth curve in Luria-Bertani (LB) medium that was similar to that of the wild-type control. However, Δ*nfuA* strains that also carried *isc* operon gene deletions displayed an impaired growth rate (40) Because *E. coli* can incorporate exogenous lipoic acid present in rich or LB media into LCPs via a pathway that is independent of LipA, we investigated whether an *E. coli* Δ*nfuA* strain could grow in M9 minimal medium lacking lipoic acid and using glucose as a carbon source. The Δ*nfuA* strain did not exhibit pronounced growth defects relative to the control; moreover, neither the addition of exogenous lipoic acid nor succinate plus acetate (which bypasses the requirement for lipoic acid) had a measurable effect on the overall growth rate **(Figure 2-7, Panel A).** By contrast, *E. coli lipA* mutants could not grow under these conditions. These results differ from the extreme phenotypes observed in humans or yeast for *NFU1* or *BOLA3* deletion strains (31,33,45).

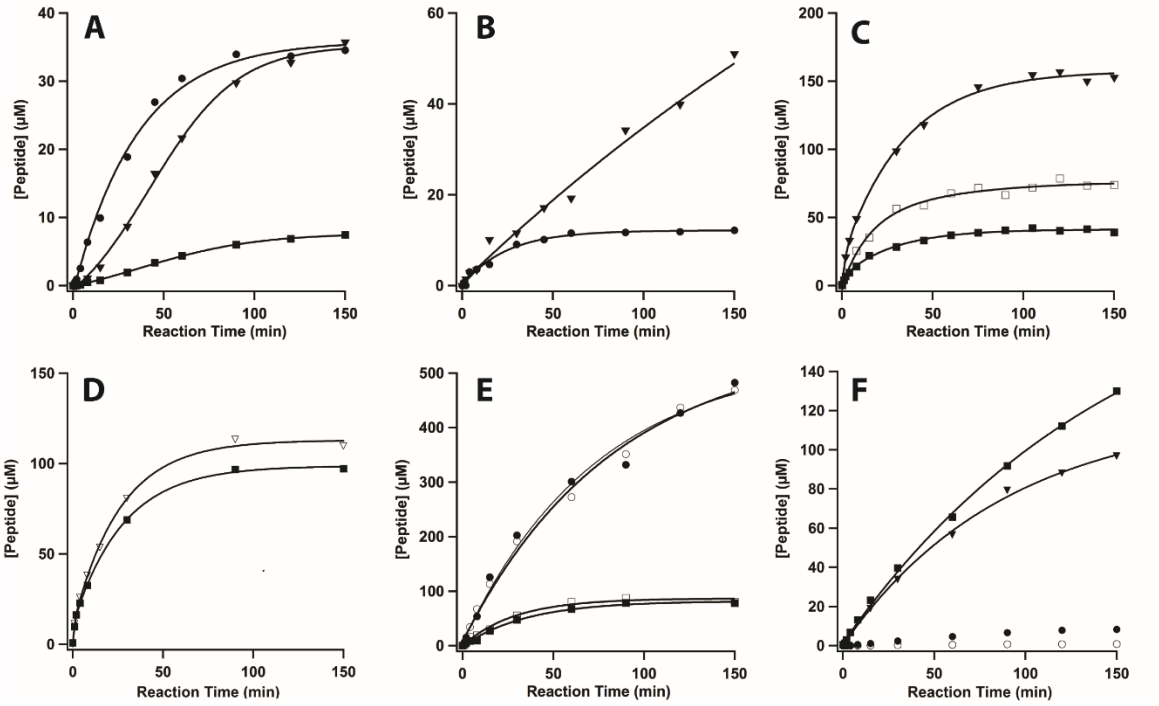

Figure **2-6**: **(A)** Formation of lipoyllysyl product in the presence of NfuA reconstituted with ^{34}S-labeled sulfide. (^{32}S,^{32}S)-containing lipoyllysyl product (closed circles); (^{34}S,^{34}S)-containing lipoyllysyl product (closed triangles); (^{32}S,^{34}S)-containing lipoyllysyl product (closed squares)**;** total lipoyllysyl product (open squares). The reaction contained 20 μM LipA, 100 μM ^{34}S-labeled NfuA, 600 μM peptide substrate analog, 0.5 μM SAH nucleosidase, 2 mM dithionite and 1 mM SAM. **(B)** Formation of lipoyllysyl product in the presence of NfuA reconstituted with ^{34}S-labeled sulfide and under catalytic conditions. The reaction conditions were as described above, except that the concentration of LipA was 10 μM and the concentration of ^{34}S-labeled NfuA was 400 μM. (^{32}S,^{32}S)-containing lipoyllysyl product (closed circles); (^{34}S,^{34}S)-containing lipoyllysyl product (closed triangles). **(C)** Effect of extraneous iron and sulfide on the activity of LipA. LipA reaction (50 μM) in the absence of NfuA or iron and sulfide (closed squares). LipA reaction in the presence of 0.8 mM $FeCl_3$ and 0.8 mM Na_2S (open squares). LipA reaction in the presence of 200 μM NfuA (closed triangles). Other reaction components were as described above in panel A. **(D)** Effect of IscS on the LipA reaction. LipA reaction in the presence of IscS (open triangles). LipA reaction in the absence of IscS (closed squares). Reactions were described as above (panel A), except they contained 100 μM LipA, 200 μM IscS, 5 mM cysteine, 5 mM DTT, and no NfuA. (**E**) Effect of citrate on NfuA's enhancement of LipA catalysis. Reactions included 100 μM LipA (open squares); 100 μM LipA + 5 mM citrate (closed squares); 100 μM LipA + 1 mM NfuA (open circles); 100 μM LipA + 1 mM NfuA + 5 mM citrate (closed circles). (**F**) Reaction of 25 μM LipA + 400 μM NfuA (closed squares); 25 μM LipA, and 400 μM NfuA in the presence of 1 mM $Na_2{}^{34}S$ (closed triangles) in which the lipoic acid product containing two ^{32}S atoms is monitored. Reaction of 25 μM LipA + 400 μM NfuA in the presence of 1 mM $Na_2{}^{34}S$ monitoring the ^{32}S/^{34}S mixed-labeled product (closed circles) and the ^{34}S/^{34}S-labeled product (open circles).

The observation that *E. coli* Δ*nfuA* strains do not exhibit severe growth defects in the absence of lipoic acid suggests that a second pathway exists for the regeneration of LipA's auxiliary cluster in *E. coli.* Given that an exacerbated effect was previously observed in an Δ*nfuA:*Δ*iscU* strain relative to strains harboring single deletions of the two genes, we assessed whether *E. coli* IscU could render LipA catalytic in the absence of NfuA (39). *E. coli* IscU was overproduced and isolated in its apo form, and its [4Fe-4S] cluster was then reconstituted using previously established methods (37). Indeed, when *E. coli* IscU containing a [4Fe-4S] cluster was included in excess of LipA, additional turnover was observed **(Figure 2-7, Panel B).** The cochaperones HscA and HscB, encoded within the *isc* gene operon, function in facilitating cluster transfer from *E. coli* IscU to its recipient proteins, including NfuA (39,46). However, no increase in rate or product formation was observed when HscA, HscB, $MgCl_2$, and adenosine triphosphate (ATP) were included in the reaction with holo IscU or holo NfuA; in fact, the inclusion of HscA and HscB was slightly inhibitory **(Figure 2-7, Panels C and D).**

We also carried out a similar scrambling study of the effect of IscU on LipA catalysis. When the reaction was conducted with unlabeled IscU and unlabeled LipA in the presence of 1 mM $Na_2{}^{34}S$, almost all of the resulting lipoyl product contained two ^{32}S atoms; very little contained the mixed $^{32}S/^{34}S$ or the $^{34}S/^{34}S$ product **(Figure 2-7, Panel E).** The effect of citrate on the enhancement of the LipA reaction by IscU could not be studied because IscU's cluster was unstable under those conditions **(Figure 2-8, Panel C).**

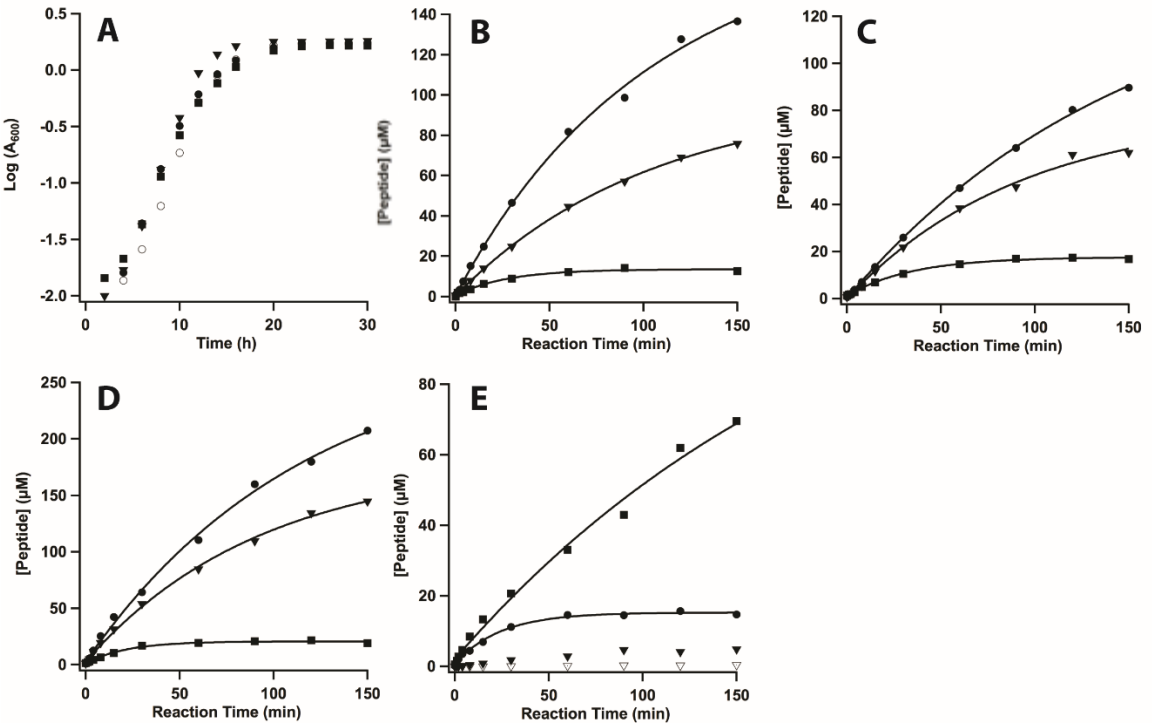

Figure **2-7**: **(A)** Effect of NfuA on growth of *E. coli* in M9 minimal medium using glucose as a carbon source. Wild-type *BW25113* (closed circles), *BW25113*:Δ*nfuA* (solid squares), *BW25113*:Δ*nfuA* + 25 μM lipoic acid (open circles), and *BW25113*:Δ*nfuA* + 5 mM succinate/5 mM acetate (black triangles). **(B)** Effect of IscU on LipA catalysis. LipA only (solid squares). LipA + IscU (solid triangles). LipA + NfuA (solid circles). **(C)** Effect of IscU, HscA, and HscB on LipA catalysis. LipA only (solid squares). LipA + IscU (solid circles). LipA + IscU + HscA and HscB (solid triangles). **(D)** Effect of NfuA, HscA, and HscB on LipA catalysis. LipA only (solid squares). LipA + NfuA (solid circles). LipA + NfuA + HscA and HscB (solid triangles). Reactions contained 20 μM LipA, 400 μM octanoyllysyl-containing peptide substrate, 2 mM SAM, 2 mM dithionite, 2 mM ATP, 100 mM $MgCl_2$, and 0.5 μM SAH nucleosidase. When appropriate, IscU, HscA, and HscB were each added to a final concentration of 200 μM. (**E**) Reaction of 25 μM LipA + 400 μM IscU (closed squares); 25 μM LipA, and 400 μM IscUin the presence of 1 mM $Na_2{}^{34}S$ (closedsquares) in which the lipoic acid product containing two ^{32}S atoms is monitored. Reaction of 25 μM LipA + 400 μM IscU in the presence of 1 mM $Na_2{}^{34}S$ monitoring the $^{32}S/^{34}S$ mixed-labeled product (closed triangles) and the $^{34}S/^{34}S$ doubled-labeled product (open triangles).

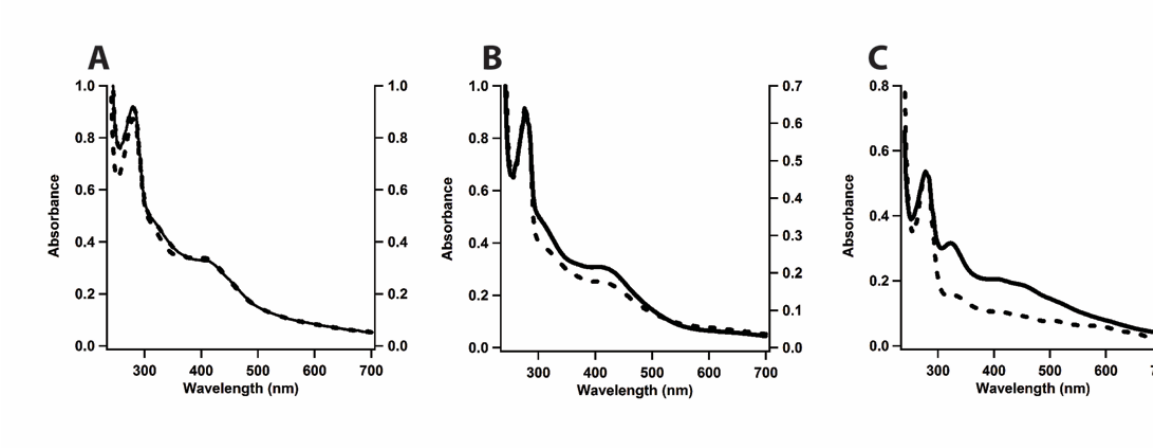

Figure **2-8**: UV-visible spectra of Citrate-treated E. coli LipA, NfuA, and IscU. (A) 30 µM LipA before incubation with excess citrate (solid line) and after (dashed line). (B) 30 µM NfuA before (solid line) and after citrate incubation (dashed line). (C) 30 µM IscU before (solid line) and after citrate incubation (dashed line).

Conclusions

The resistance to the idea that an Fe-S cluster can act as a sulfur source during the radical-mediated sulfhydrylation of unactivated carbon centers is largely due to the consequence of the enzyme inactivating itself after only one turnover. Our finding that *E. coli* NfuA or IscU can reinstall the Fe-S cluster in *E. coli* LipA after each turnover, in a process that is not rate-limiting, suggests that this concern is no longer warranted. Our studies also most likely explain why patients with defects in NFU1, the mammalian ortholog of NfuA, display phenotypes that are consistent with lipoic acid deficiency.

References

1. Reed, L. J., De, B. B., Gunsalus, I. C., and Hornberger, C. S., Jr. (1951) Crystalline alpha-lipoic acid; a catalytic agent associated with pyruvate dehydrogenase. *Science (New York, N.Y.)* **114**, 93-94
2. Reed, L. J., Gunsalus, I. C., Schnakenberg, G. H. F., Soper, Q. F., Boaz, H. E., Kern, S. F., and Parke, T. V. (1953) Isolation, Characterization and Structure of α-Lipoic Acid1. *Journal of the American Chemical Society* **75**, 1267-1270
3. Reed, L. J. (1974) Multienzyme complexes. *Accounts of Chemical Research* **7**, 40-46
4. Reed, L. J. (2001) A trail of research from lipoic acid to alpha-keto acid dehydrogenase complexes. *The Journal of biological chemistry* **276**, 38329-38336
5. E.S. Billgren, R. M. C., N.M. Nesbitt, S.J. Booker. (2010) *Lipoic acid biosynthesis and enzymology*, Elsevier
6. Perham, R. N. (2000) Swinging Arms and Swinging Domains in Multifunctional Enzymes: Catalytic Machines for Multistep Reactions. *Annual review of biochemistry* **69**, 961-1004
7. Landgraf, B. J., McCarthy, E. L., and Booker, S. J. (2016) Radical S-Adenosylmethionine Enzymes in Human Health and Disease. *Annual review of biochemistry* **85**, 485-514
8. Yi, X., and Maeda, N. (2005) Endogenous Production of Lipoic Acid Is Essential for Mouse Development. *Molecular and Cellular Biology* **25**, 8387-8392
9. Cronan, J. E. (2016) Assembly of Lipoic Acid on Its Cognate Enzymes: an Extraordinary and Essential Biosynthetic Pathway. *Microbiology and Molecular Biology Reviews* **80**, 429-450
10. Cronan, J. E., Zhao, X., and Jiang, Y. (2005) Function, Attachment and Synthesis of Lipoic Acid in Escherichia coli. in *Advances in microbial physiology* (Poole, R. K. ed.), Academic Press. pp 103-146
11. Miller, J. R., Busby, R. W., Jordan, S. W., Cheek, J., Henshaw, T. F., Ashley, G. W., Broderick, J. B., Cronan, J. E., Jr., and Marletta, M. A. (2000) Escherichia coli LipA is a lipoyl synthase: in vitro biosynthesis of lipoylated pyruvate dehydrogenase complex from octanoyl-acyl carrier protein. *Biochemistry* **39**, 15166-15178
12. Zhao, X., Miller, J. R., Jiang, Y., Marletta, M. A., and Cronan, J. E. (2003) Assembly of the covalent linkage between lipoic acid and its cognate enzymes. *Chem Biol* **10**, 1293-1302
13. Spalding, M. D., and Prigge, S. T. (2010) Lipoic acid metabolism in microbial pathogens. *Microbiology and molecular biology reviews : MMBR* **74**, 200-228
14. Schonauer, M. S., Kastaniotis, A. J., Kursu, V. A., Hiltunen, J. K., and Dieckmann, C. L. (2009) Lipoic acid synthesis and attachment in yeast mitochondria. *The Journal of biological chemistry* **284**, 23234-23242
15. Douglas, P., Kriek, M., Bryant, P., and Roach, P. L. (2006) Lipoyl synthase inserts sulfur atoms into an octanoyl substrate in a stepwise manner. *Angewandte Chemie (International ed. in English)* **45**, 5197-5199
16. Lanz, N. D., Pandelia, M. E., Kakar, E. S., Lee, K. H., Krebs, C., and Booker, S. J. (2014) Evidence for a catalytically and kinetically competent enzyme-substrate cross-linked intermediate in catalysis by lipoyl synthase. *Biochemistry* **53**, 4557-4572
17. McLaughlin, M. I., Lanz, N. D., Goldman, P. J., Lee, K. H., Booker, S. J., and Drennan, C. L. (2016) Crystallographic snapshots of sulfur insertion by lipoyl synthase.

Proceedings of the National Academy of Sciences of the United States of America **113**, 9446-9450
18. Cicchillo, R. M., Iwig, D. F., Jones, A. D., Nesbitt, N. M., Baleanu-Gogonea, C., Souder, M. G., Tu, L., and Booker, S. J. (2004) Lipoyl synthase requires two equivalents of S-adenosyl-L-methionine to synthesize one equivalent of lipoic acid. *Biochemistry* **43**, 6378-6386
19. Booker, S. J., and Grove, T. L. (2010) Mechanistic and functional versatility of radical SAM enzymes. *F1000 biology reports* **2**, 52
20. Frey, P. A., and Booker, S. J. (2001) Radical mechanisms of S-adenosylmethionine-dependent enzymes. in *Advances in Protein Chemistry*, Academic Press. pp 1-45
21. Cicchillo, R. M., Lee, K. H., Baleanu-Gogonea, C., Nesbitt, N. M., Krebs, C., and Booker, S. J. (2004) Escherichia coli lipoyl synthase binds two distinct [4Fe-4S] clusters per polypeptide. *Biochemistry* **43**, 11770-11781
22. Harmer, J. E., Hiscox, M. J., Dinis, P. C., Fox, S. J., Iliopoulos, A., Hussey, J. E., Sandy, J., Van Beek, F. T., Essex, J. W., and Roach, P. L. (2014) Structures of lipoyl synthase reveal a compact active site for controlling sequential sulfur insertion reactions. *The Biochemical journal* **464**, 123-133
23. Bryant, P., Kriek, M., Wood, R. J., and Roach, P. L. (2006) The activity of a thermostable lipoyl synthase from Sulfolobus solfataricus with a synthetic octanoyl substrate. *Anal Biochem* **351**, 44-49
24. Booker, S. J. (2009) Anaerobic functionalization of unactivated C-H bonds. *Current opinion in chemical biology* **13**, 58-73
25. Frazzon, J., Fick, J. R., and Dean, D. R. (2002) Biosynthesis of iron-sulphur clusters is a complex and highly conserved process. *Biochemical Society transactions* **30**, 680-685
26. Johnson, D. C., Dean, D. R., Smith, A. D., and Johnson, M. K. (2005) Structure, function, and formation of biological iron-sulfur clusters. *Annual review of biochemistry* **74**, 247-281
27. Maio, N., and Rouault, T. A. (2015) Iron-sulfur cluster biogenesis in mammalian cells: New insights into the molecular mechanisms of cluster delivery. *Biochimica et biophysica acta* **1853**, 1493-1512
28. Fontecave, M., and Ollagnier-de-Choudens, S. (2008) Iron-sulfur cluster biosynthesis in bacteria: Mechanisms of cluster assembly and transfer. *Archives of biochemistry and biophysics* **474**, 226-237
29. Ayala-Castro, C., Saini, A., and Outten, F. W. (2008) Fe-S cluster assembly pathways in bacteria. *Microbiology and molecular biology reviews : MMBR* **72**, 110-125, table of contents
30. Lill, R., and Muhlenhoff, U. (2006) Iron-sulfur protein biogenesis in eukaryotes: components and mechanisms. *Annual review of cell and developmental biology* **22**, 457-486
31. Cameron, Jessie M., Janer, A., Levandovskiy, V., MacKay, N., Rouault, Tracey A., Tong, W.-H., Ogilvie, I., Shoubridge, Eric A., and Robinson, Brian H. (2011) Mutations in Iron-Sulfur Cluster Scaffold Genes NFU1 and BOLA3 Cause a Fatal Deficiency of Multiple Respiratory Chain and 2-Oxoacid Dehydrogenase Enzymes. *American Journal of Human Genetics* **89**, 486-495
32. Navarro-Sastre, A., Tort, F., Stehling, O., Uzarska, M. A., Arranz, J. A., Del Toro, M., Labayru, M. T., Landa, J., Font, A., Garcia-Villoria, J., Merinero, B., Ugarte, M., Gutierrez-Solana, L. G., Campistol, J., Garcia-Cazorla, A., Vaquerizo, J., Riudor, E., Briones, P., Elpeleg, O., Ribes, A., and Lill, R. (2011) A fatal mitochondrial disease is

associated with defective NFU1 function in the maturation of a subset of mitochondrial Fe-S proteins. *Am J Hum Genet* **89**, 656-667

33. Melber, A., Na, U., Vashisht, A., Weiler, B. D., Lill, R., Wohlschlegel, J. A., and Winge, D. R. (2016) Role of Nfu1 and Bol3 in iron-sulfur cluster transfer to mitochondrial clients. *eLife* **5**, e15991
34. Bradford, M. M. (1976) A rapid and sensitive method for the quantitation of microgram quantities of protein utilizing the principle of protein-dye binding. *Analytical Biochemistry* **72**, 248-254
35. Beinert, H. (1978) Micro methods for the quantitative determination of iron and copper in biological material. *Methods in enzymology* **54**, 435-445
36. Beinert, H. (1983) Semi-micro methods for analysis of labile sulfide and of labile sulfide plus sulfane sulfur in unusually stable iron-sulfur proteins. *Analytical Biochemistry* **131**, 373-378
37. Agar, J. N., Krebs, C., Frazzon, J., Huynh, B. H., Dean, D. R., and Johnson, M. K. (2000) IscU as a scaffold for iron-sulfur cluster biosynthesis: sequential assembly of [2Fe-2S] and [4Fe-4S] clusters in IscU. *Biochemistry* **39**, 7856-7862
38. Cicchillo, R. M., and Booker, S. J. (2005) Mechanistic Investigations of Lipoic Acid Biosynthesis in Escherichia coli: Both Sulfur Atoms in Lipoic Acid are Contributed by the Same Lipoyl Synthase Polypeptide. *Journal of the American Chemical Society* **127**, 2860-2861
39. Angelini, S., Gerez, C., Ollagnier-de Choudens, S., Sanakis, Y., Fontecave, M., Barras, F., and Py, B. (2008) NfuA, a new factor required for maturing Fe/S proteins in Escherichia coli under oxidative stress and iron starvation conditions. *The Journal of biological chemistry* **283**, 14084-14091
40. Bandyopadhyay, S., Naik, S. G., O'Carroll, I. P., Huynh, B. H., Dean, D. R., Johnson, M. K., and Dos Santos, P. C. (2008) A proposed role for the Azotobacter vinelandii NfuA protein as an intermediate iron-sulfur cluster carrier. *The Journal of biological chemistry* **283**, 14092-14099
41. Jin, Z., Heinnickel, M., Krebs, C., Shen, G., Golbeck, J. H., and Bryant, D. A. (2008) Biogenesis of iron-sulfur clusters in photosystem I: holo-NfuA from the cyanobacterium Synechococcus sp. PCC 7002 rapidly and efficiently transfers [4Fe-4S] clusters to apo-PsaC in vitro. *The Journal of biological chemistry* **283**, 28426-28435
42. Ding, H., Clark, R. J., and Ding, B. (2004) IscA mediates iron delivery for assembly of iron-sulfur clusters in IscU under the limited accessible free iron conditions. *The Journal of biological chemistry* **279**, 37499-37504
43. Farrar, C. E., Siu, K. K., Howell, P. L., and Jarrett, J. T. (2010) Biotin synthase exhibits burst kinetics and multiple turnovers in the absence of inhibition by products and product-related biomolecules. *Biochemistry* **49**, 9985-9996
44. Boutigny, S., Saini, A., Baidoo, E. E., Yeung, N., Keasling, J. D., and Butland, G. (2013) Physical and functional interactions of a monothiol glutaredoxin and an iron sulfur cluster carrier protein with the sulfur-donating radical S-adenosyl-L-methionine enzyme MiaB. *The Journal of biological chemistry* **288**, 14200-14211
45. Navarro-Sastre, A., Tort, F., Stehling, O., Uzarska, Marta A., Arranz, José A., del Toro, M., Labayru, M T., Landa, J., Font, A., Garcia-Villoria, J., Merinero, B., Ugarte, M., Gutierrez-Solana, Luis G., Campistol, J., Garcia-Cazorla, A., Vaquerizo, J., Riudor, E., Briones, P., Elpeleg, O., Ribes, A., and Lill, R. (2011) A Fatal Mitochondrial Disease Is Associated with Defective NFU1 Function in the Maturation of a Subset of Mitochondrial Fe-S Proteins. *American Journal of Human Genetics* **89**, 656-667

46. Reyda, M. R., Fugate, C. J., and Jarrett, J. T. (2009) A complex between biotin synthase and the iron-sulfur cluster assembly chaperone HscA that enhances in vivo cluster assembly. *Biochemistry* **48**, 10782-10792

Chapter 3

The A-type domain in *Escherichia coli* NfuA is required for regenerating the auxiliary [4Fe–4S] cluster in *Escherichia coli* lipoyl synthase

This chapter was partially reproduced from "McCarthy, E.L., Rankin, A.N., Dill, Z.R., and Booker, S.J. The A-type domain in Escherichia coli NfuA is required for regenerating the auxiliary [4Fe–4S] cluster in Escherichia coli lipoyl synthase. The Journal of Biological Chemistry. 2019; 294(5): 1609-1617."

Abstract

The lipoyl cofactor plays an integral role in several essential biological processes. The last step in its *de novo* biosynthetic pathway, the attachment of two sulfur atoms at C6 and C8 of an *n*-octanoyl-lysyl chain, is catalyzed by lipoyl synthase (LipA), a member of the radical SAM superfamily. In addition to the [4Fe–4S] cluster common to all radical SAM enzymes, LipA contains a second [4Fe–4S] auxiliary cluster, which is sacrificed during catalysis to supply the requisite sulfur atoms, rendering the protein inactive for further turnovers. Recently, it was shown that the Fe–S cluster carrier protein NfuA from *Escherichia coli* can regenerate the auxiliary cluster of *E. coli* LipA after each turnover, but the molecular mechanism is incompletely understood. Herein, using protein–protein interaction and kinetic assays as well as site-directed mutagenesis, we provide further insight into the mechanism of NfuA-mediated cluster regeneration. In particular,

we show that the N-terminal A-type domain of *E. coli* NfuA is essential for its tight interaction with LipA. Further, we demonstrate that NfuA from *Mycobacterium tuberculosis* can also regenerate the auxiliary cluster of *E. coli* LipA. However, an Nfu protein from *Staphylococcus aureus*, which lacks the A-type domain, was severely diminished in facilitating cluster regeneration. Of note, addition of the N-terminal domain of *E. coli* NfuA to *S. aureus* Nfu, fully restored cluster-regenerating activity. These results expand our understanding of the newly discovered mechanism by which the auxiliary cluster of LipA is restored after each turnover.

Introduction

Since its initial identification by Sofia, *et al.* in 2001, the radical *S*-adenosylmethionine (RS) superfamily has expanded to include almost 114,000 individual sequences representing more than 85 distinct reactions (1,2). Members of the RS superfamily coordinate a [4Fe–4S] which, in its reduced state, is used to fragment *S*-adenosylmethionine (SAM) to methionine and a 5′-deoxyadenosin 5′-radical (5′-dA•) (3). Lipoyl synthase (LipA) uses the 5′-dA• intermediate to catalyze the last step of the *de novo* pathway for the biosynthesis of the lipoyl cofactor, which is the attachment of sulfur atoms at C6 and C8 of an *n*-octanoyllysyl chain on a lipoyl carrier protein. LipA belongs to a subclass of RS enzymes that contain additional auxiliary iron-sulfur (Fe-S) clusters, which further diversifies the chemical repertoire of the superfamily (4). The [4Fe–4S] auxiliary cluster of LipA has been shown to be cannibalized by the protein during catalysis to provide the sulfur atoms in the lipoyl product. Although this sacrificial role for an Fe-S cluster has been controversial, given that its destruction inactivates the protein, an abundance of biochemical, spectroscopic, and crystallographic evidence support it (5-10).

All organisms have established and highly regulated pathways for Fe-S cluster assembly, which share some basic components (11-13), and it seemed likely that these pathways might be involved in regenerating LipA's auxiliary cluster after each turnover. Briefly, a cysteine desulfurase provides sulfur from cysteine, while a still-debated source supplies iron to a general scaffold protein upon which an Fe-S cluster is assembled. In a poorly understood process, the scaffold protein transfers a cluster to targeting proteins, which recognize their targets and transfer newly assembled clusters to them. Defects in Fe-S cluster assembly in humans result in a number of prevalent disorders, such as Friedrich's Ataxia and Multiple Mitochondrial Dysfunctions Disorder (14).

Recently, *E. coli* NfuA, a previously characterized intermediate Fe-S cluster carrier protein, was shown to restore the auxiliary cluster in LipA after each turnover in a process that does not limit the overall rate of catalysis (15-17). *E. coli* NfuA is composed of two distinct domains: a 'degenerate' A-type N-terminal domain and an Nfu-like C-terminal domain, and previous studies have provided evidence for a role for both of these two domains in NfuA's function (18). Because LipA has now been established as a target for NfuA, we can exploit this system to better understand the roles of these two domains in Fe-S protein targeting and Fe-S cluster regeneration.

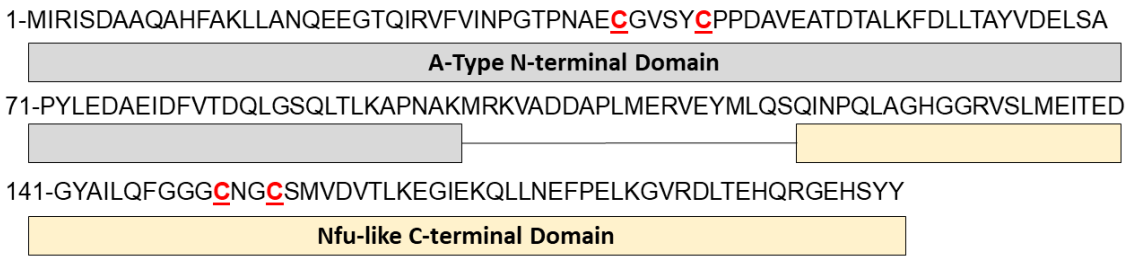

Figure 3-1: Amino acid sequence and domain architecture of *E. coli* NfuA. NfuA is composed of two distinct domains: an N-terminal A-type domain (grey) and a C-terminal Nfu-like domain (pale yellow). The sequence contains four cysteinyl residues (red): two in the N-terminal domain and two in the C-terminal domain.

Materials and Methods

General methods and procedures—The polymerase chain reaction was conducted using a BioRad S1000 thermocycler. DNA sequencing was performed at the Penn State Genomics Core Facility. Amino acid analysis was performed at the UC Davis Proteomics Core Facility. UV-visible spectra were recorded on a Cary 50 spectrometer from Varian (Walnut Creek, CA) with the associated WinUV software package. All anaerobic experiments were conducted in a Coy anaerobic chamber (Grass Lakes, MI). High-performance Liquid Chromatography (HPLC) with detection by mass spectrometry (LC-MS) was conducted using an Agilent Technologies (Santa Clara, CA) 1200 system coupled to an Agilent Technologies 6410 QQQ mass spectrometer. Data collection and analysis were performed using the associated MassHunter software. Analytical molecular sieve chromatography was performed on an *Ä*KTA system (GE Healthcare) housed in a Coy anaerobic chamber equipped with a HiPrep 16/60 Sephacryl HR S-200 column (GE Healthcare). Sodium dodecyl sulfate-polyacrylamide gel electrophoresis (SDS-PAGE) was performed using a mini vertical electrophoresis unit from Hoefer (Holliston, MA).

Cloning of genes encoding E. coli LipA, E. coli NfuA, and E. coli NfuA C39A, C44A, C149A, C152A and C39A,C44A variants into pET28a— The construction of the *E. coli lipA*-pET28a and *E. coli nfuA*-pET28a expression vectors has been described previously (5,17). *E. coli nfuA*-pET28a C39A, C44A, C149A, and C152A variants were constructed by site-directed mutagenesis using the Stratagene QuikChange II kit (Agilent Technologies) along with primers listed in **Table 3-1**. However, *Pfu* polymerase was substituted with Vent polymerase in the polymerase chain reaction (PCR). *E. coli nfuA*-pET28a plasmid DNA was used as the DNA template, and DNA sequencing was used to confirm the desired substitutions. For the *E. coli* NfuA C39A, C44A double variant construct, the double-stranded DNA was purchased as a gBlock from IDT with flanking NdeI and

XhoI cut sites. The gene fragments were digested and ligated into a pET28a vector digested with the same enzymes.

Cloning of genes corresponding to E. coli NfuA N-terminal and C-terminal domains and truncated NfuA aa 51-191 into pET28a— The gene fragments corresponding to *E. coli* NfuA N-terminal domain (amino acid residues 1-97) and C-terminal domain (amino acid residues 98-191) were PCR-amplified using the *E. coli nfuA*-pET28a plasmid as a DNA template. The primers used for amplification of the N terminal domain and C terminal domain introduced an NdeI restriction site at the 5′ end of the gene and a XhoI restriction site at the 3′ end. For the *E. coli* NfuA aa 51-191 construct, the double-stranded DNA was purchased as a gBlock from IDT with flanking NdeI and XhoI cut sites. The gene fragments were digested and ligated into a pET28a vector digested with the same enzymes. Primers used for the constructs can be found in **Table 3-1.**

Table 3-1: Oligonucleotides used for plasmid construction.

Gene	**Vector**		**Oligonucleotide**
nfuA	pET28a	for	5' CGC GGC GTC AAG CTT ATG ATC CGT ATT TCC GAT GCT GC 3'
		rev	5' CGC GGC GTC CTC GAG TTA GTA GTA GGA GTG TTC GCC GC 3'
lipA	pET28a	for	5' GCG GCG TCC ATA TGA GTA AAC CCA TTG TGA TGG AAC GC 3'
		rev	5′ GCC GGA ATT CTT ACT TAA CTT CCA TCC CTT TCG 3′
nfuA N terminal domain	pET28a	for	5′ CGC GGC GTC CAT ATG ATC CGT ATT TCC GAT GCT GCA CAA GC 3′
		rev	5′ CGC GGC GTC CTC GAG TTA TTT GGC GTT CGG GGC TTT CAG CG 3′
nfuA C terminal domain	pET28a	for	5′ CGC GGC GTC CAT ATG ATG CGT AAA GTG GCA GAC GAT GC 3′
		rev	5′ CGC GC GTC CTC GAG TTA GTA GTA GGA GTG TTC GCC GC 3′
Cys39Ala	pET28a	for	5' ACG CCT AAC GCT GAA GCT GGC GTT TCT TAT TGT 3'
		rev	5' ACA ATA AGA AAC GCC AGC TTC AGC GTT AGG CGT 3'
Cys44Ala	pET28a	for	5' TGT GGC GTT TCT TAT GCT CCG CCG GAC GCT GTG 3'
		rev	5' CAC AGC GTC CGG CGG AGC ATA AGA AAC GCC ACA 3'
Cys149Ala	pET28a	for	5' CAA TTT GGC GGC GGC GCT AAC GGT TGT TCC ATG 3'
		rev	5' CAT GGA ACA ACC GTT AGC GCC GCC GCC AAA TTG 3'
Cys152Ala	pET28a	for	5' GGC GGC TGT AAC GGT GCT TCC ATG GTC GAT GTG 3'

		rev	5' CAC ATC GAC CAT GGA AGC ACC GTT ACA GCC GCC 3'	

Cloning of the Mycobacterium tuberculosis nfuA gene— The gene encoding NfuA from *Mycobacterium tuberculosis* (*Mt*) was codon-optimized for expression in *E. coli* by GeneArt Gene Synthesis (Thermo Fisher Scientific) and was received as a construct in plasmid pMA-T. The gene contained an *Nde*I restriction site at the 5′ end and an *Xho*I restriction site at the 3′ end. The gene was digested with these two enzymes and then ligated into a pET28a vector that was similarly digested. The desired construct was confirmed by DNA sequencing.

Cloning of S. aureus Nfu, S. aureus Nfu—E. coli NfuA N-terminal domain fusion protein, and Human NFU—E. coli NfuA N-terminal domain fusion protein into pET28a—. Genes encoding Nfu (SAUSA300_0839) from *Staphylococcus aureus (S. aureus)* and a genetic fusion consisting of the N-terminal domain of *E. coli* NfuA (aa 1-117) attached to *S. aureus* Nfu or Human NFU1 were codon-optimized for expression in *E. coli* and received as constructs in plasmid pMA-T from GeneArt Gene Synthesis (Thermo Fisher Scientific). All received genes contained an *Nde*I restriction site at the 5′ end and an *Xho*I restriction site at the 3′ end. They were each digested with *Nde*I and *Xho*I and then ligated into pET28a that was similarly digested. The desired constructs were confirmed by DNA sequencing.

Overproduction of wt E. coli NfuA, NfuA truncations, and NfuA variants, as well as Mt NfuA, S. aureus Nfu, the E. coli NfuA N-terminal domain—Human NFU1 fusion protein, and the E. coli NfuA N-terminal domain—S. aureus Nfu fusion protein— The overproduction of full-length *E. coli* NfuA has been previously described (17). *E. coli* NfuA C39A, C44A, C149A, C152A, NfuA C39A, C44A double variant, NfuA N-terminal domain, NfuA C-terminal domain, NfuA aa 51-191, *Mt*

NfuA, *S. aureus* Nfu, the *E. coli* NfuA N-terminal domain—Human NFU1 fusion protein, and the *E. coli* NfuA N-terminal domain—*S. aureus* Nfu fusion were overproduced exactly as described for the full-length *E. coli* NfuA. Briefly, BL21(DE3) cells were co-transformed with the construct encoding the desired gene and plasmid pDB1282, which encodes the genes in the *isc* operon from *Azotobacter vinelandii* (19,20)**.** A single colony was used to inoculate 200 mL lysogeny broth (LB) supplemented with 50 µg/mL kanamycin and 100 µg/mL ampicillin, and the starter culture was incubated overnight at 37 °C with shaking at 250 rpm. The following day, 20 mL of the starter culture was used to inoculate four 6 L flasks containing 4 L M9 minimal media supplemented with 50 µg/mL kanamycin and 100 µg/mL ampicillin. The *E. coli* strains were cultured at 37 °C with shaking at 180 rpm. At an OD_{600}=0.3, 0.2% arabinose was added to induce expression of the genes encoded in the pDB1282 plasmid. At an OD_{600}=0.6, 50 µM $FeCl_3$ was added to the cultures, and the flasks were placed in an ice-water bath for ~30 min. Once chilled, expression of the desired gene was induced by the addition of 200 µM IPTG (final concentration) and allow to proceed for ~18 h at 18 °C with shaking at 180 rpm. Bacterial cells were harvested by centrifugation at 7,500 × g for 12 min. The resulting cellular pellet was flash-frozen in liquid N_2 and stored in liquid N_2 until further use.

Isolation of wt E. coli NfuA,, NfuA truncations, and NfuA variants, as well as Mt NfuA, S. aureus Nfu, the E. coli NfuA N-terminal domain—Human NFU1 fusion protein, and the E. coli NfuA N-terminal domain—S. aureus Nfu fusion protein— The purification of *E. coli* wt NfuA has been previously described (17). NfuA C39A, C44A, C139A, C152A, NfuA C39A, C44A double variant, NfuA N-terminal domain, NfuA C-terminal domain, *Mt* NfuA, *S. aureus* Nfu, the *E. coli* NfuA N-terminal domain—Human NFU1 fusion protein, and the *E. coli* NfuA N-terminal domain—*S. aureus* Nfu fusion protein were purified exactly as described for wt *E. coli* NfuA. All purification steps were carried out in an anaerobic chamber containing <1 ppm O_2 (Coy Laboratory Products,

Grass Lake, Michigan), with the exception of the centrifugation steps. In these instances, solutions were loaded into bottles that were then tightly sealed before being removed from the chamber for centrifugation. The cell pellet was re-suspended in Lysis Buffer (50 mM HEPES, pH 7.5, 300 mM KCl, 20 mM imidazole, and 10 mM β-mercaptoethanol). Lysozyme (1 mg/mL) and DNAse I (0.1 mg/mL) were added, and the solution was stirred at room temperature for 30 min. The cells were lysed by sonic disruption, and the lysate was centrifuged at 45,000 × g for 1 h. The supernatant was applied to a nickel-nitrilotriacetic acid (Ni-NTA) resin (Qiagen) column pre-equilibrated in Buffer A. The column was washed with Buffer B (50 mM HEPES, pH 7.5, 300 mM KCl, 45 mM imidazole, 10 mM β-mercaptoethanol, and 10% glycerol), and the protein was eluted using Buffer C (50 mM HEPES, pH 7.5, 300 mM KCl, 500 mM imidazole, 10 mM β-mercaptoethanol, and 10% glycerol). The protein was concentrated to 2.5 mL and then exchanged into Storage Buffer (50 mM HEPES, pH 7.5, 300 mM KCl, 1 mM DTT, 15% glycerol) using a PD-10 column (GE Healthcare). The protein was aliquoted, flash-frozen in liquid N_2, and stored in liquid N_2 until further use. The *E. coli* NfuA N-terminal domain was further purified by size-exclusion chromatography using a HiPrep 16/60 Sephacryl HR S-200 column (GE Healthcare) connected to an *Ä*KTA FPLC system housed within an anaerobic chamber. The column was equilibrated in Storage Buffer (50 mM HEPES, pH 7.5, 300 mM KCl, 1 mM DTT, 15% glycerol) at a constant flow-rate of 0.5 mL/min before application and subsequent elution of the protein at the same flow-rate. The purity of the isolated proteins was analyzed by SDS-PAGE (12.5% gel) and determined to be >95%. The protein concentration was determined via the Bradford method (21). Amino acid analysis revealed that the Bradford method overestimates the protein concentration of *E. coli* NfuA by a factor of 1.18, *Mt* NfuA by a factor of 1.03, *S. aureus* Nfu by a factor of 1.26, and the *E. coli* C-terminal domain by a factor of 1.24 (UC Davis Proteomics Core). Colorimetric iron and sulfide analyses were used to estimate the iron and sulfide content per polypeptide (22,23).

Overproduction and isolation of E. coli LipA — The overproduction and isolation of *E. coli* LipA has been previously described (5). This method was performed exactly as described with the following amendment. In the overproduction of *E. coli* LipA, the M9 minimal media was inoculated with 0.2 mL of starter culture, which was allowed to grow overnight at 37 °C with shaking at 180 rpm. The following day, expression of genes on pDB1282 was induced by addition of arabinose (0.2% final concentration) at OD_{600}=0.3. At an OD_{600}=0.6, 50 μM $FeCl_3$ was added to the cultures, and the flasks were placed in an ice-water bath for ~30 min. Once chilled, expression of the *lipA* gene was induced by the addition of IPTG (200 μM final concentration) and allowed to proceed for ~18 h at 18 °C with shaking at 180 rpm. Bacterial cells were harvested by centrifugation at 7,500 × g for 12 min. The resulting cell pellet was flash-frozen in liquid N_2 and stored in liquid N_2 until further use. *E. coli* LipA was isolated using methods previously described with no modifications (5).

Analytical molecular sieve chromatography— Physical interactions between *E. coli* LipA and truncated versions of *E. coli* NfuA , as well as *E. coli* NfuA variants, and *E. coli* LipA, were probed by analytical molecular sieve chromatography. A 500 μL mixture of standards composed of cytochrome c, carbonic anhydrase, bovine serum album, alcohol dehydrogenase, β-amylase, and blue dextran was applied to a HiPrep 16/60 Sephacryl HR S-200 column (GE Healthcare) connected to an *Ä*KTA FPLC system housed within an anaerobic chamber (<1 ppm O_2). The column was equilibrated in 50 mM HEPES, pH 7.5, 300 mM KCl, 15% glycerol, and 5 mM DTT (freshly prepared immediately before use) at a constant flow-rate of 0.5 mL/min before applying and eluting protein samples. The log molecular weight (MW) of each standard was plotted against its elution volume after correcting for the void volume of the column. The linear equation was then used to estimate the MW of each sample. The chromatogram of the standards as well as the standard curve used for experimental calculations are shown in **Figure 3-2.** The samples included the

following in a total 500 µL volume: 100 µM LipA only, 100 µM full-length NfuA only, 100 µM NfuA N-terminal domain only, 100 µM NfuA C-terminal domain only, a mixture of 100 µM LipA + 100 µM NfuA N-terminal domain, a mixture of 100 µM LipA + 100 µM NfuA C-terminal domain, 100 µM NfuA aa 51-191 only, a mixture of 100 µM LipA + 100 µM NfuA aa 51-191, 100 µM NfuA C39A only, 100 µM NfuA C44A only, 100 µM NfuA C39A, C44A, 100 µM LipA + 100 µM NfuA C39A, 100 µM LipA + 100 µM NfuA C44A, and 100 µM LipA + 100 µM NfuA C39A, C44A. The interaction was determined by the presence of a shift in the elution volume of samples as well as by the calculated experimental weights for each of the peaks. Fractions corresponding to each peak were subjected to SDS-PAGE to determine the presence of each protein.

LC-MS activity determinations— The experimental setup and assay conditions were described in detail in previous publications with a few notable amendments (8,20). The reactions were conducted under strictly anaerobic conditions in a Coy anaerobic glovebox. Reactions of NfuA variants C39A, C44A, C149A, and C152A **(Figure 3-4)** contained 25 µM LipA, 400 µM NfuA variant or wild-type protein, 600 µM peptide substrate (Glu-Ser-Val-[N^6-octanoyl]Lys-Ala-Ala-Ser-Asp), 0.5 µM S-adenosylhomocysteine (SAH) nucleosidase, and 1 mM SAM. Reactions testing LipA activity in the presence of NfuA C39A, C44A contained 25 µM Ec LipA, 600 µM Ec NfuA or Ec NfuA C39A C44A, 400 µM octanoyl pep, 0.5 µM SAH nucleosidase, and 1 mM SAM **(Figure 3-5).** Reactions testing LipA activity in the presence of NfuA truncations **(Figure 3-7 and Figure 3-17)** included 25 µM LipA, 400 µM wild-type NfuA or NfuA domain, 400 µM peptide substrate, 1 mM SAM, and 0.5 µM SAH nucleosidase. Reactions comparing the effects of *E. coli* NfuA and *Mt* NfuA **(Figure 3-13)** contained 20 µM LipA, 400 µM *E. coli* NfuA or *Mt* NfuA, 400 µM peptide substrate, 700 µM SAM, and 0.5 µM SAH nucleosidase. The reaction using the 8-thio-octanoyl peptide substrate analog **(Figure 3-14)** included 75 µM LipA, 400 µM NfuA, 400 µM

peptide substrate (control) or 8-thio-octanoyl-containing peptide substrate, 0.5 μM SAH nucleosidase, and 1 mM SAM. Reactions testing the effect of *S. aureus* Nfu or the *E. coli* NfuA N-terminal Domain—*S. aureus* Nfu fusion protein **(Figure 3-16)** contained 25 μM LipA, 400 μM *S. aureus* Nfu or fusion protein, 400 μM peptide substrate, 0.5 μM SAH nucleosidase, and 1 mM SAM. Reactions testing the effect of Human LIAS or *E. coli* LipA in the presence of the *E. coli* NfuA N-terminal Domain—*Human NFU1* fusion protein **(Figure 3-19)** included 20 μM LipA/LIAS protein, 300 μM *E. coli* NfuA or fusion, 500 μM peptide substrate, 0.5 μM SAH nucleosidase, and 1 mM SAM. Reactions were conducted at room temperature and were initiated by addition of sodium dithionite to a final concentration of 2 mM. The reactions were quenched at appropriate times with H_2SO_4 at a final concentration of 100 mM. Reactions were performed in triplicate when indicated. Detection of substrates and products was performed using electrospray ionization mass spectrometry in positive mode (ESI^+-MS) with the following parameters: a nitrogen gas temperature of 340 °C and flow rate of 9.0 L/min, a nebulizer pressure of 40 PSI and a capillary voltage of 4000 V. Substrates and products were detected using multiple reaction monitoring **(Table 3-2).** The reaction mixture was separated on an Agilent Technologies Zorbax Extend-C18 Rapid Resolution HT column (4.6 mm × 50 mm, 1.8 μm particle size) equilibrated in 98% Solvent A (0.1% formic acid, pH 2.6) and 2% Solvent B (100% acetonitrile). A gradient of 2-23% solvent B was applied from 0.8 min to 3.5 min and maintained at 23% solvent B until 8 min, before returning to solvent B to 2% from 8 min to 10 min. A flow-rate of 0.4 mL/min was maintained throughout the method. The column was allowed to re-equilibrate for 2 min under the initial conditions between sample injections.

Table 3-2: Parameters for LC-MS/MS analysis of unlabeled reaction intermediate and product.

Compound	Parent Ion	Fragmentator Voltage	Product Ion 1	P
Octanoyl Peptide	932.5	240	552.3 (37)	
6-Thio-octanoyl Peptide	964.5	240	584.3 (37)	
Lipoyl Peptide	996.5	240	616.4 (37)	
AtsA Peptide (IS)	474.4	135	229.1 (12)	
Tryptophan (IS)	188.0	130	146.1 (10)	

*Respective collision energies are in parentheses

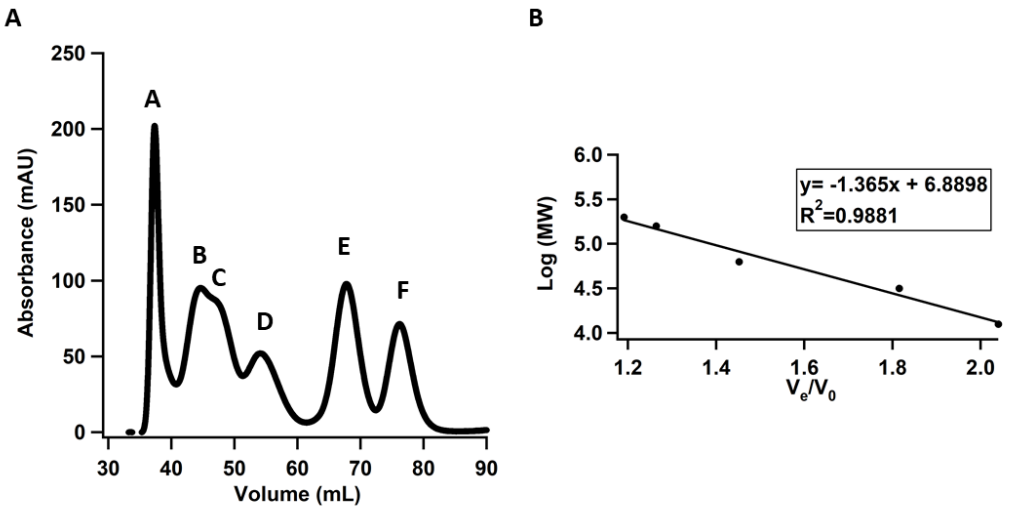

Figure 3-2: Suite of Standards Used in Analytical Molecular Sieve Chromatography. (A) Chromatogram of the standards used for standard curve generation, monitoring their absorbance at 280 nm: (A) Blue Dextran 2000 kDa, (B) β-Amylase 200 kDa, (C) Alcohol Dehydrogenase 150 kDa, (D) Bovine Serum Albumin 66 kDa, (E) Carbonic Anhydrase 29 kDa, and (F) Cytochrome C, 12.4 kDa. (B) The elution volume of each standard corrected for the void volume of the column was plotted versus the log molecular weight of each of the standards. The linear equation was used to estimate the respective size of each unknown protein based on its elution volume.

Results

Role of NfuA cysteine residues in cluster coordination and transfer. NfuA contains four cysteine residues, two of which are in its N-terminal A-type domain (Cys39 and Cys44), and two of which are in its C-terminal Nfu-like domain (Cys149 and Cys152) (**Figure 3-1**). To assess the importance of each of the cysteine residues on NfuA's ability to enhance LipA catalysis, each was individually changed to an alanine residue, yielding four variant proteins. When Cys39 or Cys44

is changed to alanine, the resulting variant protein is as capable as wild-type NfuA of ligating a [4Fe–4S] cluster (**Figure 3-3, Panel A**) and can enhance LipA turnover, though to a lesser extent (**Figure 3-4**). In the absence of NfuA, 25 μM LipA catalyzes formation of ~20 μM lipoyl product in 2.5 h (**Figure 3-4**, closed circles). In the presence of 400 μM (200 μM active dimer) NfuA variant, 25 μM LipA catalyzes formation of 140 μM (C44A) or 120 μM (C39A) lipoyl product in 2.5 h, while 170 μM product is formed in the presence of wild-type (wt) NfuA (**Figure 3-4**, closed triangles, C39A variant; closed squares, C44A variant; open squares, wild-type NfuA), indicating that the variant proteins can restore LipA's auxiliary cluster. An NfuA double variant in which both N-terminal cysteinyl residues are exchanged with alanine C39A, C44A also has an unaltered ability to activate LipA **(Figure 3-5).** By contrast, when Cys149 or Cys152 is changed to alanine, the ability of the variant protein to ligate a [4Fe–4S] cluster (**Figure 3-3, Panel B**) and to enhance LipA turnover (**Figure 3-4,** blue open circles and red open triangles) is abrogated. In these instances, LipA catalyzes significantly less than one turnover, suggesting that these NfuA variants inhibit LipA turnover. These results confirm the role of the two C-terminal cysteines in [4Fe–4S] cluster coordination and show that that the two N-terminal cysteines do not function in cluster transfer to LipA under the given reaction conditions. An earlier study in which the two N-terminal cysteine residues were substituted with serine residues reported that these variants could still coordinate a cluster (15). However, this observed difference may be due to the fact that serine residues can participate in cluster coordination, as is the case for the auxiliary cluster of LipA as well as other variants of Fe-S proteins (24,25).

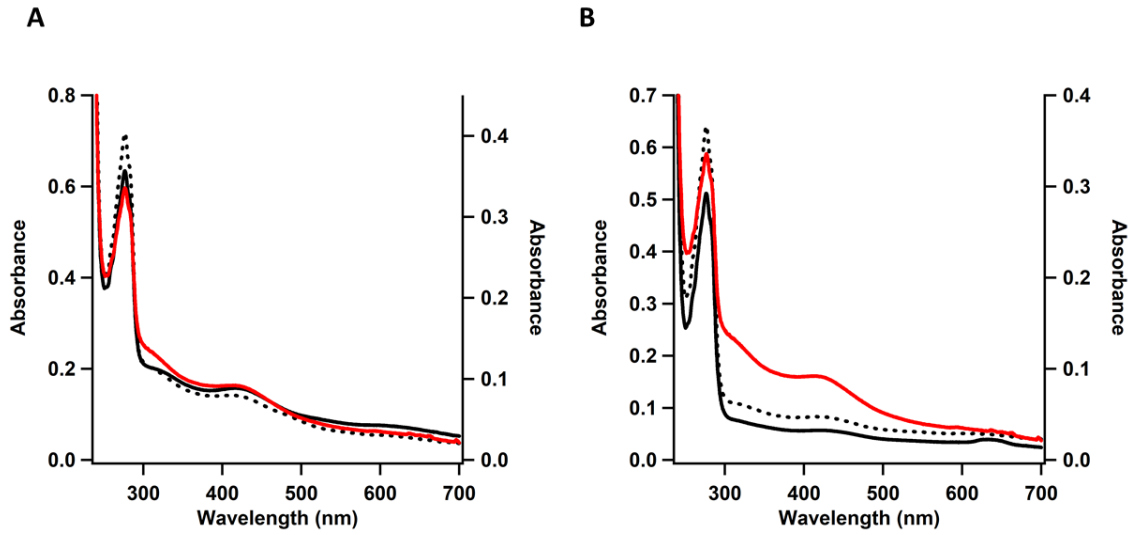

Figure 3-3: UV-visible Spectra of *E. coli* NfuA C39A, C44A, C149A, and C152A Variants. UV-visible spectrum of (A) 15 µM as-isolated *E. coli* NfuA C39A (black solid trace), C44A (black dotted trace) compared to wild-type NfuA (red solid trace). (B) 15 µM as-isolated *E. coli* NfuA C149A (black solid trace), C152A (black dotted trace), compared to wild-type NfuA (red solid trace).

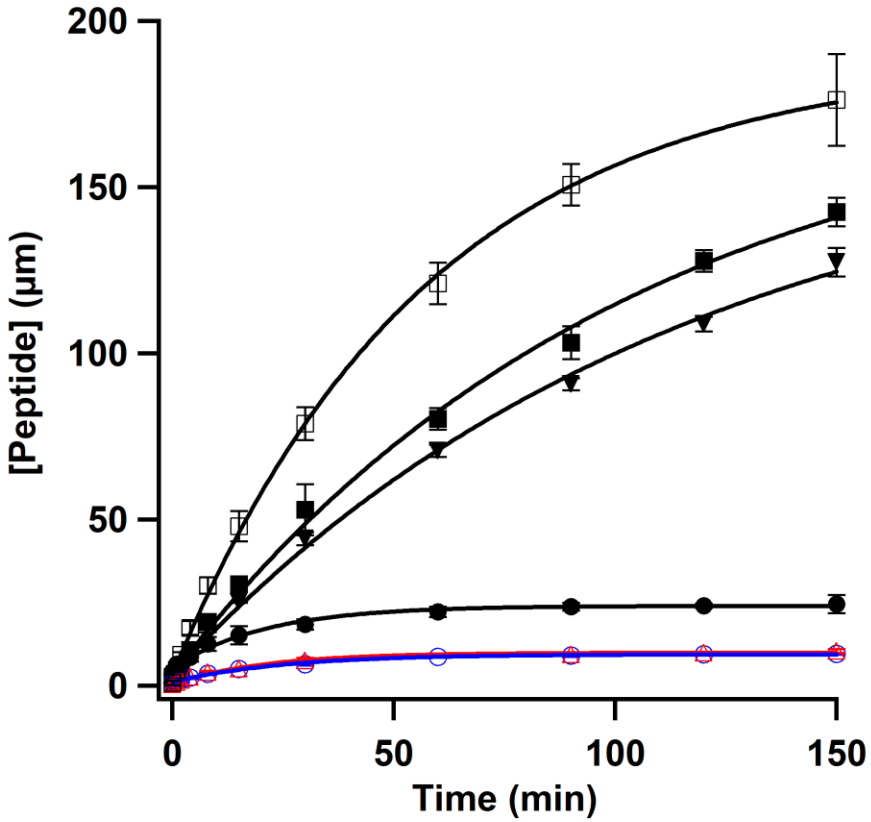

Figure 3-4: (A) Effect of NfuA C39A (closed triangles), C44A (closed squares), C149A (blue open circles), and C152A (red open triangles) variants on LipA catalysis. LipA only control (closed circles). LipA and NfuA control (open squares). Reactions were performed at room temperature and included 25 µM LipA, 400 µM NfuA variant or wild-type protein, 400 µM peptide substrate, 1 mM SAM, and 0.5 µM SAH nucleosidase. Reactions were initiated by the addition of 2 mM dithionite and quenched at various times with H_2SO_4 at a final concentration of 100 mM. Error bars represent the mean ± SD (standard deviation) of three replicates.

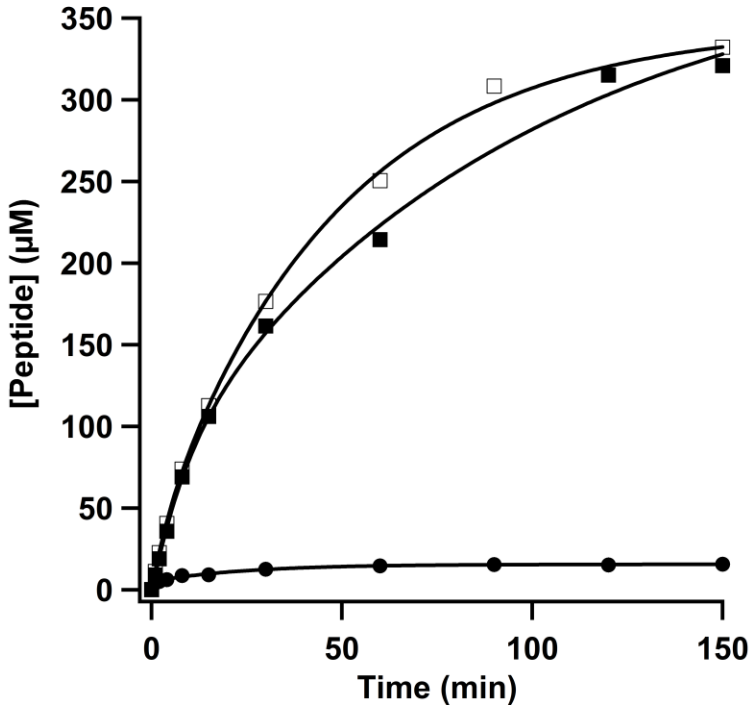

Figure 3-5: (A) Effect of NfuA C39A, C44A double variant (closed squares) on LipA catalysis. LipA only control (closed circles). LipA and NfuA control (open squares). Reactions were performed at room temperature and included 25 µM LipA, 600 µM NfuA variant or wild-type protein, 400 µM peptide substrate, 1 mM SAM, and 0.5 µM SAH nucleosidase. Reactions were initiated by the addition of 2 mM dithionite and quenched at various times with H_2SO_4 at a final concentration of 100 mM.

E. coli NfuA N-terminal domain is essential for tightly interacting with LipA. Currently, there is no well-defined function for the so-called 'degenerate' A-type N-terminal domain of *E. coli* NfuA, although it has been proposed to play a role in protein-protein interactions (18). We investigated the role of the N-terminal domain in regenerating the auxiliary cluster of LipA by isolating and characterizing a fragment of NfuA (N-terminal domain) containing amino acid residues 1-97. This truncated domain has been shown to exhibit a far-UV CD spectrum that is identical to that of the full-length protein (18). We subjected the NfuA N-terminal domain to UV-visible spectroscopy

and analyzed its effect on the activity of LipA. As expected, the UV-visible spectrum of the NfuA N-terminal domain shows no features that are indicative of an Fe-S cluster **(Figure 3-6**).

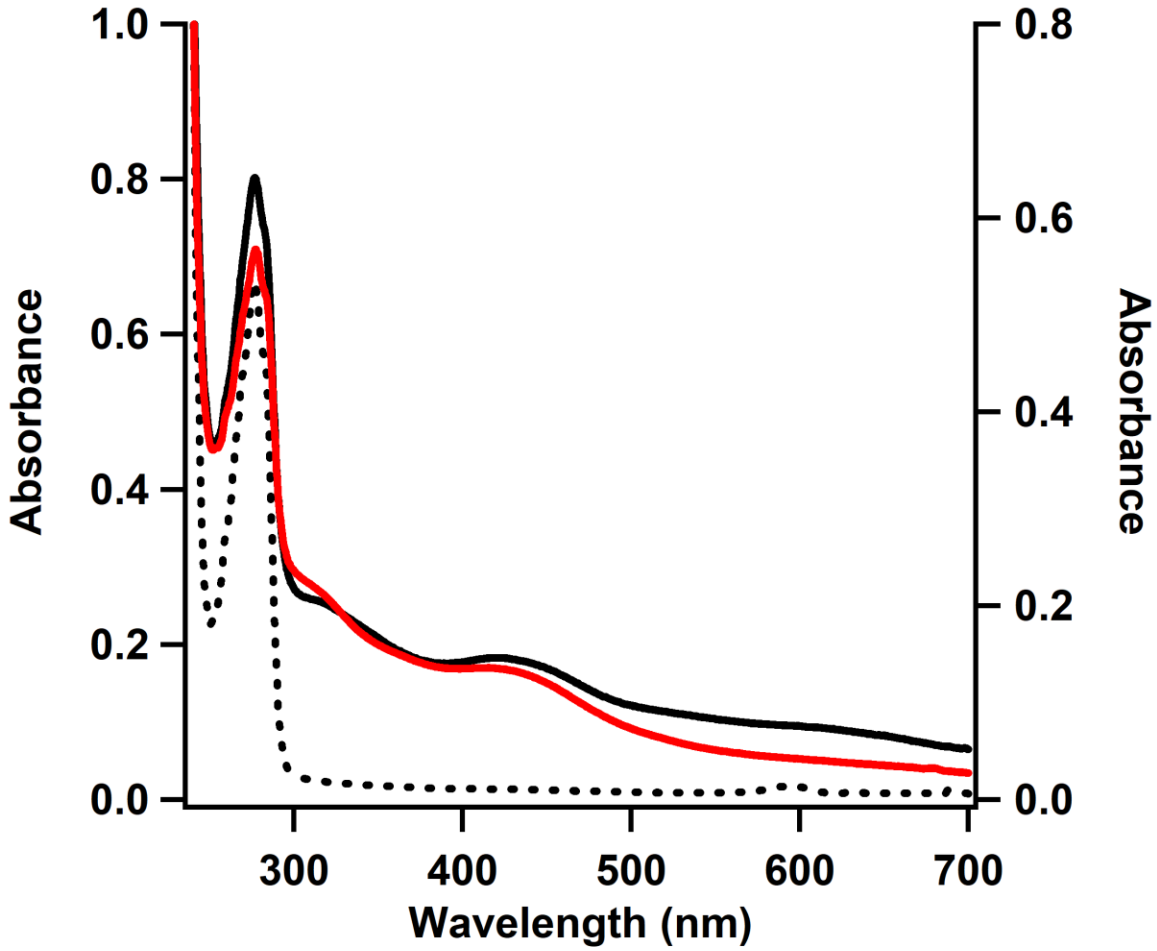

Figure 3-6: *E. coli* NfuA C-terminal domain, but not the N-terminal domain, coordinates a [4Fe–4S] cluster. UV-visible spectrum of 30 µM as-isolated *E. coli* NfuA N-terminal domain (black dotted trace), 30 µM as-isolated *E. coli* NfuA C-terminal domain (black solid trace), and full-length *E. coli* NfuA (solid red trace).

Further, the N-terminal domain does not have any apparent effect on LipA's activity **(Figure 3-7).** In the presence of 400 µM (200 µM active dimer) wt NfuA, 25 µM LipA catalyzes formation of almost 200 µM lipoyl product in 2.5 h (**Figure 3-7**, closed black squares). By contrast,

in the absence of NfuA (**Figure 3-7**, closed red circles), or when full-length NfuA is replaced by its N-terminal domain (**Figure 3-7**, closed blue circles), 25 μM LipA catalyzes formation of slightly less than 25 μM product. To determine if the N-terminal domain of NfuA might be involved in protein–protein interactions, as has been suggested previously (18), its tight association with LipA was assessed by molecular-sieve chromatography (**Figure 3-8, Panel A**). LipA alone (dotted trace) elutes at 60.6 mL, corresponding to an experimental mass of 44.3 kDa (theoretical mass is 38.2 kDa). The N-terminal domain of NfuA elutes at 75.3 mL (dashed trace), corresponding to an experimental mass of 12.5 kDa (theoretical mass is 12.6 kDa). The sample containing an equimolar mixture of LipA and the NfuA N-terminal domain (solid trace) elutes at 58.6 mL as a major peak, corresponding to an experimental mass of 52.4 kDa, which suggests a 1:1 complex between the two proteins (theoretical mass is 50.8 kDa). Fractions corresponding to the major peak were subjected to analysis by SDS-PAGE, and two bands corresponding to the masses of LipA and NfuA are observed (**Figure 3-8, Panel B**). Therefore, although the C-terminal domain of NfuA is essential for the protein's activity, it is dispensable for the interaction between NfuA and LipA. In an attempt to further identify the potential binding site of NfuA and LipA, another NfuA truncation was created that encoded amino acid residues 51-191. When subjected to molecular sieve chromatography, LipA alone (black solid trace) eluted at 60.9 mL, corresponding to an experimental mass of 43.6 kDa (theoretical mass is 38.2 kDa). The NfuA aa 51-191 only control (black dashed trace) eluted at 67.7 mL, corresponding to an experimental mass of 25.7 kDa (theoretical mass is 17.9 kDa). The sample containing equimolar mixture of LipA and NfuA aa 51-191 (red dashed trace) contained two peaks, at 61.1 mL and 67.3 mL corresponding to experimental masses of 42.6 kDa and 25.4 kDa, respectively. No shift in elution volume was observed, consistent with no interaction between LipA and the NfuA aa 51-191 protein **(Figure 3-9, Panel A).** Further, when subjected to SDS-PAGE analysis, NfuA aa 51-191 was not present in the fractions containing LipA **(Figure 3-9, Panel B).** This data suggests that the amino acid residues essential for interacting

with LipA are contained within the first 1-50 residues of *E. coli* NfuA. Unfortunately, subsequent truncated versions of NfuA (aa 11-191, 21-191, 31-191, and 41-191) proved to be unstable for subsequent analysis (data not shown). While further truncating NfuA to identify interacting residues was found to be unfeasible, it was observed that the second CXXXXC motif was found within the 1-50 amino acid residues that were shown to be essential for the LipA/NfuA interaction. Because there is still no defined function for these two cysteinyl residues that are a relic of the three cysteinyl residues conserved in A-type proteins, we subjected the NfuA C39A, the NfuA C44A, and a NfuA C39A, C44A double variant to molecular sieve chromatography as well. In all cases, a tight interaction was still observed between LipA and the NfuA variant proteins, confirmed by both the elution volume shift and SDS-PAGE analysis, indicating these residues are not essential for the interaction **(Figure 3-10).** The robust binding of the variants is supported by the similar LipA activity in the presence of each of the NfuA variants when compared to the wild-type NfuA control **(Figure 3-4 and Figure 3-5).**

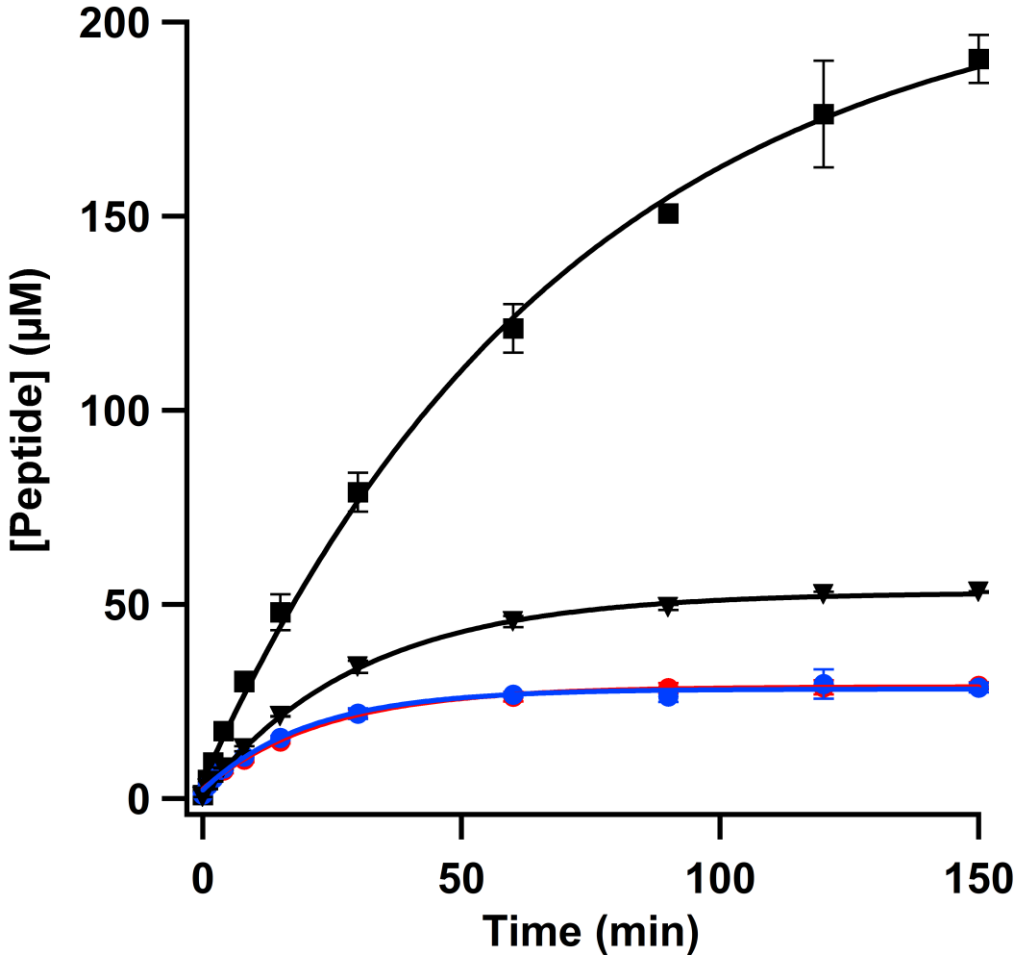

Figure 3-7: Effect of NfuA truncations on LipA activity. Effect of *E. coli* NfuA N-terminal domain and C-terminal domain on LipA activity. LipA only control (closed red circles), LipA + NfuA N-terminal domain (closed blue circles), LipA + wild-type NfuA control (closed black squares), LipA + NfuA C-terminal domain (closed black triangles). For both panels, reactions included 25 μM LipA, 400 μM NfuA or NfuA domain, 400 μM peptide substrate, 1 mM SAM, and 0.5 μM SAH nucleosidase. Reactions were conducted at room temperature, and were initiated by the addition of 2 mM dithionite before quenching with a final concentration of 100 mM H_2SO_4 at various times. Error bars represent the mean ± SD (standard deviation) of three replicates.

E. coli NfuA C-terminal domain coordinates a [4Fe–4S] cluster but does not bind tightly to E. coli LipA. A wealth of evidence has supported a role for [4Fe–4S**]** cluster coordination at a

dimer interface by two conserved cysteinyl residues in the Nfu-like C-terminal domain of NfuA (15,16). We therefore explored whether the C-terminal domain could still coordinate its cluster in the absence of the N-terminal domain. We first overproduced, isolated, and characterized a truncated version of *E. coli* NfuA lacking the N-terminal domain (residues 98-191). Similar to the N-terminal domain, the Nfu-like C-terminal domain was also shown to have a far-UV CD spectrum identical to that of the full-length NfuA protein (18). The C-terminal domain was stable and was overproduced in high yields for analysis. The UV-visible spectrum of the as-isolated protein reveals features of a [4Fe–4S**]** cluster that are nearly identical to those of the full-length wild-type protein **(Figure 3-6).** We then tested the effect of the C-terminal domain on LipA's activity. Surprisingly, although the C-terminal domain coordinates a [4Fe–4S**]** cluster, its ability to restore LipA's auxiliary cluster in a catalytic fashion is largely diminished **(Figure 3-7,** closed triangles**)**. Interestingly, however, the NfuA C-terminal domain allows for one additional turnover, albeit at a rate that is 6 to 9 times slower than that in the presence of full-length NfuA **(**compare **Figure 3-7,** closed triangles and closed squares**).** This additional turnover may result from complete destruction of the auxiliary [4Fe-4S] cluster on LipA after one turnover, and the subsequent relatively slow reconstitution of a new [4Fe-4S] cluster during catalysis at the expense of the NfuA C-terminal domain [4Fe-4S] cluster.

Given that the N-terminal domain of NfuA is found to interact with LipA in the absence of the NfuA C-terminal domain, we hypothesized that the C-terminal domain alone may be unable to recognize LipA or does so poorly. Therefore, a similar interaction analysis by molecular-sieve chromatography was conducted to assess whether LipA and the NfuA C-terminal domain interact tightly **(Figure 3-8, Panel C).** LipA alone (dotted trace) elutes at 61.1 mL, corresponding to an experimental mass of 45.2 kDa (theoretical mass is 38.2 kDa). The C-terminal domain of NfuA alone elutes at 77.0 mL (dashed trace), corresponding to an experimental mass of 11.8 kDa (theoretical mass is 12.8 kDa). The sample containing an equimolar mixture of LipA and the NfuA

C-terminal domain (solid trace) contains two major peaks: one peak at 60.9 mL and another at 77.0 mL. The first peak corresponds to LipA alone, whereas the second peak corresponds to the NfuA C-terminal domain. The absence of a shift in the elution volumes suggests that the two proteins do not form a tight complex as was previously observed for the full-length NfuA and LipA (17), and for the NfuA N-terminal domain and LipA, as demonstrated in this work. Fractions corresponding to the major peak were analyzed by SDS-PAGE, confirming that the two proteins do not co-elute (**Figure 3-8, Panel D**). The inability to interact tightly with LipA may explain the observation that the C-terminal domain alone has a limited effect on LipA's activity, despite the observation that it coordinates a [4Fe–4S] cluster. Together, our analysis suggests that the NfuA N-terminal domain is essential for recognizing LipA and interacting with it, and that in its absence, NfuA is unable to regenerate LipA's auxiliary cluster in a catalytic fashion.

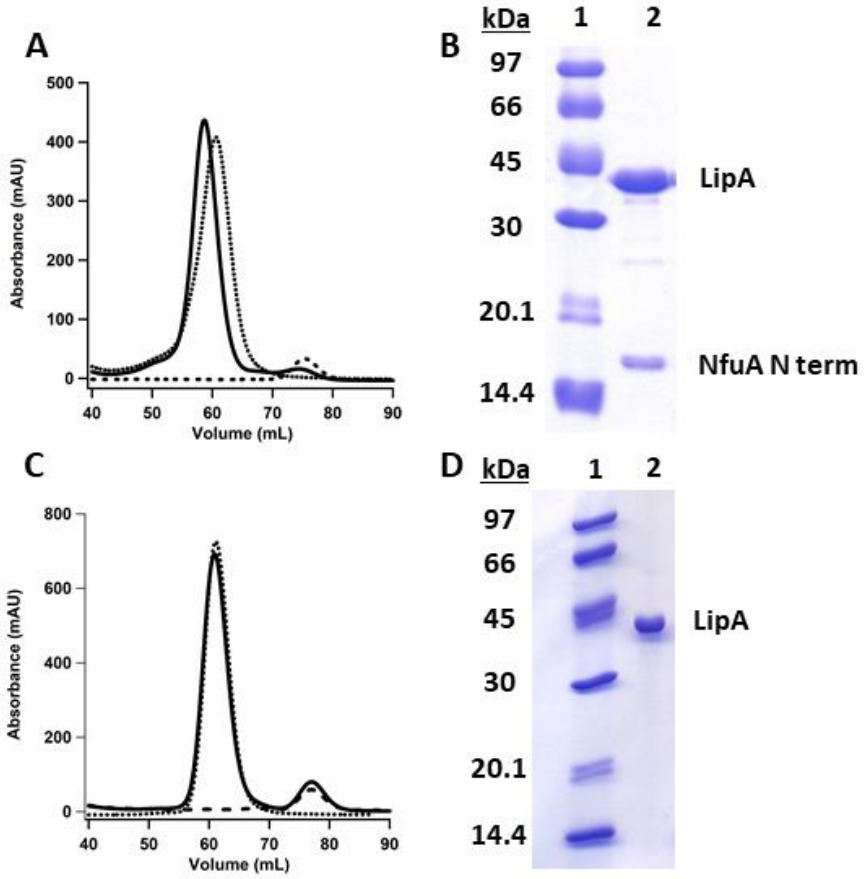

Figure 3-8: N-terminal domain of *E. coli* NfuA alone interacts with *E. coli* LipA. (A) A control sample containing 100 µM LipA (dotted trace) eluted at 60.6 mL with an experimental calculated size of 44.3 kDa (theoretical size 38.2 kDa). A second control sample containing 100 µM NfuA N-terminal domain (dashed trace) eluted at 75.3 mL, with an experimental calculated size of 12.5 kDa (theoretical size 12.6 kDa). A sample containing LipA + the NfuA N-terminal domain (solid trace) eluted at 58.6 mL, corresponding to a calculated size of 52.4 kDa (theoretical size of complex 50.8 kDa). (B) SDS-PAGE analysis of the LipA + NfuA N-terminal domain fractions, confirming the presence of both proteins. Lane 1: molecular weight ladder, Lane 2: LipA + NfuA N-terminal domain fractions. (C) A control sample containing 100 µM LipA (dotted trace) eluted at 61.1 mL, with an experimental calculated size of 45.2 kDa (theoretical size 38.2 kDa). A second control sample containing 100 µM NfuA C-terminal domain (dashed trace) eluted at 77.0 mL, with an experimental calculated size of 11.8 kDa (theoretical size 12.8 kDa). The sample containing LipA + the NfuA C-terminal domain (solid trace) contained two peaks eluting at 60.9 mL and 77.0 mL, corresponding to calculated sizes of 47.3 kDa and 12.3 kDa, respectively (theoretical size of complex 51.0 kDa). (D) SDS-PAGE analysis of the LipA + NfuA C-terminal domain fractions, confirming the absence of the NfuA C-terminal domain in fractions containing LipA. Lane 1: Molecular weight ladder, Lane 2: LipA fraction.

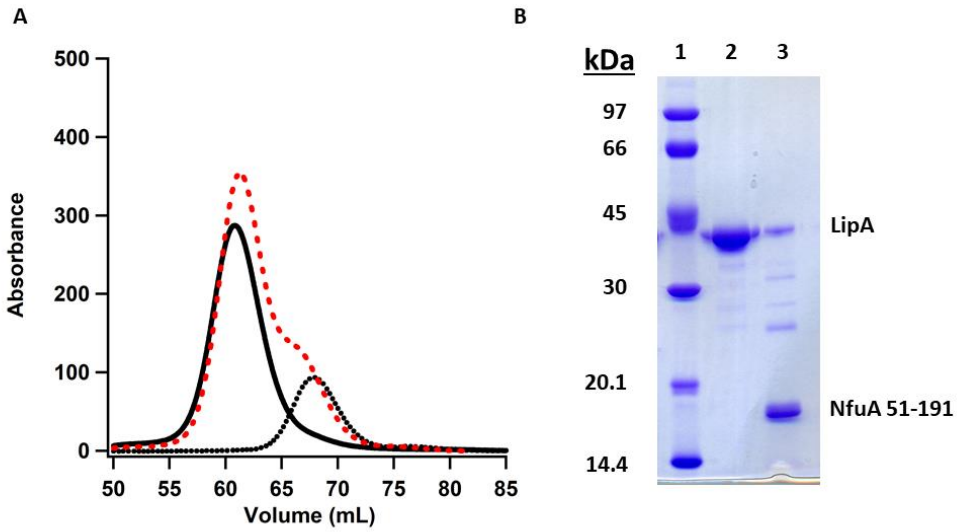

Figure 3-9: *E. coli* NfuA aa 51-191 does not interact with *E. coli* LipA. (A) A control sample containing 100 µM LipA (solid trace) eluted at 60.9 mL with an experimental calculated size of 44.6 kDa (theoretical size 38.2 kDa). A second control sample containing 100 µM NfuA aa 51-191 (dashed black trace) eluted at 67.8 mL, with an experimental calculated size of 25.7 kDa (theoretical size 17.9 kDa). A sample containing LipA + the NfuA aa 51-191 (dashed red trace) eluted in two peaks at 61.1 mL and 67.2 mL. (B) SDS-PAGE analysis of the LipA + NfuA aa 51-191 fractions, confirming the absence of both proteins. Lane 1: molecular weight ladder, Lane 2: LipA + NfuA aa 51-191 peak 1 fractions and Lane 3: LipA + NfuA aa 51-191 peak 2 fractions.

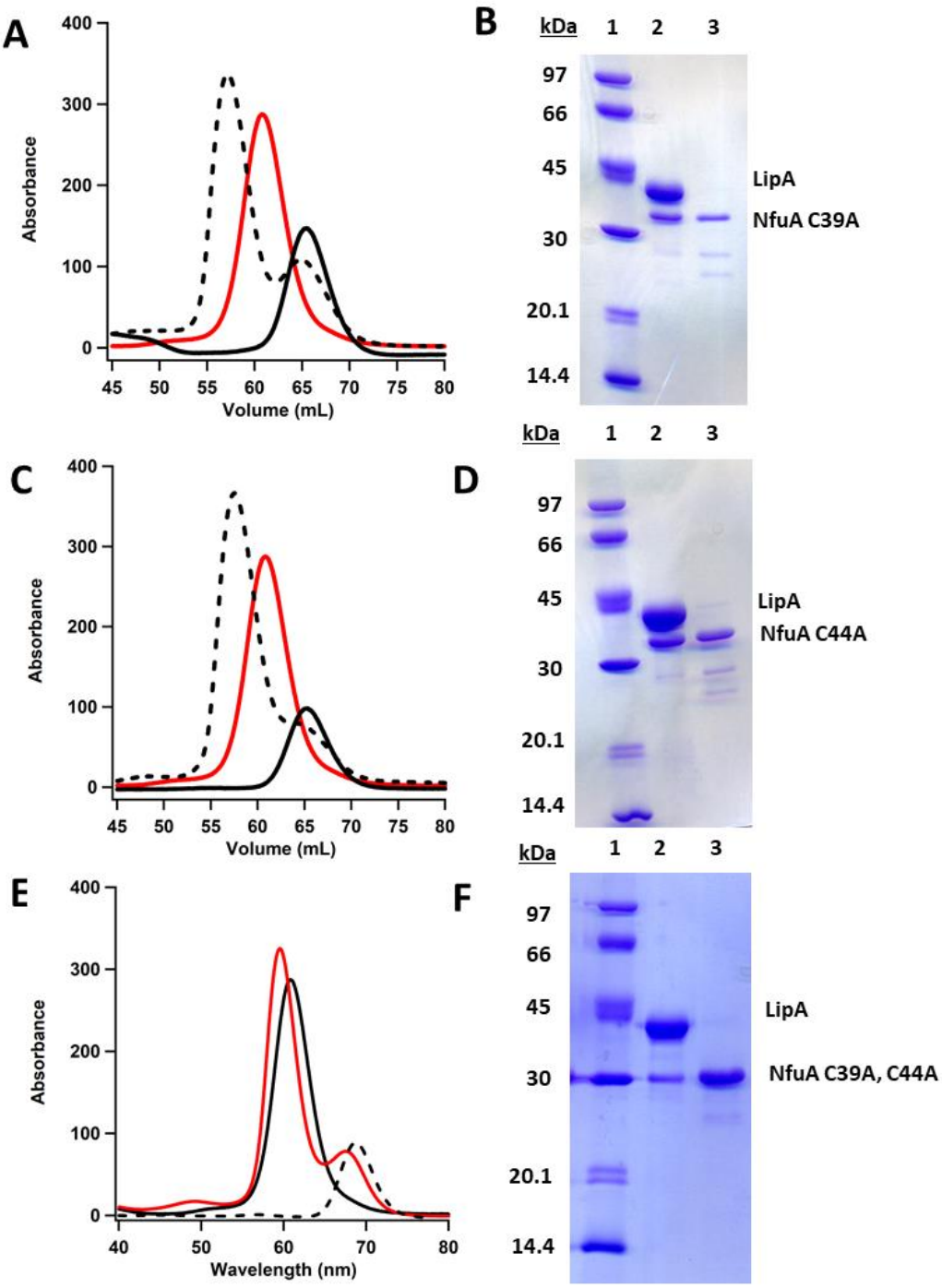

Figure 3-10: *E. coli* NfuA C39A, *E. coli* NfuA C44A, and *E. coli* NfuA C39A, C44A tightly interact with *E. coli* LipA. (A) A control sample containing 100 µM LipA (solid red trace). A second control sample containing 100 µM NfuA C39A (solid black trace). A sample containing LipA + the NfuA C39A (dashed black trace). (B) SDS-PAGE analysis of the LipA + NfuA C39A fractions, confirming the presence of both proteins. Lane 1: molecular weight ladder, Lane 2: LipA

+ NfuA C39A peak 1 fractions and Lane 3: LipA + NfuA C39A peak 2 fractions. (C) A control sample containing 100 μM LipA (solid red trace). A second control sample containing 100 μM NfuA C44A (solid trace). A sample containing LipA + the NfuA C44A (dashed black trace). (D) SDS-PAGE analysis of the LipA + NfuA C44A fractions, confirming the presence of both proteins. Lane 1: molecular weight ladder, Lane 2: LipA + NfuA 44A peak 1 fractions and Lane 3: LipA + NfuA C44A peak 2 fractions. (E) A control sample containing 100 μM LipA (solid black trace). A second control sample containing 100 μM NfuA C39A, C44A (dashed black trace). A sample containing LipA + the NfuA C39A, C44A (solid red trace). (B) SDS-PAGE analysis of the LipA + NfuA C39A, C44A fractions, confirming the presence of both proteins. Lane 1: molecular weight ladder, Lane 2: LipA + NfuA C39A, C44A peak 1 fractions and Lane 3: LipA + NfuA C39A, C44A peak 2 fractions.

NfuA from Mycobacterium tuberculosis also activates E. coli LipA. Given the structural studies that have been carried out on LipA from *Mycobacterium tuberculosis* (*Mt*) (10), we assessed whether *Mt* NfuA can also regenerate *E. coli* LipA's auxiliary Fe/S cluster. Inspection of an alignment of the two protein sequences shows that the primary structure of *Mt* NfuA shares 89% amino acid identity with the primary structure of *E. coli* NfuA, containing two domains corresponding to the N-terminal A-type domain and the C-terminal Nfu-like domain **(Figure 3-11).** The UV-visible spectrum of as-isolated *Mt* NfuA contains features that are consistent with those of a [4Fe–4S] cluster (**Figure 3-12**). Further, when *Mt* NfuA is included in LipA activity assays, product formation is nearly identical to that in reactions containing *E. coli* NfuA **(Figure 3-13).** In this experiment, 20 μM LipA catalyzes formation of 10 μM lipoyl product after 2.5 h in the absence of NfuA. In the presence of *E. coli* NfuA (closed squares) or *Mt* NfuA (closed triangles), 20 μM *E. coli* LipA catalyzes formation of approximately 100 μM lipoyl product in each case. These results suggest that NfuA from other organisms with a similar domain architecture as that of *E. coli* NfuA can fulfill a similar role in LipA catalysis.

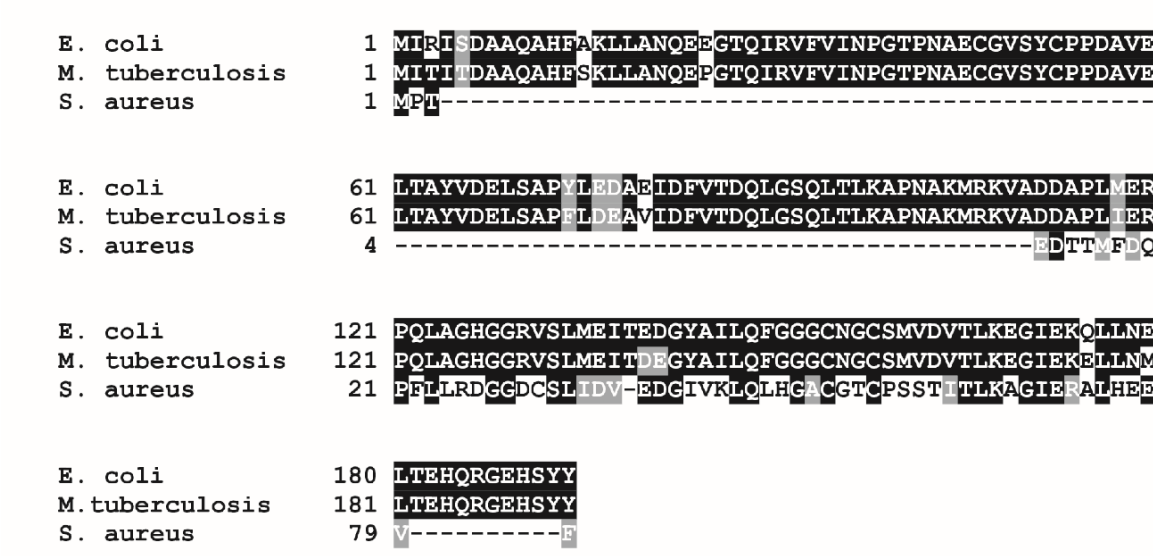

Figure 3-11: Sequence alignment of NfuA/Nfu from *Escherichia coli (E. coli)*, *Mycobacterium tuberculosis (M. tuberculosis)*, and *Staphylococcus aureus (S. aureus)*.

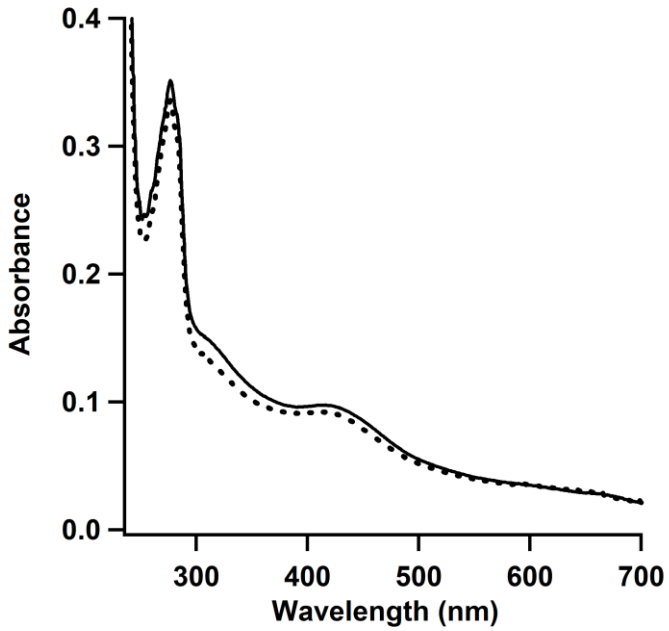

Figure 3-12: **UV-visible Spectrum of *Mt* NfuA.** UV-visible spectrum of 15 µM as-isolated NfuA from *Mycobacterium tuberculosis* (solid line) compared to 15 µM as-isolated *E. coli* NfuA (dashed line).

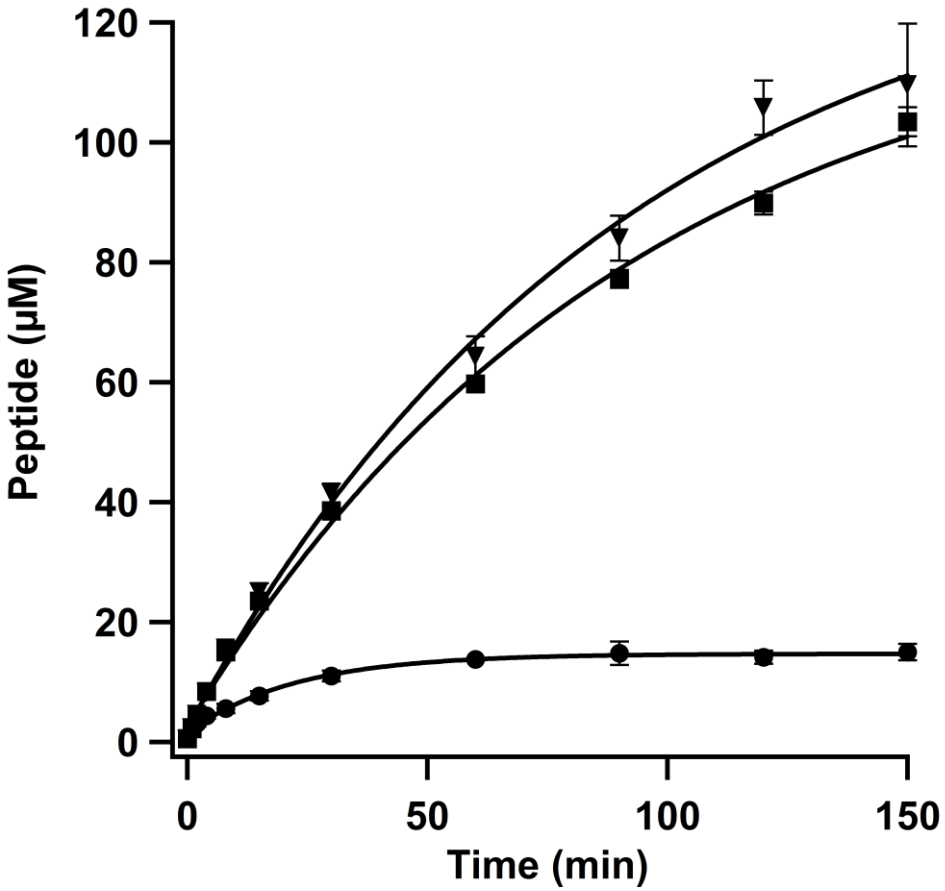

Figure 3-13: Effect of *Mt* NfuA on LipA activity. LipA only control (closed circles). LipA + *E. coli* NfuA control (closed squares). LipA + *Mt* NfuA (closed triangles). Reactions included 20 μM LipA, 400 μM *E. coli* NfuA or *Mt* NfuA, 400 μM peptide substrate, 700 μM SAM, and 0.5 μM SAH nucleosidase. Reactions were conducted at room temperature and were initiated by the addition of dithionite to a final concentration of 2 mM. At designated times, samples were removed and the reaction was quenched by addition of H_2SO_4 to a final concentration of 100 mM. Error bars represent the mean ± the standard deviation of three replicates.

LipA turnover is not enhanced by NfuA when using a peptide substrate containing an 8-thiooctanoyllysyl moiety. Early studies of lipoic acid biosynthesis showed that 8-thiooctanoic acid is converted into lipoic acid when administered to growing *E. coli*, but not as well as when octanoic acid is administered (26-28). **Figure 3-14** shows lipoyl product formation when a peptide substrate containing an 8-thiooctanoyllysyl amino acid residue is acted upon by LipA in the presence of 400 μM NfuA. As can be observed, the lipoyl product levels off at a concentration that is nearly stoichiometric with that of LipA (75 μM) in the reaction (closed circles). By contrast, when a peptide substrate containing an octanoyllysyl amino acid is used (closed squares), additional turnovers take place. Our model predicts that in the absence of chemistry that results in sulfur insertion at C8, the 8-thiooctanoyl substrate is converted to a lipoyl product that is still bonded to the auxiliary Fe-S cluster. This appendage, and/or the lack of partial or full destruction of the auxiliary cluster, is expected to inhibit cluster transfer from NfuA to LipA.

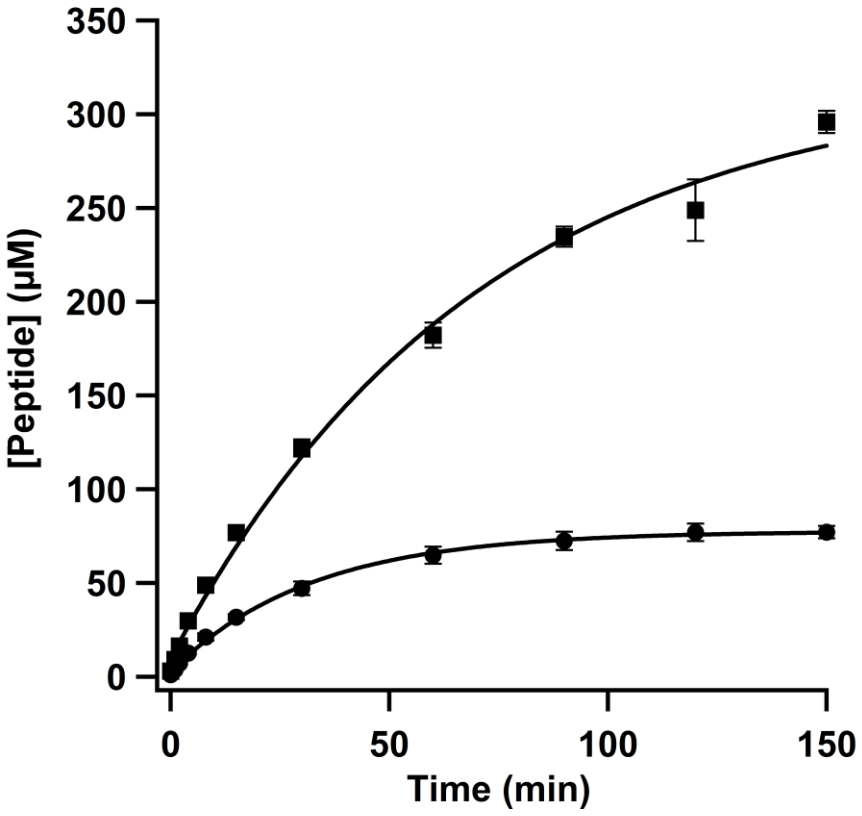

Figure 3-14: **Effect of an 8-thiooctanoyllysyl peptide substrate on catalysis.** The reaction (closed circles) contained 75 μM LipA, 400 μM NfuA, 400 μM 8-thiooctanoyllysyl peptide substrate, 700 μM SAM, and 0.5 μM SAH nucleosidase. A control reaction using the normal peptide substrate (400 μM) under the same reaction conditions is also shown (closed squares). Reactions were conducted at room temperature and were initiated by the addition of dithionite to a final concentration of 2 mM. At designated times, samples were removed and the reaction was quenched by addition of H_2SO_4 to a final concentration of 100 mM. Error bars represent the mean ± the standard deviation of three replicates.

The addition of an A-type domain to S. aureus Nfu supports multiple turnover by LipA

The observation that the *E. coli* NfuA N-terminal domain is required to regenerate *E. coli* LipA lead us to ask whether other Nfu type proteins that lacked this domain could restore *E. coli* LipA's auxiliary cluster during catalysis. To address this question, we initially overproduced and isolated Nfu from *Staphylococcus aureus* and used it in LipA reactions. The sequence homology between

E. coli NfuA and *S. aureus* Nfu is limited to the C-terminal domain **(Figure 3-11).** The UV-visible spectrum of *S. aureus* Nfu in its as-isolated state contains features that support the presence of a [4Fe–4S] cluster (**Figure 3-15**), consistent with what was previously reported (29). However, when *S. aureus* Nfu is included in activity assays, its effect on LipA's activity is minimal, as shown in **Figure 3-16.** In the presence of 400 µM *S. aureus* NfuA, 25 µM LipA catalyzes formation of ~25 µM product (**Figure 3-16**, closed triangles), while in its absence, it catalyzes formation of ~15 µM product (**Figure 3-16**, closed circles).

The effect of *S. aureus* Nfu on the LipA reaction is similar to that of the C-terminal domain of *E. coli* NfuA. The A-type domain in *E. coli* NfuA, which is shown to be essential in this work, is absent in *S. aureus* Nfu. We therefore created a fusion protein consisting of the *E. coli* NfuA N-terminal domain (residues 1-117) attached to *S. aureus* Nfu. Upon addition of the *E. coli* NfuA N-terminal domain-*S. aureus* Nfu fusion to an *E. coli* LipA reaction, significant enhancement of lipoyl product formation is observed, providing more evidence for the essential role of this domain. Now, 25 µM LipA catalyzes formation of greater than 250 µM lipoyl product in 2.5 h (**Figure 3-16,** closed squares). Robust activity has not been observed when Human NFU1, the homologue of NfuA, is used in assays with Human lipoyl synthase (LIAS). Sequence alignment has also revealed poor homology to the N-terminal domain of *E. coli* NfuA. As a result, a new construct was made again fusing the *E. coli* NfuA N-terminal domain to the gene encoding human NFU1. When the *E. coli* NfuA N-terminal domain-human NFU1fusion protein was used in activity assays with *E. coli* LipA, robust catalysis was observed **(Figure 3-18, Panel A).** However, at the time this assay was performed, quality NFU1 protein was unavailable to use as a control, so this preliminary data will need to be further investigated with appropriate controls. Unfortunately, the same effect was not observed when the activity Human LIAS was analyzed in the presence of the *E. coli* NfuA N-terminal domain-human NFU1fusion protein **(Figure 3-18, Panel B).**

Due to the observed effect of the fusion of the *E. coli* NfuA N-terminal domain to the C-terminal like Nfu protein from *S. aureus*, we performed an assay in which both the N-terminal and C-terminal domains of E. coli NfuA were added to test if they could function as individual proteins. As shown in **Figure 3-17,** the *E. coli* NfuA N-terminal domain has no apparent effect on LipA activity whereas the C-terminal domain alone results in ~1.5 eq. of additional activity as has been observed previously. However, inclusion of both the N-terminal domain and C-terminal domain together in a reaction results in less product formation than the C-terminal domain alone, indicating that these domains cannot result in a functional NfuA protein if added individually.

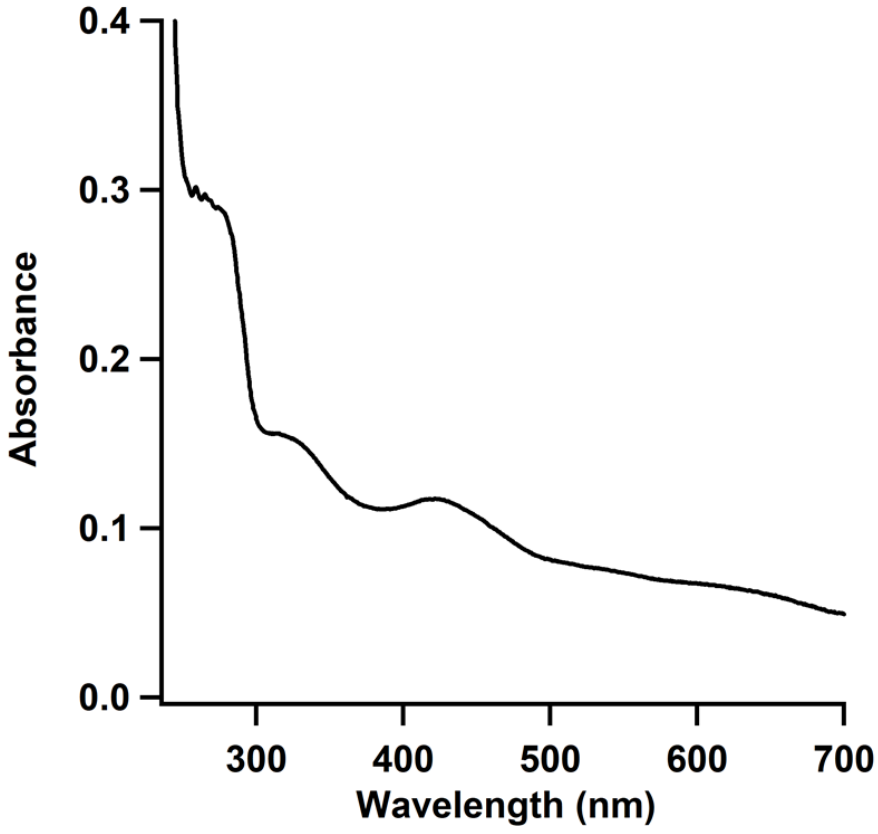

Figure 3-15: UV-visible spectrum of 15 µM as-isolated Nfu from *Staphylococcus aureus* (SAUSA300_0839).

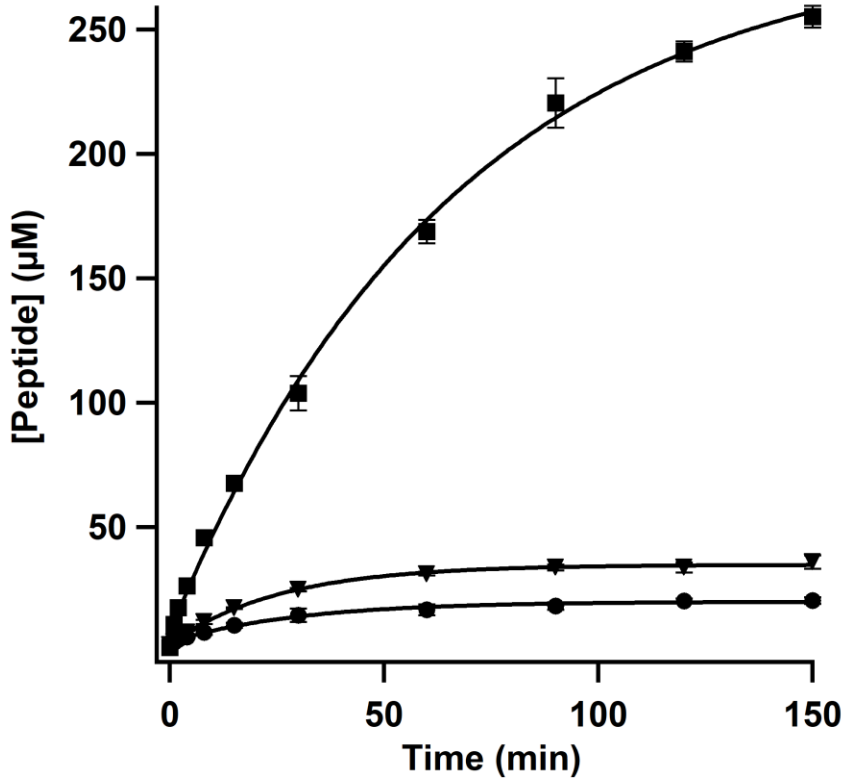

Figure 3-16: Effect of *S. aureus* Nfu and *E. coli* NfuA N-terminal Domain—*S. aureus* Nfu Fusion Protein on *E. coli* LipA Activity. LipA only control (closed circles). LipA + *S. aureus* Nfu (closed triangles). LipA + *E. coli* NfuA N-terminal domain—*S. aureus* Nfu fusion protein (closed squares). Reactions included 25 μM LipA, 400 μM peptide substrate, 1 mM SAM, and 0.5 μM SAH nucleosidase. When appropriate 400 μM *S. aureus* Nfu or 400 μM *E. coli* NfuA N-terminal domain—*S. aureus* Nfu fusion protein were included. Reactions were conducted at room temperature and were initiated by the addition of dithionite to a final concentration of 2 mM. At designated times, samples were removed and the reaction was quenched by addition of H_2SO_4 to a final concentration of 100 mM. Error bars represent the mean ± the standard deviation of three replicates.

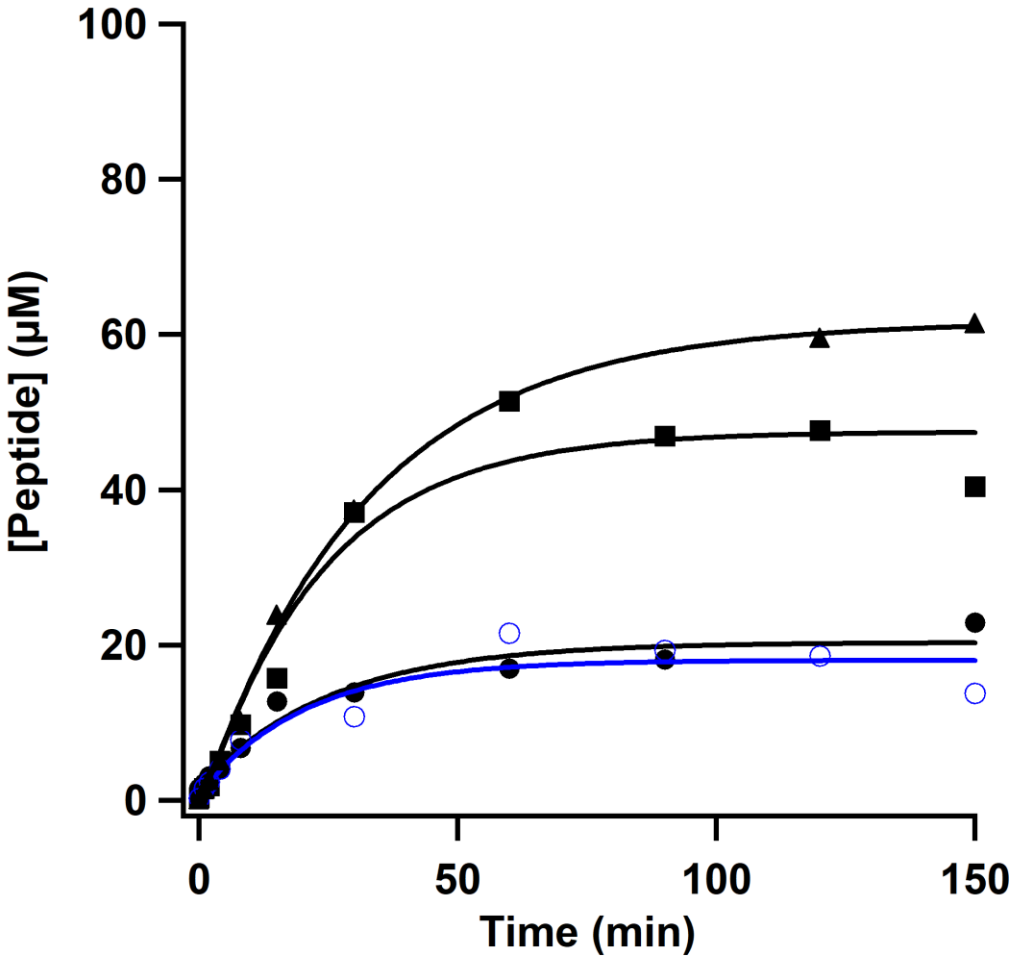

Figure 3-17: Effect of NfuA N terminal and C terminal truncations together on LipA activity. LipA only control (closed red circles), LipA + NfuA N-terminal domain (open blue circles), LipA + NfuA C-terminal domain (closed black triangles), LipA + both NfuA N-terminal domain and NfuA C-terminal domain (closed black squares). Reactions included 25 μM LipA, 400 μM NfuA domain, 400 μM peptide substrate, 1 mM SAM, and 0.5 μM SAH nucleosidase. Reactions were conducted at room temperature, and were initiated by the addition of 2 mM dithionite before quenching with a final concentration of 100 mM H_2SO_4 at various times.

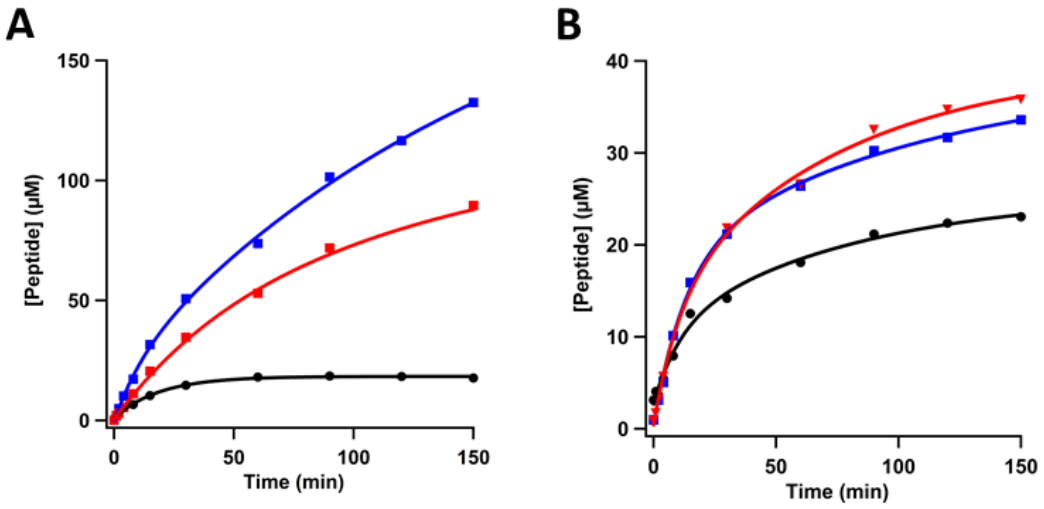

Figure 3-18: *E. coli* LipA or Human LIAS activity in the presence of the *E. coli* NfuA N-terminal domain-Human NFU1 Fusion protein. (A) *E. coli* LipA in the presence of *E. coli* NfuA or the *E. coli* NfuA N-terminal domain-Human NFU1 Fusion protein. *E. coli* LipA only control (black closed circles). *E. coli* LipA + *E. coli* NfuA control (closed blue squares). *E. coli* LipA + the *E. coli* NfuA N-terminal domain-Human NFU1 Fusion protein (red closed squares). Reactions included 20 μM LipA, 300 μM NfuA or fusion protein, 500 μM peptide substrate, 1 mM SAM, and 0.5 μM SAH nucleosidase. (B) Human LIAS in the presence of *E. coli* NfuA or the *E. coli* NfuA N-terminal domain-Human NFU1 Fusion protein. Human LIAS only control (closed black circles). Human LIAS + *E. coli* NfuA (closed blue squares). Human LIAS + the *E. coli* NfuA N-terminal domain-Human NFU1 Fusion protein (red closed triangles). All reactions were conducted at room temperature, and were initiated by the addition of 2 mM dithionite before quenching with a final concentration of 100 mM H_2SO_4 at various times.

Discussion

The recent demonstration that *E. coli* NfuA affords multiple turnovers by *E. coli* LipA by restoring its Fe-S cluster cofactor provided the groundwork for expanding our understanding of this complex system. In this work, we confirm the critical role of the cysteinyl residues in the C-terminal domain of *E. coli* NfuA as coordinating ligands to an Fe-S cluster that is housed at the interface between two NfuA monomers, and show that the cysteinyl residues in the N-terminal domain have no apparent effect on cluster coordination, binding, or cluster transfer to LipA. In addition, we provide a detailed investigation of the essential role of the *E. coli* NfuA N-terminal domain in interacting with *E. coli* LipA, which was previously proposed to aid in protein-protein interactions (18). Further, we have shown that the first 50 amino acids of the *E. coli* NfuA domain are required for the tight interaction. The C-terminal domain, which is homologous to many Nfu proteins, is fully capable of coordinating its cluster in the absence of the N-terminal domain, yet is unable to allow LipA to become catalytic, likely because it lacks the domain responsible for recognizing and interacting with *E. coli* LipA. *Mt* NfuA, which is highly homologous to the *E. coli* NfuA, is another NfuA that also contains the A-type domain, and engenders an identical effect on *E. coli* LipA. Interestingly, Nfu from *S. aureus*, which lacks the N-terminal A-type domain, does not affect the activity of *E. coli* LipA, while a genetic fusion that adds the *E. coli* NfuA N-terminal domain to the *S. aureus* Nfu protein engenders catalytic activity by *E. coli* LipA. It is tempting to consider the possibility that the domain architecture of *E. coli* NfuA is organized to contain two components with separate essential functions.

Cumulatively, our results highlight the role of the so-called ‘degenerate’ A-type N-terminal domain as having an essential function. Although our results provide further insight into the

regeneration of *E. coli* LipA's auxiliary cluster, significant gaps still remain in our understanding of the cluster restoration by NfuA. Our initial evidence that *E. coli* LipA can use an 8-thiooctanoyllysyl-containing peptide as a substrate, but not in a catalytic fashion, suggests that its cluster must be significantly (a [2Fe–2S] cluster or smaller) degraded before NfuA intervenes. Studies to provide a more detailed mechanism of the state of the cluster on NfuA as it is being transferred to LipA are currently underway.

References

1. Broderick, J. B., Duffus, B. R., Duschene, K. S., and Shepard, E. M. (2014) Radical S-Adenosylmethionine Enzymes. *Chemical Reviews* **114**, 4229-4317
2. Sofia, H. J., Chen, G., Hetzler, B. G., Reyes-Spindola, J. F., and Miller, N. E. (2001) Radical SAM, a novel protein superfamily linking unresolved steps in familiar biosynthetic pathways with radical mechanisms: functional characterization using new analysis and information visualization methods. *Nucleic acids research* **29**, 1097-1106
3. Frey, P. A., and Booker, S. J. (2001) Radical mechanisms of S-adenosylmethionine-dependent enzymes. in *Advances in Protein Chemistry*, Academic Press. pp 1-45
4. Lanz, N. D., and Booker, S. J. (2015) Auxiliary iron-sulfur cofactors in radical SAM enzymes. *Biochimica et biophysica acta* **1853**, 1316-1334
5. Cicchillo, R. M., Iwig, D. F., Jones, A. D., Nesbitt, N. M., Baleanu-Gogonea, C., Souder, M. G., Tu, L., and Booker, S. J. (2004) Lipoyl synthase requires two equivalents of S-adenosyl-L-methionine to synthesize one equivalent of lipoic acid. *Biochemistry* **43**, 6378-6386
6. Cicchillo, R. M., Lee, K. H., Baleanu-Gogonea, C., Nesbitt, N. M., Krebs, C., and Booker, S. J. (2004) Escherichia coli lipoyl synthase binds two distinct [4Fe-4S] clusters per polypeptide. *Biochemistry* **43**, 11770-11781
7. Douglas, P., Kriek, M., Bryant, P., and Roach, P. L. (2006) Lipoyl synthase inserts sulfur atoms into an octanoyl substrate in a stepwise manner. *Angewandte Chemie (International ed. in English)* **45**, 5197-5199
8. Lanz, N. D., Pandelia, M. E., Kakar, E. S., Lee, K. H., Krebs, C., and Booker, S. J. (2014) Evidence for a catalytically and kinetically competent enzyme-substrate cross-linked intermediate in catalysis by lipoyl synthase. *Biochemistry* **53**, 4557-4572
9. Lanz, N. D., Rectenwald, J. M., Wang, B., Kakar, E. S., Laremore, T. N., Booker, S. J., and Silakov, A. (2015) Characterization of a Radical Intermediate in Lipoyl Cofactor Biosynthesis. *Journal of the American Chemical Society* **137**, 13216-13219

10. McLaughlin, M. I., Lanz, N. D., Goldman, P. J., Lee, K. H., Booker, S. J., and Drennan, C. L. (2016) Crystallographic snapshots of sulfur insertion by lipoyl synthase. *Proceedings of the National Academy of Sciences of the United States of America* **113**, 9446-9450
11. Ayala-Castro, C., Saini, A., and Outten, F. W. (2008) Fe-S cluster assembly pathways in bacteria. *Microbiology and molecular biology reviews : MMBR* **72**, 110-125, table of contents
12. Fontecave, M., and Ollagnier-de-Choudens, S. (2008) Iron-sulfur cluster biosynthesis in bacteria: Mechanisms of cluster assembly and transfer. *Archives of biochemistry and biophysics* **474**, 226-237
13. Johnson, D. C., Dean, D. R., Smith, A. D., and Johnson, M. K. (2005) Structure, function, and formation of biological iron-sulfur clusters. *Annual review of biochemistry* **74**, 247-281
14. Rouault, T. A., and Tong, W. H. (2008) Iron–sulfur cluster biogenesis and human disease. *Trends in genetics : TIG* **24**, 398-407
15. Angelini, S., Gerez, C., Ollagnier-de Choudens, S., Sanakis, Y., Fontecave, M., Barras, F., and Py, B. (2008) NfuA, a new factor required for maturing Fe/S proteins in Escherichia coli under oxidative stress and iron starvation conditions. *The Journal of biological chemistry* **283**, 14084-14091
16. Bandyopadhyay, S., Naik, S. G., O'Carroll, I. P., Huynh, B. H., Dean, D. R., Johnson, M. K., and Dos Santos, P. C. (2008) A proposed role for the Azotobacter vinelandii NfuA protein as an intermediate iron-sulfur cluster carrier. *The Journal of biological chemistry* **283**, 14092-14099
17. McCarthy, E. L., and Booker, S. J. (2017) Destruction and reformation of an iron-sulfur cluster during catalysis by lipoyl synthase. *Science (New York, N.Y.)* **358**, 373-377
18. Py, B., Gerez, C., Angelini, S., Planel, R., Vinella, D., Loiseau, L., Talla, E., Brochier-Armanet, C., Garcia Serres, R., Latour, J. M., Ollagnier-de Choudens, S., Fontecave, M., and Barras, F. (2012) Molecular organization, biochemical function, cellular role and evolution of NfuA, an atypical Fe-S carrier. *Molecular microbiology* **86**, 155-171
19. Lanz, N. D., Grove, T. L., Gogonea, C. B., Lee, K. H., Krebs, C., and Booker, S. J. (2012) RlmN and AtsB as models for the overproduction and characterization of radical SAM proteins. *Methods in enzymology* **516**, 125-152
20. McCarthy, E. L., and Booker, S. J. (2018) Biochemical Approaches for Understanding Iron-Sulfur Cluster Regeneration in Escherichia coli Lipoyl Synthase During Catalysis. *Methods in enzymology* **606**, 217-239
21. Bradford, M. M. (1976) A rapid and sensitive method for the quantitation of microgram quantities of protein utilizing the principle of protein-dye binding. *Analytical Biochemistry* **72**, 248-254
22. Beinert, H. (1978) Micro methods for the quantitative determination of iron and copper in biological material. *Methods in enzymology* **54**, 435-445
23. Beinert, H. (1983) Semi-micro methods for analysis of labile sulfide and of labile sulfide plus sulfane sulfur in unusually stable iron-sulfur proteins. *Analytical Biochemistry* **131**, 373-378
24. Hurley, J. K., Weber-Main, A. M., Hodges, A. E., Stankovich, M. T., Benning, M. M., Holden, H. M., Cheng, H., Xia, B., Markley, J. L., Genzor, C., Gomez-Moreno, C., Hafezi, R., and Tollin, G. (1997) Iron-sulfur cluster cysteine-to-serine mutants of Anabaena -2Fe-2S- ferredoxin exhibit unexpected redox properties and are competent in electron transfer to ferredoxin:NADP+ reductase. *Biochemistry* **36**, 15109-15117

25. Subramanian, S., Duin, E. C., Fawcett, S. E. J., Armstrong, F. A., Meyer, J., and Johnson, M. K. (2015) Spectroscopic and redox studies of valence-delocalized [Fe2S2](+) centers in thioredoxin-like ferredoxins. *Journal of the American Chemical Society* **137**, 4567-4580
26. Hayden, M. A., Huang, I. Y., Iliopoulos, G., Orozco, M., and Ashley, G. W. (1993) Biosynthesis of lipoic acid: Characterization of the lipoic acid auxotrophs Escherichia coli W1485-lip2 and JRG33-lip9. *Biochemistry* **32**, 3778-3782
27. Reed, K. E., and Cronan, J. E. (1993) Lipoic acid metabolism in Escherichia coli: sequencing and functional characterization of the lipA and lipB genes. *Journal of Bacteriology* **175**, 1325-1336
28. White, R. H. (1980) Biosynthesis of lipoic acid: extent of incorporation of deuterated hydroxy- and thiooctanoic acids into lipoic acid. *Journal of the American Chemical Society* **102**, 6605-6607
29. Mashruwala, A. A., Pang, Y. Y., Rosario-Cruz, Z., Chahal, H. K., Benson, M. A., Anzaldi-Mike, L. L., Skaar, E. P., Torres, V. J., Nauseef, W. M., and Boyd, J. M. (2015) Nfu facilitates the maturation of iron-sulfur proteins and participates in virulence in Staphylococcus aureus. *Molecular microbiology* **95**, 383-409

Chapter 4

Biosynthesis of Selenolipoic Acid by *E. coli* Lipoyl Synthase

Abstract

Lipoyl synthase (LipA) catalyzes the final step in the *de novo* biosynthesis of the lipoyl cofactor: the attachment of two sulfur atoms at C6 and C8 of an *n*-octanoyllysyl chain of a lipoyl carrier protein. LipA is a member of the radical *S*-adenosylmethionine (SAM) superfamily and, as such, coordinates a [4Fe–4S] cluster that it uses to catalyze the reductive cleavage of SAM to afford the common intermediate 5'-deoxyadenos-5'-yl (5'-dA•). LipA contains an additional [4Fe–4S] auxiliary cluster that has been shown to be degraded during its reaction cycle to provide the attached sulfur atoms. In the absence of a means to regenerate the cluster after each turnover, only 1 equivalent of lipoyl cofactor is formed in *in vitro* reactions, resulting in the release of four Fe^{2+} ions and two S^{2-} ions into solution. Recently, it was shown that *E. coli* NfuA can regenerate the auxiliary cluster of *E. coli* LipA after each turnover, allowing the enzyme to catalyze multiple turnovers. However, the mechanism by which this is accomplished is unclear, as is the fate of the remaining sulfur atoms and iron ions from LipA's destroyed cluster. Herein, we report that NfuA reconstituted with a [4Fe–4Se] cluster can deliver the cluster to LipA during turnover, allowing for the production of selenolipoic acid. We also provide additional evidence that LipA can mobilize all four sulfur atoms in its [4Fe–4S] cluster during catalysis to allow for two equivalents of lipoic acid formation

before selenolipoic acid is produced. These studies now set the stage for deciphering the mechanism of iron-sulfur cluster regeneration in LipA. The fate of the original iron ions remains unclear.

Introduction

Lipoic acid is an eight-carbon straight-chain fatty acid containing sulfhydryl groups at C6 and C8, which can reversibly undergo oxidation to the disulfide-containing dithiolane form, a characteristic that is essential for its role as a redox cofactor in a number of multienzyme complexes that are involved in energy and amino acid metabolism.. In its biologically relevant form, lipoic acid is covalently attached to a specific lysyl residue of a lipoyl carrier protein (LCP), affording a 14 Å appendage (1). This so-called "swinging arm" allows for the transport of reaction intermediates to successive active sites within the multienzyme complexes that require the lipoyl cofactor. In *E. coli,* two pathways exist for forming the lipoyl cofactor. In the exogenous pathway, lipoic acid is scavenged from the environment and activated by lipoate protein ligase A (LplA) in an ATP-dependent manner. The same protein then catalyzes the transfer of the lipoyl group to one of three LCPs to produce the lipoyl cofactor. In *E. coli*, these LCPs include the E_2 subunits of the pyruvate and α-ketoglutarate dehydrogenase complexes as well as the H protein of the glycine cleavage system. Alternatively, the lipoyl cofactor can be synthesized *de novo* in what is termed the endogenous pathway, which involves two dedicated enzymes. In this pathway, an octanoyltransferase, LipB, first transfers an octanoyl group from octanoyl-acyl carrier protein to an LCP. Subsequently, lipoyl synthase (LipA) attaches sulfur atoms at C6 and C8 of the octanoyl chain to generate the final lipoyl product.

LipA is a member of the radical *S*-adenosylmethionine (SAM) superfamily and, as such, coordinates a [4Fe–4S] cluster that it uses to cleave SAM reductively to form a 5′ deoxyadenosyl 5'-radical (5'-dA•). The 5'-dA• is a potent oxidant that can abstract hydrogen atoms from C–H

bonds having homolytic bond-dissociation energies of 98 kcal/mol or more (2-4). LipA contains a second 'auxiliary' [4Fe–4S] cluster, which is sacrificed during turnover to provide the sulfur atoms that are attached to the organic substrate (5-13). The destruction of the auxiliary cluster renders LipA catalytically inactive. As a result, the enzyme can only perform one turnover in the absence of a means to regenerate the auxiliary cluster.

Recently, the intermediate iron-sulfur (FeS) cluster carrier protein from *E. coli*, NfuA, was shown to regenerate the auxiliary cluster of LipA in a non-rate-limiting step, demonstrating LipA catalysis for the first time *in vitro* (14). In order to trace the origin of the sulfur in the nascent lipoyl group, experiments were performed using NfuA reconstituted to contain a [4Fe–4^{34}S] cluster, and LipA containing [4Fe–4^{32}S] (i.e. natural abundance) clusters. The expectation was that LipA would use two of the sulfur atoms from its auxiliary cluster to form one equivalent of lipoyllysine, as has been observed in the past in the absence of NfuA, and then all subsequently produced lipoyllysine would be labeled with ^{34}S originating from NfuA's cluster. Unexpectedly, in the presence of NfuA, almost two equivalents of ^{32}S-containing lipoyllysine were observed before production of ^{34}S-containing lipoyllysine, indicating that all four of the sulfur atoms within the auxiliary cluster can be transferred to the organic substrate. Additionally, a distinct lag in the production of ^{34}S-containing lipoyllysine was observed while the auxiliary cluster was consumed. This unexpected but interesting result lead us to perform subsequent experiments using NfuA coordinating an iron-selenium cluster.

A seminal study in the Cronan laboratory reported the use of selenolipoic acid to investigate the *in vivo* biosynthesis of lipoic acid (15). In this study, selenolipoic acid, or lipoic acid with selenium atoms at C6 and C8 instead of sulfur, was found to inhibit wild-type *E. coli* growth. Conversely, replacement of either the C6 or C8 sulfur atom of the lipoic acid molecule with selenium creating lipoic acid with a selenium/sulfur mixed species had no apparent biological consequence. Labeling experiments using [^{75}Se] selenolipoic acid revealed that the selenolipoic

acid could be efficiently incorporated into α-ketoacid dehydrogenase complexes. The observed growth inhibition was proposed to be a result of the protein-bound selenolipoate being irreversibly oxidized, and, as a result, unable to perform its essential role in the reductive acylation step in the catalytic cycle of the α-ketoacid dehydrogenase.

To date, the ability of LipA to synthesize selenolipoic acid has never been shown. Given the interesting results that were previously observed using ^{34}S-labeled clusters, we were motivated to further probe the mechanism of cluster regeneration using [4Fe–4Se] loaded NfuA through biochemical and spectroscopic characterization. [4Fe–4Se] clusters are routinely reconstituted on iron-sulfur cluster proteins, including radical SAM enzymes (16). One advantage in using selenium is that it has a much larger atomic radii, such that its electron density can be differentiated from sulfur. This could allow us to track the location of selenium from NfuA to LipA at various stages of turnover by X-ray crystallography. A similar experiment was recently published from the Rees laboratory, in which selenium was incorporated into the iron-molybdenum cofactor of nitrogenase (17). The authors found that the selenium migrated as a function of catalysis to various positions in the cofactor.

Materials and Methods

Materials.

Kanamycin, arabinose, isopropyl β-D-thiogalactopyranoside (IPTG), dithiothreitol (DTT), tris(2-carboxyethyl)phosphine (TCEP), and ampicillin were from Gold Biotechnology (St. Louis, MO). Sodium dithionite, sodium selenite, $FeCl_3$, Dnase I, β-mercaptoethanol (BME), and (1,10)-phenanthroline were purchased from Sigma Co. (St. Louis, MO). N-(2-

Hydroxyethyl)piperazine-N′-2-ethanesulfonic acid (HEPES) and potassium chloride were from Dot Scientific (Burton, MI). Imidazole and lysozyme were from Alfa Aesar (Haverhill, MA). Coomassie brilliant blue dye was from Amresco (Fountain Parkway Solon, OH). Glycerol, Coomassie Plus Protein Assay Reagent for protein concentration determination as well as the bovine serum albumin standard were from Thermofisher Scientific (Rockford, IL). *S*-Adenosylhomocysteine nucleosidase (SAHN) and *S*-adenosylmethionine (SAM) were prepared as described previously (18,19).

General Procedures.

The polymerase chain reaction was conducted using a BioRad S1000 thermocycler. DNA sequencing was performed at the Huck Institutes Genomics Core Facility at Penn State University. Amino acid analysis was performed at the UC Davis Proteomics Core Facility. UV-visible spectra were recorded on a Cary 50 spectrometer from Varian (Walnut Creek, CA) using the associated WinUV software package. All anaerobic experiments were conducted in a Coy anaerobic chamber (Grass Lake, MI). Ultra Performance Liquid Chromatography (UPLC) with detection by mass spectrometry (UPLC-MS) was conducted using an Agilent Technologies (Santa Clara, CA) 1290 Infinity II system coupled to an Agilent Technologies 6470 QQQ mass spectrometer. Data collection and analysis were performed using the associated MassHunter software. Size-exclusion chromatography was performed on an *Ä*KTA system (GE Healthcare) housed in a Coy anaerobic chamber equipped with a HiPrep 16/60 Sephacryl HR S-200 column (GE Healthcare). Sodium dodecyl sulfate-polyacrylamide gel electrophoresis (SDS-PAGE) was performed using a mini vertical electrophoresis unit from Hoefer (Holliston, MA).

Plasmid Construction.

The construction of the *E. coli lipA*-pET28a and *E. coli nfuA*-pET28a expression vectors used in this study has been described previously (6,14).

Overproduction of E. coli LipA.

E. coli LipA was overproduced as previously described (14,20). BL21(DE3) cells were co-transformed with the construct encoding the desired gene and plasmid pDB1282, which encodes the genes in the *isc* operon from *Azotobacter vinelandii* (6). A single colony was used to inoculate 200 mL lysogeny broth (LB) supplemented with 50 µg/mL kanamycin and 100 µg/mL ampicillin, and the starter culture was incubated overnight at 37 °C with shaking at 250 rpm. The following day, M9 minimal media (4 × 6 L flasks containing 4 L media each) pre-equilibrated to 37 °C was inoculated with 0.2 mL starter culture, and was incubated at 37 °C with shaking at 180 rpm. At an OD_{600}=0.3 (~14-18 h post-inoculation), expression of genes on pDB1282 was induced by addition of arabinose (0.2% final concentration). At an OD_{600}=0.6, 50 µM $FeCl_3$ was added to the cultures and the flasks were placed in an ice-water bath for ~30 min. Once chilled, expression of the *lipA* gene was induced by the addition of IPTG (200 µM final concentration) and allowed to proceed for ~18 h at 18 °C with shaking at 180 rpm. Bacterial cells were harvested by centrifugation at 7,500 × g for 12 min. The resulting cell pellet was flash-frozen in liquid N_2 and stored in liquid N_2 until further use.

Overproduction of Holo and Apo E. coli NfuA.

Holo (i.e., FeS-cluster loaded) and apo *E. coli* NfuA were overproduced as previously described (14,20). For overproduction of holo *E. coli* NfuA, BL21(DE3) cells were co-transformed with the *E. coli nfuA*-pET28a and pDB1282 expression vectors. A single colony was used to inoculate 200 mL lysogeny broth (LB) supplemented with 50 µg/mL kanamycin and 100 µg/mL ampicillin, and the starter culture was incubated overnight at 37 °C with shaking at 250 rpm. The

following day, 20 mL of the starter culture was used to inoculate four 6 L flasks containing 4 L M9 minimal media supplemented with 50 µg/mL kanamycin and 100 µg/mL ampicillin. The *E. coli* strains were cultured at 37 °C with shaking at 180 rpm. At an OD_{600}=0.3, 0.2% arabinose was added to induce expression of the genes encoded in the pDB1282 plasmid. At an OD_{600}=0.6, 50 µM $FeCl_3$ was added to the cultures, and the flasks were placed in an ice-water bath for ~30 min. Once chilled, expression of the *E. coli nfuA* gene was induced by the addition of 200 µM IPTG (final concentration) and allowed to proceed for ~18 h at 18 °C with shaking at 180 rpm. A similar procedure was followed for the overproduction of apo *E. coli* NfuA, with the following modifications. BL21(DE3) cells were transformed with the *nfuA*-pET28a construct in the absence of pDB1282, and ampicillin was omitted in the culture media . For overproduction of apo-NfuA, cultures were supplemented with a metal mix (3 nM $(NH_4)_2Mo_7O_{24}$, 30 nM $CoCl_2$•$6H_20$, 400 nM H_3BO_3, 10 nM $CuSO_4$•$5H_2O$, 80 nM $MnCl_2$•$4H_20$, and 10 nM $ZnSO_4$•$7H_20$). At an OD_{600}=0.3, the flasks were supplemented with an amino acid mixture containing alanine (800 µM), arginine (400 µM), asparagine (400 µM), aspartic acid (400 µM), cysteine (100 µM), glutamic acid (600 µM), glutamine (600 µM), glycine (800 µM), histidine (200 µM), isoleucine (400 µM), leucine (800 µM), lysine (400 µM), methionine (200 µM), phenylalanine (400 µM), proline (400 µM), serine (10 mM), threonine (400 µM), tryptophan (100 µM), tyrosine (200 µM), and valine (600 µM). At an OD_{600}=0.6, 75 µM 1,10-phenanthroline was added to the flasks, which were subsequently chilled on ice for 2 h. Expression of apo *nfuA* was induced by the addition of 200 µM IPTG (final concentration) and allowed to proceed for ~18 h at 18 °C with shaking at 180 rpm. In all cases, bacterial cells were harvested by centrifugation at 7,500 × g for 12 min. The resulting cellular pellet was flash-frozen in liquid N_2 and stored in liquid N_2 until further use.

Isolation of apo E. coli NfuA, holo E. coli NfuA, and E. coli LipA.

Apo *E. coli* NfuA, holo *E. coli* NfuA, and *E. coli* LipA were isolated as previously described (14,20). All purification steps were carried out in a Coy anaerobic chamber containing <1 ppm O_2, except that centrifugation steps were carried out outside of the chamber with samples in tightly sealed tubes. Apo *E. coli* NfuA, holo *E. coli* NfuA, and *E. coli* LipA were purified by immobilized metal affinity chromatography (IMAC) using the following procedure. The cellular pellet containing the NfuA protein was re-suspended in Buffer A (50 mM HEPES, pH 7.5, 300 mM KCl, 20 mM imidazole, 10 mM β-mercaptoethanol). Lysozyme (1 mg/mL) and Dnase I (0.1 mg/mL) were added, and the solution was stirred for 30 min at room temperature. The cells were lysed by sonic disruption, and the resulting lysate was centrifuged at 45,000 × g for 1 h. The supernatant was applied to a column of Ni-NTA resin pre-equilibrated in Buffer A, and the column was washed with Buffer B (50 mM HEPES, pH 7.5, 300 mM KCl, 45 mM imidazole, 10 mM β-mercaptoethanol, and 10% glycerol). The protein was eluted with Buffer C (50 mM HEPES, pH 7.5, 300 mM KCl, 500 mM imidazole, 10 mM β-mercaptoethanol, and 10% glycerol) and then concentrated to 2.5 mL before exchanging into storage buffer (50 mM Hepes, pH 7.5, 300 mM KCl, 5 mM DTT, 15% glycerol) using a PD-10 column (GE Healthcare Life Sciences). For *E. coli* LipA, the buffer conditions were identical, with the exceptions that Buffer B, C, and D contained 20% glycerol and Buffer C contained 250 mM imidazole. The protein was aliquoted, flash-frozen, and stored in liquid N_2 until use. SDS-PAGE (12.5%) analysis with staining with Coomassie brilliant blue revealed that the final protein was >95% pure. The protein concentration was determined using the Bradford method. Amino acid analysis, performed by the UC Davis Proteomics Core (21), revealed that the Bradford method overestimates the protein concentration of *E. coli* NfuA and *E. coli* LipA by a factor of 1.18 and 1.47, respectively. Colorimetric iron analysis normalized to protein concentration were used to estimate the iron content per polypeptide (22).

Isolation of pSUMO-Gly-E. coli LipA (native).

The purification of native *E. coli* LipA was performed in a Coy anaerobic chamber. The cellular pellet (~50 mgs) was resuspended in 150 mL Lysis Buffer (100 mM HEPES, pH 7.5, 300 mM KCl, 20 mM Imidazole, and 10 mM BME). Lysozyme (1 mg/mL) and DNAse I (0.1 mg/mL) was added, and the solution was slowly stirred for 30 min. at room temperature. The solution was placed in an ice-water bath, and the cells were lysed by sonic disruption. The lysate was placed into centrifuge tubes and tightly sealed, then removed from the anaerobic chamber and centrifuged at 45,000 x g for 1 h. The supernatant was applied to a column containing Ni-NTA resin equilibrated in the Lysis buffer. Once loaded, the column was washed with 200 mL Wash Buffer (100 mM HEPES, pH 7.5, 300 mM KCl, 40 mM Imidazole, 20% glycerol and 10 mM BME). The protein was eluted from the column using Elution Buffer (100 mM HEPES, pH 7.5, 300 mM KCl, 250 mM Imidazole, 20% glycerol, and 10 mM BME). The protein was concentrated in tightly sealed 10 kDa centricons to approximately 5 mL. The protein was then gel-filtered into Cleavage Buffer (100 mM HEPES, pH 7.5, 300 mM KCl, 20% glycerol, and 10 mM BME) using a PD-10 column (performed twice for a total volume of 7 mL). The SUMO protease, ULP1, was added and the protein was incubated on ice overnight to generate native LipA. The following day, the protein was re-applied to the Ni-NTA column and washed with Cleavage Wash Buffer (100 mM HEPES, pH 7.5, 500 mM KCl, 40 mM Imidazole, 20% glycerol, and 10 mM BME). The flow-through containing native LipA was collected, concentrated, and buffer exchanged into Storage Buffer (100 mM HEPES, pH 7.5, 300 mM KCl, 20% glycerol, and 1 mM DTT. The protein was determined to be >95% pure judged by SDS-PAGE analysis, and the concentration was determined via the Bradford method, using the previously calculated amino acid correction factor 1.47.

Selenium Reconstitution of Apo E. coli NfuA.

Apo *E. coli NfuA* was chemically reconstituted with reductant, iron, and selenide to produce a [4Fe–4Se] loaded NfuA. A 15 mL reaction containing 100 µM as-isolated NfuA was slowly stirred on ice. DTT (5 mM final concentration) was added in three increments every 20 min, and the solution was incubated for 1 h. Following reduction, $FeCl_3$ (1 mM final concentration) was added in five increments every 5 min, and the solution was incubated for 30 min. A 50 mM sodium selenide (Se^{2-}) stock was generated by dissolving 8 mg solid sodium selenite (Na_2SeO_3) in 1 mL 500 mM DTT solution and incubating it for 15 min at room temperature. The selenide solution was added in five increments every 30 min (1 mM final concentration), and the reaction was incubated on ice overnight. The following day, precipitation was removed by centrifugation at 45,000 × g for 10 min and the supernatant was concentrated to 2 mL using an Amicon cecntrifugal filter with a 10 kDa molecular weight cutoff. Aggregates and non-specifically bound molecules were removed by applying the reaction to a HiPrep 16/60 Sephacryl HR S-200 column (GE Healthcare) equilibrated in storage buffer (flow-rate of 0.5 mL/min). For the ^{57}Fe–Se reconstituted apo NfuA, an identical procedure was followed, with the exception that $^{57}FeCl_3$ was used.

Synthesis of selenolipoyllysyl-peptide product standard for LC-MS.

A disodium diselenide solution (1 M in DMF) was prepared according to a previously reported procedure (23). Disodium diselenide is oxygen sensitive, so all the reactions were performed in degassed solvent. To accomplish this, a solution of 6,8-dichlorooctanoic acid (1.1 g, 5.0 mmol, 1 equiv) in DMF (10 mL) in a 50 mL Schlenk flask was thoroughly frozen by liquid nitrogen, followed by vacuum for 10 s to remove the residual air in the flask. The solution in the Schlenk flask was thawed thoroughly using a warm water bath. This procedure was repeated a total of three times. The disodium diselenide solution (10.0 mL, 10.0 mmol, 2.0 equiv) was added to the resulting degassed solution and the resulting reaction mixture was stirred at room temperature overnight. After completion, the reaction mixture was diluted with ethyl acetate (150 mL) and

washed thoroughly with water. The organic layer was concentrated *in vacuo*, and the resulting residue was purified on a silica gel column (dichloromethane : methanol = 30:1), giving 1.0 g product as a brown solid in a 67% yield. The product was analyzed using an LC-MS scan method in negative ion mode. Once synthesized, the selenolipoic acid was shipped to Proimmune Ltd. (Oxford, UK) to custom synthesize a selenolipoyl-peptide standard for LC-MS (Glu-Ser-Val-[N^6-selenolipoyl]Lys-Ala-Ala-Ser-Asp).

Synthesis of $^{57}FeCl_3$.

Approximately 142 mg $^{57}Fe_2O_3$ (Cambridge Isotopes) was placed in a small vial and dissolved in 2.8 mL 5 M HCl in a Coy anaerobic chamber. 1.2 mL oxygen-free distilled and deonized water (ddH_20) was added to the solution, and the vial was tightly sealed. The reaction was placed in a small crystallization dish filled with silicon oil and placed on a heat block within the glovebox. The vial was submerged in the oil, which was heated to 70 °C and incubated at that temperature for ~16 h. The following day, the concentration (~400 mM) was determined by a colorimetric procedure for iron analysis (22). The solution was stored in the anaerobic chamber until its use.

Mössbauer Cluster Transfer.

The regeneration of the auxiliary cluster of *E. coli* LipA was analyzed using Mössbauer spectroscopy. An *E. coli* LipA reaction was performed in a Coy anaerobic chamber containing 250 µM native LipA isolated with natural abundance iron, 400 mM octanoyl peptide substrate (Glu-Ser-Val-[N^6-octanoyl]Lys-Ala-Ala-Ser-Asp), 0.5 mM SAH nucleosidase, and 1 mM SAM to a total volume of 1 mL, in Buffer A (100 mM HEPES, pH 7.5, 300 mM KCl, 15% glycerol, and 1 mM TCEP). The reaction was initiated by the addition of 2 mM sodium dithionite and proceeded at room temperature for 120 min. The reaction was then buffer exchanged using a NAP-10 column

equilibrated in Buffer A to remove reaction components and quench the reaction. After gel filtration, 3.5 eq. ^{57}Fe NfuA was added to native LipA and incubated for 15 min. at room temperature. The mixture was then applied to a column containing Ni-NTA resin equilibrated in Buffer B (100 mM HEPES, pH 7.5, 300 mM KCl, 10 mM BME, and 15% glycerol). The column was washed with Buffer C (100 mM HEPES, pH 7.5, 500 mM KCl, 45 mM Imidazole, 10 mM BME, and 15% glycerol). The flow-through (containing native LipA) was collected and concentrated using a tightly sealed 10 kDa centricon., and a M*össbauer sample containing approximately 1 mM total ^{57}Fe (~250* µM LipA) was prepared in the anaerobic chamber for subsequent analysis. A second sample containing ^{57}Fe NfuA before the cluster transfer was also prepared to a final concentration of 1 mM *total ^{57}Fe (~500* µM NfuA). SDS-PAGE analysis of the flow-through and elution was performed to ensure that the two proteins were successfully separated.

Generation of [3Fe-4S]^{0} Intermediate.

An *E. coli* LipA reaction (1 mL total volume) containing 350 µM native LipA isolated with natural abundance iron, 450 octanoyl peptide substrate (Glu-Ser-Val-[N^6-octanoyl]Lys-Ala-Ala-Ser-Asp), 0.5 mM SAH nucleosidase, and 1 mM SAM in Buffer A (100 mM HEPES, pH 7.5, 300 mM KCl, 15% glycerol, and 1 mM TCEP) was performed in a Coy anaerobic chamber. The reaction was initiated by the addition of 2 mM sodium dithionite and proceeded at room temperature for 120 min. The reaction was quenched and reaction components were removed by buffer exchanging the reaction into Buffer B (100 mM HEPES, pH 7.5, 300 mM KCl, 10 mM BME, and 15% glycerol) using a NAP-10 column. LipA (post-reaction) was then incubated with 3.5 eq. ^{57}Fe NfuA at room temperature for 15 min. A column containing Ni-NTA resin was equilibrated in Buffer B. The LipA/NfuA reaction was then applied to the column. Once loaded, the column was washed with Buffer C (100 mM HEPES, pH 7.5, 500 mM KCl, 45 mM Imidazole,

10 mM BME, and 15% glycerol). The flow-through, containing LipA was collected and concentrated using a 10 kDA molecular weight cutoff centricon. The concentration of LipA post-cluster transfer was determined via the Bradford method. A new reaction (800 µL total volume) was containing 230 µM LipA post-cluster transfer, 400 µM 8,8,8-deutero-octanoyl peptide substrate, and 1 mM SAM in Buffer A. The reaction was initiated with 2 mM dithionite and proceeded for 60 min. at room temperature. After 60 min., the reaction was concentrated to ~400 µL using 10 kDA molecular weight cutoff spin centricons in the anaerobic chamber. A Mössbauer sample was then prepared without further chromatography.

Analysis of E. coli LipA post reaction with [4Fe-4Se] loaded E. coli NfuA.

An *E. coli* LipA reaction (320 μL total volume) containing 350 µM native LipA isolated with natural abundance iron, 1800 octanoyl peptide substrate (Glu-Ser-Val-[N^6-octanoyl]Lys-Ala-Ala-Ser-Asp), 1300 µM *E. coli* NfuA reconstituted with [^{57}Fe-4Se] cluster, 0.5 mM SAH nucleosidase, and 1 mM SAM in Buffer A (100 mM HEPES, pH 7.5, 300 mM KCl, 15% glycerol, and 1 mM TCEP) was performed in a Coy anaerobic chamber. Mössbauer sample NfuA22 was made as an unreacted control. Mössbauer sample NfuA23 was made using identical conditions as described for NfuA22, with the exception that the reaction was initiated using 2 mM dithionite and proceeded to react for 2.5 hr at room temperature before flash-freezing in liquid nitrogen without further chromatography.

For Mössbauer sample NfuA24, an *E. coli* LipA reaction (640 μL total volume) containing 350 µM native LipA isolated with natural abundance iron, 1800 octanoyl peptide substrate (Glu-Ser-Val-[N^6-octanoyl]Lys-Ala-Ala-Ser-Asp), 1300 µM *E. coli* NfuA reconstituted with [^{57}Fe-4Se] cluster, 0.5 mM SAH nucleosidase, and 1 mM SAM in Buffer A (100 mM HEPES, pH 7.5, 300 mM KCl, 15% glycerol, and 1 mM TCEP) was performed in a Coy anaerobic chamber. The reaction was initiated with the addition of 2 mM dithionite and proceeded to react for 2.5 hr at room

temperature. At t=2.5 hr, the reaction was quenched and reaction components were removed by buffer exchanging the reaction into Buffer B (100 mM HEPES, pH 7.5, 300 mM KCl, 10 mM BME, and 15% glycerol) using a NAP-10 column. A column containing Ni-NTA resin was equilibrated in Buffer B. The LipA/NfuA reaction was then applied to the column. Once loaded, the column was washed with Buffer C (100 mM HEPES, pH 7.5, 500 mM KCl, 45 mM Imidazole, 10 mM BME, and 15% glycerol). The flow-through, containing LipA was collected and concentrated using a 10 kDA molecular weight cutoff centricon. The concentrated protein was gel-filtered into Buffer A using a Nick column. The concentration of LipA protein was then re-determined using the Bradford method, and sample NfuA24 was prepared (final concentration of sample ~340 μM).

For Mössbauer sample NfuA25, an *E. coli* LipA reaction (320 μL total volume) containing 450 μM native LipA isolated with natural abundance iron, 1800 octanoyl peptide substrate (Glu-Ser-Val-[N^6-octanoyl]Lys-Ala-Ala-Ser-Asp), 990 μM *E. coli* NfuA reconstituted with [^{57}Fe-4Se] cluster, 0.5 mM SAH nucleosidase, and 1 mM SAM in Buffer A (100 mM HEPES, pH 7.5, 300 mM KCl, 15% glycerol, and 1 mM TCEP) was performed in a Coy anaerobic chamber. The reaction was initiated with the addition of 2 mM dithionite and proceeded to react for 2.5 hr at room temperature. Sample NfuA25 was made without further chromatography.

Analysis by Mössbauer Spectroscopy.

Mössbauer spectra were recorded on a spectrometer from SEE Co. (Edina, MN) equipped with a Janis (Woburn, MA) SVT-400 variable-temperature cryostat. An external magnetic field of 53 mT was applied parallel to the γ radiation. The reported isomer shifts were referenced relative to the centroid of the spectrum of α-iron metal recorded at room temperature. Simulations of the Mössbauer spectra were carried out using the WMOSS spectral analysis software from SEE Co. (www.wmoss.org; Edina, MN).

Enzyme Reactions.

Reactions were performed in an anaerobic chamber containing <1 ppm O_2. Reactions contained either 15 µM *E. coli* LipA only (control) or 15 µM *E. coli* LipA in the presence of 600 µM [4Fe–4Se]-loaded *E. coli* NfuA. Additional reaction components included 600 µM octanoyl peptide substrate analogue (Glu-Ser-Val-[N^6-octanoyl]Lys-Ala-Ala-Ser-Asp), 0.5 µM SAH nucleosidase, and 1 mM SAM. The reaction was initiated by addition of 2 mM (final concentration) sodium dithionite and quenched at various times in a final concentration of 100 mM H_2SO_4 containing 20 µM peptide internal standard (Pro-Met-Ser-Ala-Pro-Ala-Arg-Ser-Met). The quenched reactions were removed from the anaerobic chamber and centrifuged at 14,000 × g for 30 min. The supernatant was loaded into autosampler vials and subsequently analyzed by LC-MS. Products were separated on an Agilent Technologies Zorbax Rapid Resolution Eclipse Plus C18 column (2.1 × 50mm 1.8 micron) equilibrated in 92% solvent A (0.1% formic acid, pH 2.6) and 8% solvent B (acetonitrile). A gradient of 8-25% solvent B was applied from 0-0.5 min followed by 25-27% B from 0.5-2 min before returning back to 8% B from 2-3 min. The column was allowed to re-equilibrate for 1 min under the initial conditions before subsequent sample injections. A constant flow-rate of 0.300 mL/min was maintained throughout the procedure. A scan method was used to qualitatively monitor the formation of selenolipoic acid over time by sweeping from 1080-1100 *m/z* values. The external peptide standard, lipoyl peptide, and selenolipoyl peptide were detected by MS2 selected-ion monitoring at *m/z* ratios 474.4, 996.5, and 1090.3, respectively. Detection of each species was performed using electrospray-ionization in positive mode (ESI^+) with the following parameters: a nitrogen gas temperature of 350 °C with a flow-rate of 5 L/min, a nebulizer pressure of 45 PSI, and a capillary voltage of 4000 V. The fragmentor voltage was optimized for each compound and was determined to be 112 V for the external standard peptide and 208 V for the lipoyl and selenolipoyl peptides.

Results

E. coli NfuA can coordinate a [4Fe–4Se] Cluster.

We recently discovered that *E. coli* NfuA, an intermediate FeS cluster carrier protein, targets *E. coli* LipA and regenerates its auxiliary [4Fe–4S] in a non-rate-limiting step in catalysis (14). However, the details of how NfuA is targeted to LipA and the mechanism of Fe/S cluster transfer or regeneration are largely unknown. Unexpectedly, we discovered that in the presence of NfuA, all four sulfide ions in the auxiliary cluster of LipA can be incorporated into the organic substrate, a finding that differs from what is observed in the absence of NfuA, wherein only one equivalent of the lipoyl cofactor is made per equivalent of LipA polypeptide, which leaves four Fe^{2+} and two S^{2-} ions to be released into solution. To address the mechanism of cluster transfer from NfuA to LipA, we sought to use a selenium-labeling strategy, which might allow for the observation of intermediates in the future via X-ray crystallography. Selenium is just beneath sulfur in the periodic table and exhibits many of the same characteristics of sulfur in a biological context. For example, selenocysteine (24), selenomethionine (25), and Se-adenosylselenomethionine (26) all function similarly to their sulfur-containing counterparts, albeit with slightly different properties (27). Moreover, selenium has been incorporated into FeS clusters (e.g. [4Fe–4Se] and [2Fe–2Se]), where the protein containing the selenium-labeled cluster was able to perform its typical reaction (16,27)

To determine whether *E. coli* NfuA can transfer a selenium-containing cluster to *E. coli* LipA during turnover, NfuA was first overproduced and isolated in its apo form and then chemically reconstituted with iron and selenide to contain a [4Fe–4Se] cluster. As shown in **Figure**

4-1, the UV-visible spectrum of the reconstituted *E. coli* NfuA protein is consistent with incorporation of a [4Fe–4Se] cluster, containing a broad shoulder at 320 nm and distinct features in the 400 nm region. Iron analysis revealed that the protein contained 2.2 ± 0.1 iron ions per NfuA monomer, indicative of a [4Fe–4Se] cluster coordinated at the NfuA dimer interface as has been previously established (28,29). To confirm the presence of a [4Fe–4Se] cluster and ensure robust cofactor incorporation following the chemical reconstitution procedure, a [4^{57}Fe–4Se] was also reconstituted into apo NfuA for analysis by Mössbauer spectroscopy using $^{57}FeCl_3$ as an iron source. Mössbauer analysis of this NfuA protein, shown in **Figure 4-2,** indicated the presence of two quadrupole doublets with δ = 0.47 mm/s and ΔE_Q = 1.16 mm/s; and δ = 1.28 mm/s; ΔE_Q = 2.41 mm/s accounting for 87% and 13% of the total intensity. The major contribution is attributed to the $[4Fe\text{-}4Se]^{2+}$ cluster, shown in red. These parameters closely relate to the δ = 0.45 mm/s and ΔE_Q = 1.13 mm/s previously reported for the $[4Fe–4S]^{2+}$ coordinated by *E. coli* NfuA (28).

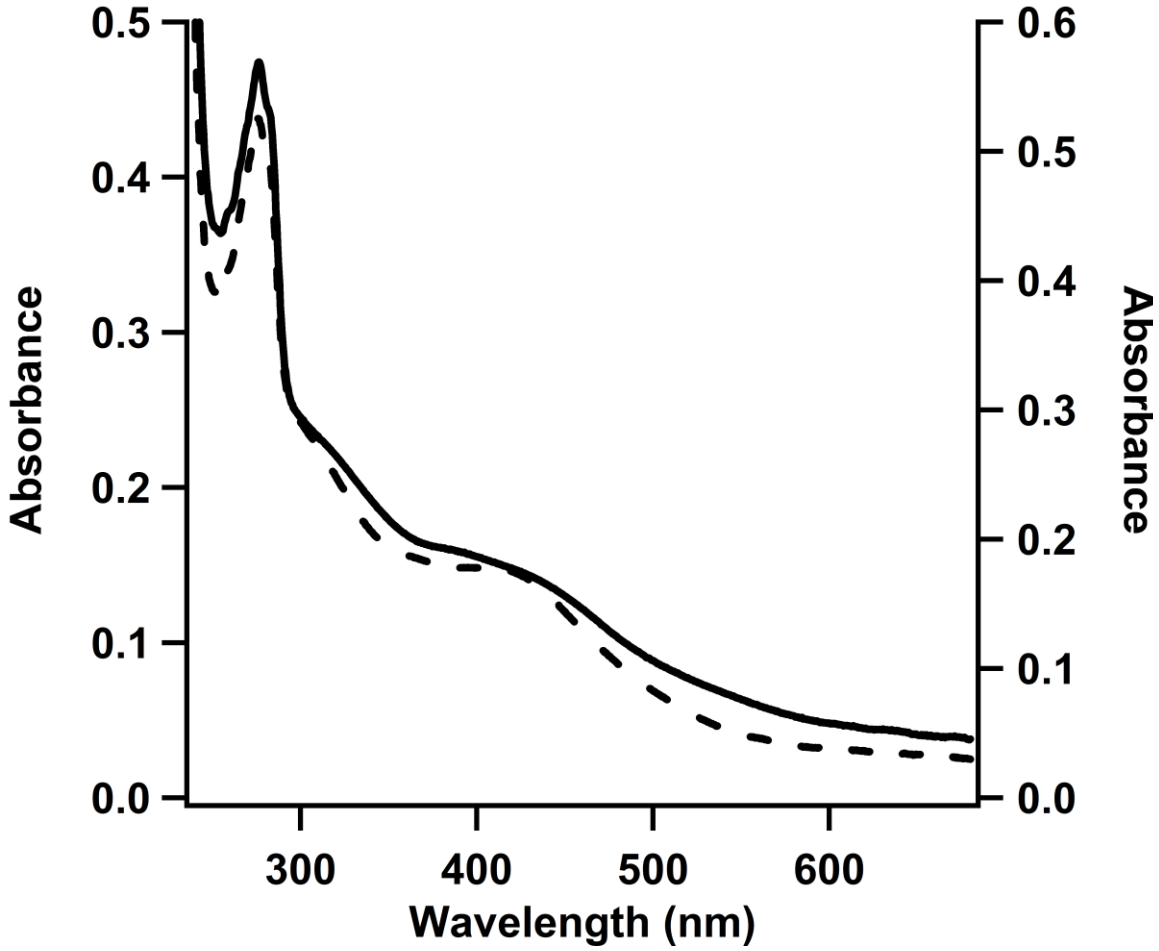

Figure 4-1: UV-visible spectrum of 15 µM Apo reconstituted [4Fe–4Se] *E. coli* NfuA (solid trace) and 15 µM [4Fe–4S] *E. coli* NfuA (dashed trace)**.**

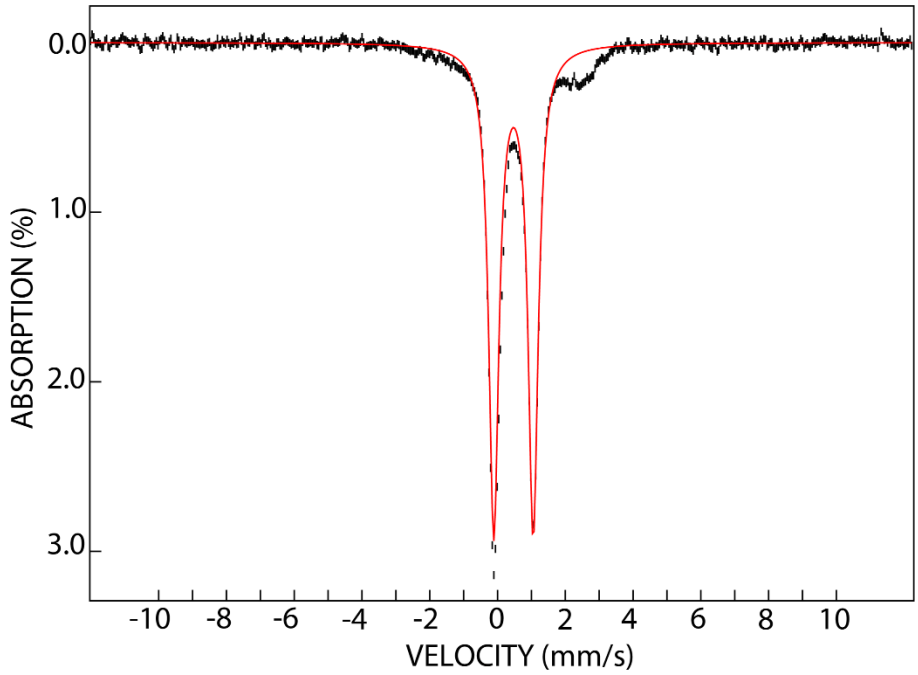

Figure 4-2: Mössbauer analysis of apo-reconstituted [4Fe–4Se] *E. coli* NfuA. 4.2 K Mössbauer spectrum of NfuA reconstituted with $^{57}FeCl_3$ and selenide recorded in an externally applied field of 53 mT oriented parallel to the gamma beam (vertical bars). The contribution of the quadrupole doublet assigned to the $[4Fe\text{-}4Se]^{2+}$ cluster (δ = 0.47 mm/s and ΔE_Q = 1.16 mm/s; 87 % of total intensity) is shown red.

E. coli LipA catalyzes formation of selenolipoic acid.

E. coli LipA consumes its [4Fe–4S] auxiliary cluster to use as a sulfur source for production of the lipoyl cofactor. In *in vitro* reactions wherein NfuA is omitted, only one equivalent of the lipoyl cofactor is produced, which requires the mobilization of only two of the sulfide ions and the elimination of one iron ion from the auxiliary cluster. The state and fate of the remaining iron and sulfide is largely unknown. Our previous studies revealed that in the presence of NfuA, one LipA polypeptide can produce two equivalents of lipoic acid, requiring the mobilization of all four of the sulfide ions in the auxiliary cluster (14). To investigate this observed effect in greater detail, we used [4Fe–4Se]-containing NfuA to reconstitute a [4Fe–4Se] cluster on LipA for use in reactions.

In a reaction containing 15 μM *E. coli* LipA and 600 μM [4Fe–4Se]-containing *E. coli* NfuA, as well as all other required reaction components, product analysis by mass spectrometry using single ion monitoring (SIM) reveals the time-dependent formation of a selenolipoyl product **(Figure 4-3, Panel B)** that exhibits a distinct isotopic distribution pattern that is nearly identical to that of a chemically synthesized selenolipoyl standard **(Figure 4-3, Panel A).** Selenium consists of six stable isotopes: ^{74}Se (0.86%), ^{76}Se (9.23%), ^{77}Se (7.60%), ^{78}Se (23.69%), ^{80}Se (49.80%), and ^{82}Se (8.82%). The reaction was then repeated using a single-ion monitoring (SIM) LC-MS method wherein the synthesized selenolipoyl peptide standard and a lipoyl peptide standard at natural abundance were used to quantify the reaction products. In a reaction containing 15 μM *E. coli* LipA only, ~10 μM unlabeled lipoyl product is observed **(Figure 4-3, Panel C),** consistent with the presence of sulfide at natural abundance on the protein and the fact that only one turnover is observed in the absence of NfuA**.** However, in the presence of 600 μM [4Fe–4Se]-containing *E. coli* NfuA, *E. coli* LipA produces ~22 μM unlabeled lipoyl product—or about two-fold more. This result is consistent with our previous report that *E. coli* LipA can use all four of the sulfide ions in its auxiliary cluster to produce two equivalents of lipoic acid in the presence of *E. coli* NfuA.

When the same reaction is monitored for the selenolipoyl peptide product, no selenolipoyl product is observed in the LipA only control (i.e. no NfuA present), as expected **(Figure 4-3, Panel D).** By contrast, when 600 μM [4Fe–4Se] loaded *E. coli* NfuA is included in the reaction, the selenolipoyl peptide product is observed, indicating that *E. coli* NfuA can transfer a [4Fe–4Se] cluster to *E. coli* LipA, which it can subsequently use to form selenolipoic acid. Surprisingly, exactly only one equivalent of the selenolipoyl product is observed in this reaction, despite the presence of a vast excess (40-fold) of [4Fe–4Se]-containing NfuA in the reaction. This observation is in stark contrast to the robust catalysis observed when [4Fe–4S]-containing *E. coli* NfuA is included in the reaction (14,30). Additionally, a pronounced lag is observed in the formation of selenolipoyl product, compared to the burst observed in the formation of lipoyl peptide **(Figure 4-**

13, compare Panels C and D closed circles). The Mössbauer analysis of the [4Fe–4Se]-containing NfuA indicates nearly full cofactor incorporation, suggesting that the reaction is not limited by the cofactor availability.

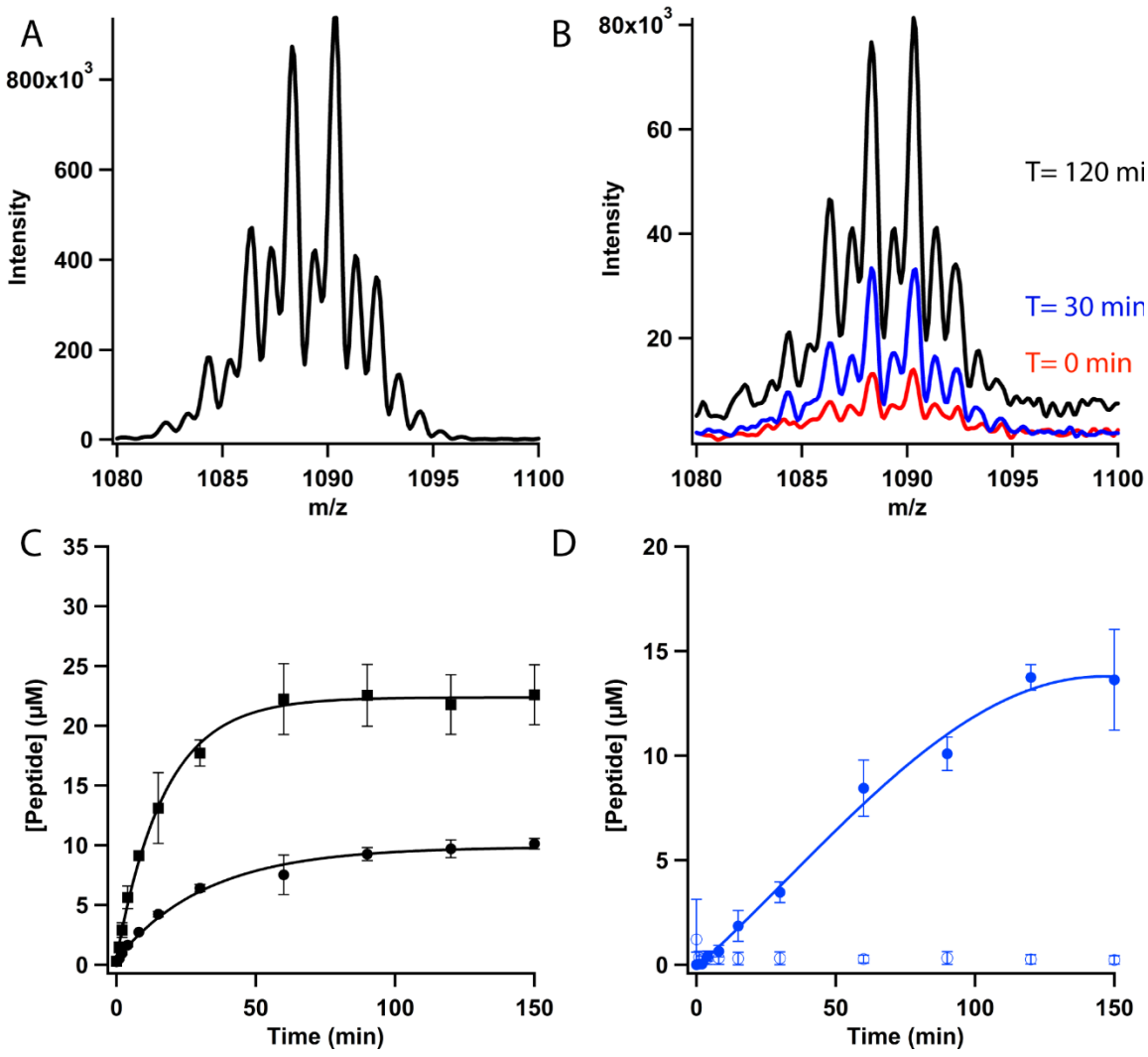

Figure 4-3: **Formation of the selenolipoyl product.** (A) Mass spectrum of synthesized selenolipoyl-peptide standard (500 μM). (B) LipA-catalyzed formation of selenolipoyl-peptide product. The reaction included 15 μM *E. coli* LipA, 600 μM [4Fe–4Se]-containing *E. coli* NfuA, 600 μM octanoyl-peptide substrate analogue (Glu-Ser-Val-[N^6-octanoyl]Lys-Ala-Ala-Ser-Asp), 0.5 μM SAH nucleosidase, and 1 mM SAM. The reaction was initiated with sodium dithionite (2 mM final concentration, and was quenched with H_2SO_4 at a final concentration of 100 mM .(C) Time-dependent formation of lipoyl product at natural abundance. Reaction included either 15 μM LipA only control (closed circles) or 15 μM LipA, 600 μM [4Fe–4Se]-containing *E. coli* NfuA, 600 μM octanoyl-peptide substrate analogue (Glu-Ser-Val-[N^6-octanoyl]Lys-Ala-Ala-Ser-Asp), 0.5 μM SAH nucleosidase, and 1 mM SAM. Error bars represent the mean ± standard deviation of three replicates. (D) Selenolipoyl product formation over time. Analysis of the same reaction shown in Panel C, instead monitoring for formation of the selenolipoyl product. Error bars represent the mean ± standard deviation of three replicates.

Cluster Transfer from E. coli NfuA to E. coli LipA.

The recent finding that *E. coli* NfuA can regenerate the auxiliary cluster of *E. coli* LipA after each round of turnover expands our understanding of the biosynthesis of the lipoyl cofactor, and more generally, how sulfurs can be attached to completely unactivated carbon centers. However, significant gaps with respect to the detailed molecular mechanism by which the auxiliary cluster is replenished still remain. In our previous work, we employed an isotopic labeling strategy to show that LipA catalyzes the formation of the lipoyl cofactor using sulfur derived from the cluster on *E. coli* NfuA after sulfide ions in its own auxiliary cluster have been consumed. However, this experiment did not conclusively exclude the possibility of a repair mechanism, wherein the sulfide ions from NfuA could be used to rebuild the auxiliary cluster using LipA's remaining iron ions in a fashion that does not involve intact or partial cluster transfer. To test this hypothesis, we used Mössbauer spectroscopy to assess the state of the cluster on LipA after its reaction with NfuA. Native *E. coli* LipA (i.e. LipA without a hexahistidine tag) was isolated and allowed to react to completion. Following its incubation with hexahistidine-tagged and ^{57}Fe-containing NfuA, LipA and NfuA were separated using a Ni-NTA column. Samples of ^{57}Fe NfuA before the cluster transfer

and LipA post-cluster transfer were analyzed by Mössbauer Spectroscopy. As shown in **Figure 4-4** (top), the spectrum of ^{57}Fe NfuA revealed a dominant quadrupole doublet feature with an isomer shift of 0.45 mm/s and quadrupole splitting value of 1.10 mm/s, indicative of a $[4Fe\text{-}4S]^{2+}$ cluster and representing 93% of the total iron. The post-cluster transfer spectrum of LipA (bottom) also was dominated by a quadrupole doublet $[4Fe\text{-}4S]^{2+}$ cluster with an isomer shift of 0.46 mm/s and quadruple splitting 1.17 mm/s, also characteristic of a $[4Fe\text{-}4S]^{2+}$ cluster, and representing 80% of the total iron. The post-cluster transfer LipA spectrum had another feature with an isomer shift of 0.32 mm/s and quadruple splitting of 0.66 mm/s accounting for the remaining 20% of the total iron, which may be small amounts of $[2Fe\text{-}2S]^{2+}$ cluster, though this feature does not appear to grow in when comparing the spectra before and after cluster transfer. As a result, this feature is not a direct result of the cluster transfer reaction. Ultimately, this experiment did not give evidence for a novel intermediate, though it does show cluster transfer from *E. coli* NfuA to *E. coli* LipA.

Generation of $[3Fe\text{-}4S]^{0}$ Intermediate.

In early studies by Cicchillo, *et al.*, a species consistent with a single sulfur insertion was observed in LipA reactions when using an [octanoyl-$^{2}H_{15}$] H protein substrate (6). Consistent with this observation, ~50% of the expected concentration of 5′-dA was formed when using the [octanoyl-$^{2}H_{15}$] H protein substrate compared to the substrate at natural abundance. Further work by Douglas, *et al.*, demonstrated that deuterium incorporation at the C8 position of an N^{6}-(octanoy)l-lysyl residue within a tripeptide substrate significantly hindered formation of the lipoyl product and established that sulfur insertion at C6 occurs first and is followed by sulfur insertion at C8 (8). Collectively, these observations suggested a strategy for generating large quantities of a potential intermediate in the LipA reaction after one sulfur insertion has taken place using either an 8,8,8-d_3-octanoyl substrate or 1 equivalent of SAM in the reaction. Mössbauer spectroscopy with

complementary biochemical techniques provided evidence for the formation of a [3Fe–3S–1(6-thiooctanoyl)LCP] cluster, in which the organic substrate is cross-linked at C6 to a sulfide ion in a [3Fe-4S] cluster. Moreover, biochemical studies showed that this cross-linked intermediate is both chemically and kinetically competent to proceed to product (11). Further, the intermediate was captured using X-ray crystallography, verifying what had been described by Mössbauer spectroscopy (13).

Upon showing cluster transfer from NfuA to LipA, we then tested whether LipA could then use this [4Fe-4S]-containing cluster to form the aforementioned monothiolated intermediate. In this experiment, native LipA isolated with natural abundance iron was first reacted to completion to remove its auxiliary cluster. Reacted LipA was then incubated with ^{57}Fe-labeled NfuA that contained a hexahistidine tag. After incubation, the proteins were separated by IMAC using Ni-NTA resin. LipA, which was not tagged, did not adhere to the resin and was collected in the flow-through. This protein was then reacted with the 8,8,8-d_3-octanoyl peptide substrate used in previous studies to arrest the reaction after the first sulfur insertion (6,8,31). The state of the auxiliary cluster was then analyzed using Mössbauer spectroscopy. The Mössbauer spectra from this experiment are shown in **Figure 4-5,** and were analyzed using the previously published parameters (11). Comparison of spectra recorded in zero-field and small applied field (53 mT) reveal the broadening of features in the presence of a weak field, indicative of the [3Fe-4S]^0-like cluster **(Figure 4-5, Panel A).** By contrast, features associated with a [4Fe−4S]$^{2+}$ cluster should remain unchanged in the presence of a small field. The behavior of the 3Fe cluster intermediate is apparent in the [0−53 mT] difference spectrum **(Figure 4-5, Panel B).** The zero-field reference spectrum of the LipA [3Fe-4S]^0 cluster is shown in **Figure 4-5, Panel C.** The green and blue doublets represent the Fe^{3+} site (7%) and the $Fe_2^{2.5+}$ pair (14%) of the [3Fe-4S]^0 cluster, respectively, simulated using the published parameters. The field strength dependence, the characteristic [0−53 mT] difference spectrum, as well as the 2:1 ratio for the Fe^{3+} site and the $Fe_2^{2.5+}$ pair together support the assignment

of this species as the $[3Fe\text{-}4S]^0$-like cluster previously characterized in the LipA reaction (11). However, due to the harsh sample preparation conditions and the complexity of the system involving three [4Fe-4S] clusters, the data could be improved with sample optimization. The amount of $[3Fe\text{-}4S]^0$ cluster only accounts for ~21% of the total iron, whereas an additional 21% is associated with a valence-delocalized $[4Fe\text{-}4S]^{2+}$ cluster which could be due to either unreacted auxiliary cluster or to transfer of the ^{57}Fe -labeled cluster from NfuA into the RS cluster site on LipA. Indeed, a surprisingly high amount of site-differentiated $[4Fe\text{-}4S]^{2+}$ was observed. In future experiments, the use of chemically reconstituted LipA may decrease the amount of cluster shuffling by starting with LipA that has the highest cofactor incorporation as possible. Additionally, the conditions of the experiment could be altered to avoid partial breakdown of the clusters during sample preparation, though the reaction is slow and occurs at room temperature, so it is unclear how much this can be minimized.

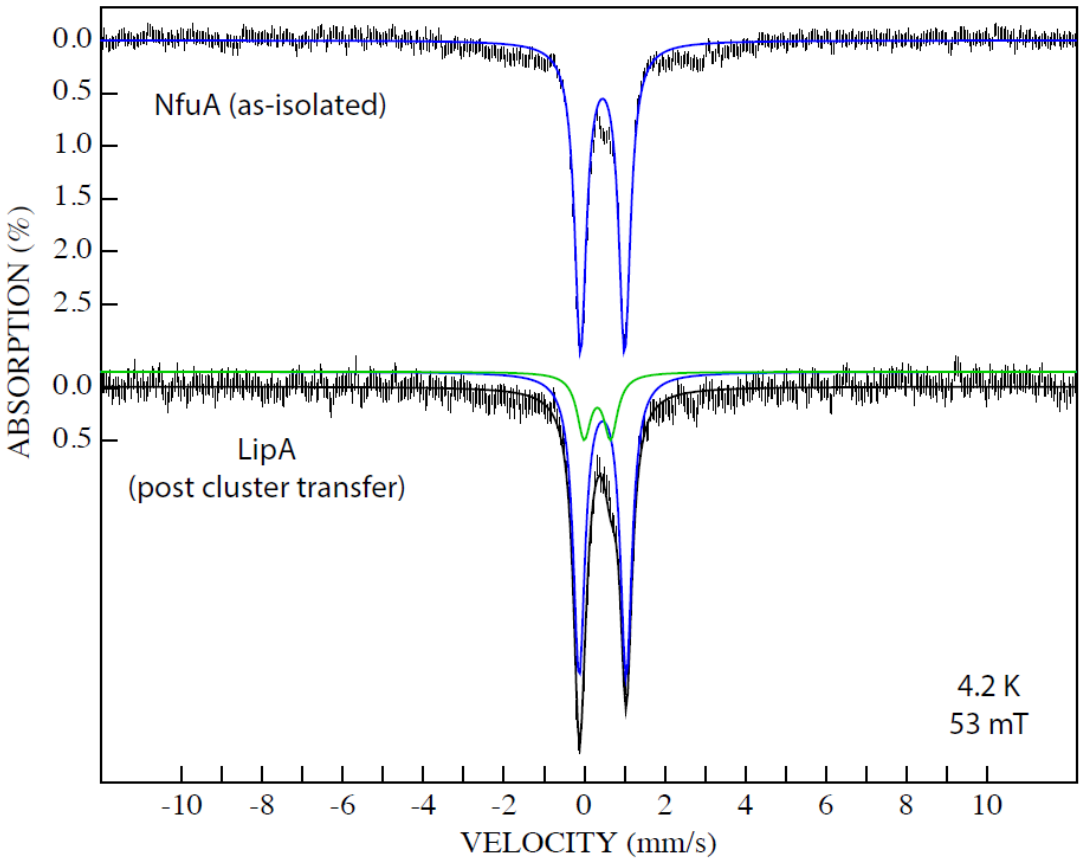

Figure 4-4: **Mössbauer Spectroscopic Characterization of Cluster Transfer from NfuA to LipA.** 4.2 K/ 53 mT spectrum of as-isolated *E. coli* NfuA (top). 4.2 K/ 53 mT spectrum of *E. coli* LipA post-cluster transfer (bottom). The features associated with $[4Fe\text{-}4S]^{2+}$ cluster are shown in blue (93% total iron in top spectrum, 80% total iron in bottom spectrum).

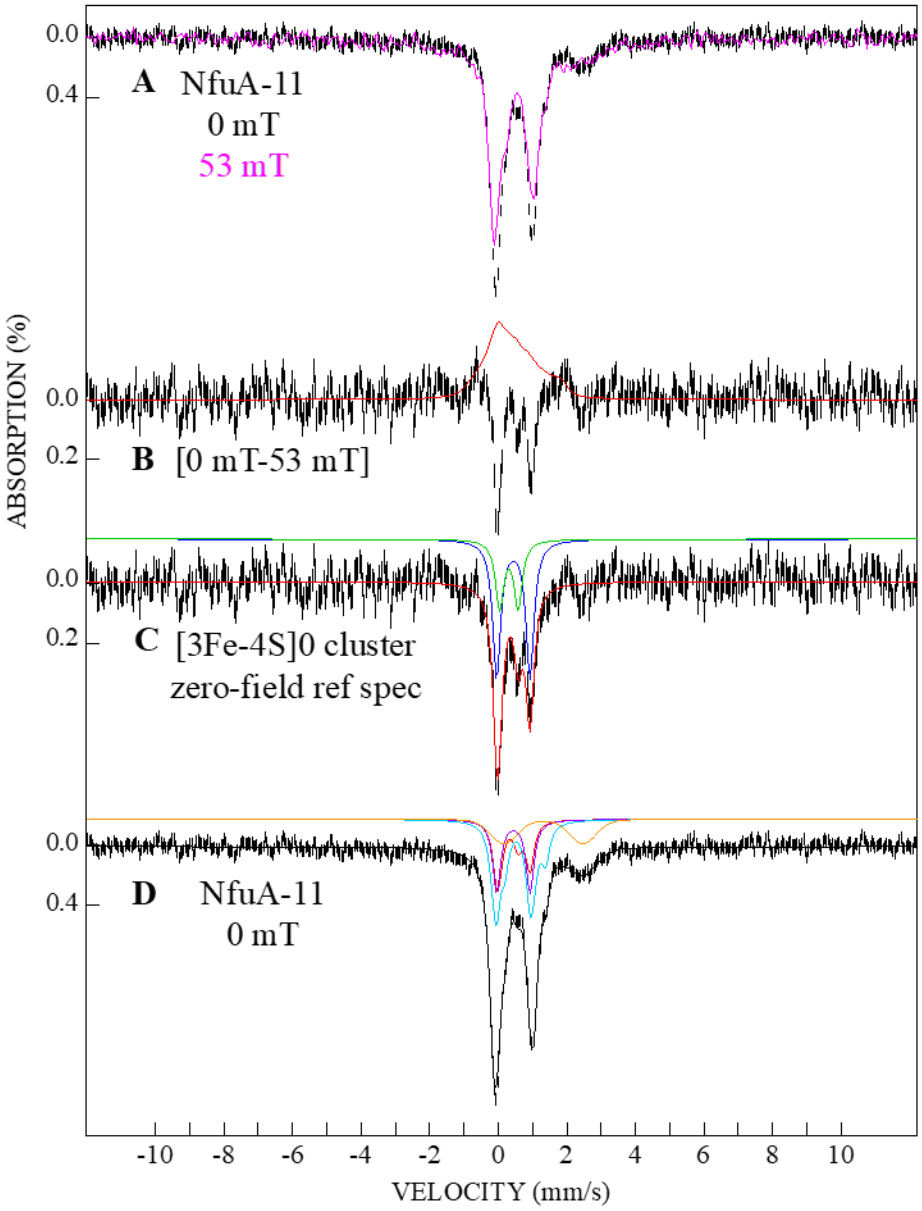

Figure 4-5: **Mössbauer Spectroscopic Characterization of [3Fe-4S]^0 Intermediate Following Cluster Transfer by NfuA.** 4.2K Mössbauer spectra (A) Comparison of spectra recorded in zero field (vertical bars) and 53mT applied magnetic field (pink line). (B) Difference spectrum generated by subtracting the 53-mT spectrum from that of zero-field spectrum. The red line is theoretical simulation of LipA [3Fe-4S]^0 cluster using the published parameters, scaled to -21% of total ^{57}Fe absorption. (C) The zero-field reference spectrum of the LipA [3Fe-4S]^0 cluster in sample NfuA11. The green and blue doublets represent the Fe^{3+} site (7%) and the $Fe_2^{2.5+}$ pair (21%) of the [3Fe-4S]^0 cluster, respectively, simulated using the published parameters. The red line represents the added contribution of the green and blue doublets. (D) Simulation of the zero-field spectrum.

Table 4-1. Parameters used for simulation of spectrum in Figure 4-5.

Species	Parameter		Amount of total ^{57}Fe	Color in figure
$[3Fe\text{-}4Fe]^0$ cluster	Fe^{3+}	$\delta = 0.31$ mm/s $\Delta E_Q = 0.55$ mm/s	21%	red
	$Fe_2^{2.5+}$	$\delta = 0.44$ mm/s $\Delta E_Q = 0.98$ mm/s		
Valence-delocalized $[4Fe\text{-}4S]^{2+}$ cluster	$Fe_2^{2.5+}$	$\delta = 0.45$ mm/s $\Delta E_Q = 1.18$ mm/s	21%	purple
Site-differentiated $[4Fe\text{-}4S]^{2+}$ cluster	$Fe_2^{2.5+}$	$\delta = 0.45$ mm/s $\Delta E_Q = 1.18$ mm/s	41%	Light blue
	Fe^{3+}-like site	$\delta = 0.43$ mm/s $\Delta E_Q = 0.94$ mm/s		
	Fe^{2+}-like site	$\delta = 0.79$ mm/s $\Delta E_Q = 1.19$ mm/s		
Fe^{II}	$\delta = 1.32$ mm/s $\Delta E_Q = 2.31$ mm/s		17%	orange

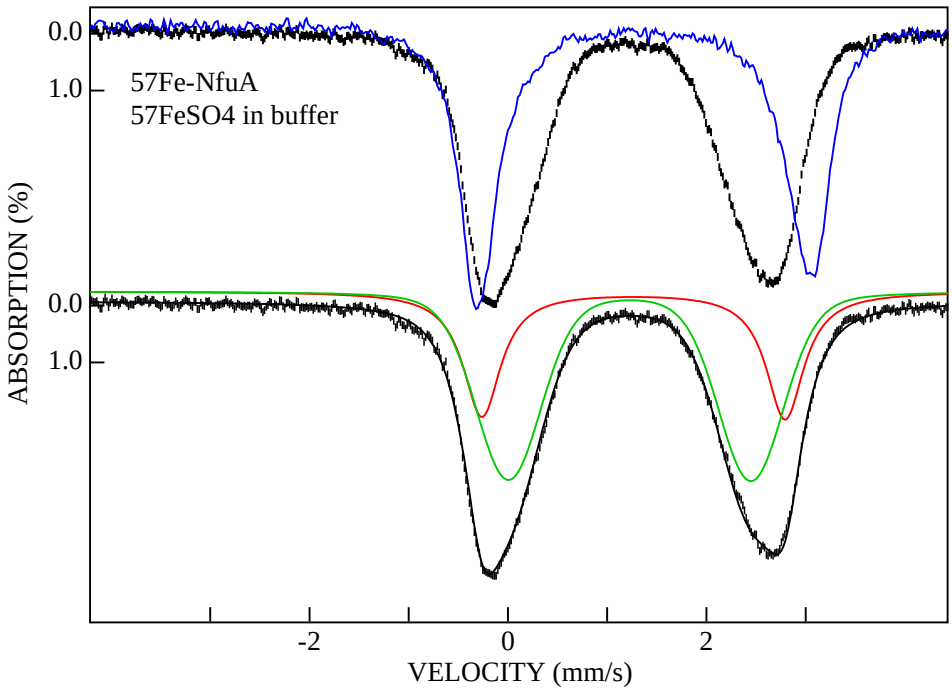

Figure 4-6: **Iron Binding by Apo *E. coli* NfuA.** 4.2K/53mT Mössbauer spectrum of apo NufA after incubation with $^{57}FeSO_4$. (Top panel) Comparison of the spectrum of apo NufA after incubation with $^{57}FeSO_4$ (vertical bars) and that of free $^{57}FeSO_4$ in solution (blue line). (Lower panel) The spectrum of Fe-bound form of NfuA can be analysed as superposition of two quadrupole doublets with the following parameter: δ_1 = 1.23 mm/s ΔE_{Q1} = 2.44 mm/s (66% of total ^{57}Fe absorption, green) and δ_2 = 1.27 mm/s ΔE_{Q2} = 3.06 mm/s (34% of total ^{57}Fe absorption, red). The black line is the added contribution of the two doublets.

Probing iron binding of Apo NfuA.

Labelling strategies using $^{34}S^{2-}$ and selenium have provided evidence of consumption of all four of the sufide ions within the auxiliary cluster of LipA. A remaining question is what is the fate of the residual iron that is liberated upon mobilization of the sulfide ions within the cluster? One possible model is that NfuA fulfills a dual-function in the regeneration of the auxiliary cluster, both reinserting the newly assembled cluster while also trapping the iron that is released. Fe-loaded NfuA could then return to the IscU scaffold where Fe/S clusters are initially assembled and supply the requisite iron. Indeed, the source of iron for assembly of iron sulfur clusters is still debated, and

recent studies have shown that Nfu1 and IscU interact. We have also observed a weak interaction between *E. coli* NfuA and *E. coli* IscU *in vivo* using bacterial two hybrid screening (unpublished). To explore this possibility, we compared a Mössbauer spectra of two samples prepared in tandem: free $^{57}FeSO_4$ in solution and $^{57}FeSO_4$ in the presence of apo *E. coli* NfuA. Comparison of the two spectra revealed significant changes between the spectrum of free iron and that from a sample containing both free iron and apo *E. coli* NfuA **(Figure 4-6, top panel).** The iron-bound form of NfuA **(Figure 4-6, bottom panel)** is broad and can be modeled with two quadrupole doublets with the following parameters: δ_1 = 1.23 mm/s ΔE_{Q1} = 2.44 mm/s (66% of total ^{57}Fe absorption, green line) and δ_2 = 1.27 mm/s ΔE_{Q2} = 3.06 mm/s (34% of total ^{57}Fe absorption, red line), which are typical of high-spin Fe^{II}. Importantly, less than ~10% of Fe^{II} is bound by NfuA, thus revealing that NfuA can bind Fe^{II} tightly. Though preliminary, this observation supports this possible dual-function for NfuA; further experiments are required to probe the possible role of Fe^{II} binding by NfuA during LipA catalysis.

Analysis of E. coli LipA post reaction with [4Fe-4Se]-loaded E. coli NfuA.

Activity assays of *E. coli* LipA performed in the presence of excess [4Fe-4Se] loaded *E. coli* NfuA lead to the surprising observation that *E. coli* LipA can produce only one equivalent of selenolipoyl product, compared to the robust 10-15 turnovers over 150 minutes observed when using sulfur. This observation prompted the characterization of this species using Mössbauer spectroscopy. In the first sample, the *E. coli* LipA reaction (640 μL total volume) contained 350 µM native LipA isolated with natural abundance iron, 1800 octanoyl peptide substrate (Glu-Ser-Val-[N^6-octanoyl]Lys-Ala-Ala-Ser-Asp), 1300 µM *E. coli* NfuA reconstituted with [^{57}4Fe-4Se] cluster, 0.5 mM SAH nucleosidase, and 1 mM SAM in Buffer A (100 mM HEPES, pH 7.5, 300 mM KCl, 15% glycerol, and 1 mM TCEP). The reaction was initiated with the addition of 2 mM dithionite and proceeded to react for 2.5 h at room temperature. At the end of the reaction, LipA

was isolated via affinity chromatography and analyzed using Mössbauer spectroscopy (Sample NfuA24). Analysis of these spectra revealed that an overwhelming majority of the iron in the sample was in the form of $[^{57}4Fe\text{-}4Se]^{2+}$ cluster (approximately 80% of total iron). The [0-53mT] difference spectrum reveals ~11% of the total iron is in the form of $[^{57}3Fe\text{-}4Se]^{0}$ cluster **(Figure 4-7 and Table 4-2)**. The observation that the broadening in a 53-mT magnetic field appears broader than that observed for the $[3Fe\text{-}4S]^{0}$-like native intermediate of LipA suggests that this species could represent a chemically distinct state with a $[3Fe\text{-}4Se]^{0}$-like cluster, possibly 340 cluster. It is conceivable that this complex might have the selenolipoyl product coordinating the 3Fe cluster and that product release is very slow, thus arresting the reaction. The weak absorption at ~2.6 mm/s is likely due to a small amount of high spin ferrous iron.

The reaction conditions were adjusted to reduce the amount of excess NfuA present, such that there is approximately one [4Fe-4Se] cluster on NfuA per LipA protein. In theory, LipA would consume its auxiliary cluster and subsequently receive a $[4^{57}Fe\text{-}4Se]$ cluster from NfuA, rendering NfuA apo/ Mössbauer silent. In the sample preparation, the *E. coli* LipA reaction (320 μL total volume) contained 450 µM native LipA isolated with natural abundance iron, 1800 octanoyl peptide substrate (Glu-Ser-Val-[N^6-octanoyl]Lys-Ala-Ala-Ser-Asp), 990 µM *E. coli* NfuA reconstituted with $[^{57}Fe\text{-}4Se]$ cluster, 0.5 mM SAH nucleosidase, and 1 mM SAM in Buffer A (100 mM HEPES, pH 7.5, 300 mM KCl, 15% glycerol, and 1 mM TCEP) was performed in a Coy anaerobic chamber. The reaction was initiated with the addition of 2 mM dithionite and proceeded to react for 2.5 hr at room temperature. Mössbauer sample NfuA25 was then prepared without further chromatography. Analysis of the spectra for sample NfuA25 again revealed unusually high levels of $[^{57}4Fe\text{-}4Se]^{2+}$ cluster (approximately 50% of total iron). Approximately 16-17% of the total iron is identified as $[^{57}3Fe\text{-}4Se]^{0}$ cluster **(Figure 4-8 and Table 4-3),** whereas 30% ferrous is present ($\delta = 1.27$, $\Delta E_Q = 2.62$).

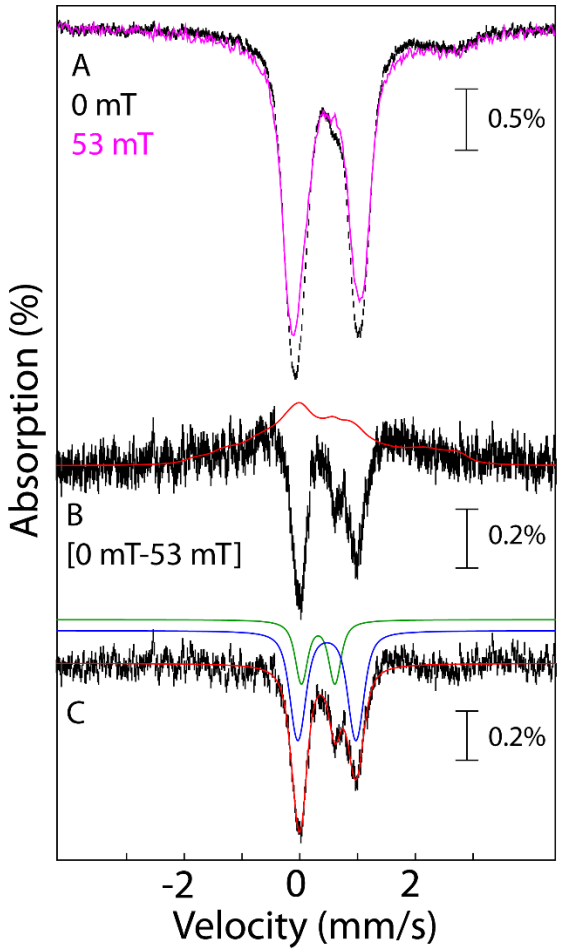

Figure 4-7 Mössbauer Spectroscopic Characterization of [^{57}Fe-4Se] loaded *E. coli* NfuA and *E. coli* LipA Reaction. The *E. coli* LipA reaction (640 μL total volume) contained 350 µM native LipA isolated with natural abundance iron, 1800 octanoyl peptide substrate (Glu-Ser-Val-[N^6-octanoyl]Lys-Ala-Ala-Ser-Asp), 1300 µM *E. coli* NfuA reconstituted with [^{57}Fe-4Se] cluster, 0.5 mM SAH nucleosidase, and 1 mM SAM in Buffer A (100 mM HEPES, pH 7.5, 300 mM KCl, 15% glycerol, and 1 mM TCEP). The reaction was initiated with the addition of 2 mM dithionite and proceeded to react for 2.5 hr at room temperature. LipA was isolated via affinity chromatography and analyzed using Mössbauer spectroscopy (Sample NfuA24). (A) Comparison of spectra recorded in zero field (vertical bars) and 53mT applied magnetic field (pink line). (B) Difference spectrum generated by subtracting the 53-mT spectrum from that of zero-field spectrum. The red line is theoretical simulation of [3Fe-4S]0 cluster using the parameters mentioned in the text, scaled to -11% of total ^{57}Fe absorption using the published parameters except for a smaller ZFS parameter, D = -2.5 cm^{-1}, that results in the greater experimentally observed broadening in a 53-mT magnetic field. (C) The zero-field reference spectrum of the [3Fe-4S]0 cluster in sample NfuA 24 generated by adding 11% of the theoretical 53 mT spectrum of [3Fe-4S]^0 cluster to spectrum B. The green and blue doublets represent the Fe^{3+} site (3.5%) and the $Fe_2^{2.5+}$ pair (7%) of

the [3Fe-4S]0 cluster, respectively, simulated using the parameters mentioned in the text. The red line represents the added contribution of the green and blue doublets.

Table 4-2. Parameters used for simulation of spectrum in Figure 4-7.

Sample	Parameters		Amount of ^{57}Fe	Color
$[3Fe\text{-}4Se]^0$ 0mT	Fe^{3+}	d = 0.31 mm/s DEq = 0.50 mm/s	3.5%	green
	$Fe_2^{2.5+}$	d = 0.46 mm/s DEq = 0.95 mm/s	7%	blue

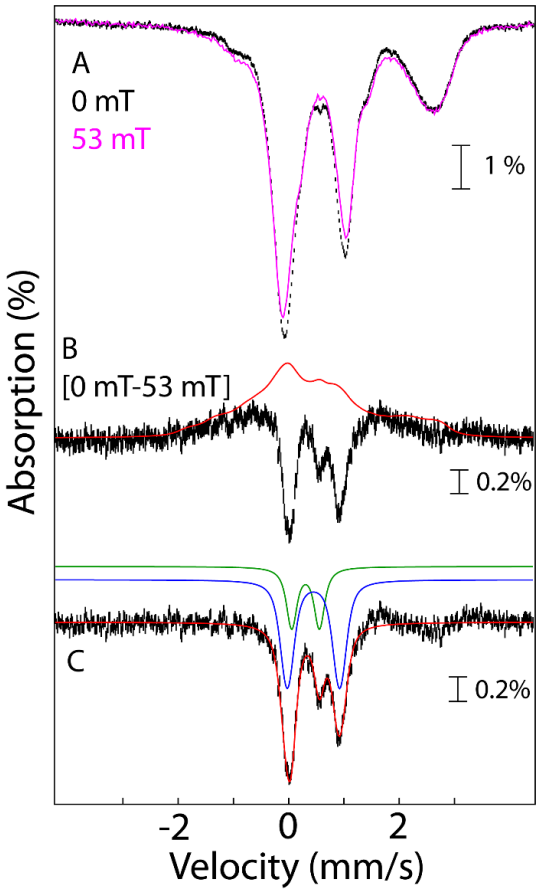

Figure 4-8 Mössbauer Spectroscopic Characterization of [^{57}Fe-4Se] loaded *E. coli* NfuA and *E. coli* LipA Reaction Without Separation. The *E. coli* LipA reaction (320 μL total volume) containing 450 µM native LipA isolated with natural abundance iron, 1800 octanoyl peptide substrate (Glu-Ser-Val-[N^6-octanoyl]Lys-Ala-Ala-Ser-Asp), 990 µM *E. coli* NfuA reconstituted with [^{57}Fe-4Se] cluster, 0.5 mM SAH nucleosidase, and 1 mM SAM in Buffer A (100 mM HEPES, pH 7.5, 300 mM KCl, 15% glycerol, and 1 mM TCEP) was performed in a Coy anaerobic chamber. The reaction was initiated with the addition of 2 mM dithionite and proceeded to react for 2.5 hr at room temperature. Mössbauer sample NfuA25 was prepared without further chromatography. (A) Comparison of spectra recorded in zero field (vertical bars) and 53 mT applied magnetic field (pink line). (B) Difference spectrum generated by subtracting the 53 mT spectrum from that of zero-field spectrum. The red line is theoretical simulation of [3Fe-4S]^0 cluster at 53 mT using the parameters mentioned in the text and using the published parameters except for a smaller ZFS parameter, D = -2.5 cm^{-1}, that results in the greater experimentally observed broadening in a 53-mT magnetic field. (C) The zero-field reference spectrum of the [3Fe-4S]^0 cluster in sample NfuA 25 generated by adding 15% of the theoretical 53 mT spectrum of [3Fe-4S]^0 cluster to spectrum B. The green and blue doublets represent the Fe^{3+} site (5.5%) and the $Fe_2^{2.5+}$ pair (11%) of the [3Fe-4S]^0 cluster, respectively, simulated using the parameters mentioned in the text. The red line represents the added contribution of the green and blue doublets.

Table 4-3. Parameters used for simulation of spectrum in Figure 4-8.

Sample	Parameters		Amount of ^{57}Fe	Color
[3Fe-4Se]^{0} 0mT	Fe^{3+}	d = 0.32 mm/s DEq = 0.58 mm/s	5.5%	green
	$Fe_2^{2.5+}$	d = 0.47 mm/s DEq = 1.0 mm/s	11%	blue

Discussion

The work described in this chapter incorporated various biochemical, molecular biology, and spectroscopic methods to probe fundamental outstanding questions in the mechanism of cofactor regeneration in *E. coli* LipA. Previous to this work, no more than one equivalent of lipoyl product formation was observed in *in vitro* LipA activity assays due to the obligate destruction of its auxiliary cluster to supply sulfur. In Chapter 2, the identification of *E. coli* NfuA was described, which efficiently restored the cofactor for catalysis. Interestingly, when using NfuA with ^{34}S labelled cluster in the reaction, two equivalents of unlabeled lipoyl product were observed before formation of 34S incorporated product. This data suggested that, only in the presence of NfuA, LipA could consume its entire cluster. This observation prompted the use of a selenium labelling strategy, where selenium was incorporated into NfuA's cluster. When using the [4Fe–4Se] loaded NfuA in LipA activity assays, it was demonstrated for the first time that LipA could use selenium rather than sulfur to produce selenolipoic acid. However, even when [4Fe–4Se]-loaded NfuA was supplied in vast excess of LipA, no more than one equivalent of selenolipoic acid was observed. Mössbauer analysis of the [4Fe–4Se] incorporated NfuA revealed that the cofactor incorporation

was not limiting in the reaction. An intriguing possibility is that we have inadvertently trapped an intermediate species in the reaction that is a consequence of using selenium rather than sulfur in the reaction. We are excited to exploit this system in future research by characterizing this species using Mössbauer spectroscopy and in crystallographic studies. Preliminary studies analyzing the species at the end of the selenolipoyl product reaction were inconclusive. The large amounts of $[4^{57}Fe\text{-}4Se]^{2+}$ cluster present in NfuA24 and NfuA25 is still unclear, given that this cluster would not lead to selenolipoyl product formation regardless of whether the cluster was transferred to LipA's radical SAM site, the auxiliary site, or still resided on NfuA/was not transferred. No amount of [2Fe-2Se] cluster was observed in any sample analysis. While the possibility of a chemically distinct $[3^{57}Fe\text{-}4Se]^{0}$ cluster seemed possible, the large amount of ferrous iron (30% in NfuA25) would likely come from the iron lost from the auxiliary site to form this intermediate, which is more than the one equivalent of selenolipoyl product formation observed in the reaction. One explanation for the high levels of ferrous iron could be due to the degradation of the clusters because of increased oxygen sensitivity of the [4Fe–4Se] clusters which has been reported, compared to [4Fe–4S] clusters. Moreover, at this time, it is still unclear what the state of the cluster is during these reactions, which will warrant substantial additional experiments to untangle.

[4Fe–4Se] clusters are have previously been reconstituted on iron-sulfur cluster proteins to probe their reaction mechansim, including radical SAM enzymes such as biotin synthase (16). When assaying [2Fe–2Se]-loaded biotin synthase, selenobiotin formation was observed. However, the turnovers were much lower (~0.1-0.3) than when assayed with [2Fe–2S]-loaded biotin synthase (turnover ~1). The reasons for the sluggish activity were discussed in detail. One possibility is that the [2Fe–2Se]-loaded biotin synthase could have been less efficiently reconstituted than the [2Fe–2S]-loaded biotin synthase, which would result in lower activity due to lower cofactor incorporation. Our Mössbauer studies of [4Fe–4Se]-loaded NfuA indicate that we have sufficient

cofactor incorporation, making this possibility less likely. Secondly, they have suggested that [Fe-Se] clusters are more oxygen-sensitive than their [Fe-S] cluster counterparts (27). Our experiments using [4Fe–4Se]-loaded NfuA were performed under anaerobic conditions (<5 ppm O_2); however, we cannot exclude the possibility that the [4Fe–4Se] clusters are being degraded to a greater extent under these conditions. Lastly, the authors comment that the reduction potentials of [4Fe–4Se] clusters and [4Fe–4S] clusters are different. As such, it could be possible that the [4Fe–4Se] cluster may not be efficiently reduced to reductively cleave SAM, given that our Mössbauer experiments have shown that clusters can be inserted in the radical SAM site as well.

We also performed experiments using ^{57}Fe incorporated NfuA and demonstrated that at the end of the reaction, LipA coordinates a [4Fe–4S] cluster that it receives from NfuA, though the intermediary steps which are of great interest are unknown. Further, we have shown that LipA can use this cluster to make the same [3Fe–3S–1(6-thiooctanoyl)LCP] cluster intermediate that was previously characterized in detail using Mössbauer spectroscopy and X-ray crystallography. A detailed spectroscopic study of the LipA reaction during catalysis in the presence of NfuA remains to be performed, as preliminary studies provided little novel insight. In addition, it was shown that apo NfuA binds iron and its spectroscopic properties are distinct from free iron in solution. This preliminary evidence supports one hypothesis that NfuA could remove the residual iron from the auxiliary site. Additional experiments, either using Mössbauer spectroscopy or 55Fe tracing, could provide more insight.

References

1. Cronan, J. E. (2016) Assembly of Lipoic Acid on Its Cognate Enzymes: an Extraordinary and Essential Biosynthetic Pathway. *Microbiology and Molecular Biology Reviews* **80**, 429-450
2. Booker, S. J. (2009) Anaerobic functionalization of unactivated C-H bonds. *Current opinion in chemical biology* **13**, 58-73
3. Booker, S. J., and Grove, T. L. (2010) Mechanistic and functional versatility of radical SAM enzymes. *F1000 biology reports* **2**, 52
4. Broderick, J. B., Duffus, B. R., Duschene, K. S., and Shepard, E. M. (2014) Radical S-Adenosylmethionine Enzymes. *Chemical Reviews* **114**, 4229-4317
5. Cicchillo, R. M., and Booker, S. J. (2005) Mechanistic Investigations of Lipoic Acid Biosynthesis in Escherichia coli: Both Sulfur Atoms in Lipoic Acid are Contributed by the Same Lipoyl Synthase Polypeptide. *Journal of the American Chemical Society* **127**, 2860-2861
6. Cicchillo, R. M., Iwig, D. F., Jones, A. D., Nesbitt, N. M., Baleanu-Gogonea, C., Souder, M. G., Tu, L., and Booker, S. J. (2004) Lipoyl synthase requires two equivalents of S-adenosyl-L-methionine to synthesize one equivalent of lipoic acid. *Biochemistry* **43**, 6378-6386
7. Cicchillo, R. M., Lee, K.-H., Baleanu-Gogonea, C., Nesbitt, N. M., Krebs, C., and Booker, S. J. (2004) Escherichia coli Lipoyl Synthase Binds Two Distinct [4Fe−4S] Clusters per Polypeptide. *Biochemistry* **43**, 11770-11781
8. Douglas, P., Kriek, M., Bryant, P., and Roach, P. L. (2006) Lipoyl synthase inserts sulfur atoms into an octanoyl substrate in a stepwise manner. *Angewandte Chemie (International ed. in English)* **45**, 5197-5199
9. Harmer, J. E., Hiscox, M. J., Dinis, P. C., Fox, S. J., Iliopoulos, A., Hussey, J. E., Sandy, J., Van Beek, F. T., Essex, J. W., and Roach, P. L. (2014) Structures of lipoyl synthase reveal a compact active site for controlling sequential sulfur insertion reactions. *The Biochemical journal* **464**, 123-133
10. Lanz, N. D., and Booker, S. J. (2015) Auxiliary iron-sulfur cofactors in radical SAM enzymes. *Biochimica et biophysica acta* **1853**, 1316-1334
11. Lanz, N. D., Pandelia, M. E., Kakar, E. S., Lee, K. H., Krebs, C., and Booker, S. J. (2014) Evidence for a catalytically and kinetically competent enzyme-substrate cross-linked intermediate in catalysis by lipoyl synthase. *Biochemistry* **53**, 4557-4572
12. Lanz, N. D., Rectenwald, J. M., Wang, B., Kakar, E. S., Laremore, T. N., Booker, S. J., and Silakov, A. (2015) Characterization of a Radical Intermediate in Lipoyl Cofactor Biosynthesis. *Journal of the American Chemical Society* **137**, 13216-13219
13. McLaughlin, M. I., Lanz, N. D., Goldman, P. J., Lee, K. H., Booker, S. J., and Drennan, C. L. (2016) Crystallographic snapshots of sulfur insertion by lipoyl synthase. *Proceedings of the National Academy of Sciences of the United States of America* **113**, 9446-9450
14. McCarthy, E. L., and Booker, S. J. (2017) Destruction and reformation of an iron-sulfur cluster during catalysis by lipoyl synthase. *Science (New York, N.Y.)* **358**, 373-377
15. Reed, K. E., Morris, T. W., and Cronan, J. E. (1994) Mutants of Escherichia coli K-12 that are resistant to a selenium analog of lipoic acid identify unknown genes in lipoate metabolism. *Proceedings of the National Academy of Sciences* **91**, 3720-3724
16. Tse Sum Bui, B., Mattioli, T. A., Florentin, D., Bolbach, G., and Marquet, A. (2006) Escherichia coli Biotin Synthase Produces Selenobiotin. Further Evidence of the

Involvement of the [2Fe-2S]2+ Cluster in the Sulfur Insertion Step. *Biochemistry* **45**, 3824-3834
17. Spatzal, T., Perez, K. A., Howard, J. B., and Rees, D. C. (2015) Catalysis-dependent selenium incorporation and migration in the nitrogenase active site iron-molybdenum cofactor. *eLife* **4**, e11620
18. Iwig, D. F., and Booker, S. J. (2004) Insight into the Polar Reactivity of the Onium Chalcogen Analogues of S-Adenosyl-l-methionine. *Biochemistry* **43**, 13496-13509
19. Iwig, D. F., Grippe, A. T., McIntyre, T. A., and Booker, S. J. (2004) Isotope and Elemental Effects Indicate a Rate-Limiting Methyl Transfer as the Initial Step in the Reaction Catalyzed by Escherichia coli Cyclopropane Fatty Acid Synthase. *Biochemistry* **43**, 13510-13524
20. McCarthy, E. L., and Booker, S. J. (2018) Biochemical Approaches for Understanding Iron-Sulfur Cluster Regeneration in Escherichia coli Lipoyl Synthase During Catalysis. *Methods in enzymology* **606**, 217-239
21. Lanz, N. D., Grove, T. L., Gogonea, C. B., Lee, K. H., Krebs, C., and Booker, S. J. (2012) RlmN and AtsB as models for the overproduction and characterization of radical SAM proteins. *Methods in enzymology* **516**, 125-152
22. Beinert, H. (1978) Micro methods for the quantitative determination of iron and copper in biological material. *Methods in enzymology* **54**, 435-445
23. Thompson, D. P., and Boudjouk, P. (1988) A convenient synthesis of alkali metal selenides and diselenides in tetrahydrofuran and the reactivity differences exhibited by these salts toward organic bromides. Effect of ultrasound. *The Journal of Organic Chemistry* **53**, 2109-2112
24. Greene, B. L., Stubbe, J., and Nocera, D. G. (2019) Selenocysteine Substitution in a Class I Ribonucleotide Reductase. *Biochemistry*
25. Linscott, J. A., Kapilashrami, K., Wang, Z., Senevirathne, C., Bothwell, I. R., Blum, G., and Luo, M. (2016) Kinetic isotope effects reveal early transition state of protein lysine methyltransferase SET8. *Proceedings of the National Academy of Sciences of the United States of America* **113**, E8369-e8378
26. Thompson, S., McMahon, S. A., Naismith, J. H., and O'Hagan, D. (2016) Exploration of a potential difluoromethyl-nucleoside substrate with the fluorinase enzyme. *Bioorganic Chemistry* **64**, 37-41
27. Meyer, J., Moulis, J.-M., Gaillard, J., and Lutz, M. (1992) Replacement Of Sulfur By Selenium In Iron—Sulfur Proteins. in *Advances in Inorganic Chemistry* (Cammack, R. ed.), Academic Press. pp 73-115
28. Angelini, S., Gerez, C., Ollagnier-de Choudens, S., Sanakis, Y., Fontecave, M., Barras, F., and Py, B. (2008) NfuA, a new factor required for maturing Fe/S proteins in Escherichia coli under oxidative stress and iron starvation conditions. *The Journal of biological chemistry* **283**, 14084-14091
29. Py, B., Gerez, C., Angelini, S., Planel, R., Vinella, D., Loiseau, L., Talla, E., Brochier-Armanet, C., Garcia Serres, R., Latour, J. M., Ollagnier-de Choudens, S., Fontecave, M., and Barras, F. (2012) Molecular organization, biochemical function, cellular role and evolution of NfuA, an atypical Fe-S carrier. *Molecular microbiology* **86**, 155-171
30. McCarthy, E. L., Rankin, A. N., Dill, Z. R., and Booker, S. J. (2019) The A-type domain in Escherichia coli NfuA is required for regenerating the auxiliary [4Fe-4S] cluster in Escherichia coli lipoyl synthase. *The Journal of biological chemistry* **294**, 1609-1617
31. Bryant, P., Kriek, M., Wood, R. J., and Roach, P. L. (2006) The activity of a thermostable lipoyl synthase from Sulfolobus solfataricus with a synthetic octanoyl substrate. *Analytical Biochemistry* **351**, 44-49

1. Cronan, J. E. (2016) Assembly of Lipoic Acid on Its Cognate Enzymes: an Extraordinary and Essential Biosynthetic Pathway. *Microbiology and Molecular Biology Reviews* **80**, 429-450
2. Booker, S. J. (2009) Anaerobic functionalization of unactivated C-H bonds. *Current opinion in chemical biology* **13**, 58-73
3. Booker, S. J., and Grove, T. L. (2010) Mechanistic and functional versatility of radical SAM enzymes. *F1000 biology reports* **2**, 52
4. Broderick, J. B., Duffus, B. R., Duschene, K. S., and Shepard, E. M. (2014) Radical S-Adenosylmethionine Enzymes. *Chemical Reviews* **114**, 4229-4317
5. Cicchillo, R. M., and Booker, S. J. (2005) Mechanistic Investigations of Lipoic Acid Biosynthesis in Escherichia coli: Both Sulfur Atoms in Lipoic Acid are Contributed by the Same Lipoyl Synthase Polypeptide. *Journal of the American Chemical Society* **127**, 2860-2861
6. Cicchillo, R. M., Iwig, D. F., Jones, A. D., Nesbitt, N. M., Baleanu-Gogonea, C., Souder, M. G., Tu, L., and Booker, S. J. (2004) Lipoyl synthase requires two equivalents of S-adenosyl-L-methionine to synthesize one equivalent of lipoic acid. *Biochemistry* **43**, 6378-6386
7. Cicchillo, R. M., Lee, K.-H., Baleanu-Gogonea, C., Nesbitt, N. M., Krebs, C., and Booker, S. J. (2004) Escherichia coli Lipoyl Synthase Binds Two Distinct [4Fe−4S] Clusters per Polypeptide. *Biochemistry* **43**, 11770-11781
8. Douglas, P., Kriek, M., Bryant, P., and Roach, P. L. (2006) Lipoyl synthase inserts sulfur atoms into an octanoyl substrate in a stepwise manner. *Angewandte Chemie (International ed. in English)* **45**, 5197-5199
9. Harmer, J. E., Hiscox, M. J., Dinis, P. C., Fox, S. J., Iliopoulos, A., Hussey, J. E., Sandy, J., Van Beek, F. T., Essex, J. W., and Roach, P. L. (2014) Structures of lipoyl synthase reveal a compact active site for controlling sequential sulfur insertion reactions. *The Biochemical journal* **464**, 123-133
10. Lanz, N. D., and Booker, S. J. (2015) Auxiliary iron-sulfur cofactors in radical SAM enzymes. *Biochimica et biophysica acta* **1853**, 1316-1334
11. Lanz, N. D., Pandelia, M. E., Kakar, E. S., Lee, K. H., Krebs, C., and Booker, S. J. (2014) Evidence for a catalytically and kinetically competent enzyme-substrate cross-linked intermediate in catalysis by lipoyl synthase. *Biochemistry* **53**, 4557-4572
12. Lanz, N. D., Rectenwald, J. M., Wang, B., Kakar, E. S., Laremore, T. N., Booker, S. J., and Silakov, A. (2015) Characterization of a Radical Intermediate in Lipoyl Cofactor Biosynthesis. *Journal of the American Chemical Society* **137**, 13216-13219
13. McLaughlin, M. I., Lanz, N. D., Goldman, P. J., Lee, K. H., Booker, S. J., and Drennan, C. L. (2016) Crystallographic snapshots of sulfur insertion by lipoyl synthase. *Proceedings of the National Academy of Sciences of the United States of America* **113**, 9446-9450
14. McCarthy, E. L., and Booker, S. J. (2017) Destruction and reformation of an iron-sulfur cluster during catalysis by lipoyl synthase. *Science (New York, N.Y.)* **358**, 373-377
15. Reed, K. E., Morris, T. W., and Cronan, J. E. (1994) Mutants of Escherichia coli K-12 that are resistant to a selenium analog of lipoic acid identify unknown genes in lipoate metabolism. *Proceedings of the National Academy of Sciences* **91**, 3720-3724
16. Tse Sum Bui, B., Mattioli, T. A., Florentin, D., Bolbach, G., and Marquet, A. (2006) Escherichia coli Biotin Synthase Produces Selenobiotin. Further Evidence of the

Involvement of the [2Fe-2S]2+ Cluster in the Sulfur Insertion Step. *Biochemistry* **45**, 3824-3834
17. Spatzal, T., Perez, K. A., Howard, J. B., and Rees, D. C. (2015) Catalysis-dependent selenium incorporation and migration in the nitrogenase active site iron-molybdenum cofactor. *eLife* **4**, e11620
18. Iwig, D. F., and Booker, S. J. (2004) Insight into the Polar Reactivity of the Onium Chalcogen Analogues of S-Adenosyl-l-methionine. *Biochemistry* **43**, 13496-13509
19. Iwig, D. F., Grippe, A. T., McIntyre, T. A., and Booker, S. J. (2004) Isotope and Elemental Effects Indicate a Rate-Limiting Methyl Transfer as the Initial Step in the Reaction Catalyzed by Escherichia coli Cyclopropane Fatty Acid Synthase. *Biochemistry* **43**, 13510-13524
20. McCarthy, E. L., and Booker, S. J. (2018) Biochemical Approaches for Understanding Iron-Sulfur Cluster Regeneration in Escherichia coli Lipoyl Synthase During Catalysis. *Methods in enzymology* **606**, 217-239
21. Lanz, N. D., Grove, T. L., Gogonea, C. B., Lee, K. H., Krebs, C., and Booker, S. J. (2012) RlmN and AtsB as models for the overproduction and characterization of radical SAM proteins. *Methods in enzymology* **516**, 125-152
22. Beinert, H. (1978) Micro methods for the quantitative determination of iron and copper in biological material. *Methods in enzymology* **54**, 435-445
23. Thompson, D. P., and Boudjouk, P. (1988) A convenient synthesis of alkali metal selenides and diselenides in tetrahydrofuran and the reactivity differences exhibited by these salts toward organic bromides. Effect of ultrasound. *The Journal of Organic Chemistry* **53**, 2109-2112
24. Greene, B. L., Stubbe, J., and Nocera, D. G. (2019) Selenocysteine Substitution in a Class I Ribonucleotide Reductase. *Biochemistry*
25. Linscott, J. A., Kapilashrami, K., Wang, Z., Senevirathne, C., Bothwell, I. R., Blum, G., and Luo, M. (2016) Kinetic isotope effects reveal early transition state of protein lysine methyltransferase SET8. *Proceedings of the National Academy of Sciences of the United States of America* **113**, E8369-e8378
26. Thompson, S., McMahon, S. A., Naismith, J. H., and O'Hagan, D. (2016) Exploration of a potential difluoromethyl-nucleoside substrate with the fluorinase enzyme. *Bioorganic Chemistry* **64**, 37-41
27. Meyer, J., Moulis, J.-M., Gaillard, J., and Lutz, M. (1992) Replacement Of Sulfur By Selenium In Iron—Sulfur Proteins. in *Advances in Inorganic Chemistry* (Cammack, R. ed.), Academic Press. pp 73-115
28. Angelini, S., Gerez, C., Ollagnier-de Choudens, S., Sanakis, Y., Fontecave, M., Barras, F., and Py, B. (2008) NfuA, a new factor required for maturing Fe/S proteins in Escherichia coli under oxidative stress and iron starvation conditions. *The Journal of biological chemistry* **283**, 14084-14091
29. Py, B., Gerez, C., Angelini, S., Planel, R., Vinella, D., Loiseau, L., Talla, E., Brochier-Armanet, C., Garcia Serres, R., Latour, J. M., Ollagnier-de Choudens, S., Fontecave, M., and Barras, F. (2012) Molecular organization, biochemical function, cellular role and evolution of NfuA, an atypical Fe-S carrier. *Molecular microbiology* **86**, 155-171
30. McCarthy, E. L., Rankin, A. N., Dill, Z. R., and Booker, S. J. (2019) The A-type domain in Escherichia coli NfuA is required for regenerating the auxiliary [4Fe-4S] cluster in Escherichia coli lipoyl synthase. *The Journal of biological chemistry* **294**, 1609-1617
31. Bryant, P., Kriek, M., Wood, R. J., and Roach, P. L. (2006) The activity of a thermostable lipoyl synthase from Sulfolobus solfataricus with a synthetic octanoyl substrate. *Analytical Biochemistry* **351**, 44-49

Chapter 5

Efforts Towards Understanding the Target Specificity and Recognition Mechanism of *E. coli* NfuA

Abstract

It has been established that *E. coli* NfuA targets *E. coli* LipA and regenerates its auxiliary cluster to support catalysis *in vitro.* However, *E. coli* bacterial strains in which the *nfuA* gene had been replaced with a blank cassette did not display any growth phenotype, contrary to the dramatic defects observed in the human homologue NFU1. In this chapter, we sought to provide evidence of this protein-protein interaction *in vivo,* as well as identify other unknown targets of *E. coli* NfuA. *E. coli* NfuA and *E. coli* LipA were co-immunoprecipitated to identify proteins that interact with them *in vivo*. Intriguingly, *E. coli* LipA was pulled out of the cell when using NfuA-FLAG as a target, and *E. coli* NfuA was pulled out of the cell when using *E. coli* LipA as the target. Microscale thermophoresis was used to measure the dissociation constant, Kd, of *E. coli* LipA and *E. coli* NfuA. Further, we investigated whether *E. coli* NfuA targets *E. coli* MiaB, a protein that also pulled down with *E. coli* NfuA and could perform a similar sacrificial mechanism. Lastly, we provided evidence that *E. coli* NfuA and *E. coli* LipA form a complex in the cell using bacterial two hybrid screening. Through library construction and screening of NfuA and LipA variants, we have predicted that the tight interaction between the two is dependent upon a single isoleucine residue in NfuA and an isoleucine-proline-valine motif in LipA.

Introduction

The trafficking of iron-sulfur (FeS) clusters in the cell is an emerging field in biology. The mechanism by which newly assembled FeS clusters are targeted and subsequently transferred to their apo-protein acceptors is poorly understood. Although many intermediate FeS cluster carrier proteins have been identified, the ultimate protein acceptors of their cofactors are still unknown in many cases. We have recently shown that *E. coli* NfuA targets and regenerates the auxiliary FeS cluster of *E. coli* LipA, which is consumed during catalysis to supply sulfur during the *de novo* biosynthesis of the lipoyl cofactor. This new insight, along with our established methods for biochemically analyzing the reaction mechanism of *E. coli* LipA *in vitro,* provides us a unique opportunity to address fundamental outstanding questions, such as the specificity of FeS cluster carrier proteins for a given target. We can also begin to understand how these intermediate carrier proteins recognize their apo- protein targets and how they sense that cluster delivery to a target is needed.

Recent work by the Lill and Rouault laboratories provides an example of how to address these outstanding questions (1,2). In studies performed in yeast, a single amino acid substitution of a C-terminal tryptophan residue with alanine in Lto1 prevented the adaptor protein complex Yae1-Lto1 from forming a complex with the cytosolic iron-sulfur protein assembly (CIA) targeting complex (1). Interestingly, through a similar strategy, the radical SAM enzyme viperin relies on a conserved C-terminal tryptophan residue to associate with the CIA targeting complex. Substitution of this residue abolishes viperin's ability to interact with the CIA targeting complex. This work provides precedent that a single amino acid motif is sufficient to mediate protein-protein interactions for iron-sulfur cluster assembly in eukaryotes.

Studies by the Rouault laboratory identified an LYR/IYR motif as a targeting sequence for the co-chaperone HSC20 to recognize succinate dehydrogenase, with the implication that this motif

may be wide-spread among eukaryotic FeS cluster containing proteins (2). Using yeast two hybrid screening, truncations of succinate dehydrogenase were screened against HSC20 to identify the LYR/IYR motif. Interestingly, within the motif, a single isoleuecine residue was found to be absolutely essential for the interaction. While this paper represented a significant advance in our understanding of target recognition in FeS cluster assembly systems, the paper lacked *in vitro* validation of the proposed residues that were identified in genetic screens as essential for the interaction.

In this current work, we performed co-immunoprecipitation experiments using NfuA-FLAG and LipA-FLAG constructs and identified interacting proteins by mass spectrometry. We aimed to identify new metalloprotein targets that NfuA can recognize, as well as identify other proteins that may be involved in the iron-sulfur cluster assembly process. In these efforts, we were able to pull out NfuA with LipA-FLAG, and alternately LipA with NfuA-FLAG, without the use of a crosslinker. Consequently, we performed binding experiments using microscale thermophoresis to calculate the Kd of the interaction. Further, inspired by the accomplishments by the Rouault laboratory, we used bacterial two-hybrid screening to show an interaction between *E. coli* NfuA and *E. coli* LipA *in vivo.* The observed robust interaction between the wild-type proteins allowed us to follow a similar strategy and make a library of NfuA and LipA truncations and screen for binding. Ultimately, a single isoleucine residue within the N-terminal domain of NfuA and an "isoleucine-proline-valine" motif within LipA were identified as essential binding residues. We further validated the importance of these residues *in vitro* using a combination of analytical techniques, including analytical size-exclusion chromatography and microscale thermophoresis, as well as activity assays. Collectively, this work provides the first *in vivo* evidence for a strong complex formation between *E. coli* NfuA and *E. coli* LipA and identifies previously unknown amino acid residues that are essential for this interaction.

Materials and Methods

General Procedures

The polymerase chain reaction was conducted using a BioRad S1000 thermocycler or an Eppendorf Nexus MX2 thermocycler. DNA concentration was determined using a Nanodrop 2000c Spectrophotometer (Thermo Fisher, Waltham, MA). DNA sequencing was performed at the Penn State Huck Life Sciences Genomics Core Facility. Protein identification was performed at the Penn State Huck Life Sciences Proteomics Core Facility.

C39A, C44A, E. coli LipA, E. coli H protein, E. coli NfuA truncations, E. coli LipA truncations, E. coli MiaB, and E. coli Glutathione S-transferase into bacterial two hybrid vectors. Genes encoding *E. coli* NfuA, NfuA Cys39Ala, Cys44Ala, NfuA N-terminal domain, NfuA C-terminal domain, *E. coli* NfuA truncations, *E. coli* LipA truncations, *E. coli* LipA, *E. coli* H protein (*gcvH*), *E. coli* MiaB and *E. coli* Glutathione S-transferase (*gstB*) were PCR-amplified to introduce flanking attB sites using previously cloned *nfuA*-pET28a (3), *nfuA Cys39Ala,Cys44Ala*-pET28a (4), *nfuA N-term*-pET28a (4), *nfuA C-term*-pET28a (4), *lipA*-pET28a (5,6), *gcvH*-pET28a (this study), *miaB*-pET28a (this study), and *gstB*-pSUMO (this study) plasmid DNA as a template for the reaction and the primers listed in **Table 5-1.** Following gel purification, the attB-flanked DNA (150 ng) was mixed with pDONR221 DNA (150 ng) and BP clonase enzyme mix to initiate BP recombination and incubated at 4 °C overnight. The following day, the reaction was quenched by the addition of proteinase K. The DNA mixture was used to transform *E. coli* DH5α, and the desired constructs were confirmed by DNA sequencing. The entry construct (150 ng) was mixed with the bacterial two hybrid vectors (pUT18C-DEST or pST25-DEST, 150 ng), and the LR clonase enzyme mix was added to initiate LR recombination. The reaction was incubated at room temperature for 2 h before stopping it by the addition of proteinase K. DH5α cells were transformed with the DNA mixture, and the desired constructs were confirmed by DNA sequencing.

Cloning of E. coli NfuA Ile4Ala, E. coli NfuA Ser5Ala, E. coli Ile4Ala, Ser5Ala, E. coli LipA Leu21Ala, E. coli LipA Ile22Ala, E. coli LipA Pro23Ala, E. coli LipA Val24Ala, E. coli LipA Lys25Arg, and E. coli LipA Lys25Ala into bacterial two hybrid vectors. Site-directed mutagenesis was performed using the QuikChange Site Directed Mutagenesis kit (Agilent Technologies, Santa Clara, CA) using the primers listed in **Table 5-1.** The *E. coli nfuA*-pDONR221 entry vector plasmid DNA and *E. coli lipA*-pDONR221 entry vector plasmid DNA were used as DNA templates for the reaction. Following sequence confirmation, the entry construct (150 ng) was mixed with the bacterial two hybrid vectors (pUT18C-DEST or pST25-DEST, 150 ng), and the LR clonase enzyme mix was added to initiate LR recombination. The reaction was incubated at room temperature for 2 h before stopping it by the addition of proteinase K. DH5α cells were transformed with the DNA mixture, and the desired constructs were confirmed by DNA sequencing.

Subcloning of E. coli NfuA Ile4Ala, E. coli LipA Ile22Ala, E. coli LipA Pro23Ala, and E. coli LipA Val24Ala into pET28a. The genes encoding *E. coli* NfuA Ile4Ala, *E. coli* LipA Ile22Ala, *E. coli* LipA Pro23Ala, and *E. coli* LipA Val24Ala were amplified via the polymerase chain reaction using the primers in **Table 5-1**, which added an *Nde*I restriction site at the 5' end and an *Xho*I restriction site at the 3' end. Following digestion, the DNA was ligated into a pET28a vector digested with the same restriction enzymes. DH5α cells were transformed with the DNA mixture, and the desired constructs were confirmed by DNA sequencing.

Plasmid Construction of E. coli LipA Ile22Ala, Pro23Ala, Val24Ala triple variant into pET28a.

The gene encoding the *E. coli* LipA Ile22Ala, Pro23Ala, Val24Ala triple variant was ordered as a gBlock from Integrated DNA Technologies with a 5′ *Nde*I cut site and a 3′ *Xho*I cut site. Following digestion, the DNA was ligated into pET28a vector DNA digested with the same restriction

enzymes. DH5α cells were transformed with the DNA mixture, and the desired constructs were confirmed by DNA sequencing.

Plasmid Construction of E. coli miaB-pET28a, E. coli nfuA-FLAG, and E. coli lipA-FLAG.

The gene encoding *E. coli* MiaB was amplified by PCR technology using *E. coli* miaB-pET26b (7) as a DNA template with the following primers: Forward: 5′ CGC GGC GTC CAT ATG ATG ACC AAA AAA CTC CAT ATT AAA ACC 3′ (*NdeI* restriction site underlined) Reverse: 5′ CGC GGC GTC CTC GAG TTA CGG CTG ATA ATA ACC CAC GCC AAG 3′ (*XhoI* restriction site underlined). The amplified DNA was digested with *Nde*I and *Xho*I and then ligated into pET28a that had been digested with the same restriction enzymes. DH5α cells were then transformed with the construct. For the *E. coli nfuA*-FLAG construct, the gene encoding *E. coli* NfuA was amplified by PCR technology using *E. coli nfuA*-pET28a as a DNA template with the following primers: Forward: 5′ CGC GGC GTC AAG CTT ATG ATC CGT ATT TCC GAT GCT GC 3′ (*Hin*dIII restriction site underlined) Reverse: 5′ CGC GGC GTC GAG CTC TTA GTA GGA GTG TTC GCC GC 3′ (*Sac*I restriction site underlined). The amplified DNA was digested with *Hin*dIII and *Sac*I and then ligated into a FLAG vector encoding an N-terminal DYKDDDDK epitope tag (pT7-FLAG-1 Expression Vector, Sigma) that had been digested with the same restriction enzymes. *E. coli* DH5α cells was then transformed with the construct. For the *E. coli lipA*-FLAG construct, the gene encoding *E. coli* LipA was amplified by PCR technology using *E. coli lipA*-pET28a as a DNA template with the following primers: Forward: 5′ CGC GGC GTC GAA TTC ATG AGT AAA CCC ATT GTG ATG GAA CGC 3′ (*Eco*RI restriction site underlined) Reverse: 5′ CGC GGC GTC GAG CTC TTA CTT AAC TTC CAT CCC TTT CGC CTG C 3′ (*Sac*I restriction site underlined). The amplified DNA was digested with *Eco*RI and *Sac*I and then ligated into a FLAG

vector (pT7-FLAG-1 Expression Vector, Sigma) that had been digested with the same restriction enzymes. *E. coli* DH5α was then transformed with the construct.

Co-immunoprecipitation of E. coli NfuA and E. coli LipA.

E. coli NfuA or *E. coli* LipA containing a FLAG epitope tag (DYKDDDDK) was used for co-immunoprecipitation studies. BL21(DE3) cells were transformed with the *E. coli nfuA*-FLAG construct or the *E. coli lipA*-FLAG construct. A single colony was used to inoculate 200 mL lysogeny broth (LB) supplemented with 100 μg/mL ampicillin, and the starter culture was incubated overnight at 37 °C with shaking at 250 rpm. The following day, LB (4- 6 L flasks containing 4 L media) pre-equilibrated to 37 °C was inoculated with 20 mL of starter culture and then incubated at 37 °C with shaking at 180 rpm. At OD_{600}=0.6, the flasks were placed in an ice-water bath for ~30 min. The cells were allowed to grow for an additional ~14-18 h at 18 °C with shaking at 180 rpm without IPTG induction. Significant leaky expression was observed using the overnight growth procedure. As a result, the protocol was also performed by inoculating the LB media with 40 mL overnight starter culture and allowing growth to proceed for only 7 h at 37 °C with shaking at 180 rpm. Bacteria were harvested by centrifugation at 7,500 × g for 12 min, and the resulting cell pellet was flash-frozen in liquid N_2 and stored in liquid N_2 until further use. The lysate used for co-immunoprecipitation was prepared in the absence of oxygen in a Coy anaerobic chamber. Approximately half of the collected cells (~35 g frozen cell paste from a total of 70 g frozen cell paste) were re-suspended in phosphate-buffered saline (PBS) buffer, pH 7.4. Lysozyme (1 mg/mL), a SigmaFAST EDTA-free protease inhibitor tablet, and Dnase I (0.1 mg/mL) were added, and the solution was stirred for 30 min at room temperature. The cells were lysed by sonic disruption, and the resulting lysate was centrifuged at 45,000 × g for 1 h. A 1 mL aliquot of the crude protein mixture was incubated with 100 μL anti-flag affinity resin in an Eppendorf tube with

gentle agitation for 2 g at room temperature. After incubation, the resin/lysate mixture was transferred to a Pierce spin column and centrifuged at 700 × g for 1 min. The resin was then washed (3 times) by adding 500 μL ice-cold PBS and then centrifuging at 700 × g for 1 min. The resin was then incubated with 100 μL of 100 μg/mL flag peptide for 10 min at room temperature to elute the protein from the resin. This step was performed twice to give a final elution volume of 200 μL. Samples of the cellular pellet, the crude supernatant, the flow-through, the washes, and the elution were collected for SDS-PAGE analysis. The resulting SDS-PAGE gel was stained with Coomassie Blue, and the lanes containing the pure eluted protein were also visualized using silver stain with the Pierce Silver Stain Mass Spectrometry compatible kit (ThermoFisher; Waltham, MA). Bands of interest were excised, subjected to trypsin digestion and submitted for protein identification at the Penn State Proteomics and Mass Spectrometry Core Facility.

Bacterial two hybrid binding analysis. Adenylate cyclase deficient cells BTH101 were co-transformed with the following pairs of plasmids: *nfuA*-pUT18C + *lipA*-pST25; *nfuA C39A/C44A*-pUT18C + *lipA*-pST25; *nfuA N term*-pUT18C + *lipA*-pST25; *nfuA C term*-pUT18C + *lipA*-pST25; *nfuA*-pUT18C + *miaB*-pST25; *zip*-pUT18C + *zip*-pST25 (positive control); and *gcvH*-pUT18C + *gstB*-pST25. The co-transformed cells were plated on LB agar containing 40 μg/μL galactosidase and 0.5 mM IPTG with the respective selective antibiotics (100 μg/μL spectinomycin or 50 μg/μL kanamycin and 100 μg/μL ampicillin). The plates were incubated at 30 °C for 48 h while monitoring for the development of a blue color, indicating a protein-protein interaction. A table of all protein pairs screened using this methodology can be found in **Appendix C.**

Expression and Isolation of E. coli NfuA Ile4Ala, E. coli LipA Ile22Ala, E. coli LipA Pro23Ala, E. coli LipA Val24Ala, and E. coli LipA Ile22Ala–Pro23Ala–Val24Ala triple variant. The *E. coli*

NfuA and *E. coli* LipA variants studied in this chapter were prepared exactly as described for wild-type *E. coli* NfuA and *E. coli* LipA described in published procedures (8).

Chemical Reconstitution of E. coli NfuA Ile4Ala, E. coli LipA Ile22Ala, E. coli LipA Pro23Ala, and E. coli LipA Val24Ala. E. coli NfuA Ile4Ala, *E. coli* LipA Ile22Ala, *E. coli* LipA Pro23Ala, and *E. coli* LipA Val24Ala were chemically reconstituted with reductant (DTT), iron, and sodium sulfide to improve cofactor incorporation. A reaction containing 100 µM as-isolated protein was slowly stirred on ice. DTT (5 mM final concentration) was added in three increments every 20 min, and the solution was incubated further for 1 h. Following treatment with DTT, $FeCl_3$ was added in five increments every 5 min to give a final concentration of 400 µM, and the solution was incubated for 30 min. Sodium sulfide was then added in five increments every 30 min to give a final concentration of 400 µM, and the reaction was incubated on ice overnight. The following day, protein precipitation was removed by centrifugation at 45,000 × g for 10 min, and the protein was concentrated to 2 mL using an Amicon centrifugal filter with a 10 kDa molecular weight cutoff. Aggregates and non-specifically bound substances were removed by applying the protein preparation to a HiPrep 16/60 Sephacryl HR S-200 column (GE Healthcare) equilibrated in storage buffer (100 mM HEPES, pH 7.5, 300 mM KCl, 5 mM DTT, 15% glycerol) at a flow-rate of 0.5 mL/min.

Determination of the Binding Affinity of E. coli LipA with E. coli NfuA using Microscale Thermophoresis. Microscale thermophoresis was used to measure the dissociation constant (K_d) for the interaction between *E. coli* LipA and *E. coli* NfuA. All steps were performed in an anaerobic chamber until the capillaries were sealed and removed for analysis. *E. coli* LipA (100 µL) was centrifuged for 5 min at 14,000 × g and transferred to a fresh Eppendorf

tube. The protein was then exchanged into NHS labeling buffer (130 mM $NaHCO_3$, 50 mM NaCl, pH 8.2) using a Nick column (GE Healthcare), yielding 400 μL of protein at a concentration of 192 μM. The protein was centrifuged again for 5 min at 14,000 × g and transferred to a fresh Eppendorf tube. This stock was further diluted to make 200 μL of a 10 μM *E. coli* LipA stock. A 600 μM RED-NHS dye stock was made by resuspending the lyophilized dye supplied from Nanotemper (Monolith Protein Labeling Kit RED-NHS 2nd Generation, 10 μg) in 25 μL DMSO. A 300 μM RED-NHS dye working solution was made by mixing 7 μL of the 600 μM dye stock with 7 μL of NHS labeling buffer. 90 μL of the 10 μM *E. coli* LipA stock was mixed with 10 μL of the 300 μM RED-NHS dye working-solution (3:1 dye:protein ratio, final protein concentration is 9 μM) and incubated for 30 min at room temperature in the dark. While the protein/dye incubated, an NHS column supplied with the labeling kit was equilibrated with four column volumes of MST buffer (50 mM HEPES, pH 7.5, 150 mM KCl, 5% glycerol, and 0.05% Tween 20). When the incubation was complete, the dye/protein mixture was loaded onto the column. 550 μL of MST buffer was added to the resin and allowed to fully settle. Finally, 450 μL additional MST buffer was used to elute the labeled LipA. The NHS-labeled LipA (final concentration 2 μM) was centrifuged for 5 min at 14,000 × g and transferred to a fresh Eppendorf tube. The unlabeled *E. coli* NfuA ligand was centrifuged for 5 min at 14,000 × g and transferred to a fresh Eppendorf tube. The *E. coli* NfuA protein ligand was exchanged into MST buffer using a Nick column (GE Healthcare), yielding a 431 μM protein solution in a final volume of 400 μL. The 431 μM stock was centrifuged for 5 min at 14,000 × g and transferred to a fresh Eppendorf tube.

A protein-labeling pre-test was performed to ensure that the fluorescence intensity of the labeled LipA was adequate for the binding experiment. 100 μL of 1 μM NHS-labeled LipA was prepared (7.5 μL of 2 μM NHS labeled LipA protein + 192.5 μL MST buffer) in a 0.6 mL low-retention microcentrifuge tube (Fisher). 10 μL of 1 μM NHS-labeled LipA was mixed with 10 μL MST buffer in each of four 0.6 mL low-retention microcentrifuge tubes to give a 500 nM final concentration in each tube. Two standard and two premium capillaries were each loaded with a 500 nM NHS-labeled LipA solution. Using a Monolith NT.115 Microscale Thermophoresis instrument, the pre-test was selected and the samples were measured at 40% LED/excitation power with medium MST power (40% MST power in NT.Control). Based on the pre-test analysis, no adsorption or aggregation was observed in the standard capillaries. The curves in the standard capillaries and in the premium capillaries appeared identical. Further, the fluorescence was ~300. All quality checks indicated that the experimental conditions were optimal, and that the binding event could be assessed.

In order to perform the binding assay, 100 μL of 200 μM NfuA (ligand) in MST buffer was prepared in a 0.6 mL low-retention microcentrifuge tube. 250 μL 1 μM NHS-labeled LipA in MST buffer was also prepared in a 0.6 mL low-retention microcentrifuge tube. 18 0.6 mL low retention microcentrifuge tubes were aligned in a microcentrifuge tube rack, and 10 μL MST buffer was added to tubes 2-18. 20 μL of 200 μM NfuA was added to tube 1. 10 μL of solution was removed from tube 1 and mixed with tube 2, and this serial dilution was repeated for tubes 3-18. 10 μL was removed from tube 18 and discarded so each tube had a final volume of 10 μL. 10 μL of 1 μM NHS-labeled LipA was added to

each tube and carefully mixed. The solution from each tube was loaded into a standard capillary, carefully sealed, and placed in the capillary chip. The sealed capillaries were then removed from the anaerobic chamber and measured using 40% LED/excitation power and medium MST power.

Unfortunately, ligand induced fluorescence changes were observed, preventing the MST curves from being used to determine the K_d. However, the K_d can be robustly obtained from the initial fluorescence data if the fluorescence changes can be shown to depend on a specific protein-protein interaction. The standard way to show that the fluorescence is due to a protein-protein interaction is to perform a specificity test, which was conducted in the following manner. The remaining mixtures from tubes 1-3 and tubes 14-16 were centrifuged for 10 min at 14,000 × g. 7 μL of each sample was carefully removed and mixed with 7 μL of SD mix (4% SDS, 40 mM DTT) before incubating the tubes for 5 min at 95 °C to denature the protein. Each sample was placed in a standard capillary, sealed and analyzed using the + SD test function in the MST instrument. The binding assay with the associated specificity test was performed in triplicate and analyzed with the associated MO analysis software to obtain the K_d.

Determination of the Binding Affinity of E. coli LipA with E. coli NfuA Ile4Ala using Microscale Thermophoresis. Microscale thermophoresis was used to calculate the K_d for the interaction of *E. coli* LipA with *E. coli* NfuA Ile4Ala. All steps were performed in an anaerobic chamber until the capillaries were sealed and removed for analysis. The NHS-labeled protein was prepared exactly as described above for the wild-type *E. coli* LipA and *E. coli* NfuA measurements. The unlabeled *E. coli* NfuA Ile4Ala ligand was centrifuged

for 5 min at 14,000 × g and transferred to a fresh Eppendorf tube. *E. coli* NfuA was exchanged into MST buffer using a Nick column (GE Healthcare), yielding 400 μL of an 840 μM protein solution. This 840 μM protein stock was centrifuged for 5 min at 14,000 × g and transferred to a fresh Eppendorf tube.

A protein-labeling pre-test was performed to ensure that the fluorescence intensity of labeled LipA was adequate for the binding experiment. 100 μL of 1 μM NHS-labeled LipA was prepared (7.5 μL of 2 μM NHS-labeled LipA protein + 192.5 μL MST buffer) in a 0.6 mL low-retention microcentrifuge tube (Fisher). 10 μL of the 1 μM NHS-labeled LipA protein was mixed with 10 μL MST buffer in four 0.6 mL low-retention microcentrifuge tubes (500 nM final concentration). Two standard and two premium capillaries were loaded with the 500 nM NHS-labeled LipA. Using a Monolith NT.115 Microscale Thermophoresis instrument, the pre-test was selected and the samples were measured at 40% LED/excitation power with medium MST power (40% MST power in NT.Control). In the pre-test, no adsorption was observed in the standard capillaries, and no aggregation was observed. The curves obtained using the standard appeared identical to those obtained with the premium capillaries. Further, the fluorescence was ~500. All quality checks indicated that the experimental conditions were optimal, and that the binding event could be assessed.

In order to perform the binding assay, 100 μL of 660 μM NfuA in MST buffer was prepared in a 0.6 mL low-retention microcentrifuge tube. 250 μL of 1 μM NHS-labeled LipA in MST buffer was also prepared in a 0.6 mL low-retention microcentrifuge tube. 16 0.6 mL low-retention microcentrifuge tubes were aligned in a tube rack, and 10 μL MST

buffer was added to tubes 2-16. 20 μL of 660 μM NfuA was added to tube 1. 10 μL of the 660 μM NfuA protein ligand was removed from tube 1 and mixed with tube 2, and the serial dilution was repeated for tubes 3-16. 10 μL was removed from tube 16 and discarded so that each tube contained a final volume of 10 μL. 10 μL of the 1 μM NHS-labeled LipA stock was added to each tube and carefully mixed. The solution from each tube was loaded into a standard capillary, carefully sealed and placed in the capillary chip. The sealed capillaries were then removed from the anaerobic chamber and binding was measured using 40% LED/excitation power and medium MST power.

Unfortunately, ligand induced fluorescence changes were observed, preventing the MST curves from being used to determine the K_d. However, the K_d can be robustly obtained from the initial fluorescence data if the fluorescence changes can be shown to depend on a specific protein-protein interaction. The standard way to show that the fluorescence is due to a protein-protein interaction is to perform a specificity test, which was conducted in the following manner. The remaining mixtures from tubes 1-3 and tubes 14-16 were centrifuged for 10 min at 14,000 × g. 7 μL of each sample was carefully removed and mixed with 7 μL of SD mix (4% SDS, 40 mM DTT) before incubating the tubes for 5 min at 95 °C to denature the protein. Each sample was placed in a standard capillary, sealed and analyzed using the + SD test function in the MST instrument. The binding assay with the associated specificity test was performed in triplicate and analyzed with the associated MO analysis software to obtain the K_d.

Determination of the Binding Affinity of E. coli LipA Ile22Ala and E. coli NfuA using Microscale Thermophoresis.

Microscale thermophoresis was used to calculate the K_d for the interaction of *E. coli* LipA Ile22Ala with *E. coli* NfuA. All steps were performed in an anaerobic chamber until the capillaries were sealed and removed for analysis. The NHS-labeled protein was prepared exactly as described above for the wild-type *E. coli* LipA and *E. coli* NfuA measurements. The unlabeled *E. coli* NfuA Ile4Ala ligand was centrifuged for 5 min at 14,000 × g and transferred to a fresh Eppendorf tube. *E. coli* NfuA was exchanged into MST buffer using a Nick column (GE Healthcare), yielding 400 μL of a 431 μM protein solution. This 431 μM protein stock was centrifuged for 5 min at 14,000 × g and transferred to a fresh Eppendorf tube.

A protein-labeling pre-test was performed to ensure that the fluorescence intensity of labeled LipA was adequate for the binding experiment. 100 μL of 1.5 μM NHS-labeled LipA protein was prepared in a 0.6 mL low-retention microcentrifuge tube (Fisher). 10 μL of the 1.5 μM NHS-labeled LipA protein was mixed with 10 μL MST buffer in four 0.6 mL low-retention microcentrifuge tubes (750 nM final concentration). Two standard and two premium capillaries were loaded with the 500 nM NHS-labeled LipA. Using a Monolith NT.115 Microscale Thermophoresis instrument, the pre-test was selected and the samples were measured at 40% LED/excitation power with medium MST power (40% MST power in NT.Control). No adsorption was observed in the standard capillaries, and no aggregation was not observed in the MST traces. The curves obtained using the standard capillaries appeared identical to those obtained with the premium capillaries. However, the

fluorescence was only ~180. Therefore, the excitation power was increased to 60%, which resulted in a fluorescence of ~250, a value that is suitable for binding analysis. All quality checks indicated that the experimental conditions were optimal, and that the binding event could be assessed.

In order to perform the binding assay, 100 μL of 200 μM NfuA in MST buffer was prepared in a 0.6 mL low-retention microcentrifuge tube. 250 μL of 1 μM NHS-labeled LipA in MST buffer was also prepared in a 0.6 mL low retention microcentrifuge tube. 16 0.6 mL low-retention microcentrifuge tubes were aligned in a tube rack, and 10 μL MST buffer was added to tubes 2-16. 20 μL of 200 μM NfuA protein ligand was added to tube 1. 10 μL of the 200 μM NfuA protein ligand was removed from tube 1 and mixed with tube 2, and the serial dilution was repeated for tubes 3-16. 10 μL was removed from tube 16 and discarded so that each tube contained a final volume of 10 μL. 10 μL of the 1 μM NHS-labeled LipA stock was added to each tube and carefully mixed. The solution from each tube was loaded into a standard capillary, carefully sealed and placed in the capillary chip. The sealed capillaries were then removed from the anaerobic chamber and measured using 60% LED/excitation power and medium MST power. The binding assay was performed in triplicate; however, binding could not be detected in all three replicates.

Determination of the Binding Affinity of E. coli LipA Pro23Ala and E. coli NfuA using Microscale Thermophoresis.

Microscale thermophoresis was used to calculate the K_d for the interaction of *E. coli* LipA Pro23Ala with *E. coli* NfuA. All steps were performed in an anaerobic chamber until the capillaries were sealed and removed for analysis. The NHS-labeled protein was prepared exactly as described above for the wild-type *E. coli* LipA and *E. coli* NfuA measurements. The unlabeled *E. coli* NfuA ligand was centrifuged for 5 min at 14,000 × g and transferred to a fresh Eppendorf tube. *E. coli* NfuA was exchanged into MST buffer using a Nick column (GE Healthcare), yielding 400 μL of a 430 μM protein solution. This 430 μM protein stock was centrifuged for 5 min at 14,000 × g and transferred to a fresh Eppendorf tube.

A protein-labeling pre-test was performed to ensure that the fluorescence intensity of labeled LipA Pro23Ala was adequate for the binding experiment. 100 μL of 1 μM NHS-labeled LipA Pro23Ala protein was prepared in a 0.6 mL low-retention microcentrifuge tube (Fisher). 10 μL of the 1 μM NHS-labeled LipA protein was mixed with 10 μL MST buffer in four 0.6 mL low-retention microcentrifuge tubes (500 nM final concentration). Two standard and two premium capillaries were loaded with the 500 nM NHS-labeled LipA Pro23Ala. Using a Monolith NT.115 Microscale Thermophoresis instrument, the pre-test was selected and the samples were measured at 40% LED/excitation power with medium MST power (40% MST power in NT.Control). No adsorption or aggregation was observed in the standard capillaries during the pre-test. The curves obtained using the standard capillaries appeared identical to those obtained with the premium capillaries and the fluorescence was ~300. All quality checks indicated that the experimental conditions were optimal, and that the binding event could be assessed.

In order to perform the binding assay, 30 μL of 430 μM NfuA in MST buffer was prepared in a 0.6 mL low-retention microcentrifuge tube. 220 μL of 1 μM NHS-labeled LipA Pro23Ala in MST buffer was also prepared in a 0.6 mL low retention microcentrifuge tube. 16 0.6 mL low-retention microcentrifuge tubes were aligned in a tube rack, and 10 μL MST buffer was added to tubes 2-16. 20 μL of 430 μM NfuA protein ligand was added to tube 1. 10 μL of the 430 μM NfuA protein ligand was removed from tube 1 and mixed with tube 2, and the serial dilution was repeated for tubes 3-16. 10 μL was removed from tube 16 and discarded so that each tube contained a final volume of 10 μL. 10 μL of the 1 μM-NHS-labeled LipA Pro23Ala stock was added to each tube and carefully mixed. The solution from each tube was loaded into a standard capillary, carefully sealed and placed in the capillary chip. The sealed capillaries were then removed from the anaerobic chamber and measured using 40% LED/excitation power and medium MST power.

Unfortunately, ligand induced fluorescence changes were observed, preventing the MST curves from being used to determine the K_d. A specificity test was performed to assess whether the initial fluorescence data could be used to determine a K_d. The remaining mixtures from tubes 1-3 and tubes 14-16 were centrifuged for 10 min at 14,000 × g. 7 μL of each sample was carefully removed and mixed with 7 μL of SD mix (4% SDS, 40 mM DTT) before incubating the tubes for 5 min at 95 °C to denature the protein. Each sample was placed in a standard capillary, sealed and analyzed using the + SD test function in the MST instrument. The binding assay with the associated specificity test was performed in triplicate and analyzed with the associated MO analysis software to obtain the K_d.

Kd Determination of E. coli LipA Val24Ala and E. coli NfuA using Microscale Thermophoresis.

Microscale thermophoresis was used to calculate the K_d for the interaction of *E. coli* LipA *Val24Ala* with *E. coli* NfuA. All steps were performed in an anaerobic chamber until the capillaries were sealed and removed for analysis. The NHS-labeled protein was prepared exactly as described above for the wild-type *E. coli* LipA and *E. coli* NfuA measurements. The unlabeled *E. coli* NfuA ligand was centrifuged for 5 min at 14,000 × g and transferred to a fresh Eppendorf tube. *E. coli* NfuA was exchanged into MST buffer using a Nick column (GE Healthcare), yielding 400 μL of a 431 μM protein solution. This 431 μM protein stock was centrifuged for 5 min at 14,000 × g and transferred to a fresh Eppendorf tube.

A protein-labeling pre-test was performed to ensure that the fluorescence intensity of labeled LipA was adequate for the binding experiment. 100 μL of 1 μM NHS-labeled LipA Val24Ala was prepared in a 0.6 mL low-retention microcentrifuge tube (Fisher). 10 μL of the 1 μM NHS-labeled LipA Val24Ala protein was mixed with 10 μL MST buffer in four 0.6 mL low-retention microcentrifuge tubes (500 nM final concentration). Two standard and two premium capillaries were loaded with the 500 nM NHS-labeled LipA Val24Ala. Using a Monolith NT.115 Microscale Thermophoresis instrument, the pre-test was selected and the samples were measured at 40% LED/excitation power with medium MST power (40% MST power in NT.Control). No adsorption or aggregation was observed in the standard capillaries during the pre-test. The curves obtained using the standard appeared identical to those obtained with the premium capillaries. Further, the fluorescence was ~450. All quality checks indicated that the experimental conditions were optimal, and that the binding event could be assessed.

In order to perform the binding assay, 30 μL of 430 μM NfuA in MST buffer was prepared in a 0.6 mL low-retention microcentrifuge tube. 220 μL of 1 μM NHS-labeled LipA Val24Ala in MST buffer was also prepared in a 0.6 mL low retention microcentrifuge tube. 16 0.6 mL low-retention microcentrifuge tubes were aligned in a tube rack, and 10 μL MST buffer was added to tubes 2-16. 20 μL of 430 μM NfuA protein ligand was added to tube 1. 10 μL of the 430 μM NfuA protein ligand was removed from tube 1 and mixed with tube 2, and the serial dilution was repeated for tubes 3-16. 10 μL was removed from tube 16 and discarded so that each tube contained a final volume of 10 μL. 10 μL of the 1 μM-NHS-labeled LipA Val24Ala stock was added to each tube and carefully mixed. The solution from each tube was loaded into a standard capillary, carefully sealed and placed in the capillary chip. The sealed capillaries were then removed from the anaerobic chamber and measured using 40% LED/excitation power and medium MST power.

Unfortunately, ligand induced fluorescence changes were observed, preventing the MST curves from being used to determine the K_d. A specificity test was performed to assess whether the initial fluorescence data could be used to determine a K_d. The remaining mixtures from tubes 1-3 and tubes 14-16 were centrifuged for 10 min at 14,000 × g. 7 μL of each sample was carefully removed and mixed with 7 μL of SD mix (4% SDS, 40 mM DTT) before incubating the tubes for 5 min at 95 °C to denature the protein. Each sample was placed in a standard capillary, sealed and analyzed using the + SD test function in the MST instrument. The binding assay with the associated specificity test was performed in triplicate and analyzed with the associated MO analysis software to obtain the K_d.

Binding of E. coli NfuA Ile4Ala to E. coli LipA Ile22Ala, E. coli LipA Pro23Ala, E. coli LipA Val24Ala, and the E. coli LipA Ile22Ala, Pro23Ala, Val24Ala triple variant using analytical molecular sieve chromatography.

The interactions between protein variants identified in bacterial two-hybrid screens were validated using analytical molecular-sieve chromatography. A 500 μL mixture of standards composed of cytochrome c (12.4 kDa), carbonic anhydrase (29 kDa), bovine serum albumin (66 kDa), alcohol dehydrogenase (150 kDa), α-amylase (200 kDa), and blue dextran (2000 kDa) was applied to a HiPrep 16/60 Sephacryl HR S-200 column (GE Healthcare) housed in a Coy anaerobic chamber under anoxic conditions (<1 ppm O_2) equilibrated in freshly prepared buffer (50 mM HEPES, pH 7.5, 150 mM KCl, 15% glycerol, and 1 mM DTT). The log MW of each standard was plotted against their respective elution volumes after correcting for the void volume of the column. A linear fit to the data was then used to estimate the molecular weight of each sample. The following samples were applied to the column in a 500 μL volume: 100 μM wild-type NfuA; 100 μM wild-type LipA; a mixture of 100 μM wild-type LipA and 100 μM wild-type NfuA; 100 μM LipA Ile22Ala; 100 μM NfuA Ile4Ala; 100 μM LipA Pro23Ala; 100 μM LipA Val24Ala; 100 μM LipA Ile22Ala, Pro23Ala, Val24Ala triple variant; 100 μM wild-type LipA + 100 μM NfuA Ile4Ala; 100 μM LipA Ile22Ala + 100 μM wild-type NfuA; 100 μM LipA Pro23Ala + 100 μM wild-type NfuA; 100 μM LipA Val24Ala + 100 μM wild-type NfuA; 100 μM LipA Ile22Ala, Pro23Ala, Val24Ala triple variant + 100 μM wild-type NfuA; and 100 μM LipA Ile22Ala, Pro23Ala, Val24Ala triple variant + 100 μM NfuA Ile4Ala. The interaction was judged both by the calculated experimental size of each of the peaks as well as by a shift in the elution volume. The identity of protein(s) contained in the corresponding fractions was confirmed by SDS-PAGE.

Table 5-1: Oligonucleotides used for plasmid construction of genes screened using bacterial two hybrid analysis.

Gene	Vector		Oligonucleotide
nfuA	pDONR221	for	5'GCCGCACAAGTTTGTACAAAAAAGCAGGCTTTATGATGATCCGTATTTCCGATG C 3'
		rev	5' GCGGACCACTTTGTACAAGAAAGCTGGGTT TTA GTA GTA GGA GTG TTC GC 3'
lipA	pDONR221	for	5' GCCGCACAAGTTTGTACAAAAAAGCAGGCTTTATG ATG AGT AAA CCC ATT GTG ATG 3'
		rev	5' GCGGACCACTTTGTACAAGAAAGCTGGGTT TTA CTT AAC TTC CAT CCC TTT C 3'
gcvH	pDONR221	for	5' GCCGCACAAGTTTGTACAAAAAAGCAGGCTTT ATG ATT ACG CTG TGG GGT CGG 3'
		rev	5' GCGGACCACTTTGTACAAGAAAGCTGGGTT TTA GCT AAC GGG AAT CAT CAC 3'
gstB	pDONR221	for	5' GCCGCACAAGTTTGTACAAAAAAGCAGGCTTT ATG AGC AAC GTA CCA GCA GAA 3'
		rev	5' GCGGACCACTTTGTACAAGAAAGCTGGGTT TTA CTC GTC TTC TAA CAA TGC 3'
nfuA C39A, C44A	pDONR221	for	5'GCCGCACAAGTTTGTACAAAAAAGCAGGCTTTATGATGATCCGTATTTCCGATG C 3'
		rev	5' GCGGACCACTTTGTACAAGAAAGCTGGGTT TTA GTA GTA GGA GTG TTC GC 3'
nfuA N terminal domain	pDONR221	for	5′ GCCGCACAAGTTTGTACAAAAAAGCAGGCTTT ATG ATC CGT ATT TCC GAT GCT GCA CAA GC 3′
		rev	5′ GCGGACCACTTTGTACAAGAAAGCTGGGTT TTA TTT GGC GTT CGG GGC TTT CAG CG 3′
nfuA C terminal domain	pDONR221	for	5′ GCCGCACAAGTTTGTACAAAAAAGCAGGCTTT ATG ATG CGT AAA GTG GCA GAC GAT GC 3′
		rev	5′ GCGGACCACTTTGTACAAGAAAGCTGGGTT TTA GTA GTA GGA GTG TTC GCC GC 3′
miaB	pDONR221	for	5′ GCCGCACAAGTTTGTACAAAAAAGCAGGCTTT ATG ACC AAA AAA CTC CAT ATT AAA ACC 3′
		rev	5′ GCGGACCACTTTGTACAAGAAAGCTGGGTT TTA CGG CTG ATA ATA ACC CAC GCC AAG 3′
nfuA 3-191	pDONR221	for	5′ GCCGCACAAGTTTGTACAAAAAAGCAGGCTTT ATGCGTATTTCCGATGCT 3′
		rev	5′ GCGGACCACTTTGTACAAGAAAGCTGGGTT TTAGTAGTAGGAGTGTTC 3′
nfuA 4-191	pDONR221	for	5′ GCCGCACAAGTTTGTACAAAAAAGCAGGCTTT ATGATTTCCGATGCTGCACAAGC 3′
		rev	5′ GCGGACCACTTTGTACAAGAAAGCTGGGTT TTAGTAGTAGGAGTGTTC 3′
nfuA 6-191	pDONR221	for	5′ GCCGCACAAGTTTGTACAAAAAAGCAGGCTTT ATGGATGCTGCACAAGCGCAC 3′
		rev	5′ GCGGACCACTTTGTACAAGAAAGCTGGGTT TTAGTAGTAGGAGTGTTC 3′
nfuA 8-191	pDONR221	for	5′ GCCGCACAAGTTTGTACAAAAAAGCAGGCTTT ATG GCA CAA GCG CAC TTT GCC3′
		rev	5′ GCGGACCACTTTGTACAAGAAAGCTGGGTT TTAGTAGTAGGAGTGTTC 3′
nfuA 11-191	pDONR221	for	5′ GCCGCACAAGTTTGTACAAAAAAGCAGGCTTT ATGCACTTTGCCAAACTGCTG 3′
		rev	5′ GCGGACCACTTTGTACAAGAAAGCTGGGTT TTAGTAGTAGGAGTGTTC 3′
nfuA 21-191	pDONR221	for	5′ GCCGCACAAGTTTGTACAAAAAAGCAGGCTTT ATGGAAGGGACACAAATCCGC 3′
		rev	5′ GCGGACCACTTTGTACAAGAAAGCTGGGTT TTAGTAGTAGGAGTGTTC 3′

nfuA 31-191	pDONR221	for	5′ GCCGCACAAGTTTGTACAAAAAAGCAGGCTTT ATGAACCCTGGCACGCCTAAC 3′
		rev	5′ GCGGACCACTTTGTACAAGAAAGCTGGGTT TTA GTA GTA GGA GTG TTC GC 3′
nfuA 41-191	pDONR221	for	5′ GCCGCACAAGTTTGTACAAAAAAGCAGGCTTT ATGGTTTCTTATTGTCCGCCG 3′
		rev	5′ GCGGACCACTTTGTACAAGAAAGCTGGGTT TTA GTA GTA GGA GTG TTC GC 3′
nfuA 51-191	pDONR221	for	5′ GCCGCACAAGTTTGTACAAAAAAGCAGGCTTT ATGGCCACCGACACAGCCCTG 3′
		rev	5′ GCGGACCACTTTGTACAAGAAAGCTGGGTT TTA GTA GTA GGA GTG TTC GC 3′
lipA 6-321	pDONR221	for	5′ GCCGCACAAGTTTGTACAAAAAAGCAGGCTTT ATG GTG ATG GAA CGC GGT G 3′
	pDONR221	rev	5′ GCGGACCACTTTGTACAAGAAAGCTGGGTT TTACTTAACTTCCATCCC 3′
lipA 11-321	pDONR221	for	5′ GCCGCACAAGTTTGTACAAAAAAGCAGGCTTT ATG GTT AAA TAC CGC GAT G 3′
		rev	5′ GCGGACCACTTTGTACAAGAAAGCTGGGTT TTACTTAACTTCCATCCC 3′
lipA 16-321	pDONR221	for	5′ GCCGCACAAGTTTGTACAAAAAAGCAGGCTTT ATG GCC GAT AAG ATG GCC C 3′
		rev	5′ GCGGACCACTTTGTACAAGAAAGCTGGGTT TTACTTAACTTCCATCCC 3′
lipA 21-321	pDONR221	for	5′ GCCGCACAAGTTTGTACAAAAAAGCAGGCTTT ATG CTT ATC CCG GTT AAA AAC 3′
		rev	5′ GCGGACCACTTTGTACAAGAAAGCTGGGTT TTACTTAACTTCCATCCC 3′
lipA 26-321	pDONR221	for	5′ GCCGCACAAGTTTGTACAAAAAAGCAGGCTTT ATG AACGTGGCAACAGAGCGC 3′
		rev	5′ GCGGACCACTTTGTACAAGAAAGCTGGGTT TTACTTAACTTCCATCCC 3′
lipA 51-321	pDONR221	for	5′ GCCGCACAAGTTTGTACAAAAAAGCAGGCTTT ATGCGTATCCAGGGCATCAAAG 3′
		rev	5′ GCGGACCACTTTGTACAAGAAAGCTGGGTT TTACTTAACTTCCATCCC 3′
lipA 76-321	pDONR221	for	5′ GCCGCACAAGTTTGTACAAAAAAGCAGGCTTT ATG CTGGCGGAATGCTTCAAC 3′
		rev	5′ GCGGACCACTTTGTACAAGAAAGCTGGGTT TTACTTAACTTCCATCCC 3′
lipA 101-321	pDONR221	for	5′ GCCGCACAAGTTTGTACAAAAAAGCAGGCTTT ATG TGTGATGTTGCCCACGGTC 3′
		rev	5′ GCGGACCACTTTGTACAAGAAAGCTGGGTT TTACTTAACTTCCATCCC 3′
lipA 126-321	pDONR221	for	5′ GCCGCACAAGTTTGTACAAAAAAGCAGGCTTT ATG ATGGCGCTGCGTTATGTG 3′
		rev	5′ GCGGACCACTTTGTACAAGAAAGCTGGGTT TTACTTAACTTCCATCCC 3′
lipA 151-321	pDONR221	for	5′ GCCGCACAAGTTTGTACAAAAAAGCAGGCTTT ATG GATTGCATTACTGCCATTC 3′
		rev	5′ GCGGACCACTTTGTACAAGAAAGCTGGGTT TTACTTAACTTCCATCCC 3′
lipA 176-321	pDONR221	for	5′ GCCGCACAAGTTTGTACAAAAAAGCAGGCTTTATG ATG GATC GTGCT CTGGATA TTC 3′
		rev	5′ GCGGACCACTTTGTACAAGAAAGCTGGGTT TTACTTAACTTCCATCCC 3′
lipA 201-321	pDONR221	for	5′ GCCGCACAAGTTTGTACAAAAAAGCAGGCTTT ATG ATTTACCGTCAGGTACGG 3′
		rev	5′ GCGGACCACTTTGTACAAGAAAGCTGGGTT TTACTTAACTTCCATCCC 3′
lipA 226-321	pDONR221	for	5′ GCCGCACAAGTTTGTACAAAAAAGCAGGCTTT ATGCCGGAAATCCCGACCAAG 3′
		rev	5′ GCGGACCACTTTGTACAAGAAAGCTGGGTT TTACTTAACTTCCATCCC 3′
nfuA Ile4Ala	pDONR221	for	5′ GGC TTT ATG ATC CGT GCG TCC GAT G CT G CA C AA G 3′

		rev	5′ CTT GTG CAG CAT CGG A CGC ACGGATCATAAAGCC 3′
nfuA Ser5Ala	pDONR221	for	5′ C TTT ATG ATC CGT ATT GCC GAT GCT GCA CAA GCG 3′
		rev	5′ CGCTTGTGCAGCATCGGCAATACGGATCATAAAG 3′
nfuA Ile4Ala, Ser5Ala	pDONR221	for	5′ GGC TTT ATG ATC CGT GCG GCC GAT GCT GCA CAA GCG 3′
		rev	5′ CGCTTGTGCAGCATCGGCCGCACGGATCATAAAGCC 3′
lipA Leu21ALa	pDONR221	for	5′ GCC GAT AAG ATG GCC GCG ATC CCG GTT AAA AAC 3′
		rev	5′ GTTTTTAACCGGGATCGCGGCCATCTTATCGGC 3′
lipA Ile22Ala	pDONR221	for	5′ GAT AAG ATG GCC CTT GCC CCG GTT AAA AAC GTG 3′
		rev	5′ CACGTTTTTAACCGGGGCAAGGGCCATCTTATC 3′
lipA Pro23Ala	pDONR221	for	5′ GAT AAG ATG GCC CTT ATC GCG GTT AAA AAC GTG GCA AC 3′
		rev	5′ GTTGCCACGTTTTTAACCGCGATAAGGGCCATCTTATC 3′
lipA Val24Ala	pDONR221	for	5′ G ATG GCC CTT ATC CCG GCG AAA AAC GTG GCA ACA G 3′
		rev	5′ CTGTTGCCACGTTTTTCGCCGGGATAAGGGCCATC 3′
lipA Lys25Arg	pDONR221	for	5′ GCC CTT ATC CCG GTT CGT AAC GTG GCA ACA GAG 3′
		rev	5′ CTCTGTTGCCACGTTACGAACCGGGATAAGGGC 3′
lipA Lys25Ala	pDONR221	for	5′ GCC CTT ATC CCG GTT GCG AAC GTG GCA ACA GAG 3′
		rev	5′ CTCTGTTGCCACGTTCGCAACCGGGATAAGGGC 3′

LipA Enzyme Reactions.

Ultra-Performance Liquid Chromatography (UPLC) with detection by mass spectrometry (UPLC-MS) was conducted using an Agilent Technologies (Santa Clara, CA) 1290 Infinity II system coupled to an Agilent Technologies 6470 QQQ mass spectrometer or an Agilent Technologies 1200 system coupled to an Agilent Technologies 6410 QQQ mass spectrometer. Data collection and analysis were performed using the associated MassHunter software. Detection of substrates and products was performed using electrospray ionization mass spectrometry in positive mode (ESI^+-MS) with the following parameters: a nitrogen gas temperature of 350 °C and flow

rate of 59.0 L/min, a nebulizer pressure of 45 PSI and a capillary voltage of 4000 V. Substrates and products were detected using multiple-reaction-monitoring **(Table 5-2).** The reaction mixture was separated on an Agilent Technologies Zorbax Eclipse Plus-C18 Rapid Resolution HD column (2.1 mm × 50 mm, 1.8 μm particle size) equilibrated in 98% Solvent A (0.1% formic acid, pH 2.6) and 2% Solvent B (100% acetonitrile). A gradient of 25-27% solvent B was applied from 0.5 min to 2.0 min before returning solvent B to 8% from 2 min to 2.5 min. A flow-rate of 0.3 mL/min was maintained throughout the method. The column was allowed to re-equilibrate for 1 min under the initial conditions between sample injections.

The reaction monitoring the activity of the protein variants included 25 μM *E. coli* LipA Ile22Ala, 400 μM [4Fe–4S]-containing *E. coli* NfuA, 600 μM octanoyl-peptide substrate analogue (Glu-Ser-Val-[N^6-octanoyl]Lys-Ala-Ala-Ser-Asp), 0.5 μM SAH nucleosidase, and 1 mM SAM. The reaction was initiated with sodium dithionite (2 mM final concentration) and was quenched with H_2SO_4 at a final concentration of 100 mM in the presence of a final concentration of 20 μM AtsA peptide (REF) (internal standard). Error bars represent the mean ± standard deviation of three replicates.

Table 5-2: Fragmentation Products of LipA Reaction Monitored by LC-MS.

Compound	Parent Ion*	Product Ion 1	Product Ion 2
AtsA (IS)	474.4(112)	201.1 (18)	153 (26)
Lipoyl peptide	996.5 (208)	776.3 (30)	274.1 (46)
6-thiooctanoyl peptide	964.5 (220)	744.4 (30)	242.1 (46)

*Respective fragmentor voltages in parenthesis

Respective collision energies in parenthesis

Overproduction of Holo E. coli MiaB.

E. coli BL21(DE3) cells were co-transformed with the *E. coli* miaB-pET28a construct encoding the desired gene and plasmid pDB1282, which encodes the genes in the *isc* operon from *Azotobacter vinelandii* (5). A single colony was used to inoculate 200 mL lysogeny broth (LB) supplemented with 50 µg/mL kanamycin and 100 µg/mL ampicillin, and the starter culture was incubated overnight at 37 °C with shaking at 250 rpm. The following day, 20 mL of the starter culture was used to inoculate four 6 L flasks containing 4 L M9 minimal media supplemented with 50 µg/mL kanamycin and 100 µg/mL ampicillin. The *E. coli* strains were cultured at 37 °C with shaking at 180 rpm. At an OD_{600}=0.3, 0.2% (final concentration) arabinose was added to induce expression of the genes encoded in the pDB1282 plasmid. At an OD_{600}=0.6, 50 µM (final concentration) $FeCl_3$ was added to the cultures, and the flasks were placed in an ice-water bath for ~30 min. Once chilled, expression of the desired gene was induced by the addition of 200 µM IPTG (final concentration) and allow to proceed for ~18 h at 18 °C with shaking at 180 rpm. Bacterial cells were harvested by centrifugation at 7,500 × g for 12 min. The resulting cellular pellet was flash-frozen in liquid N_2 and stored in liquid N_2 until further use.

Isolation of E. coli MiaB.

All purification steps were carried out in an anaerobic chamber containing <1 ppm O_2 (Coy Laboratory Products, Grass Lake, MI), with the exception of the centrifugation steps, which were conducted outside of the chamber in tightly sealed tubes. *E. coli* MiaB was purified by immobilized metal affinity chromatography (IMAC) using the following procedure. The cellular pellet containing overproduced protein was re-suspended in Buffer A (50 mM HEPES, pH 7.5, 300 mM KCl, 10 mM imidazole, 10 mM β-mercaptoethanol). Lysozyme (1 mg/mL) and DNase I (0.1 mg/mL) were added and the solution was stirred for 30 min at room temperature. The cells were lysed by sonic disruption, and the resulting lysate was centrifuged at 45,000 × g for 1 h. The

supernatant was applied to a column of Ni-NTA resin pre-equilibrated in Buffer A, and the column was washed with Buffer B (50 mM HEPES, pH 7.5, 300 mM KCl, 20 mM imidazole, 10 mM β-mercaptoethanol, and 10% glycerol). The protein was eluted with Buffer C (50 mM HEPES, pH 7.5, 300 mM KCl, 500 mM imidazole, 10 mM β-mercaptoethanol, and 10% glycerol) and then concentrated to 2.5 mL and exchanged into storage buffer (50 mM HEPES, pH 7.5, 300 mM KCl, 5 mM DTT, 15% glycerol) using a PD-10 column (GE Healthcare Life Sciences). The protein was aliquoted, flash-frozen, and stored in liquid N_2 until use. An SDS-PAGE (12.5%) gel stained with Coomassie brilliant blue revealed that the final protein was >95% pure. The protein concentration was determined using the Bradford method. No amino acid correction factor was available for *E. coli* MiaB, so the correction factor for Tm MiaB was used (1.53). Colorimetric iron analysis normalized to protein concentration was used to estimate the iron content per polypeptide (9).

Chemical Reconstitution of E. coli MiaB.

E. coli MiaB was chemically reconstituted using DTT, iron, and sodium sulfide to improve cofactor incorporation. A reaction containing 100 µM as-isolated MiaB was slowly stirred on ice. DTT (5 mM final concentration) was added in three increments every 20 min, and the solution was incubated for 1 hr. Following reduction, $FeCl_3$ (800 µM final concentration) was added in five increments every 5 min, and the solution was incubated for 30 min. The sodium sulfide was added in five increments every 30 min (800 µM final concentration), and the reaction was incubated on ice overnight. The following day, precipitation was removed by centrifugation at 45,000 × g for 10 min, and the protein in the supernatant was concentrated to 2 mL. Aggregates and non-specifically bound substances were removed by applying the reaction to a HiPrep 16/60 Sephacryl HR S-200 column (GE Healthcare) equilibrated in storage buffer (flow-rate of 0.5 mL/min).

Association of E.coli NfuA and E. coli MiaB using molecular sieve chromatography.

The ability of *E. coli* MiaB and *E. coli* NfuA to associate was investigated using size-exclusion chromatography. A 500 μL mixture of standards composed of cytochrome c (12.4 kDa), carbonic anhydrase (29 kDa), bovine serum albumin (66 kDa), alcohol dehydrogenase (150 kDa), α-amylase (200 kDa), and blue dextran (2000 kDa) was applied to a HiPrep 16/60 Sephacryl HR S-200 column (GE Healthcare) housed in a Coy anaerobic glovebox under strictly anaerobic conditions (<1 ppm O_2) equilibrated in freshly prepared buffer (50 mM HEPES, pH 7.5, 150 mM KCl, 15% glycerol, and 1 mM DTT). The log MW of each standard was plotted against their respective elution volumes after correcting for the void-volume of the column. A linear fit to the data was then used to estimate the molecular weight of each sample. The following samples were applied to the column in a 500 μL volume: 100 μM NfuA, 100 μM MiaB, and a mixture of 100 μM MiaB and 100 μM NfuA. The interaction was judged both by the calculated experimental size of each of the peaks as well as by a shift in the elution volume. The identity of protein(s) contained in the corresponding fractions was confirmed by SDS-PAGE.

E. coli MiaB Activity Assays.

Activity assays were performed as previously described (7). Detection of substrates and products was performed using electrospray ionization in positive mode (ESI+) with the following parameters: a nitrogen gas temperature of 350 °C and flow rate of 9.0 L/min, a nebulizer pressure of 45 PSI and a capillary voltage of 4000 V. Substrates and products were detected using multiple reaction monitoring **(Table 5-3).** The assay mixture was separated on an Agilent Technologies Zorbax Extend-C18 column Rapid Resolution HT (4.6 mm × 50 mm, 1.8 μm particle size) equilibrated in 98% Solvent A (40 mM ammonium acetate, pH 6.2) and 2% Solvent B (100% acetonitrile). A gradient of 2-50% solvent B was applied from 0.3 min to 2.0 min and maintained at 50% solvent B until 3.0 min before returning to 2% solvent B from 3 min to 3.5 min. A flow-

rate of 0.5 mL/min was maintained throughout the method. The column was allowed to re-equilibrate for 2 min under the initial conditions between sample injections. Reactions contained either 25 µM *E. coli* MiaB only (control) or 25 µM *E. coli* MiaB in the presence of 200 µM [4Fe–4S] loaded *E. coli* NfuA. Additional reaction components included 300 µM i^6A 17-mer substrate (7), reaction buffer (50 mM HEPES, pH 7.5, 300 mM KCl, 10 mM $MgCl_2$, 3.3 mM Trp (internal standard), and 1 mM SAM. The reaction was initiated using 2 mM sodium dithionite. At the selected time points, 10 µL of the reaction was quenched in 10 µL 200 mM H_2SO_4 . At the end of the assay, the quenched samples were removed from the anaerobic chamber, and 40 µL 10× P1 buffer and 0.8 units of Nuclease P1 (2 µL of 0.2 units/ µL stock) were added to each sample. After incubating at 45 °C for 2 h, *C. adamanteus* phosphodiesterase was added (0.002 U) in its reaction buffer (50 mM Tris-HCl pH 9.3, 1 mM $MgCl_2$, 0.1 $ZnCl_2$, and 1 mM spermidine) and the reaction was incubated at 37 °C for 2 h. Calf-intestinal alkaline phosphatase (2 U) was then added, and the reaction was incubated at 37 °C for 1 h. The pH was then adjusted to 6.0 using 0.1 mM H_2SO_4. The reaction was centrifuged at 14,000 × g for 30 min. The supernatant was loaded into autosampler vials and subsequently analyzed.

Table 5-3: Fragmentation Products in MiaB Reaction Monitored by LC-MS.

Compound	Parent Ion*	Product Ion 1□	Product Ion 2□
Trp	188 (130)	146.1 (10)	118 (21)
ms^2i^6A	382.2 (135)	250.1 (13)	194 (25)
i^6A	336.2 (135)	204.1 (13)	148.1 (25)

*Respective fragmentor voltages in parenthesis

□Respective collision energies in parenthesis

Results

Co-immunoprecipitation of E. coli NfuA and E. coli LipA.

Many gaps remain in our understanding of *E. coli* NfuA and its role in FeS cluster maturation. One outstanding question is whether NfuA specifically targets LipA or whether it targets multiple proteins in the cell. A second fundamental question is whether there is a defined recognition motif within the primary sequence of NfuA's targets. In order to gain more insight into both of these questions, initial studies focused on co-immunoprecipitation experiments. A construct encoding the *nfuA* gene with a flag epitope tag was used to produce the NfuA-FLAG protein, which could subsequently be captured from cells using an anti-flag antibody resin. The resin-protein mixture was carefully washed with physiological salt conditions (137 mM NaCl and 2.7 mM KCl) to minimize loss of interacting proteins, and the target protein was eluted using a flag peptide. Proteins that were "pulled-down" with our NfuA target were visualized using SDS-PAGE with visualization using either Coomassie staining **(Figure 5-1, Panel A)** or silver staining procedures **(Figure 5-1, Panels B and C)**. The corresponding region of the gel was excised, and the proteins therein were typsin-digested and identified using mass spectrometry. A total of 10 bands were submitted for identification **(Figure 5-1, Panel C).** We anticipated that the co-immunoprecipitation would reveal additional protein targets. An extensive list of proteins **(Appendix A)** identified by mass spectrometry provided a robust amount of useful data. As we had hoped, we pulled-down LipA with NfuA-FLAG, providing convincing *in vivo* evidence of their tight association. Several of the lipoylated protein complexes also co-immunoprecipitated with NfuA, including components of the

pyruvate dehydrogenase complex and 2-oxoglutarate dehydrogenase complex. Components that are hypothesized to play a role in the regulation of lipoic acid biosynthesis also were captured, such as ClpX, as well as other iron-sulfur carrier proteins and proteins involved in iron sulfur cluster assembly, such as IscS and Mrp. Surprisingly, several other RS enzymes co-immunoprecipitated with NfuA, including MiaB and RimO, which also catalyze sulfur-insertion reactions and have auxiliary clusters that might undergo destruction during catalysis (10). To gain further insight, the *lipA* gene was used to create a construct with an encoded flag epitope tag. This new construct was used to perform an identical experiment as described for *nfuA*-FLAG instead using LipA as the target. Following elution from the antibody resin with FLAG peptide, an SDS-PAGE gel was run and visualized using silver stain **(Figure 5-2).** The same protein sample was visualized using Coomassie stain for better sensitivity with mass spectrometry analysis. A total of 11 bands were submitted for protein identification. Again, an extensive list of proteins **(Appendix B)** were identified in the pull-down mixture. Excitingly, of these identified proteins, *E. coli* NfuA was present, confirming the tight interaction of *E. coli* LipA and *E. coli* NfuA in the cell. No other protein involved with iron-sulfur cluster biosynthesis pulled down with LipA. However, components of protein complexes that are lipoylated in the cell were also among the list of identified proteins. One potential downfall of this technique is that it is difficult to capture weak or transient interactions. To overcome this issue in future work, a crosslinking reagent could be used in a similar experiment to stabilize these protein-protein complexes.

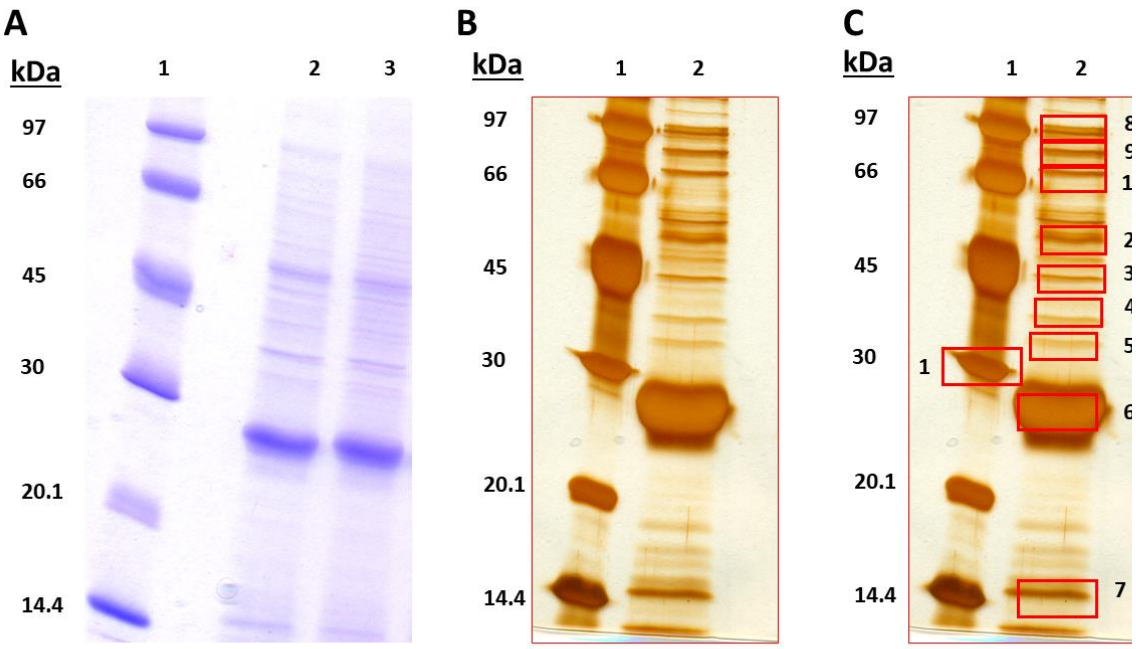

Figure 5-1: **Co-immunoprecipitation of *E. coli* NfuA.** *E. coli* flag-tagged NfuA protein was pulled out of the cell using anti-flag resin. After mild washing, the NfuA protein and any potential interactors were eluted following incubation of the protein-resin complex with flag peptide. (A) SDS-PAGE analysis of the eluted protein with visualization by Coomassie stain. Lane 1: molecular weight ladder Lane 2: eluted protein Lane 3: eluted protein (B) SDS-PAGE analysis of the eluted protein with visualization by silver stain Lane 1: molecular weight ladder Lane 2: eluted protein (C) Same gel presented in panel B, with red boxes indicating the bands that were excised for identification by mass spectrometry.

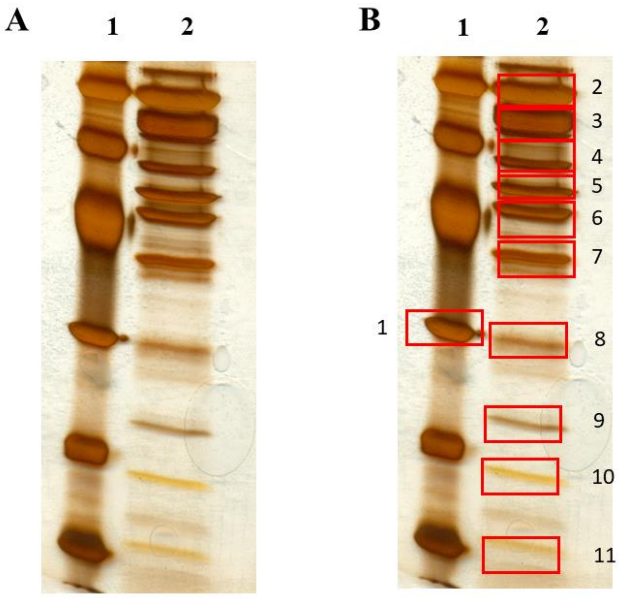

Figure 5-2: **Co-immunoprecipitation of *E. coli* LipA.** *E. coli* flag-tagged LipA protein was pulled out of the cell using anti-flag resin. After mild washing, the LipA protein and any potential interactors were eluted following incubation of the protein-resin complex with flag peptide. (A) SDS-PAGE analysis of the eluted protein with visualization by silver stain Lane 1: molecular weight ladder Lane 2: eluted protein (B) Same gel presented in panel B, with red boxes indicating the bands that were excised for identification by mass spectrometry.

Kd Determination of E. coli LipA and E. coli NfuA using Microscale Thermophoresis.

The previously reported complex of *E. coli* LipA and *E. coli* NfuA determined by analytical molecular-sieve chromatography is consistent with a stable and tight association between the two proteins *in vitro*. Interestingly, when performing *in vivo* co-immunoprecipitation studies, NfuA and LipA could be pulled out of the cell together without the use of a crosslinker. Our qualitative binding studies lead us to calculate the dissociation constant (K_d), of the interaction, which we accomplished using microscale thermophoresis. *E. coli* LipA was fluorescently labeled using an amine reactive dye, while the unlabeled *E. coli* NfuA protein was titrated against it. Unfortunately, ligand induced fluorescence changes were observed at high concentrations of the NfuA ligand,

which precluded the use of the MST traces to calculate the K_d. However, a specificity test was performed that indicated that the fluorescence changes were a direct result of the protein-protein interaction, which allowed a K_d to be determined directly from the fluorescence data. **(Figure 5-3).** The binding assay was performed in triplicate, and each replicate was accompanied by a specificity test. The resulting K_d was calculated to be 950 nM ± 110 nM **(Figure 5-4).**

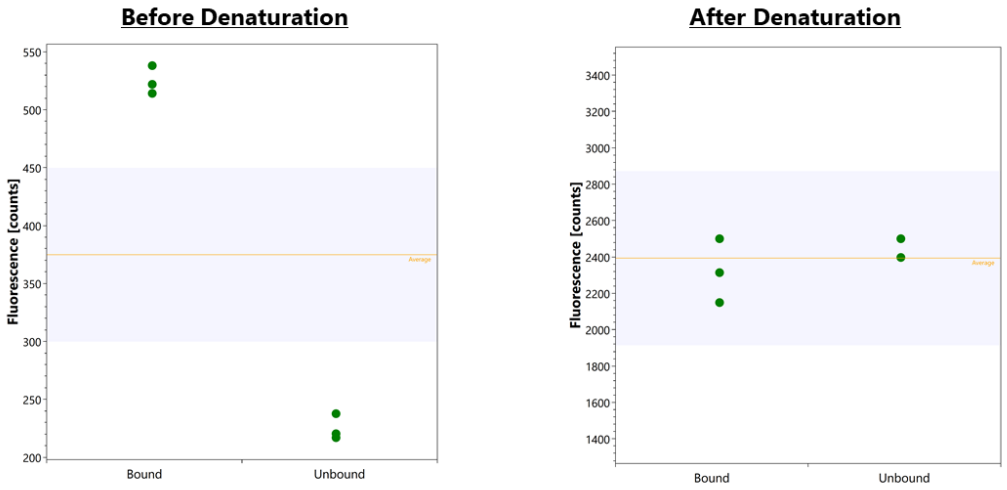

Figure 5-3: Specificity Test from the *E. coli* LipA/*E. coli* NfuA MST Experiment. Ligand induced fluorescence changes were observed in the MST data. A specificity test was performed for each replicate to assess whether initial fluorescence data could be used to calculate the K_d. Upon denaturation, the fluorescence changes were not observed, consistent with the changes in fluorescence being a direct result of the protein-protein interaction.

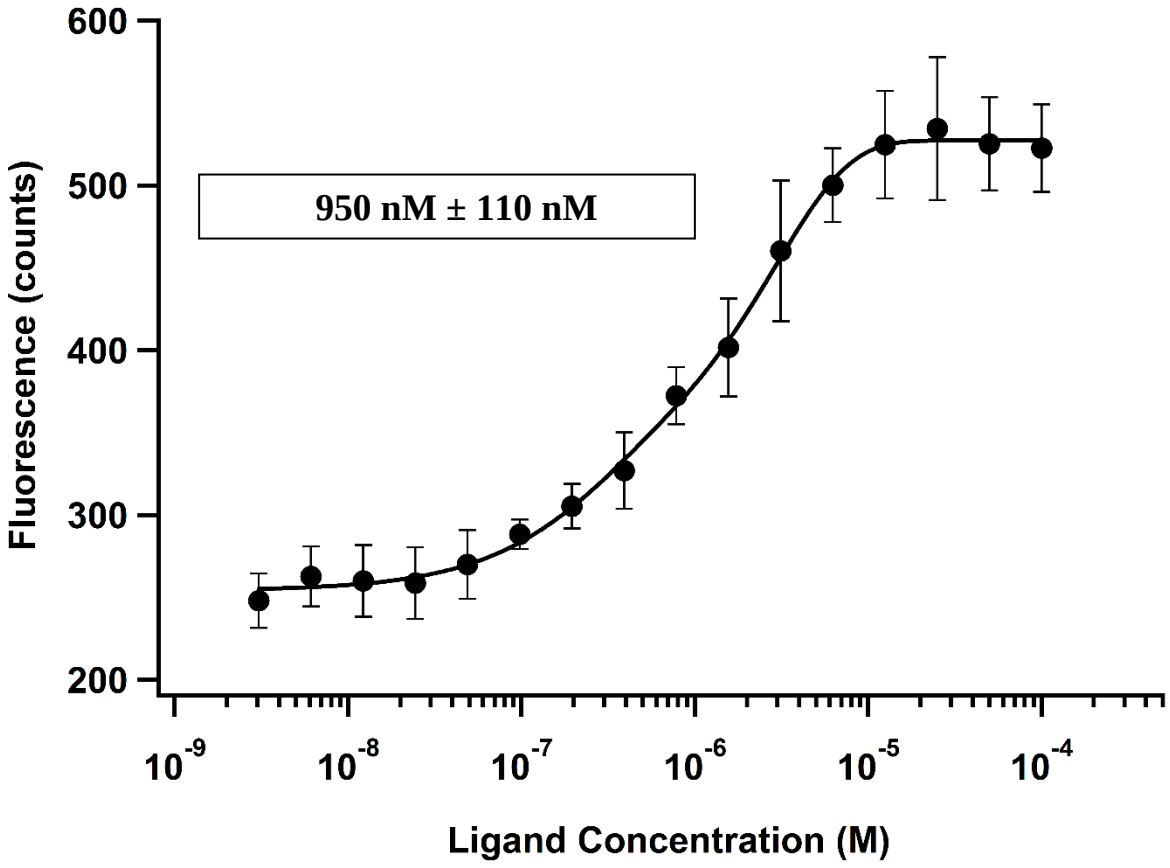

Figure 5-4: K_d Determination of *E. coli* LipA and *E. coli* NfuA association using MST. *E. coli* LipA (500 nM final protein concentration) was labeled with a fluorescent amine-reactive dye. Unlabeled *E. coli* NfuA ligand was serial diluted from 100 µM (first point) across 16 tubes. Error bars represent the data obtained from triplicate experiments, and a specificity test was performed for each replicate.

E. coli NfuA binds E. coli LipA in vivo. We have previously shown that *E. coli* NfuA, specifically the N terminal domain, and *E. coli* LipA form a tight complex *in vitro* using analytical molecular sieve chromatography (3,4). To show that this is a physiologically relevant complex, a bacterial adenylate cyclase two hybrid system was used. This system takes advantage of the two catalytic domains of *Bordetella pertussis* adenylate cyclase (CyaA) toxin, which can be fused separately to proteins of interest (11). If the proteins of interest interact, then the adenylate cyclase domains will

be brought in close proximity to each other, reconstituting cyclic AMP (cAMP) production **(Figure 5-5).** In *E. coli*, cAMP is a regulator of gene transcription, and binds to the catabolite activator protein (CAP). The resulting cAMP/CAP complex can then activate the transcription of catabolite genes, which upregulates β-galactosidase expression. As a result, interacting proteins can be screened by the development of blue color in the presence of X-gal. The following constructs were assembled using gateway cloning technology: *gstB*-pUT18C, *gcvH*-pST25, *nfuA*-pUT18C, and *lipA*-pST25. Two domains of the leucine zipper zip-pUT18C and zip-pKT25 were a gift from Dr. Scot Ouellette, University of Nebraska Medical Center. *E. coli* adenylate cyclase deficient BTH101 cells were co-transformed with the following pairs of plasmids: *gstB*-pUT18C + *gcvH*-pST25 (negative control), zip-pUT18C + zip-pKT25 (positive control), and *nfuA*-pUT18C + *lipA*-pST25. The cells were plated on LB agar plates containing IPTG and x-gal. After incubation at 30 °C for 48 h, robust blue colonies were observed on both the *zip*-pUT18C + *zip*-pKT25 control plates and the *nfuA*-pUT18C + *lipA*-pST25 plates compared to the color of the *gstB*-pUT18C + *gcvH*-pST25 negative control plates indicating an interaction **(Figure 5-6, Panels A-C).** The binding of *E. coli* LipA and the *E. coli* NfuA N terminal domain, as well as the lack of binding of the *E. coli* NfuA C terminal domain were also confirmed *in vivo* using this approach **(Figure 5-6, Panels D and E).** Moreover, this data provides the foundation for the development of a genetic screen to probe important outstanding questions, such as identifying essential residues for the interaction between NfuA and LipA using a library of variants. β-galactosidase assays were not performed to quantify the interaction *in vivo* and can be an additional future research direction.

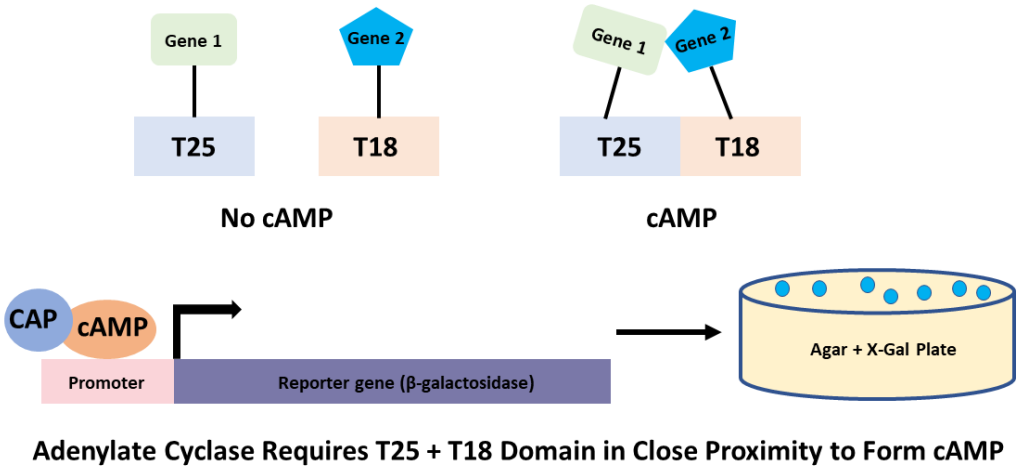

Figure 5-5: **Overview of Bacterial Two Hybrid Method.** Bacterial two hybrid screening relies on the fact that adenylate cyclase requires its T25 and T18 domains in close proximity to form cAMP. The method fuses each of the domains individually to two proteins of interest. If the proteins of interest interact, then the adenylate cyclase domains will be brought in close proximity to each other, reconstituting cyclic AMP (cAMP) production. In *E. coli*, cAMP is a regulator of gene transcription and binds to the catabolite activator protein (CAP), and then the cAMP/CAP complex can activate the transcription of catabolite genes and upregulates β-galactosidase expression. As a result, positively interacting proteins can be screened by the development of blue color in the presence of X-gal.

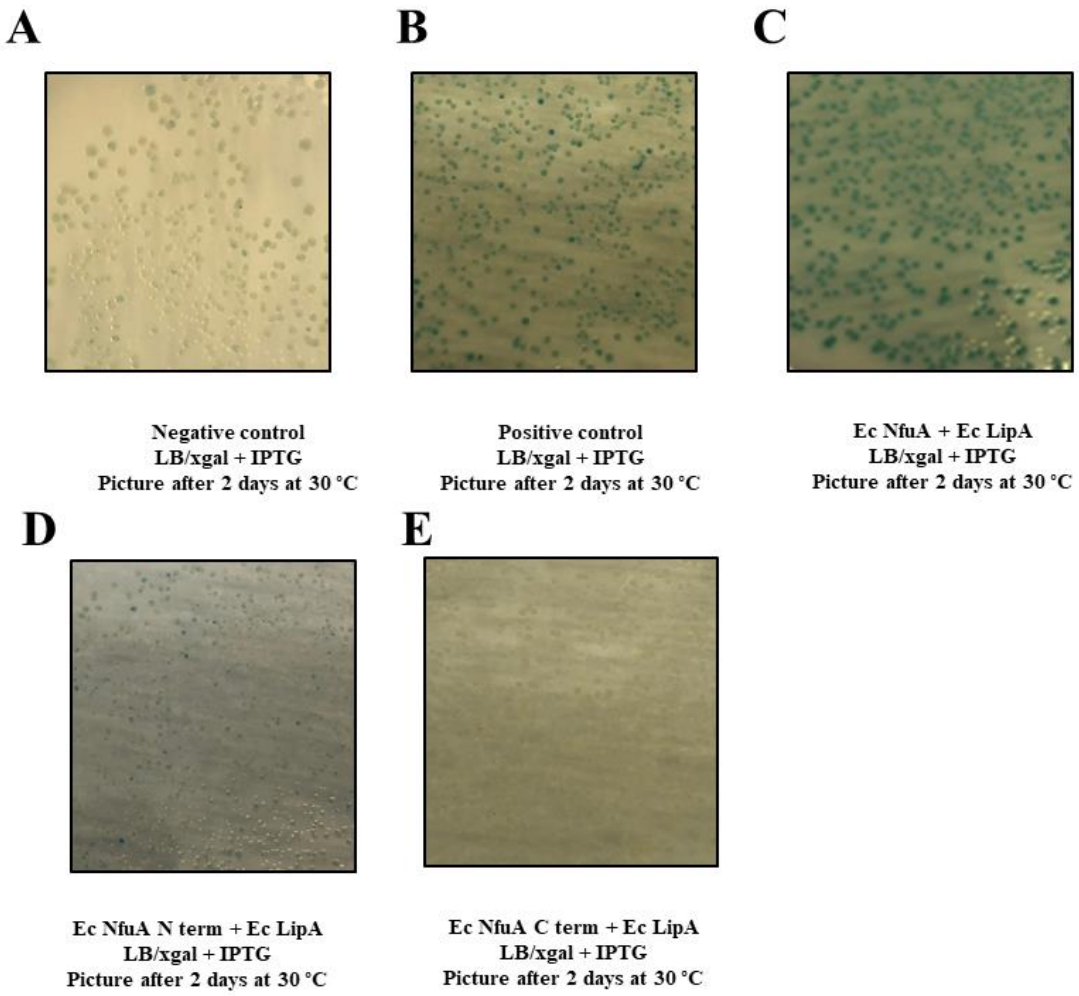

Figure 5-6: Bacterial two hybrid screening of *E. coli* NfuA and *E. coli* LipA. Adenylate cyclase deficient cells strain BTH101 were co-transformed bacterial two hybrid plasmids and spread on LB agar plates containing 40 μg/μL galactosidase and 0.5 mM IPTG with the respective selective antibiotics (100 μg/μL spectinomycin or 50 μg/μL kanamycin and 100 μg/μL ampicillin) . (A) Negative control containing two non-interacting proteins *E. coli gcvH*-pUT18C and *E. coli gstB*-pST25. (B) Positive control containing two domains of leucine zipper: *zip*-pUT18C and *zip*-pKT25 (C) *E. coli nfuA*-pUT18C and *E. coli lipA*-pST25. (D) *E.coli nfuA N term*-pUT18C and *E. coli lipA*-pST25. (E) *E.coli nfuA C term*-pUT18C and *E. coli lipA*-pST25.

Bacterial two hybrid screening of E. coli NfuA and E. coli LipA truncations.

A robust interaction was observed between *E. coli* NfuA and *E. coli* LipA *in vivo* using bacterial two-hybrid screening. This result provided a unique opportunity to probe the interaction

in further detail using this methodology and identify the amino acids that are essential for tight binding. A recent paper from the Rouault laboratory identified an L/IYR motif that is essential for the targeting of succinate dehydrogenase by the co-chaperone HSC20 (2). This was accomplished by creating a library of succinate dehydrogenase truncations and screening them against wild-type HSC20 using a similar yeast two-hybrid approach. Inspired by this success, we adopted a similar strategy and created a library of *E. coli* LipA truncations and screened them against wild-type *E. coli* NfuA **(Figure 5-7).** We observed robust binding between wild-type NfuA and full-length LipA, LipA aa 6-321, LipA aa 11-321, LipA aa 16-321, and LipA aa 21-321 **(Figure 5-7, Panels C-G).** However, no binding was observed between wild-type NfuA and LipA aa 26-321, LipA aa 51-321, LipA aa 76-321, LipA aa 101-321, LipA aa 126-321, LipA 151-321, LipA 176-321, LipA 201-321, LipA 226-321, or LipA 251-321 **(Figure 5-7, Panels H-Q).** Comparing the sequences between *E. coli* LipA aa 21-321 where robust binding with *E. coli* NfuA was observed, and *E. coli* LipA aa 26-321 where binding with *E. coli* NfuA was abolished, the amino acid motif was determined to be "LIPVK."

The reciprocal experiment was performed in which a library of *E. coli* NfuA variants was screened against wild-type *E. coli* LipA **(Figure 5-8).** Because of our previous knowledge that the interaction is dependent upon the N-terminal domain of *E. coli* NfuA, we limited our library to this region. Robust binding was observed between wild-type *E. coli* LipA and full-length *E. coli* NfuA, NfuA aa 3-191, and NfuA aa 4-191 **(Figure 5-8, Panels C-E).** However, no binding was observed between wild-type *E. coli* LipA and NfuA aa 6-191, 8-191, 11-191, 21-191, 31-191, 41-191, or 51-191 **(Figure 5-8, Panels F-L).** Comparing the sequences between NfuA aa 4-191 where robust binding was observed with NfuA aa 6-191, where binding was abolished, an isoleucine-serine motif was discovered.

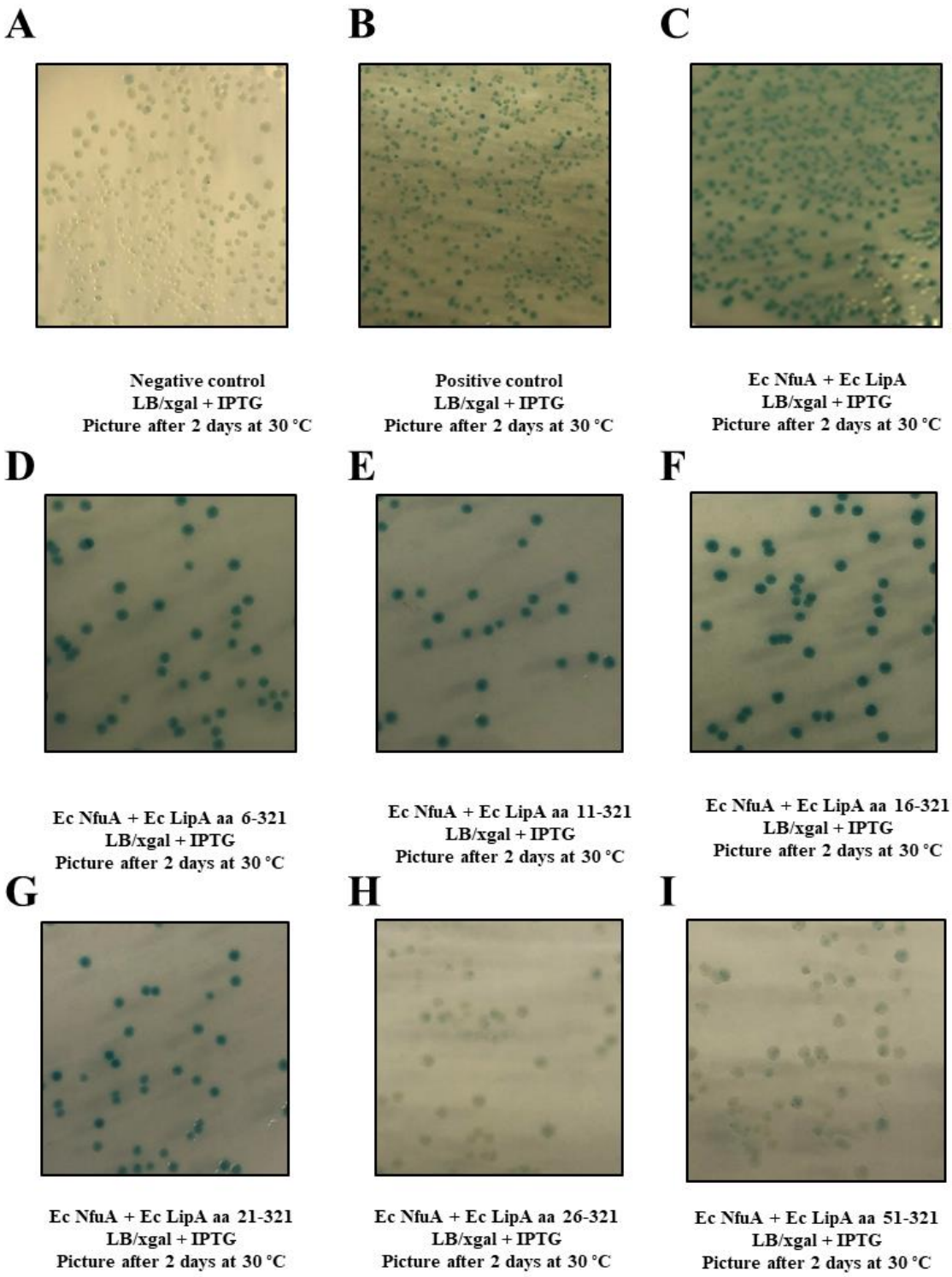
A
B
C
Negative control
LB/xgal + IPTG
Picture after 2 days at 30 °C
Positive control
LB/xgal + IPTG
Picture after 2 days at 30 °C
Ec NfuA + Ec LipA
LB/xgal + IPTG
Picture after 2 days at 30 °C
D
E
F
Ec NfuA + Ec LipA aa 6-321
LB/xgal + IPTG
Picture after 2 days at 30 °C
Ec NfuA + Ec LipA aa 11-321
LB/xgal + IPTG
Picture after 2 days at 30 °C
Ec NfuA + Ec LipA aa 16-321
LB/xgal + IPTG
Picture after 2 days at 30 °C
G
H
I
Ec NfuA + Ec LipA aa 21-321
LB/xgal + IPTG
Picture after 2 days at 30 °C
Ec NfuA + Ec LipA aa 26-321
LB/xgal + IPTG
Picture after 2 days at 30 °C
Ec NfuA + Ec LipA aa 51-321
LB/xgal + IPTG
Picture after 2 days at 30 °C

J

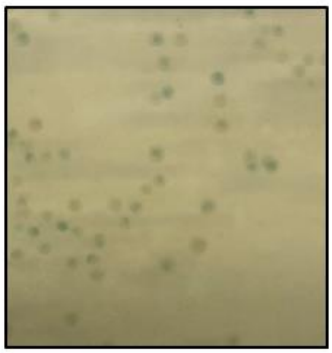

Ec NfuA + Ec LipA aa 76-321
LB/xgal + IPTG
Picture after 2 days at 30 °C

K

Ec NfuA + Ec LipA aa 101-321
LB/xgal + IPTG
Picture after 2 days at 30 °C

L

Ec NfuA + Ec LipA aa 126-321
LB/xgal + IPTG
Picture after 2 days at 30 °C

M

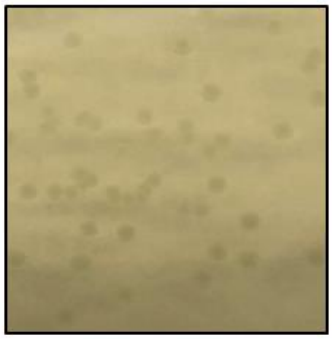

Ec NfuA + Ec LipA aa 151-321
LB/xgal + IPTG
Picture after 2 days at 30 °C

N

Ec NfuA + Ec LipA aa 176-321
LB/xgal + IPTG
Picture after 2 days at 30 °C

O

Ec NfuA + Ec LipA aa 201-321
LB/xgal + IPTG
Picture after 2 days at 30 °C

P

Ec NfuA + Ec LipA aa 226-321
LB/xgal + IPTG
Picture after 2 days at 30 °C

Q

Ec NfuA + Ec LipA aa 251-321
LB/xgal + IPTG
Picture after 2 days at 30 °C

Figure 5-7: Bacterial two hybrid screening of *E. coli* LipA truncations against wild-type *E. coli* NfuA. Adenylate cyclase deficient cells strain BTH101 were co-transformed bacterial two hybrid plasmids and spread on LB agar plates containing 40 μg/μL galactosidase and 0.5 mM IPTG with the respective selective antibiotics (100 μg/μL spectinomycin or 50 μg/μL kanamycin and 100 μg/μL ampicillin) . (A) Negative control containing two non-interacting proteins *E. coli gcvH*-pUT18C and *E. coli gstB*-pST25. (B) Positive control containing two domains of leucine zipper: *zip*-pUT18C and *zip*-pKT25 (C) *E. coli nfuA*-pUT18C and wild-type *E. coli lipA*-pST25. (D) *E. coli nfuA*-pUT18C and *E. coli lipA aa 6-321*-pST25. (E) *E. coli nfuA*-pUT18C and *E. coli lipA aa 11-321*-pST25. (F) *E. coli nfuA*-pUT18C and *E. coli lipA aa 16-321*-pST25. (G) *E. coli nfuA*-pUT18C and *E. coli lipA aa 21-321*-pST25. (H) *E. coli nfuA*-pUT18C and *E. coli lipA aa 26-321*-pST25. (I) *E. coli nfuA*-pUT18C and *E. coli lipA aa 51-321*-pST25. (J) *E. coli nfuA*-pUT18C and *E. coli lipA aa 76-321*-pST25. (K) *E. coli nfuA*-pUT18C and *E. coli lipA aa 101-321*-pST25. (L) *E. coli nfuA*-pUT18C and *E. coli lipA aa 126-321*-pST25. (M) *E. coli nfuA*-pUT18C and *E. coli lipA aa 151-321*-pST25. (N) *E. coli nfuA*-pUT18C and *E. coli lipA aa 176-321*-pST25. (O) *E. coli nfuA*-pUT18C and *E. coli lipA aa 201-321*-pST25. (P) *E. coli nfuA*-pUT18C and *E. coli lipA aa 226-321*-pST25. (Q) *E. coli nfuA*-pUT18C and *E. coli lipA aa 251-321*-pST25.

A

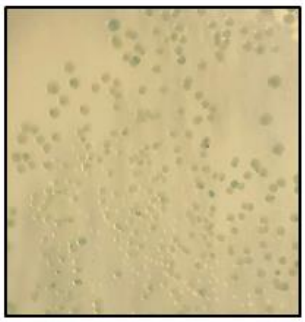

Negative control
LB/xgal + IPTG
Picture after 2 days at 30 °C

B

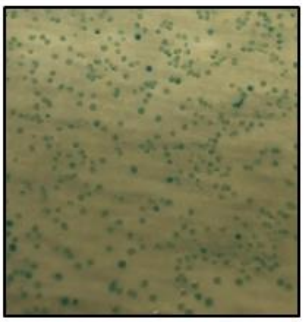

Positive control
LB/xgal + IPTG
Picture after 2 days at 30 °C

C

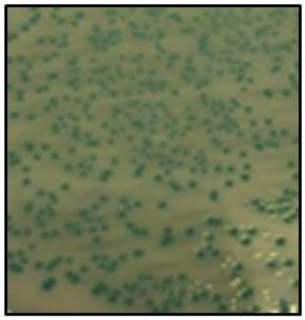

Ec NfuA + Ec LipA
LB/xgal + IPTG
Picture after 2 days at 30 °C

D

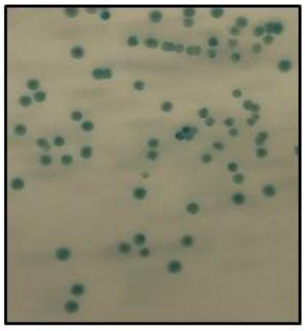

Ec NfuA aa 3-191 + Ec LipA
LB/xgal + IPTG
Picture after 2 days at 30 °C

E

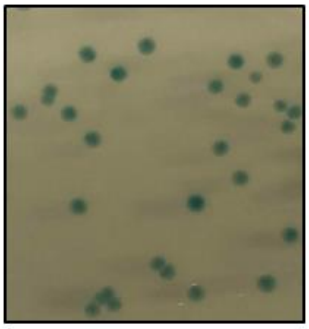

Ec NfuA aa 4-191 + Ec LipA
LB/xgal + IPTG
Picture after 2 days at 30 °C

F

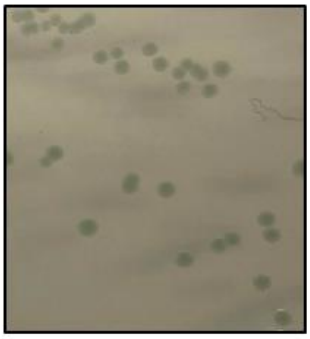

Ec NfuA aa 6-191 + Ec LipA
LB/xgal + IPTG
Picture after 2 days at 30 °C

G

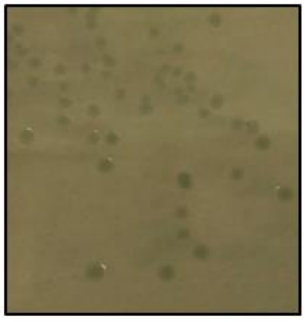

Ec NfuA aa 8-191 + Ec LipA
LB/xgal + IPTG
Picture after 2 days at 30 °C

H

Ec NfuA aa 11-191 + Ec LipA
LB/xgal + IPTG
Picture after 2 days at 30 °C

I

Ec NfuA aa 21-191 + Ec LipA
LB/xgal + IPTG
Picture after 2 days at 30 °C

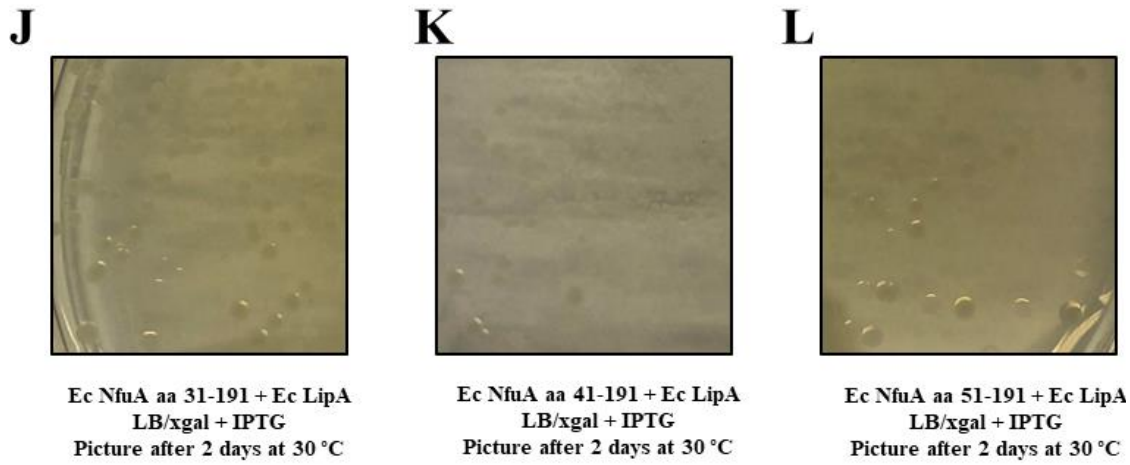

Figure 5-8: Bacterial two hybrid screening of *E. coli* NfuA truncations against wild-type *E. coli* LipA. Adenylate cyclase deficient cells strain BTH101 were co-transformed bacterial two hybrid plasmids and spread on LB agar plates containing 40 μg/μL galactosidase and 0.5 mM IPTG with the respective selective antibiotics (100 μg/μL spectinomycin or 50 μg/μL kanamycin and 100 μg/μL ampicillin). (A) Negative control containing two non-interacting proteins *E. coli gcvH*-pUT18C and *E. coli gstB*-pST25. (B) Positive control containing two domains of leucine zipper: *zip*-pUT18C and *zip*-pKT25 (C) *E. coli nfuA*-pUT18C and wild-type *E. coli lipA*-pST25. (D) *E. coli nfuA aa 3-191*-pUT18C and *E. coli lipA*-pST25. (E) *E. coli nfuA aa 4-191*-pUT18C and *E. coli lipA*-pST25. (F) *E. coli nfuA aa 6-191*-pUT18C and *E. coli lipA*-pST25. (G)) *E. coli nfuA aa 8-191*-pUT18C and *E. coli lipA*-pST25. (H) *E. coli nfuA aa 11-191*-pUT18C and *E. coli lipA*-pST25. (I) *E. coli nfuA aa 21-191*-pUT18C and *E. coli lipA*-pST25. (J) *E. coli nfuA aa 31-191*-pUT18C and *E. coli lipA*-pST25. (K) *E. coli nfuA aa 41-191*-pUT18C and *E. coli lipA*-pST25. (L) *E. coli nfuA aa 51-191*-pUT18C and *E. coli lipA*-pST25.

Bacterial two hybrid screening of E. coli NfuA Ile4Ala, E. coli NfuA Ser5Ala, E. coli NfuA Ile4A, Ser5Ala, E. coli LipA Leu21Ala, E. coli LipA Ile22Ala, E. coli LipA Pro23Ala, E. coli LipA Val24Ala, E. coli LipA Lys25Arg, and E. coli LipA Lys25Ala.

The bacterial hybrid screen of *E. coli* LipA truncations and *E. coli* NfuA truncations led to the discovery of a five-amino acid motif “LIPVK” within LipA and a two-amino acid motif “IS” within NfuA that are essential for tight binding. The importance of each

amino acid within the motifs was then investigated by making single amino acid substitutions within the motif and subsequently re-screening for binding **(Figure 5-9).** When the *E. coli* LipA leucine residue at position 21 was exchanged for an alanine, the binding with wild-type *E. coli* NfuA was unaffected **(Figure 5-9, Panel G).** Similarly, when the *E. coli* LipA lysine residue at position 25 was exchanged for an alanine or an arginine, binding was not disrupted **(Figure 5-9, Panels K and L).** However, when the *E. coli* LipA isoleucine at position 22, the proline at position 23, or the valine at position 24 was substituted with an alanine, binding with wild-type NfuA was abrogated **(Figure 5-9, Panels H-J).** Alternatively, when the *E. coli* NfuA isoleucine at position 4 was replaced with an alanine, binding with wild-type *E. coli* LipA was not observed **(Figure 5-9, Panel D).** When the *E. coli* NfuA serine at position 5 was replaced with an alanine, binding with wild-type was unaffected **(Figure 5-9, Panel E).** The double substitution of the *E. coli* NfuA isoleucine at position 4 and the serine at position 5 for alanine residues reflected what was observed for the isoleucine only substitution **(Figure 5-9, Panel F).** Collectively, this data suggests that a single isoleucine residue at position 4 on *E. coli* NfuA is essential for complex formation with wild-type *E. coli* LipA.

A

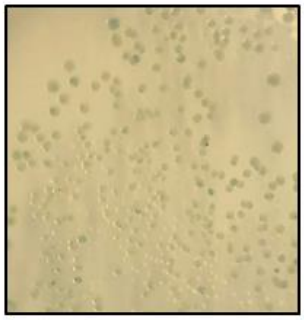

Negative control
LB/xgal + IPTG
Picture after 2 days at 30 °C

B

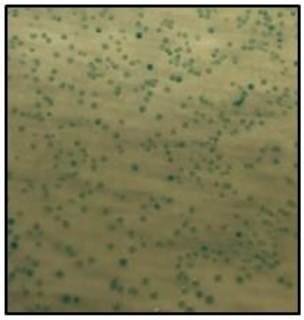

Positive control
LB/xgal + IPTG
Picture after 2 days at 30 °C

C

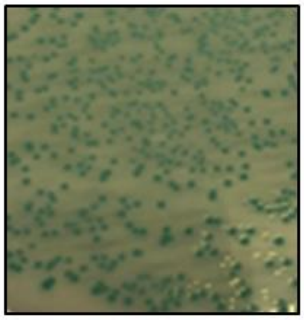

Ec NfuA + Ec LipA
LB/xgal + IPTG
Picture after 2 days at 30 °C

D

Ec NfuA Ile4Ala + Ec LipA
LB/xgal + IPTG
Picture after 2 days at 30 °C

E

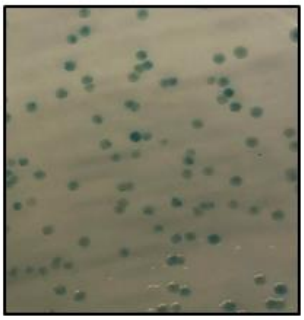

Ec NfuA Ser5Ala + Ec LipA
LB/xgal + IPTG
Picture after 2 days at 30 °C

F

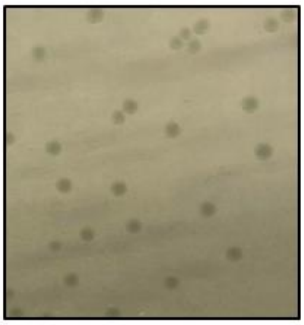

Ec NfuA Ile4Ala, Ser5Ala
+ Ec LipA LB/xgal + IPTG
Picture after 2 days at 30 °C

G

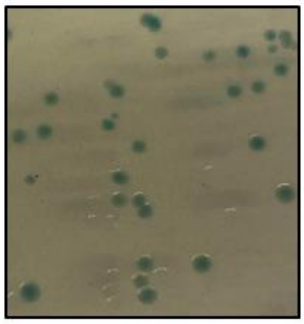

Ec NfuA + Ec LipA Leu21Ala
LB/xgal + IPTG
Picture after 2 days at 30 °C

H

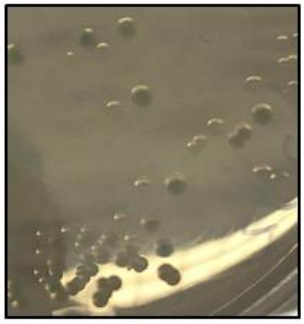

Ec NfuA + Ec LipA Ile22Ala
LB/xgal + IPTG
Picture after 2 days at 30 °C

I

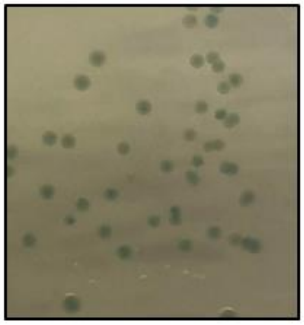

Ec NfuA + Ec LipA Pro23Ala
LB/xgal + IPTG
Picture after 2 days at 30 °C

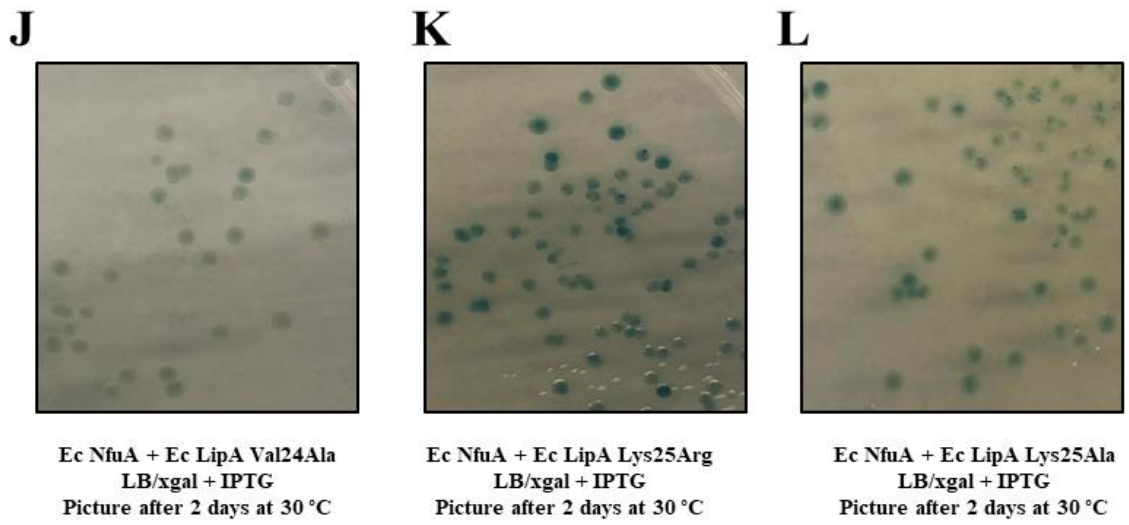

Figure 5-9: Bacterial two hybrid screening of *E. coli* NfuA variants and *E. coli* LipA variants of amino acid identified in library screen. Adenylate cyclase deficient cells strain BTH101 were co-transformed bacterial two hybrid plasmids and spread on LB agar plates containing 40 μg/μL galactosidase and 0.5 mM IPTG with the respective selective antibiotics (100 μg/μL spectinomycin or 50 μg/μL kanamycin and 100 μg/μL ampicillin). (A) Negative control containing two non-interacting proteins *E. coli gcvH*-pUT18C and *E. coli gstB*-pST25. (B) Positive control containing two domains of leucine zipper: *zip*-pUT18C and *zip*-pKT25 (C) *E. coli nfuA*-pUT18C and wild-type *E. coli lipA*-pST25. (D) *E. coli nfuA Ile4Ala*-pUT18C and *E. coli lipA*-pST25. (E) *E. coli nfuA Ser5Ala*-pUT18C and *E. coli lipA*-pST25. (F) *E. coli nfuA Ile4Ala, Ser5Ala*-pUT18C and *E. coli lipA*-pST25. (G) *E. coli nfuA*-pUT18C and *E. coli lipA Leu21Ala*-pST25. (H) *E. coli nfuA*-pUT18C and *E. coli lipA Ile22Ala*-pST25. (I) *E. coli nfuA*-pUT18C and *E. coli lipA Pro23Ala*-pST25. (J) *E. coli nfuA*-pUT18C and *E. coli lipA Val24Ala*-pST25. (K) *E. coli nfuA*-pUT18C and *E. coli lipA Lys25Arg*-pST25. (K) *E. coli nfuA*-pUT18C and *E. coli lipA Lys25Ala*-pST25.

Isolation and Characterization of E. coli NfuA Ile4Ala, E. coli LipA Ile22Ala, E. coli LipA Pro23Ala, E. coli LipA Val24Ala, and E. coli LipA Ile22Ala, Pro23Ala, Val24Ala triple mutant.

The genes encoding *E. coli* NfuA Ile4Ala, *E. coli* LipA Ile22Ala, *E. coli* LipA Pro23Ala, *E. coli* LipA Val24Ala, and *E. coli* LipA Ile22Ala, Pro23Ala, Val24Ala triple mutant were subcloned into a pET28a vector, and the variant proteins were subsequently overproduced and isolated using the described protocol for preparing the wild-type *E. coli* NfuA and *E. coli* LipA. In

all cases, the variant proteins were soluble and behaved similarly to what is observed for the wild-type proteins. *E. coli* NfuA Ile4Ala was successfully overproduced and isolated to >95% homogeneity when analyzed by SDS-PAGE **(Figure 5-10).** The UV-visible spectrum of the as-isolated protein had features consistent with coordination of a [4Fe-4S] cluster **(Figure 5-11, solid trace).** Colorimetric iron analysis revealed the protein contained 1.6 ± 0.09 Fe per polypeptide. In order to ensure complete cofactor incorporation, the protein was chemically reconstituted using iron, sulfide, and reductant. After removal of the aggregates and non-specifically bound metals by size exclusion chromatography, the UV-visible spectrum had more pronounced features **(Figure 5-11, dashed trace)** compared to the as-isolated spectrum. Colorimetric iron analysis of the reconstituted protein revealed the protein contained 3.2 ± 0.2 Fe per polypeptide. The wild-type *E. coli* NfuA typically contains almost full [4Fe-4S] cluster incorporation in its as-isolated state. However, when reconstituted in the past, it has been shown to elute with an extra iron atom in addition to the expected 2 Fe atoms per polypeptide.

E. coli LipA Ile22Ala was overproduced and isolated to >95% homogeneity when analyzed by SDS-PAGE **(Figure 5-12).** Upon isolation, there are dramatic features in the 330 nM and 400 nM region corresponding to the two [4Fe-4S] clusters **(Figure 5-13, solid trace).** Colorimetric iron analysis revealed the protein contained 6.9 ± 0.26 Fe per polypeptide. After chemical reconstitution and removal of the aggregates and non-specifically bound metals by size exclusion chromatography, the UV-visible spectrum had more pronounced features **(Figure 5-13, dashed trace)** compared to the as-isolated spectrum. Colorimetric iron analysis of the reconstituted protein revealed the protein contained 8.4 ± 2.8 Fe per polypeptide which is in agreement with the theoretical amount of iron for the fully reconstituted protein (8 Fe per polypeptide). Similarly, *E. coli* LipA Pro23Ala and *E. coli* LipA Val24Ala were overproduced and isolated **(Figure 5-14 and Figure 5-16).** Colorimetric iron analysis revealed the protein contained 5.4 ± 0.26 Fe per polypeptide, and 5.2 ± 0.15 Fe per polypeptide, respectively. The features at 330 nM and 400 nM

in the UV-visible spectra for *E. coli* LipA Pro23Ala and *E. coli* LipA Val24Ala became more pronounced after chemical reconstitution **(Figure 5-15 and Figure 5-17, compare solid trace and dashed trace).** The *E. coli* LipA IPV -> AAA triple variant was also successfully overproduced and isolated **(Figure 5-18 and Figure 5-19).**

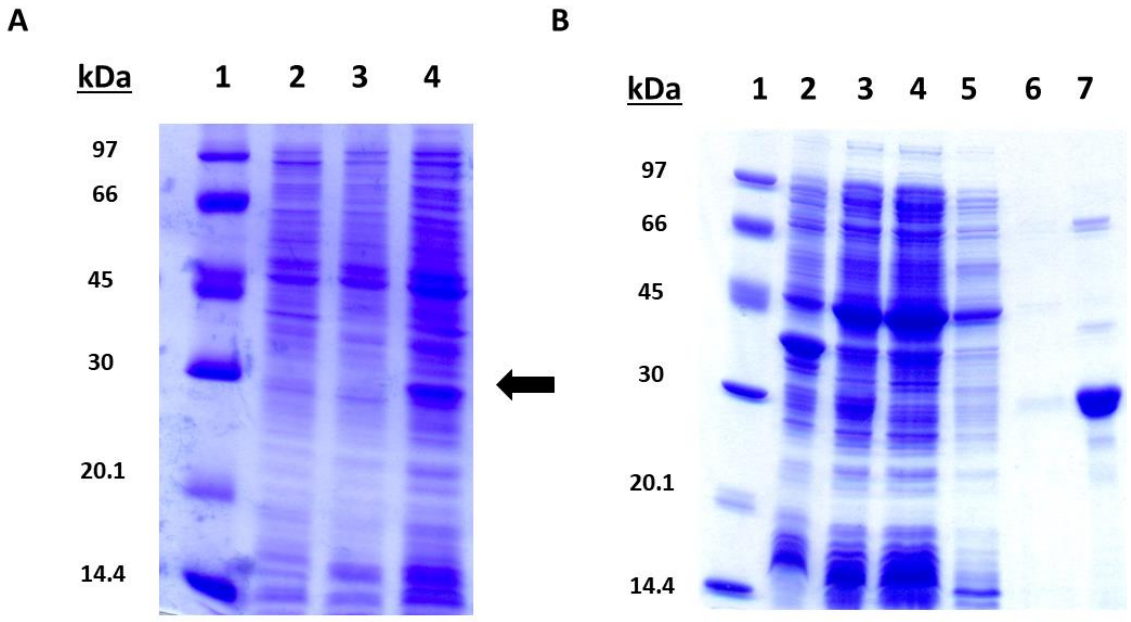

Figure 5-10: (A) SDS-PAGE gel monitoring overproduction of *E. coli* NfuA Ile4Ala. Lanes are as follows: 1- molecular weight ladder 2-uninduced 3-arabinose induced 4-IPTG induced (B) SDS-PAGE gel monitoring the isolation of *E. coli* NfuA Ile4Ala. Lanes are as follows: 1-molecular weight ladder 2-cellular pellet 3-supernatant 4-flowthrough 5-wash 1 6-wash 2 7-pure protein

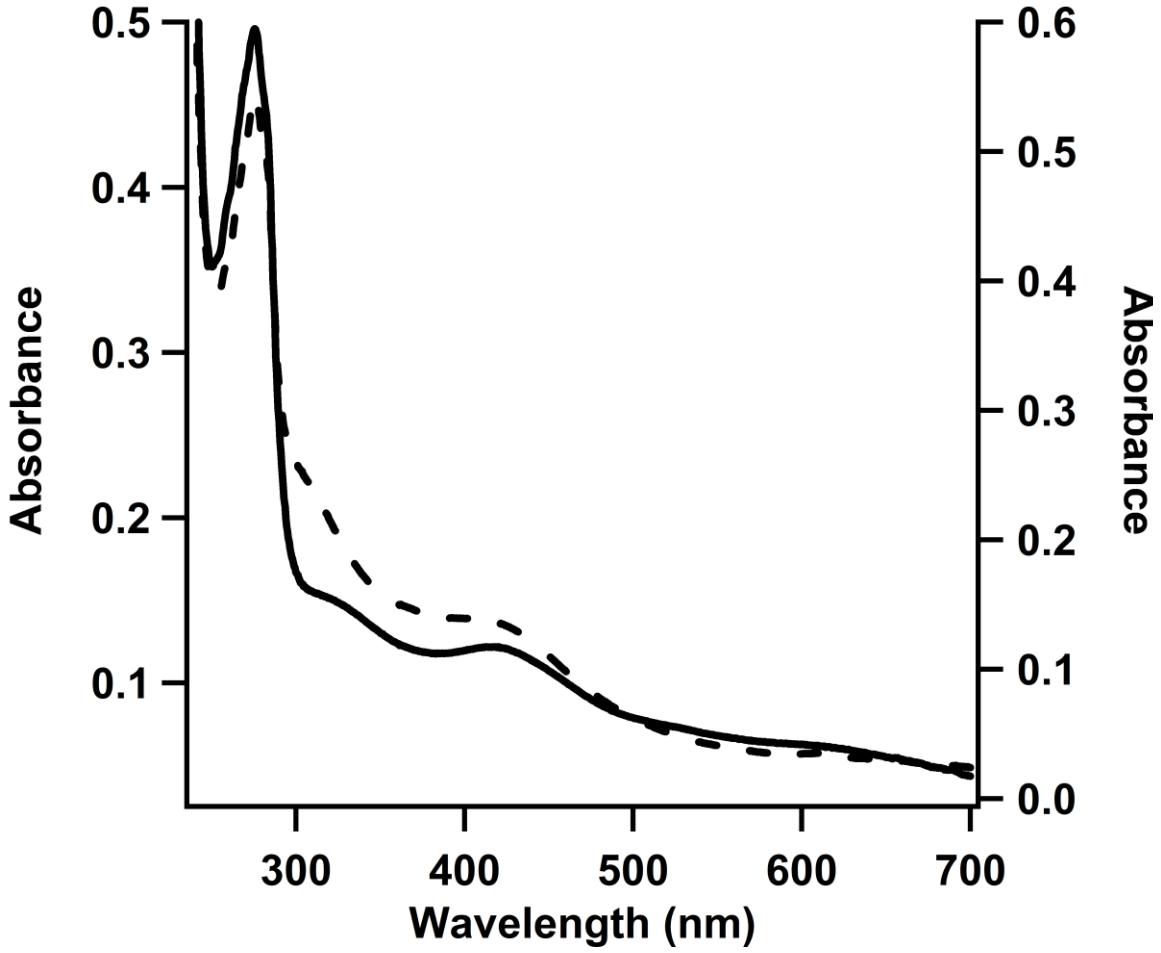

Figure 5-11: UV-visible spectrum of 10 µM *E. coli* NfuA Ile4Ala as-isolated (solid trace) and after chemical reconstitution. (dashed trace)

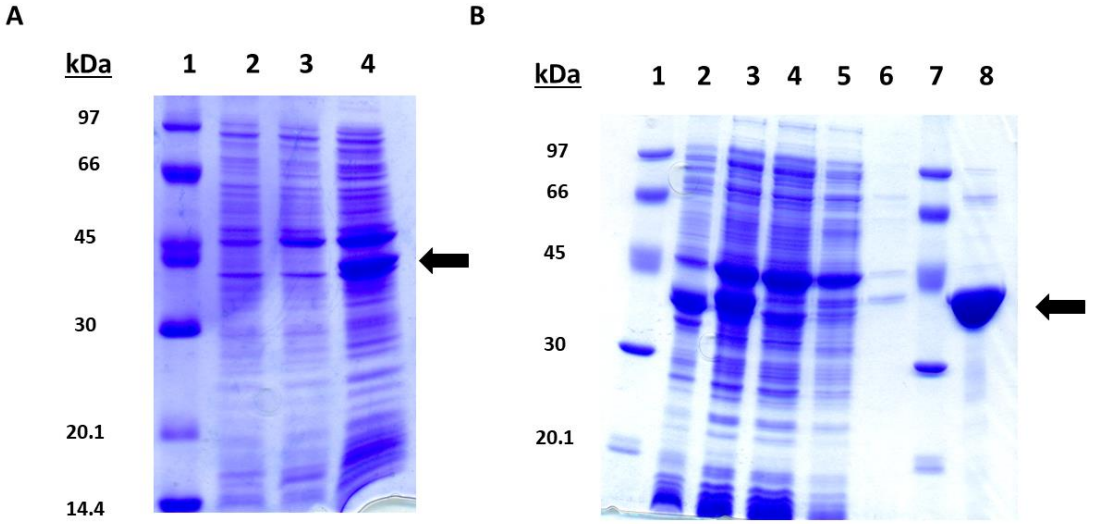

Figure 5-12: SDS-PAGE gel monitoring overproduction of *E. coli* LipA Ile22Ala Lanes are as follows: 1- molecular weight ladder 2-uninduced 3-arabinose induced 4-IPTG induced (B) SDS-PAGE gel monitoring the isolation of *E. coli* LipA Ile22Ala. Lanes are as follows: 1-molecular weight ladder 2-cellular pellet 3-supernatant 4-flowthrough 5-wash 1 6-wash 2 7-molecular weight ladder 8-pure protein

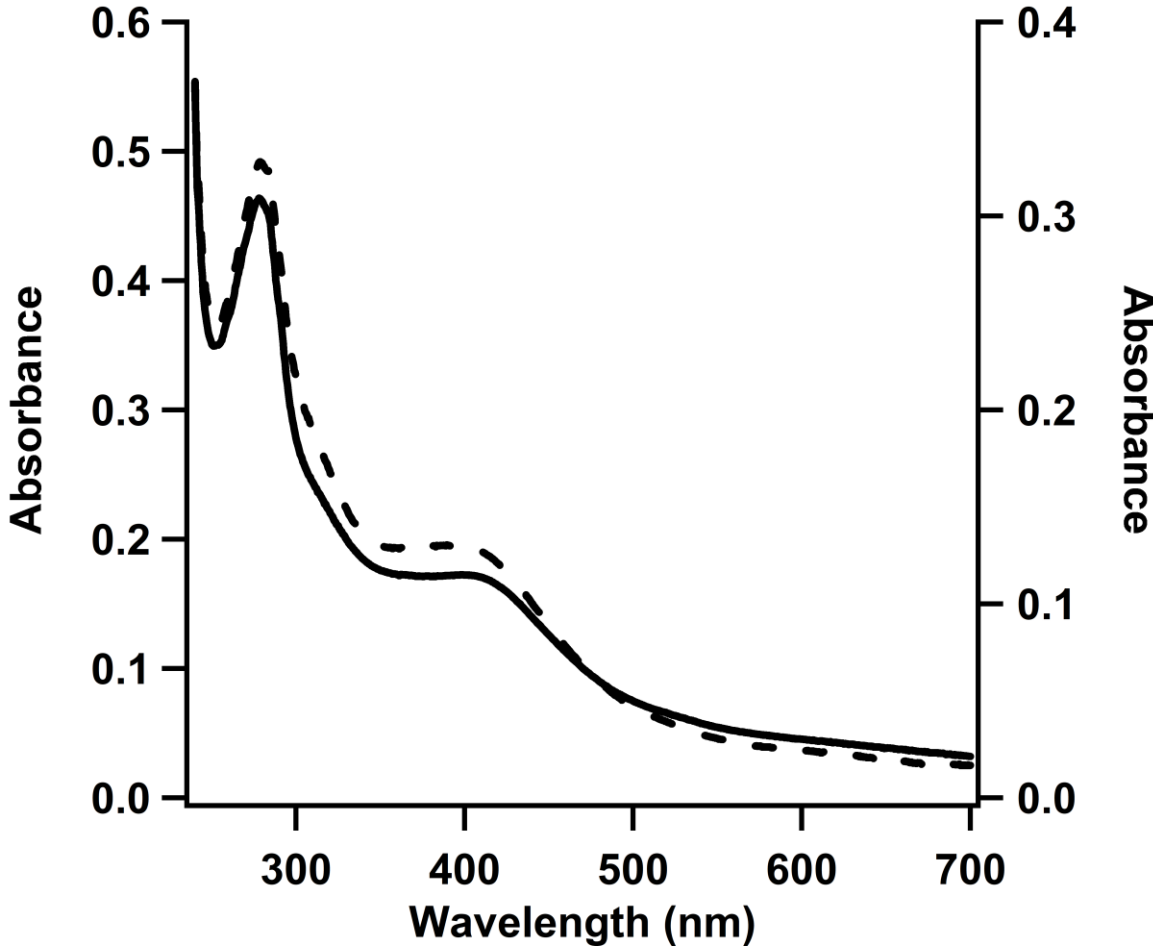

Figure 5-13: UV-visible spectrum of 6 *μM E. coli* LipA Ile22Ala as-isolated (solid trace*)* and after chemical reconstitution (dashed trace).

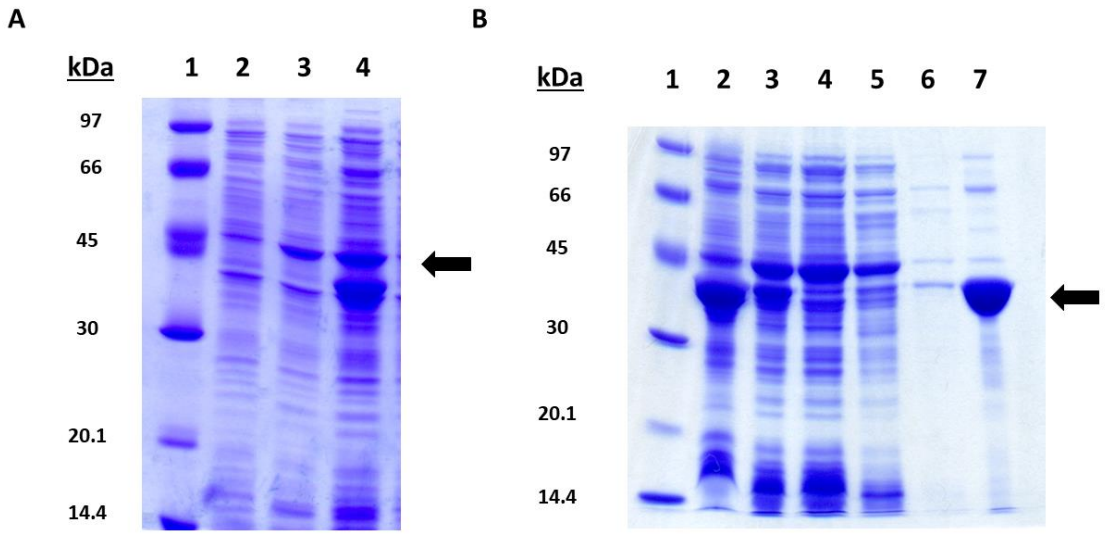

Figure 5-14: SDS-PAGE gel monitoring overproduction of *E. coli* LipA Pro23Ala Lanes are as follows: 1- molecular weight ladder 2-uninduced 3-arabinose induced 4-IPTG induced (B) SDS-PAGE gel monitoring the isolation of *E. coli* LipA Ile22Ala. Lanes are as follows: 1-molecular weight ladder 2-cellular pellet 3-supernatant 4-flowthrough 5-wash 1 6-wash 2 7-pure protein

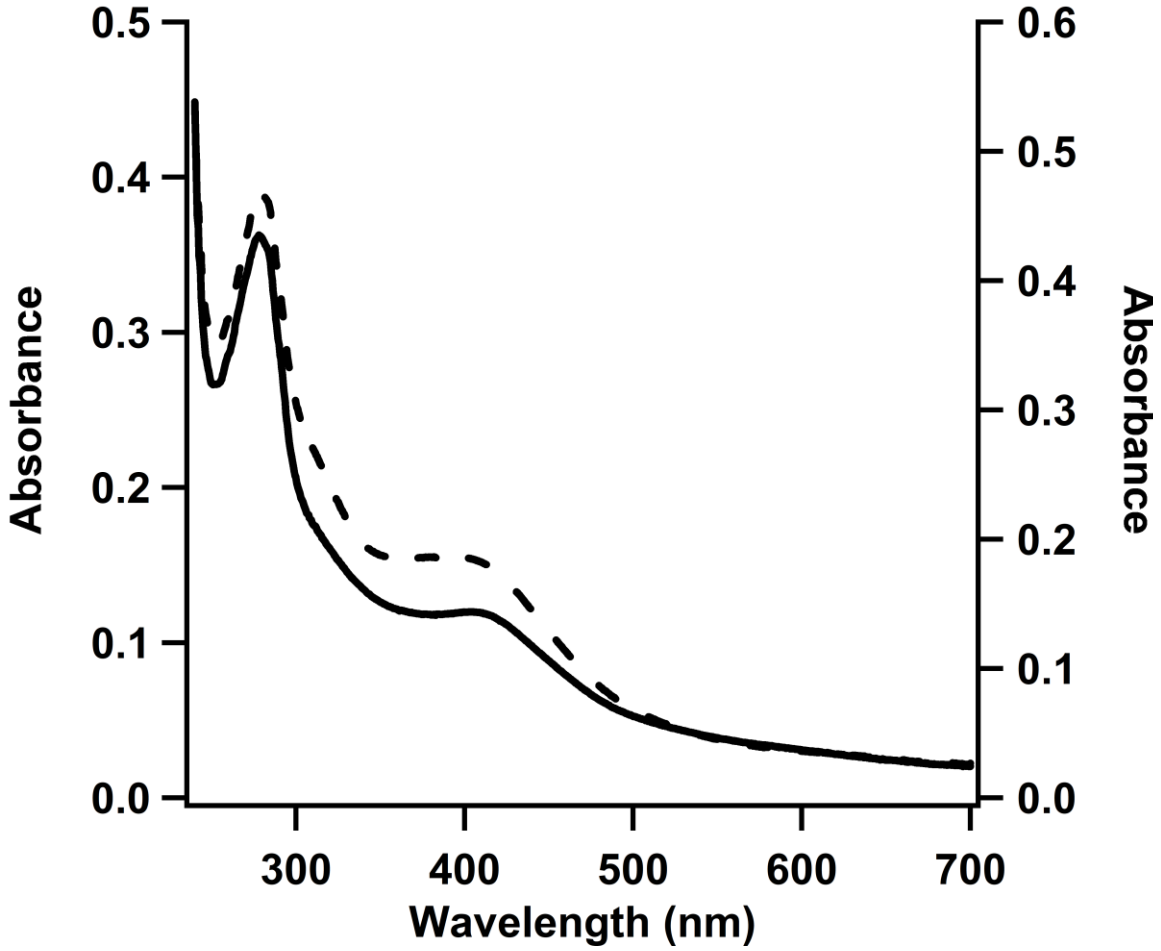

Figure 5-15: UV-visible spectrum of 6 μM as-isolated *E. coli* LipA Pro23Ala (solid trace) and after chemical reconstitution (dashed trace).

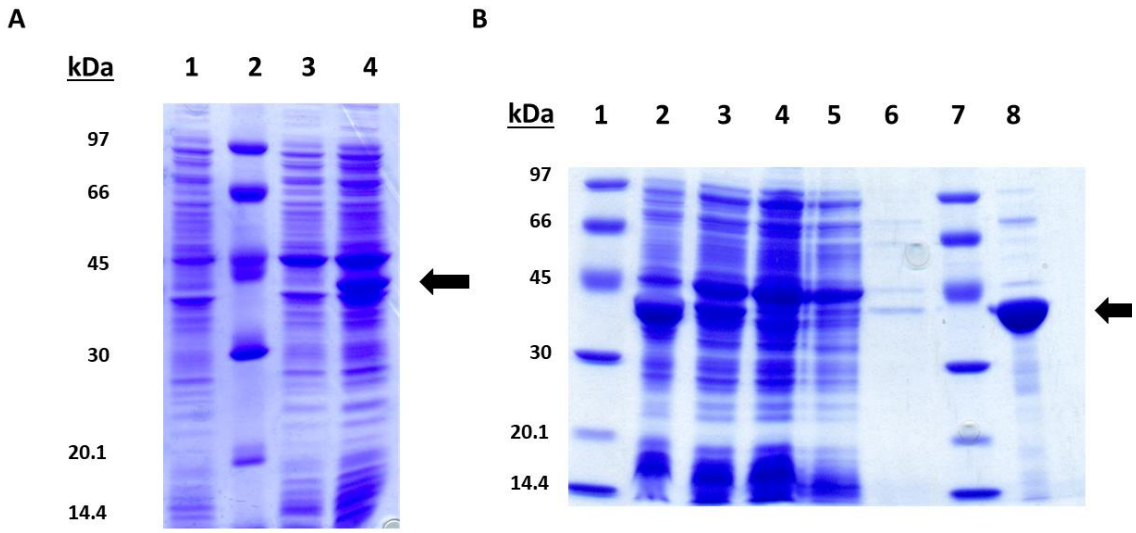

Figure 5-16: SDS-PAGE gel monitoring overproduction of *E. coli* LipA Val24Ala Lanes are as follows: 1- uninduced 2- molecular weight ladder 3-arabinose induced 4-IPTG induced (B) SDS-PAGE gel monitoring the isolation of *E. coli* LipA Ile22Ala. Lanes are as follows: 1-molecular weight ladder 2-cellular pellet 3-supernatant 4-flowthrough 5-wash 1 6-wash 2 7-molecular weight ladder 8-pure protein

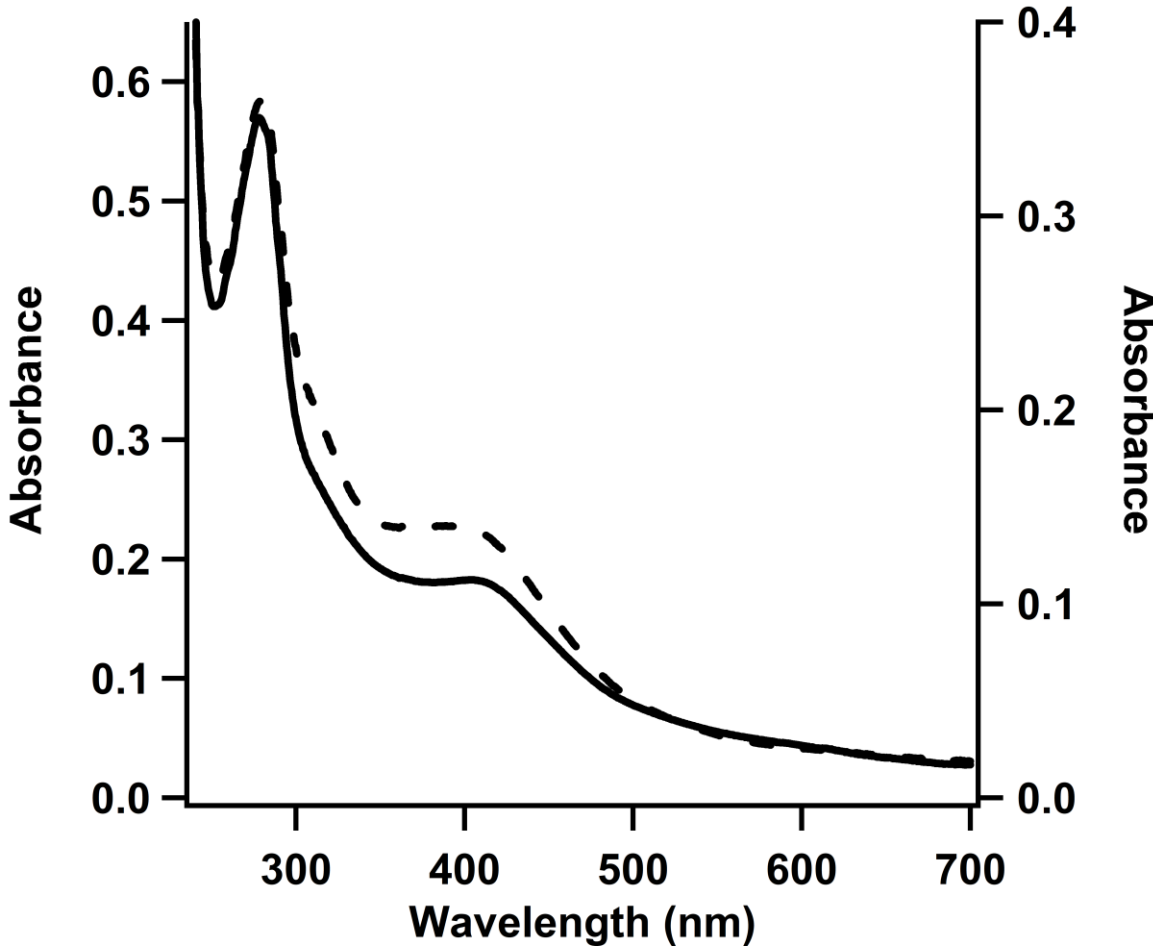

Figure 5-17: UV-visible spectrum of as-isolated *E. coli* LipA Val24Ala (solid trace) and after chemical reconstitution (dashed trace).

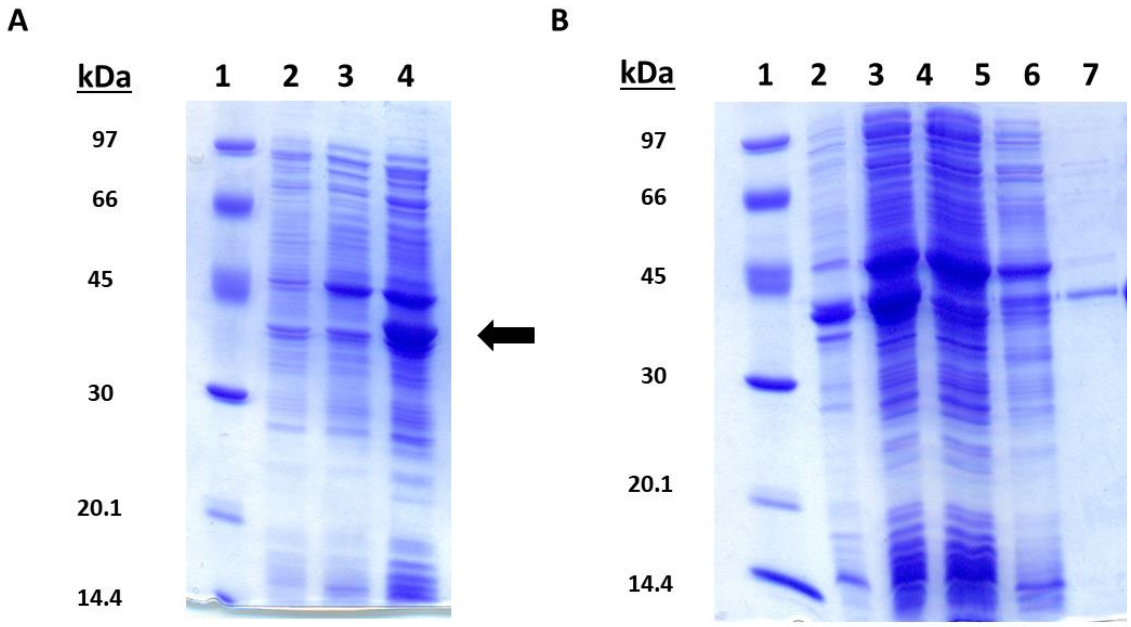

Figure 5-18: SDS-PAGE gel monitoring overproduction of *E. coli* LipA Ile22Ala, Pro23Ala, Val24Ala triple variant. Lanes are as follows: 1- molecular weight ladder 2-uninduced 3-arabinose induced 4-IPTG induced (B) SDS-PAGE gel monitoring the isolation of *E. coli* LipA Ile22Ala. Lanes are as follows: 1-molecular weight ladder 2-cellular pellet 3-supernatant 4-flowthrough 5-wash 1 6-wash 2 7-pure protein

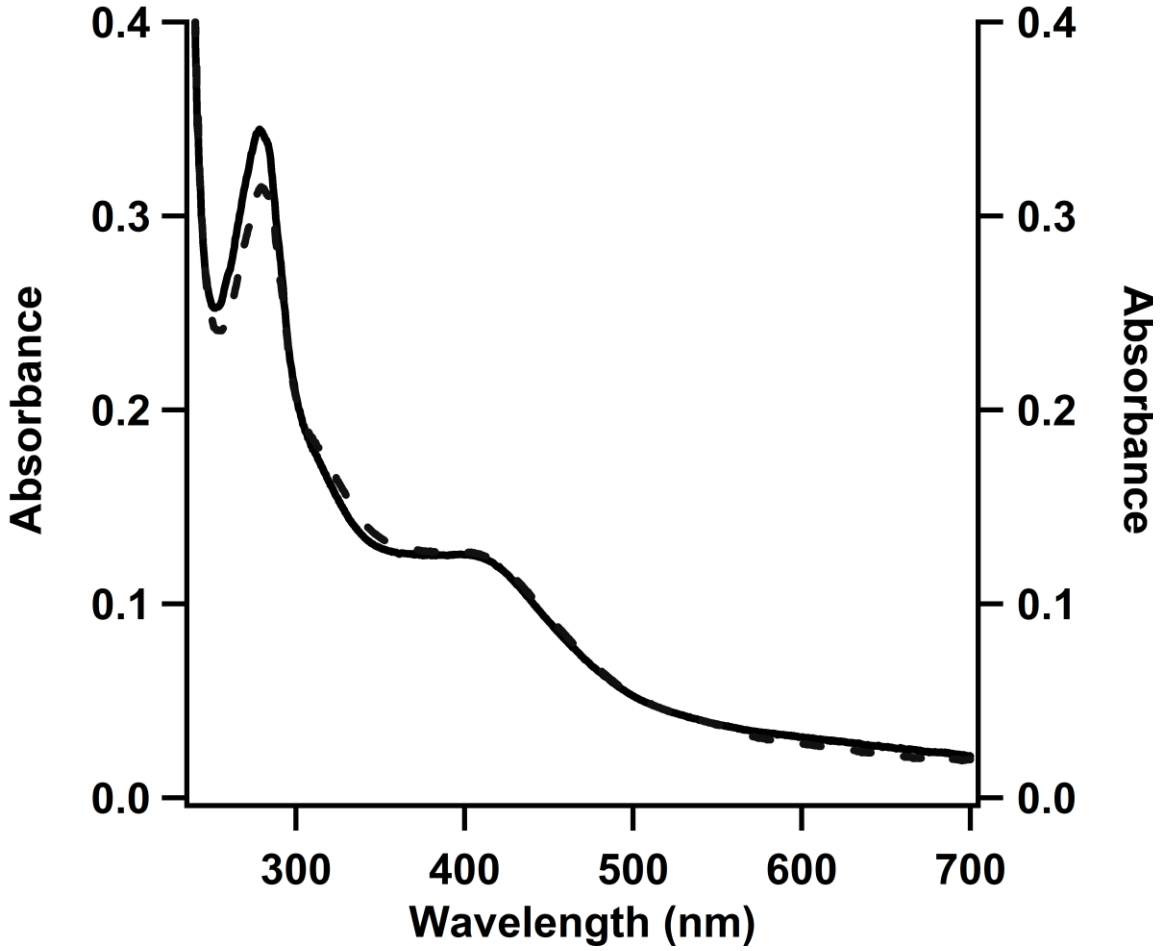

Figure 5-19: UV-visible spectrum of 6 *μM* as-isolated *E. coli* LipA Ile22Ala, Pro23Ala, Val24Ala triple mutant before (solid trace) and after chemical reconstitution (dashed trace).

Assessment of Binding of E. coli NfuA Ile4Ala, E. coli LipA Ile22Ala, E. coli LipA Pro23Ala, E. coli LipA Val24Ala, and E. coli LipA Ile22Ala, Pro23Ala, Val24Ala triple mutant using Microscale Thermophoresis and Analytical Molecular Sieve Chromatography

Bacterial two hybrid screening was used to identify an isoleucine at position 4 on NfuA and an isoleucine-proline-valine motif at positions 22-24 on LipA that were essential for the protein-protein interaction. A similar approach was used in a recent study by the Rouault laboratory

which successfully identified an LYR/IYR motif on succinate dehydrogenase that was essential for recognition by the iron-sulfur cluster chaperone protein HSC20 (2). However, these predictions were not validated using *in vitro* methods. In this particular study, we have subcloned the genes encoding the NfuA Ile4Ala, LipA Ile22Ala, LipA Pro23Ala, and LipA Val24Ala variants into a pET28a construct. These variant proteins were overproduced and isolated and subsequently characterized using *in vitro* methods for binding, including microscale thermophoresis and analytical sieve chromatography, and activity assessment. The binding constant for wild-type *E. coli* LipA and wild-type *E. coli* NfuA was calculated to be 950 nM ± 110 nM **(Figure 5-4).** Consistent with this tight interaction, when an equimolar mixture of NfuA and LipA are loaded onto a size exclusion column, a major peak corresponding to a 1:1 complex between LipA and NfuA is observed **(Figure 5-20, Panel A, Peak A).** When the fractions corresponding to the peak were subjected to SDS-PAGE analysis, two major bands are observed corresponding to *E. coli* LipA and *E. coli* NfuA **(Figure 5-20, Panel B).** This result was initially reported in Chapter 2, but was reproduced as a control experiment in this chapter.

The binding between wild-type *E. coli* LipA and *E. coli* NfuA Ile4Ala was probed by microscale thermophoresis using fluorescently labeled LipA and unlabeled NfuA Ile4Ala as a ligand. The Kd was calculated to be 2.5 ± 0.37 µM **(Figure 5-21),** approximately 2.5 fold higher than the calculated Kd for wild-type LipA and wild-type NfuA **(Table 5-3).** Similarly, an equimolar mix of LipA and NfuA Ile4Ala was applied to the column, and a slightly shifted peak was observed, compared to the LipA only control and NfuA Ile4Ala only control **(Figure 5-22, Panel A).** When the fractions corresponding to peak A were subjected to SDS-PAGE, two bands were observed corresponding to LipA and NfuA Ile4Ala. However, the amount of NfuA Ile4Ala present in these fractions is significantly less than what is observed with the wild-type LipA and wild-type NfuA control **(Figure 5-22, Panel B),** which is consistent with the weakened interaction calculated by microscale thermophoresis.

The interaction between *E. coli* LipA Ile22Ala and wild-type *E. coli* NfuA was probed by microscale thermophoresis using fluorescently labeled LipA Ile22Ala and unlabeled wild-type NfuA as a ligand. Triplicate experiments were performed; however, binding could not be detected in this assay. This suggests that the LipA isoleucine at position 22 is absolutely required for complex formation between NfuA and LipA. When an equimolar mixture of the LipA Ile22Ala variant and wild-type NfuA were applied to the size exclusion column, the major peak directly coincided with the LipA Ile22Ala only control **(Figure 5-23, Panel A).** The absence of a shift in the elution volume is consistent with no stable complex formation between LipA Ile22Ala and NfuA. When the fractions corresponding to the major peak were subjected to SDS-PAGE, a single band was observed corresponding to LipA, confirming that no complex formed between LipA Ile22Ala and wild-type NfuA **(Figure 5-23, Panel B).**

Microscale thermophoresis experiments probing the binding of *E. coli* LipA Pro23Ala or *E. coli* LipA Val24Ala with wild-type NfuA revealed approximately a 10-fold increase in the binding constant compared to wild-type *E. coli* LipA and wild-type *E. coli* NfuA **(Figure 5-24 and Figure 5-26, Table 5-4).** When the molecular sieve chromatography experiments were performed using equimolar mixtures of wild-type NfuA and either *E. coli* LipA Pro23Ala or *E. coli* LipA Val24Ala, small shifts were observed in the elution volumes **(Figure 5-25, Panel A, and Figure 5-27, Panel A).** When the major peak was subjected to SDS-PAGE analysis, a major band corresponding to the LipA variant protein was observed and a second band corresponding to a small amount of NfuA was present **(Figure 5-25, Panel B and Figure 5-27, Panel B).** This observation is also consistent with a weakened, but not entirely disrupted, complex formation.

.

Table 5-4: Calculated Binding Constants using Microscale Thermophoresis.

Protein 1	Protein 2	Kd
E. coli LipA	*E. coli* NfuA	950 ± 110 nM
E. coli LipA	*E. coli* NfuA Ile4Ala	2.5 ± 0.37 µM
E. coli LipA Ile22Ala	*E. coli* NfuA	N.D.*
E. coli LipA Pro23Ala	*E. coli* NfuA	10.0 ± 1.44 µM
E. coli LipA Val24Ala	*E. coli* NfuA	10.1 ± 0.97 µM

*N.D.= Not Determined; could not be calculated under conditions tested

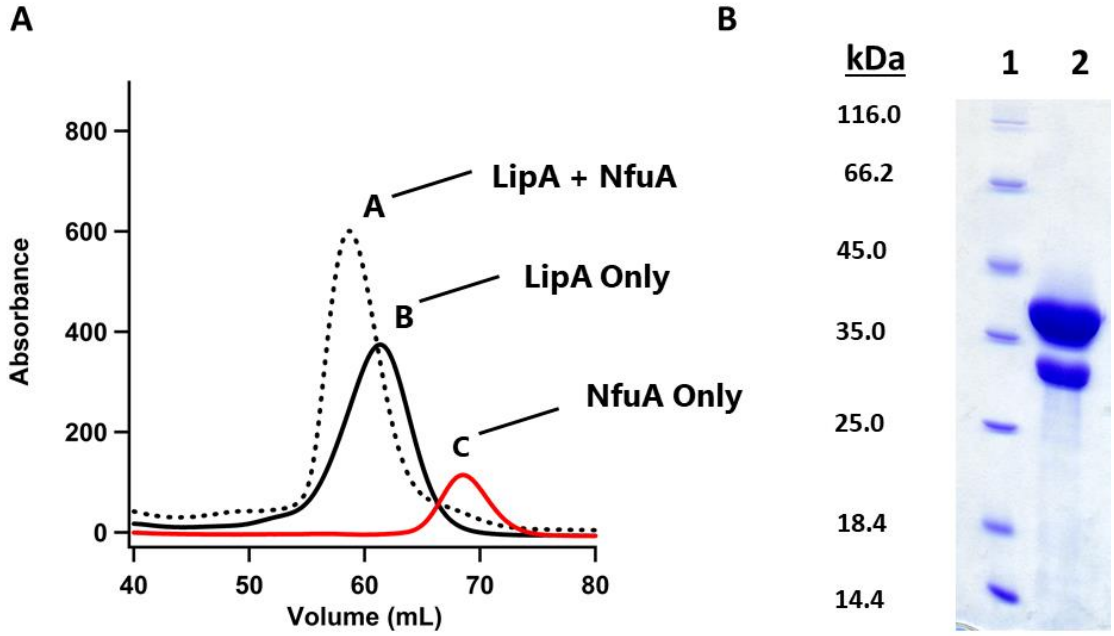

Figure 5-20: (A) Interaction between wild-type *E. coli* LipA wild-type and wild-type *E. coli* NfuA monitored by molecular sieve chromatography**.** Red solid line, 100 µM NfuA alone. NfuA elutes (68.5 mL) with an experimentally calculated molecular mass of 26.8 kDa (theoretical mass, 25.6 kDa). Solid black line, 100 µM *E. coli* LipA alone. LipA elutes (61.3 mL) with an experimentally calculated molecular mass of 48.5 kDa (theoretical mass, 38.2 kDa). Black dashed line, 100 µM *E. coli* LipA + 100 µM wild-type *E. coli* NfuA. A major peak elutes at 58.7 mL with an experimentally calculated molecular mass of 62.2 kDa (theoretical mass of 1:1 complex is 63.8 kDa). (B) SDS-PAGE of fractions corresponding to the main peak, contain two major bands corresponding to LipA and NfuA.

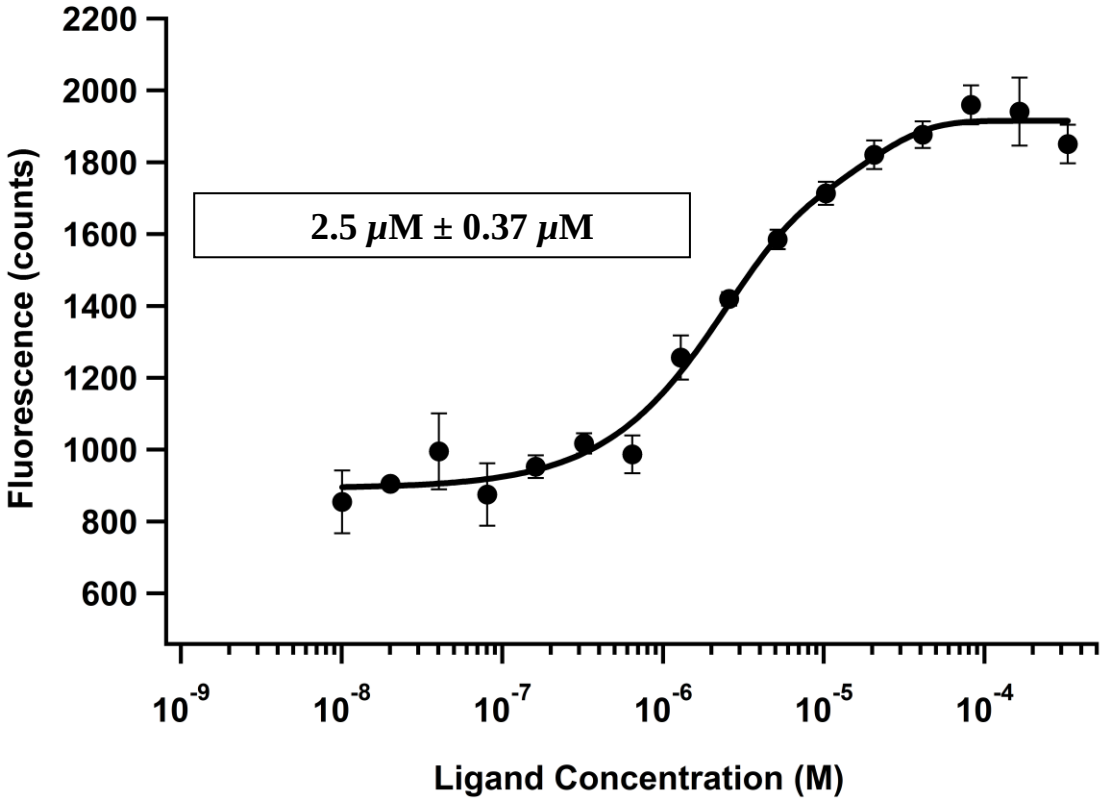

Figure 5-21: Kd Determination of *E. coli* LipA and *E. coli* NfuA Ile4Ala using Microscale Thermophoresis. *E. coli* LipA (500 nM final protein concentration) was labeled with a fluorescent amine reactive dye. Unlabeled *E. coli* NfuA ligand was serial diluted from 100 µM (first point) across 16 tubes. Error bars represent the data obtained from triplicate experiments, and a specificity test was performed for each replicate.

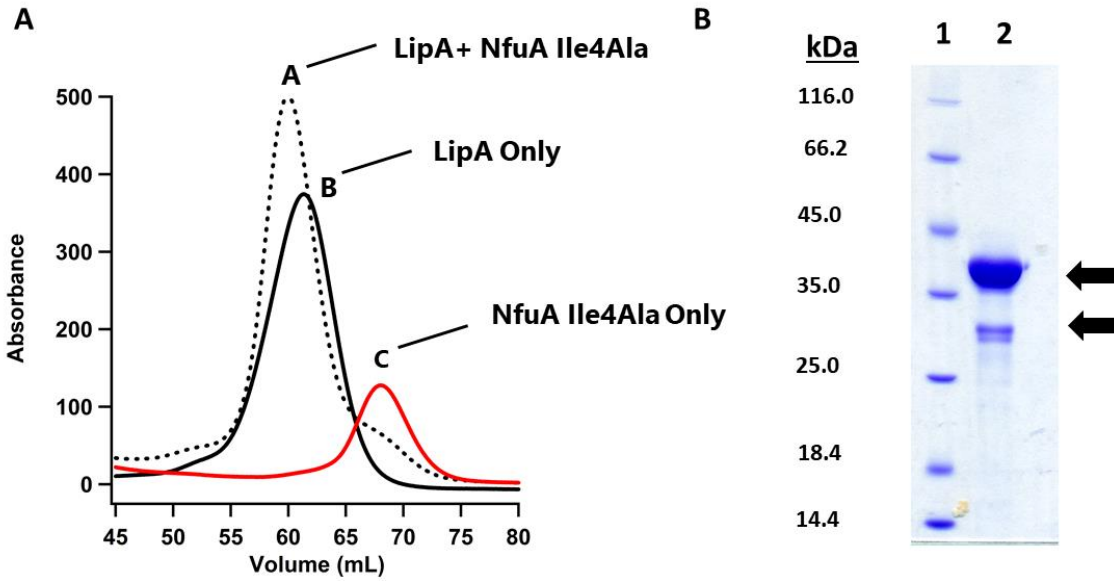

Figure 5-22: (A) Interaction between wild-type *E. coli* LipA wild-type and *E. coli* NfuA Ile4Ala monitored by molecular sieve chromatography**.** Red solid line, 100 µM NfuA Ile4Ala alone. NfuA Ile4Ala elutes (68.2 mL) with an experimentally calculated molecular mass of 27.4 kDa (theoretical mass, 25.6 kDa). Solid black line, 100 µM *E. coli* LipA alone. LipA elutes (61.3 mL) with an experimentally calculated molecular mass of 48.5 kDa (theoretical mass, 38.2 kDa). Black dashed line, 100 µM *E. coli* LipA + 100 µM *E. coli* NfuA Ile4Ala. Two peaks are observed at 60.0 mL and 68.1 mL. (B) SDS-PAGE of fractions corresponding to the main peak, contain two major bands corresponding to LipA and a small band of NfuA Ile4Ala.

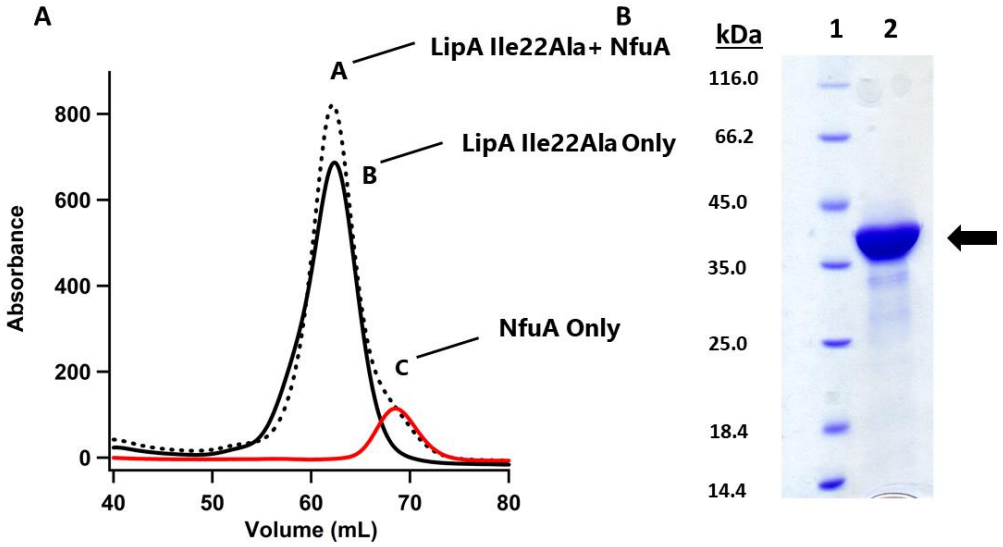

Figure 5-23: (A) Interaction between *E. coli* LipA Ile22Ala and wild-type *E. coli* NfuA monitored by molecular sieve chromatography**.** Red solid line, 100 µM NfuA alone. NfuA elutes (68.5 mL) with an experimentally calculated molecular mass of 26.8 kDa (theoretical mass, 25.6 kDa). Solid black line, 100 µM *E. coli* LipA Ile22Ala alone. LipA Ile22Ala elutes (62.4 mL) with an experimentally calculated molecular mass of 44.3 kDa (theoretical mass, 38.2 kDa). Black dashed line, 100 µM *E. coli* LipA Ile22Ala + 100 µM wild-type *E. coli* NfuA. Two peaks overlaying the control samples elute at 62.2 mL and 68.1 mL.. (B) SDS-PAGE of fractions corresponding to the main peak, contain only one major band corresponding to *E. coli* LipA Ile22Ala.

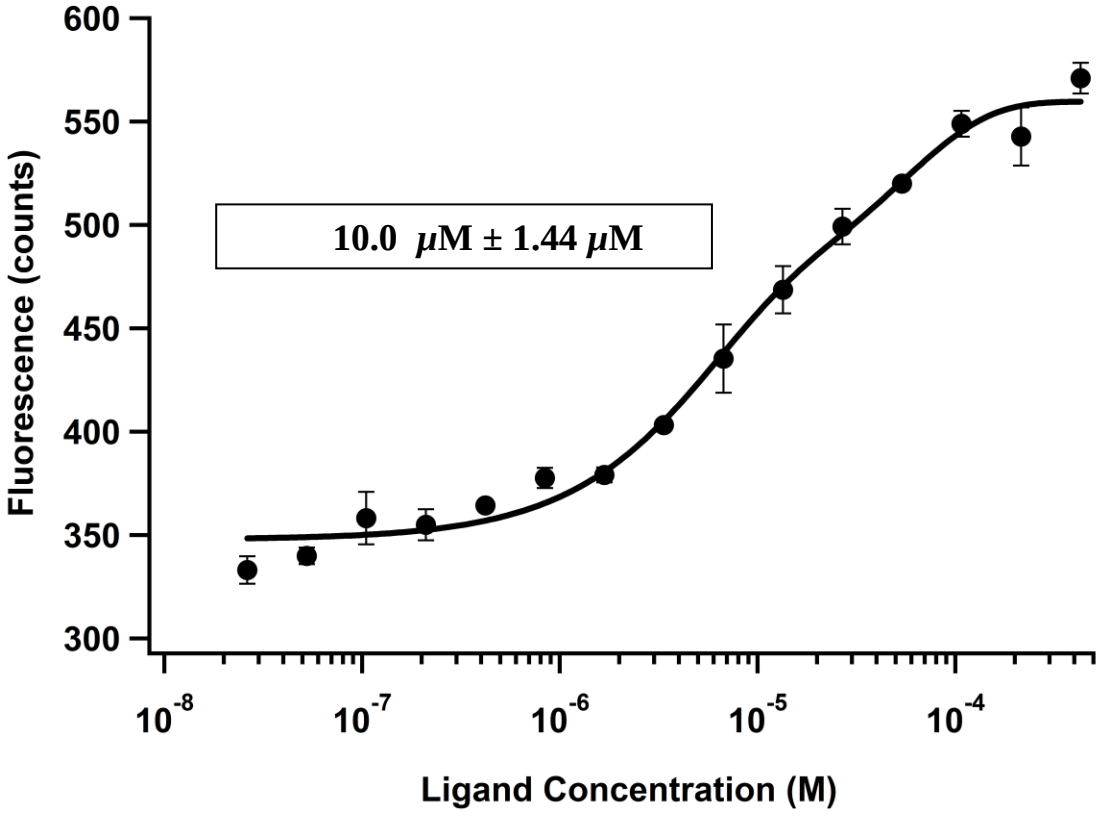

Figure 5-24: Kd Determination of *E. coli* LipA Pro23Ala and *E. coli* NfuA using Microscale Thermophoresis. *E. coli* LipA Pro23Ala (500 nM final protein concentration) was labeled with a fluorescent amine reactive dye. Unlabeled *E. coli* NfuA ligand was serial diluted from 430 μM (first point) across 15 tubes. Error bars represent the data obtained from triplicate experiments, and a specificity test was performed for each replicate.

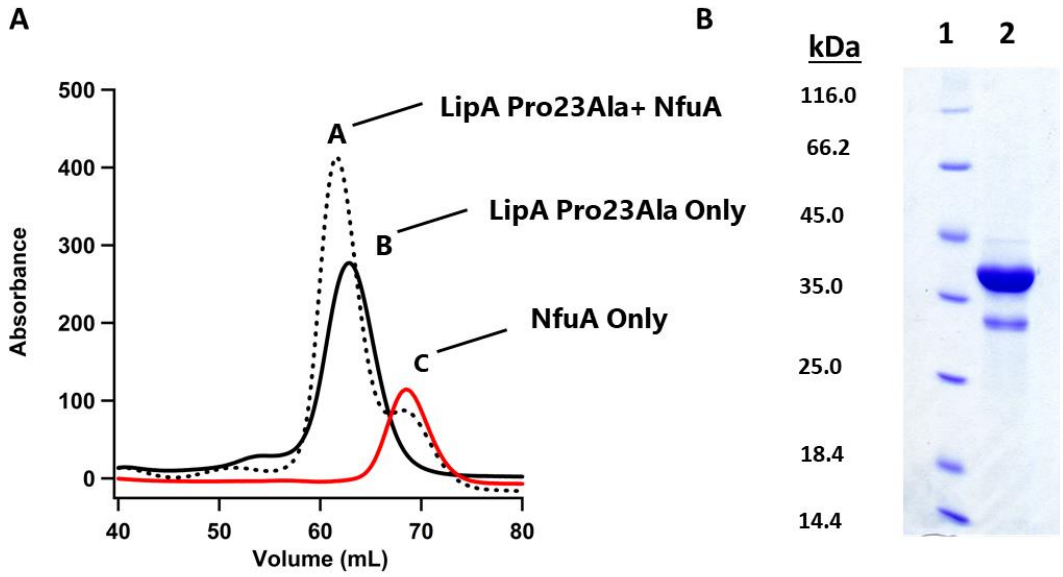

Figure 5-25: (A) Interaction between *E. coli* LipA Pro23Ala and wild-type *E. coli* NfuA monitored by molecular sieve chromatography**.** Red solid line, 100 µM NfuA alone. NfuA elutes (68.5 mL) with an experimentally calculated molecular mass of 26.8 kDa (theoretical mass, 25.6 kDa). Solid black line, 100 µM *E. coli* LipA Pro23Ala alone. LipA Pro23Ala elutes (62.8 mL) with an experimentally calculated molecular mass of 42.5 kDa (theoretical mass, 38.2 kDa). Black dashed line, 100 µM *E. coli* LipA Pro23Ala + 100 µM wild-type *E. coli* NfuA. Two peaks overlaying the control samples elute at 61.6 mL and 68.4 mL. (B) SDS-PAGE of fractions corresponding to the main peak, contain two major bands corresponding to LipA Pro23Ala and a small band of NfuA.

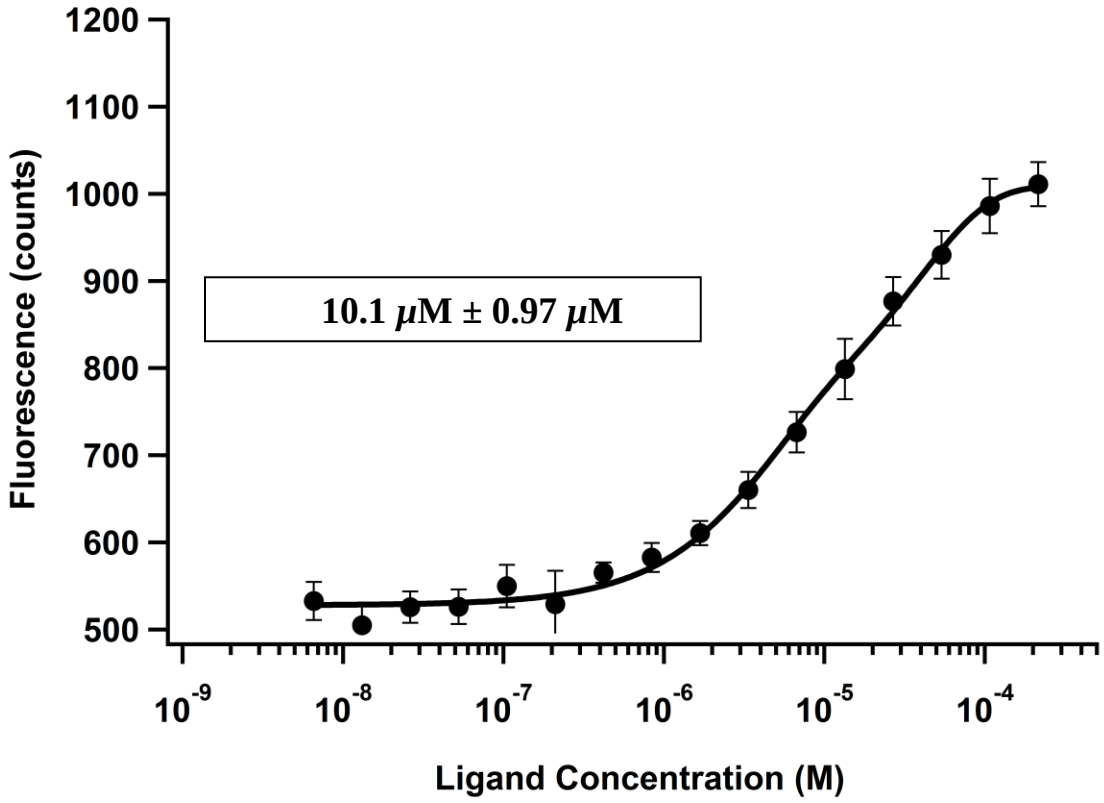

Figure 5-26: Kd Determination of *E. coli* LipA Val24Ala and *E. coli* NfuA using Microscale Thermophoresis. *E. coli* LipA Val24Ala (500 nM final protein concentration) was labeled with a fluorescent amine reactive dye. Unlabeled *E. coli* NfuA ligand was serial diluted from 215 µM (first point) across 16 tubes. Error bars represent the data obtained from triplicate experiments, and a specificity test was performed for each replicate.

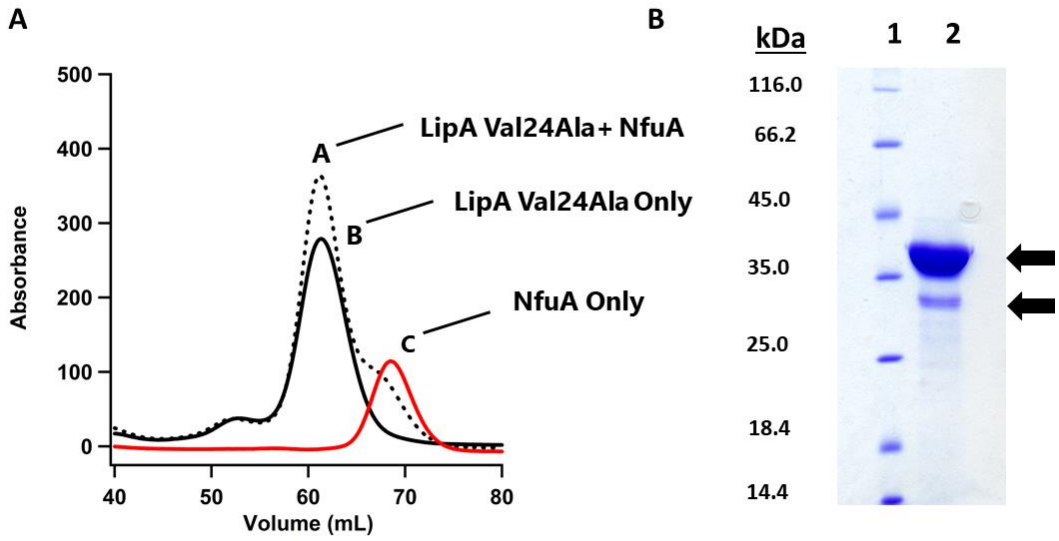

Figure 5-27: (A) Interaction between *E. coli* LipA Val24Ala and wild-type *E. coli* NfuA monitored by molecular sieve chromatography**.** Red solid line, 100 µM NfuA alone. NfuA elutes (68.5 mL) with an experimentally calculated molecular mass of 26.8 kDa (theoretical mass, 25.6 kDa). Solid black line, 100 µM *E. coli* LipA Val24Ala alone. LipA Val24Ala elutes (61.4 mL) with an experimentally calculated molecular mass of 48.1 kDa (theoretical mass, 38.2 kDa). Black dashed line, 100 µM *E. coli* LipA Val24Ala + 100 µM wild-type *E. coli* NfuA. Two peaks elute at 61.3 mL and 67.3 mL.(B) SDS-PAGE of fractions corresponding to the main peak, contain two major bands corresponding to LipA Val24Ala and a small band of NfuA

Enzyme Activity of E. coli LipA wild-type + E. coli NfuA Ile4Ala, E. coli LipA Ile22Ala, E. coli LipA Pro23Ala, and E. coli LipA Val24Ala variants.

The enzyme activity of the protein variants was tested *in vitro* in order to determine if tight complex formation was required for lipoyl product formation. However, it should be noted that the protein concentrations in the assay are above the binding constants reported in this work (**Table 5-3**), which make it difficult to untangle the effect of binding on activity. When 25 µM wild-type *E.*

coli LipA was analyzed under normal assay conditions, approximately one equivalent of lipoyl product formation was observed as expected **(Figure 5-28, closed circles).** However, when 400 µM of either wild-type *E. coli* NfuA (open circles) or *E. coli* NfuA Ile4Ala (closed squares) was included in the reaction, similar levels of catalysis was observed. Similarly, when wild-type *E. coli* LipA or *E. coli* LipA Ile22Ala were reacted in the presence of wild-type *E. coli* NfuA, catalysis was observed though to a slightly lesser extent in the *E. coli* LipA Ile22Ala variant reaction. Reactions including 25 µM wild-type *E. coli* LipA **(Figure 5-29, closed circles)** or *E. coli* LipA Ile22Ala **(Figure 5-29, open squares)** catalyzed approximately one equivalent of lipoyl product. Inclusion of 400 µM wild-type *E. coli* NfuA in the wild-type *E. coli* LipA reaction **(Figure 5-29, open circles)** resulted in ~200 µM lipoyl product, whereas reactions including *E. coli* LipA Ile22Ala and wild-type *E. coli* NfuA catalyzed formation of ~150 µM lipoyl product **(Figure 5-29, closed squares).** Similar results were observed in reactions containing *E. coli* LipA Pro23Ala or *E. coli* LipA Val24Ala. A reaction including 25 µM *E. coli* LipA Pro23Ala **(Figure 5-30, open squares),** displayed almost full activity, catalyzing approximately one equivalent of lipoyl product, whereas addition of 400 µM wild-type *E. coli* NfuA resulted in ~200 µM lipoyl product **(Figure 5-30, closed squares).** Reactions including 25 µM *E. coli* LipA Val24Ala only catalyzed approximately one equivalent of lipoyl product **(Figure 5-31, open squares)** while addition of 400 µM wild-type *E. coli* NfuA **(Figure 5-31, closed squares)** catalyzed similar levels of lipoyl product as the wild-type *E. coli* LipA + wild-type *E. coli* NfuA control reaction **(Figure 5-31, open circles).** In all cases, the disruption of the motif responsible for tight complex formation did not have drastic effects on enzyme activity.

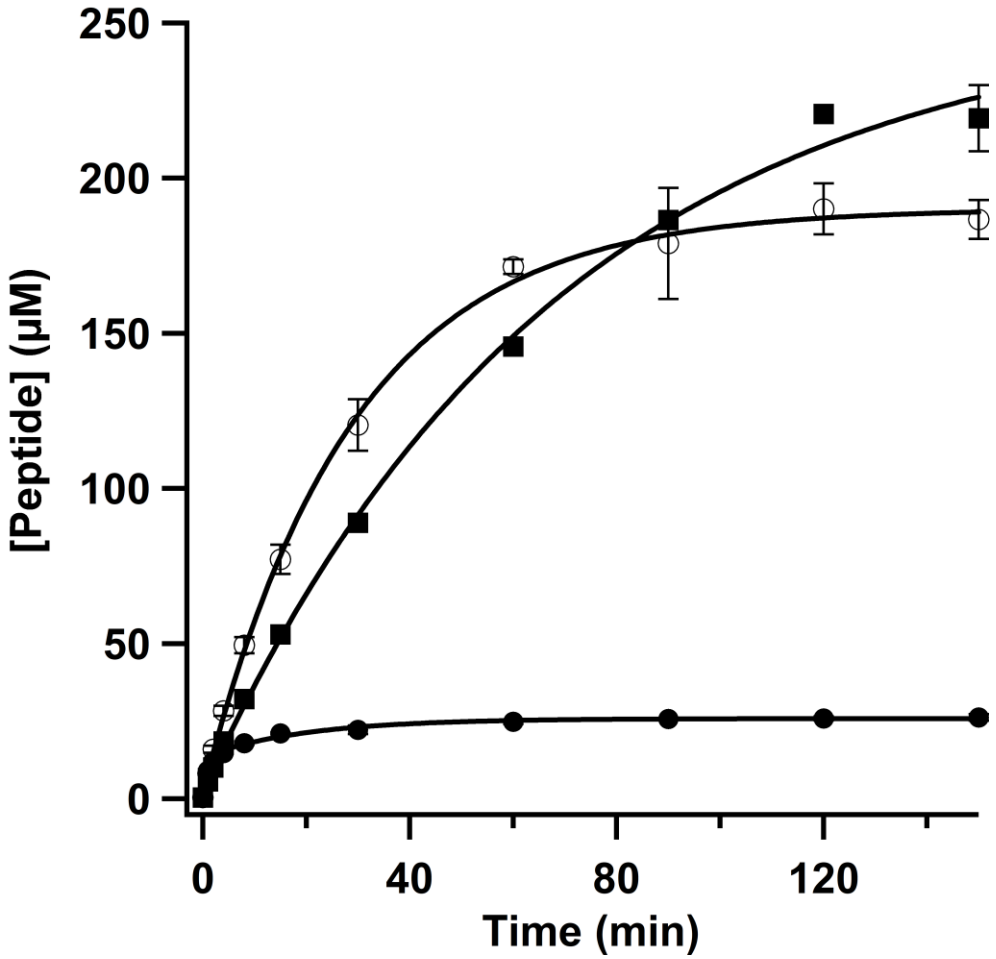

Figure 5-28: Activity of wild-type *E. coli* LipA in presence of *E. coli* NfuA Ile4Ala. Wild-type LipA only (closed circles). Wild-type *E. coli* LipA + wild-type *E. coli* NfuA (open circles). Wild-type *E. coli* LipA + *E. coli* NfuA Ile4Ala (closed squares). The reaction included 25 μM wild-type *E. coli* LipA, 400 μM [4Fe–4S]-containing wild-type *E. coli* NfuA or *E. coli* NfuA Ile4Ala, 600 μM octanoyl-peptide substrate analogue (Glu-Ser-Val-[N^6-octanoyl]Lys-Ala-Ala-Ser-Asp), 0.5 μM SAH nucleosidase, and 1 mM SAM. The reaction was initiated with sodium dithionite (2 mM final concentration, and was quenched with H_2SO_4 at a final concentration of 100 mM . Error bars represent the mean ± standard deviation of three replicates.

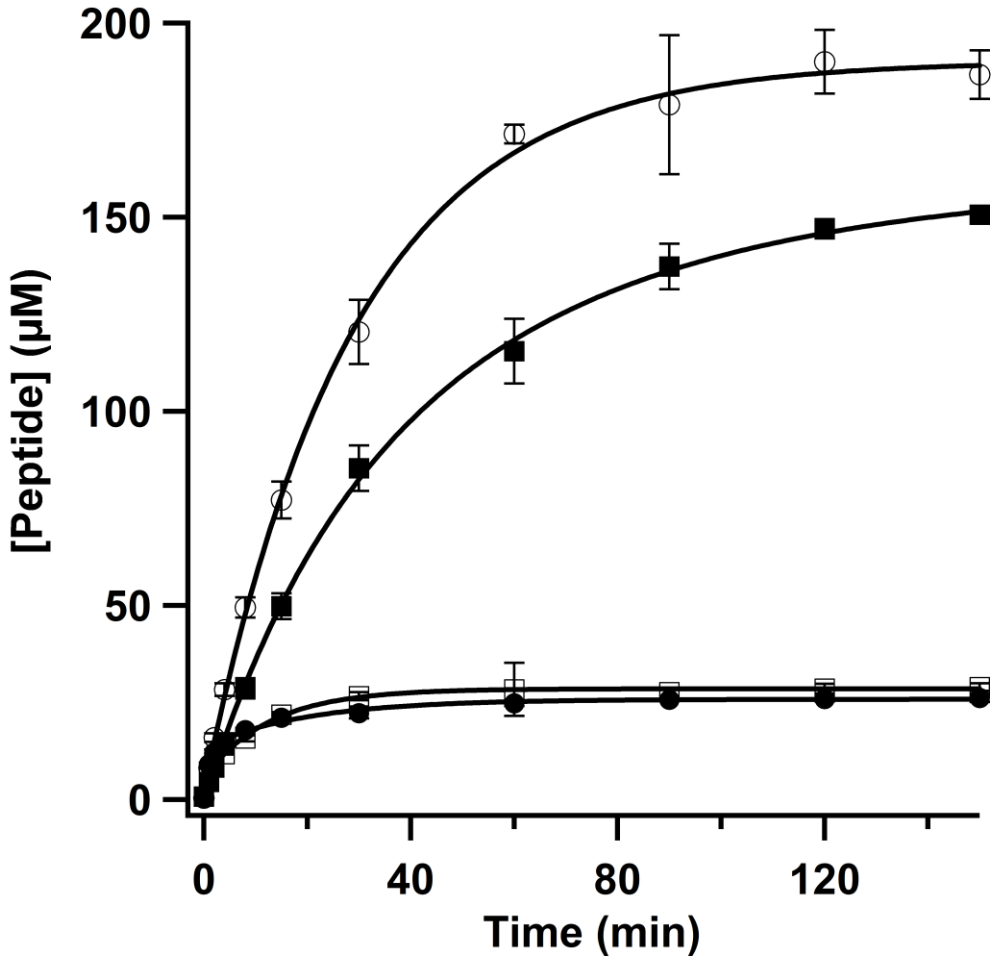

Figure 5-29: Activity of *E. coli* LipA Ile22Ala. Wild-type LipA only (closed circles). Wild-type *E. coli* LipA + wild-type *E. coli* NfuA (open circles). *E. coli* LipA Ile22Ala only (open squares). *E. coli* LipA Ile22Ala + wild-type *E. coli* NfuA (closed squares). The reaction included 25 μM wild-type *E. coli* LipA or *E. coli* LipA Ile22Ala, 400 μM [4Fe–4S]-containing *E. coli* NfuA, 600 μM octanoyl-peptide substrate analogue (Glu-Ser-Val-[N^6-octanoyl]Lys-Ala-Ala-Ser-Asp), 0.5 μM SAH nucleosidase, and 1 mM SAM. The reaction was initiated with sodium dithionite (2 mM final concentration, and was quenched with H_2SO_4 at a final concentration of 100 mM . Error bars represent the mean ± standard deviation of three replicates. Wild-type *E. coli* LipA and wild-type *E. coli* NfuA reproduced from Figure 5-28 for comparison.

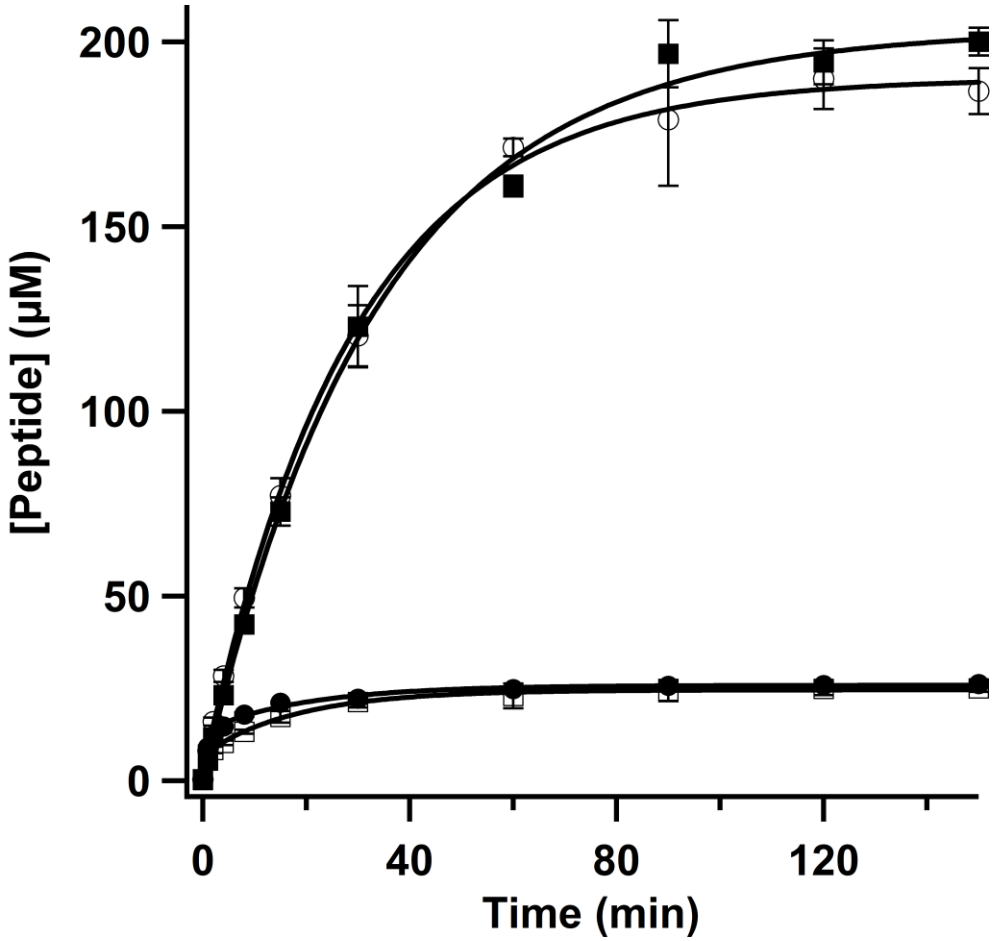

Figure 5-30: Activity of *E. coli* LipA Pro23Ala. Wild-type LipA only (closed circles). Wild-type *E. coli* LipA + wild-type *E. coli* NfuA (open circles). *E. coli* LipA Pro23Ala only (open squares). *E. coli* LipA Pro23AlaAla + wild-type *E. coli* NfuA (closed squares). The reaction included 25 μM wild-type *E. coli* LipA or *E. coli* LipA Pro23AlaAla, 400 μM [4Fe–4S]-containing *E. coli* NfuA, 600 μM octanoyl-peptide substrate analogue (Glu-Ser-Val-[N^6-octanoyl]Lys-Ala-Ala-Ser-Asp), 0.5 μM SAH nucleosidase, and 1 mM SAM. The reaction was initiated with sodium dithionite (2 mM final concentration, and was quenched with H_2SO_4 at a final concentration of 100 mM . Error bars represent the mean ± standard deviation of three replicates. Wild-type *E. coli* LipA and wild-type *E. coli* NfuA reproduced from Figure 5-28 for comparison.

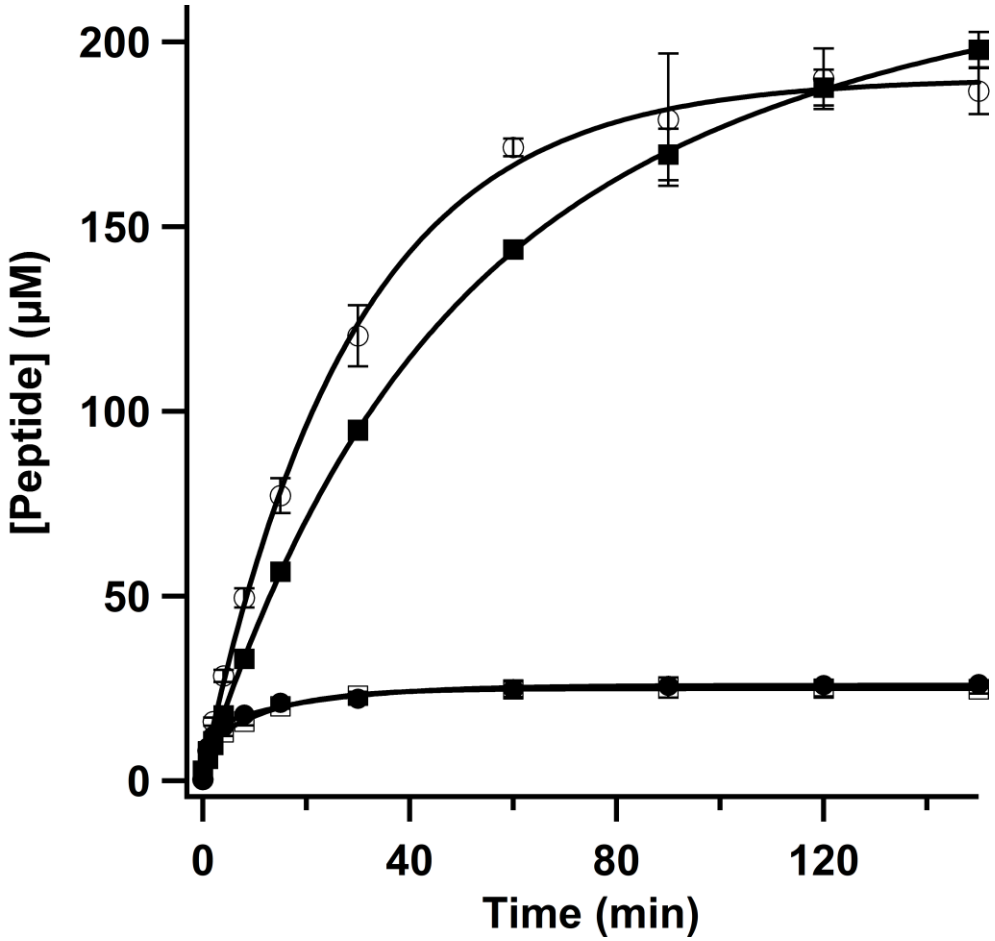

Figure 5-31: Activity of *E. coli* LipA Val24Ala. Wild-type LipA only (closed circles). Wild-type *E. coli* LipA + wild-type *E. coli* NfuA (open circles). *E. coli* LipA Val24Ala only (open squares). *E. coli* LipA Val24Ala + wild-type *E. coli* NfuA (closed squares). The reaction included 25 μM wild-type *E. coli* LipA or *E. coli* LipA Val24Ala, 400 μM [4Fe–4S]-containing *E. coli* NfuA, 600 μM octanoyl-peptide substrate analogue (Glu-Ser-Val-[N^6-octanoyl]Lys-Ala-Ala-Ser-Asp), 0.5 μM SAH nucleosidase, and 1 mM SAM. The reaction was initiated with sodium dithionite (2 mM final concentration, and was quenched with H_2SO_4 at a final concentration of 100 mM . Error bars represent the mean ± standard deviation of three replicates. Wild-type *E. coli* LipA and wild-type *E. coli* NfuA reproduced from Figure 5-28 for comparison.

Sequence alignments and homology modeling.

Sequence alignments of lipoyl synthases from a selection of organisms revealed that the IPV motif and generally the N-terminal domain of *E. coli* LipA is not well conserved **(Figure 5-32).** We conclude that this interaction is a unique feature of *E. coli* LipA and *E. coli* NfuA. We have discovered that in some organisms, this tight complex formation is not observed, such as between LipA and NfuA from *T. elongatus* (unpublished data, Vivian Robert Jeyachandran). Because the crystal structure of *E. coli* LipA is not available, we constructed a homology model using I-TASSER (12-14). The resulting model was superimposed with the published crystal structure of LipA from *Thermosynechococcus elongatus* (PDB 4u0p) and found that the predicted structure of *E. coli* LipA aligned reasonably well. The N-terminal domain of *E. coli* LipA is mostly predicted to be a flexible loop region. However, the IPV motif is in a predicted helix loop helix region. Intriguingly, this motif is predicted to be on the surface of *E. coli* LipA within close proximity of the auxiliary cluster that is regenerated by *E. coli* NfuA **(Figure 5-33).** From the model, we can predict that the proline might play a structural role, helping to project the valine and isoleucine residue outwards towards the surface to interact with NfuA **(Figure 5-33).** This predicted model supports the experimental evidence for the IPV motif within *E. coli* LipA as being critical for complex formation with *E. coli* NfuA.

The significance of the domain architecture of *E. coli* NfuA is still being unraveled. However, alignment of several NfuA sequences with the similar two domain components show very strong sequence similarity, including the isoleucine residue at position 4 **(Figure 5-34).** In some organisms, such as *T. elongatus* and *S. aureus*, only the C-terminal domain is present, and as such, they are named Nfu, distinguishing them from Nfu**A**s which have an A-type domain appended to the N-terminus. The presence of the additional A-type domain has been postulated by others and ourselves as playing a role in enhancing protein-protein interactions and cluster insertion (4,15).

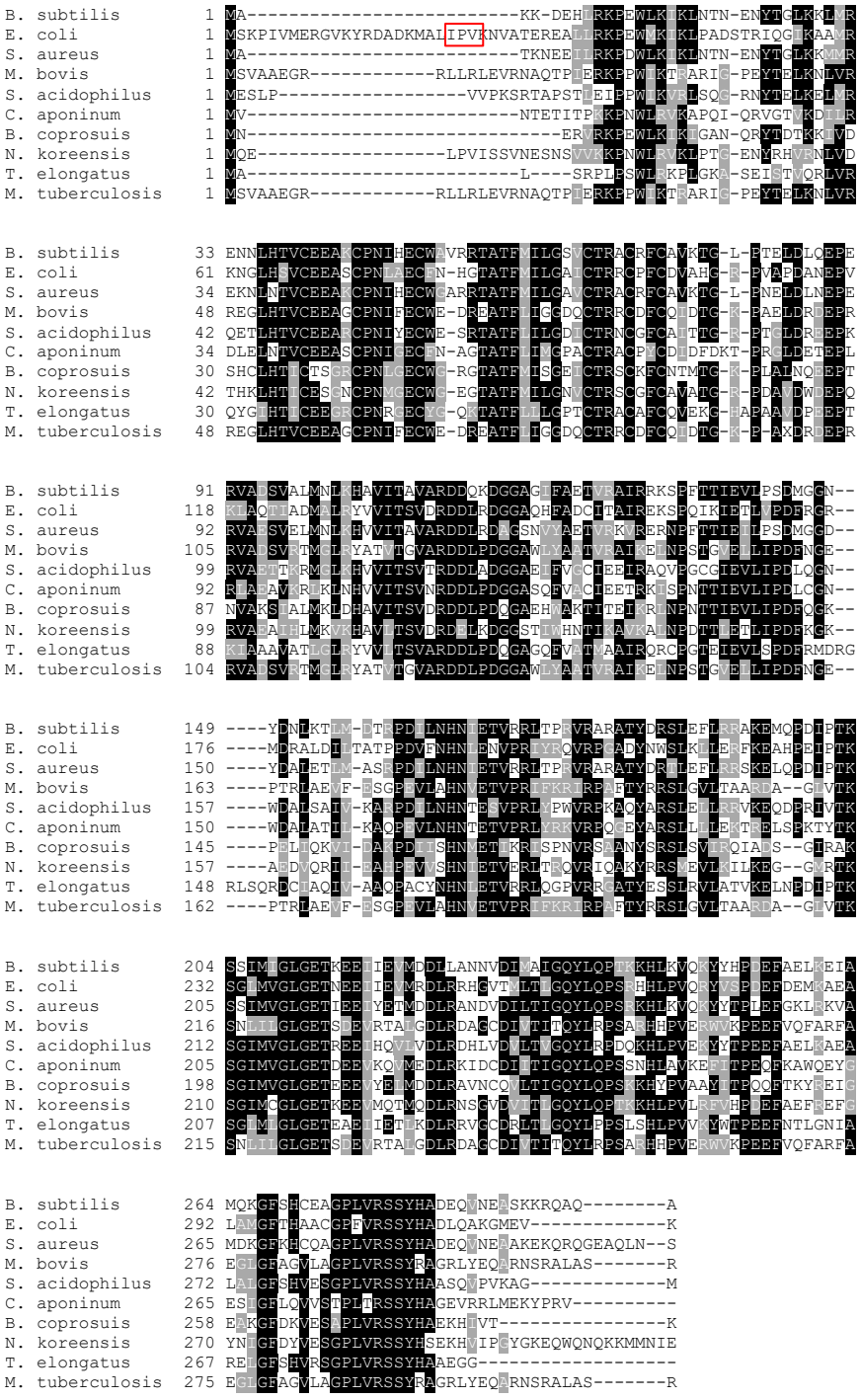

Figure 5-32: Sequence alignment of lipoyl synthases from various organisms: *Bacillus subtilis* (*B. subtilus*), *Escherichia coli* (*E. coli*), *Staphylococcus aureus* (*S. aureus*), *Mycobacterium bovis* (*M. bovis*), *Sulfobacillus acidophilus* (*S. acidophilus*), *Cyanobacterium aponinum* (*C. aponinum*), *Bacteroides coprosuis* (*B. coprosuis*), *Niastella koreensis* (*N. koreensis*), *Thermosynechococcus elongatus* (*T. elongatus*), and *Mycobacterium tuberculosis* (*M. tuberculosis*).

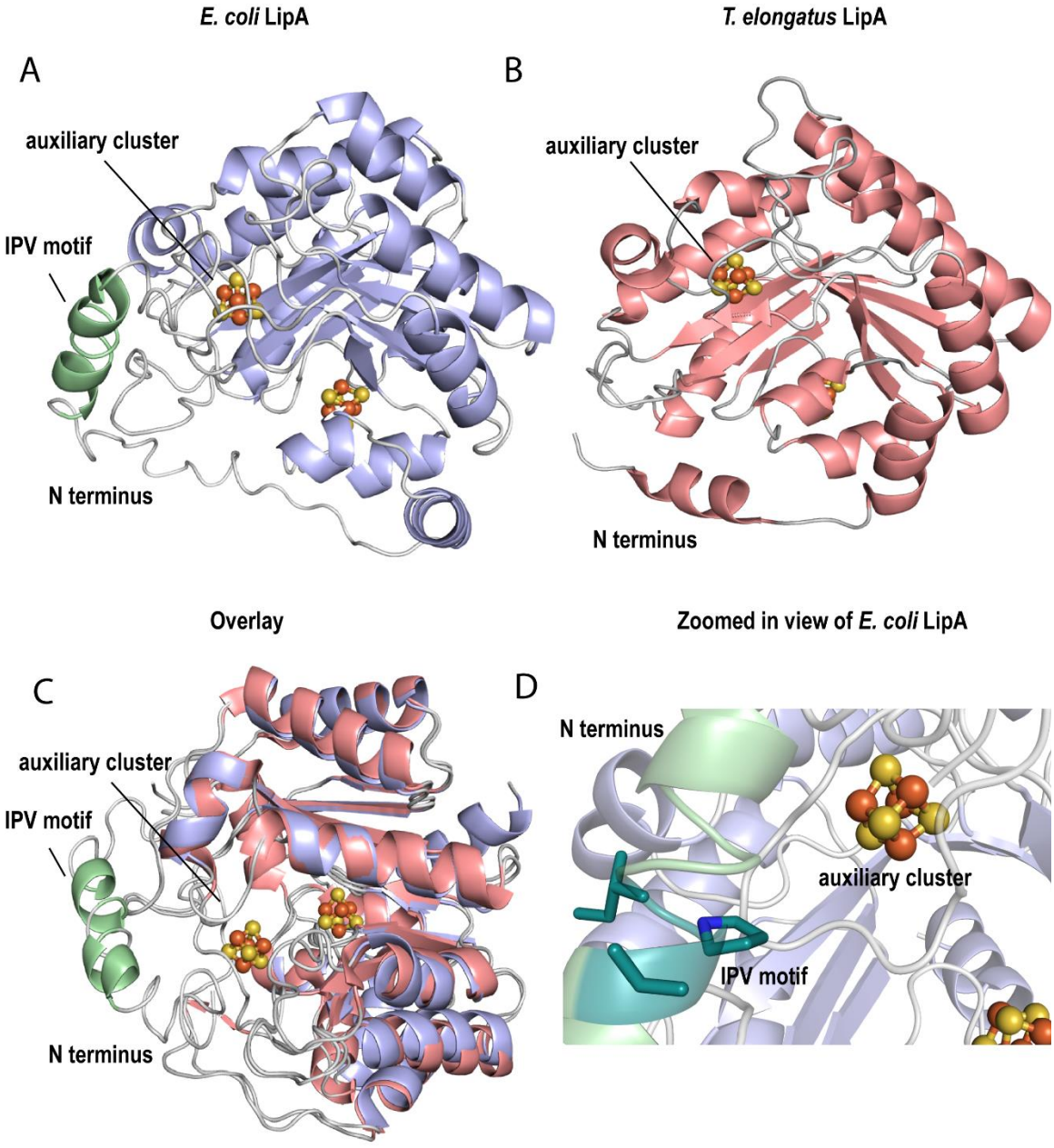

Figure 5-33: (A) Homology model of *E. coli* LipA (light blue) generated using I-TASSER (Zhang lab, University of Michigan). Extended N-terminal domain with IPV motif is shown in pale green. (B) Published crystal structure of LipA from *T. elongatus* (PDB 4u0p, pink). (C) *E. coli* LipA homology model (light blue) with the extended N-terminal domain (pale green) superimposed with published crystal structure of LipA from *T. elongatus* (pink). (D) Zoomed in view of Panel A focusing on the extended N-terminal domain that contains the IPV motif.

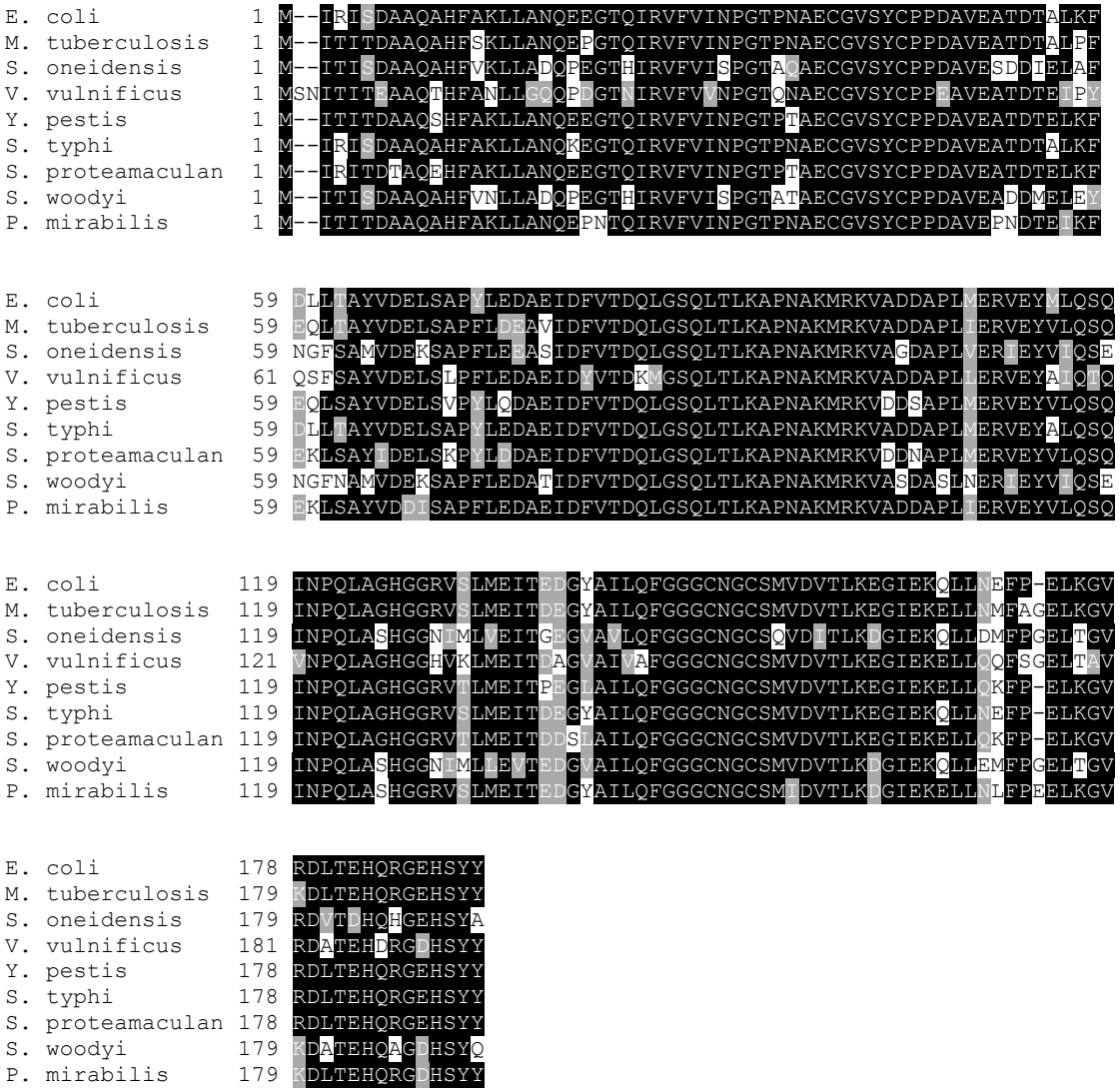

Figure 5-34: Sequence alignment NfuA's from various organisms: *Escherichia coli* (*E. coli*), *Mycobacterium tuberculosis* (*M. tuberculosis*), *Shewanella oneidensis* (*S. oneidensis*), *Vibrio vulnificus* (*V. vulnificus*), *Yersinia pestis* (*Y. pestis),* *Salmonella typhi* (*S. typhi*), *Serratia proteamaculans* (*S. proteamaculans),* *Shewanella woodyi* (*S. woodyi*), and *Proteus mirabilis* (*P. mirabilis*).

Characterization of E. coli MiaB

The published findings that *E. coli* NfuA could restore the cofactor in *E. coli* LipA revealed that enzymes that sacrifice their auxiliary clusters during their reaction mechanism could be regenerated for catalysis. An outstanding question following this discovery is whether NfuA is specifically targeted to LipA or whether it is targeted to several proteins that require metal cofactors. An additional protein that contains an auxiliary [4Fe-4S] cluster is *E. coli* MiaB, which catalyzes the methylthiolation of of N^6-(isopentenyl)adenosine. It is still unclear whether MiaB performs a sacrificial mechanism consuming its auxiliary cluster. Intriguingly, *E. coli* MiaB was amongst the proteins identified in mixture of proteins that pulled-down in the co-immunoprecipitation of *E. coli* NfuA. To this end, we proceeded to isolate *E. coli* MiaB in an attempt to address this open question. Previous work by our laboratory attempted to purify *E. coli* MiaB but found it to be only 10% pure (unpublished). Other laboratories also reported that *E. coli* MiaB was unsuitable for robust biochemical analysis and utilized MiaB from *Thermotoga maritima* (7,16,17). Nevertheless, a new expression construct *E. coli miaB*-pET28a was created to overproduce *E. coli* MiaB with a hexahistidine tag at the N terminus. Upon overproduction using the protocol described in the materials and methods, a robust expression band corresponding to the size of MiaB was observed when analyzed by SDS-PAGE **(Figure 5-35, Panel A).** Further, the protein was able to be isolated to ~80 percent purity following a one-step affinity purification **(Figure 5-35 Panel B).** While the protein was determined to be of sufficient purity for initial analysis, the cofactor incorporation was suboptimal, though UV-visible spectroscopy revealed the as-isolated protein contained some cofactor incorporation **(Figure 5-36, dashed line).** Colorimetric iron analysis estimated a total of 4.7 iron +/- 0.4 iron atoms per protein. In order to improve the cofactor incorporation, a chemical reconstitution of the iron-sulfur cluster was performed. Following size-exclusion chromatography to remove protein aggregates and non-specifically

bound metals, more pronounced features of a [4Fe-4S] cluster are observed in the UV-visible spectrum **(Figure 5-37, solid line).** Colorimetric iron analysis of the reconstituted protein estimated a total of 8.9 iron +/- 0.7 iron atoms per protein.

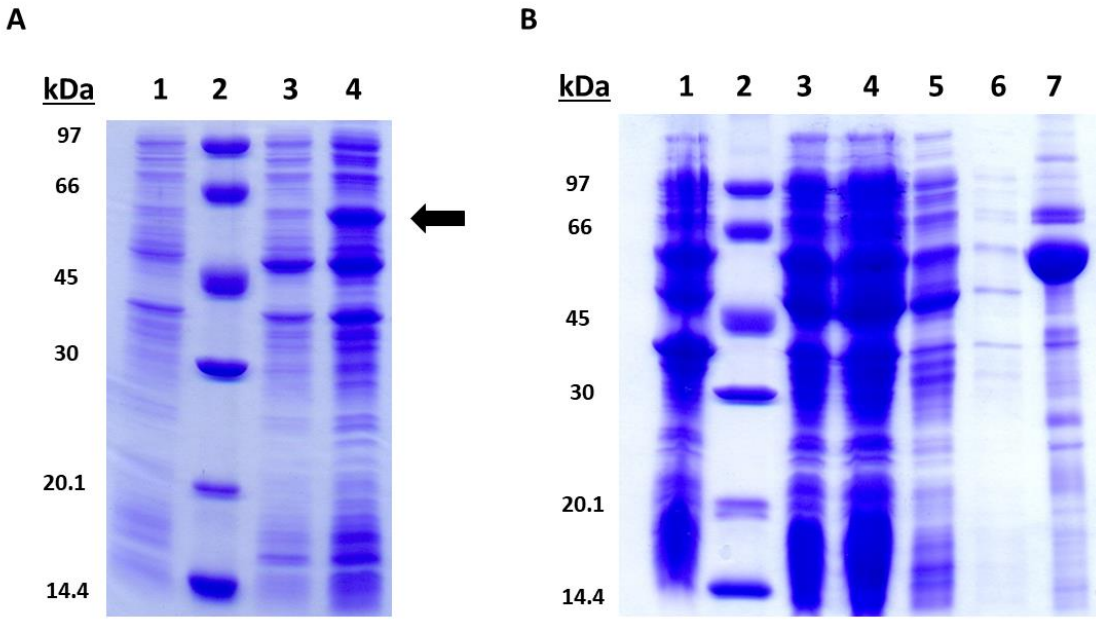

Figure 5-35: **Overproduction and isolation of *E. coli* MiaB.** (A) SDS-PAGE of overexpression of the *E. coli miaB* gene. Lanes are as follows: 1- uninduced 2- molecular weight ladder 3- post-arabinose 4- post-IPTG (B) SDS-PAGE of isolation of *E. coli* MiaB. Lanes are as follows: 1- cellular pellet 2- molecular weight ladder 3- crude supernatant 4- flow-through 5- wash 1 6- wash 2 7- pure protein

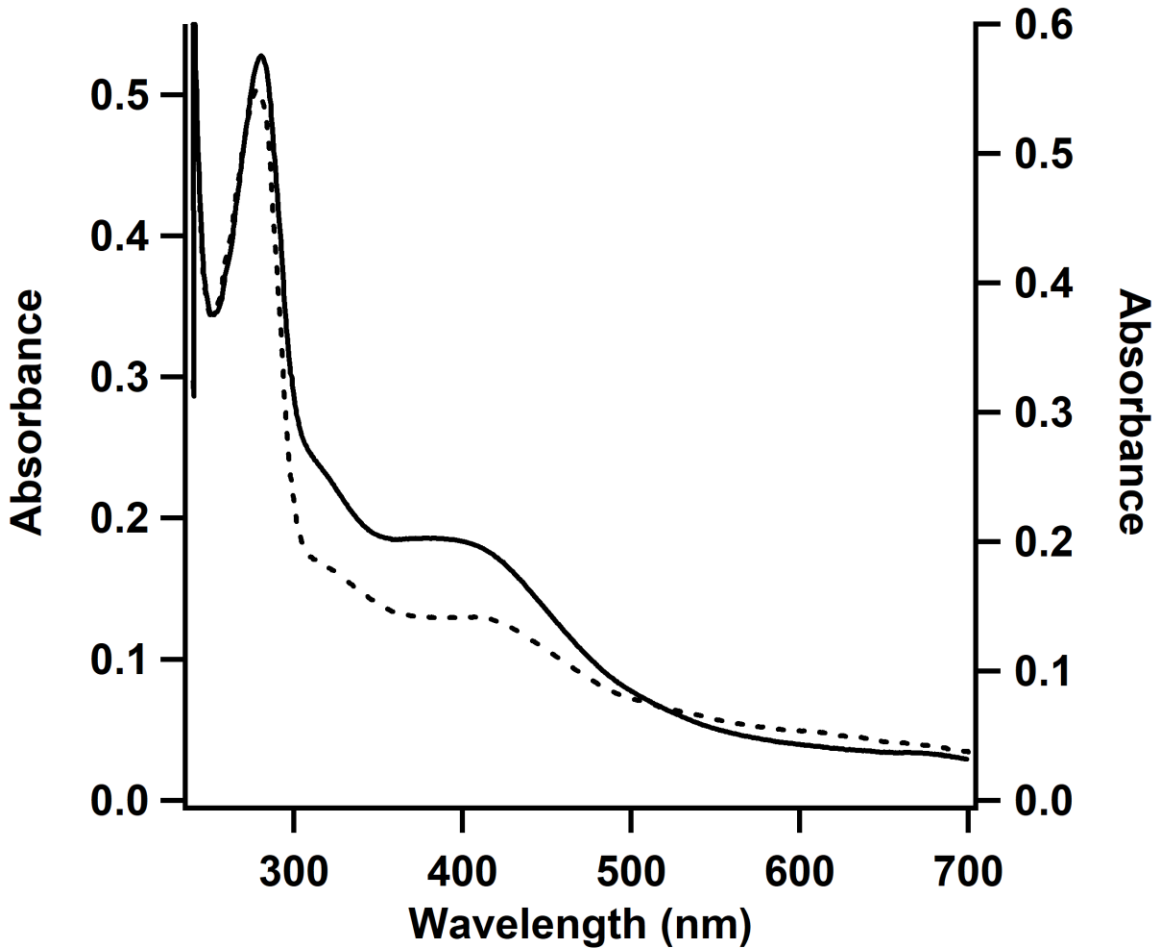

Figure 5-36: **UV-visible spectra of *E. coli* MiaB.** As-isolated protein (dashed line) and chemically reconstituted protein (solid line).

Binding of E.coli NfuA and E. coli MiaB using molecular sieve chromatography.

A report in the literature describes an interaction between Apo *E. coli* NfuA and Apo *E. coli* MiaB using a variety of methods, including surface plasmon resonance, affinity co-purification, and molecular sieve chromatography (18). In order to test the hypothesis that *E. coli* NfuA also targets *E. coli* MiaB, we performed a similar analytical molecular sieve chromatography experiment to probe the interaction between the two proteins, instead using both holo NfuA and holo MiaB **(Figure 5-37).** *E. coli* MiaB alone (solid black trace) elutes at 67.2 mL, corresponding

to an experimental mass of 53.6 kDa (theoretical mass is 56.7 kDa). *E. coli* NfuA alone (solid blue trace) elutes at 77.0 mL, corresponding to an experimental mass of 27.9 kDa (theoretical mass is 25.7 kDa). The sample containing an equimolar mixture of MiaB and NfuA (dotted red trace) resulted in two peaks at 67.3 mL and 76.5 mL. No shift in the elution times for the peaks were observed compared to the samples, suggesting no complex formation under the conditions tested. The fractions corresponding to each of the peaks were subjected to SDS-PAGE analysis confirmed the absence of a protein complex.

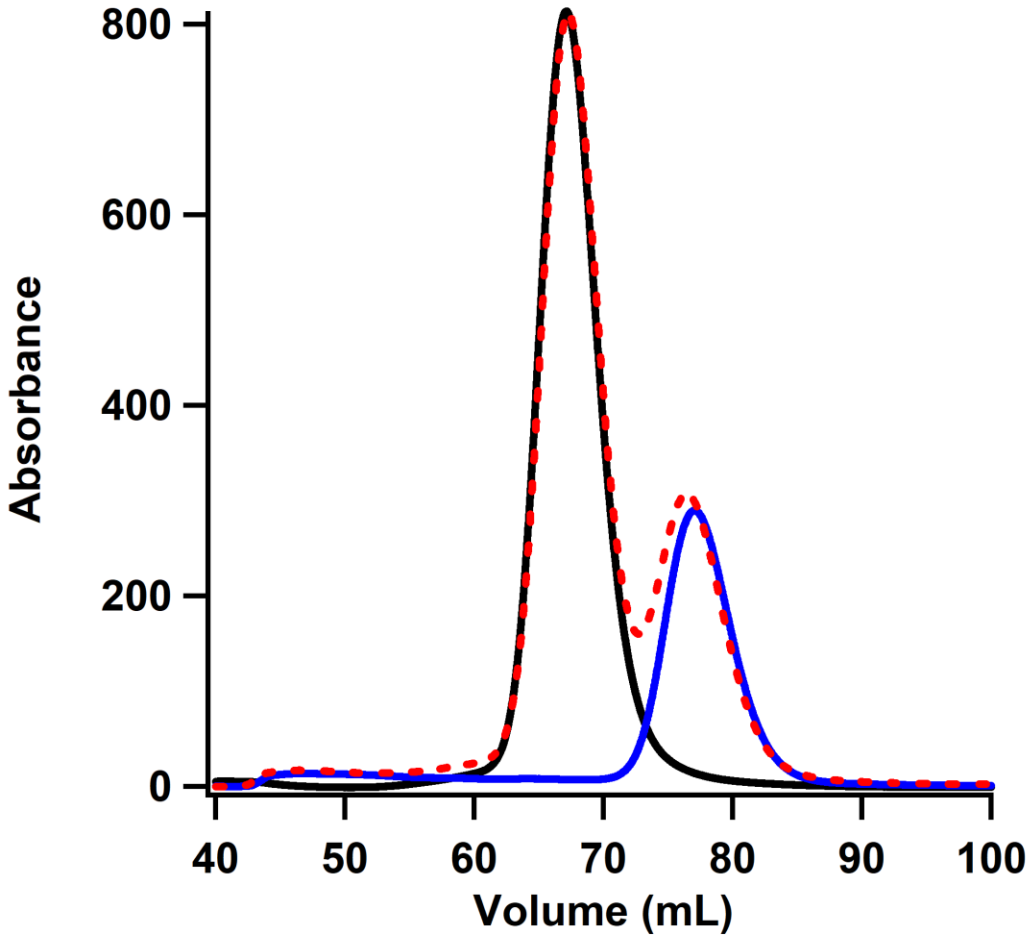

Figure 5-37: **Analytical molecular sieve chromatography of *E. coli* MiaB and *E. coli* NfuA.** Interaction between MiaB and NfuA monitored by molecular sieve chromatography**.** Blue solid

line, 100 µM NfuA alone. NfuA elutes (77.0 mL) with an experimentally calculated molecular mass of 27.9 kDa (theoretical mass, 25.6 kDa). Sold black line, 100 µM MiaB alone. MiaB elutes (67.2 mL) with an experimentally calculated molecular mass of 53.6 kDa (theoretical mass, 56.7 kDa). Red dashed line, 100 µM MiaB + 100 µM NfuA. Two peaks overlaying the control samples elute at 67.3 mL and 76.5 mL.

Binding of E.coli NfuA and E. coli MiaB using bacterial two hybrid screening.

The lack of observed binding of *E. coli* NfuA and *E. coli* MiaB in our experiments using analytical molecular sieve chromatography deviates from the previous published data that suggested an interaction between the two proteins (18). One possibility is the difference in cofactor incorporation between the two studies. In the previous study, apo proteins were used in the binding experiments, whereas our experiments utilized holo forms of the two enzymes. Further, if the association is weak between the two proteins, we may not have been able to pull-down a stable complex like we have observed for *E. coli* NfuA and *E. coli* LipA using this particular technique, though it does not exclude the possibility of a transient interaction. We then moved to a more physiological *in vivo* bacterial two hybrid binding assay described in detail above. The following constructs were assembled using gateway cloning technology: *gstB*-pUT18C, *gcvH*-pST25, *nfuA*-pUT18C, and *miaB*-pST25. *E. coli* adenylate cyclase deficient BTH101 cells were co-transformed with the following pairs of plasmids: *gstB*-pUT18C + *gcvH*-pST25 (negative control), zip-pUT18C + zip-pKT25 (positive control), and *nfuA*-pUT18C + *miaB*-pST25. The cells were plated on LB agar plates containing IPTG and x-gal. After incubation at 30 °C for 48 hours, robust blue colonies were observed on the *zip*-pUT18C + *zip*-pKT25 control plates, as expected **(Figure 5-38, Panel C).** However, no color was observed in the colonies on both the *gstB*-pUT18C + *gcvH*-pST25 (negative control) and *nfuA*-pUT18C + *miaB*-pST25 plates **(Figure 5-38, Panels A and C)**, indicative of no interaction between the proteins *in vivo.*

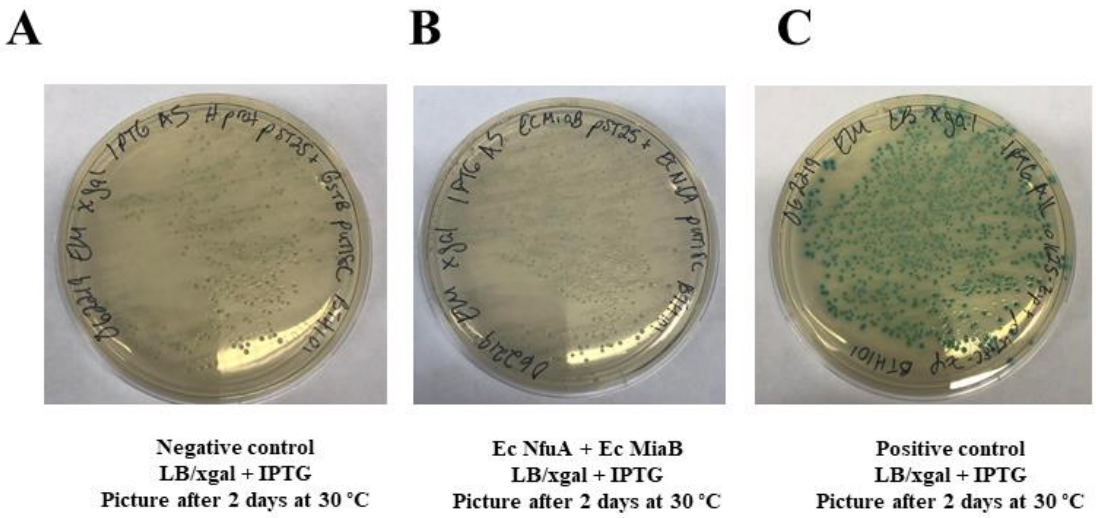

Figure 5-38: **Bacterial two hybrid screening of *E. coli* NfuA and *E. coli* MiaB.** Adenylate cyclase deficient cells strain BTH101 were co-transformed bacterial two hybrid plasmids and spread on LB agar plates containing 40 µg/µL galactosidase and 0.5 mM IPTG with the respective selective antibiotics (100 µg/µL spectinomycin or 50 µg/µL kanamycin and 100 µg/µL ampicillin) . (A) Negative control containing two non-interacting proteins *E. coli gcvH*-pST25 and *E. coli gstB*-pUT18C. (B) *E. coli* n*fuA*-pUT18C and *E. coli miaB*-pST25. (C) Positive control containing two domains of leucine zipper: *zip*-pUT18C and *zip*-pKT25.

E. coli MiaB Activity Assays.

Previously, the activity of *E. coli* MiaB had previously reported to be very poor *in vitro*, which prompted the use of a thermophilic homolog with enhanced activity and cofactor incorporation for biochemical and spectroscopic analysis. In addition to the various experiments described that were performed to probe the potential complex formation between *E. coli* NfuA and *E. coli* MiaB, *in vitro* activity assays were also performed to test whether the inclusion of *E. coli* NfuA had any effect on the activity of *E. coli* MiaB. *E. coli* MiaB (25 µM) catalyzed only approximately 4 µM ms^2i^6A product over 120 min **(Figure 5-39, black closed circles).** When *E. coli* NfuA was included in the assay (200 µM), even less ms^2i^6A product was observed under the same reaction conditions **(Figure 5-39, red closed circles).** While the reason for the decrease in

product formation in the presence of NfuA is unknown, it is clear that under the described experimental conditions, *E. coli* NfuA does not significantly enhance the activity of *E. coli* MiaB, consistent with the lack of binding observed both *in vitro* and *in vivo.*

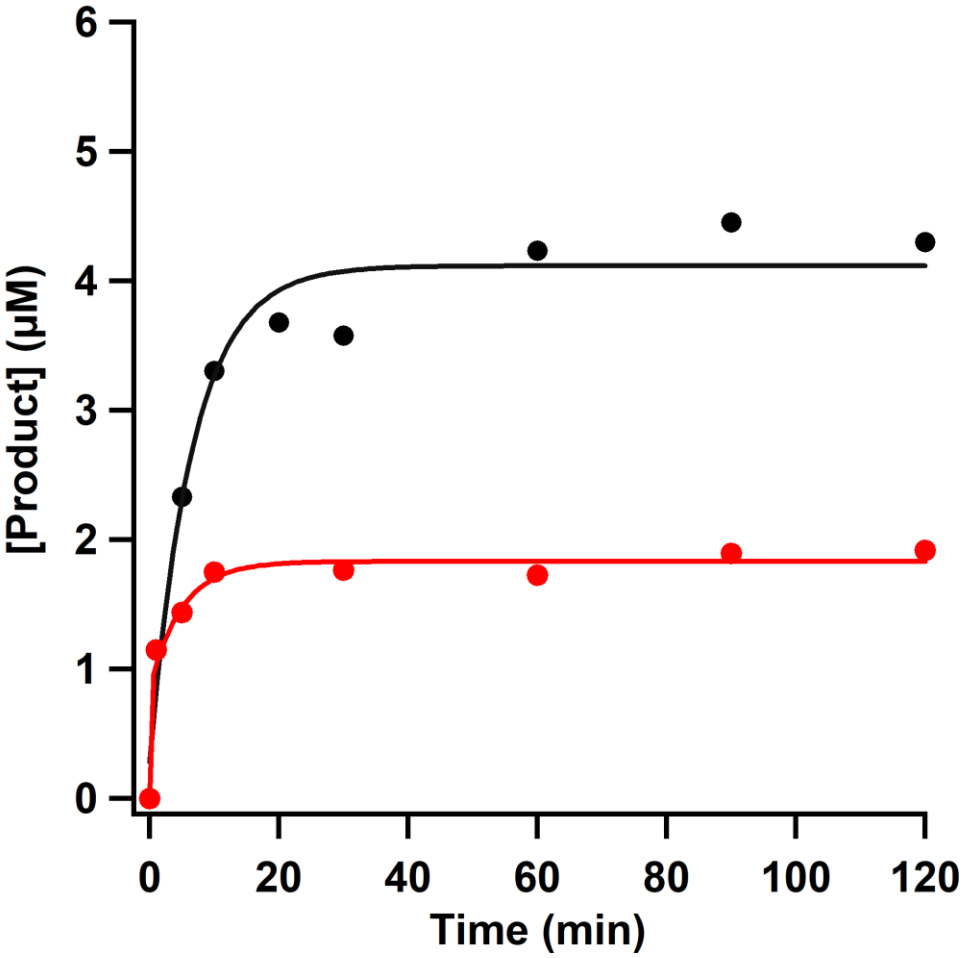

Figure 5-39: **Activity assay of *E. coli* MiaB in the absence and presence of *E. coli* NfuA.** Formation of ms^2i^6A product over time. Reaction included either 25 μM *E. coli* MiaB only control (black closed circles) or 25 μM *E. coli* MiaB in the presence of 200 μM *E. coli* NfuA (closed red circles). Additional reaction components included 300 μM Tm i^6A 17mer RNA substrate and 1 mM SAM in reaction buffer (50 mM HEPES, pH 7.5, 300 mM KCl, 10 mM $MgCl_2$). Reactions were performed at room temperature, initiated with 1 mM dithionite, and acid-quenched with 100 mM H_2SO_4 at the indicated times.

Discussion

In this work, we seek understanding of the specificity of iron-sulfur carrier proteins for their intended target, and the mechanism of binding and recognition of their apo-protein recipient. *In vitro* analysis, using analytical molecular sieve chromatography, showed that a tight complex forms between *E. coli* LipA and *E. coli* NfuA (3). Our co-immunoprecipitation studies validated these findings, showing that *E. coli* LipA and *E. coli* NfuA can be pulled out of the cell together without the need for a crosslinker. This surprising result lead us to speculate that *E. coli* NfuA and *E. coli* LipA could exist as a stable complex in the cell. Consistent with this hypothesis, our bacterial two hybrid analysis revealed a robust positive interaction between *E. coli* NfuA and *E. coli* LipA *in vivo.* We calculated the binding constant to be ~1 μM using microscale thermophoresis. In our binding studies, we are typically using iron-sulfur cluster loaded protein. One interesting idea that remains to be tested is that the binding affinity could be modulated based on the cluster occupancy of the two proteins. For example, the binding affinity between iron-sulfur cluster loaded NfuA and LipA after its auxiliary cluster has been destroyed could be higher than when its auxiliary cluster is intact. Such a strategy would allow for "sensing of" when NfuA needs to provide a newly assembled iron-sulfur cluster. NfuA coordinates its iron-sulfur cluster at a dimer interface, and it is believed to disassociate to its monomeric form in its apo state. Interestingly, analytical molecular sieve chromatography revealed a 1:1 complex between LipA and NfuA. The experiment used iron-sulfur cluster loaded LipA and NfuA, but NfuA has been shown to lose its cofactor at low protein concentration when subjected to the conditions of the column (room temperature for 2.5 hr). Moreover, we envision a model in which the binding affinity of NfuA for LipA could be enhanced when NfuA is in its holo form and LipA's auxiliary cluster has been destroyed. Once the auxiliary

cluster of LipA has been replenished, rendering NfuA apo, the binding affinity could decrease allowing for facile dissociation.

Using bacterial two hybrid screening, we were able to identify an Ile at position 4 on NfuA and an Ile-Pro-Val motif on LipA at positions 22-24 that were involved in the protein-protein interaction. The binding of these variant proteins were probed *in vitro* using microscale thermophoresis and analytical molecular sieve chromatography. While the effect of the NfuA Ile4Ala variant was modest, demonstrating ~2.5 fold increase in the binding constant, the LipA Pro23Ala and LipA Val24Ala variants increased the binding constant ~10-fold. Interestingly, binding between LipA Ile22Ala and wild-type NfuA could not be detected using microscale thermophoresis, and no complex could be observed using analytical molecular sieve chromatography. This single isoleucine residue in LipA is absolutely required for complex formation. This finding is consistent with the literature precedent described by the Rouault laboratory for succinate dehydrogenase, in which a single isoleucine residue is required for recognition by the iron-sulfur cluster co-chaperone HSC20. When the activity of each of the variant proteins was tested, surprisingly, all variants could stimulate catalytic activity, though these experiments were performed at concentrations above the calculated dissociation constant. This result supports an unpublished observation that Nfu from *Thermosynechococcus elongatus* (Te) can still activate Te LipA, though tight complex formation is not observed between these two proteins. Consequently, the exact role of the tight complex formation between NfuA and LipA in *E. coli* is not well understood. It is clear from the *in vivo* bacterial two hybrid screening interaction and through co-immunoprecipitation of the complex without the use of a crosslinker that this complex is physiologically relevant. One possibility is that NfuA stabilizes and protects LipA from degradation during its catalytic cycle *in vivo* **(Figure 5-40).** It has been reported that loss of iron-sulfur clusters as a result of catalysis in *E. coli* biotin synthase promotes unfolding and degradation (19). Another possibility is that NfuA forms a complex with LipA to allow facile delivery of iron-

sulfur clusters during its catalytic mechanism, presumably receiving its clusters from the scaffold IscU.

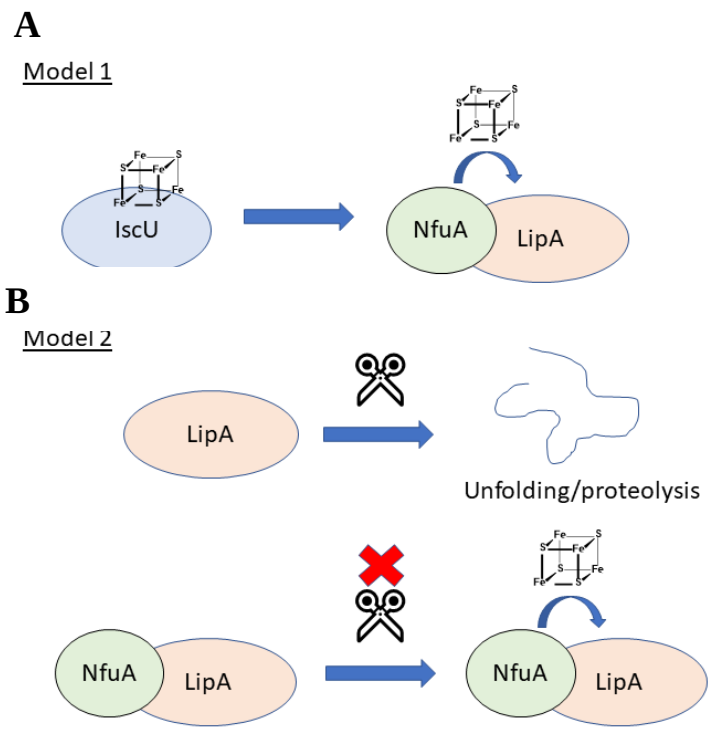

Figure 5-40: Possible biological roles for the tight complex formation between *E. coli* LipA and *E. coli* NfuA. (A) In one model, NfuA remains in close proximity of LipA to allow facile transfer of iron-sulfur clusters to the auxiliary site during LipA's catalytic mechanism. (B) A second model for complex formation suggests a role for NfuA in stabilizes LipA from proteolysis and unfolding as a result of the destruction of its auxiliary cluster, as has been observed for the closely related biotin synthase.

Excitingly, one of the proteins that was identified in the co-immunoprecipiation of *E. coli* NfuA was *E. coli* MiaB, which catalyzes the methylthiolation of of N^6-(isopentenyl)adenosine. Similar to LipA, MiaB coordinates an auxiliary [4Fe-4S] cluster. While MiaB also catalyzes a sulfur insertion mechanism, is still unclear whether it performs a sacrificial mechanism consuming its auxiliary cluster. An interesting publication provided evidence for complex formation between *E. coli* NfuA and *E. coli* MiaB *in vitro* (18). This evidence, along with our co-immunoprecipitation results, motivated us to further study the possible connection between these two proteins. *E. coli* MiaB was not successfully isolated from our lab, which noted difficulty obtaining quality protein for robust biochemical and spectroscopic analysis, consistent with reports from other laboratories (16,17). After re-cloning *E. coli* MiaB into a construct that encoded an N-terminal hexahistidine tag, we were able to obtain moderately pure protein. After chemical reconstitution and further purification by size exclusion chromatography, we were able to produce suitable protein for biochemical analysis. However, when binding between *E. coli* NfuA and *E. coli* MiaB was assessed by analytical molecular sieve chromatography, no complex formation was observed. This contradicts the published complex formation between the two proteins using the same method; however, the published experiment used apo-MiaB while this experiment used holo MiaB (18). As discussed, the state of the cluster may affect binding affinities which could explain the discrepancy. When *E. coli* MiaB was screened against *E. coli* NfuA using the bacterial two hybrid method, no evidence of binding was observed. This experiment was performed with each protein with a domain of the adenylate cyclase protein fused to the N-terminus. Therefore, the experiment should be repeated with the domain moved to the C-terminus to rule out the possibility that the fusion location is disrupting binding. Lastly, assays testing the activity of *E. coli* MiaB revealed very poor activity, consistent with what was previously reported. This activity was further diminished in the presence of NfuA. Indeed, more experiments will need to be performed in order to conclusively determine any connection between NfuA and MiaB.

References

1. Paul, V. D., Mühlenhoff, U., Stümpfig, M., Seebacher, J., Kugler, K. G., Renicke, C., Taxis, C., Gavin, A.-C., Pierik, A. J., and Lill, R. (2015) The deca-GX3 proteins Yae1-Lto1 function as adaptors recruiting the ABC protein Rli1 for iron-sulfur cluster insertion. *eLife* **4**, e08231-e08231
2. Maio, N., Singh, A., Uhrigshardt, H., Saxena, N., Tong, W. H., and Rouault, T. A. (2014) Cochaperone binding to LYR motifs confers specificity of iron sulfur cluster delivery. *Cell metabolism* **19**, 445-457
3. McCarthy, E. L., and Booker, S. J. (2017) Destruction and reformation of an iron-sulfur cluster during catalysis by lipoyl synthase. *Science (New York, N.Y.)* **358**, 373-377
4. McCarthy, E. L., Rankin, A. N., Dill, Z. R., and Booker, S. J. (2019) The A-type domain in Escherichia coli NfuA is required for regenerating the auxiliary [4Fe-4S] cluster in Escherichia coli lipoyl synthase. *The Journal of biological chemistry* **294**, 1609-1617
5. Cicchillo, R. M., Iwig, D. F., Jones, A. D., Nesbitt, N. M., Baleanu-Gogonea, C., Souder, M. G., Tu, L., and Booker, S. J. (2004) Lipoyl synthase requires two equivalents of S-adenosyl-L-methionine to synthesize one equivalent of lipoic acid. *Biochemistry* **43**, 6378-6386
6. Cicchillo, R. M., Lee, K. H., Baleanu-Gogonea, C., Nesbitt, N. M., Krebs, C., and Booker, S. J. (2004) Escherichia coli lipoyl synthase binds two distinct [4Fe-4S] clusters per polypeptide. *Biochemistry* **43**, 11770-11781
7. Landgraf, B. J., Arcinas, A. J., Lee, K.-H., and Booker, S. J. (2013) Identification of an Intermediate Methyl Carrier in the Radical S-Adenosylmethionine Methylthiotransferases RimO and MiaB. *Journal of the American Chemical Society* **135**, 15404-15416
8. McCarthy, E. L., and Booker, S. J. (2018) Biochemical Approaches for Understanding Iron-Sulfur Cluster Regeneration in Escherichia coli Lipoyl Synthase During Catalysis. *Methods in enzymology* **606**, 217-239
9. Beinert, H. (1978) Micro methods for the quantitative determination of iron and copper in biological material. *Methods in enzymology* **54**, 435-445
10. Zhang, B., Arcinas, A. J., Radle, M. I., Silakov, A., Booker, S. J., and Krebs, C. (2020) First Step in Catalysis of the Radical S-Adenosylmethionine Methylthiotransferase MiaB Yields an Intermediate with a [3Fe-4S]0-Like Auxiliary Cluster. *Journal of the American Chemical Society* **142**, 1911-1924
11. Olson, M. G., Goldammer, M., Gauliard, E., Ladant, D., and Ouellette, S. P. (2018) A Bacterial Adenylate Cyclase-Based Two-Hybrid System Compatible with Gateway((R)) Cloning. *Methods in molecular biology (Clifton, N.J.)* **1794**, 75-96
12. Roy, A., Kucukural, A., and Zhang, Y. (2010) I-TASSER: a unified platform for automated protein structure and function prediction. *Nat Protoc* **5**, 725-738
13. Yang, J., Yan, R., Roy, A., Xu, D., Poisson, J., and Zhang, Y. (2015) The I-TASSER Suite: protein structure and function prediction. *Nature methods* **12**, 7-8
14. Yang, J., and Zhang, Y. (2015) I-TASSER server: new development for protein structure and function predictions. *Nucleic acids research* **43**, W174-W181
15. Py, B., Gerez, C., Angelini, S., Planel, R., Vinella, D., Loiseau, L., Talla, E., Brochier-Armanet, C., Garcia Serres, R., Latour, J. M., Ollagnier-de Choudens, S., Fontecave, M.,

and Barras, F. (2012) Molecular organization, biochemical function, cellular role and evolution of NfuA, an atypical Fe-S carrier. *Molecular microbiology* **86**, 155-171
16. Pierrel, F., Bjork, G. R., Fontecave, M., and Atta, M. (2002) Enzymatic modification of tRNAs: MiaB is an iron-sulfur protein. *The Journal of biological chemistry* **277**, 13367-13370
17. Pierrel, F., Douki, T., Fontecave, M., and Atta, M. (2004) MiaB protein is a bifunctional radical-S-adenosylmethionine enzyme involved in thiolation and methylation of tRNA. *The Journal of biological chemistry* **279**, 47555-47563
18. Boutigny, S., Saini, A., Baidoo, E. E., Yeung, N., Keasling, J. D., and Butland, G. (2013) Physical and functional interactions of a monothiol glutaredoxin and an iron sulfur cluster carrier protein with the sulfur-donating radical S-adenosyl-L-methionine enzyme MiaB. *The Journal of biological chemistry* **288**, 14200-14211
19. Reyda, M. R., Dippold, R., Dotson, M. E., and Jarrett, J. T. (2008) Loss of iron-sulfur clusters from biotin synthase as a result of catalysis promotes unfolding and degradation. *Archives of biochemistry and biophysics* **471**, 32-41
1. Paul, V. D., Mühlenhoff, U., Stümpfig, M., Seebacher, J., Kugler, K. G., Renicke, C., Taxis, C., Gavin, A.-C., Pierik, A. J., and Lill, R. (2015) The deca-GX3 proteins Yae1-Lto1 function as adaptors recruiting the ABC protein Rli1 for iron-sulfur cluster insertion. *eLife* **4**, e08231-e08231
2. Maio, N., Singh, A., Uhrigshardt, H., Saxena, N., Tong, W. H., and Rouault, T. A. (2014) Cochaperone binding to LYR motifs confers specificity of iron sulfur cluster delivery. *Cell metabolism* **19**, 445-457
3. McCarthy, E. L., and Booker, S. J. (2017) Destruction and reformation of an iron-sulfur cluster during catalysis by lipoyl synthase. *Science (New York, N.Y.)* **358**, 373-377
4. McCarthy, E. L., Rankin, A. N., Dill, Z. R., and Booker, S. J. (2019) The A-type domain in Escherichia coli NfuA is required for regenerating the auxiliary [4Fe-4S] cluster in Escherichia coli lipoyl synthase. *The Journal of biological chemistry* **294**, 1609-1617
5. Cicchillo, R. M., Iwig, D. F., Jones, A. D., Nesbitt, N. M., Baleanu-Gogonea, C., Souder, M. G., Tu, L., and Booker, S. J. (2004) Lipoyl synthase requires two equivalents of S-adenosyl-L-methionine to synthesize one equivalent of lipoic acid. *Biochemistry* **43**, 6378-6386
6. Cicchillo, R. M., Lee, K. H., Baleanu-Gogonea, C., Nesbitt, N. M., Krebs, C., and Booker, S. J. (2004) Escherichia coli lipoyl synthase binds two distinct [4Fe-4S] clusters per polypeptide. *Biochemistry* **43**, 11770-11781
7. Landgraf, B. J., Arcinas, A. J., Lee, K.-H., and Booker, S. J. (2013) Identification of an Intermediate Methyl Carrier in the Radical S-Adenosylmethionine Methylthiotransferases RimO and MiaB. *Journal of the American Chemical Society* **135**, 15404-15416
8. McCarthy, E. L., and Booker, S. J. (2018) Biochemical Approaches for Understanding Iron-Sulfur Cluster Regeneration in Escherichia coli Lipoyl Synthase During Catalysis. *Methods in enzymology* **606**, 217-239
9. Beinert, H. (1978) Micro methods for the quantitative determination of iron and copper in biological material. *Methods in enzymology* **54**, 435-445
10. Zhang, B., Arcinas, A. J., Radle, M. I., Silakov, A., Booker, S. J., and Krebs, C. (2020) First Step in Catalysis of the Radical S-Adenosylmethionine Methylthiotransferase MiaB Yields an Intermediate with a [3Fe-4S]0-Like Auxiliary Cluster. *Journal of the American Chemical Society* **142**, 1911-1924
11. Olson, M. G., Goldammer, M., Gauliard, E., Ladant, D., and Ouellette, S. P. (2018) A Bacterial Adenylate Cyclase-Based Two-Hybrid System Compatible with Gateway((R)) Cloning. *Methods in molecular biology (Clifton, N.J.)* **1794**, 75-96

12. Roy, A., Kucukural, A., and Zhang, Y. (2010) I-TASSER: a unified platform for automated protein structure and function prediction. *Nat Protoc* **5**, 725-738
13. Yang, J., Yan, R., Roy, A., Xu, D., Poisson, J., and Zhang, Y. (2015) The I-TASSER Suite: protein structure and function prediction. *Nature methods* **12**, 7-8
14. Yang, J., and Zhang, Y. (2015) I-TASSER server: new development for protein structure and function predictions. *Nucleic acids research* **43**, W174-W181
15. Py, B., Gerez, C., Angelini, S., Planel, R., Vinella, D., Loiseau, L., Talla, E., Brochier-Armanet, C., Garcia Serres, R., Latour, J. M., Ollagnier-de Choudens, S., Fontecave, M., and Barras, F. (2012) Molecular organization, biochemical function, cellular role and evolution of NfuA, an atypical Fe-S carrier. *Molecular microbiology* **86**, 155-171
16. Pierrel, F., Bjork, G. R., Fontecave, M., and Atta, M. (2002) Enzymatic modification of tRNAs: MiaB is an iron-sulfur protein. *The Journal of biological chemistry* **277**, 13367-13370
17. Pierrel, F., Douki, T., Fontecave, M., and Atta, M. (2004) MiaB protein is a bifunctional radical-S-adenosylmethionine enzyme involved in thiolation and methylation of tRNA. *The Journal of biological chemistry* **279**, 47555-47563
18. Boutigny, S., Saini, A., Baidoo, E. E., Yeung, N., Keasling, J. D., and Butland, G. (2013) Physical and functional interactions of a monothiol glutaredoxin and an iron sulfur cluster carrier protein with the sulfur-donating radical S-adenosyl-L-methionine enzyme MiaB. *The Journal of biological chemistry* **288**, 14200-14211
19. Reyda, M. R., Dippold, R., Dotson, M. E., and Jarrett, J. T. (2008) Loss of iron-sulfur clusters from biotin synthase as a result of catalysis promotes unfolding and degradation. *Archives of biochemistry and biophysics* **471**, 32-41

Chapter 6

Deciphering the role of A-type proteins in lipoyl synthase catalysis

Abstract

Radical SAM enzymes (RS) catalyze some of Nature's most difficult chemical transformations. To accomplish this, most RS enzymes coordinate a [4Fe-4S] cluster, which in its one electron reduced state, can reductively cleave a molecule of *S*-adenosyl-L-methionine to form a potent oxidant: 5′-dA•. Some RS enzymes, such as LipA, coordinate a second auxiliary cluster which further diversifies the chemistry they can perform. It has been extensively shown that LipA destroys its auxiliary cluster to use as a sulfur source in the biosynthesis of lipoic acid. Recently, we have shown that *E. coli* NfuA is the factor responsible for its regeneration. In this work, we address a recently proposed hypothesis that suggests that NfuA does not participate in regenerating the cluster, but rather stabilizes a different A-type protein ErpA which is the sole protein responsible for the maturation process. Herein, we have provided evidence that NfuA, and not ErpA, forms a tight complex with LipA both *in vitro* and *in vivo.* We have also provided evidence that ErpA does not catalytically affect LipA activity, and also is inhibitory when in the presence of NfuA. This observed inhibition is likely due to the observed tight complex formation between NfuA and ErpA *in vivo.* In this chapter, we also characterize LipA from *S. aureus*, an organism with profound significance in human health and seek to understand the regeneration mechanism in this pathogenic

organism. To accomplish this, we isolated and characterized an nfu-like protein from *S. aureus*, as well as an A-type protein SufA, and SufT, a factor with unknown function that has shown to be essential in cells experiencing high lipoic acid demand.

Introduction

Lipoyl synthase (LipA) is a radical SAM enzyme that cannibalizes its auxiliary iron-sulfur cluster during its reaction mechanism to supply the requisite sulfur for the biosynthesis of lipoic acid. A consequence of this reaction is that is limited to one turnover without the regeneration of its auxiliary cluster. Recently, we have provided robust evidence that *E. coli* NfuA, an intermediate iron-sulfur cluster carrier, targets *E. coli* LipA and regenerates its cluster (1). Shortly after this work was published, a group reported a new hypothesis that *E. coli* NfuA does not directly target metalloproteins that require maturation, but rather, its main function is to stabilize an alternate iron-sulfur cluster protein, *E. coli* ErpA, which is the sole protein in the cell responsible for iron-sulfur cluster maturation (2). *E. coli* ErpA is another intermediate iron-sulfur cluster carrier protein that coordinates both [2Fe-2S] clusters (~50%) and [4Fe-4S] clusters (~15-25%) (3). In cells, it is an essential protein due to its vital role in the maturation of metalloproteins utilized in respiratory metabolism. In *E. coli,* ErpA is one of three so-called A-type proteins, along with SufA and IscA, which all contain three characteristic cysteinyl residues which are hypothesized to play a role in iron binding or iron-sulfur cluster coordination. Interestingly, *E. coli* NfuA is comprised of two distinct domains, including a ‘degenerate’ N-terminal A-type domain containing only two of the A-type cysteinyl residues. This degenerate domain has been shown to be essential for tight complex formation between *E. coli* NfuA and *E. coli* LipA, and for efficient restoration of *E. coli* LipA activity *in vitro* (4). In this chapter, we sought to explore the proposed hypothesis that *E. coli* ErpA is stabilized by *E. coli* NfuA and that ErpA, not NfuA, is the sole protein responsible for targeting and maturating apo-proteins in the cell. To this end, we used a combination of molecular sieve

chromatography, bacterial two hybrid analysis, and activity assays to demonstrate that, though *E. coli* NfuA and *E. coli* ErpA do interestingly form a tight complex, all evidence suggests that *E. coli* NfuA is the ultimate protein that regenerates *E. coli* LipA. The cellular role of the complex formation between *E. coli* NfuA and *E. coli* ErpA is currently unknown, though it has been suggested that *E. coli* NfuA protects *E. coli* ErpA's cluster cofactor from oxidative damage (2).

While trying to decipher the role of this A-type protein in catalysis, it was observed that some organisms, such as the pathogenic bacteria *Staphylococcus aureus (S. aureus)*, contained nfu-like proteins that were missing the A-type domain found in *E. coli* NfuA. The pathogenic *S. aureus* bacteria is a leading cause of mortality worldwide, and one of the leading causes of infection in a hospital setting. The acquisition of iron and metal utilization is essential for *S. aureus* to colonize hosts and for disease progression (5). As such, the characterization of iron-cluster regeneration in LipA from *S. aureus* was explored because of its profound implications in human health and disease, and to gain insight into the cellular role of the A-type domain and A-type proteins. *S. aureus* LipA was successfully isolated for the first time and shown to be active *in vitro.* However, the nfu-like protein, which lacks the A-type domain, was unable to efficiently restore LipA activity, though 1-2 additional turnovers were observed. A genetic fusion of the *E. coli* NfuA N terminal domain to the *S. aureus* Nfu protein restored full activation of *S. aureus* LipA. Several hypotheses for the absence of catalytic activity of *S. aureus* LipA in the presence of *S. aureus* Nfu were proposed and tested. A newly discovered protein composed of a DUF59 domain, SufT, was found to be involved in the maturation of iron-sulfur cluster containing proteins under conditions with high iron-sulfur cluster cofactor demand in *S. aureus* (6). Intriguingly, SufT was found to be an essential iron-sulfur cluster assembly factor in cells experiencing a high demand for lipoic acid (7). The convincing *in vivo* evidence described that connected this factor to lipoic acid biosynthesis provided immense hope that this was the missing piece in lipoic acid biosynthesis in *S. aureus.*

Unfortunately, despite much effort presented in this chapter, no role for SufT in lipoic acid biosynthesis has been assigned *in vitro.*

Upon analysis of the genome neighborhood of *S. aureus* Nfu, it was realized that Nfu lies in an operon with other components of the suf operon, unlike *E. coli* NfuA which does not lie in any apparent operon. When analyzing the genes surrounding *S. aureus* Nfu, another A-type protein *S. aureus* SufA was found closely downstream. As a result, this protein was analyzed to determine what effect, if any, it plays in the biosynthesis of lipoic acid.

Materials and Methods

General methods and procedures— The polymerase chain reaction was conducted using a BioRad S1000 thermocycle. DNA sequencing was performed at the Penn State Genomics Core Facility. Amino acid analysis was performed at the UC Davis Proteomics Core Facility. UV-visible spectra were recorded on a Cary 50 spectrometer from Varian (Walnut Creek, CA) with the associated WinUV software package. All anaerobic experiments were conducted in a Coy anaerobic chamber (Grass Lakes, MI). Ultra Performance Liquid Chromatography (UPLC) with detection by mass spectrometry (UPLC-MS) was conducted using an Agilent Technologies (Santa Clara, CA) 1290 Infinity II system coupled to an Agilent Technologies 6470 QQQ mass spectrometer or Agilent Technologies (Santa Clara, CA) 1200 system coupled to an Agilent Technologies 6410 QQQ mass spectrometer. Data collection and analysis were performed using the associated MassHunter software. Analytical molecular sieve chromatography was performed on an *Ä*KTA system (GE Healthcare) housed in a Coy anaerobic chamber equipped with a HiPrep 16/60 Sephacryl HR S-200 column (GE Healthcare). Sodium dodecyl sulfate-polyacrylamide gel electrophoresis (SDS-PAGE) was performed using a mini vertical electrophoresis unit from Hoefer (Holliston, MA).

Cloning of genes encoding E. coli LipA, E. coli NfuA, E. coli ErpA, S. aureus LipA, S. aureus SufT, S. aureus Nfu, S. aureus SufA, E. coli NfuA N term- S. aureus Nfu Fusion, S. aureus SufT-S. aureus Nfu pCOLADUET, and S. aureus SufA-S. aureus Nfu pCOLADUET— The gene constructs used in this study for *E. coli* LipA, *E. coli* NfuA, *S. aureus* Nfu, and *E. coli* NfuA N term- *S. aureus* Nfu Fusion have previously been described (1,4,8). The gene encoding ErpA was amplified from *E. coli* genomic DNA (K12 W3110) using the polymerase chain reaction with the following primers: Forward 5′—CGC GGC GTC GGTCTC G AGGT ATG AGT GAT GAC GTA GCA CTG CC—3′ and Reverse 5′—CGC GGC GTC GGTCTC CTCGAG TTA GAT ACT AAA GGA AGA ACC GC—3′. The amplified DNA was digested with BsaI-HF restriction enzyme, while the pSUMO construct was digested with BsaI-HF and XhoI restrictions enzymes. The resulting digested DNA was gel-purified, ligated, and DH5α competent cells were transformed with the mixture. The codon-optimized genes encoding *S. aureus* LipA, *S. aureus* SufT, and *S. aureus* SufA were purchased from GeneArt (ThermoFisher) and supplied in a pMA-T background vector with NdeI and XhoI cut sites. In order to subclone the supplied genes into their destination vector, the pMA-T-gene constructs as well as pET28a vector DNA were digested with NdeI and XhoI restriction enzymes, gel-purified, ligated, and DH5α competent cells were transformed with the mixture. The *S. aureus* SufT-*S. aureus* Nfu pCOLA-DUET co-expression construct was created by first digesting *S. aureus* Nfu-pET28a plasmid DNA and empty pCOLA-DUET vector with NdeI and XhoI restriction enzymes. Following ligation, DH5α competent cells were transformed with the mixture. DNA was isolated from the resulting colonies and confirmed by DNA sequencing. *S. aureus* SufT-pET28a plasmid DNA was used as a template in a polymerase chain reaction with the following primers: Forward 5′—CGC GGC GTC GGA TCC A ATG GTG ATT GAT CCG GAA C—3′ and Reverse 5′— CGC GGC GTC AAG CTT TTA GCT AAC ACC CAG TGC—3′. The amplified DNA and the *S. aureus* Nfu-pCOLA-DUET DNA were digested with BamHI and HindIII restriction enzymes and ligated together using standard procedures. Following ligation, DH5α

competent cells were transformed with the mixture. In order to make the *S. aureus* SufA-*S. aureus* Nfu pCOLA-DUET co-expression construct, the gene encoding *S. aureus* SufA was amplified from the *sufA*-pET28a template DNA using the polymerase chain reaction with the following primers: Forward: 5′—CGCGGCGTCGGATCCAATGCCGACCGTTATTCTGAC—3′ and Reverse 5′—CGCGGCGTC AAG CTTTTAGCAATTTTCCGGATTAC—3′. The amplified DNA and the *S. aureus* Nfu-pCOLA-DUET plasmid DNA were digested with BamHI and HindIII restriction enzymes and ligated together. DH5α competent cells were transformed with the mixture. In all cases, the final construct was verified at the Penn State Genomics Core Facility (University Park, PA).

Cloning of bacterial two hybrid constructs—The construction of *E. coli nfuA*-pUT18C, *E. coli lipA*-pST25, *E. coli nfuA*-pST25, *zip*-pUT18C, *zip*-pST25, *gcvH*-pUT18C, and *gstB*-pST25 were described in Chapter 3. Genes encoding *E. coli* ErpA, *S. aureus* LipA, *S. aureus* SufA, and *S. aureus* Nfu were PCR amplified to introduce flanking attB sites using previously cloned *E. coli erpA*-pSUMO, *S. aureus lipA*-pET28a, *S. aureus sufA*-pET28a, and *S. aureus nfu*-pET28a plasmid DNA as a template. The following primers were used for amplification: Forward (*E. coli erpA*-pSUMO) 5′—GCC GCA CAA GTT TGT ACA AAA AAG CAG GCT TTA TGA GTG ATG ACG TAG CAC TG—3′ and Reverse (*E. coli erpA*-pSUMO) 5′—GCG GAC CAC TTT GTA CAA GAA AGC TGG GTT TTA GAT ACT AAA GGA AGA ACC—3′, Forward (*S. aureus lipA*-pET28a) 5′—GCC GCA CAA GTT TGT ACA AAA AAG CAG GCT TT ATG GCC ACC AAA AAC GAA G—3′ and Reverse (*S. aureus lipA*-pET28a) 5′—GCG GAC CAC TTT GTA CAA GAA AGC TGG GTT TTAGCTATTCAGCTGTGC—3′, Forward (*S. aureus nfu*-pET28a) 5′—GCC GCA CAA GTT TGT ACA AAA AAG CAG GCT TT ATG CCG ACC GAA GAT ACC—3′ and Reverse (*S. aureus nfu*-pET28a) 5′—GCG GAC CAC TTT GTA CAA GAA AGC TGG GTT TTA AAA CAC CTG TTC AAC—3′, Forward (*S. aureus sufA*-pET28a) 5′—GCC GCA CAA GTT

TGT ACA AAA AAG CAG GCT TT ATG CCG ACC GTT ATT CTG AC—3′ and Reverse (*S. aureus sufA*-pET28a) 5′—GCG GAC CAC TTT GTA CAA GAA AGC TGG GTT TTA GCA ATT TTC CGG ATT AC—3′. Following gel purification, the attB-flanked DNA (150 ng) was mixed with pDONR221 DNA (150 ng) and BP clonase enzyme mix to initiate BP recombination and incubated at 4 °C overnight. The following day, the reaction was quenched by the addition of proteinase K, and DH5α cells were transformed with the DNA mixture, and the desired constructs were confirmed by DNA sequencing. The entry construct (150 ng) was mixed with the bacterial two hybrid vectors (pUT18C-DEST or pST25-DEST, 150 ng) and LR clonase enzyme mix was added to initiate LR recombination, and the reaction proceeded for 2 hr at room temperature and arrested by the addition of proteinase K. DH5α cells were transformed with the DNA mixture, and the desired constructs were confirmed by DNA sequencing.

Overproduction of E. coli LipA, E. coli NfuA, E. coli ErpA, S. aureus LipA, S. aureus SufT, S. aureus Nfu, S. aureus SufA, E. coli NfuA N term- S. aureus Nfu Fusion, S. aureus SufT-S. aureus Nfu pCOLADUET, and S. aureus SufA-S. aureus Nfu pCOLADUET— The overproduction of *E. coli* LipA, *E. coli* NfuA, *S. aureus* Nfu, and *E. coli* NfuA N term- *S. aureus* Nfu Fusion was previously described (1,4,8). *E. coli* ErpA, *S. aureus* LipA, *S. aureus* SufA, *S. aureus* SufT from co-expression with *S. aureus* Nfu, and *S. aureus* SufA from co-expression with *S. aureus* Nfu were overproduced using a similar procedure. BL21(DE3) cells were co-transformed with the construct encoding the desired gene and plasmid pDB1282, which encodes the genes in the *isc* operon from *Azotobacter vinelandii* (8). A single colony was used to inoculate 200 mL lysogeny broth (LB) supplemented with 50 µg/mL kanamycin and 100 µg/mL ampicillin, and the starter culture was incubated overnight at 37 °C with shaking at 250 rpm. The following day, M9 minimal media (4-6L flasks containing 4 L media) pre-equilibrated to 37 °C was inoculated with 20 mL of starter culture, and was incubated at 37 °C with shaking at 180 rpm. At OD_{600}=0.3, expression of genes

on pDB1282 was induced by addition of arabinose (0.2% final concentration). At an OD_{600}=0.6, 50 µM $FeCl_3$ was added to the cultures, and the flasks were placed in an ice-water bath for ~30 min. Once chilled, expression of the desired gene was induced by the addition of IPTG (200 µM final concentration) and allowed to proceed for ~18 h at 18 °C with shaking at 180 rpm. Overproduction of *S. aureus* SufT was overproduced with significant differences. BL21(DE3) cells were transformed with the *S. aureus* sufT-pET28a construct. single colony was used to inoculate 200 mL lysogeny broth (LB) supplemented with 50 µg/mL kanamycin, and the starter culture was incubated overnight at 37 °C with shaking at 250 rpm. The following day, LB media (4- 6L flasks containing 4 L media) pre-equilibrated to 37 °C was inoculated with 20 mL of starter culture, and was incubated at 37 °C with shaking at 180 rpm. At an OD_{600}=0.6, the flasks were placed in an ice-water bath for ~30 min. Once chilled, expression of the desired gene was induced by the addition of IPTG (200 µM final concentration) and allowed to proceed for ~18 h at 18 °C with shaking at 180 rpm. In all cases, bacterial cells were harvested by centrifugation at 7,500 × g for 12 min. The resulting cell pellet was flash-frozen in liquid N_2 and stored in liquid N_2 until further use.

Isolation of E. coli LipA, E. coli NfuA, E. coli ErpA, S. aureus LipA, S. aureus SufT, S. aureus Nfu, S. aureus SufA, E. coli NfuA N term- S. aureus Nfu Fusion, S. aureus SufT-S. aureus Nfu pCOLADUET, and S. aureus SufA-S. aureus Nfu pCOLADUET— The isolation of *E. coli* LipA, *E. coli* NfuA, *S. aureus* Nfu, and *E. coli* NfuA N term- *S. aureus* Nfu Fusion was previously described (1,4,8). Isolation of *S. aureus* LipA, *S. aureus* SufA, *S. aureus* SufT from co-expression with *S. aureus* Nfu, and *S. aureus* SufA from co-expression with *S. aureus* Nfu was performed in an identical procedure with no modifications. *S. aureus* SufT was isolated in an exact procedure with one modification. Following isolation using affinity chromatography, the SufT protein was further purified by size-exclusion chromatography performed on an *Ä*KTA system (GE Healthcare) housed in a Coy anaerobic chamber equipped with a HiPrep 16/60 Sephacryl HR S-200 column

(GE Healthcare) equilibrated in storage buffer (50 mM HEPES, pH 7.5, 300 mM KCl, 1 mM DTT, and 15% glycerol) with a flow-rate of 0.5 mL/min. *E. coli* ErpA was isolated in the exact procedure with the exception of a second purification step in which the SUMO tag was cleaved. Briefly, after isolation, the SUMO protease, ULP1, was added and the protein was incubated on ice overnight to generate native ErpA. The following day, the protein was re-applied to the Ni-NTA column and washed with Cleavage Wash Buffer (100 mM HEPES, pH 7.5, 500 mM KCl, 40 mM Imidazole, 20% glycerol, and 10 mM BME). The flow-through containing native ErpA was collected, concentrated, and buffer exchanged into Storage Buffer (100 mM HEPES, pH 7.5, 300 mM KCl, 20% glycerol, and 1 mM DTT.

Chemical Reconstitution of S. aureus LipA and S. aureus SufA—.

S. aureus LipA and *S. aureus* SufA were chemically reconstituted with reductant, iron, and sodium sulfide to improve cofactor incorporation. A reaction containing 100 µM as-isolated LipA was slowly stirred on ice. DTT (5 mM final concentration) was added in three increments every 20 min., and the solution was incubated for 1 h. Following reduction, $FeCl_3$ (400 µM final concentration) was added in five increments every 5 min., and the solution was incubated for 30 min. The sodium sulfide was added in five increments every 30 min (400 µM final concentration), and the reaction was incubated on ice overnight. The following day, protein precipitation was removed by centrifugation at 45,000 × g for 10 min and concentrated to ~2 mL. Aggregates and non-specifically bound substances were removed by applying the reaction to a HiPrep 16/60 Sephacryl HR S-200 column (GE Healthcare) equilibrated in storage buffer (flow-rate of 0.5 mL/min). S. aureus SufA was chemically reconstituted via the same general method, with the exception that a final protein concentration of 300 µM was used as well as a 1 mM final concentration of $FeCl_3$ and sodium sulfide.

Analytical molecular sieve chromatography—Physical interactions between *E. coli* NfuA and *E. coli* MiaB, as well as *E. coli* NfuA, *E. coli* ErpA, and *E. coli* LipA, were probed by analytical molecular sieve chromatography. The monomeric state of *S. aureus* LipA was also determined using this method. A 500 µL mixture of standards composed of cytochrome c, carbonic anhydrase, bovine serum album, alcohol dehydrogenase, β-amylase, and blue dextran was applied to a HiPrep 16/60 Sephacryl HR S-200 column (GE Healthcare) connected to an *Ä*KTA FPLC system housed within an anaerobic chamber (<1 ppm O_2). The column was equilibrated in 50 mM HEPES, pH 7.5, 300 mM KCl, 15% glycerol, and 5 mM DTT (freshly prepared immediately before use) at a constant flow-rate of 0.5 mL/min before applying and eluting protein samples. The log molecular weight (MW) of each standard was plotted against its elution volume after correcting for the void volume of the column. The linear equation was then used to estimate the MW of each sample. The samples included the following in a total 500 µL volume: 100 µM *S. aureus* LipA only, 100 µM *E. coli* NfuA only, 100 µM *E. coli* MiaB only, a mixture of 100 µM *E. coli* NfuA + 100 µM *E. coli* MiaB, 100 µM *E. coli* ErpA only, 100 µM *E. coli* LipA only, a mixture of 100 µM *E. coli* ErpA + 100 µM *E. coli* LipA, a mixture of 100 µM *E. coli* ErpA + 100 µM *E. coli* NfuA, and a mixture of 100 µM *E. coli* ErpA + 100 µM *E. coli* NfuA + 100 µM *E. coli* LipA. The interaction was determined by the presence of a shift in the elution volume of samples as well as by the calculated experimental weights for each of the peaks. Fractions corresponding to each peak were subjected to SDS-PAGE to determine the presence of each protein, except in cases where the protein standards co-elute with possible complex formation.

Bacterial two hybrid analysis—Adenylate cyclase deficient cells BTH101 were co-transformed with the following pairs of plasmids: *E. coli nfuA*-pUT18C + *E. coli lipA*-pST25, *zip*-pUT18C + *zip*-pST25 (positive control), and *gcvH*-pUT18C + *gstB*-pST25 (negative control), *E. coli nfuA*-pST25 + *E. coli erpA*-pUT18C, *E. coli erpA*-pUT18C + *E. coli lipA*-pST25, *S. aureus nfu*-pUT18C

+ *S. aureus lipA*-pST25, *S. aureus sufA*-pUT18C + *S. aureus lipA*-pST25, and *S. aureus sufA*-pUT18C + *S. aureus nfu*- pST25. The co-transformed cells were plated on LB agar plates containing 40 μg/μL galactosidase and 0.5 mM IPTG with the respective selective antibiotics (100 μg/μL spectinomycin or 50 μg/μL kanamycin and 100 μg/μL ampicillin). The plates were incubated at 30 °C for 48 hr, and observed for the presence of a blue color indicative of a positive interaction.

LC-MS activity determinations— Ultra Performance Liquid Chromatography (UPLC) with detection by mass spectrometry (UPLC-MS) was conducted using an Agilent Technologies (Santa Clara, CA) 1290 Infinity II system coupled to an Agilent Technologies 6470 QQQ mass spectrometer or Agilent Technologies (Santa Clara, CA) 1200 system coupled to an Agilent Technologies 6410 QQQ mass spectrometer. Data collection and analysis were performed using the associated MassHunter software. Detection of substrates and products was performed using electrospray ionization mass spectrometry in positive mode (ESI^+-MS) with the following parameters: a nitrogen gas temperature of 350 °C and flow rate of 59.0 L/min, a nebulizer pressure of 45 PSI and a capillary voltage of 4000 V. Substrates and products were detected using multiple reaction monitoring **(Table 6-1).** The reaction mixture was separated on an Agilent Technologies Zorbax Eclipse Plus-C18 Rapid Resolution HD column (2.1 mm × 50 mm, 1.8 μm particle size) equilibrated in 98% Solvent A (0.1% formic acid, pH 2.6) and 2% Solvent B (100% acetonitrile). A gradient of 25-27% solvent B was applied from 0.5 min to 2.0 min, before returning to solvent B to 8% from 2 min to 2.5 min. A flow-rate of 0.3 mL/min was maintained throughout the method. The column was allowed to re-equilibrate for 1 min under the initial conditions between sample injections. Reactions testing the effect of *E. coli* ErpA on *E. coli* LipA activity **(Figure 6-4)** contained 15 μM LipA, 300 μM NfuA, or 300 μM ErpA, or both, 600 μM peptide substrate (Glu-Ser-Val-[N^6-octanoyl]Lys-Ala-Ala-Ser-Asp), 0.5 μM *S*-adenosylhomocysteine (SAH) nucleosidase, and 1 mM SAM. Reactions testing the activity of *S. aureus* LipA **(Figure 6-9)**

contained 150 µM RCN Sa LipA, 300 µM peptide substrate, 0.5 µM SAH nucleosidase, and 1 mM SAM. Reactions testing the activity of *S. aureus* LipA in the presence of *S. aureus* Nfu **(Figure 6-12)** included 25 µM RCN Sa LipA, 400 µM Sa Nfu, 400 µM peptide substrate, 0.5 µM SAH nucleosidase, and 1 mM SAM. Reactions testing the effect of S. aureus SufT on S. aureus LipA activity (Figure 5-15) included 25 µM RCN Sa LipA and 350 µM Sa Nfu with or without the addition of 350 µM Sa SufT, 400 µM peptide substrate, 0.5 µM SAH nucleosidase, and 1 mM SAM. Reactions testing the effect of the *E. coli* NfuA N-terminal domain-*Sa* Nfu fusion on the activity of *E. coli* or Sa LipA **(Figure 6-17)** included 25 µM of either *E. coli* LipA or Sa LipA, 500 µM *E. coli* NfuA N-terminal domain-Sa Nfu fusion, 400 µM peptide substrate, 0.5 µM SAH nucleosidase, and 1 mM SAM. Reactions testing the activity of *S. aureus* LipA in the presence of *S. aureus* SufA and *S. aureus* Nfu **(Figure 6-23)** included 25 µM Sa LipA and when applicable, 400 µM Sa Nfu and/or 400 µM Sa SufA, 400 µM peptide substrate, 0.5 µM SAH nucleosidase, and 1 mM SAM. Reactions testing the effect of Sa SufT on the enhanced activity of Sa LipA observed when Sa SufA and Sa Nfu are present **(Figure 6-24)** contained 10 µM Sa LipA, and when applicable, 250 µM Sa Nfu, 250 µM Sa SufA, and 250 µM Sa SufT, 400 µM peptide substrate, 0.5 µM SAH nucleosidase, and 1 mM SAM. **Figure 6-25, Panel A** displays a reaction in which Sa LipA and Sa Nfu were reacted to completion (t=150 min) following the injection of Sa SufA to the reaction, whereas **Figure 6-25, Panel B** displays a reaction in which Sa LipA and Sa SufA were reacted to completion (t=150 min) following the injection of Sa Nfu to the reaction, though it is a qualitative assessment due to inaccuracies in quantification. All reactions were conducted at room temperature and were initiated by addition of sodium dithionite to a final concentration of 2 mM. The reactions were quenched at appropriate times with H_2SO_4 at a final concentration of 100 mM.

Table 6-1: Parameters for LC-MS/MS analysis of unlabeled reaction intermediate and product.

Compound	**Parent Ion**	**Fragmentator Voltage**	**Product Ion 1**	**Product Ion 2**
6-Thio-octanoyl Peptide	964.5	220	744.4 (30)	242.1 (46)
Lipoyl Peptide	996.5	208	776.3 (30)	274.1 (46)
AtsA Peptide (IS)	474.4	112	201.1 (18)	153 (26)

*Respective collision energies are in parentheses

Results

Isolation and characterization of E. coli ErpA.

E. coli ErpA was previously characterized as an A-type intermediate iron-sulfur cluster carrier protein (3). ErpA, which was found to coordinate both [2Fe-2S] and [4Fe-4S] clusters, is an essential protein due to its role in the maturation of metalloproteins in respiratory metabolism. Recently, new research suggested that NfuA does not participate in the re-insertion of iron-sulfur clusters, but rather, its role is to stabilize the iron-sulfur cluster cofactors on ErpA (2). In this hypothesis, they propose that ErpA is the sole protein in the cell responsible for targeting all apo-proteins that require an iron-sulfur cluster cofactor. We sought to decipher the role of ErpA in our recently reported mechanism of cluster regeneration in LipA by NfuA. To accomplish this, the gene encoding ErpA was cloned into a pSUMO construct, allowing for facile purification by affinity chromatography as well as a robust way to generate native protein after tag removal. *E. coli* ErpA was overproduced and isolated as described in the materials and methods. The resulting protein was >95% pure as evidenced by SDS-PAGE analysis **(Figure 6-1).** The UV-visible spectrum of the protein revealed distinct features at 330 nm, 410 nm, and 456 nm **(Figure 6-2).** The prominent feature at 330 nm as well as 456 nm indicates the protein coordinates mostly [2Fe-2S] cluster which aligns with what is reported in the literature. The additional feature at 410 nm could be the small amount of [4Fe-4S] cluster which is also observed in the previously reported Mössbauer analysis. Iron analysis of the protein corrected by amino acid analysis revealed 1.2 +/- 0.08 Fe per polypeptide, consistent with one [2Fe-2S] cluster coordinated by a protein dimer.

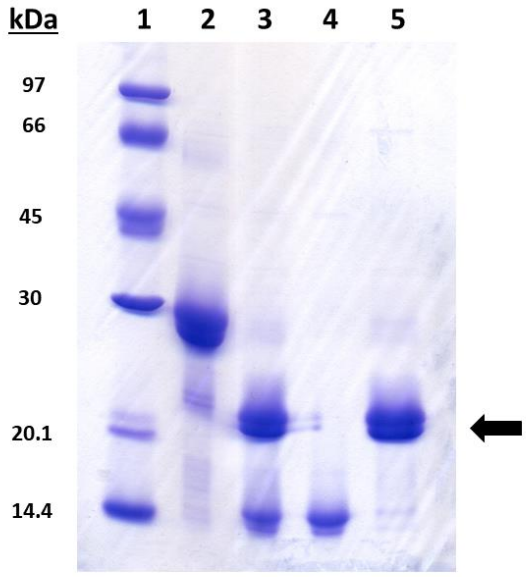

Figure 6-1: SDS-PAGE of as-isolated *E. coli* ErpA. Lanes are as follows: 1- molecular weight ladder 2- pure protein before SUMO tag removal 3-pure protein after cleavage with SUMO protease (before reapplication to Ni-NTA resin) 4- post-cleavage eluate 5- post-cleavage flow-through containing final pure protein

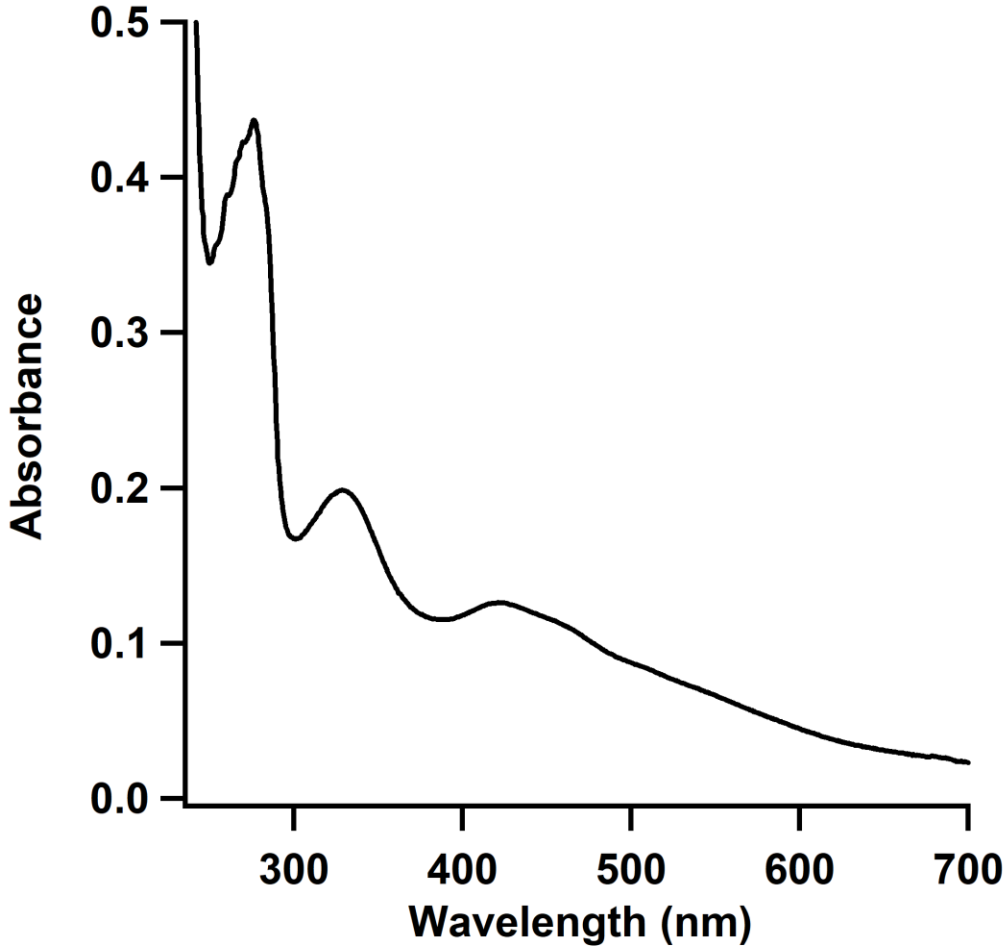

Figure 6-2: UV-visible spectrum of as-isolated *E. coli* ErpA (20 μM).

Molecular Sieve Chromatography of E. coli LipA, E.coli ErpA, and E. coli NfuA.

Upon isolation of *E. coli* ErpA, we then probed whether *E. coli* ErpA can form a complex with *E. coli* LipA using molecular sieve chromatography. As shown in **Figure 6-3, Panel A,** an ErpA only control (solid black trace) exhibits two peaks at 64.7 mL and 75.0 mL, with experimentally calculated molecular masses of 31.4 kDa and 12.4 kDa, respectively. This likely represents different oligomeric states of ErpA, as a monomer in its apo form and as a dimer

coordinating its cofactor. An *E. coli* LipA only control (black dotted trace) elutes at 60.6 mL with an experimentally calculated molecular mass of 44.3 kDa (theoretical mass, 38.2 kDa). An equimolar mixture of ErpA and LipA displays two peaks at 60.5 mL and 75.0 mL with experimentally calculated masses of 44.7 kDa and 13.1 kDa, respectively. These peaks overlay the control samples and no shift in elution volume is observed, consistent with no tight complex formation between LipA and ErpA. The interaction between *E. coli* ErpA and *E. coli* NfuA was also explored using this method **(Figure 6-3, Panel B).** The ErpA only control (black solid line) elutes at the same volume it did in the first experiment. The NfuA only control (black dotted line) elutes at 65.6 mL with an experimentally calculated molecular mass of 29.1 kDa (theoretical mass, 25.7 kDa). An equimolar mixture of ErpA and NfuA (red solid trace) results in two peaks at 64.3 mL and 74.4 mL with experimentally calculated masses of 32.5 kDa and 13.9 kDa, respectively. The theoretical size of a NfuA + ErpA complex is 37.9 kDa. A small shift in the elution volume is observed as well as an increase in protein absorbance, which is consistent with an interaction. However, the shift is very small, which is what is expected due to the small size of the ErpA protein. Unfortunately, because the potential complex elution volume overlays with where the control samples elute, this could not be confirmed by SDS-PAGE analysis. As a result, a complex between ErpA and NfuA cannot be unambiguously assigned using this method. Lastly, an experiment was performed in which complex formation between LipA, ErpA, and NfuA was investigated **(Figure 6-3, Panel C).** The ErpA only control (black solid line), the NfuA only control (dotted black line), and the LipA only control (solid red trace) elute at the same respective volumes did in the previous experiments. An equimolar mixture of LipA, NfuA, and ErpA (solid blue trace) exhibited three peaks at 55.9 mL, 31.6 mL, and 13.3 mL with experimentally calculated masses of 65.4 kDa, 31.6 kDa, and 13.3 kDa, respectively. A significant shift in the major fraction was observed and the experimentally determined size 65.4 kDa is close to the theoretical size of a 1:1 complex of LipA and NfuA. The fractions corresponding to this major peak were subjected to SDS-PAGE analysis,

and the presence of both LipA and NfuA, but not ErpA, were confirmed **(Figure 6-3, Panel D).** Together, this data indicates that ErpA does not form a complex with LipA, even when NfuA is present, though it could potentially form a complex with NfuA. If it does form a complex with NfuA, NfuA preferentially binds LipA.

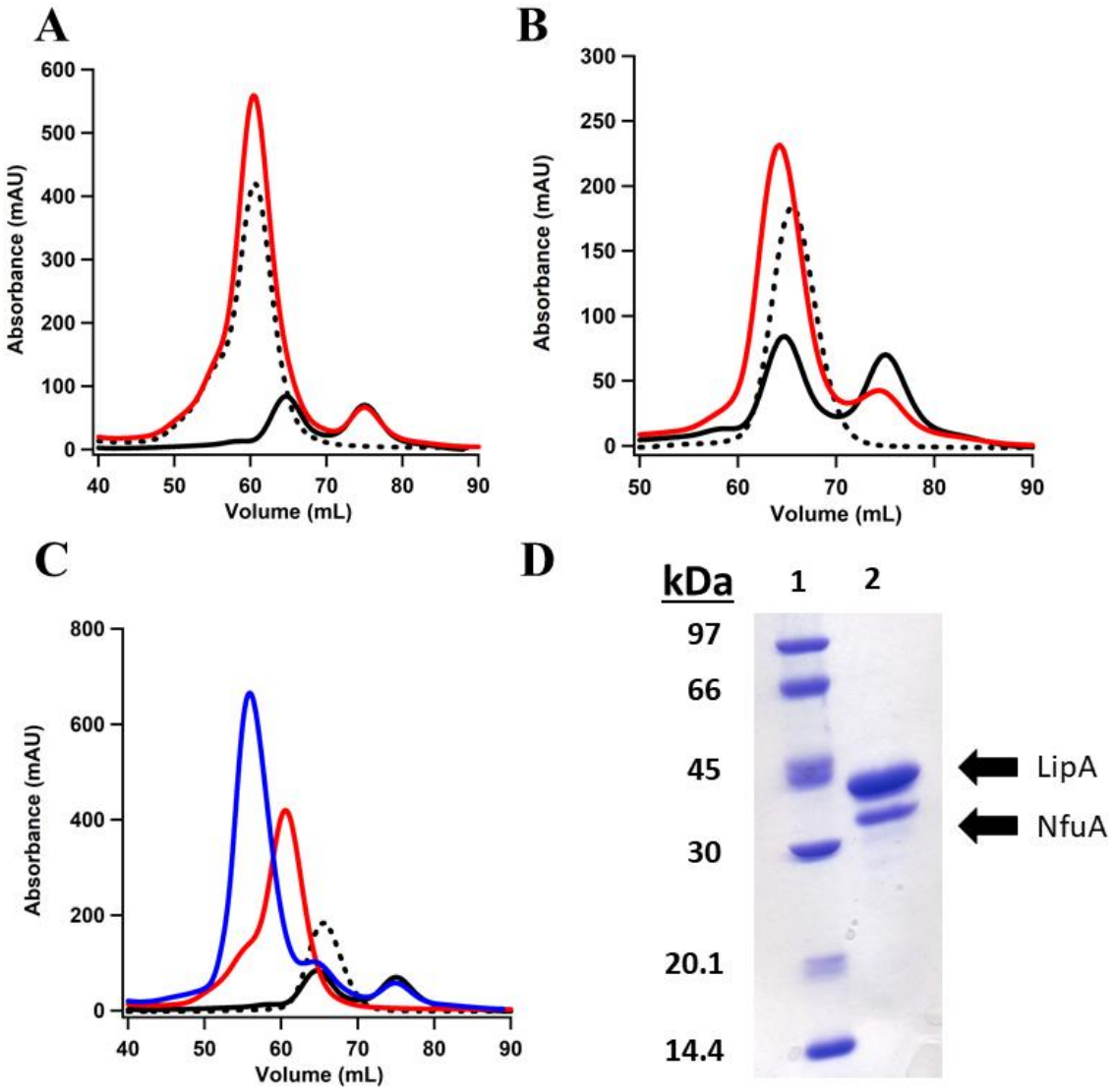

Figure 6-3: Analytical Molecular Sieve Chromatography of *E. coli* ErpA and *E. coli* LipA or *E. coli* NfuA. (A) Interaction between *E. coli* LipA and *E. coli* ErpA monitored by molecular sieve chromatography**.** Black solid line, 100 µM *E. coli* ErpA alone. ErpA displays two peaks at 64.7 mL and 75.0 mL with experimentally calculated molecular masses of 31.4 kDa and 12.4 kDa, respectively (theoretical mass of monomer, 12.2 kDa). Dotted black line, 100 µM LipA alone. LipA

elutes (60.6 mL) with an experimentally calculated molecular mass of 44.3 kDa (theoretical mass, 38.2 kDa). Red solid line, 100 µM ErpA + 100 µM LipA. Two peaks overlaying the control samples elute at 60.5 mL and 75.0 mL with experimentally calculated masses of 44.7 kDa and 13.1 kDa, respectively. (B) Interaction between *E. coli* NfuA and *E. coli* ErpA monitored by molecular sieve chromatography. Black solid line, 100 µM *E. coli* ErpA alone. Dotted black line, 100 µM NfuA alone. NfuA elutes (65.6 mL) with an experimentally calculated molecular mass of 29.1 kDa (theoretical mass, 25.7 kDa). Red solid line, 100 µM ErpA + 100 µM NfuA. Two peaks are observed at 64.3 mL and 74.4 mL with experimentally calculated masses of 32.5 kDa and 13.9 kDa, respectively. (C) Interaction between *E. coli* LipA and *E. coli* ErpA and *E. coli* NfuA monitored by molecular sieve chromatography. Black solid line, 100 µM *E. coli* ErpA alone. Dotted black line, 100 µM NfuA alone. Red solid line, 100 µM LipA alone. Blue solid line, 100 µM ErpA + 100 µM LipA + 100 µM NfuA. Three peaks elute at 55.9 mL, 31.6 mL, and 13.3 mL with experimentally calculated masses of 65.4 kDa, 31.6 kDa, and 13.3 kDa, respectively. (D) SDS-PAGE of fractions from the blue solid peak described in (C). Lanes are as follows: 1- molecular weight ladder 2- blue fraction from (C).

Bacterial two hybrid analysis of E. coli LipA, E. coli NfuA, and E. coli ErpA.

To further investigate the potential binding of ErpA to LipA or NfuA *in vivo* under physiological conditions, bacterial two hybrid screening was used. As described in Chapter 3, this system relies on the fusion of each partner protein to components of adenylate cyclase. If the proteins of interest interact, then the adenylate cyclase domains will be brought in close proximity to each other, reconstituting cyclic AMP (cAMP) production. In *E. coli*, cAMP is a regulator of gene transcription and binds to the catabolite activator protein (CAP), and then the cAMP/CAP complex can activate the transcription of catabolite genes and upregulates β-galactosidase expression. As a result, positively interacting proteins can be screened by the development of blue color in the presence of x-gal in an adenylate cyclase deficient strain of *E. coli*. The following constructs were assembled using gateway cloning technology: *gstB*-pUT18C, *gcvH*-pST25, *nfuA*-pUT18C, *nfuA*-pST25, *erpA*-pUT18C and *lipA*-pST25. Two domains of the leucine zipper zip-pUT18C and zip-pKT25 were used as positive controls. As shown in **Figure 6-5,** robust blue color can be observed in the positive control (Panel C), whereas no color is observed in the *gstB*-pUT18C + *gcvH*-pST25 negative control, as expected. As indicated in previous chapters, a robust color is

observed in the *nfuA*-pUT18C + *lipA*-pST25 plate, confirming a strong *in vivo* interaction. (Panel B) However, no color is observed on the plates with cells containing *erpA*-pUT18C + *lipA*-pST25 (Panel E), confirmed no interaction as reported from the analytical molecular sieve chromatography as well. Interestingly, the plate with cells containing *erpA*-pUT18C + *nfuA*-pST25 (Panel D) also display a tight interaction between these two proteins, a reproduced experiment from a previously reported result (2). While the complex formation between NfuA and ErpA is interesting, no evidence presented supports a possible interaction between ErpA and LipA.

Activity of E. coli LipA in the presence of E. coli ErpA.

Though no evidence of a complex between LipA and ErpA was observed in i*n vitro* or *in vivo* binding assays, the effect of ErpA on LipA activity was tested **(Figure 6-4).** In this experiment, a reaction contained 15 µM LipA with all other necessary reaction components. The control reaction (black closed circles) showed that the LipA protein was fully active. When 300 µM ErpA was added to the reaction (black closed triangles), approximately one additional equivalent of lipoyl product formation was observed. When 300 µM NfuA was included in the reaction with LipA, approximately 140 µM lipoyl product was observed (black closed squares). Interestingly, when both NfuA and ErpA were included in a reaction with LipA, only approximately 80 µM lipoyl product was observed (black open circles). This product inhibition is possibly due to ErpA binding NfuA and preventing its cluster transfer during the reaction. In any case, ErpA does not enhance the rate or the total lipoyl product formed. This evidence does not support a role for ErpA in the maturation of LipA.

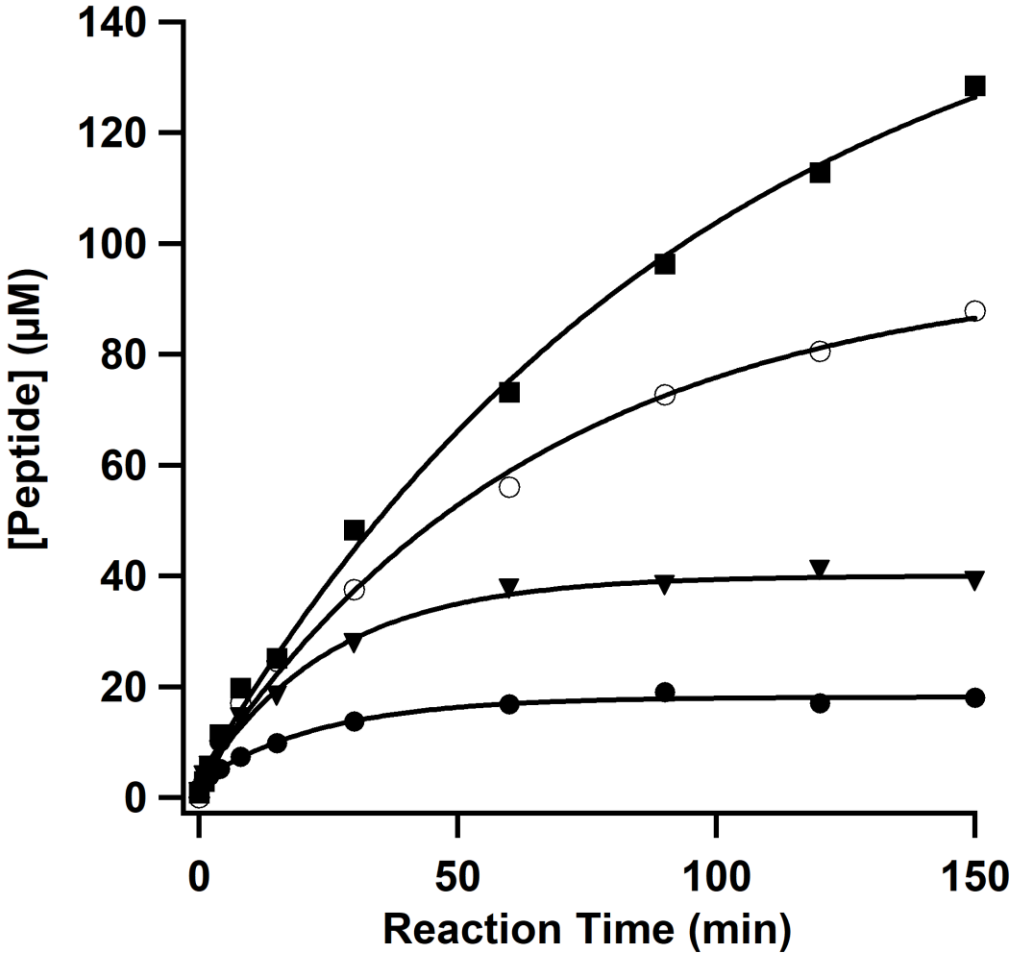

Figure 6-4: Activity determination of *E. coli* LipA in the presence of *E. coli* ErpA. Reaction included 15 μM *E. coli* LipA and either 300 μM ErpA, 300 μM NfuA, or 300 μM of both, 600 μM peptide substrate, 0.5 μM SAH nucleosidase, and 1 mM SAM in buffer (50 mM HEPES, pH 7.5, 300 mM KCl, 10% glycerol). Reactions were conducted at room temperature, and were initiated by the addition of 2 mM dithionite before quenching with a final concentration of 100 mM H_2SO_4 at various times. LipA only control (black circles). LipA + NfuA control (black squares). LipA + ErpA (black triangles). LipA + NfuA + ErpA (open circles).

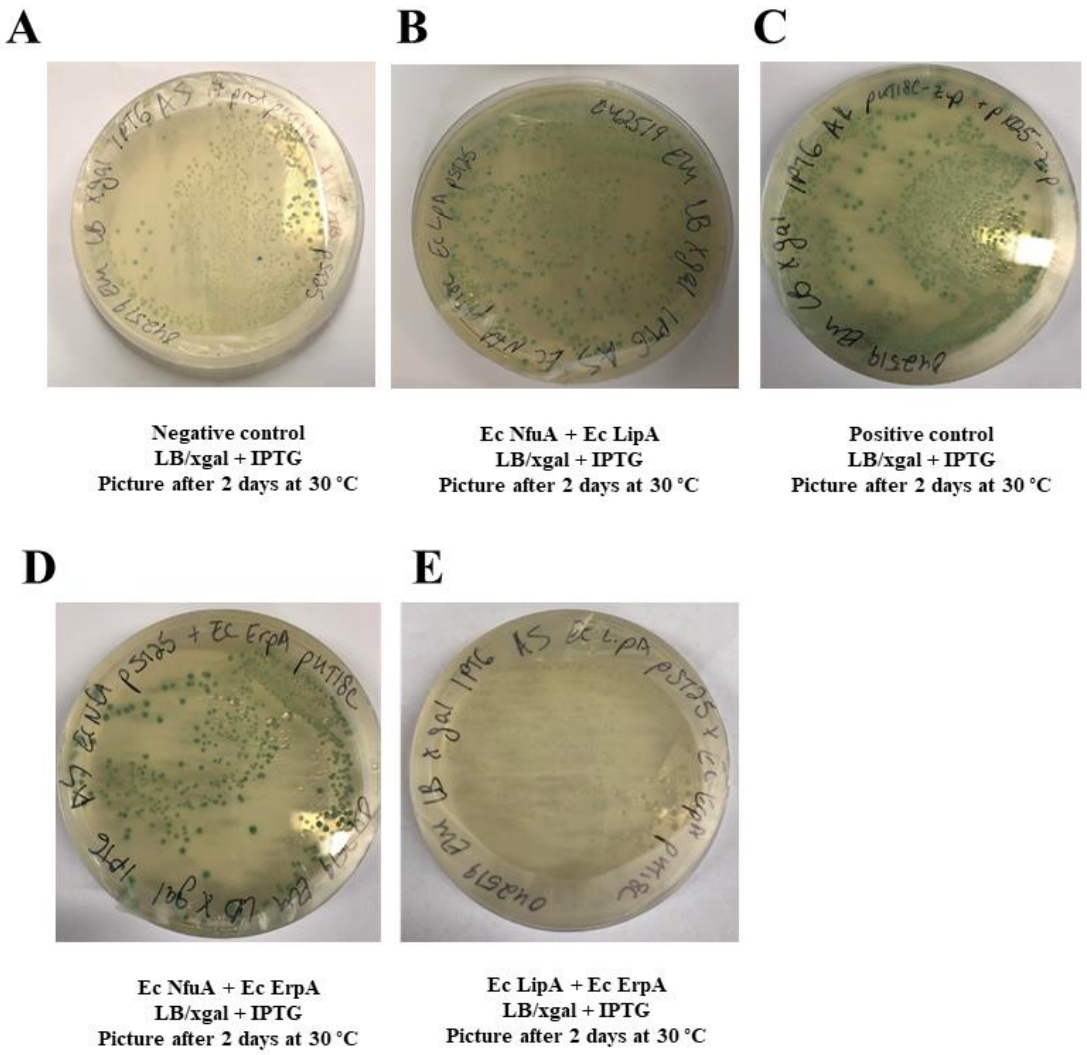

Figure 6-5: Bacterial two hybrid screening of *E. coli* NfuA, *E. coli* ErpA, and *E.coli* LipA. Adenylate cyclase deficient cells strain BTH101 were co-transformed bacterial two hybrid plasmids and spread on LB agar plates containing 40 µg/µL galactosidase and 0.5 mM IPTG with the respective selective antibiotics (100 µg/µL spectinomycin or 50 µg/µL kanamycin and 100 µg/µL ampicillin) . (A) Negative control containing two non-interacting proteins *E. coli gcvH*-pST25 and *E. coli gstB*-pUT18C. (B) *E. coli* n*fuA*-pUT18C and *E. coli lipA*-pST25. (C) Positive control containing two domains of leucine zipper: *zip*-pUT18C and *zip*-pKT25. (D) *E. coli* n*fuA*-pST25 + *E. coli erpA*-pUT18C (E) *E. coli lipA*-pST25 + *E. coli erpA*-pUT18C.

Isolation and characterization of S. aureus LipA.

Because of its medical relevance and our interest in the role of A-type domains/A-type proteins in lipoic acid biosynthesis, LipA from *Staphylococcus aureus* was cloned, overproduced, and isolated for the first time. As shown in **Figure 6-6**, *S. aureus* LipA was purified to homogeneity using affinity chromatography. An amino acid correction factor was obtained for accurate protein concentration determination which indicated that Bradford analysis overestimates the protein concentration of *S. aureus* LipA by a factor of 1.46. In its as-isolated state (without the correction factor), colorimetric iron analysis revealed 3.9 +/- 0.6 Fe per protein which is significantly lower than the theoretical of 8 Fe per protein. As a result, the LipA protein was chemically reconstituted in order to improve cofactor incorporation. After aggregates and non-specifically bound metals were removed by size exclusion chromatography, nearly full iron incorporation was achieved as judged by iron analysis with the new correction factor.

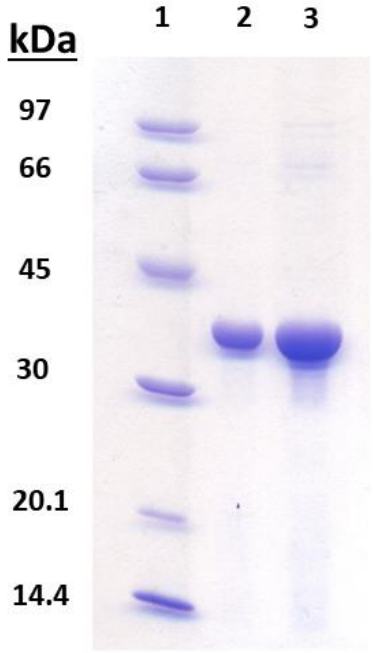

Figure 6-6: SDS-PAGE of as-isolated LipA from *Staphylococcus aureus.* Lanes are as follows: 1-molecular weight ladder 2- pure protein 3-pure protein.

The UV-visible spectrum of the final chemically reconstituted *S. aureus* LipA protein **(Figure 6-7)** shows characteristic features of [4Fe-4S] clusters which is pronounced in LipA due to the presence of two [4Fe-4S] clusters. The oligomeric state of the final *S. aureus* LipA protein was determined using analytical molecular sieve chromatography. As observed in **Figure 6-8,** a clear single peak is observed at 63.3 mL corresponding to an experimentally calculated size of 35.2 kDa (theoretical size 37.0 kDa). This result indicates that the oligomeric state of *S. aureus* LipA is entirely monomeric. A reaction testing the activity of the final *S. aureus* LipA protein was performed **(Figure 6-9)** monitoring formation and decay of the monothiolated intermediate as well as formation of the lipoyl product. When 150 µM reconstituted *S. aureus* LipA was reacted with 300 µM peptide substrate, approximately 100 µM lipoyl product is formed over 150 min.

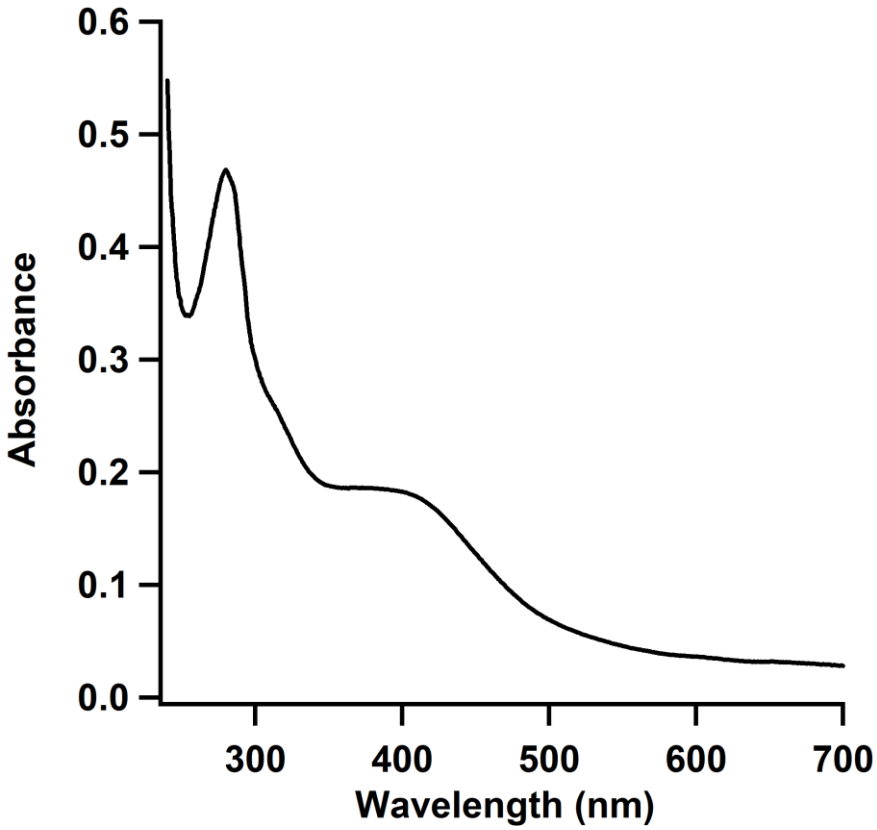

Figure 6-7: UV-visible spectrum of reconstituted LipA (6 µM) from *Staphylococcus aureus.*

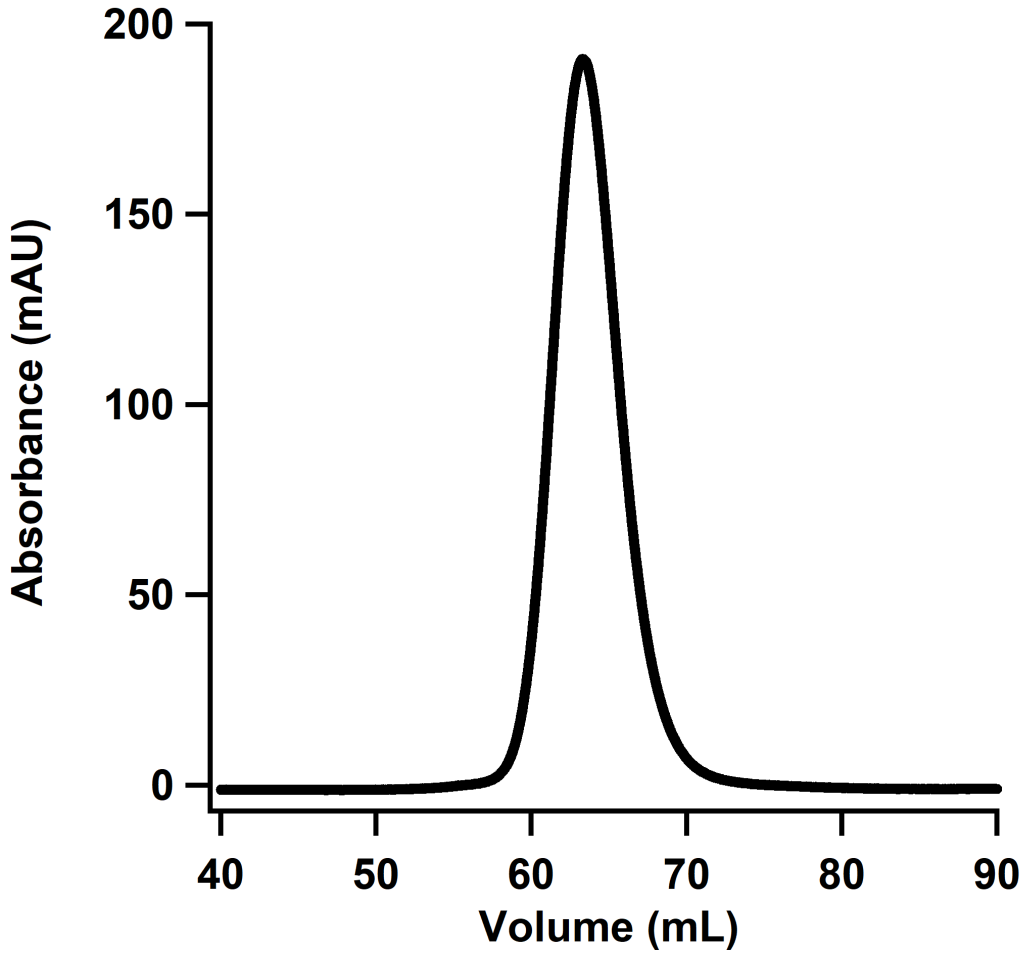

Figure 6-8: Oligomeric state of LipA from *Staphylococcus aureus.* A sample containing 100 µM LipA eluted at 63.3 mL with an experimental calculated size of 35.2 kDa (theoretical size 37.0 kDa).

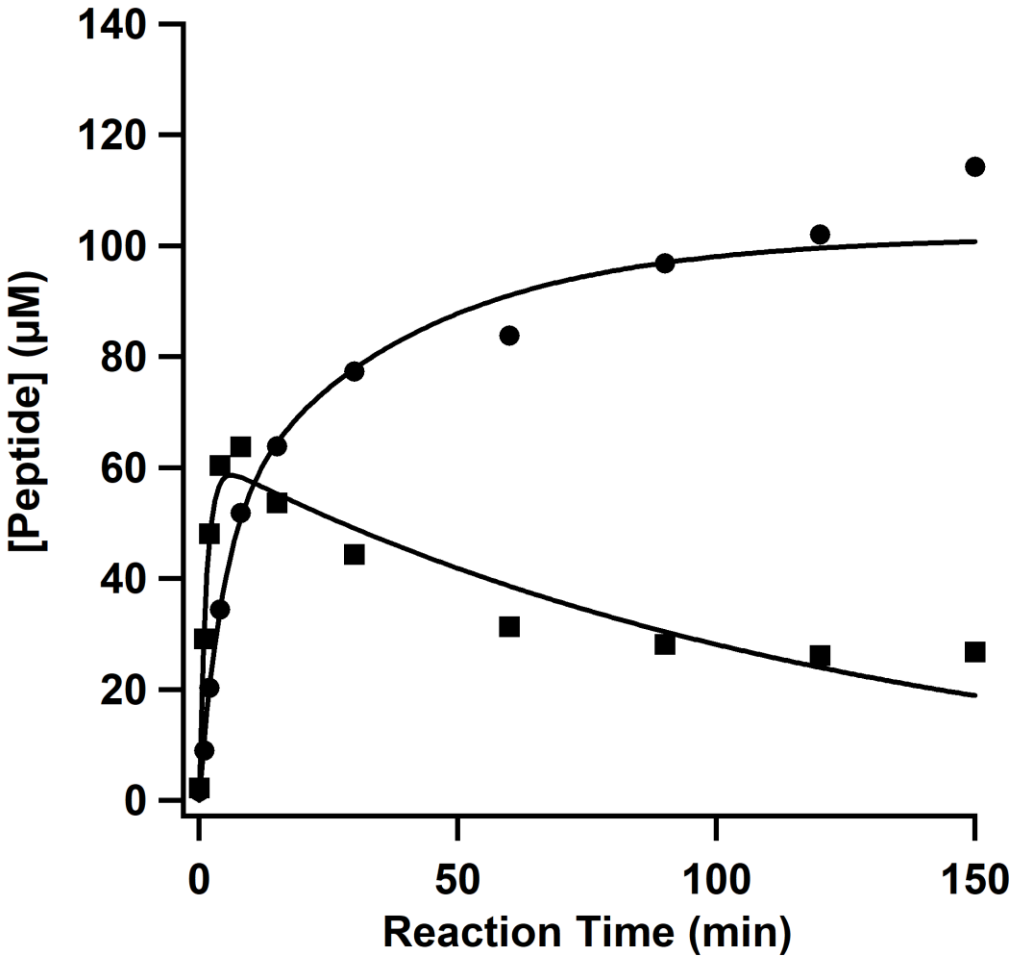

Figure 6-9: Activity of LipA from *Staphylococcus aureus.* Reaction included 150 μM RCN Sa LipA, 300 μM peptide substrate, 0.5 μM SAH nucleosidase, and 1 mM SAM in buffer (50 mM HEPES, pH 7.5, 300 mM KCl, 10% glycerol). Reactions were conducted at room temperature, and were initiated by the addition of 2 mM dithionite before quenching with a final concentration of 100 mM H_2SO_4 at various times. Intermediate formation is shown in black squares, and lipoyl product is shown in black circles.

Isolation and characterization of S. aureus Nfu.

In Chapter 3, it was shown that *S. aureus* Nfu was unable to activate *E. coli* LipA. In this section, we characterize *S. aureus* Nfu and determine its effect on the activity of *S. aureus* LipA. To this end, *S. aureus* Nfu was cloned, overproduced, and isolated. Upon purification by affinity chromatography, *S. aureus* Nfu was found to be >90% pure by SDS-PAGE analysis **(Figure 6-10).** An amino acid correction factor was obtained for S. aureus Nfu in order to accurately quantify the protein concentration. This analysis revealed that Bradford analysis overestimated the concentration of protein by a factor of 1.26. The UV-visible spectrum of the as-isolated protein **(Figure 6-11)** revealed distinct features at 320 nm and 400 nm which are indicative of a [4Fe-4S] cluster cofactor. Due to the unusual amino acid composition of *S. aureus* Nfu which lacks tryptophan and tyrosine residues, a unique UV-visible spectrum is observed which is consistent with previously published literature (9). Colorimetric iron analysis with the amino acid correction factor reveals 1.9 +/- 0.3 Fe per protein which is consistent with a [4Fe-4S] cluster coordinated at a dimer interface similarly to what is observed in *E. coli* NfuA. While it was shown in Chapter 3 that S. aureus Nfu could not efficiently activate *E. coli* LipA, its effect on the activity of *S. aureus* LipA was unknown. Therefore, assays were performed in which the activity of *S. aureus* LipA was monitored in the absence and presence of *S. aureus* Nfu **(Figure 6-12).** Reactions included 25 μM *S. aureus* LipA, 400 μM octanoyl pep, 0.5 μM SAH nucleosidase, and 1 mM SAM. A *S. aureus* LipA only control reaction (closed black circles) formed approximately 14 μM lipoyl product over 150 min. When 400 μM *S. aureus* Nfu (closed blue squares) was included in the assay, approximately 30 μM, or about one additional turnover, was observed. As previously indicated **(Figure 6-18),** the homology between *S. aureus* Nfu and *E. coli* NfuA is limited to the C-terminal domain. In Chapter 3, when a genetic fusion of the *E. coli* NfuA N-terminal domain was added to *S. aureus* Nfu, the protein fusion was able to activate *E. coli* LipA. We sought to test whether this

same *E. coli* NfuA N terminal domain- *S. aureus* Nfu fusion protein could similarly activate S. aureus LipA **(Figure 6-17).** In this reaction, assays included 25 µM of either *E. coli* LipA (red circles) or *S. aureus* LipA (black squares) in the presence of 500 µM *E. coli* NfuA N terminal domain- *S. aureus* Nfu fusion protein. Interestingly, the *E. coli* NfuA N terminal domain- *S. aureus* Nfu fusion protein was able to efficiently regenerate *S. aureus* LipA to the same extent as *E. coli* LipA.

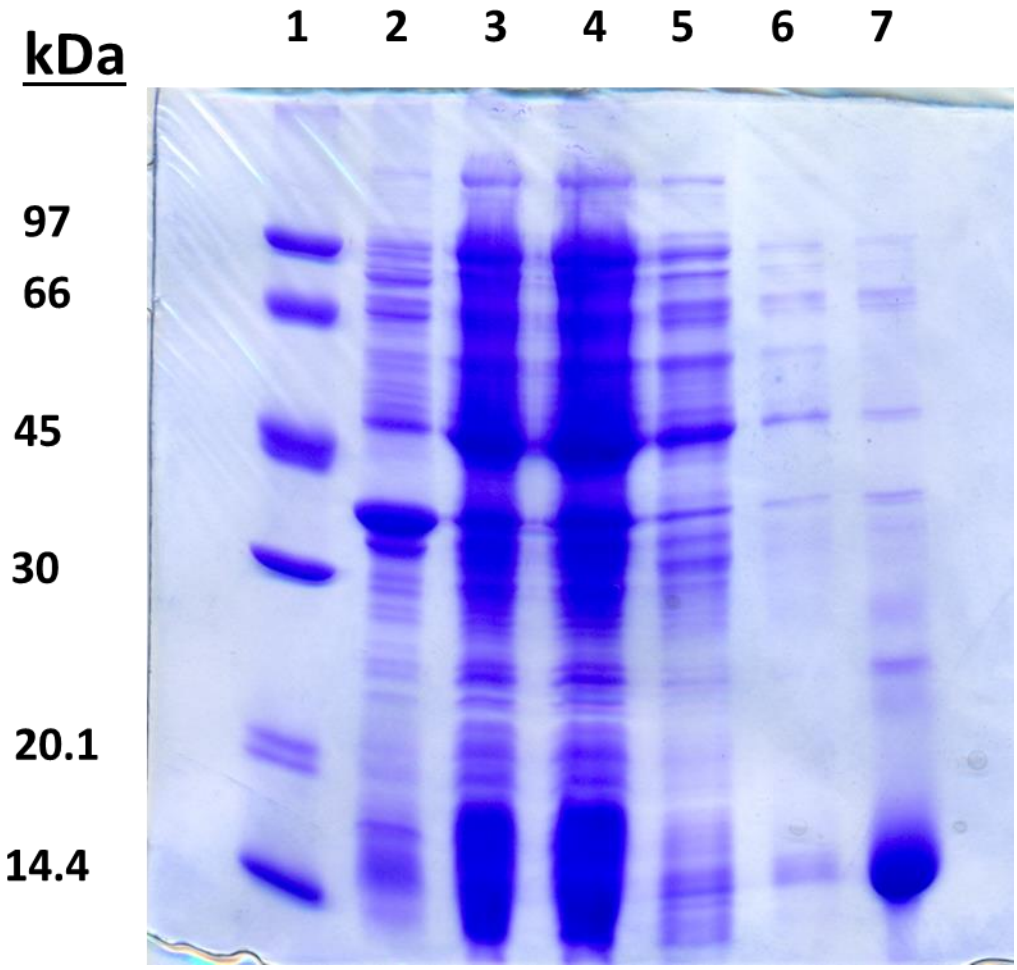

Figure 6-10: SDS-PAGE of as-isolated Nfu from *Staphylococcus aureus.* Lanes are as follows: 1- molecular weight ladder 2- pellet 3-supernatant 4- flow-through 5- wash 1 6-wash 2 7-pure protein.

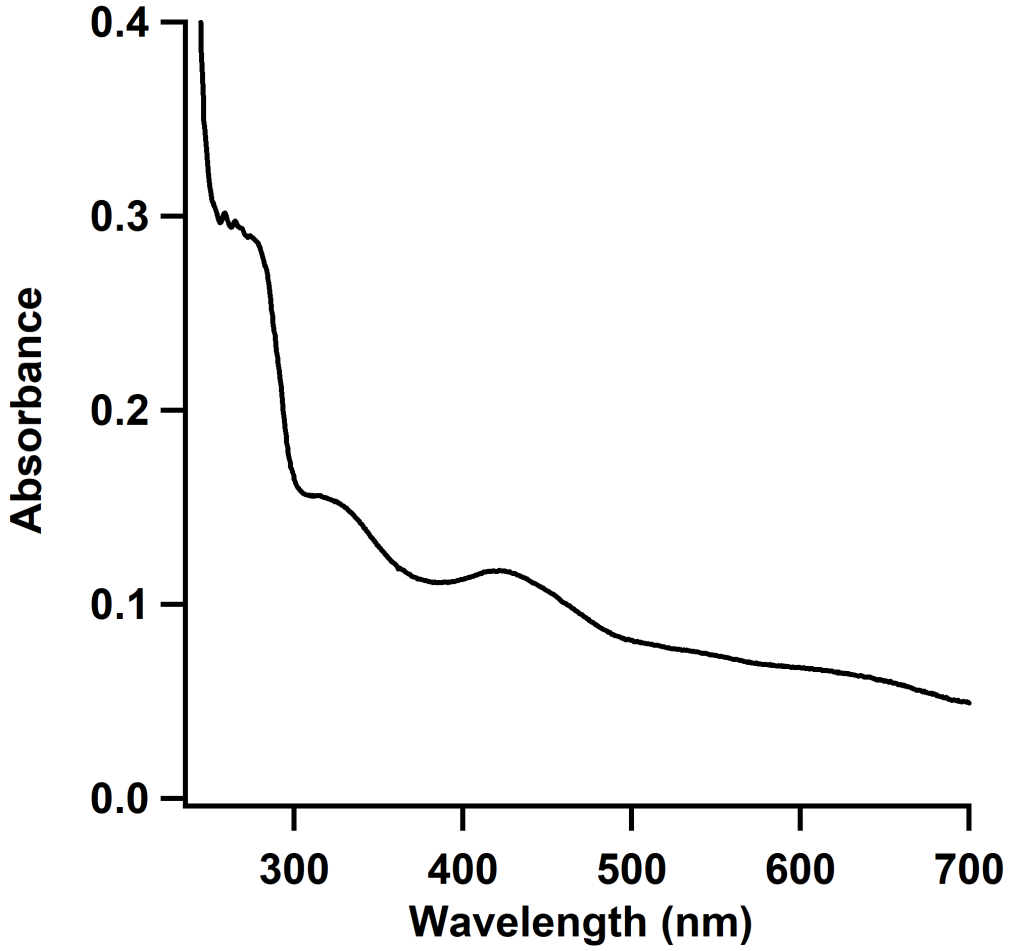

Figure 6-11: UV-visible spectrum of 15 µM as-isolated Nfu (SAUSA300_0839) from *Staphylococcus aureus*.

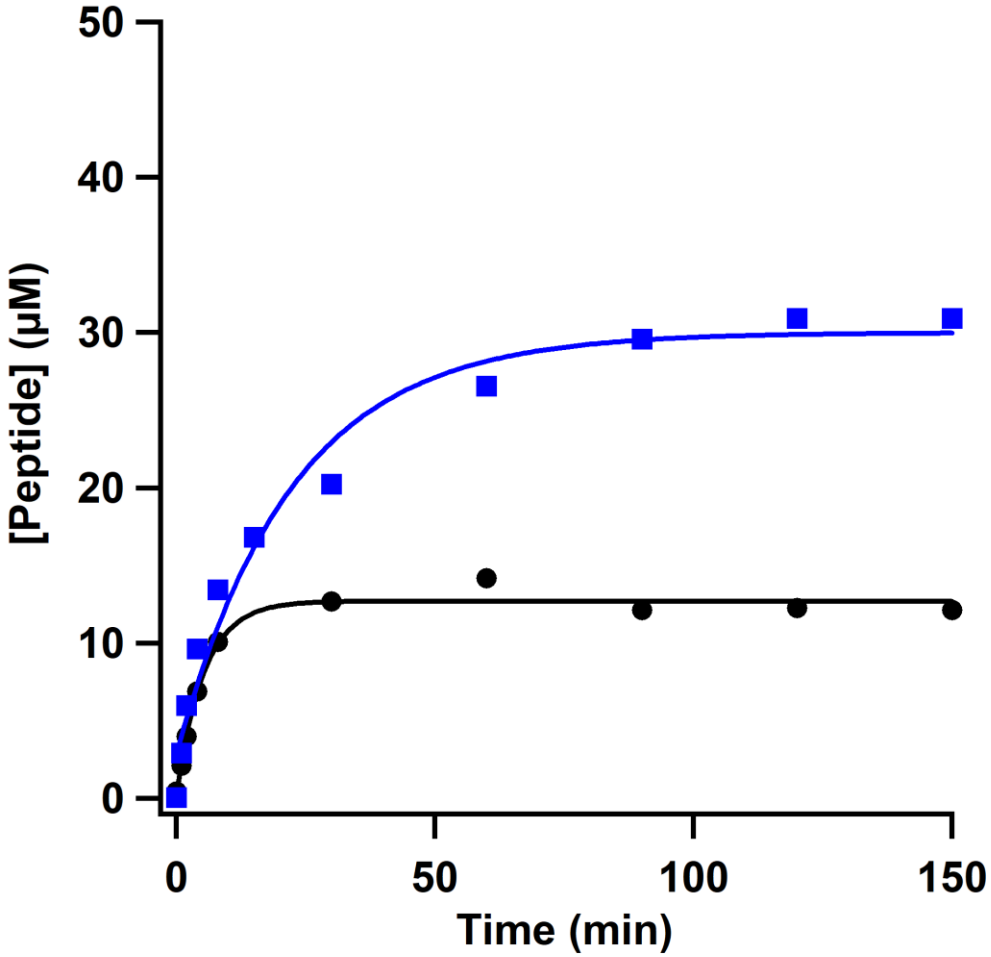

Figure 6-12: Activity of *S. aureus* LipA in the presence of *S. aureus* Nfu. Reactions included 25 μM Sa LipA, 400 μM Sa Nfu, 400 μM octanoyl pep, 0.5 μM SAH nucleosidase, and 1 mM SAM. Sa LipA only control (black circles). Sa LipA + Sa Nfu (blue squares). Reactions were conducted at room temperature, and were initiated by the addition of 2 mM dithionite before quenching with a final concentration of 100 mM H_2SO_4 at various times

Isolation and characterization of S. aureus SufT.

The absence of enhanced *S. aureus* LipA activity observed in the presence of *S. aureus* Nfu lead us to the hypothesis that a second, yet unknown, factor was involved that was essential for the cluster regeneration event. Intriguingly, a series of two papers described a novel protein factor, SufT, which was shown to be essential *in vivo* under conditions with an increased demand for lipoic acid (6,7). The *in vivo* defects described were compelling that this factor is somehow involved in lipoic acid biosynthesis. To test whether this was the missing piece to the *S. aureus* LipA regeneration, we cloned, overproduced, and isolated *S. aureus* SufT. Initial attempts to isolate *S. aureus* SufT were unsuccessful. No obvious overexpression band was observed in SDS-PAGE analysis of the cells in which SufT had been overproduced. However, when switching the culture medium from M9 minimal media to LB media, we were able to isolate protein from the cells. The protein following affinity chromatography remained very impure, requiring a second purification step by size exclusion chromatography to yield protein suitable for analysis **(Figure 6-13).** The isolated protein was colorless and did not appear to coordinate a cofactor, though it contains two cysteinyl residues, one of which is essential. The UV-visible spectrum of the purified protein **(Figure 6-14)** had no indication of cofactor coordination, and its absorbance is shifted to 260 nm due to the lack of tryptophan and tyrosine residues. Attempts to incorporate a cofactor by co-expressing the *isc* machinery or by chemical reconstitution methods were unsuccessful. Colorimetric iron analysis of the as-isolated protein indicated the absence of any quantifiable iron in the protein. Unfortunately, *S. aureus* SufT did not appear to affect the activity of S. aureus LipA in the presence of *S. aureus* Nfu **(Figure 6-15).** In this reaction, 15 µM S. aureus LipA + 350 µM *S. aureus* Nfu (closed circles) catalyzed the formation of approximately 25 µM lipoyl product. When 350 µM *S. aureus* SufT was included in the reaction, approximately 30 µM lipoyl product was observed, indicating no significant product enhancement. Further, co-expression of *S. aureus*

SufT with *S. aureus* Nfu was unable to produce a stable pure complex that might indicate synergism **(Figure 6-16).**

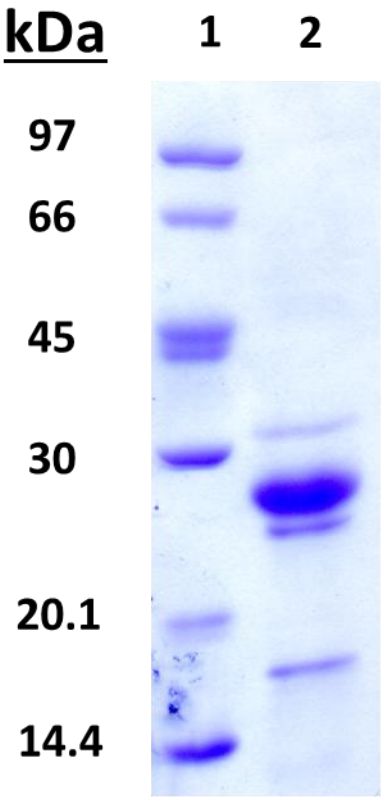

Figure 6-13: SDS-PAGE of as-isolated post-S200 SufT from *Staphylococcus aureus.* Lanes are as follows: 1- molecular weight ladder 2- pure protein

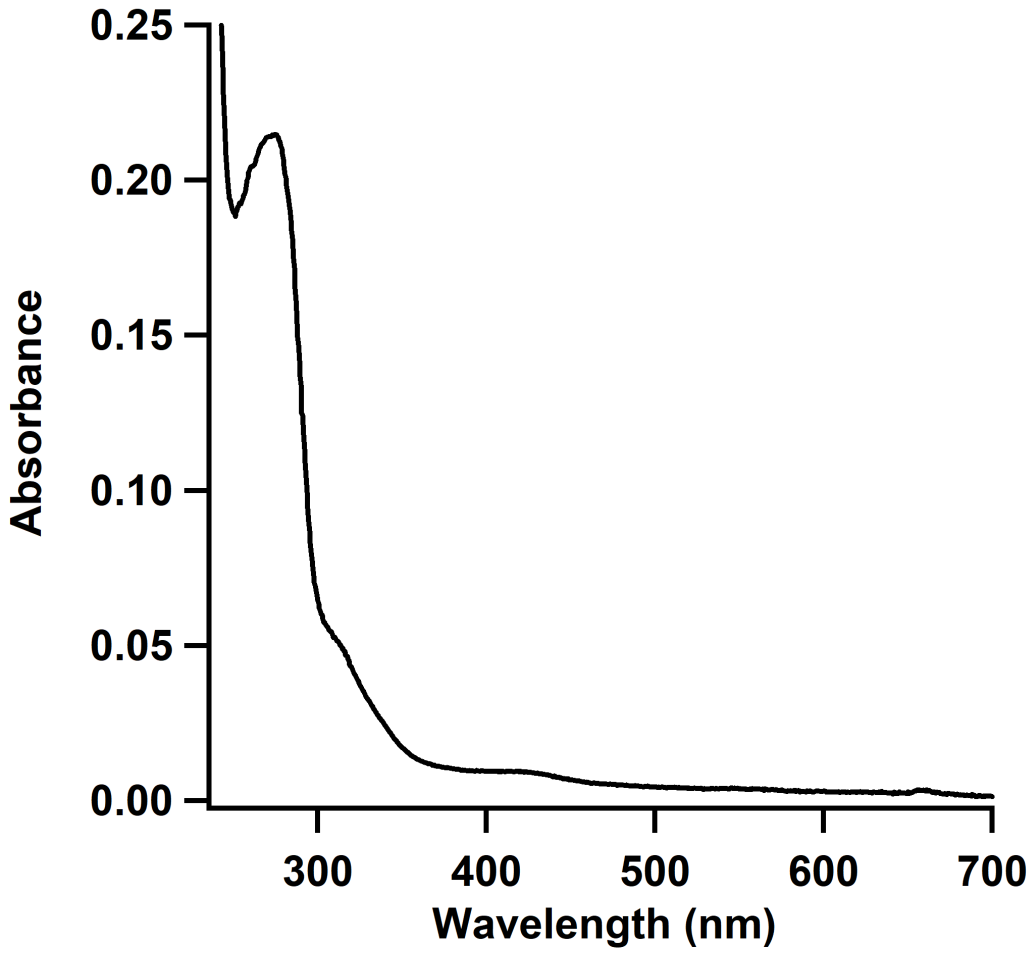

Figure 6-14: UV-visible spectrum of SufT from *Staphylococcus aureus* (SAUSA300_0875).

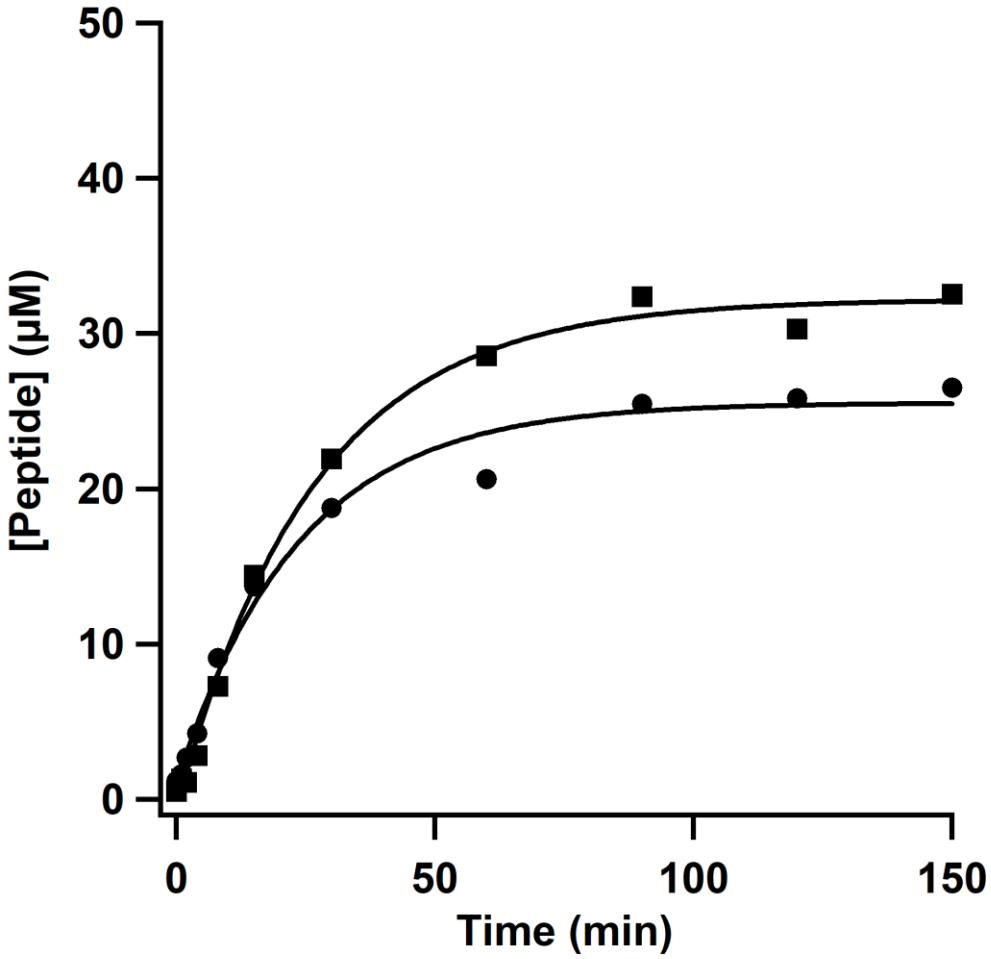

Figure 6-15: Activity of *S. aureus* LipA (open circles) in presence of *S. aureus* Nfu + *S. aureus* SufT (closed squares). Assays include: 15 µM RCN *S. aureus* LipA, 350 µM *S. aureus* Nfu and *S. aureus* SufT, 400 µM OctH substrate, 0.5 µM SAH nucleosidase, and 1 mM SAM. Buffer (50 mM HEPES, pH 7.5, 300 mM KCl, 10% glycerol). Reactions were conducted at room temperature, and were initiated by the addition of 2 mM dithionite before quenching with a final concentration of 100 mM H_2SO_4 at various times.

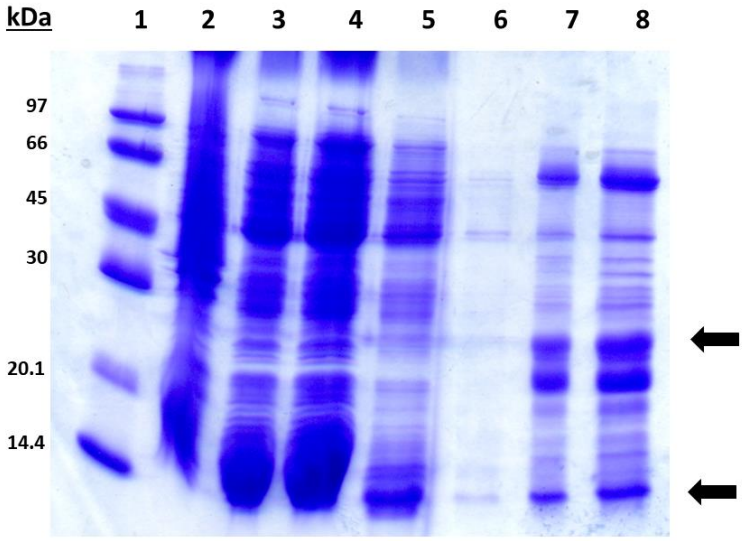

Figure 6-16: SDS-PAGE of isolation of *S. aureus* SufT and *S. aureus* Nfu from cells in which the two genes were co-expressed in LB media. Lanes are as follows: 1- molecular weight ladder 2- cellular pellet 3- supernatant 4- flowthrough 5-wash 1 6- wash 2 7- "pure" 2 µL 8- "pure" 4 µL.

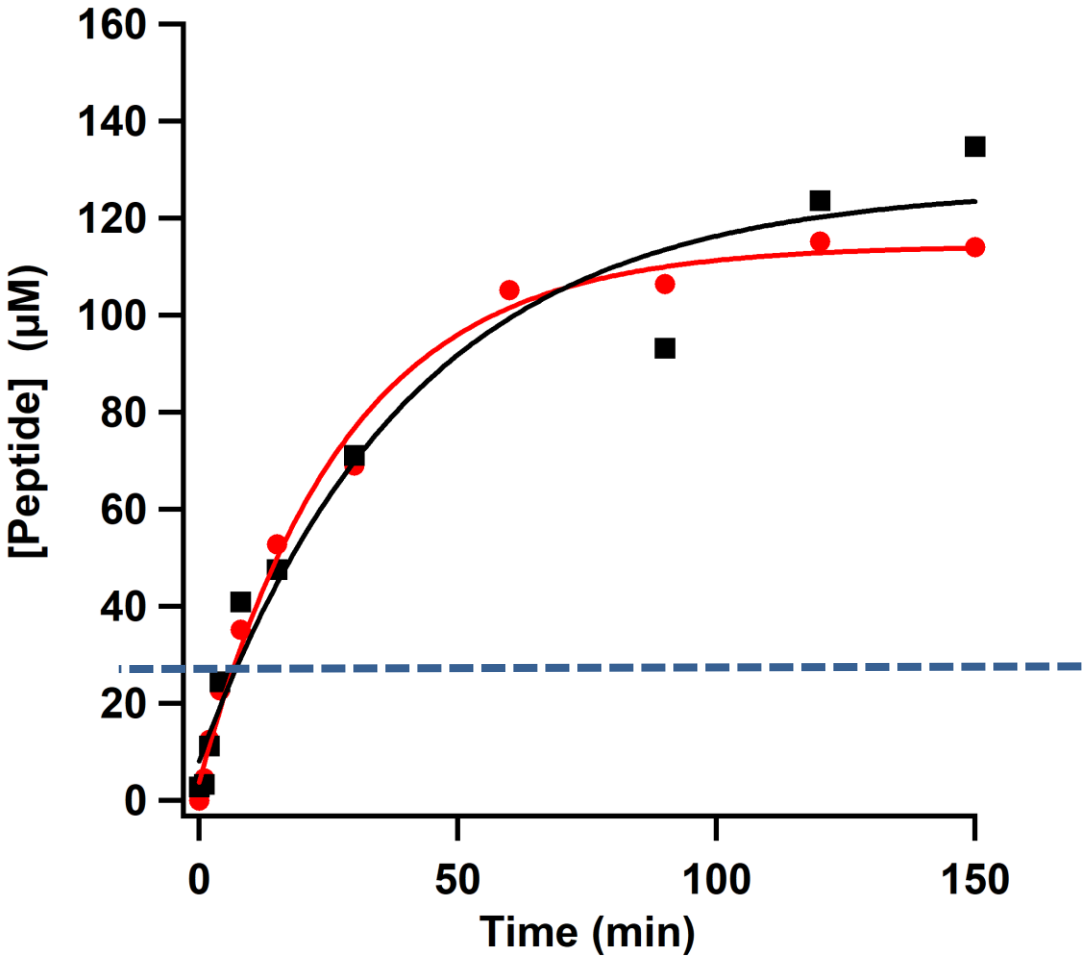

Figure 6-17: Activity of Ec LipA (red circles) or Sa LipA (black squares) in presence of Sa Nfu-Ec NfuA N terminal domain fusion. Assays included: 25 μM Ec LipA or Sa LipA, 500 μM Sa Nfu-Ec NfuA N terminal domain fusion, 400 μM OctH substrate, 0.5 μM SAH nucleosidase, and 1 mM SAM. Buffer (50 mM HEPES, pH 7.5, 300 mM KCl, 10% glycerol). Reactions were conducted at room temperature, and were initiated by the addition of 2 mM dithionite before quenching with a final concentration of 100 mM H_2SO_4 at various times.

Figure 6-18: Sequence alignment of NfuA/Nfu from *Escherichia coli (E. coli), Mycobacterium tuberculosis (M. tuberculosis)*, and *Staphylococcus aureus (S. aureus)*.

Isolation and characterization of S. aureus SufA.

The realization that *S. aureus* SufT was not the missing factor in the regeneration mechanism of *S. aureus* LipA lead to a new approach. A hypothesis reasoned that since *S. aureus* Nfu was missing the A-type domain present in *E. coli* NfuA, an additional separate A-type protein may fulfill a similar role. A BLAST search of the *E. coli* NfuA N-terminal domain against the *S. aureus* genome did not generate a suitable candidate. However, analysis of the genetic context of *S. aureus* Nfu provided some insight. In many organisms, genes with similar functions are arranged in operons. *E. coli* NfuA, however, is found randomly in the genome. *S. aureus* Nfu is found in the suf operon, the sole pathway for iron-sulfur cluster assembly in *S. aureus.* This operon also contains an additional gene that encodes SufA, an A-type protein similar to the degenerate N terminal domain of *E. coli* NfuA **(Figure 6-19).**

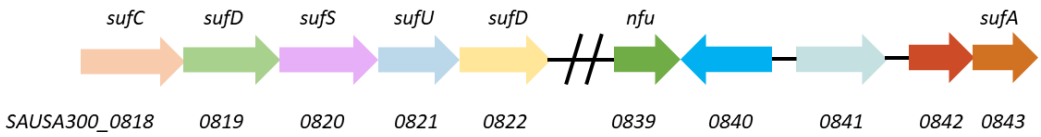

Figure 6-19: Genetic context of *S. aureus* Nfu and *S. aureus* SufA.

We explored the possibility that this A-type protein, SufA, could function together with *S. aureus* Nfu. To this end, we cloned, overproduced, and isolated *S. aureus* SufA. Although the isolation of *S. aureus* SufA was successful, the as-isolated protein was relatively impure as judged by SDS-PAGE analysis **(Figure 6-20).** The as-isolated protein was brown in color, and the UV-visible spectrum had features of a [4Fe-4S] cluster **(Figure 6-22, Panel A).** Colorimetric iron analysis revealed that the protein contained 0.6 +/- 0.03 Fe per protein, though this was without an amino correction factor using the relatively impure protein. Amino acid analysis of this protein was performed in order to obtain a more accurate determination of protein concentration. It was determined that Bradford analysis overestimated the amount of protein by a factor of 1.16. In order to improve both the protein purity and cofactor incorporation, a chemical reconstitution was performed. Following removal of aggregates and non-specifically bound metals, the protein was a distinctive new reddish color. The protein was significantly more pure as can be seen in the post-size exclusion SDS-PAGE gel **(Figure 6-21).** In addition to the increased purity and color change, colorimetric iron analysis using the amino acid correction factor revealed 0.9 Fe +/- 0.2 per protein. The UV-visible spectrum of the reconstituted protein was drastically different than the spectrum obtained from the as-isolated protein **(Figure 6-22, Panel B).** SufA has been described by contradicting characterizations in the literature indicating that it could coordinate [4Fe-4S] clusters,

or alternately, could be an iron binding protein (10,11). It is currently unclear what the identity of the cofactor within *S. aureus* SufA is and whether the UV-visible features are indicative of that cofactor or due to degradation during the size exclusion purification step.

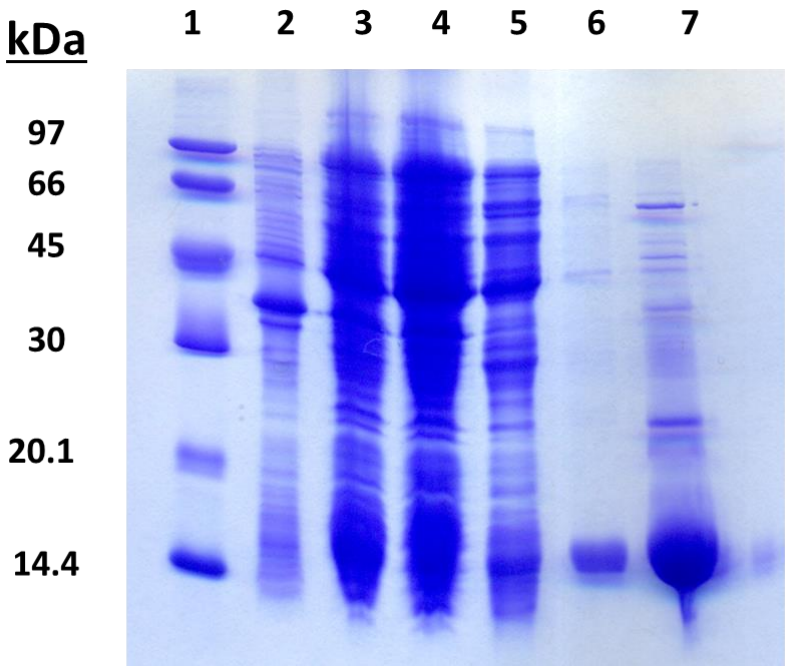

Figure 6-20: SDS-PAGE of SufA from *Staphylococcus aureus*.. Lanes are as follows: 1- molecular weight ladder 2- pellet 3- supernatant 4- flow-through 5- wash 1 6- wash 2 7- pure protein

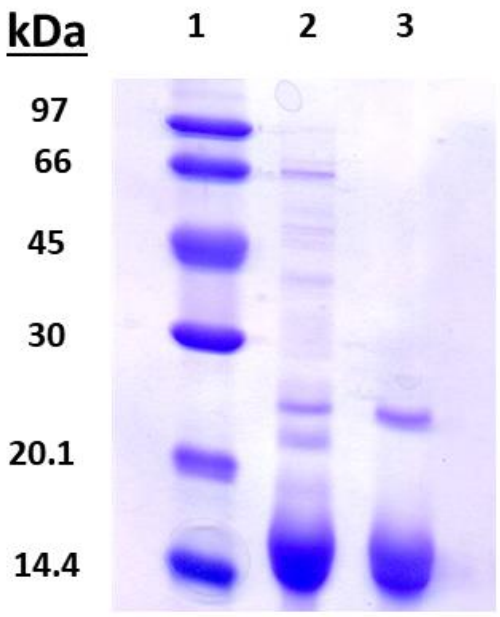

Figure 6-21: *S. aureus* SufA as-isolated versus reconstituted/S200 SDS-PAGE. Lanes are as follows: 1- molecular weight marker 2- *S. aureus* SufA as-isolated 3- *S. aureus* SufA following chemical reconstitution and size-exclusion chromatography.

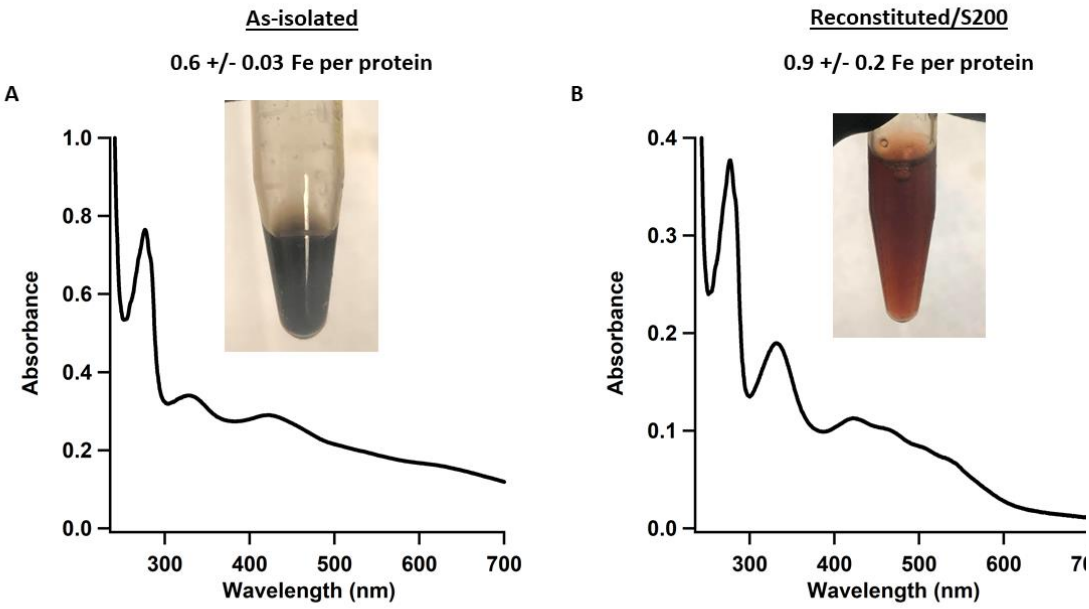

Figure 6-22: UV-visible spectrum of as-isolated versus reconstituted *S. aureus* SufA. (A) UV-visible spectrum of as-isolated *S. aureus* SufA. Pictured above is the as-isolated protein sample. (B) UV-visible spectra of the chemically reconstituted S. aureus SufA protein following size-exclusion chromatography. Pictured above is the reconstituted protein sample.

Assays were performed to assess what effect, if any, *S. aureus* SufA has on the activity of *S. aureus* LipA **(Figure 6-23).** This experiment contained 25 µM *S. aureus* LipA as well as all other required reaction components, and either 400 µM *S. aureus* SufA, 400 µM *S. aureus* Nfu, or 400 µM of both. The LipA only control (closed black circles) catalyzed the formation of approximately 12 µM lipoyl product, whereas the inclusion of 400 µM SufA (red open triangles) or Nfu (blue closed squares) resulted in approximately 30 µM lipoyl product. However, when both SufA and Nfu were present (black closed squares), approximately 65 µM lipoyl product was observed, and the product was continuing to increase at the end of the reaction (t=150 min).

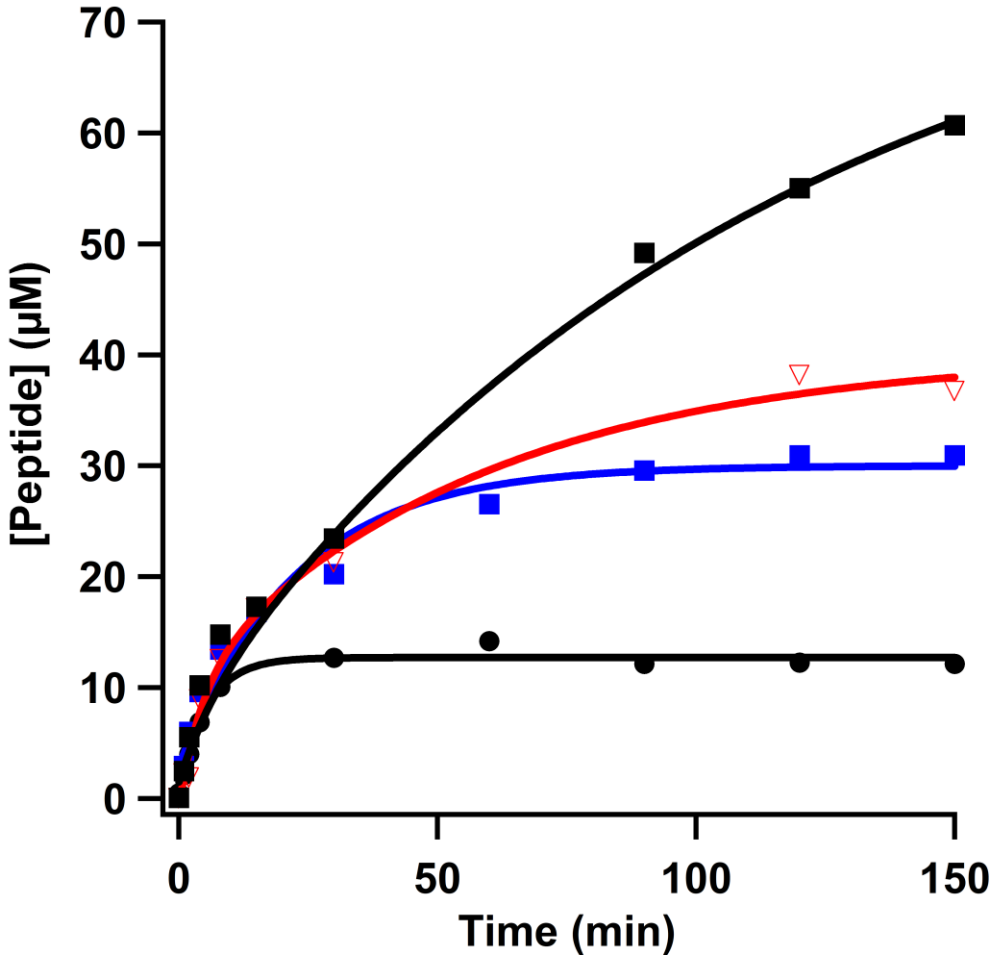

Figure 6-23: Activity of *S. aureus* LipA in the presence of *S. aureus* SufA and *S. aureus* Nfu. Assays included: 25 µM Sa LipA and, when applicable, 400 µM Sa Nfu and/or 400 µM Sa SufA, 400 µM OctH substrate, 0.5 µM SAH nucleosidase, and 1 mM SAM. Buffer (50 mM HEPES, pH 7.5, 300 mM KCl, 10% glycerol). Reactions were conducted at room temperature, and were initiated by the addition of 2 mM dithionite before quenching with a final concentration of 100 mM H_2SO_4 at various times. *S. aureus* LipA only control (black closed circles). *S. aureus* LipA + *S. aureus* Nfu (blue closed squares). *S. aureus* LipA + *S. aureus* SufA (red open triangles). *S. aureus* LipA + *S. aureus* Nfu + *S. aureus* SufA (black closed squares).

Because hope still lingered for a role for SufT in the reaction, the experiment was repeated in order to assess if SufT had an effect when both SufA and Nfu were present **(Figure 6-24).** This reaction contained 10 µM S. aureus LipA and, when applicable, 250 µM Sa Nfu, 250 µM Sa SufA, and/or 250 µM Sa SufT. A LipA only control reaction (closed black circles) catalyzed the formation

of approximately 10 µM lipoyl product. When Nfu and SufA were included in the reaction (closed black squares), approximately 80 µM lipoyl product was observed. When SufT was included with SufA and Nfu in the LipA reaction, only approximately 40 µM lipoyl product was observed, indicating product inhibition in the presence of SufT. This could indicate that SufT binds/interacts with one of the proteins in the assay.

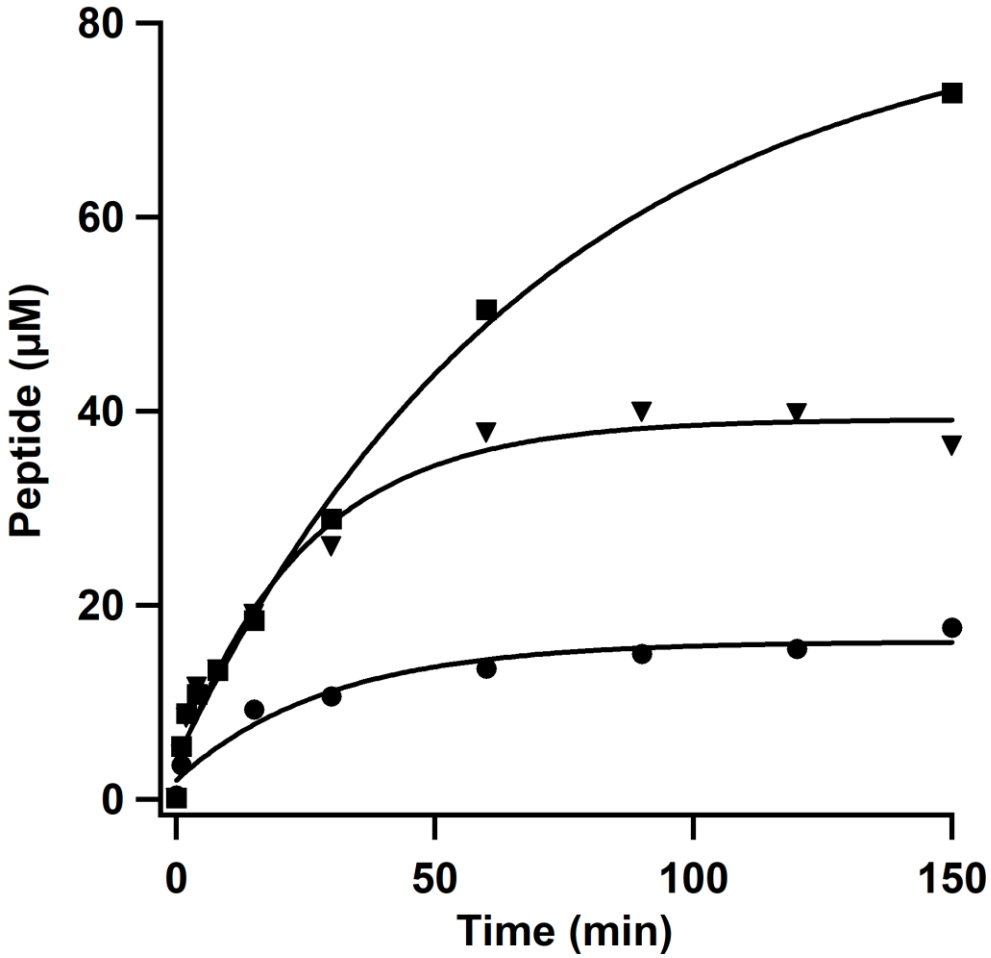

Figure 6-24: Activity of *S. aureus* LipA in the presence of *S. aureus* SufA and *S. aureus* Nfu and *S. aureus* SufT. Assays included: 10 µM Sa LipA and, when applicable, 250 µM Sa Nfu, 250 µM Sa SufA, and/or 250 µM Sa SufT, 400 µM OctH substrate, 0.5 µM SAH nucleosidase, and 1 mM SAM. Buffer (50 mM HEPES, pH 7.5, 300 mM KCl, 10% glycerol). Reactions were conducted at room temperature, and were initiated by the addition of 2 mM dithionite before

quenching with a final concentration of 100 mM H_2SO_4 at various times. *S. aureus* LipA only control (black closed circles). *S. aureus* LipA + *S. aureus* Nfu + *S. aureus* SufA (black closed squares). *S. aureus* LipA + *S. aureus* Nfu + *S. aureus* SufA + *S. aureus* SufT (black closed triangles).

In order to gain more insight to the cooperativity between SufA and Nfu, an experiment was performed in which LipA's activity was assayed over time in the presence of either SufA or Nfu **(Figure 6-25).** At the end of the reaction (t=150 min) the other protein partner was injected into the reaction, and its effect was monitored. In both cases, the LipA activity had leveled off at t=150 min indicating the reaction was complete. However, upon either the addition of SufA **(Figure 6-25, Panel A)** or Nfu **(Figure 6-25, Panel B),** lipoyl product formation begins occurring again. Unfortunately, issues with quantification during this experiment prevent the concentration values from being reliable; however, qualitatively, it is clear that an effect is observed.

Finally, as an attempt to obtain a stable complex between SufA and Nfu, the genes expressing the two proteins were co-expressed **(Figure 6-26).** Upon isolation of the protein, several protein bands are observed but a robust protein complex between the two proteins is not observed.

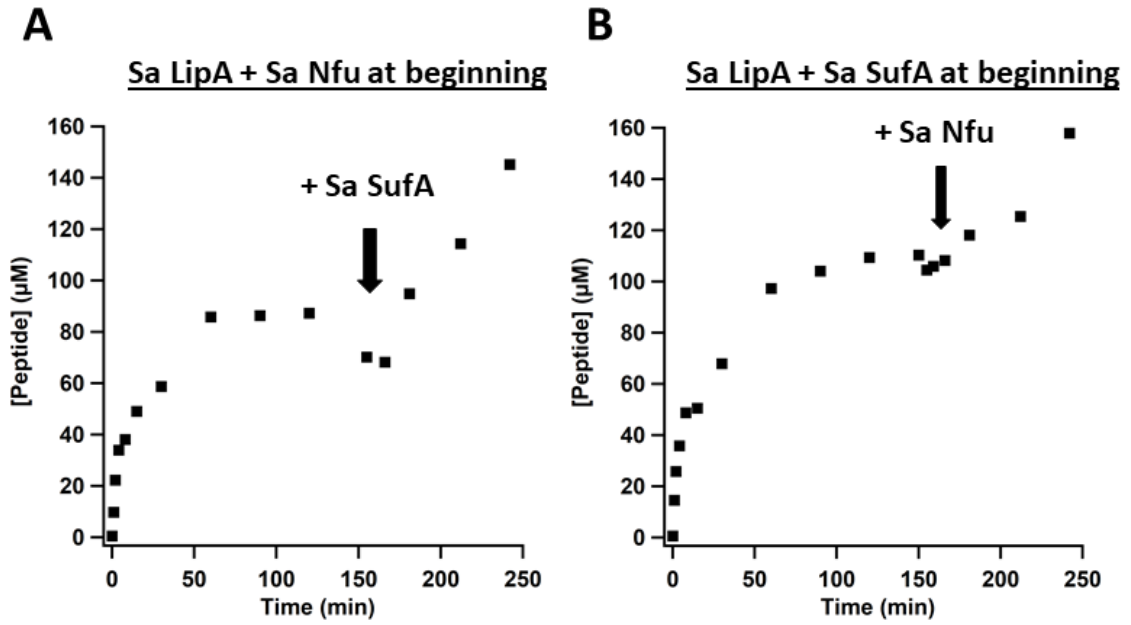

Figure 6-25: Activity of *S. aureus* LipA in the presence of *S. aureus* SufA with S. aureus spiked in and vice versa. Note: the data presented is qualitative due to inaccurate quantification. (A) *S. aureus* LipA in the presence of *S. aureus* Nfu. At t=251 min, *S. aureus* SufA was added to the reaction. (B) *S. aureus* LipA in the presence of *S. aureus* SufA. At t=251 min, *S. aureus* Nfu was added to the reaction.

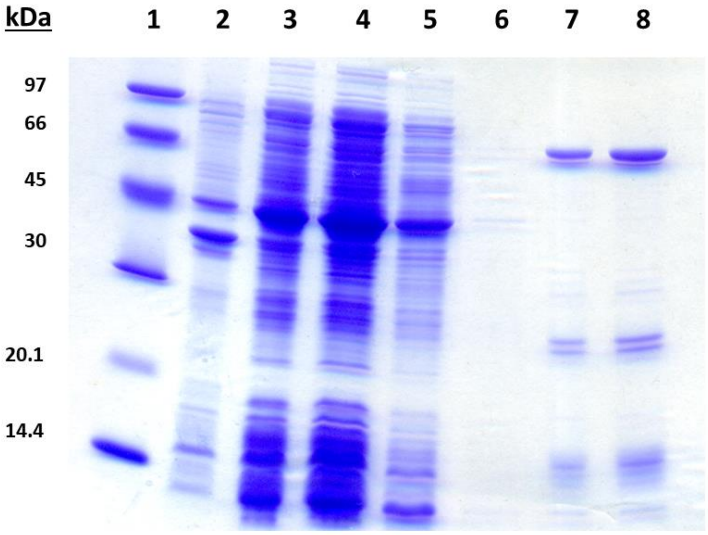

Figure 6-26: SDS-PAGE of isolation of *S. aureus* SufA and *S. aureus* Nfu from cells in which the two genes were co-expressed. Lanes are as follows: 1- molecular weight ladder 2- cellular pellet 3- supernatant 4- flowthrough 5- wash 1 6- wash 2 7- eluate 5 µL 8- eluate 10 µL.

Bacterial two hybrid screening of S. aureus LipA, S. aureus Nfu, and S. aureus SufA.

Bacterial two hybrid screening was used to uncover whether *S. aureus* LipA, *S. aureus* Nfu, and *S. aureus* SufA form complexes *in vivo.* Using the same method previously described, the following constructs were assembled using gateway cloning technology: *S. aureus lipA*-pUT18C, *S. aureus nfu*-pUT18C, *S. aureus sufA*-pST25, *S. aureus lipA*-pST25, and *S. aureus nfu*-pST25. The same negative controls (*E. coli gcvH*-pST25 + *E. coli gstB*-pUT18C) and positive controls (*zip*-pUT18C + *zip*-pKT25) were used. As shown in **Figure 6-27,** no color was observed in the negative control (Panel A), and robust color was observed in the positive control (Panel C), as expected. When BTH101 cells were co-transformed with *S. aureus nfu*-pUT18C and *S. aureus lipA*-pST25 (Panel B), no color was observed. The cells co-transformed with *S. aureus lipA-pUT28C* + *S. aureus sufA*-pST25 (Panel D) also showed no color. Finally, cells maintaining *S.*

aureus nfu-pST25 + *S. aureus sufA*-pUT18C (Panel E) were colorless. In all cases, no complex formation could be observed *in vivo.*

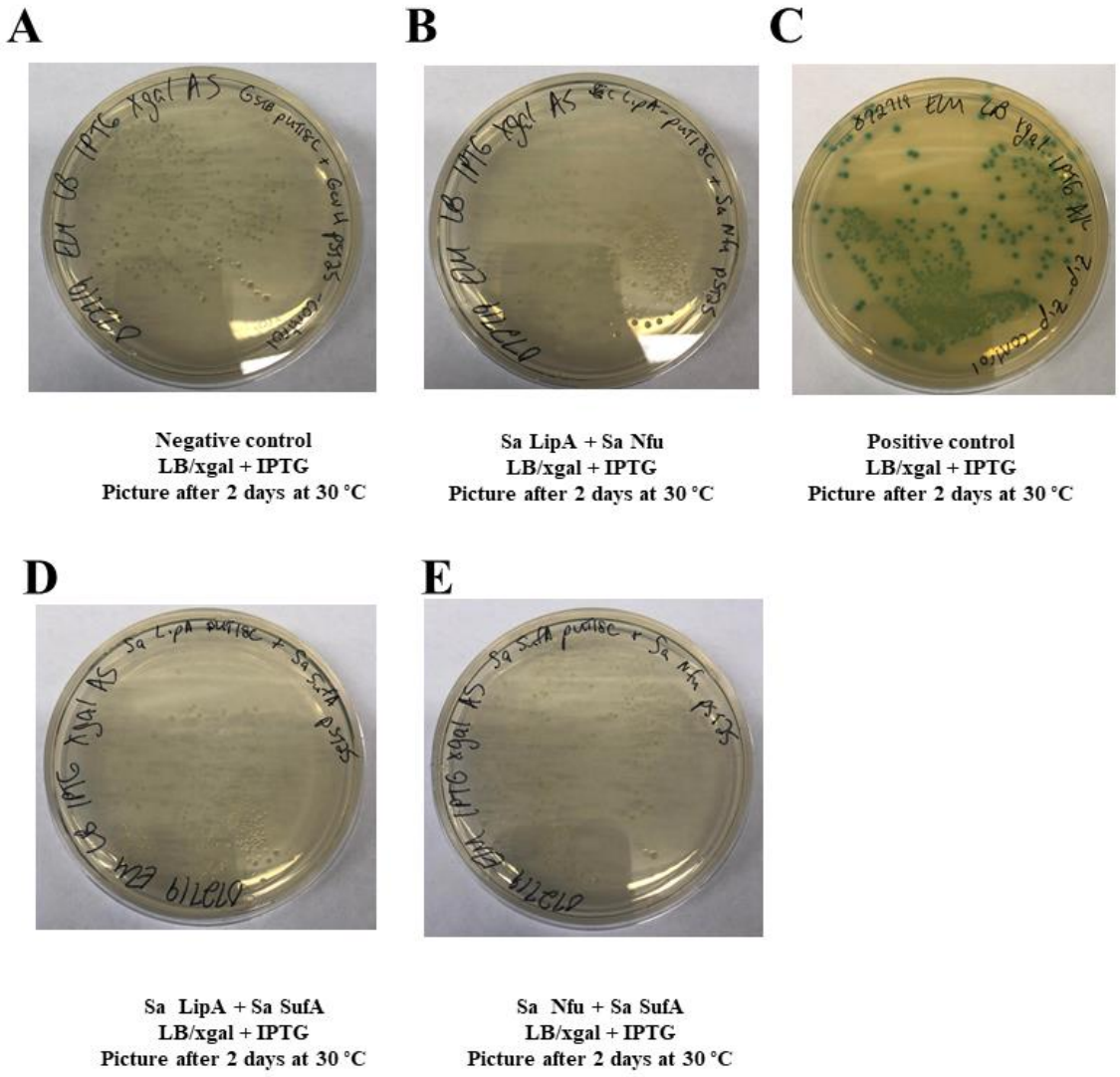

Figure 6-27: Bacterial two hybrid screening of *S. aureus* LipA, *S. aureus* Nfu, and *S. aureus* SufA. Adenylate cyclase deficient cells strain BTH101 were co-transformed bacterial two hybrid plasmids and spread on LB agar plates containing 40 µg/µL galactosidase and 0.5 mM IPTG with the respective selective antibiotics (100 µg/µL spectinomycin or 50 µg/µL kanamycin and 100 µg/µL ampicillin) . (A) Negative control containing two non-interacting proteins *E. coli gcvH*-pST25 and *E. coli gstB*-pUT18C. (B) *S. aureus nfu*-pUT18C and *S. aureus lipA*-pST25. (C) Positive control containing two domains of leucine zipper: *zip*-pUT18C and *zip*-pKT25. (D) *S. aureus lipA-pUT28C* + *S. aureus sufA*-pST25 (E) *S. aureus nfu*-pST25 + *S. aureus sufA*-pUT18C.

Discussion

This work sought to address several outstanding questions in the regeneration mechanism of LipA. The first part of this chapter rigorously addresses a hypothesis that NfuA is not responsible for inserting iron-sulfur clusters into apo-proteins that require them. This hypothesis directly contradicts all of the data obtained in this thesis providing a direct role for *E. coli* NfuA in targeted *E. coli* LipA and restoring its auxiliary cluster. Because of this, substantial effort was devoted to understanding what role, if any, the alternative proposed iron sulfur cluster carrier protein ErpA played in the biosynthesis of lipoic acid. In vitro and in vivo binding assays indicate a robust complex formation between *E. coli* NfuA and *E. coli* LipA, whereas no binding is observed between LipA and ErpA using these methods. Interestingly, a tight complex formation has been discovered between *E. coli* ErpA and *E. coli* NfuA, reproducing an observation in a previous study (2). While the role of this complex is not understood, NfuA has been found to interact with other intermediate iron-sulfur cluster carriers as well, such as Mrp, also known as AbpC, which is one of the proteins that pulled down with NfuA in the co-immunoprecipitation studies. The binding data, in conjunction with the activity assays performed with ErpA in this chapter, do not support the claim that ErpA is the sole iron-sulfur cluster carrier in the cell. It seems unlikely that one singular protein would be responsible and able to target every metalloprotein in the cell.

The second main focus of this chapter involved understanding lipoic acid biosynthesis in the pathogenic organism *S. aureus.* Understanding lipoic acid biosynthesis in S. aureus has profound implications in human health and disease, as *S. aureus* is one of the leading causes of infection in a hospital setting. With the rise of methicillin resistant Staphylococcus aureus (MRSA), new potential avenues for antibiotic therapy are critical. One such method to kill resistant bacteria, such as *S. aureus,* is to interrupt biologically essential pathways, such as lipoic acid biosynthesis. As such, *S. aureus* LipA was isolated and its activity was determined *in vitro.*

The observation that *S. aureus* Nfu did not catalytically affect the activity of *S. aureus* LipA indicated there might by an additional, yet identified, protein target. One promising candidate, SufT, a factor that was shown to be essential in cells experiencing a high demand for lipoic acid, did not appear to play a role in the maturation of LipA. Nevertheless, the *in vivo* data is compelling that is plays a still unknown role in lipoic acid biosynthesis. One hypothesis that has not been tested is that it performs a role upstream of *S. aureus* Nfu which would result in the same defect in lipoic acid biosynthesis. For example, SufT could be a regulatory factor and/or essential for the transfer of the newly assembled iron-sulfur cluster from the SufBCD scaffold to the intermediate proteins that target the cluster to apo-proteins.

Lastly, the preliminary data presented with *S. aureus* SufA could be expanded upon to unravel its potential role in the process. Of particular importance, the identity of the cofactor coordinated within SufA is critical information. If SufA is indeed an iron-binding protein, it could function to remove the residual iron from the auxiliary site of LipA, allowing for cluster insertion by Nfu. In addition to identifying the cofactor on SufA, the assays could be performed in the absence of SufA but in the presence of an iron chelator to determine if this is its role. Alternately, if SufA coordinates a [4Fe-4S] cluster, it is possible that it is either directly transferring a cluster to LipA or that it is transferring a [4Fe-4S] to Nfu after it has handed off its cluster. Moreover, much work remains to be performed to untangle this complicated process in this organism.

References

1. McCarthy, E. L., and Booker, S. J. (2017) Destruction and reformation of an iron-sulfur cluster during catalysis by lipoyl synthase. *Science (New York, N.Y.)* **358**, 373-377

2. Py, B., Gerez, C., Huguenot, A., Vidaud, C., Fontecave, M., Ollagnier de Choudens, S., and Barras, F. (2018) The ErpA/NfuA complex builds an oxidation-resistant Fe-S cluster delivery pathway. *The Journal of biological chemistry* **293**, 7689-7702
3. Loiseau, L., Gerez, C., Bekker, M., Ollagnier-de Choudens, S., Py, B., Sanakis, Y., Teixeira de Mattos, J., Fontecave, M., and Barras, F. (2007) ErpA, an iron sulfur (Fe S) protein of the A-type essential for respiratory metabolism in Escherichia coli. *Proceedings of the National Academy of Sciences of the United States of America* **104**, 13626-13631
4. McCarthy, E. L., Rankin, A. N., Dill, Z. R., and Booker, S. J. (2019) The A-type domain in Escherichia coli NfuA is required for regenerating the auxiliary [4Fe-4S] cluster in Escherichia coli lipoyl synthase. *The Journal of biological chemistry* **294**, 1609-1617
5. Skaar, E. P., Humayun, M., Bae, T., DeBord, K. L., and Schneewind, O. (2004) Iron-source preference of Staphylococcus aureus infections. *Science (New York, N.Y.)* **305**, 1626-1628
6. Mashruwala, A. A., Bhatt, S., Poudel, S., Boyd, E. S., and Boyd, J. M. (2016) The DUF59 Containing Protein SufT Is Involved in the Maturation of Iron-Sulfur (FeS) Proteins during Conditions of High FeS Cofactor Demand in Staphylococcus aureus. *PLoS genetics* **12**, e1006233
7. Mashruwala, A. A., Roberts, C. A., Bhatt, S., May, K. L., Carroll, R. K., Shaw, L. N., and Boyd, J. M. (2016) Staphylococcus aureus SufT: an essential iron-sulphur cluster assembly factor in cells experiencing a high-demand for lipoic acid. *Molecular microbiology* **102**, 1099-1119
8. Cicchillo, R. M., Iwig, D. F., Jones, A. D., Nesbitt, N. M., Baleanu-Gogonea, C., Souder, M. G., Tu, L., and Booker, S. J. (2004) Lipoyl synthase requires two equivalents of S-adenosyl-L-methionine to synthesize one equivalent of lipoic acid. *Biochemistry* **43**, 6378-6386
9. Mashruwala, A. A., Pang, Y. Y., Rosario-Cruz, Z., Chahal, H. K., Benson, M. A., Mike, L. A., Skaar, E. P., Torres, V. J., Nauseef, W. M., and Boyd, J. M. (2015) Nfu facilitates the maturation of iron-sulfur proteins and participates in virulence in Staphylococcus aureus. *Molecular microbiology* **95**, 383-409
10. Lu, J., Yang, J., Tan, G., and Ding, H. (2008) Complementary roles of SufA and IscA in the biogenesis of iron-sulfur clusters in Escherichia coli. *The Biochemical journal* **409**, 535-543
11. Wada, K., Hasegawa, Y., Gong, Z., Minami, Y., Fukuyama, K., and Takahashi, Y. (2005) Crystal structure of Escherichia coli SufA involved in biosynthesis of iron–sulfur clusters: Implications for a functional dimer. *FEBS Letters* **579**, 6543-6548

Chapter 7

Conclusions and Future Directions

The work presented in this thesis contributes to our understanding of how enzymes that destroy their essential metal cofactors during their reaction mechanism get regenerated in order to support catalysis. In particular, this work focused on lipoyl synthase, a radical SAM enzyme that catalyzes the second step of the *de novo* biosynthesis of lipoic acid, an essential cofactor known for its prominent roles in energy metabolism and the degradation of certain amino acids, among others. Lipoyl synthase coordinates a second 'auxiliary' cluster that has been shown to be sacrificed as a sulfur source during catalysis, leaving LipA in an inactive state in the absence of a system to regenerate it (1). This controversial role for an iron-sulfur cluster has been firmly established (2-5). The fundamental question this work addressed is whether there is a system in the cell to target LipA and either repair or replace its auxiliary cluster for subsequent turnover. Given that the cell has established pathways for the biosynthesis and trafficking of iron-sulfur clusters, it was likely that an undiscovered pathway existed.

Chapter 2 described the successful identification of the protein factor, *E. coli* NfuA, that afforded *E. coli* LipA catalysis. The identification of NfuA relied on the observation of clinical reports in the literature describing patients with mutations in the human homolog of NfuA, NFU1, that resulted in a fatal condition associated with lipoic acid deficiency (6-8). To this end, we were able to isolate *E. coli* NfuA with full incorporation of [4Fe–4S] cluster cofactor without the need for chemical reconstitution methods. Using our established methods for monitoring *E. coli* LipA

activity i*n vitro,* we were able to show robust catalysis for the first time in the presence of *E. coli* NfuA (9). We labeled the NfuA cluster with 34S as a method to demonstrate the *E. coli* LipA utilized the sulfur atoms from NfuA to produce lipoic acid. Using this method, we could distinguish lipoyl product produced from the unlabeled cluster that was coordinated by LipA produced with natural abundance sulfur from lipoyl product produced from the 34S incorporated cluster residing on NfuA. To our surprise, we were able to observe two equivalents of unlabeled lipoyl product in these experiments, indicating that LipA can mobilize all four of its sulfur atoms in the presence of NfuA. A growth study that was performed indicated that an *E. coli* strain in which the gene encoding NfuA had been knockout out exhibited the same growth rate as a wild-type strain, deviating from the drastic phenotypes observed in humans. We reasoned that a second redundant factor in *E. coli* could exist to support the lipoic acid levels requisite for growth. Indeed, we discovered that IscU, the scaffold protein upon which iron-sulfur clusters are assembled, could also directly transfer clusters to LipA. This observation provided several pathways in which LipA could be regenerated; either directly from the IscU scaffold, or from NfuA, which presumably receives its cluster from IscU. Future work seeks to understand the differences between the drastic phenotype observed in the human mutant NFU1 as compared to the *E. coli* NfuA that displays no growth phenotype. One insightful experiment would be to probe lipoic acid levels in the wild-type *E. coli* strain compared to the NfuA knockout strain by performing a Western Blot of normalized cells blotting against lipoic acid to which we have antibodies. It is possible that in the knockout strain there are reduced lipoylation levels in the cell, but, as the cellular requirements for lipoic acid are low, a growth phenotype is not observed. In humans, mutations in other genes have given rise to similar lipoic acid deficient conditions, such as the human factors IBA57, GLRX5 and BOLA3 (6,10). Other research in our laboratory has shown that Human NFU1 cannot activate Human LIAS to the same extent. It was our hypothesis that these other essential factors are involved, but to this

date, no role for these factors have been assigned, despite their drastic defects in lipoic acid biosynthesis.

Chapter 3 describes efforts towards understanding the pathway by which *E. coli* NfuA recognizes *E. coli* LipA. In this work, we have realized that *E. coli* NfuA has a distinct architecture composed of two domains: an N-terminal A-type domain and a C-terminal Nfu-like domain (11). We have shown that the degenerate cysteinyl residues in the N-terminal domain are not essential for binding or activating *E. coli* LipA, while the C- terminal cysteinyl residues are absolutely required for cluster coordination and activity, but not binding. Further, we have found that the N-terminal domain is essential for the tight complex formation with *E. coli* LipA that is described in Chapter 2. NfuA from *Mycobacterium tuberculosis,* which also has an N-terminal A-type domain, was able to activate *E. coli* LipA, whereas Nfu from *S. aureus* which lacks this domain was unable to. A genetic fusion of the *E. coli* NfuA N terminal domain to either *S. aureus* Nfu or Human NFU1 afforded the proteins the ability to activate *E. coli* LipA. Lastly, it was shown that NfuA was not able to catalytically activate LipA when an 8-thiooctanoyl-lysyl peptide substrate mimic was used, indicating that the cluster must be degraded to a [2Fe–2S] or smaller in order for cluster regeneration to occur.

Chapter 4 describes strategies towards understanding the mechanism by which the iron-sulfur cluster in *E. coli* LipA is regenerated, as well as the specificity of *E. coli* NfuA towards *E. coli* LipA. In the absence of NfuA, only 1 equivalent of lipoic acid requiring two sulfur atoms had previously been observed in *in vitro* assays due to its destruction. The unexpected observation in Chapter 2 that LipA could produce two equivalents of lipoic acid from its auxiliary cluster in the presence of NfuA lead us to perform additional labelling experiments. In this chapter, we report that NfuA reconstituted with a [4Fe–4Se] cluster can deliver the cluster to LipA during turnover, allowing for the production of selenolipoic acid. We also provide additional evidence that LipA can mobilize all four sulfur atoms in its [4Fe–4S] cluster during catalysis to allow for two

equivalents of lipoic acid formation before selenolipoic acid is produced. These studies now set the stage for deciphering the mechanism of iron-sulfur cluster regeneration in LipA. An important question is what the state of the auxiliary cluster is on LipA following the production of one equivalent of selenolipoic acid. To accomplish this, a 57Fe-Se loaded NfuA was produced, and reacted with LipA to completion. At the end of the reaction, the sample was flash-frozen for Mössbauer analysis to determine its identity which is still be unraveled. Alternately, in collaboration with the laboratory of Professor Amie Boal, attempts to obtain a crystal structure of this seleno-incorporated LipA protein are ongoing by graduate student Vivian Robert Jeyachandran. The fate of the iron lost from the cluster as the sulfur atoms are being consumed is also unclear. In the cell, iron is highly regulated due to its potential toxicity at high concentrations. As a result, it is unlikely that the iron is simply dispelled into solution. One hypothesis is that the degenerate A-type domain, which contains two cysteinyl residues of yet unknown function, is responsible for removing the iron from the auxiliary site and recycle the iron to the protein scaffold for new cluster assembly. Some preliminary evidence has shown that apo NfuA can tightly bind iron by Mössbauer analysis. This hypothesis will need to be more rigorously tested.

Chapter 5 sought to understand the specificity of *E. coli* NfuA for *E. coli* LipA. In order to address this question, NfuA was produced with a FLAG epitope tag, allowing it to be "pulled out" of the cell using anti-flag antibody based resin with endogenously interacting proteins that could subsequently be identified by mass spectrometry. LipA was one of the interacting proteins identified providing additional direct *in vivo* evidence for the complex. The list also included lipoylated proteins in the cell, such as the pyruvate dehydrogenase complex, and proteins involved in lipoic acid regulation such as ClpX. Other proteins involved in iron-sulfur cluster biogenesis and trafficking were also identified, including IscS and Mrp/AbpC. Surprisingly, other Fe–S cluster containing proteins, including RimO, MiaB, and RlmN, were also pulled down with NfuA. This could indicate that NfuA is also involved in the delivery of clusters to other RS enzymes in the cell.

Preliminary data with MiaB was inconclusive, but this hypothesis will need to be more rigorously tested. The reciprocal experiment in which LipA has an encoded FLAG tag and pulled out of the cell has also been performed, and the interacting proteins were identified by mass spectrometry. In this reciprocal experiment, NfuA was also successfully pulled out of the cell with LipA-FLAG. One potential downfall of the co-immunoprecipitation technique is that it is difficult to capture transient or weak interactions. To circumvent this, future experiments can be repeated in the presence of an amine crosslinker. Chapter 5 also provided direct *in vivo* evidence for the complex formation between *E. coli* NfuA and *E. coli* LipA bacterial two hybrid screening. This method was also used to confirm *in vivo* that the tight complex is reliant upon specifically the N terminal domain, whereas the C-terminal domain is dispensable. Further, a small library of NfuA and LipA constructs were screened to identify the amino acids essential for the protein-protein interaction. Through this method, we discovered an isoleucine-serine motif in NfuA, and a LIPVK motif in LipA, that are essential for the binding event.

Chapter 6 describes the characterization of *E. coli* ErpA, a factor that was alternately proposed to function as the sole protein responsible for Fe-S cofactor delivery (12). This chapter also focuses on understanding the potential similarities and differences in the maturation mechanism in *S. aureus* LipA, which could serve as a biochemical pathway to exploit for the development of new antibiotics. In this chapter, we have shown that *E. coli* ErpA does not interact with *E. coli* LipA using molecular sieve chromatography *(in vitro)* as well as bacterial two hybrid (*in vivo*). Analysis of the activity of LipA in the presence of ErpA indicated only one additional turnover, in stark contrast to the catalysis observed when NfuA is present. Interestingly, *E. coli* ErpA and *E. coli* NfuA form a complex *in vivo,* but the role of this interaction is unknown. When both ErpA and NfuA are included in a reaction with LipA, decreased product formation is observed which may be due to inhibition caused by the interaction of NfuA and ErpA. In this chapter, we were also able to isolate LipA from *S. aureus* and demonstrate its activity for the first time *in vitro.*

We found that upon isolation and characterization of *S. aureus* Nfu, it was unable to activate *S. aureus* LipA to the same extent as what is observed in the *E. coli* system. Convincing *in vivo* evidence implicating a new factor, SufT in lipoic acid biosynthesis is *S. aureus* lead us to isolate it and determine its role (13,14). However, despite substantial effort, no role was discovered. A leading hypothesis is that it is an element that is involved with interacting with the SufBCD scaffold complex and transferring the cluster to intermediate iron-sulfur cluster delivery proteins, but this remains to be tested. The observation that the gene encoding *S. aureus* Nfu lies in an operon nearby another A-type protein, SufA, lead us to isolate and characterize SufA as well. In the literature, conflicting reports indicate that SufA can either coordinate a [4Fe–4S] cluster or act as an iron binding protein (15,16). The UV-visible spectrum of the as-isolated, relatively impure SufA protein, shows features of a [4Fe–4S] cluster. Chemical reconstitution and subsequent size exclusion chromatography yields a more pure protein, though a distinct color change from brown to red is observed, as well as dramatic changes in the UV-visible spectrum. This could be a result of degradation of the cofactor in the size exclusion step, or could indicate an iron metal center. When the chemically reconstituted *S. aureus* SufA protein was included in activity assays with *S. aureus* LipA, approximately the same amount of product was observed as when only *S. aureus* Nfu was included. However, when both *S. aureus* SufA and *S. aureus* Nfu were included in a reaction with *S. aureus* LipA, approximately six or more lipoyl product equivalents were observed. The identification of the cofactor coordinated by *S. aureus* SufA is critical to understanding its role in the reaction. It could be removing the residual iron from the auxiliary site to allow new cluster insertion by *S. aureus* Nfu. Alternately, it could be replenishing the cofactor on *S. aureus* Nfu if it coordinates a [4Fe–4S] cluster. The preliminary data, while interesting, needs to be more robustly investigated.

Collectively, our work sheds light on many important biochemical questions, such as how the lipoyl cofactor is biosynthesized in the cell, the mechanism by which enzymes can catalyze the

appendage of sulfur to an unactivated carbon center, and lastly, the mechanism by which newly assembled Fe-S clusters are targeted and subsequently transferred to proteins that use these metal cofactors for catalysis.

References

1. Lanz, N. D., and Booker, S. J. (2015) Auxiliary iron-sulfur cofactors in radical SAM enzymes. *Biochimica et biophysica acta* **1853**, 1316-1334
2. Cicchillo, R. M., and Booker, S. J. (2005) Mechanistic Investigations of Lipoic Acid Biosynthesis in Escherichia coli: Both Sulfur Atoms in Lipoic Acid are Contributed by the Same Lipoyl Synthase Polypeptide. *Journal of the American Chemical Society* **127**, 2860-2861
3. McLaughlin, M. I., Lanz, N. D., Goldman, P. J., Lee, K. H., Booker, S. J., and Drennan, C. L. (2016) Crystallographic snapshots of sulfur insertion by lipoyl synthase. *Proceedings of the National Academy of Sciences of the United States of America* **113**, 9446-9450
4. Lanz, N. D., Pandelia, M. E., Kakar, E. S., Lee, K. H., Krebs, C., and Booker, S. J. (2014) Evidence for a catalytically and kinetically competent enzyme-substrate cross-linked intermediate in catalysis by lipoyl synthase. *Biochemistry* **53**, 4557-4572
5. Lanz, N. D., Rectenwald, J. M., Wang, B., Kakar, E. S., Laremore, T. N., Booker, S. J., and Silakov, A. (2015) Characterization of a Radical Intermediate in Lipoyl Cofactor Biosynthesis. *Journal of the American Chemical Society* **137**, 13216-13219
6. Cameron, Jessie M., Janer, A., Levandovskiy, V., MacKay, N., Rouault, Tracey A., Tong, W.-H., Ogilvie, I., Shoubridge, Eric A., and Robinson, Brian H. (2011) Mutations in Iron-Sulfur Cluster Scaffold Genes NFU1 and BOLA3 Cause a Fatal Deficiency of Multiple Respiratory Chain and 2-Oxoacid Dehydrogenase Enzymes. *American Journal of Human Genetics* **89**, 486-495
7. Mayr, J. A., Feichtinger, R. G., Tort, F., Ribes, A., and Sperl, W. (2014) Lipoic acid biosynthesis defects. *Journal of inherited metabolic disease* **37**, 553-563
8. Navarro-Sastre, A., Tort, F., Stehling, O., Uzarska, Marta A., Arranz, José A., del Toro, M., Labayru, M T., Landa, J., Font, A., Garcia-Villoria, J., Merinero, B., Ugarte, M., Gutierrez-Solana, Luis G., Campistol, J., Garcia-Cazorla, A., Vaquerizo, J., Riudor, E., Briones, P., Elpeleg, O., Ribes, A., and Lill, R. (2011) A Fatal Mitochondrial Disease Is Associated with Defective NFU1 Function in the Maturation of a Subset of Mitochondrial Fe-S Proteins. *American Journal of Human Genetics* **89**, 656-667
9. McCarthy, E. L., and Booker, S. J. (2017) Destruction and reformation of an iron-sulfur cluster during catalysis by lipoyl synthase. *Science (New York, N.Y.)* **358**, 373-377
10. Baker, P. R., 2nd, Friederich, M. W., Swanson, M. A., Shaikh, T., Bhattacharya, K., Scharer, G. H., Aicher, J., Creadon-Swindell, G., Geiger, E., MacLean, K. N., Lee, W. T., Deshpande, C., Freckmann, M. L., Shih, L. Y., Wasserstein, M., Rasmussen, M. B., Lund, A. M., Procopis, P., Cameron, J. M., Robinson, B. H., Brown, G. K., Brown, R.

M., Compton, A. G., Dieckmann, C. L., Collard, R., Coughlin, C. R., 2nd, Spector, E., Wempe, M. F., and Van Hove, J. L. (2014) Variant non ketotic hyperglycinemia is caused by mutations in LIAS, BOLA3 and the novel gene GLRX5. *Brain : a journal of neurology* **137**, 366-379

11. McCarthy, E. L., Rankin, A. N., Dill, Z. R., and Booker, S. J. (2019) The A-type domain in Escherichia coli NfuA is required for regenerating the auxiliary [4Fe-4S] cluster in Escherichia coli lipoyl synthase. *The Journal of biological chemistry* **294**, 1609-1617
12. Py, B., Gerez, C., Huguenot, A., Vidaud, C., Fontecave, M., Ollagnier de Choudens, S., and Barras, F. (2018) The ErpA/NfuA complex builds an oxidation-resistant Fe-S cluster delivery pathway. *The Journal of biological chemistry* **293**, 7689-7702
13. Mashruwala, A. A., Bhatt, S., Poudel, S., Boyd, E. S., and Boyd, J. M. (2016) The DUF59 Containing Protein SufT Is Involved in the Maturation of Iron-Sulfur (FeS) Proteins during Conditions of High FeS Cofactor Demand in Staphylococcus aureus. *PLoS genetics* **12**, e1006233
14. Mashruwala, A. A., Roberts, C. A., Bhatt, S., May, K. L., Carroll, R. K., Shaw, L. N., and Boyd, J. M. (2016) Staphylococcus aureus SufT: an essential iron-sulphur cluster assembly factor in cells experiencing a high-demand for lipoic acid. *Molecular microbiology* **102**, 1099-1119
15. Lu, J., Yang, J., Tan, G., and Ding, H. (2008) Complementary roles of SufA and IscA in the biogenesis of iron-sulfur clusters in Escherichia coli. *The Biochemical journal* **409**, 535-543
16. Wada, K., Hasegawa, Y., Gong, Z., Minami, Y., Fukuyama, K., and Takahashi, Y. (2005) Crystal structure of Escherichia coli SufA involved in biosynthesis of iron–sulfur clusters: Implications for a functional dimer. *FEBS Letters* **579**, 6543-6548

Appendix A

List of Proteins Identified in NfuA-FLAG Co-Immunoprecipitation

Accession	Protein
BAND 2	
P0C8J8	D-tagatose-1,6-bisphosphate aldolase subunit GatZ GN=gatZ PE=1 SV=1 - [GATZ_ECOLI]
P0ABB4	ATP synthase subunit beta GN=atpD PE=1 SV=2 - [ATPB_ECOLI]
P06720	Alpha-galactosidase GN=melA PE=1 SV=1 - [AGAL_ECOLI]
P02930	Outer membrane protein TolC GN=tolC PE=1 SV=3 - [TOLC_ECOLI]
P0A9P0	Dihydrolipoyl dehydrogenase GN=lpdA PE=1 SV=2 - [DLDH_ECOLI]
P0A6H5	ATP-dependent protease ATPase subunit HslU GN=hslU PE=1 SV=1 - [HSLU_ECOLI]
P76658	Bifunctional protein HldE GN=hldE PE=1 SV=1 - [HLDE_ECOLI]
P63020	Fe/S biogenesis protein NfuA GN=nfuA PE=1 SV=1 - [NFUA_ECOLI]
P0AFG6	Dihydrolipoyllysine-residue succinyltransferase component of 2-oxoglutarate dehydrogenase complex GN=sucB
P0A6U8	Glycogen synthase GN=glgA PE=1 SV=1 - [GLGA_ECOLI]
P25553	Lactaldehyde dehydrogenase GN=aldA PE=1 SV=2 - [ALDA_ECOLI]
P21513	Ribonuclease E GN=rne PE=1 SV=6 - [RNE_ECOLI]
P39342	Uncharacterized protein YjgR GN=yjgR PE=4 SV=1 - [YJGR_ECOLI]
P0AC38	Aspartate ammonia-lyase GN=aspA PE=1 SV=1 - [ASPA_ECOLI]
P0A9P6	ATP-dependent RNA helicase DeaD GN=deaD PE=1 SV=2 - [DEAD_ECOLI]
P0ADR8	LOG family protein YgdH GN=ygdH PE=3 SV=1 - [YGDH_ECOLI]
P24182	Biotin carboxylase GN=accC PE=1 SV=2 - [ACCC_ECOLI]
P0A853	Tryptophanase GN=tnaA PE=1 SV=1 - [TNAA_ECOLI]
P0A850	Trigger factor GN=tig PE=1 SV=1 - [TIG_ECOLI]
P0A6F3	Glycerol kinase GN=glpK PE=1 SV=2 - [GLPK_ECOLI]
P37349	Protein-lysine deacetylase GN=dhaM PE=1 SV=3 - [DHAM_ECOLI]
P0ACB0	Replicative DNA helicase GN=dnaB PE=1 SV=1 - [DNAB_ECOLI]
P0A8M0	Asparagine--tRNA ligase GN=asnS PE=1 SV=2 - [SYN_ECOLI]
P0A6E4	Argininosuccinate synthase GN=argG PE=1 SV=2 - [ASSY_ECOLI]
P0AFK0	Metalloprotease PmbA GN=pmbA PE=1 SV=1 - [PMBA_ECOLI]
P0AG30	Transcription termination factor Rho GN=rho PE=1 SV=1 - [RHO_ECOLI]
P0A8L1	Serine--tRNA ligase GN=serS PE=1 SV=1 - [SYS_ECOLI]
P27306	Soluble pyridine nucleotide transhydrogenase GN=sthA PE=1 SV=5 - [STHA_ECOLI]
P0AGG8	Metalloprotease TldD GN=tldD PE=1 SV=1 - [TLDD_ECOLI]

P16095	L-serine dehydratase 1 GN=sdaA PE=1 SV=3 - [SDHL_ECOLI]
P02943	Maltoporin GN=lamB PE=1 SV=1 - [LAMB_ECOLI]
P0AGI8	Trk system potassium uptake protein TrkA GN=trkA PE=1 SV=1 - [TRKA_ECOLI]
P77671	Allantoinase GN=allB PE=1 SV=1 - [ALLB_ECOLI]
P37648	Protein YhjJ GN=yhjJ PE=1 SV=1 - [YHJJ_ECOLI]
P0AAG8	Galactose/methyl galactoside import ATP-binding protein MglA GN=mglA PE=1 SV=1 - [MGLA_ECOLI]
P0A821	L-seryl-tRNA(Sec) selenium transferase GN=selA PE=1 SV=1 - [SELA_ECOLI]
P0ABH9	ATP-dependent Clp protease ATP-binding subunit ClpA GN=clpA PE=1 SV=1 - [CLPA_ECOLI]
P25526	Succinate-semialdehyde dehydrogenase [NADP(+)] GabD GN=gabD PE=1 SV=1 - [GABD_ECOLI]
P23830	CDP-diacylglycerol--serine O-phosphatidyltransferase GN=pssA PE=1 SV=2 - [PSS_ECOLI]
P06710	DNA polymerase III subunit tau GN=dnaX PE=1 SV=1 - [DPO3X_ECOLI]
P0A705	Translation initiation factor IF-2 GN=infB PE=1 SV=1 - [IF2_ECOLI]
P0A9W3	Energy-dependent translational throttle protein EttA GN=ettA PE=1 SV=2 - [ETTA_ECOLI]
P0AFU4	Transcriptional regulatory protein GlrR GN=glrR PE=1 SV=1 - [GLRR_ECOLI]
P42588	Putrescine aminotransferase GN=patA PE=1 SV=2 - [PAT_ECOLI]
P23886	ATP-binding/permease protein CydC GN=cydC PE=3 SV=2 - [CYDC_ECOLI]
P0C0V0	Periplasmic serine endoprotease DegP GN=degP PE=1 SV=1 - [DEGP_ECOLI]
P0AC41	Succinate dehydrogenase flavoprotein subunit GN=sdhA PE=1 SV=1 - [SDHA_ECOLI]
P0A6C5	Amino-acid acetyltransferase GN=argA PE=1 SV=1 - [ARGA_ECOLI]
P0A6Z3	Chaperone protein HtpG GN=htpG PE=1 SV=1 - [HTPG_ECOLI]
P32132	GTP-binding protein TypA/BipA GN=typA PE=1 SV=2 - [TYPA_ECOLI]
P0A7V3	30S ribosomal protein S3 GN=rpsC PE=1 SV=2 - [RS3_ECOLI]
P21165	Xaa-Pro dipeptidase GN=pepQ PE=1 SV=2 - [PEPQ_ECOLI]
P0ABB0	ATP synthase subunit alpha GN=atpA PE=1 SV=1 - [ATPA_ECOLI]
P0A6Y8	Chaperone protein DnaK GN=dnaK PE=1 SV=2 - [DNAK_ECOLI]
P0AEI4	Ribosomal protein S12 methylthiotransferase RimO GN=rimO PE=1 SV=1 - [RIMO_ECOLI]
P19934	Protein TolA GN=tolA PE=1 SV=1 - [TOLA_ECOLI]
P0A6F5	60 kDa chaperonin GN=groL PE=1 SV=2 - [CH60_ECOLI]
P0ABI8	Cytochrome bo(3) ubiquinol oxidase subunit 1 GN=cyoB PE=1 SV=1 - [CYOB_ECOLI]
P0AGD7	Signal recognition particle protein GN=ffh PE=1 SV=1 - [SRP54_ECOLI]
P05793	Ketol-acid reductoisomerase (NADP(+)) GN=ilvC PE=1 SV=4 - [ILVC_ECOLI]
P21179	Catalase HPII GN=katE PE=1 SV=1 - [CATE_ECOLI]
P0A6J5	D-amino acid dehydrogenase GN=dadA PE=1 SV=1 - [DADA_ECOLI]
P0AAI3	ATP-dependent zinc metalloprotease FtsH GN=ftsH PE=1 SV=1 - [FTSH_ECOLI]
P02931	Outer membrane protein F GN=ompF PE=1 SV=1 - [OMPF_ECOLI]
P0AG67	30S ribosomal protein S1 GN=rpsA PE=1 SV=1 - [RS1_ECOLI]

BAND 3

P02943	Maltoporin GN=lamB PE=1 SV=1 - [LAMB_ECOLI]
P0AG30	Transcription termination factor Rho GN=rho PE=1 SV=1 - [RHO_ECOLI]
P0A853	Tryptophanase GN=tnaA PE=1 SV=1 - [TNAA_ECOLI]

P39099	Periplasmic pH-dependent serine endoprotease DegQ GN=degQ PE=1 SV=1 - [DEGQ_ECOLI]
P0ABB4	ATP synthase subunit beta GN=atpD PE=1 SV=2 - [ATPB_ECOLI]
P0A6P9	Enolase GN=eno PE=1 SV=2 - [ENO_ECOLI]
P0A9G6	Isocitrate lyase GN=aceA PE=1 SV=1 - [ACEA_ECOLI]
P0A6H1	ATP-dependent Clp protease ATP-binding subunit ClpX GN=clpX PE=1 SV=2 - [CLPX_ECOLI]
P0A6J5	D-amino acid dehydrogenase GN=dadA PE=1 SV=1 - [DADA_ECOLI]
P0C8J8	D-tagatose-1,6-bisphosphate aldolase subunit GatZ GN=gatZ PE=1 SV=1 - [GATZ_ECOLI]
P0C0V0	Periplasmic serine endoprotease DegP GN=degP PE=1 SV=1 - [DEGP_ECOLI]
P0A6E4	Argininosuccinate synthase GN=argG PE=1 SV=2 - [ASSY_ECOLI]
P00934	Threonine synthase GN=thrC PE=1 SV=1 - [THRC_ECOLI]
P08200	Isocitrate dehydrogenase [NADP] GN=icd PE=1 SV=1 - [IDH_ECOLI]
P0AES6	DNA gyrase subunit B GN=gyrB PE=1 SV=2 - [GYRB_ECOLI]
P0ABZ6	Chaperone SurA GN=surA PE=1 SV=1 - [SURA_ECOLI]
P63020	Fe/S biogenesis protein NfuA GN=nfuA PE=1 SV=1 - [NFUA_ECOLI]
P0A7D4	Adenylosuccinate synthetase GN=purA PE=1 SV=2 - [PURA_ECOLI]
P00350	6-phosphogluconate dehydrogenase, decarboxylating GN=gnd PE=1 SV=2 - [6PGD_ECOLI]
P0A8J8	ATP-dependent RNA helicase RhlB GN=rhlB PE=1 SV=2 - [RHLB_ECOLI]
P0ABC7	Modulator of FtsH protease HflK GN=hflK PE=1 SV=1 - [HFLK_ECOLI]
P09127	Putative uroporphyrinogen-III C-methyltransferase GN=hemX PE=1 SV=1 - [HEMX_ECOLI]
P31979	NADH-quinone oxidoreductase subunit F GN=nuoF PE=1 SV=3 - [NUOF_ECOLI]
P0A850	Trigger factor GN=tig PE=1 SV=1 - [TIG_ECOLI]
P21513	Ribonuclease E GN=rne PE=1 SV=6 - [RNE_ECOLI]
P0A8M0	Asparagine--tRNA ligase GN=asnS PE=1 SV=2 - [SYN_ECOLI]
P0CE47	Elongation factor Tu 1 GN=tufA PE=1 SV=1 - [EFTU1_ECOLI]
P0ABH9	ATP-dependent Clp protease ATP-binding subunit ClpA GN=clpA PE=1 SV=1 - [CLPA_ECOLI]
P00393	NADH dehydrogenase GN=ndh PE=1 SV=2 - [DHNA_ECOLI]
P60293	Chromosome partition protein MukF GN=mukF PE=1 SV=1 - [MUKF_ECOLI]
P77581	Succinylornithine transaminase GN=astC PE=1 SV=1 - [ASTC_ECOLI]
P60906	Histidine--tRNA ligase GN=hisS PE=1 SV=2 - [SYH_ECOLI]
P0A9P6	ATP-dependent RNA helicase DeaD GN=deaD PE=1 SV=2 - [DEAD_ECOLI]
P02930	Outer membrane protein TolC GN=tolC PE=1 SV=3 - [TOLC_ECOLI]
P0A705	Translation initiation factor IF-2 GN=infB PE=1 SV=1 - [IF2_ECOLI]
P0AEI1	tRNA-2-methylthio-N(6)-dimethylallyladenosine synthase GN=miaB PE=1 SV=1 - [MIAB_ECOLI]
P0A6U8	Glycogen synthase GN=glgA PE=1 SV=1 - [GLGA_ECOLI]
P0A6M8	Elongation factor G GN=fusA PE=1 SV=2 - [EFG_ECOLI]
P77552	Uncharacterized protein YdhQ GN=ydhQ PE=4 SV=1 - [YDHQ_ECOLI]
P0A7V8	30S ribosomal protein S4 GN=rpsD PE=1 SV=2 - [RS4_ECOLI]
P08192	Bifunctional protein FolC GN=folC PE=1 SV=2 - [FOLC_ECOLI]
P66948	Beta-barrel assembly-enhancing protease GN=bepA PE=1 SV=1 - [BEPA_ECOLI]
P0AG67	30S ribosomal protein S1 GN=rpsA PE=1 SV=1 - [RS1_ECOLI]
P0A6F5	60 kDa chaperonin GN=groL PE=1 SV=2 - [CH60_ECOLI]

P07001	NAD(P) transhydrogenase subunit alpha GN=pntA PE=1 SV=2 - [PNTA_ECOLI]
P0AEW6	Inosine-guanosine kinase GN=gsk PE=1 SV=1 - [INGK_ECOLI]
P24182	Biotin carboxylase GN=accC PE=1 SV=2 - [ACCC_ECOLI]
P0AGD7	Signal recognition particle protein GN=ffh PE=1 SV=1 - [SRP54_ECOLI]
P0ADR8	LOG family protein YgdH GN=ygdH PE=3 SV=1 - [YGDH_ECOLI]
P0A9W3	Energy-dependent translational throttle protein EttA GN=ettA PE=1 SV=2 - [ETTA_ECOLI]
P24228	D-alanyl-D-alanine carboxypeptidase DacB GN=dacB PE=1 SV=2 - [DACB_ECOLI]
P16095	L-serine dehydratase 1 GN=sdaA PE=1 SV=3 - [SDHL_ECOLI]
P0A6Y8	Chaperone protein DnaK GN=dnaK PE=1 SV=2 - [DNAK_ECOLI]
P76658	Bifunctional protein HldE GN=hldE PE=1 SV=1 - [HLDE_ECOLI]
P0ABH0	Cell division protein FtsA GN=ftsA PE=1 SV=1 - [FTSA_ECOLI]
P06710	DNA polymerase III subunit tau GN=dnaX PE=1 SV=1 - [DPO3X_ECOLI]
P07012	Peptide chain release factor RF2 GN=prfB PE=1 SV=3 - [RF2_ECOLI]
P00968	Carbamoyl-phosphate synthase large chain GN=carB PE=1 SV=2 - [CARB_ECOLI]
P69874	Spermidine/putrescine import ATP-binding protein PotA GN=potA PE=1 SV=1 - [POTA_ECOLI]
P0AE45	UPF0053 inner membrane protein YtfL GN=ytfL PE=1 SV=1 - [YTFL_ECOLI]
P31677	Alpha,alpha-trehalose-phosphate synthase [UDP-forming] GN=otsA PE=1 SV=3 - [OTSA_ECOLI]
P11447	Argininosuccinate lyase GN=argH PE=1 SV=3 - [ARLY_ECOLI]
P31120	Phosphoglucosamine mutase GN=glmM PE=1 SV=3 - [GLMM_ECOLI]
P0ABJ9	Cytochrome bd-I ubiquinol oxidase subunit 1 GN=cydA PE=1 SV=1 - [CYDA_ECOLI]
P76216	N-succinylarginine dihydrolase GN=astB PE=1 SV=1 - [ASTB_ECOLI]
P03004	Chromosomal replication initiator protein DnaA GN=dnaA PE=1 SV=2 - [DNAA_ECOLI]
P00909	Tryptophan biosynthesis protein TrpCF GN=trpC PE=1 SV=4 - [TRPC_ECOLI]
P39830	Inner membrane protein YbaL GN=ybaL PE=1 SV=2 - [YBAL_ECOLI]
P03023	Lactose operon repressor GN=lacI PE=1 SV=3 - [LACI_ECOLI]
P06720	Alpha-galactosidase GN=melA PE=1 SV=1 - [AGAL_ECOLI]
P0A6H5	ATP-dependent protease ATPase subunit HslU GN=hslU PE=1 SV=1 - [HSLU_ECOLI]
P02921	Melibiose carrier protein GN=melB PE=1 SV=2 - [MELB_ECOLI]
P25522	tRNA modification GTPase MnmE GN=mnmE PE=1 SV=3 - [MNME_ECOLI]
P10384	Long-chain fatty acid transport protein GN=fadL PE=1 SV=5 - [FADL_ECOLI]
P0AC41	Succinate dehydrogenase flavoprotein subunit GN=sdhA PE=1 SV=1 - [SDHA_ECOLI]
P69776	Major outer membrane lipoprotein Lpp GN=lpp PE=1 SV=1 - [LPP_ECOLI]
P00370	NADP-specific glutamate dehydrogenase GN=gdhA PE=1 SV=1 - [DHE4_ECOLI]
P0AFU4	Transcriptional regulatory protein GlrR GN=glrR PE=1 SV=1 - [GLRR_ECOLI]
P16659	Proline--tRNA ligase GN=proS PE=1 SV=4 - [SYP_ECOLI]
P0AAZ4	Replication-associated recombination protein A GN=rarA PE=1 SV=1 - [RARA_ECOLI]
P0A6Z3	Chaperone protein HtpG GN=htpG PE=1 SV=1 - [HTPG_ECOLI]
P24554	DNA repair protein RadA GN=radA PE=1 SV=1 - [RADA_ECOLI]
P30744	L-serine dehydratase 2 GN=sdaB PE=2 SV=2 - [SDHM_ECOLI]
P0A9T0	D-3-phosphoglycerate dehydrogenase GN=serA PE=1 SV=2 - [SERA_ECOLI]
P23367	DNA mismatch repair protein MutL GN=mutL PE=1 SV=2 - [MUTL_ECOLI]

P30871	Inorganic triphosphatase GN=ygiF PE=1 SV=1 - [3PASE_ECOLI]
P32131	Oxygen-independent coproporphyrinogen III oxidase GN=hemN PE=1 SV=4 - [HEMN_ECOLI]
P0A7I0	Peptide chain release factor RF1 GN=prfA PE=1 SV=1 - [RF1_ECOLI]
P00957	Alanine--tRNA ligase GN=alaS PE=1 SV=2 - [SYA_ECOLI]
P10100	Endolytic peptidoglycan transglycosylase RlpA GN=rlpA PE=1 SV=1 - [RLPA_ECOLI]
P0ABF1	Poly(A) polymerase I GN=pcnB PE=1 SV=2 - [PCNB_ECOLI]
P0AB67	NAD(P) transhydrogenase subunit beta GN=pntB PE=1 SV=1 - [PNTB_ECOLI]
P36929	Ribosomal RNA small subunit methyltransferase B GN=rsmB PE=1 SV=2 - [RSMB_ECOLI]
P11880	UDP-N-acetylmuramoyl-tripeptide--D-alanyl-D-alanine ligase GN=murF PE=1 SV=2 - [MURF_ECOLI]
P14375	Transcriptional regulatory protein ZraR GN=zraR PE=1 SV=2 - [ZRAR_ECOLI]
P0A9Q7	Aldehyde-alcohol dehydrogenase GN=adhE PE=1 SV=2 - [ADHE_ECOLI]
P0ABH7	Citrate synthase GN=gltA PE=1 SV=1 - [CISY_ECOLI]
P0AB89	Adenylosuccinate lyase GN=purB PE=1 SV=1 - [PUR8_ECOLI]
P77671	Allantoinase GN=allB PE=1 SV=1 - [ALLB_ECOLI]

BAND 4

P03023	Lactose operon repressor GN=lacI PE=1 SV=3 - [LACI_ECOLI]
P0A9A6	Cell division protein FtsZ GN=ftsZ PE=1 SV=1 - [FTSZ_ECOLI]
P77690	UDP-4-amino-4-deoxy-L-arabinose--oxoglutarate aminotransferase GN=arnB PE=1 SV=3 - [ARNB_ECOLI]
P0A853	Tryptophanase GN=tnaA PE=1 SV=1 - [TNAA_ECOLI]
P63020	Fe/S biogenesis protein NfuA GN=nfuA PE=1 SV=1 - [NFUA_ECOLI]
P0A7G6	Protein RecA GN=recA PE=1 SV=2 - [RECA_ECOLI]
P0ABH9	ATP-dependent Clp protease ATP-binding subunit ClpA GN=clpA PE=1 SV=1 - [CLPA_ECOLI]
P0AEX9	Maltose-binding periplasmic protein GN=malE PE=1 SV=1 - [MALE_ECOLI]
P62620	4-hydroxy-3-methylbut-2-en-1-yl diphosphate synthase (flavodoxin) GN=ispG PE=1 SV=1 - [ISPG_ECOLI]
P0A799	Phosphoglycerate kinase GN=pgk PE=1 SV=2 - [PGK_ECOLI]
P0A7Z4	DNA-directed RNA polymerase subunit alpha GN=rpoA PE=1 SV=1 - [RPOA_ECOLI]
P0C0V0	Periplasmic serine endoprotease DegP GN=degP PE=1 SV=1 - [DEGP_ECOLI]
P0AEB2	D-alanyl-D-alanine carboxypeptidase DacA GN=dacA PE=1 SV=1 - [DACA_ECOLI]
P23893	Glutamate-1-semialdehyde 2,1-aminomutase GN=hemL PE=1 SV=2 - [GSA_ECOLI]
P0A9K3	PhoH-like protein GN=ybeZ PE=3 SV=2 - [PHOL_ECOLI]
P77581	Succinylornithine transaminase GN=astC PE=1 SV=1 - [ASTC_ECOLI]
P0A836	Succinate--CoA ligase [ADP-forming] subunit beta GN=sucC PE=1 SV=1 - [SUCC_ECOLI]
P08506	D-alanyl-D-alanine carboxypeptidase DacC GN=dacC PE=1 SV=2 - [DACC_ECOLI]
P63284	Chaperone protein ClpB GN=clpB PE=1 SV=1 - [CLPB_ECOLI]
P0CE47	Elongation factor Tu 1 GN=tufA PE=1 SV=1 - [EFTU1_ECOLI]
P0AE37	Arginine N-succinyltransferase GN=astA PE=2 SV=1 - [ASTA_ECOLI]
P0A7B5	Glutamate 5-kinase GN=proB PE=1 SV=1 - [PROB_ECOLI]
P0A9G6	Isocitrate lyase GN=aceA PE=1 SV=1 - [ACEA_ECOLI]
P75863	Uncharacterized protein YcbX GN=ycbX PE=1 SV=1 - [YCBX_ECOLI]
P68187	Maltose/maltodextrin import ATP-binding protein MalK GN=malK PE=1 SV=1 - [MALK_ECOLI]

P0AB77	2-amino-3-ketobutyrate coenzyme A ligase GN=kbl PE=1 SV=1 - [KBL_ECOLI]
P02921	Melibiose carrier protein GN=melB PE=1 SV=2 - [MELB_ECOLI]
P0C8J8	D-tagatose-1,6-bisphosphate aldolase subunit GatZ GN=gatZ PE=1 SV=1 - [GATZ_ECOLI]
P21507	ATP-dependent RNA helicase SrmB GN=srmB PE=1 SV=1 - [SRMB_ECOLI]
P0A9H7	Cyclopropane-fatty-acyl-phospholipid synthase GN=cfa PE=1 SV=2 - [CFA_ECOLI]
P0AAI3	ATP-dependent zinc metalloprotease FtsH GN=ftsH PE=1 SV=1 - [FTSH_ECOLI]
P64612	Cell division protein ZapE GN=zapE PE=1 SV=1 - [ZAPE_ECOLI]
P77258	N-ethylmaleimide reductase GN=nemA PE=2 SV=1 - [NEMA_ECOLI]
P27248	Aminomethyltransferase GN=gcvT PE=1 SV=3 - [GCST_ECOLI]
P0A9J8	P-protein GN=pheA PE=1 SV=1 - [PHEA_ECOLI]
P0A6H1	ATP-dependent Clp protease ATP-binding subunit ClpX GN=clpX PE=1 SV=2 - [CLPX_ECOLI]
P0AEI1	tRNA-2-methylthio-N(6)-dimethylallyladenosine synthase GN=miaB PE=1 SV=1 - [MIAB_ECOLI]
P13009	Methionine synthase GN=metH PE=1 SV=5 - [METH_ECOLI]
P0A6F5	60 kDa chaperonin GN=groL PE=1 SV=2 - [CH60_ECOLI]
P69924	Ribonucleoside-diphosphate reductase 1 subunit beta GN=nrdB PE=1 SV=2 - [RIR2_ECOLI]
P08390	USG-1 protein GN=usg PE=1 SV=1 - [USG_ECOLI]
P0A7V3	30S ribosomal protein S3 GN=rpsC PE=1 SV=2 - [RS3_ECOLI]
P00509	Aspartate aminotransferase GN=aspC PE=1 SV=1 - [AAT_ECOLI]
P18133	Nicotinate phosphoribosyltransferase GN=pncB PE=1 SV=3 - [PNCB_ECOLI]
P33232	L-lactate dehydrogenase GN=lldD PE=1 SV=1 - [LLDD_ECOLI]
P00946	Mannose-6-phosphate isomerase GN=manA PE=1 SV=1 - [MANA_ECOLI]
P0A959	Glutamate-pyruvate aminotransferase AlaA GN=alaA PE=1 SV=1 - [ALAA_ECOLI]
P04693	Aromatic-amino-acid aminotransferase GN=tyrB PE=1 SV=1 - [TYRB_ECOLI]
P03004	Chromosomal replication initiator protein DnaA GN=dnaA PE=1 SV=2 - [DNAA_ECOLI]
P0A7V8	30S ribosomal protein S4 GN=rpsD PE=1 SV=2 - [RS4_ECOLI]
P02916	Maltose transport system permease protein MalF GN=malF PE=1 SV=1 - [MALF_ECOLI]
P0ACB7	Protein HemY GN=hemY PE=1 SV=1 - [HEMY_ECOLI]
P0ABB4	ATP synthase subunit beta GN=atpD PE=1 SV=2 - [ATPB_ECOLI]
P0AG30	Transcription termination factor Rho GN=rho PE=1 SV=1 - [RHO_ECOLI]
P0A6Z3	Chaperone protein HtpG GN=htpG PE=1 SV=1 - [HTPG_ECOLI]
P0A6Y8	Chaperone protein DnaK GN=dnaK PE=1 SV=2 - [DNAK_ECOLI]
P0ABJ9	Cytochrome bd-I ubiquinol oxidase subunit 1 GN=cydA PE=1 SV=1 - [CYDA_ECOLI]
P0AF08	Iron-sulfur cluster carrier protein GN=mrp PE=3 SV=1 - [APBC_ECOLI]
P0A6B7	Cysteine desulfurase IscS GN=iscS PE=1 SV=1 - [ISCS_ECOLI]
P0A6B4	Alanine racemase, biosynthetic GN=alr PE=1 SV=1 - [ALR1_ECOLI]
P10441	Lipid-A-disaccharide synthase GN=lpxB PE=1 SV=2 - [LPXB_ECOLI]
P00961	Glycine--tRNA ligase beta subunit GN=glyS PE=1 SV=4 - [SYGB_ECOLI]
P0A6F3	Glycerol kinase GN=glpK PE=1 SV=2 - [GLPK_ECOLI]
P0ABC7	Modulator of FtsH protease HflK GN=hflK PE=1 SV=1 - [HFLK_ECOLI]
P0AFG6	Dihydrolipoyllysine-residue succinyltransferase comp. of 2-oxoglutarate dehydrogenase complex GN=sucB - [ODO2_ECOLI]
P0AB71	Fructose-bisphosphate aldolase class 2 GN=fbaA PE=1 SV=2 - [ALF_ECOLI]

P75728	2-octaprenyl-3-methyl-6-methoxy-1,4-benzoquinol hydroxylase GN=ubiF PE=1 SV=1 - [UBIF_ECOLI]
P76440	NAD-dependent dihydropyrimidine dehydrogenase subunit PreT GN=preT PE=1 SV=1 - [PRET_ECOLI]
P27306	Soluble pyridine nucleotide transhydrogenase GN=sthA PE=1 SV=5 - [STHA_ECOLI]
P0A6H5	ATP-dependent protease ATPase subunit HslU GN=hslU PE=1 SV=1 - [HSLU_ECOLI]
P00888	Phospho-2-dehydro-3-deoxyheptonate aldolase, Tyr-sensitive GN=aroF PE=1 SV=1 - [AROF_ECOLI]
P00393	NADH dehydrogenase GN=ndh PE=1 SV=2 - [DHNA_ECOLI]
P0AB58	Lipopolysaccharide assembly protein B GN=lapB PE=1 SV=1 - [LAPB_ECOLI]
P37759	dTDP-glucose 4,6-dehydratase 1 GN=rfbB PE=3 SV=2 - [RMLB1_ECOLI]
P27833	dTDP-4-amino-4,6-dideoxygalactose transaminase GN=wecE PE=1 SV=2 - [WECE_ECOLI]
P02943	Maltoporin GN=lamB PE=1 SV=1 - [LAMB_ECOLI]
P0AES6	DNA gyrase subunit B GN=gyrB PE=1 SV=2 - [GYRB_ECOLI]
P24182	Biotin carboxylase GN=accC PE=1 SV=2 - [ACCC_ECOLI]
P0ABU2	Ribosome-binding ATPase YchF GN=ychF PE=1 SV=2 - [YCHF_ECOLI]
P0A6E4	Argininosuccinate synthase GN=argG PE=1 SV=2 - [ASSY_ECOLI]
P16676	Sulfate/thiosulfate import ATP-binding protein CysA GN=cysA PE=3 SV=2 - [CYSA_ECOLI]
P0A6F1	Carbamoyl-phosphate synthase small chain GN=carA PE=1 SV=1 - [CARA_ECOLI]
P16926	Cell shape-determining protein MreC GN=mreC PE=1 SV=1 - [MREC_ECOLI]
P36683	Aconitate hydratase B GN=acnB PE=1 SV=3 - [ACNB_ECOLI]
P76586	Uncharacterized protein YphH GN=yphH PE=3 SV=2 - [YPHH_ECOLI]
P0ABB0	ATP synthase subunit alpha GN=atpA PE=1 SV=1 - [ATPA_ECOLI]
P06720	Alpha-galactosidase GN=melA PE=1 SV=1 - [AGAL_ECOLI]
P36979	Dual-specificity RNA methyltransferase RlmN GN=rlmN PE=1 SV=1 - [RLMN_ECOLI]
P76035	Uncharacterized protein YciW GN=yciW PE=4 SV=2 - [YCIW_ECOLI]
P21179	Catalase HPII GN=katE PE=1 SV=1 - [CATE_ECOLI]

BAND 5

P02931	Outer membrane protein F GN=ompF PE=1 SV=1 - [OMPF_ECOLI]
P63284	Chaperone protein ClpB GN=clpB PE=1 SV=1 - [CLPB_ECOLI]
P03023	Lactose operon repressor GN=lacI PE=1 SV=3 - [LACI_ECOLI]
P0A9A6	Cell division protein FtsZ GN=ftsZ PE=1 SV=1 - [FTSZ_ECOLI]
P63020	Fe/S biogenesis protein NfuA GN=nfuA PE=1 SV=1 - [NFUA_ECOLI]
P33920	Nucleoid-associated protein YejK GN=yejK PE=1 SV=3 - [NDPA_ECOLI]
P00963	Aspartate--ammonia ligase GN=asnA PE=1 SV=1 - [ASNA_ECOLI]
P0C8J8	D-tagatose-1,6-bisphosphate aldolase subunit GatZ GN=gatZ PE=1 SV=1 - [GATZ_ECOLI]
P0AEX9	Maltose-binding periplasmic protein GN=malE PE=1 SV=1 - [MALE_ECOLI]
P0CE47	Elongation factor Tu 1 GN=tufA PE=1 SV=1 - [EFTU1_ECOLI]
P0A9X4	Rod shape-determining protein MreB GN=mreB PE=1 SV=1 - [MREB_ECOLI]
P0A870	Transaldolase B GN=talB PE=1 SV=2 - [TALB_ECOLI]
P0A7Z4	DNA-directed RNA polymerase subunit alpha GN=rpoA PE=1 SV=1 - [RPOA_ECOLI]
P0A812	Holliday junction ATP-dependent DNA helicase RuvB GN=ruvB PE=1 SV=1 - [RUVB_ECOLI]
P07639	3-dehydroquinate synthase GN=aroB PE=1 SV=1 - [AROB_ECOLI]

P67910	ADP-L-glycero-D-manno-heptose-6-epimerase GN=hldD PE=1 SV=1 - [HLDD_ECOLI]
P0AB71	Fructose-bisphosphate aldolase class 2 GN=fbaA PE=1 SV=2 - [ALF_ECOLI]
P0AEP3	UTP--glucose-1-phosphate uridylyltransferase GN=galU PE=1 SV=2 - [GALU_ECOLI]
P0ABC3	Modulator of FtsH protease HflC GN=hflC PE=1 SV=1 - [HFLC_ECOLI]
P0ABH9	ATP-dependent Clp protease ATP-binding subunit ClpA GN=clpA PE=1 SV=1 - [CLPA_ECOLI]
P0A7G6	Protein RecA GN=recA PE=1 SV=2 - [RECA_ECOLI]
P77690	UDP-4-amino-4-deoxy-L-arabinose--oxoglutarate aminotransferase GN=arnB PE=1 SV=3 - [ARNB_ECOLI]
P77735	Uncharacterized oxidoreductase YajO GN=yajO PE=3 SV=2 - [YAJO_ECOLI]
P0A9S3	Galactitol-1-phosphate 5-dehydrogenase GN=gatD PE=1 SV=1 - [GATD_ECOLI]
P39406	Ribosomal RNA small subunit methyltransferase C GN=rsmC PE=1 SV=3 - [RSMC_ECOLI]
P23893	Glutamate-1-semialdehyde 2,1-aminomutase GN=hemL PE=1 SV=2 - [GSA_ECOLI]
P0A993	Fructose-1,6-bisphosphatase class 1 GN=fbp PE=1 SV=1 - [F16PA_ECOLI]
P0ABB4	ATP synthase subunit beta GN=atpD PE=1 SV=2 - [ATPB_ECOLI]
P76372	Chain length determinant protein GN=wzzB PE=1 SV=2 - [WZZB_ECOLI]
P0AG30	Transcription termination factor Rho GN=rho PE=1 SV=1 - [RHO_ECOLI]
P30011	Nicotinate-nucleotide pyrophosphorylase [carboxylating] GN=nadC PE=3 SV=7 - [NADC_ECOLI]
P77488	1-deoxy-D-xylulose-5-phosphate synthase GN=dxs PE=1 SV=3 - [DXS_ECOLI]
P17443	UDP-N-acetylglucosamine--N-acetylmuramyl-(pentapeptide) pyrophosphoryl-undecaprenol N-acetylglucosamine transferase GN=murG
P75777	UPF0194 membrane protein YbhG GN=ybhG[YBHG_ECOLI]
P0AAC0	Universal stress protein E GN=uspE PE=1 SV=2 - [USPE_ECOLI]
P69831	PTS system galactitol-specific EIIC component GN=gatC PE=1 SV=1 - [PTKC_ECOLI]
P02921	Melibiose carrier protein GN=melB PE=1 SV=2 - [MELB_ECOLI]
P75863	Uncharacterized protein YcbX GN=ycbX PE=1 SV=1 - [YCBX_ECOLI]
P0A853	Tryptophanase GN=tnaA PE=1 SV=1 - [TNAA_ECOLI]
P22333	Adenosine deaminase GN=add PE=3 SV=2 - [ADD_ECOLI]
P0A7B5	Glutamate 5-kinase GN=proB PE=1 SV=1 - [PROB_ECOLI]
P0A991	Fructose-bisphosphate aldolase class 1 GN=fbaB PE=1 SV=2 - [ALF1_ECOLI]
P00960	Glycine--tRNA ligase alpha subunit GN=glyQ PE=1 SV=2 - [SYGA_ECOLI]
P0AEI1	tRNA-2-methylthio-N(6)-dimethylallyladenosine synthase GN=miaB PE=1 SV=1 - [MIAB_ECOLI]
P77774	Outer membrane protein assembly factor BamB GN=bamB PE=1 SV=1 - [BAMB_ECOLI]
P08839	Phosphoenolpyruvate-protein phosphotransferase GN=ptsI PE=1 SV=1 - [PT1_ECOLI]
P0A7V3	30S ribosomal protein S3 GN=rpsC PE=1 SV=2 - [RS3_ECOLI]
P08312	Phenylalanine--tRNA ligase alpha subunit GN=pheS PE=1 SV=2 - [SYFA_ECOLI]
P0AGJ5	Uncharacterized tRNA/rRNA methyltransferase YfiF GN=yfiF PE=3 SV=1 - [YFIF_ECOLI]
P77256	Uncharacterized oxidoreductase YdjG GN=ydjG PE=3 SV=1 - [YDJG_ECOLI]
P75949	Beta-hexosaminidase GN=nagZ PE=1 SV=1 - [NAGZ_ECOLI]
P0AGB0	Phosphoserine phosphatase GN=serB PE=1 SV=1 - [SERB_ECOLI]
P0A910	Outer membrane protein A GN=ompA PE=1 SV=1 - [OMPA_ECOLI]
P02943	Maltoporin GN=lamB PE=1 SV=1 - [LAMB_ECOLI]
P78061	Gamma-glutamylputrescine synthetase PuuA GN=puuA PE=1 SV=2 - [PUUA_ECOLI]
P06999	ATP-dependent 6-phosphofructokinase isozyme 2 GN=pfkB PE=1 SV=2 - [PFKB_ECOLI]

P0AGA2	Protein translocase subunit SecY GN=secY PE=1 SV=1 - [SECY_ECOLI]
P0A6Y8	Chaperone protein DnaK GN=dnaK PE=1 SV=2 - [DNAK_ECOLI]
P60716	Lipoyl synthase GN=lipA PE=1 SV=1 - [LIPA_ECOLI]
P06983	Porphobilinogen deaminase GN=hemC PE=1 SV=2 - [HEM3_ECOLI]
P0AG67	30S ribosomal protein S1 GN=rpsA PE=1 SV=1 - [RS1_ECOLI]
P77757	Undecaprenyl-phosphate 4-deoxy-4-formamido-L-arabinose transferase GN=arnC PE=1 SV=1 - [ARNC_ECOLI]
P77529	L-cystine transporter YdjN GN=ydjN PE=3 SV=1 - [YDJN_ECOLI]
P0AG00	ECA polysaccharide chain length modulation protein GN=wzzE PE=1 SV=2 - [WZZE_ECOLI]
P10441	Lipid-A-disaccharide synthase GN=lpxB PE=1 SV=2 - [LPXB_ECOLI]
P0A6Z3	Chaperone protein HtpG GN=htpG PE=1 SV=1 - [HTPG_ECOLI]
P0A6H1	ATP-dependent Clp protease ATP-binding subunit ClpX GN=clpX PE=1 SV=2 - [CLPX_ECOLI]
P0AFG6	Dihydrolipoyllysine-residue succinyltransferase component of 2-oxoglutarate dehydrogenase complex GN=sucB PE=1 SV=2 - [ODO2_ECOLI]
P76113	NADPH-dependent curcumin reductase GN=curA PE=1 SV=3 - [CURA_ECOLI]
P0AAI3	ATP-dependent zinc metalloprotease FtsH GN=ftsH PE=1 SV=1 - [FTSH_ECOLI]
P69811	Multiphosphoryl transfer protein GN=fruB PE=1 SV=1 - [PTFAH_ECOLI]
P00888	Phospho-2-dehydro-3-deoxyheptonate aldolase, Tyr-sensitive GN=aroF PE=1 SV=1 - [AROF_ECOLI]
P37313	Dipeptide transport ATP-binding protein DppF GN=dppF PE=3 SV=1 - [DPPF_ECOLI]
P0ADC3	Lipoprotein-releasing system transmembrane protein LolC GN=lolC PE=1 SV=1 - [LOLC_ECOLI]
P0AAE0	D-serine/D-alanine/glycine transporter GN=cycA PE=1 SV=1 - [CYCA_ECOLI]
P0A9B2	Glyceraldehyde-3-phosphate dehydrogenase A GN=gapA PE=1 SV=2 - [G3P1_ECOLI]
P69776	Major outer membrane lipoprotein Lpp GN=lpp PE=1 SV=1 - [LPP_ECOLI]
P0ADE8	tRNA-modifying protein YgfZ GN=ygfZ PE=1 SV=2 - [YGFZ_ECOLI]
P76193	Probable L,D-transpeptidase YnhG GN=ynhG PE=1 SV=1 - [YNHG_ECOLI]
P0A7V8	30S ribosomal protein S4 GN=rpsD PE=1 SV=2 - [RS4_ECOLI]
P0ADV5	Uncharacterized protein YhbW GN=yhbW PE=4 SV=1 - [YHBW_ECOLI]
P0A6F3	Glycerol kinase GN=glpK PE=1 SV=2 - [GLPK_ECOLI]
Q46851	L-glyceraldehyde 3-phosphate reductase GN=gpr PE=1 SV=1 - [GPR_ECOLI]
P0A7E1	Dihydroorotate dehydrogenase (quinone) GN=pyrD PE=1 SV=1 - [PYRD_ECOLI]
P0A9P0	Dihydrolipoyl dehydrogenase GN=lpdA PE=1 SV=2 - [DLDH_ECOLI]
P77581	Succinylornithine transaminase GN=astC PE=1 SV=1 - [ASTC_ECOLI]
P23871	Ferrochelatase GN=hemH PE=1 SV=3 - [HEMH_ECOLI]
P08622	Chaperone protein DnaJ GN=dnaJ PE=1 SV=3 - [DNAJ_ECOLI]
P76440	NAD-dependent dihydropyrimidine dehydrogenase subunit PreT GN=preT PE=1 SV=1 - [PRET_ECOLI]
P29131	Cell division protein FtsN GN=ftsN PE=1 SV=3 - [FTSN_ECOLI]
P76055	tRNA 2-thiocytidine biosynthesis protein TtcA GN=ttcA PE=1 SV=1 - [TTCA_ECOLI]
P60422	50S ribosomal protein L2 GN=rplB PE=1 SV=2 - [RL2_ECOLI]
P06720	Alpha-galactosidase GN=melA PE=1 SV=1 - [AGAL_ECOLI]
P0A698	UvrABC system protein A GN=uvrA PE=1 SV=1 - [UVRA_ECOLI]
P00934	Threonine synthase GN=thrC PE=1 SV=1 - [THRC_ECOLI]
P27247	Phosphate acyltransferase GN=plsX PE=1 SV=2 - [PLSX_ECOLI]
P39451	Alcohol dehydrogenase, propanol-preferring GN=adhP PE=1 SV=1 - [ADHP_ECOLI]

P25748	HTH-type transcriptional regulator GalS GN=galS PE=1 SV=2 - [GALS_ECOLI]
P0AES6	DNA gyrase subunit B GN=gyrB PE=1 SV=2 - [GYRB_ECOLI]
P17802	Adenine DNA glycosylase GN=mutY PE=1 SV=1 - [MUTY_ECOLI]
P76116	Uncharacterized protein YncE GN=yncE PE=1 SV=1 - [YNCE_ECOLI]
P0AFB5	Nitrogen regulation protein NR(II) GN=glnL PE=1 SV=1 - [NTRB_ECOLI]
P60785	Elongation factor 4 GN=lepA PE=1 SV=1 - [LEPA_ECOLI]
P10907	sn-glycerol-3-phosphate import ATP-binding protein UgpC GN=ugpC PE=1 SV=3 - [UGPC_ECOLI]
P08178	Phosphoribosylformylglycinamidine cyclo-ligase GN=purM PE=1 SV=3 - [PUR5_ECOLI]
P0ADQ2	Uncharacterized protein YiiD GN=yiiD PE=3 SV=1 - [YIID_ECOLI]
P76027	Oligopeptide transport ATP-binding protein OppD GN=oppD PE=3 SV=2 - [OPPD_ECOLI]
Q46802	Uncharacterized sigma-54-dependent transcriptional regulator YgeV GN=ygeV PE=3 SV=1 - [YGEV_ECOLI]
P0A9C9	Fructose-1,6-bisphosphatase 1 class 2 GN=glpX PE=1 SV=1 - [GLPX_ECOLI]
P27248	Aminomethyltransferase GN=gcvT PE=1 SV=3 - [GCST_ECOLI]
P62620	4-hydroxy-3-methylbut-2-en-1-yl diphosphate synthase (flavodoxin) GN=ispG PE=1 SV=1 - [ISPG_ECOLI]
P0A850	Trigger factor GN=tig PE=1 SV=1 - [TIG_ECOLI]
P16456	Selenide, water dikinase GN=selD PE=1 SV=1 - [SELD_ECOLI]
P27300	Tetraacyldisaccharide 4'-kinase GN=lpxK PE=1 SV=2 - [LPXK_ECOLI]
Q57261	tRNA pseudouridine synthase D GN=truD PE=1 SV=1 - [TRUD_ECOLI]
P03004	Chromosomal replication initiator protein DnaA GN=dnaA PE=1 SV=2 - [DNAA_ECOLI]
P23721	Phosphoserine aminotransferase GN=serC PE=1 SV=4 - [SERC_ECOLI]
P0A9P6	ATP-dependent RNA helicase DeaD GN=deaD PE=1 SV=2 - [DEAD_ECOLI]
P23524	Glycerate 2-kinase GN=garK PE=1 SV=2 - [GLXK1_ECOLI]
P0AG14	Probable protease SohB GN=sohB PE=1 SV=1 - [SOHB_ECOLI]
P24182	Biotin carboxylase GN=accC PE=1 SV=2 - [ACCC_ECOLI]
P11446	N-acetyl-gamma-glutamyl-phosphate reductase GN=argC PE=3 SV=1 - [ARGC_ECOLI]
P0C0V0	Periplasmic serine endoprotease DegP GN=degP PE=1 SV=1 - [DEGP_ECOLI]
P37047	Carbohydrate diacid regulator GN=cdaR PE=1 SV=2 - [CDAR_ECOLI]
P0ABU2	Ribosome-binding ATPase YchF GN=ychF PE=1 SV=2 - [YCHF_ECOLI]
P28630	DNA polymerase III subunit delta GN=holA PE=1 SV=1 - [HOLA_ECOLI]
P0A6P5	GTPase Der GN=der PE=1 SV=1 - [DER_ECOLI]
P37626	Uncharacterized protein YhiI GN=yhiI PE=3 SV=1 - [YHII_ECOLI]
P00803	Signal peptidase I GN=lepB PE=1 SV=2 - [LEP_ECOLI]
P76035	Uncharacterized protein YciW GN=yciW PE=4 SV=2 - [YCIW_ECOLI]
P37344	Psp operon transcriptional activator GN=pspF PE=1 SV=2 - [PSPF_ECOLI]
P29012	Alanine racemase, catabolic GN=dadX PE=2 SV=2 - [ALR2_ECOLI]
P75823	Low specificity L-threonine aldolase GN=ltaE PE=1 SV=1 - [LTAE_ECOLI]

BAND 6

P63020	Fe/S biogenesis protein NfuA GN=nfuA PE=1 SV=1 - [NFUA_ECOLI]
P0A7V3	30S ribosomal protein S3 GN=rpsC PE=1 SV=2 - [RS3_ECOLI]
P28635	D-methionine-binding lipoprotein MetQ GN=metQ PE=1 SV=2 - [METQ_ECOLI]

P0A858	Triosephosphate isomerase GN=tpiA PE=1 SV=1 - [TPIS_ECOLI]
P0A7L0	50S ribosomal protein L1 GN=rplA PE=1 SV=2 - [RL1_ECOLI]
P0A877	Tryptophan synthase alpha chain GN=trpA PE=1 SV=1 - [TRPA_ECOLI]
P0AA16	Transcriptional regulatory protein OmpR GN=ompR PE=1 SV=1 - [OMPR_ECOLI]
P23836	Transcriptional regulatory protein PhoP GN=phoP PE=1 SV=1 - [PHOP_ECOLI]
P07014	Succinate dehydrogenase iron-sulfur subunit GN=sdhB PE=1 SV=1 - [SDHB_ECOLI]
P76422	Hydroxymethylpyrimidine/phosphomethylpyrimidine kinase GN=thiD PE=1 SV=1 - [THID_ECOLI]
P0ABA6	ATP synthase gamma chain GN=atpG PE=1 SV=1 - [ATPG_ECOLI]
P0A6I0	Cytidylate kinase GN=cmk PE=1 SV=1 - [KCY_ECOLI]
P69805	PTS system mannose-specific EIID component GN=manZ PE=1 SV=2 - [PTND_ECOLI]
P0A910	Outer membrane protein A GN=ompA PE=1 SV=1 - [OMPA_ECOLI]
P69441	Adenylate kinase GN=adk PE=1 SV=1 - [KAD_ECOLI]
P0A7V8	30S ribosomal protein S4 GN=rpsD PE=1 SV=2 - [RS4_ECOLI]
P0A8V6	Fatty acid metabolism regulator protein GN=fadR PE=1 SV=2 - [FADR_ECOLI]
P0A6F3	Glycerol kinase GN=glpK PE=1 SV=2 - [GLPK_ECOLI]
P12758	Uridine phosphorylase GN=udp PE=1 SV=3 - [UDP_ECOLI]
P0A7V0	30S ribosomal protein S2 GN=rpsB PE=1 SV=2 - [RS2_ECOLI]
P0A7D7	Phosphoribosylaminoimidazole-succinocarboxamide synthase GN=purC PE=1 SV=1 - [PUR7_ECOLI]
P0AG30	Transcription termination factor Rho GN=rho PE=1 SV=1 - [RHO_ECOLI]
P02925	Ribose import binding protein RbsB GN=rbsB PE=1 SV=1 - [RBSB_ECOLI]
P0A9K9	FKBP-type peptidyl-prolyl cis-trans isomerase SlyD GN=slyD PE=1 SV=1 - [SLYD_ECOLI]
P0A8K1	Phosphatidylserine decarboxylase proenzyme GN=psd PE=1 SV=1 - [PSD_ECOLI]
P0AFM6	Phage shock protein A GN=pspA PE=1 SV=2 - [PSPA_ECOLI]
P07109	Histidine transport ATP-binding protein HisP GN=hisP PE=1 SV=2 - [HISP_ECOLI]
P0CE47	Elongation factor Tu 1 GN=tufA PE=1 SV=1 - [EFTU1_ECOLI]
P77739	Uncharacterized protein YniA GN=yniA PE=3 SV=1 - [YNIA_ECOLI]
P39831	NADP-dependent 3-hydroxy acid dehydrogenase YdfG GN=ydfG PE=1 SV=2 - [YDFG_ECOLI]
P00561	Bifunctional aspartokinase/homoserine dehydrogenase 1 GN=thrA PE=1 SV=2 - [AK1H_ECOLI]
P0A9A6	Cell division protein FtsZ GN=ftsZ PE=1 SV=1 - [FTSZ_ECOLI]
P0AC02	Outer membrane protein assembly factor BamD GN=bamD PE=1 SV=1 - [BAMD_ECOLI]
P0A6C8	Acetylglutamate kinase GN=argB PE=1 SV=1 - [ARGB_ECOLI]
P77756	7-cyano-7-deazaguanine synthase GN=queC PE=1 SV=1 - [QUEC_ECOLI]
P68739	Endonuclease V GN=nfi PE=1 SV=1 - [NFI_ECOLI]
P76034	Uncharacterized HTH-type transcriptional regulator YciT GN=yciT PE=3 SV=1 - [YCIT_ECOLI]
P03023	Lactose operon repressor GN=lacI PE=1 SV=3 - [LACI_ECOLI]
P0A908	MltA-interacting protein GN=mipA PE=1 SV=1 - [MIPA_ECOLI]
P10346	Glutamine transport ATP-binding protein GlnQ GN=glnQ PE=1 SV=1 - [GLNQ_ECOLI]
P60438	50S ribosomal protein L3 GN=rplC PE=1 SV=1 - [RL3_ECOLI]
P39383	Uncharacterized protein YjiL GN=yjiL PE=4 SV=2 - [YJIL_ECOLI]
P0A8W0	Transcriptional regulator NanR GN=nanR PE=3 SV=1 - [NANR_ECOLI]
P0ACA3	Stringent starvation protein A GN=sspA PE=1 SV=2 - [SSPA_ECOLI]

P0A9P9	Gluconate 5-dehydrogenase GN=idnO PE=3 SV=1 - [IDNO_ECOLI]
P04846	Lipoprotein 28 GN=nlpA PE=1 SV=1 - [NLPA_ECOLI]
P0AEN1	NAD(P)H-flavin reductase GN=fre PE=1 SV=2 - [FRE_ECOLI]
P62707	2,3-bisphosphoglycerate-dependent phosphoglycerate mutase GN=gpmA PE=1 SV=2 - [GPMA_ECOLI]
P06720	Alpha-galactosidase GN=melA PE=1 SV=1 - [AGAL_ECOLI]
P0AFC7	NADH-quinone oxidoreductase subunit B GN=nuoB PE=1 SV=1 - [NUOB_ECOLI]
P34209	Protein YdcF GN=ydcF PE=1 SV=3 - [YDCF_ECOLI]
P0C0S1	Small-conductance mechanosensitive channel GN=mscS PE=1 SV=1 - [MSCS_ECOLI]
P17854	Phosphoadenosine phosphosulfate reductase GN=cysH PE=1 SV=3 - [CYSH_ECOLI]
P31808	Uncharacterized oxidoreductase YciK GN=yciK PE=1 SV=3 - [YCIK_ECOLI]
P0ACJ8	cAMP-activated global transcriptional regulator CRP GN=crp PE=1 SV=1 - [CRP_ECOLI]
P0C8J8	D-tagatose-1,6-bisphosphate aldolase subunit GatZ GN=gatZ PE=1 SV=1 - [GATZ_ECOLI]
P77499	Probable ATP-dependent transporter SufC GN=sufC PE=1 SV=1 - [SUFC_ECOLI]
P0A9N4	Pyruvate formate-lyase 1-activating enzyme GN=pflA PE=1 SV=2 - [PFLA_ECOLI]

BAND 7

P63020	Fe/S biogenesis protein NfuA GN=nfuA PE=1 SV=1 - [NFUA_ECOLI]
P69776	Major outer membrane lipoprotein Lpp GN=lpp PE=1 SV=1 - [LPP_ECOLI]
P0A7R5	30S ribosomal protein S10 GN=rpsJ PE=1 SV=1 - [RS10_ECOLI]
P69828	PTS system galactitol-specific EIIA component GN=gatA PE=1 SV=1 - [PTKA_ECOLI]
P0A905	Outer membrane lipoprotein SlyB GN=slyB PE=2 SV=1 - [SLYB_ECOLI]
P0A7K6	50S ribosomal protein L19 GN=rplS PE=1 SV=2 - [RL19_ECOLI]
P0A7W1	30S ribosomal protein S5 GN=rpsE PE=1 SV=2 - [RS5_ECOLI]
P0AEK2	3-oxoacyl-[acyl-carrier-protein] reductase FabG GN=fabG PE=1 SV=1 - [FABG_ECOLI]
P0ADY3	50S ribosomal protein L14 GN=rplN PE=1 SV=1 - [RL14_ECOLI]
P61175	50S ribosomal protein L22 GN=rplV PE=1 SV=1 - [RL22_ECOLI]
P0AEZ3	Septum site-determining protein MinD GN=minD PE=1 SV=2 - [MIND_ECOLI]
P62768	UPF0325 protein YaeH GN=yaeH PE=3 SV=1 - [YAEH_ECOLI]
P0A6C8	Acetylglutamate kinase GN=argB PE=1 SV=1 - [ARGB_ECOLI]
P0A7K2	50S ribosomal protein L7/L12 GN=rplL PE=1 SV=2 - [RL7_ECOLI]
P0ACF8	DNA-binding protein H-NS GN=hns PE=1 SV=2 - [HNS_ECOLI]
P0A7S9	30S ribosomal protein S13 GN=rpsM PE=1 SV=2 - [RS13_ECOLI]
P0A6X3	RNA-binding protein Hfq GN=hfq PE=1 SV=2 - [HFQ_ECOLI]
P0A734	Cell division topological specificity factor GN=minE PE=1 SV=1 - [MINE_ECOLI]
P0ADE6	Uncharacterized protein YgaU GN=ygaU PE=1 SV=2 - [YGAU_ECOLI]
P0A6D0	Arginine repressor GN=argR PE=1 SV=1 - [ARGR_ECOLI]
P39831	NADP-dependent 3-hydroxy acid dehydrogenase YdfG GN=ydfG PE=1 SV=2 - [YDFG_ECOLI]
P0A780	N utilization substance protein B GN=nusB PE=1 SV=1 - [NUSB_ECOLI]
P60624	50S ribosomal protein L24 GN=rplX PE=1 SV=2 - [RL24_ECOLI]
P0A7T7	30S ribosomal protein S18 GN=rpsR PE=1 SV=2 - [RS18_ECOLI]
P0A6E6	ATP synthase epsilon chain GN=atpC PE=1 SV=2 - [ATPE_ECOLI]

P02359	30S ribosomal protein S7 GN=rpsG PE=1 SV=3 - [RS7_ECOLI]
P0A7R1	50S ribosomal protein L9 GN=rplI PE=1 SV=1 - [RL9_ECOLI]
P69441	Adenylate kinase GN=adk PE=1 SV=1 - [KAD_ECOLI]
P0ABA4	ATP synthase subunit delta GN=atpH PE=1 SV=1 - [ATPD_ECOLI]
P0A7W7	30S ribosomal protein S8 GN=rpsH PE=1 SV=2 - [RS8_ECOLI]
P0A910	Outer membrane protein A GN=ompA PE=1 SV=1 - [OMPA_ECOLI]
P0A763	Nucleoside diphosphate kinase GN=ndk PE=1 SV=2 - [NDK_ECOLI]
P76268	Transcriptional regulator KdgR GN=kdgR PE=1 SV=1 - [KDGR_ECOLI]
P0AEH5	Protein ElaB GN=elaB PE=1 SV=1 - [ELAB_ECOLI]
P0AG30	Transcription termination factor Rho GN=rho PE=1 SV=1 - [RHO_ECOLI]
P76373	UDP-glucose 6-dehydrogenase GN=ugd PE=1 SV=1 - [UDG_ECOLI]
P0C018	50S ribosomal protein L18 GN=rplR PE=1 SV=1 - [RL18_ECOLI]
P0AED0	Universal stress protein A GN=uspA PE=1 SV=2 - [USPA_ECOLI]
P0A8W2	Transcriptional regulator SlyA GN=slyA PE=3 SV=1 - [SLYA_ECOLI]

BAND 8

P0AFG8	Pyruvate dehydrogenase E1 component GN=aceE PE=1 SV=2 - [ODP1_ECOLI]
P0A9Q7	Aldehyde-alcohol dehydrogenase GN=adhE PE=1 SV=2 - [ADHE_ECOLI]
P63020	Fe/S biogenesis protein NfuA GN=nfuA PE=1 SV=1 - [NFUA_ECOLI]
P36683	Aconitate hydratase B GN=acnB PE=1 SV=3 - [ACNB_ECOLI]
P33602	NADH-quinone oxidoreductase subunit G GN=nuoG PE=1 SV=4 - [NUOG_ECOLI]
P10408	Protein translocase subunit SecA GN=secA PE=1 SV=2 - [SECA_ECOLI]
P0AES4	DNA gyrase subunit A GN=gyrA PE=1 SV=1 - [GYRA_ECOLI]
P0AFG3	2-oxoglutarate dehydrogenase E1 component GN=sucA PE=1 SV=1 - [ODO1_ECOLI]
P0A6Y8	Chaperone protein DnaK GN=dnaK PE=1 SV=2 - [DNAK_ECOLI]
P0AES6	DNA gyrase subunit B GN=gyrB PE=1 SV=2 - [GYRB_ECOLI]
P0A6M8	Elongation factor G GN=fusA PE=1 SV=2 - [EFG_ECOLI]
P05055	Polyribonucleotide nucleotidyltransferase GN=pnp PE=1 SV=3 - [PNP_ECOLI]
P10121	Signal recognition particle receptor FtsY GN=ftsY PE=1 SV=1 - [FTSY_ECOLI]
P13009	Methionine synthase GN=metH PE=1 SV=5 - [METH_ECOLI]
P0A940	Outer membrane protein assembly factor BamA GN=bamA PE=1 SV=1 - [BAMA_ECOLI]
P63284	Chaperone protein ClpB GN=clpB PE=1 SV=1 - [CLPB_ECOLI]
P0A705	Translation initiation factor IF-2 GN=infB PE=1 SV=1 - [IF2_ECOLI]
P06959	Dihydrolipoyllysine-residue acetyltransferase comp. of pyruvate dehydrogenase complex GN=aceF[ODP2_ECOLI]
P31224	Multidrug efflux pump subunit AcrB GN=acrB PE=1 SV=1 - [ACRB_ECOLI]
P00968	Carbamoyl-phosphate synthase large chain GN=carB PE=1 SV=2 - [CARB_ECOLI]
P33195	Glycine dehydrogenase (decarboxylating) GN=gcvP PE=1 SV=3 - [GCSP_ECOLI]
P23909	DNA mismatch repair protein MutS GN=mutS PE=1 SV=1 - [MUTS_ECOLI]
P00582	DNA polymerase I GN=polA PE=1 SV=1 - [DPO1_ECOLI]
P0A9P6	ATP-dependent RNA helicase DeaD GN=deaD PE=1 SV=2 - [DEAD_ECOLI]
P32176	Formate dehydrogenase-O major subunit GN=fdoG PE=1 SV=5 - [FDOG_ECOLI]

P09546	Bifunctional protein PutA GN=putA PE=1 SV=3 - [PUTA_ECOLI]
P0ABJ9	Cytochrome bd-I ubiquinol oxidase subunit 1 GN=cydA PE=1 SV=1 - [CYDA_ECOLI]
P31554	LPS-assembly protein LptD GN=lptD PE=1 SV=2 - [LPTD_ECOLI]
P0A6F5	60 kDa chaperonin GN=groL PE=1 SV=2 - [CH60_ECOLI]
P60785	Elongation factor 4 GN=lepA PE=1 SV=1 - [LEPA_ECOLI]
P0ABB8	Magnesium-transporting ATPase, P-type 1 GN=mgtA PE=1 SV=1 - [ATMA_ECOLI]
P06612	DNA topoisomerase 1 GN=topA PE=1 SV=2 - [TOP1_ECOLI]
P00957	Alanine--tRNA ligase GN=alaS PE=1 SV=2 - [SYA_ECOLI]
P0A7V3	30S ribosomal protein S3 GN=rpsC PE=1 SV=2 - [RS3_ECOLI]
P02931	Outer membrane protein F GN=ompF PE=1 SV=1 - [OMPF_ECOLI]
P0CE47	Elongation factor Tu 1 GN=tufA PE=1 SV=1 - [EFTU1_ECOLI]

BAND 9

P03023	Lactose operon repressor GN=lacI PE=1 SV=3 - [LACI_ECOLI]
P0A9A6	Cell division protein FtsZ GN=ftsZ PE=1 SV=1 - [FTSZ_ECOLI]
P77690	UDP-4-amino-4-deoxy-L-arabinose--oxoglutarate aminotransferase GN=arnB PE=1 SV=3 - [ARNB_ECOLI]
P0A853	Tryptophanase GN=tnaA PE=1 SV=1 - [TNAA_ECOLI]
P63020	Fe/S biogenesis protein NfuA GN=nfuA PE=1 SV=1 - [NFUA_ECOLI]
P0A7G6	Protein RecA GN=recA PE=1 SV=2 - [RECA_ECOLI]
P0ABH9	ATP-dependent Clp protease ATP-binding subunit ClpA GN=clpA PE=1 SV=1 - [CLPA_ECOLI]
P0AEX9	Maltose-binding periplasmic protein GN=malE PE=1 SV=1 - [MALE_ECOLI]
P62620	4-hydroxy-3-methylbut-2-en-1-yl diphosphate synthase (flavodoxin) GN=ispG PE=1 SV=1 - [ISPG_ECOLI]
P0A799	Phosphoglycerate kinase GN=pgk PE=1 SV=2 - [PGK_ECOLI]
P0A7Z4	DNA-directed RNA polymerase subunit alpha GN=rpoA PE=1 SV=1 - [RPOA_ECOLI]
P0C0V0	Periplasmic serine endoprotease DegP GN=degP PE=1 SV=1 - [DEGP_ECOLI]
P0AEB2	D-alanyl-D-alanine carboxypeptidase DacA GN=dacA PE=1 SV=1 - [DACA_ECOLI]
P23893	Glutamate-1-semialdehyde 2,1-aminomutase GN=hemL PE=1 SV=2 - [GSA_ECOLI]
P0A9K3	PhoH-like protein GN=ybeZ PE=3 SV=2 - [PHOL_ECOLI]
P77581	Succinylornithine transaminase GN=astC PE=1 SV=1 - [ASTC_ECOLI]
P0A836	Succinate--CoA ligase [ADP-forming] subunit beta GN=sucC PE=1 SV=1 - [SUCC_ECOLI]
P08506	D-alanyl-D-alanine carboxypeptidase DacC GN=dacC PE=1 SV=2 - [DACC_ECOLI]
P63284	Chaperone protein ClpB GN=clpB PE=1 SV=1 - [CLPB_ECOLI]
P0CE47	Elongation factor Tu 1 GN=tufA PE=1 SV=1 - [EFTU1_ECOLI]
P0AE37	Arginine N-succinyltransferase GN=astA PE=2 SV=1 - [ASTA_ECOLI]
P0A7B5	Glutamate 5-kinase GN=proB PE=1 SV=1 - [PROB_ECOLI]
P0A9G6	Isocitrate lyase GN=aceA PE=1 SV=1 - [ACEA_ECOLI]
P75863	Uncharacterized protein YcbX GN=ycbX PE=1 SV=1 - [YCBX_ECOLI]
P68187	Maltose/maltodextrin import ATP-binding protein MalK GN=malK PE=1 SV=1 - [MALK_ECOLI]
P0AB77	2-amino-3-ketobutyrate coenzyme A ligase GN=kbl PE=1 SV=1 - [KBL_ECOLI]
P02921	Melibiose carrier protein GN=melB PE=1 SV=2 - [MELB_ECOLI]
P0C8J8	D-tagatose-1,6-bisphosphate aldolase subunit GatZ GN=gatZ PE=1 SV=1 - [GATZ_ECOLI]

P21507	ATP-dependent RNA helicase SrmB GN=srmB PE=1 SV=1 - [SRMB_ECOLI]
P0A9H7	Cyclopropane-fatty-acyl-phospholipid synthase GN=cfa PE=1 SV=2 - [CFA_ECOLI]
P0AAI3	ATP-dependent zinc metalloprotease FtsH GN=ftsH PE=1 SV=1 - [FTSH_ECOLI]
P64612	Cell division protein ZapE GN=zapE PE=1 SV=1 - [ZAPE_ECOLI]
P77258	N-ethylmaleimide reductase GN=nemA PE=2 SV=1 - [NEMA_ECOLI]
P27248	Aminomethyltransferase GN=gcvT PE=1 SV=3 - [GCST_ECOLI]
P0A9J8	P-protein GN=pheA PE=1 SV=1 - [PHEA_ECOLI]
P0A6H1	ATP-dependent Clp protease ATP-binding subunit ClpX GN=clpX PE=1 SV=2 - [CLPX_ECOLI]
P0AEI1	tRNA-2-methylthio-N(6)-dimethylallyladenosine synthase GN=miaB PE=1 SV=1 - [MIAB_ECOLI]
P13009	Methionine synthase GN=metH PE=1 SV=5 - [METH_ECOLI]
P0A6F5	60 kDa chaperonin GN=groL PE=1 SV=2 - [CH60_ECOLI]
P69924	Ribonucleoside-diphosphate reductase 1 subunit beta GN=nrdB PE=1 SV=2 - [RIR2_ECOLI]
P08390	USG-1 protein GN=usg PE=1 SV=1 - [USG_ECOLI]
P0A7V3	30S ribosomal protein S3 GN=rpsC PE=1 SV=2 - [RS3_ECOLI]
P00509	Aspartate aminotransferase GN=aspC PE=1 SV=1 - [AAT_ECOLI]
P18133	Nicotinate phosphoribosyltransferase GN=pncB PE=1 SV=3 - [PNCB_ECOLI]
P33232	L-lactate dehydrogenase GN=lldD PE=1 SV=1 - [LLDD_ECOLI]
P00946	Mannose-6-phosphate isomerase GN=manA PE=1 SV=1 - [MANA_ECOLI]
P0A959	Glutamate-pyruvate aminotransferase AlaA GN=alaA PE=1 SV=1 - [ALAA_ECOLI]
P04693	Aromatic-amino-acid aminotransferase GN=tyrB PE=1 SV=1 - [TYRB_ECOLI]
P03004	Chromosomal replication initiator protein DnaA GN=dnaA PE=1 SV=2 - [DNAA_ECOLI]
P0A7V8	30S ribosomal protein S4 GN=rpsD PE=1 SV=2 - [RS4_ECOLI]
P02916	Maltose transport system permease protein MalF GN=malF PE=1 SV=1 - [MALF_ECOLI]
P0ACB7	Protein HemY GN=hemY PE=1 SV=1 - [HEMY_ECOLI]
P0ABB4	ATP synthase subunit beta GN=atpD PE=1 SV=2 - [ATPB_ECOLI]
P0AG30	Transcription termination factor Rho GN=rho PE=1 SV=1 - [RHO_ECOLI]
P0A6Z3	Chaperone protein HtpG GN=htpG PE=1 SV=1 - [HTPG_ECOLI]
P0A6Y8	Chaperone protein DnaK GN=dnaK PE=1 SV=2 - [DNAK_ECOLI]
P0ABJ9	Cytochrome bd-I ubiquinol oxidase subunit 1 GN=cydA PE=1 SV=1 - [CYDA_ECOLI]
P0AF08	Iron-sulfur cluster carrier protein GN=mrp PE=3 SV=1 - [APBC_ECOLI]
P0A6B7	Cysteine desulfurase IscS GN=iscS PE=1 SV=1 - [ISCS_ECOLI]
P0A6B4	Alanine racemase, biosynthetic GN=alr PE=1 SV=1 - [ALR1_ECOLI]
P10441	Lipid-A-disaccharide synthase GN=lpxB PE=1 SV=2 - [LPXB_ECOLI]
P00961	Glycine--tRNA ligase beta subunit GN=glyS PE=1 SV=4 - [SYGB_ECOLI]
P0A6F3	Glycerol kinase GN=glpK PE=1 SV=2 - [GLPK_ECOLI]
P0ABC7	Modulator of FtsH protease HflK GN=hflK PE=1 SV=1 - [HFLK_ECOLI]
P0AFG6	Dihydrolipoyllysine-residue succinyltransferase comp of 2-oxoglutarate dehydrogenase complex GN=sucB [ODO2_ECOLI]
P0AB71	Fructose-bisphosphate aldolase class 2 GN=fbaA PE=1 SV=2 - [ALF_ECOLI]
P75728	2-octaprenyl-3-methyl-6-methoxy-1,4-benzoquinol hydroxylase GN=ubiF PE=1 SV=1 - [UBIF_ECOLI]
P76440	NAD-dependent dihydropyrimidine dehydrogenase subunit PreT GN=preT PE=1 SV=1 - [PRET_ECOLI]
P27306	Soluble pyridine nucleotide transhydrogenase GN=sthA PE=1 SV=5 - [STHA_ECOLI]

P0A6H5	ATP-dependent protease ATPase subunit HslU GN=hslU PE=1 SV=1 - [HSLU_ECOLI]
P00888	Phospho-2-dehydro-3-deoxyheptonate aldolase, Tyr-sensitive GN=aroF PE=1 SV=1 - [AROF_ECOLI]
P00393	NADH dehydrogenase GN=ndh PE=1 SV=2 - [DHNA_ECOLI]
P0AB58	Lipopolysaccharide assembly protein B GN=lapB PE=1 SV=1 - [LAPB_ECOLI]
P37759	dTDP-glucose 4,6-dehydratase 1 GN=rfbB PE=3 SV=2 - [RMLB1_ECOLI]
P27833	dTDP-4-amino-4,6-dideoxygalactose transaminase GN=wecE PE=1 SV=2 - [WECE_ECOLI]
P02943	Maltoporin GN=lamB PE=1 SV=1 - [LAMB_ECOLI]
P0AES6	DNA gyrase subunit B GN=gyrB PE=1 SV=2 - [GYRB_ECOLI]
P24182	Biotin carboxylase GN=accC PE=1 SV=2 - [ACCC_ECOLI]
P0ABU2	Ribosome-binding ATPase YchF GN=ychF PE=1 SV=2 - [YCHF_ECOLI]
P0A6E4	Argininosuccinate synthase GN=argG PE=1 SV=2 - [ASSY_ECOLI]
P16676	Sulfate/thiosulfate import ATP-binding protein CysA GN=cysA PE=3 SV=2 - [CYSA_ECOLI]
P0A6F1	Carbamoyl-phosphate synthase small chain GN=carA PE=1 SV=1 - [CARA_ECOLI]
P16926	Cell shape-determining protein MreC GN=mreC PE=1 SV=1 - [MREC_ECOLI]
P36683	Aconitate hydratase B GN=acnB PE=1 SV=3 - [ACNB_ECOLI]
P76586	Uncharacterized protein YphH GN=yphH PE=3 SV=2 - [YPHH_ECOLI]
P0ABB0	ATP synthase subunit alpha GN=atpA PE=1 SV=1 - [ATPA_ECOLI]
P06720	Alpha-galactosidase GN=melA PE=1 SV=1 - [AGAL_ECOLI]
P36979	Dual-specificity RNA methyltransferase RlmN GN=rlmN PE=1 SV=1 - [RLMN_ECOLI]
P76035	Uncharacterized protein YciW GN=yciW PE=4 SV=2 - [YCIW_ECOLI]
P21179	Catalase HPII GN=katE PE=1 SV=1 - [CATE_ECOLI]

BAND 10

P0A6Y8	Chaperone protein DnaK GN=dnaK PE=1 SV=2 - [DNAK_ECOLI]
P06959	Dihydrolipoyllysine-residue acetyltransferase component of pyruvate dehydrogenase complex GN=aceF [ODP2_ECOLI]
P63020	Fe/S biogenesis protein NfuA GN=nfuA PE=1 SV=1 - [NFUA_ECOLI]
P0AG67	30S ribosomal protein S1 GN=rpsA PE=1 SV=1 - [RS1_ECOLI]
P0A6Z3	Chaperone protein HtpG GN=htpG PE=1 SV=1 - [HTPG_ECOLI]
P0AC41	Succinate dehydrogenase flavoprotein subunit GN=sdhA PE=1 SV=1 - [SDHA_ECOLI]
P33602	NADH-quinone oxidoreductase subunit G GN=nuoG PE=1 SV=4 - [NUOG_ECOLI]
P0ABH9	ATP-dependent Clp protease ATP-binding subunit ClpA GN=clpA PE=1 SV=1 - [CLPA_ECOLI]
P0AFG8	Pyruvate dehydrogenase E1 component GN=aceE PE=1 SV=2 - [ODP1_ECOLI]
P0A9M8	Phosphate acetyltransferase GN=pta PE=1 SV=2 - [PTA_ECOLI]
P63284	Chaperone protein ClpB GN=clpB PE=1 SV=1 - [CLPB_ECOLI]
P00363	Fumarate reductase flavoprotein subunit GN=frdA PE=1 SV=3 - [FRDA_ECOLI]
P0AAI3	ATP-dependent zinc metalloprotease FtsH GN=ftsH PE=1 SV=1 - [FTSH_ECOLI]
P20083	DNA topoisomerase 4 subunit B GN=parE PE=1 SV=3 - [PARE_ECOLI]
P32132	GTP-binding protein TypA/BipA GN=typA PE=1 SV=2 - [TYPA_ECOLI]
P28903	Anaerobic ribonucleoside-triphosphate reductase GN=nrdD PE=1 SV=2 - [NRDD_ECOLI]
P36683	Aconitate hydratase B GN=acnB PE=1 SV=3 - [ACNB_ECOLI]
P0A9P6	ATP-dependent RNA helicase DeaD GN=deaD PE=1 SV=2 - [DEAD_ECOLI]

P00959	Methionine--tRNA ligase GN=metG PE=1 SV=2 - [SYM_ECOLI]
P05055	Polyribonucleotide nucleotidyltransferase GN=pnp PE=1 SV=3 - [PNP_ECOLI]
P60785	Elongation factor 4 GN=lepA PE=1 SV=1 - [LEPA_ECOLI]
P0A7V3	30S ribosomal protein S3 GN=rpsC PE=1 SV=2 - [RS3_ECOLI]
P0ABJ9	Cytochrome bd-I ubiquinol oxidase subunit 1 GN=cydA PE=1 SV=1 - [CYDA_ECOLI]
P0A8T7	DNA-directed RNA polymerase subunit beta' GN=rpoC PE=1 SV=1 - [RPOC_ECOLI]
P45464	Penicillin-binding protein activator LpoA GN=lpoA PE=1 SV=1 - [LPOA_ECOLI]
P10121	Signal recognition particle receptor FtsY GN=ftsY PE=1 SV=1 - [FTSY_ECOLI]
P30850	Exoribonuclease 2 GN=rnb PE=1 SV=3 - [RNB_ECOLI]
P13009	Methionine synthase GN=metH PE=1 SV=5 - [METH_ECOLI]
P0ADY1	Peptidyl-prolyl cis-trans isomerase D GN=ppiD PE=1 SV=1 - [PPID_ECOLI]
P0A705	Translation initiation factor IF-2 GN=infB PE=1 SV=1 - [IF2_ECOLI]
P00968	Carbamoyl-phosphate synthase large chain GN=carB PE=1 SV=2 - [CARB_ECOLI]
P0A9Q7	Aldehyde-alcohol dehydrogenase GN=adhE PE=1 SV=2 - [ADHE_ECOLI]
P0A6M8	Elongation factor G GN=fusA PE=1 SV=2 - [EFG_ECOLI]
P0A8V2	DNA-directed RNA polymerase subunit beta GN=rpoB PE=1 SV=1 - [RPOB_ECOLI]
P0A9P0	Dihydrolipoyl dehydrogenase GN=lpdA PE=1 SV=2 - [DLDH_ECOLI]
P32176	Formate dehydrogenase-O major subunit GN=fdoG PE=1 SV=5 - [FDOG_ECOLI]
P37177	Phosphoenolpyruvate-dependent phosphotransferase system GN=ptsP PE=1 SV=2 - [PT1P_ECOLI]
P0CE47	Elongation factor Tu 1 GN=tufA PE=1 SV=1 - [EFTU1_ECOLI]
P09373	Formate acetyltransferase 1 GN=pflB PE=1 SV=2 - [PFLB_ECOLI]
P24230	ATP-dependent DNA helicase RecG GN=recG PE=1 SV=1 - [RECG_ECOLI]
P0AFI2	DNA topoisomerase 4 subunit A GN=parC PE=1 SV=1 - [PARC_ECOLI]
P00961	Glycine--tRNA ligase beta subunit GN=glyS PE=1 SV=4 - [SYGB_ECOLI]
P0AG20	GTP pyrophosphokinase GN=relA PE=1 SV=1 - [RELA_ECOLI]
P75864	Ribosomal RNA large subunit methyltransferase K/L GN=rlmL PE=1 SV=1 - [RLMKL_ECOLI]
P0A698	UvrABC system protein A GN=uvrA PE=1 SV=1 - [UVRA_ECOLI]
P0C8J8	D-tagatose-1,6-bisphosphate aldolase subunit GatZ GN=gatZ PE=1 SV=1 - [GATZ_ECOLI]
P0AES6	DNA gyrase subunit B GN=gyrB PE=1 SV=2 - [GYRB_ECOLI]

Appendix B

List of Proteins Identified in LipA-FLAG Co-Immunoprecipitation

Accession	Protein
BAND 2	
P0AFG8	Pyruvate dehydrogenase E1 component GN=aceE PE=1 SV=2 - [ODP1_ECOLI]
P06959	Dihydrolipoyllysine-residue acetyltransferase comp. of pyruvate dehydrogenase complex GN=aceF PE=1 SV=3 - [ODP2_ECOLI]
P0A9Q7	Aldehyde-alcohol dehydrogenase GN=adhE PE=1 SV=2 - [ADHE_ECOLI]
P0A6F5	60 kDa chaperonin GN=groL PE=1 SV=2 - [CH60_ECOLI]
P0A9M8	Phosphate acetyltransferase GN=pta PE=1 SV=2 - [PTA_ECOLI]
P0AFG3	2-oxoglutarate dehydrogenase E1 component GN=sucA PE=1 SV=1 - [ODO1_ECOLI]
P33602	NADH-quinone oxidoreductase subunit G GN=nuoG PE=1 SV=4 - [NUOG_ECOLI]
P0A698	UvrABC system protein A GN=uvrA PE=1 SV=1 - [UVRA_ECOLI]
P0A9P0	Dihydrolipoyl dehydrogenase GN=lpdA PE=1 SV=2 - [DLDH_ECOLI]
BAND 3	
P06959	Dihydrolipoyllysine-residue acetyltransferase comp of pyruvate dehydrogenase complex GN=aceF PE=1 SV=3 - [ODP2_ECOLI]
P0A6Y8	Chaperone protein DnaK GN=dnaK PE=1 SV=2 - [DNAK_ECOLI]
P0A9M8	Phosphate acetyltransferase GN=pta PE=1 SV=2 - [PTA_ECOLI]
P0AFG8	Pyruvate dehydrogenase E1 component GN=aceE PE=1 SV=2 - [ODP1_ECOLI]
P0A6F5	60 kDa chaperonin GN=groL PE=1 SV=2 - [CH60_ECOLI]
P0A9P0	Dihydrolipoyl dehydrogenase GN=lpdA PE=1 SV=2 - [DLDH_ECOLI]
P0A698	UvrABC system protein A GN=uvrA PE=1 SV=1 - [UVRA_ECOLI]
P05055	Polyribonucleotide nucleotidyltransferase GN=pnp PE=1 SV=3 - [PNP_ECOLI]
P0A6M8	Elongation factor G GN=fusA PE=1 SV=2 - [EFG_ECOLI]
P31120	Phosphoglucosamine mutase GN=glmM PE=1 SV=3 - [GLMM_ECOLI]
P0A6Z3	Chaperone protein HtpG GN=htpG PE=1 SV=1 - [HTPG_ECOLI]
P00490	Maltodextrin phosphorylase GN=malP PE=1 SV=7 - [PHSM_ECOLI]
P0AG67	30S ribosomal protein S1 GN=rpsA PE=1 SV=1 - [RS1_ECOLI]
BAND 4	
P0A6F5	60 kDa chaperonin GN=groL PE=1 SV=2 - [CH60_ECOLI]
P0A9P0	Dihydrolipoyl dehydrogenase GN=lpdA PE=1 SV=2 - [DLDH_ECOLI]
P06959	Dihydrolipoyllysine-residue acetyltransferase comp of pyruvate dehydrogenase complex GN=aceF PE=1 SV=3 - [ODP2_ECOLI]
P0AFG8	Pyruvate dehydrogenase E1 component GN=aceE PE=1 SV=2 - [ODP1_ECOLI]
P0A6Y8	Chaperone protein DnaK GN=dnaK PE=1 SV=2 - [DNAK_ECOLI]

P0A9C0	Anaerobic glycerol-3-phosphate dehydrogenase subunit A GN=glpA PE=1 SV=1 - [GLPA_ECOLI]
P0A850	Trigger factor GN=tig PE=1 SV=1 - [TIG_ECOLI]
P0A9M8	Phosphate acetyltransferase GN=pta PE=1 SV=2 - [PTA_ECOLI]
P0AC41	Succinate dehydrogenase flavoprotein subunit GN=sdhA PE=1 SV=1 - [SDHA_ECOLI]

BAND 5

P0A9P0	Dihydrolipoyl dehydrogenase GN=lpdA PE=1 SV=2 - [DLDH_ECOLI]
P0AFG6	Dihydrolipoyllysine-residue succinyltransferase component of 2-oxoglutarate dehydrogenase complex GN=sucB PE=1 SV=2 - [ODO2_E
P31120	Phosphoglucosamine mutase GN=glmM PE=1 SV=3 - [GLMM_ECOLI]
P06959	Dihydrolipoyllysine-residue acetyltransferase component of pyruvate dehydrogenase complex GN=aceF [ODP2_ECOLI]
P0A6F5	60 kDa chaperonin GN=groL PE=1 SV=2 - [CH60_ECOLI]
P15723	Deoxyguanosinetriphosphate triphosphohydrolase GN=dgt PE=1 SV=4 - [DGTP_ECOLI]
P0ABB0	ATP synthase subunit alpha GN=atpA PE=1 SV=1 - [ATPA_ECOLI]
P0AFG8	Pyruvate dehydrogenase E1 component GN=aceE PE=1 SV=2 - [ODP1_ECOLI]
P0A6F3	Glycerol kinase GN=glpK PE=1 SV=2 - [GLPK_ECOLI]
P0A6Y8	Chaperone protein DnaK GN=dnaK PE=1 SV=2 - [DNAK_ECOLI]
P0A850	Trigger factor GN=tig PE=1 SV=1 - [TIG_ECOLI]
P13035	Aerobic glycerol-3-phosphate dehydrogenase GN=glpD PE=1 SV=3 - [GLPD_ECOLI]
P0A6H5	ATP-dependent protease ATPase subunit HslU GN=hslU PE=1 SV=1 - [HSLU_ECOLI]
P0A698	UvrABC system protein A GN=uvrA PE=1 SV=1 - [UVRA_ECOLI]
P0A9M8	Phosphate acetyltransferase GN=pta PE=1 SV=2 - [PTA_ECOLI]
P0C8J8	D-tagatose-1,6-bisphosphate aldolase subunit GatZ GN=gatZ PE=1 SV=1 - [GATZ_ECOLI]
P68767	Cytosol aminopeptidase GN=pepA PE=1 SV=1 - [AMPA_ECOLI]
P06720	Alpha-galactosidase GN=melA PE=1 SV=1 - [AGAL_ECOLI]
P69776	Major outer membrane lipoprotein Lpp GN=lpp PE=1 SV=1 - [LPP_ECOLI]

BAND 6

P31120	Phosphoglucosamine mutase GN=glmM PE=1 SV=3 - [GLMM_ECOLI]
P0A6P9	Enolase GN=eno PE=1 SV=2 - [ENO_ECOLI]
P0ABB4	ATP synthase subunit beta GN=atpD PE=1 SV=2 - [ATPB_ECOLI]
P0AFG8	Pyruvate dehydrogenase E1 component GN=aceE PE=1 SV=2 - [ODP1_ECOLI]
P0A6F5	60 kDa chaperonin GN=groL PE=1 SV=2 - [CH60_ECOLI]
P06959	Dihydrolipoyllysine-residue acetyltransferase component of pyruvate dehydrogenase complex GN=aceF [ODP2_ECOLI]
P0A9P0	Dihydrolipoyl dehydrogenase GN=lpdA PE=1 SV=2 - [DLDH_ECOLI]
P0AFG6	Dihydrolipoyllysine-residue succinyltransferase comp. of 2-oxoglutarate dehydrogenase complex GN=sucB PE= [ODO2_ECOLI]
P0AG30	Transcription termination factor Rho GN=rho PE=1 SV=1 - [RHO_ECOLI]
P0A6Y8	Chaperone protein DnaK GN=dnaK PE=1 SV=2 - [DNAK_ECOLI]
P0A9G6	Isocitrate lyase GN=aceA PE=1 SV=1 - [ACEA_ECOLI]
P60716	Lipoyl synthase GN=lipA PE=1 SV=1 - [LIPA_ECOLI]

BAND 7

P60716	Lipoyl synthase GN=lipA PE=1 SV=1 - [LIPA_ECOLI]
P0AFG8	Pyruvate dehydrogenase E1 component GN=aceE PE=1 SV=2 - [ODP1_ECOLI]
P0A9P0	Dihydrolipoyl dehydrogenase GN=lpdA PE=1 SV=2 - [DLDH_ECOLI]
P06959	Dihydrolipoyllysine-residue acetyltransferase comp.t of pyruvate dehydrogenase complex GN=aceF PE=1 SV=3 - [ODP2_ECOLI]
P03023	Lactose operon repressor GN=lacI PE=1 SV=3 - [LACI_ECOLI]
P0CE47	Elongation factor Tu 1 GN=tufA PE=1 SV=1 - [EFTU1_ECOLI]
P31120	Phosphoglucosamine mutase GN=glmM PE=1 SV=3 - [GLMM_ECOLI]

BAND 8

P63020	Fe/S biogenesis protein NfuA GN=nfuA PE=1 SV=1 - [NFUA_ECOLI]
P0AFG8	Pyruvate dehydrogenase E1 component GN=aceE PE=1 SV=2 - [ODP1_ECOLI]
P0A9P0	Dihydrolipoyl dehydrogenase GN=lpdA PE=1 SV=2 - [DLDH_ECOLI]
P06959	Dihydrolipoyllysine-residue acetyltransferase comp. of pyruvate dehydrogenase complex GN=aceF PE=1 SV=3 - [ODP2_ECOLI]
P31120	Phosphoglucosamine mutase GN=glmM PE=1 SV=3 - [GLMM_ECOLI]
P28635	D-methionine-binding lipoprotein MetQ GN=metQ PE=1 SV=2 - [METQ_ECOLI]
P0A7L0	50S ribosomal protein L1 GN=rplA PE=1 SV=2 - [RL1_ECOLI]
P60716	Lipoyl synthase GN=lipA PE=1 SV=1 - [LIPA_ECOLI]
P0A6F5	60 kDa chaperonin GN=groL PE=1 SV=2 - [CH60_ECOLI]
P0A6Y8	Chaperone protein DnaK GN=dnaK PE=1 SV=2 - [DNAK_ECOLI]
P0A910	Outer membrane protein A GN=ompA PE=1 SV=1 - [OMPA_ECOLI]
P0A7V3	30S ribosomal protein S3 GN=rpsC PE=1 SV=2 - [RS3_ECOLI]

BAND 9

P0A7B8	ATP-dependent protease subunit HslV GN=hslV PE=1 SV=2 - [HSLV_ECOLI]
P0A6F5	60 kDa chaperonin GN=groL PE=1 SV=2 - [CH60_ECOLI]
P31120	Phosphoglucosamine mutase GN=glmM PE=1 SV=3 - [GLMM_ECOLI]
P0AG55	50S ribosomal protein L6 GN=rplF PE=1 SV=2 - [RL6_ECOLI]

BAND 10

P0A8W8	UPF0304 protein YfbU GN=yfbU PE=1 SV=1 - [YFBU_ECOLI]
P0A9P0	Dihydrolipoyl dehydrogenase GN=lpdA PE=1 SV=2 - [DLDH_ECOLI]
P63020	Fe/S biogenesis protein NfuA GN=nfuA PE=1 SV=1 - [NFUA_ECOLI]
P0A7W1	30S ribosomal protein S5 GN=rpsE PE=1 SV=2 - [RS5_ECOLI]
P02359	30S ribosomal protein S7 GN=rpsG PE=1 SV=3 - [RS7_ECOLI]
P0A912	Peptidoglycan-associated lipoprotein GN=pal PE=1 SV=1 - [PAL_ECOLI]
P0AEE1	Protein DcrB GN=dcrB PE=3 SV=1 - [DCRB_ECOLI]

BAND 11

P0A9P0	Dihydrolipoyl dehydrogenase GN=lpdA PE=1 SV=2 - [DLDH_ECOLI]

Appendix C

List of Interactions Tested by Bacterial Two Hybrid

Protein 1 (pUT18C)	Protein 2 (pST25)	Interaction Detected	Validated?
zip	zip	POSITIVE	positive control
E. coli gstB	E. coli gcvH	NEGATIVE	negative control
E. coli lipA	E. coli nfuA	POSITIVE	SEC, MST, Co-IP
E. coli erpA	E. coli nfuA	POSITIVE	SEC
E. coli erpA	E. coli lipA	NEGATIVE	SEC
E. coli nfuA C39A, C44A	E. coli lipA	POSITIVE	SEC
E. coli nfuA N term (aa 1-97)	E. coli lipA	POSITIVE	SEC
E. coli nfuA C term (aa 98-191)	E. coli lipA	NEGATIVE	SEC
E. coli nfuA	E. coli miaB	NEGATIVE	SEC neg.; co-IP pos.
S. aureus lipA	S. aureus nfu	NEGATIVE	No
S. aureus lipA	S. aureus sufA	NEGATIVE	No
S. aureus nfu	S. aureus sufA	NEGATIVE	No
S. aureus sufA	S. aureus nfu	NEGATIVE	No
E. coli nfuA aa 11-191	E. coli lipA	NEGATIVE	No
E. coli nfuA aa 21-191	E. coli lipA	NEGATIVE	No
E. coli nfuA aa 31-191	E. coli lipA	NEGATIVE	No
E. coli nfuA aa 41-191	E. coli lipA	NEGATIVE	No
E. coli nfuA aa 51-191	E. coli lipA	NEGATIVE	SEC
E. coli nfuA	E. coli lipA aa 26-321	NEGATIVE	No
E. coli nfuA	E. coli lipA aa 51-321	NEGATIVE	No
E. coli nfuA	E. coli lipA aa 76-321	NEGATIVE	No
E. coli nfuA	E. coli lipA aa 101-321	NEGATIVE	No
E. coli nfuA	E. coli lipA aa 126-321	NEGATIVE	No
E. coli nfuA	E. coli lipA aa 151-321	NEGATIVE	No
E. coli nfuA	E. coli lipA aa 176-321	NEGATIVE	No
E. coli nfuA	E. coli lipA aa 201-321	NEGATIVE	No
E. coli nfuA	E. coli lipA aa 226-321	NEGATIVE	No
E. coli nfuA	E. coli lipA aa 251-321	NEGATIVE	No
E. coli nfuA	E. coli lipA R107A	POSITIVE	No
E. coli nfuA	E. coli lipA RIYR AAAA	NEGATIVE	No
E. coli nfuA aa 3-191	E. coli lipA	POSITIVE	No
E. coli nfuA aa 4-191	E. coli lipA	POSITIVE	No
E. coli nfuA aa 6-191	E. coli lipA	NEGATIVE	No
E. coli nfuA aa 8-191	E. coli lipA	NEGATIVE	No
E. coli nfuA	E. coli lipA aa 6-321	POSITIVE	No

E. coli nfuA	**E. coli lipA aa 11-321**	**POSITIVE**	**No**
E. coli nfuA	**E. coli lipA aa 16-321**	**POSITIVE**	**No**
E. coli nfuA	**E. coli lipA aa 21-321**	**POSITIVE**	**No**
E. coli nfuA	**E. coli hscB**	**NEGATIVE**	**SEC**
E. coli hscB	**E. coli nfuA**	**NEGATIVE**	**SEC**
E. coli hscB	**E. coli lipA**	**NEGATIVE**	**SEC**
E. coli lipA	**E. coli hscB**	**NEGATIVE**	**SEC**
E. coli hscB	**E. coli lipA RIYR AAAA**	**NEGATIVE**	**SEC**
E. coli nfuA Ile4Ala	**E. coli lipA**	**NEGATIVE**	**SEC, MST**
E. coli nfuA Ser5Ala	**E. coli lipA**	**POSITIVE**	**No**
E. coli nfuA Ile4Ala, Ser5Ala	**E. coli lipA**	**NEGATIVE**	**No**
E. coli lipA Leu21Ala	**E. coli nfuA**	**POSITIVE**	**No**
E. coli lipA Ile22Ala	**E. coli nfuA**	**NEGATIVE**	**SEC, MST**
E. coli lipA Pro23Ala	**E. coli nfuA**	**NEGATIVE**	**SEC, MST**
E. coli lipA Val24Ala	**E. coli nfuA**	**NEGATIVE**	**SEC, MST**
E. coli lipA Lys25Arg	**E. coli nfuA**	**POSITIVE**	**No**
E. coli lipA Lys25Ala	**E. coli nfuA**	**POSITIVE**	**No**
E. coli iscU	**E. coli lipA**	**NEGATIVE**	**No**
E. coli iscU	**E. coli lipA RIYR AAAA**	**NEGATIVE**	**No**
E. coli iscU	**E. coli hscB**	**POSITIVE**	**No**
E. coli iscU	**E. coli nfuA**	**WEAK POSITIVE**	**No**
S. aureus LipA	**S. aureus SufT**	**NEGATIVE**	**No**
S. aureus Nfu	**S. aureus SufT**	**NEGATIVE**	**No**
S. aureus SufA	**S. aureus SufT**	**NEGATIVE**	**No**

Appendix D

Amino Acid Sequences of Proteins Studied

***E. coli* Lipoyl synthase (Uniprot P60716)**

MSKPIVMERGVKYRDADKMALIPVKNVATEREALLRKPEWMKIKLPADSTRIQGIKAAMR
KNGLHSVCEEASCPNLAECFNHGTATFMILGAICTRRCPFCDVAHGRPVAPDANEPVKLA
QTIADMALRYVVITSVDRDDLRDGGAQHFADCITAIREKSPQIKIETLVPDFRGRMDRAL
DILTATPPDVFNHNLENVPRIYRQVRPGADYNWSLKLLERFKEAHPEIPTKSGLMVGLGE
TNEEIIEVMRDLRRHGVTMLTLGQYLQPSRHHLPVQRYVSPDEFDEMKAEALAMGFTHAA
CGPFVRSSYHADLQAKGMEVK

***M. tuberculosis* Lipoyl synthase (Uniprot P9WK91)**

MSVAAEGRRLLRLEVRNAQTPIERKPPWIKTRARIGPEYTELKNLVRREGLHTVCEEAGC
PNIFECWEDREATFLIGGDQCTRRCDFCQIDTGKPAELDRDEPRRVADSVRTMGLRYATV
TGVARDDLPDGGAWLYAATVRAIKELNPSTGVELLIPDFNGEPTRLAEVFESGPEVLAHN
VETVPRIFKRIRPAFTYRRSLGVLTAARDAGLVTKSNLILGLGETSDEVRTALGDLRDAG
CDIVTITQYLRPSARHHPVERWVKPEEFVQFARFAEGLGFAGVLAGPLVRSSYRAGRLYE
QARNSRALASR

***S. aureus* Lipoyl synthase (Uniprot Q2FZX4)**

MATKNEEILRKPDWLKIKLNTNENYTGLKKMMREKNLNTVCEEAKCPNIHECWGARRTAT
FMILGAVCTRACRFCAVKTGLPNELDLNEPERVAESVELMNLKHVVITAVARDDLRDAGS
NVYAETVRKVRERNPFTTIEILPSDMGGDYDALETLMASRPDILNHNIETVRRLTPRVRA
RATYDRTLEFLRRSKELQPDIPTKSSIMVGLGETIEEIYETMDDLRANDVDILTIGQYLQ
PSRKHLKVQKYYTPLEFGKLRKVAMDKGFKHCQAGPLVRSSYHADEQVNEAAKEKQRQGE
AQLNS

***E. coli* NfuA (Uniprot P63020)**

MIRISDAAQAHFAKLLANQEEGTQIRVFVINPGTPNAECGVSYCPPDAVEATDTALKFDL
LTAYVDELSAPYLEDAEIDFVTDQLGSQLTLKAPNAKMRKVADDAPLMERVEYMLQSQIN
PQLAGHGGRVSLMEITEDGYAILQFGGGCNGCSMVDVTLKEGIEKQLLNEFPELKGVRDL
TEHQRGEHSYY

***M. tuberculosis* NfuA (Uniprot A0A1K3J566)**

MITITDAAQAHFSKLLANQEPGTQIRVFVINPGTPNAECGVSYCPPDAVEATDTALPFEQ
LTAYVDELSAPFLDEAVIDFVTDQLGSQLTLKAPNAKMRKVADDAPLIERVEYVLQSQIN
PQLAGHGGRVSLMEITDEGYAILQFGGGCNGCSMVDVTLKEGIEKELLNMFAGELKGVKD
LTEHQRGEHSYY

***S. aureus* Nfu (Uniprot A0A0H2XDZ0)**

MPTEDTTMFDQVAEVIERLRPFLLRDGGDCSLIDVEDGIVKLQLHGACGTCPSSTITLKA
GIERALHEEVPGVIEVEQVF

***E. coli* NfuA N terminal domain (Uniprot P63020 full-length protein)**

MIRISDAAQAHFAKLLANQEEGTQIRVFVINPGTPNAECGVSYCPPDAVEATDTALKFDL
LTAYVDELSAPYLEDAEIDFVTDQLGSQLTLKAPNAK

***E. coli* NfuA C terminal domain (Uniprot P63020 full-length protein)**

MRKVADDAPLMERVEYMLQSQINPQLAGHGGRVSLMEITEDGYAILQFGGGCNGCSMVDVTLKEG
IEKQLLNEFPELKGVRDLTEHQRGEHSYY

***E. coli* NfuA N terminal domain- *S. aureus* Nfu Fusion**

MIRISDAAQAHFAKLLANQEEGTQIRVFVINPGTPNAECGVSYCPPDAVEATDTALKFDLLTAYVD
ELSAPYLEDAEIDFVTDQLGSQLTLKAPNAKMRKVADDAPLMERVEYMLQSMPTEDTTMFDQVA
EVIERLRPFLLRDGGDCSLIDVEDGIVKLQLHGACGTCPSSTITLKAGIERALHEEVPGVIEVEQVF

Human NFU1 (Uniprot Q9UMS0)

MAATARRGWGAAAVAAGLRRRFCHMLKNPYTIKKQPLHQFVQRPLFPLPAAFYHPVRYMFIQTQ
DTPNPNSLKFIPGKPVLETRTMDFPTPAAAFRSPLARQLFRIEGVKSVFFGPDFITVTKENEELDW
NLLKPDIYATIMDFFASGLPLVTEETPSGEAGSEEDDEVVAMIKELLDTRIRPTVQEDGGDVIYKGF
EDGIVQLKLQGSCTSCPSSIITLKNGIQNMLQFYIPEVEGVEQVMDDESDEKEANSP

***E. coli* NfuA N terminal domain- Human NFU1 Fusion**

MIRISDAAQAHFAKLLANQEEGTQIRVFVINPGTPNAECGVSYCPPDAVEATDTALKFDLLTAYVD
ELSAPYLEDAEIDFVTDQLGSQLTLKAPNAKMAATARRGWGAAAVAAGLRRRFCHMLKNPYTIKK
QPLHQFVQRPLFPLPAAFYHPVRYMFIQTQDTPNPNSLKFIPGKPVLETRTMDFPTPAAAFRSPLA
RQLFRIEGVKSVFFGPDFITVTKENEELDWNLLKPDIYATIMDFFASGLPLVTEETPSGEAGSEEDD
EVVAMIKELLDTR
IRPTVQEDGGDVIYKGFEDGIVQLKLQGSCTSCPSSIITLKNGIQNMLQFYIPEVEGVEQ
VMDDESDEKEANSP

***S. aureus* SufT (Uniprot A0A0H2XI17)**

MVIDPELGIDIVNLGLVYKVNVDDEGVCTVDMTLTSMGCPMGPQIIDQVKTVLAEIPEIQ
DTEVNIVWSPPWTKDMMSRYAKIALGVS

***S. aureus* SufA (Uniprot X5DRM5)**

MPTVILTEAAAYEVKDMLKANEMPDGYLKIKVNGGGCTGLTYGMGAEEAPGENDEVLEYF
GLKVLVDKKDAPVLNGTTIDFKQSLMGGGFQIDNPNAIASCGCGSSFRTAKVAGNPENC

***M. tuberculosis* SufT (Uniprot O53157)**

MSETSAPAEELLADVEEAMRDVVDPELGINVVDLGLVYGLDVQDGDEGTVALIDMTLTSA
ACPLTDVIEDQSRSALVGSGLVDDIRINWVWNPPWGPDKITEDGREQLRALGFTV

***E. coli* IscU (Uniprot P0ACD4)**

MAYSEKVIDHYENPRNVGSFDNNDENVGSGMVGAPACGDVMKLQIKVNDEGIIEDARFKT
YGCGSAIASSSLVTEWVKGKSLDEAQAIKNTDIAEELELPPVKIHCSILAEDAIKAAIAD
YKSKREAK

***E. coli* HscA (Uniprot P0A6Z1)**

MALLQISEPGLSAAPHQRRLAAGIDLGTTNSLVATVRSGQAETLADHEGRHLLPSVVHYQ
QQGHSVGYDARTNAALDTANTISSVKRLMGRSLADIQQRYPHLPYQFQASENGLPMIETA
AGLLNPVRVSADILKALAARATEALAGELDGVVITVPAYFDDAQRQGTKDAARLAGLHVL
RLLNEPTAAAIAYGLDSGQEGVIAVYDLGGGTFDISILRLSRGVFEVLATGGDSALGGDD
FDHLLADYIREQAGIPDRSDNRVQRELLDAAIAAKIALSDADSVTVNVAGWQGEISREQF
NELIAPLVKRTLLACRRALKDAGVEADEVLEVVMVGGSTRVPLVRERVGEFFGRPPLTSI
DPDKVVAIGAAIQADILVGNKPDSEMLLLDVIPLSLGLETMGGLVEKVIPRNTTIPVARA
QDFTTFKDGQTAMSIHVMQGERELVQDCRSLARFALRGIPALPAGGAHIRVTFQVDADGL
LSVTAMEKSTGVEASIQVKPSYGLTDSEIASMIKDSMSYAEQDVKARMLAEQKVEAARVL
ESLHGALAADAALLSAAERQVIDDAAAHLSEVAQGDDVDAIEQAIKNVDKQTQDFAARRM
DQSVRRALKGHSVDEV

***E. coli* HscB (Uniprot P0A6L9)**

MDYFTLFGLPARYQLDTQALSLRFQDLQRQYHPDKFASGSQAEQLAAVQQSATINQAWQT
LRHPLMRAEYLLSLHGFDLASEQHTVRDTAFLMEQLELREELDEIEQAKDEARLESFIKR
VKKMFDTRHQLMVEQLDNETWDAAADTVRKLRFLDKLRSSAEQLEEKLLDF

***E. coli* ErpA (Uniprot P0ACC3)**

MSDDVALPLEFTDAAANKVKSLIADEDNPNLKLRVYITGGGCSGFQYGFTFDDQVNEGDM
TIEKQGVGLVVDPMSLQYLVGGSVDYTEGLEGSRFIVTNPNAKSTCGCGSSFSI

***E. coli* YgfZ (Uniprot P0ADE8)**

MAFTPFPPRQPTASARLPLTLMTLDDWALATITGADSEKYMQGQVTADVSQMAEDQHLLA
AHCDAKGKMWSNLRLFRDGDGFAWIERRSVREPQLTELKKYAVFSKVTIAPDDERVLLGV
AGFQARAALANLFSELPSKEKQVVKEGATTLLWFEHPAERFLIVTDEATANMLTDKLRGE
AELNNSQQWLALNIEAGFPVIDAANSGQFIPQATNLQALGGISFKKGCYTGQEMVARAKF
RGANKRALWLLAGSASRLPEAGEDLELKMGENWRRTGTVLAAVKLEDGQVVVQVVMNNDM
EPDSIFRVRDDANTLHIEPLPYSLEE

***E. coli* GrxD (Uniprot P0AC69)**

MSTTIEKIQRQIAENPILLYMKGSPKLPSCGFSAQAVQALAACGERFAYVDILQNPDIRA
ELPKYANWPTFPQLWVDGELVGGCDIVIEMYQRGELQQLIKETAAKYKSEEPDAE

***E. coli* IscS (Uniprot P0A6B7)**

MKLPIYLDYSATTPVDPRVAEKMMQFMTMDGTFGNPASRSHRFGWQAEEAVDIARNQIAD
LVGADPREIVFTSGATESDNLAIKGAANFYQKKGKHIITSKTEHKAVLDTCRQLEREGFE
VTYLAPQRNGIIDLKELEAAMRDDTILVSIMHVNNEIGVVQDIAAIGEMCRARGIIYHVD
ATQSVGKLPIDLSQLKVDLMSFSGHKIYGPKGIGALYVRRKPRVRIEAQMHGGGHERGMR
SGTLPVHQIVGMGEAYRIAKEEMATEMERLRGLRNRLWNGIKDIEEVYLNGDLEHGAPNI
LNVSFNYVEGESLIMALKDLAVSSGSACTSASLEPSYVLRALGLNDELAHSSIRFSLGRF
TTEEEIDYTIELVRKSIGRLRDLSPLWEMYKQGVDLNSIEWAHH

***E. coli* BolA (Uniprot P0ABE2)**

MMIRERIEEKLRAAFQPVFLEVVDESYRHNVPAGSESHFKVVLVSDRFTGERFLNRHRMI
YSTLAEELSTTVHALALHTYTIKEWEGLQDTVFASPPCRGAGSIA

***E. coli* IscA (Uniprot P0AAC8)**

MSITLSDSAAARVNTFLANRGKGFGLRLGVRTSGCSGMAYVLEFVDEPTPEDIVFEDKGV
KVVVDGKSLQFLDGTQLDFVKEGLNEGFKFTNPNVKDECGCGESFH

VITA

Erin L. McCarthy

Education:

The Pennsylvania State University, Department of Biochemistry, Molecular Biology, and Microbiology, University Park, PA, Ph.D 2014-2019
Advisor: Squire J. Booker

Mercyhurst University, Erie, PA, Bachelor of Science in Biochemistry, 2013

Publications:

Erin L. McCarthy, Ananda N. Rankin, Zerick R. Dill, and Squire J. Booker. The A-type domain in *Escherichia coli* NfuA is required for regenerating the auxiliary [4Fe–4S] cluster in *Escherichia coli* lipoyl synthase. *The Journal of Biological Chemistry*, 2019: *294*, 1609-1617.

Erin L. McCarthy and Squire J. Booker. Biochemical approaches for understanding iron-sulfur cluster regeneration in *Escherichia coli* lipoyl synthase during catalysis. *Methods in Enzymology*, 2018: *606*, 217-239.

Nicholas D. Lanz*, Anthony J. Blaszczyk*, **Erin L. McCarthy,** Bo Wang, Roy X. Wang, Brianne Jones, and Squire J. Booker. Enhanced Solubilization of Class B Radical *S*-adenosylmethionine methylases by improved cobalamin uptake in *Escherichia coli*. *Biochemistry*, 2018: *57*, 1475-1490. *contributed equally

Erin L. McCarthy and Squire J. Booker. Destruction and reformation of an iron-sulfur cluster during catalysis by lipoyl synthase. *Science*, 2017: *358*, 373-377.

Bradley J. Landgraf, **Erin L. McCarthy,** and Squire J. Booker. Radical SAM Enzymes in Human Health and Disease. *Annual Reviews of Biochemistry*, 2016: *85*, 485-514.

Erin L. McCarthy and Squire J. Booker. Bridging a gap in iron-sulfur cluster assembly. *Elife*, 2015: *4*.

Awards:

50th Enzyme Mechanisms Conference Poster Award, 2019

Paul Berg Travel Award, 2018

Richard L. and Norma L. McCarl Graduate Scholarship, 2018

Helmut Beinert Poster Prize (39th Steenbock Symposium), 2018

Paul Berg Prize in Molecular Biology, 2018

Homer F. Braddock and Nellie H. and Oscar L. Roberts Fellowship, 2014